RESEARCH AND TECHNOLOGY

GODDARD SPACE FLIGHT CENTER **R&T**

COBE's search for structure in the Big Bang

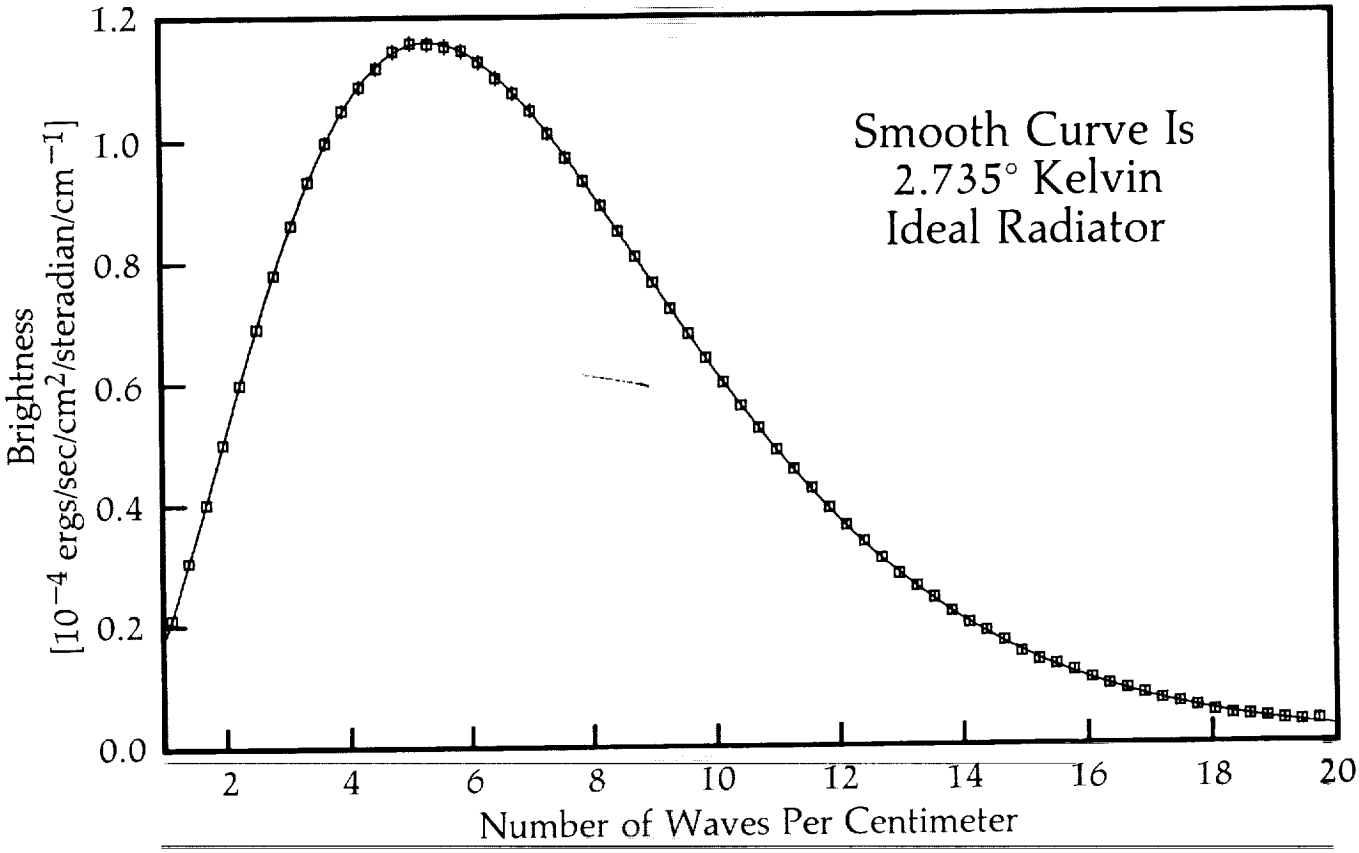

(NASA-TM-105491) RESEARCH AND TECHNOLOGY: NASA. GODDARD SPACE FLIGHT CENTER, 1989 (NASA) 279 p

N92-70705

Unclas

Z9/99 0091713

NASA

ORIGINAL PAGE
COLOR PHOTOGRAPH

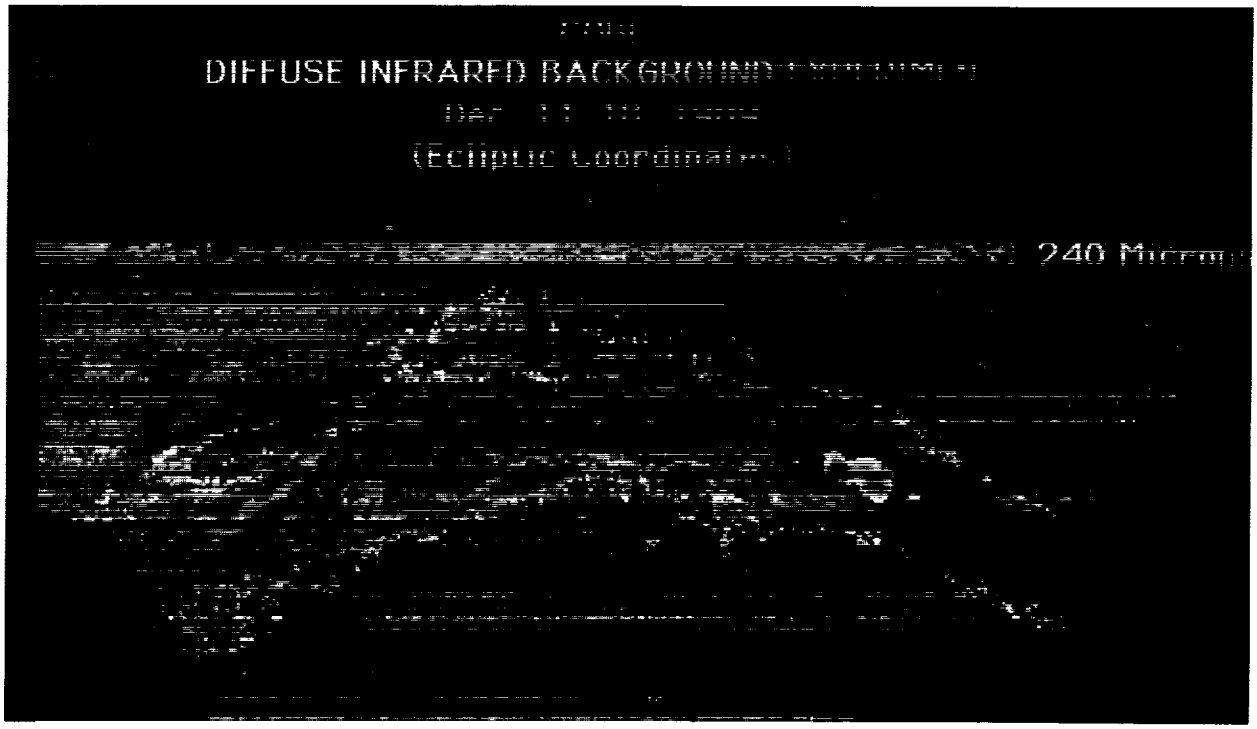

(above) The Milky Way galaxy, near the constellation Cygnus, as seen by the Diffuse Infrared Background Experiment (DIRBE) on the Cosmic Background Explorer (COBE) spacecraft. The COBE was launched November 18, 1989, to study the Big Bang, the cosmic explosion that started the present expansion of the entire universe 15 billion years ago. The DIRBE instrument maps the sky at 10 infrared wavelengths from 1 to 300 micrometers, to help us distinguish between our own astronomical neighborhood and the most distant cosmic objects. The map above was made at a wavelength of 240 micrometers and shows the brightness of cold dust grains in the space between the stars in our galaxy, but in other directions the long-sought first cosmic objects are expected to be seen. The apparent curvature of the Milky Way is due to the coordinate system in this preliminary map.

(front cover) The spectrum of the Big Bang, as measured by the Far Infrared Absolute Spectrophotometer (FIRAS) on the COBE. This spectrum shows the brightness of the Big Bang for many different wavelengths. It represents 9 minutes of flight data but already confirms the prediction of the simplest Big Bang theory to remarkable precision. The data show absolutely no hint or trace of the massive energetic processes that must have created the structure of our present universe, filled with enormous voids and huge concentrations of galaxies, such as the "Great Attractor." Further data analysis is expected to reveal these structures.

RESEARCH AND TECHNOLOGY

GODDARD SPACE FLIGHT CENTER — *R&T*

Foreword

ORIGINAL CONTAINS
COLOR ILLUSTRATIONS

The launch of Cosmic Background Explorer (COBE) and the definition of Earth Observing System (EOS)—these are two of the major events this year at Goddard Space Flight Center. COBE is typical of Goddard's style and commitment to space science. The three experiments—Differential Microwave Radiometer (DMR), Far Infrared Absolute Spectrophotometer (FIRAS), and Diffuse Infrared Background Experiment (DIRBE)—are going to be very important in measuring the "big bang." DMR measures the isotropy of the cosmic background (direction of the radiation). FIRAS looks at the spectrum over the whole sky, searching for deviations, and DIRBE operates in the infrared part of the spectrum gathering evidence of the earliest galaxy formation. By special techniques we will distinguish the radiation coming from the solar system from that of extragalactic origin. Unique graphics will be used to represent the temperature of the emitting material. Our investigators will be able to model a cosmic event of such importance that it will affect cosmological theory for generations to come.

By contrast, we are also preparing for a 20- to 25-year project to monitor changes in the Earth's geophysics during a whole solar color cycle. EOS is likely to provide the major data base on the Earth for the next several decades. Over 500 selected investigators and co-investigators assembled at Goddard for the first Investigators' Working Group to plan this important mission. We have had field trips and data conferences, made measurements from airplanes and balloons, met with our international scientific colleagues, and stimulated the public with our concern over global warming and deforestation. Now we begin on the long path which goes on until we truly understand our own home planet.

Cosmology and Earth system science are only two ends of the spectrum of interest at Goddard. We also do everything in between. We have experts in planetology, astronomy, aeronomy, solar physics, intergalactic physics, data and information theory, and biology. We design, build, and launch spacecraft, which use data systems, power systems, instruments, thermal control mechanisms, and optical instruments we have developed.

We are world class in robotics and telecommunications, in software and analytical testing. Research and technology is our profession, excellence is our goal, success is our hallmark.

Thank you, fellow employees, for surpassing NASA's and my expectations.

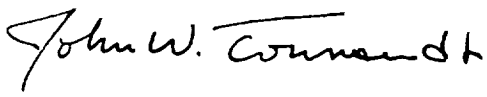

Dr. John W. Townsend, Jr.
Director

Contents

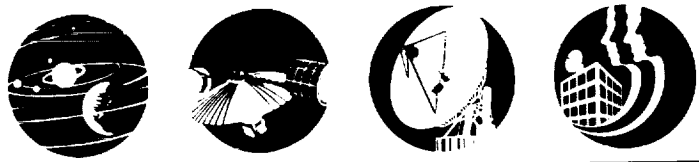

Earth Sciences

Oceans and Ice 3
Land Processes 20
Atmospheres 47

Space Sciences

Planetology 79
Solar Physics and Astronomy 82
Extraterrestrial Physics 91
High Energy Astrophysics 106

Data and Information

Data and Information 121

Flight Projects

Flight Projects 153
Space Station 169

Communications Technology

Space Communications Systems 181
System and Software Engineering 192

Engineering Technology

Sensors and Space Technology 213
Space Communications Systems 237
System and Software Engineering 239
User Space Data Systems 245
Techniques 246

Institutional Technology

Institutional Technology 257

Acronyms

Acronyms 271

Index

Index 275

ORIGINAL PAGE
COLOR PHOTOGRAPH

The challenge to Earth Sciences is to develop the capability to predict those changes that will occur in the next decade to century, both naturally and in response to human activity.

OCEANS AND ICE

ARCTIC SEA ICE VARIABILITY: 1973-1987

Polar sea ice has long been recognized as a critical element in the complex atmosphere-hydrosphere-cryosphere global climate system. Its importance derives from its considerable spatial and temporal variability and from its effectiveness in modifying surface albedo, in altering watermass properties of the underlying ocean, and in restricting exchanges of heat, mass, and momentum between the ocean and atmosphere. The largest observed spatial and temporal variation of the sea ice cover is the seasonal cycle. The Arctic sea ice extent ranges from a minimum of about 8×10^6 km^2 in September to a maximum of about 15×10^6 km^2 in March. Interannual variations of the seasonal cycle are of particular interest to climatologists as potential early indicators of climate change.

Only since the advent of satellite observations have researchers been able to monitor the variability of the sea ice cover on a global scale. The earliest satellite observations of sea ice were made nearly 30 years ago from visible and infrared imagery obtained with polar orbiting weather satellites. Manual interpretation of this imagery was generally quite reliable except when clouds or darkness obscured the view. Satellite microwave observations, which began in late 1972, allowed coverage through both darkness and cloud cover and, more importantly, permitted a quantitative determination of ice concentration through the use of computer algorithms even though individual floes and leads were not resolved. Although microwave surveillance is currently limited in spatial resolution to about 30 km, it does provide complete polar coverage with as little as 1 day of data.

The first passive microwave imaging radiometer to provide complete coverage of the polar regions was the Electrically Scanning Microwave Radiometer (ESMR) launched on the Nimbus-5 spacecraft in December 1972. Since 1972, passive microwave satellite observations have served as the single most valuable source of information on the state of global sea ice cover. In contrast to the single-channel ESMR, a Scanning Multichannel Microwave Radiometer (SMMR) was launched in October 1978, on the Nimbus-7 spacecraft. This 10-channel sensor provided the data for more accurate ice concentration determinations and yielded the first satellite observations of multiyear ice concentration and ice temperature (Cavalieri and others, 1984).

Data acquired with both the Nimbus-5 ESMR and the Nimbus-7 SMMR instruments, from 1973 to 1987, have been used to describe the seasonal, regional, and interannual variability of the Arctic sea ice cover (Parkinson and others, 1987; Gloersen and Campbell, 1988; and Parkinson and Cavalieri, 1989). Monthly mean Arctic sea ice concentration maps derived from the Nimbus-7 SMMR for February and August 1985 and

Image of Washington, DC in the spring depicting ground reflectance rather than radiance. The false color composite was created by assigning customary blue, green, and red guns to Thematic Mapper bands 1,3, and 4 respectively.

shown in the first figure illustrate the large difference in seasonal ice extent. In February, the ice cover extends across the entire Arctic Basin and over large portions of many of the peripheral seas and bays, including most of the Sea of Okhotsk, the Bering Sea, Baffin Bay, and all of Hudson Bay. Sea ice is also found along the eastern coasts of Greenland and Canada. In August, the ice cover is limited largely to the central Arctic and the Canadian Archipelago, with most of the Kara and Barents Seas ice free. Interestingly, those areas that are ice free during summer (termed seasonal sea ice zones) exhibit particularly large spatial and temporal variabilities.

For the purpose of examining these regional differences, the Arctic was divided into eight regions: the Sea of Okhotsk, Bering Sea, Hudson Bay, Baffin Bay/Davis Strait, Arctic Ocean, Canadian Archipelago, Greenland Sea, and Kara and Barents Seas (Parkinson and others, 1987). The two regions that show the greatest regional and interannual variability observed during the ESMR and SMMR years are Baffin Bay/Davis Strait and the Kara and Barents Seas. This variability is illustrated in the second figure, which shows a time series of the yearly averaged sea ice extents for the two regions and for the sum of all eight regions. (Note: There is no passive microwave coverage for 1977 or most of 1978.) Among the prominent features shown in the second figure are the upward trend in the Baffin Bay/Davis Strait ice area and the downward trend in the Kara and Barents Seas ice area. Also apparent in this figure are some out-of-phase relationships between the two regions. For example, during the ESMR years 1973 through 1975 the Baffin Bay/Davis Strait sea ice area decreases, then increases—while the Kara/Barents Sea area increases, then decreases. These and other interregional relationships have been associated with differences in atmospheric or oceanographic conditions.

Examination of the yearly averaged sea ice extent for all eight Northern Hemisphere regions shows an upward trend during the ESMR years and a smaller downward trend during the SMMR years. These data present no significant overall trend during this period. The question of whether or not the downward trend observed during the SMMR years continues, as might be expected from a scenario of global warming, will be answered only by a longer data record.

Contact: Donald J. Cavalieri (Code 671)
(301) 286-2444
Claire L. Parkinson (Code 671)
(301) 286-6507

Sponsor: Oceanic Processes Branch, NASA Headquarters

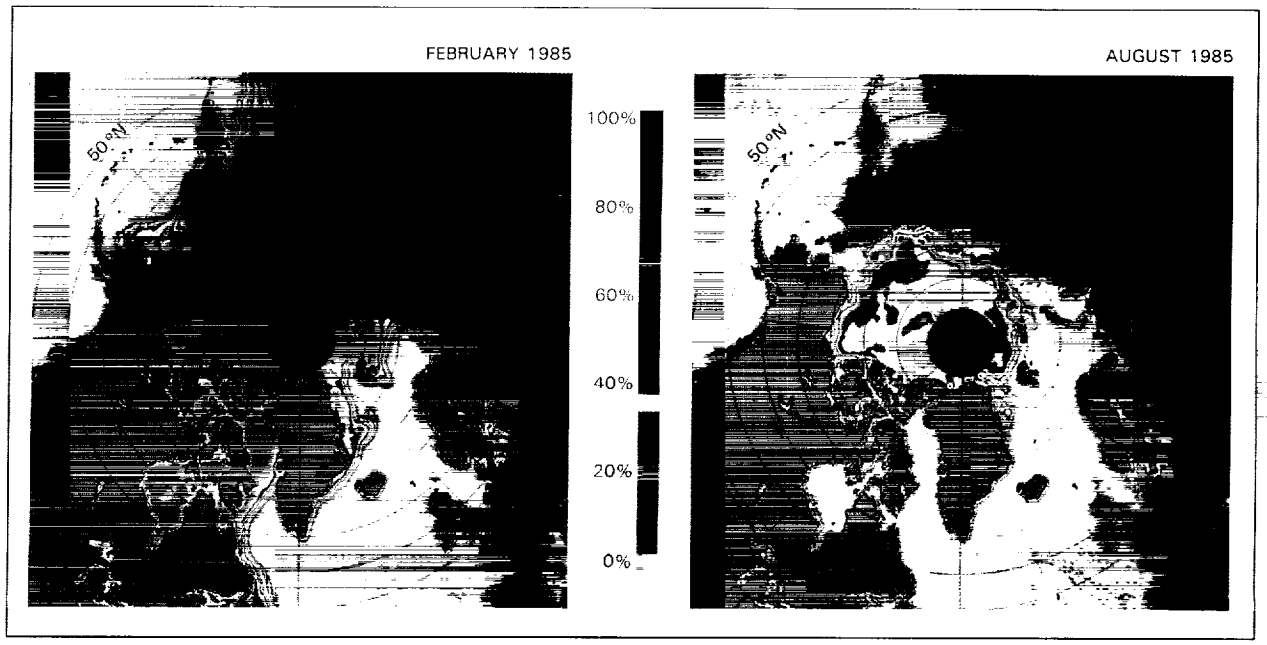

Monthly mean Arctic Sea ice concentrations derived from Nimbus-7 SMMR data for February and August 1985.

ORIGINAL PAGE
COLOR PHOTOGRAPH

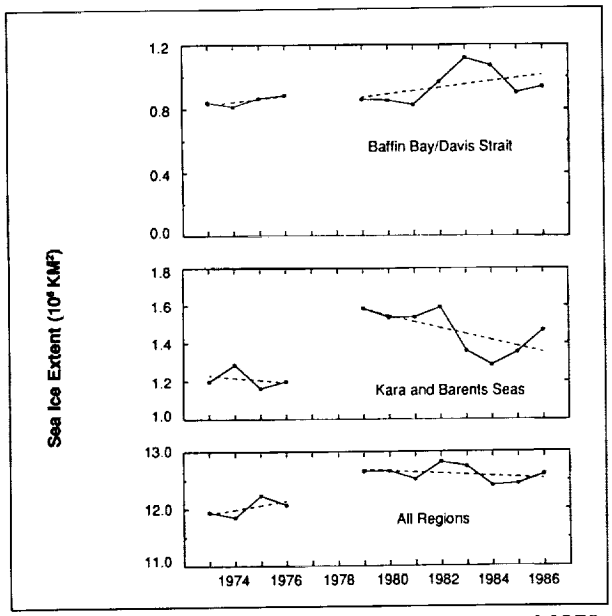

Yearly averaged sea ice extents, 1973-1976 and 1979-1986, for the Baffin Bay/Davis Strait region, the Kara and Barents Seas region, and the sum of all eight regions. The two dashed lines in each plot are the linear least-squares fits through the 1973-1976 ESMR data and the 1979-1986 SMMR data.

Dr. Donald J. Cavalieri is a physical scientist in the Oceans and Ice Branch of the Laboratory for Oceans. His research centers on development of techniques for using passive microwave satellite observations and on the application of those techniques to the study of sea ice and its interactions with the atmosphere and oceans. He has been at Goddard for 10 years and earned his PhD from New York University.

Dr. Claire L. Parkinson has been a research climatologist at Goddard for 11 years, concentrating her work on polar sea ice and its climatic connections. She has authored a book on the history of science and coauthored books on climate modeling, Arctic sea ice, and Antarctic sea ice. She received her PhD from The Ohio State University.

GROWTH OF THE GREENLAND ICE SHEET

The mass balance of the Greenland and Antarctic ice sheets is of current interest, largely because of its direct relationship to global sea level. At present, global sea level appears to be rising by 2.4 ± 0.9 mm/year. Although both thermal expansion of the ocean and melting of small glaciers contribute to sea-level rise, the major source of water for the current sea-level rise is undetermined. The possibility of enhanced ice-sheet melting in a warmer climate is also of concern. Each year, approximately 3,000 km^3 of water is exchanged between the ocean and the ice sheets of Greenland and Antarctica. This volume of exchange is equivalent to 8 mm of water from the entire surface of the world's oceans. The uncertainty in ice-sheet mass balance has been at least ± 30 percent of the annual mass exchange and is equivalent to ± 2.4 mm/year of sea-level change.

Measurement of elevation change by satellite altimetry offers a unique method of determining changes in ice volume and therefore mass balance. In 1978, ice-sheet elevations based on data from the oceanic radar altimeter on Geostationary Earth Orbiting Satellite (GEOS)-3 were reported. The 3-year operation of GEOS-3 from April 1975 to June 1978, followed by the 3-month operation of the SEASAT radar altimeter from July to September 1978, provided a time series of ice elevations, but the precision and spatial coverage of GEOS-3 was limited. GEOSAT, a U.S. Navy radar altimeter satellite, was launched in March 1985. The first 18 months of the GEOSAT data are classified for geodetic purposes, but the data over polar ice were released to NASA research. The GEOSAT ice data, processed and analyzed at Goddard, produced the Greenland ice-sheet topography in the first figure.

The first determination of regional changes in ice-sheet elevations has been made using data from GEOS-3, SEASAT, and the first 18 months of GEOSAT. Vertical velocities of the surface are determined from measured changes in surface elevations at 256,694 intersections between paths of GEOSAT during a 548-day period from 1985 to 1986 and from 5,096 intersections between GEOSAT paths in 1985 and SEASAT paths in 1978. Although the standard error at a single crossover is about 1.4 m, the error of the mean regional difference is only a few centimeters. The average of all measurements between the latitudes of 60° N and 72° N shows an increase of 0.20 ± 0.08 m/year from 1978 to 1985 and 0.28 ± 0.02 m/year from 1985 to 1986. Analysis by elevation bands shown in the second figure indicates that the surface elevation increased in both the area of net annual ablation below about 1,200 m and the area of net annual accumulation at higher elevations. For both periods, the spatially averaged increase in surface elevations is 0.23 ± 0.04 m/year.

In general, changes in ice-sheet elevation may be caused by variations in the surface balance—either accumulation or ablation—or variations in ice flow. Although it is not possible to deduce the specific cause of ice-sheet thickening, it is likely that the present ice velocities have been determined by long-term (>100-year) surface conditions and that the observed ice thickening indicates that present accumulation rates are larger than the long-term average.

The average accumulation rate on the ice sheet south of latitude 72° N is about 0.5 m/year water equivalent. Therefore, the 0.23 m/year thickness change indicates a 25- to 45-percent excess ice accumulation over the amount required to balance the outward ice flow; depending on whether the thickening is caused by recent (5 to 10 years) or longer-term (>100-year) changes, the results in sea-level equivalent are obtained by multiplying by the ratio of the ice-sheet area south of latitude 72° N to the total area of the ocean (1/600) and the relative density of ice (0.92). The implied global sea-level depletion is 0.2 to 0.4 mm/year. If a similar imbalance exists in the northern 60 percent of the ice-sheet area, the depletion is 0.35 to 0.7 mm/year. Therefore, the Greenland sheet growth is currently removing some of the water being added to the ocean from other sources.

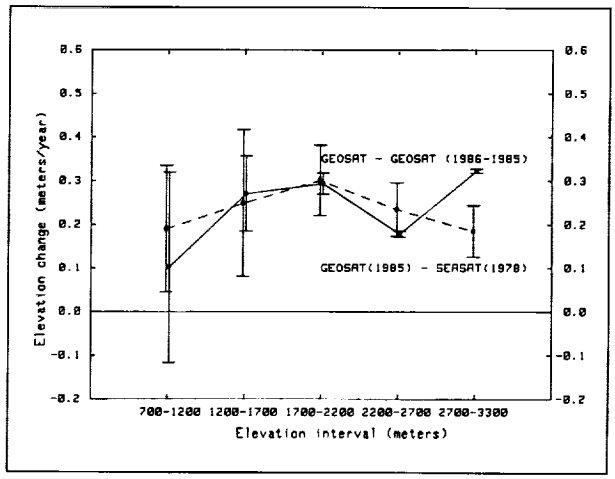

Average ice-sheet surface elevation changes in elevation bands. Ice-sheet thickening is indicated in both the ablation and accumulation zones (below and above about 1,200 m).

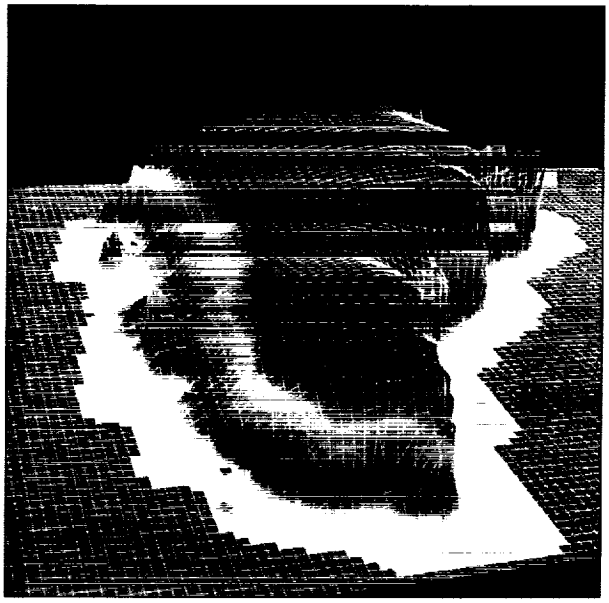

Three-dimensional surface elevation map of southern Greenland (latitude 60° to 72° N) from GEOSAT radar altimetry. The north-central part of the map is near the 3,200-m crest of the ice sheet. The surface slope indicates the direction of glacier flow. The north-south-running ice divide and the outlines of several drainage basins that discharge ice into the fjords of southeast Greenland are evident.

ORIGINAL PAGE
COLOR PHOTOGRAPH

In the future, polar ice sheets may actually grow instead of shrink because of the climate warming. In polar regions, greater precipitation is associated with warmer temperatures, with an increase of perhaps 5 to 20 percent in snowfall per degree temperature increase. Also, glaciers respond to both temperature and precipitation in such a manner that enhanced precipitation may more than offset increases in surface melting. Therefore, the dominant short-term effect is likely to be ice-sheet growth, which would continue for many years as the ice flow responds to increased driving stresses.

Over much of Antarctica, which contains 91 percent of the Earth's ice, the annual mass input is only 10 percent of the Greenland values, so that significant elevation changes may be 10 times smaller. Therefore, need for laser altimetry on a polar-orbiting satellite is critical because of its better range precision and ability to cover the critical ablation areas of Greenland where radar altimeters do not adequately follow the more irregular ice surfaces.

Contacts: H. Jay Zwally (Code 671)
(301) 286-8239
Robert A. Bindschadler (Code 671)
(301) 286-7611

Sponsor: Oceans Processes Program

Dr. H. Jay Zwally is a research scientist involved with observing and modeling the variability of polar sea ice and continental ice sheets. He received a PhD in physics from the University of Maryland. During his 16 years at Goddard, Dr. Zwally has received the NASA Group Achievement Award for his contribution as an author of the Antarctic Sea Ice Atlas *and the Goddard Exceptional Performance Award for his leadership in establishing a recognized cryospheric research program.*

Dr. Robert A. Bindschadler develops and applies techniques for studying ice sheets using remote-sensing data and conducts field research in the Antarctic. His studies focus on issues of climatic change and its effects on humans. Dr. Bindschadler, who has 10 years' experience at Goddard, has received several awards, including NASA's Exceptional Achievement Award in 1989 and the Certificate of Outstanding Performance. He holds a PhD in geophysics from the University of Washington.

DISTRIBUTION OF THE FLUORESCENT COMPONENTS OF ORGANIC MATTER IN MID-ATLANTIC SHELF AND SLOPE WATERS

One of today's most pressing Earth science problems is improving knowledge of the biogeochemical cycle of carbon. With atmospheric carbon dioxide increasing at about one part-per-million per year, the mechanisms and the capacity of the oceans to provide a sink for this apparent increased atmospheric carbon production need to be established.

While the particulate and dissolved organic matter in the oceans is a very important part of the carbon cycle, it also interferes with accurate satellite measurements of the photosynthetic contribution to the carbon budget from oceanic phytoplankton. Thus the measurement of organic matter is doubly important.

Research efforts are under way to select passive ocean color satellite sensor bands that will allow global mapping of dissolved organic matter to improve our understanding of the carbon budget and biogeochemical cycles. Potentially, this can be accomplished by analyzing airborne fluorescent components of organic matter (FCOM) data in conjunction with upwelled spectral radiances using active-passive correlation spectroscopy methods. The work described here addresses only the problem of measuring the fluorescent components of organic matter while future efforts will focus on the combined use of the data with upwelled radiances.

The FCOM are defined within the idealized laboratory laser-induced fluorescence spectrum of Mid-Atlantic Bight water shown in (a) of the accompanying figure. A similar airborne laser-induced spectrum is obtained from an altitude of 150 m by using a laser spectrometer equipped with a telescope to collect the low-intensity signals arriving at the aircraft. The excitation source used for either laboratory or airborne spectra is a frequency-tripled Nd:YAD laser with an output wavelength of 355 nm. The water Raman band (centered near 404 nm) is present in all spectra and is used to remove the variability of the water column attenuation by normalization procedures. If waterborne phytoplankton are present, then laser-induced chlorophyll fluorescence emission is found in the 685-nm

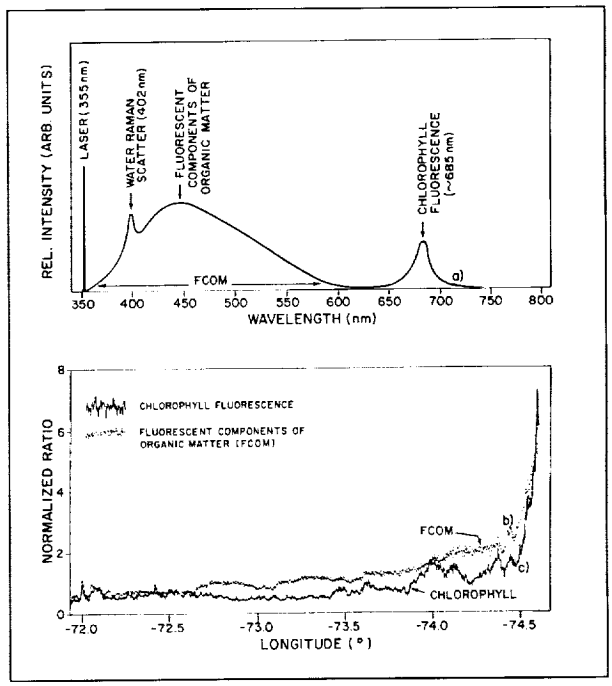

(a) Laser-induced fluorescence spectrum of unfiltered sea water. The fluorescent components of organic matter definition do not include the water Raman band at ~401 nm and phytoplankton chlorophyll fluorescence at ~685 nm. (b) Water-Raman-normalized FCOM signal recorded in the 450- to 461.25-nm band of the Airborne Oceanographic Lidar during its inbound transit toward the Virginia coast. (c) The water-Raman-normalized chlorophyll fluorescence simultaneously obtained along with the FCOM using the 355-nm laser. The chlorophyll signature was concurrently validated with a separate blue-green laser.

region of the spectrum as shown. The broad band of fluorescence from ~380 to 580 nm is due to the dissolved and particulate organic matter. This ultraviolet-stimulated blue/blue-green/orange fluorescence is defined as the fluorescent components of organic matter. The characteristic fluorescence emission in the 685-nm region is not included within the definition of the fluorescent components of organic matter. Likewise, the laser-induced water Raman band in the 403-nm region is not due to organic matter and is specifically excluded from the definition. Chlorophyll fluorescence was also obtained with a separate laser which had an output wavelength of 532 nm. The 532-nm stimulated chlorophyll fluorescence (not shown here) was in good agreement with the chlorophyll fluorescence from the 355-nm excitation. Chlorophyll fluorescence measurements made with 532-nm laser excitation have been shown to be highly correlated with chlorophyll extraction measurements made aboard surface truth vessels on numerous previous experiments.

The instrument used in this study was the NASA Airborne Oceanographic Lidar flown aboard the Goddard P-3A aircraft. The laser-induced fluorescence and water Raman backscatter from the ocean surface layer were captured with the spectrometer that contains 32 contiguous ~11.25-nm-wide channels. During the flight mission, the spectrometer was adjusted to provide spectra over a 360-nm interval between 380 and 740 nm. The Airborne Oceanographic Lidar was configured with a ~50 mJ frequency-tripled 300-nm Nd:YAG laser and fired at a 10-pulse-per-s rate. With a nominal flight speed of 100 m/s, the 10-pulse-per-s laser sample rate yielded a horizontal spatial resolution of 10 m. The airborne spectra contain the broad-spectrum organic fluorescence from 380 to 60 nm, water Raman backscatter at 401 nm and the phytoplankton chlorophyll fluorescence at 685 nm.

The flight mission observations were confined to continental shelf and slope waters of the western North Atlantic northeast of Wallops Island, Virginia. Results obtained during the flight are shown in (b) and (c) of the accompanying figure. The data were subjected to a simple 10-point average to reduce the volume of data as well as the sample-to-sample variability in the laser-induced fluorescence data. The resulting averaged data are plotted as a cross-section profile as a function of longitude. The laser-induced fluorescence of organic matter in the 450- to 461.25-nm band of the Airborne Oceanographic Lidar is shown in (b) of the figure. The FCOM signal has been normalized by the peak intensity of the laser-induced water Raman band (occurring at ~401 nm) to remove spatial variation in the fluorescence signal due to differences in the upper water column attenuation along the flight track.

The distribution of FCOM was observed [as shown in (b) of the figure] to decrease monotonically with increasing distance in the offshore direction. A surprising finding from these data and from more recent data taken at other midlatitude Atlantic shelf locations was the relatively high amount of FCOM found in the outer shelf and slope water masses. A much lower level of FCOM was expected in outer shelf and slope waters. A plot of the chlorophyll laser-induced fluorescence is shown in (c) of the figure. Notice the rather "patchy" nature of the chlorophyll distribution over these water masses. The chlorophyll distribution is distinctly noncoherent with the FCOM. The lack of coherence between FCOM and chlorophyll suggests that the primary source for FCOM in outer shelf and slope waters is not related to recent phytoplankton activities. The rather continuous distribution of FCOM from inshore to offshore, coupled with the very high levels of FCOM adjacent to the shoreline, provides a strong indication that the primary source of the FCOM in outer shelf and slope waters is of terrestrial and nearshore marine origin. The other major implication that can be drawn from this research is that the levels of organic matter in outer shelf and slope waters may be high enough to necessitate special ocean color algorithms to infer more accurately surface layer chlorophyll concentration from satellite ocean color imagery.

Contact: Frank E. Hoge (Code 672)
(804) 824-1567

Sponsor: Oceanic Processes Branch,
NASA Headquarters

Dr. Frank E. Hoge, Project Scientist for the Airborne Oceanographic Lidar, is interested in active and passive ocean color spectral variability studies. He has 8 years' experience at Goddard and 22 years at NASA. He is a member of the Optical Society of America and the American Geophysical Union.

STUDYING ICE SHEETS WITH SYNTHETIC APERTURE RADAR (SAR)

Large ice sheets are a major element of the climate system. Their volume regulates sea level, and their extent affects the circulation patterns of both the

ORIGINAL PAGE
BLACK AND WHITE PHOTOGRAPH

atmosphere and the ocean. As with other elements of the climate system, it is important to obtain a time series of data on the ice sheets to understand better how they behave in the climate system and then to monitor the major ice sheets to afford scientists the opportunity of detecting changing conditions.

The Antarctic ice sheet extends over nearly 14 million km^2, an area larger than the United States. This vastness of the ice sheets, combined with the harshness and remoteness of the polar environment, makes extensive surface-based measurements extremely difficult. Effective monitoring of these areas can only be accomplished by satellite remote sensing. The early LANDSAT sensors demonstrated how much information could be obtained on the nature of the ice sheets (Williams, 1983), and more recently the additional spectral bands of the Thematic Mapper (TM) have supplied additional opportunities to collect meaningful ice-sheet data (Orheim and Luchitta, 1988; Stephenson and Bindschadler, in press). Nevertheless, there are still large portions of major ice sheets for which adequate images do not exist (Swithinbank, 1988). The principal problem is persistent cloud cover that, for many coastal areas of ice sheets, can prevail for well over 90 percent of the sunlit season. Yet it is precisely in these coastal regions where detectable changes in the ice sheet are most likely to occur.

SAR offers the glaciologist an imaging system with spatial resolution comparable to the capability of LANDSAT imagers together with the capability of penetrating cloud cover. It also provides the capability of operating in the polar winter when the absence of sunlight renders LANDSAT useless. The first SAR images of ice sheets indicated that a wealth of information useful to the glaciologist could be gleaned from these data. This article reports on the current status of NASA's program to identify the different glaciological uses of SAR imagery for studying ice sheets.

The first figure shows a SAR image of the Greenland ice sheet taken on October 9, 1978, from the SEASAT satellite. The scene center is 64° N, 49° W and covers an area 100 km × 100 km. The size of individual pixels is 25 m × 25 m. A wide variety of features can be identified in the image. Many of these are identified in the sketch map shown in the second figure. The ice sheet flows from right to left, beginning at elevations above 1,500 m in the upper right of the image, flowing through a slush zone where extensive melting occurs, converging into channels identified by the long, sinuous stream lines, and eventually reaching the margin either by crevassed outlet glaciers or across a broad region of bare ice where numerous lakes and streams form.

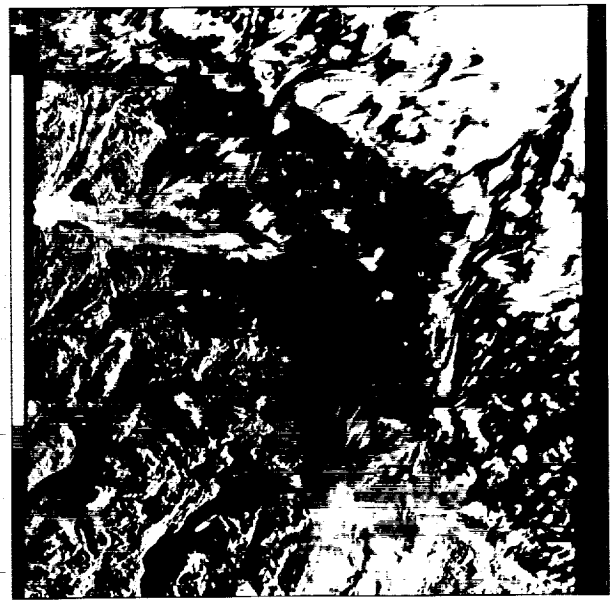

SAR image of Greenland taken on October 9, 1978. Processed by Jet Propulsion Laboratory.

The ability to identify so many different features in this image demonstrates that one of the principal uses of SAR imagery is in mapping ice-sheet features. Even today, large areas of both Greenland and Antarctica remain poorly mapped. Different features are discernible because of the differences in backscatter cross-section. These differences can be due to edges, surface roughness, topographic relief, volume scattering, or wetness. Examples of features identified by edges are crevasses, icebergs, and streams incised into the bare ice. The increased backscatter from the edges of these features makes the edges bright and the features easy to spot. By contrast, the darkness of the broad region of bare ice in the first figure is due to the smoothness of the surface relative to either the snow or the rock. This smoothness causes a more specular scatter of the radar, and less energy is scattered back to the sensor. The ice margin can be clearly seen by the difference in texture between the rock and the ice. This difference also serves to identify nunataks—isolated islands of rock surrounded by the ice sheet. This kind of mapping is being planned for the large amount of SAR data of ice sheets expected to be collected by the Earth Resources Satellite (ERS)-1.

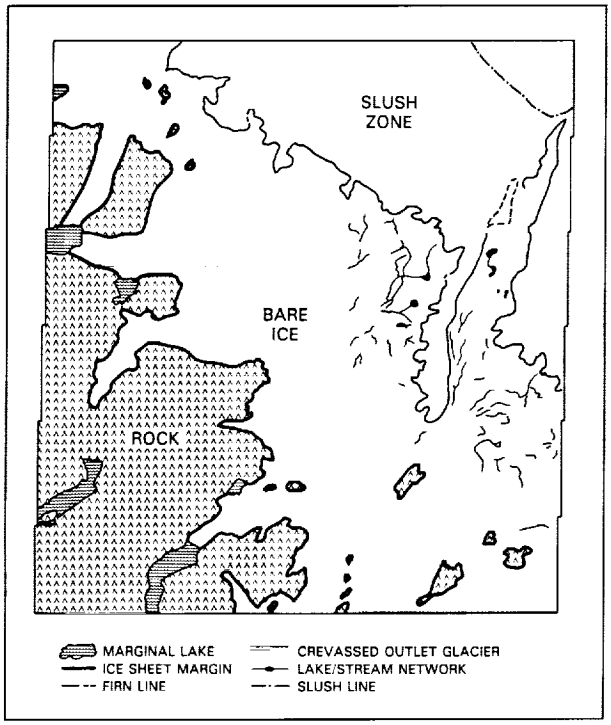

Sketch map of features in SAR image.

An ancillary application of feature mapping is repeated mapping which provides measurements of changes in the position of the margin or firn line and, along with the displacements, supplies velocities of these or other features. These can be very useful for both monitoring purposes as well as in investigations of the ice dynamics.

The upper boundary of the bare ice is termed the firn line; firn refers to snow which survives a summer. Above this boundary, melting is not intense enough to eliminate all the previous winter's snow accumulation. However, the melting that does occur can turn the snow into slush—water-saturated snow. This zone where extensive melting takes place is called the slush zone. The flow pattern of the meltwater is determined by the subtle surface undulations with troughs and hollows collecting water and the topographic highs shedding water. Wet snow appears dark in SAR imagery due to the very strong absorption of radar energy by the free water in the snow. Thus, the pattern of brighter and darker areas in the slush zone is a proxy indicator of surface topography. This correlation between the indication of ice-sheet surface topography by SAR and the actual topography was confirmed by comparing SAR data with coregistered LANDSAT TM data.

The presence of free water in firn has a second effect which affects the radar backscatter characteristics. As snow ages, it forms increasingly larger snow grains. Free water accelerates this process so that areas which have received more water are composed of larger grains. The size of snow grains is typically 0.5 to 2 mm, which means that they act as Rayleigh scatterers of radar energy. Thus, areas of relatively larger grains have a larger backscatter cross-section and appear brighter than areas of smaller grains. This is the reverse of the pattern when free water is present. Therefore, during the autumnal freeze-up period, very wet areas should switch from being darker than adjacent areas to being brighter. The SAR imager, then, delivers a means to determine not only if an area is wet but also if it has been wet and is now refrozen. This capability will prove very useful in the monitoring of the hydrology of ice sheets. If ice melting becomes more prevalent, these areas of refrozen meltwater should expand, and a monitoring program of SAR data should help identify this trend. Developing the application of SAR imagery to the ice-sheet hydrology is the central theme of continuing research in the use of SAR for studying ice sheets.

Contact: Robert A. Bindschadler (Code 671)
(301) 286-7611

Sponsor: NASA Oceans Program

Dr. Robert A. Bindschadler develops and applies techniques for studying ice sheets using remote-sensing data and conducts field research in the Antarctic. His studies focus on issues of climatic change and its effects on humans. Dr. Bindschadler, who has 10 years' experience at Goddard, has received several awards, including NASA's Exceptional Achievement Award in 1989 and the Certificate of Outstanding Performance. He holds a PhD in geophysics from the University of Washington.

MEASURING CHANGES IN LARGE-SCALE SEA-SURFACE TOPOGRAPHY FROM SPACE

One of the major goals of satellite altimetry is to measure global scale variations in sea level. Phenomena of interest at these scales include secular trends in the mean sea surface due to total mass of volume changes, hemispheric variations caused by the annual cycle of thermal expansion and contraction in the upper ocean, and basin scale fluctuations related to variability in the general circulation. The success of the GEOSAT and SEASAT

altimeter satellite missions in measuring global sea-surface topography in 1987 and 1978, respectively, has permitted the first estimate of interannual change in sea level over 9 years using spacecraft instrumentation. These instruments come from an altimeter heritage that began at Goddard with the Skylab and GEOS-3 experiments.

Accurate estimates of global scale sea level variations by satellite altimeters require precision determination of spacecraft orbit. Errors in the radial position of an altimeter satellite severely contaminate the oceanic signal at global wavelengths. The Space Geodesy Branch at Goddard has specialized in precision orbit determination and gravity field modeling for the past 2 decades and will be producing the highly accurate orbits (an estimated 10-cm rms radial position error) for the joint U.S. (NASA) and French (Centre National d'Etudes Spatiale) Ocean Topography Experiment for studies of the ocean circulation beginning in 1992. In preparation for this project, researchers at the Space Geodesy Branch have computed the radial position of GEOSAT and SEASAT using a new method that uses the altimeter range measurement as a tracking data type. In this technique, the gravity model (geoid), absolute dynamic topographic, and radial position of the satellite are simultaneously adjusted through a least-squares collocation procedure. The resulting orbits are significantly more accurate than all previous determinations of the GEOSAT and SEASAT orbit (an estimated error of 20 cm rms in radial position). At this level of orbit accuracy, estimates of changes in large-scale (>5000-km) sea-surface topography become feasible.

The success of the GEOSAT and SEASAT altimeters permits the first estimate of interannual changes in sea level over the past 10 years. For this time period, variations in air-sea heat exchange can cause surface elevation changes greater than 10 cm in the midlatitudes, and fluctuations in the tropical wind fields can lead to differences in sea level of a similar magnitude. Goddard researchers have estimated this change using the simultaneous solution technique. Solutions for the mean dynamic topography for SEASAT and GEOSAT were constructed for July-October 1978 and July-October 1987 in a geodetically consistent framework. The topographies were differenced, and the result is shown in the middle panel of the accompanying figure. This difference removes the annual cycle, which has an amplitude up to 25 cm in some locations.

It should be emphasized that this is a preliminary estimate of the change in sea level based on these two satellites with some known problems that are being corrected. This estimate includes the following known errors and omissions: inaccuracies in the GEOSAT tracking measurements that cause an error in the determination of the Earth's center of mass on the order of 10 cm (this error can be corrected by NASA laser tracking of the GEOSAT follow-on satellite to be launched in summer 1990); inaccuracies in the atmospheric refractive range delay in the GEOSAT measurements (this error can be corrected in the near future using passive microwave observations from the special sensor microwave imager on a defense mapping satellite); and omission of the solid Earth deformation by the ocean tide (a recent Goddard model will be used to correct for this phenomenon).

A major difference between 1987 and 1978 was the occurrence of an El Niño Southern Oscillation in 1986-87 but not 1977-78. This event led to high sea level in the eastern tropical Pacific in 1987 relative to 1978 because of anomalous wind-forced planetary waves in 1987. Interpolated sea level change derived from island tide gauge

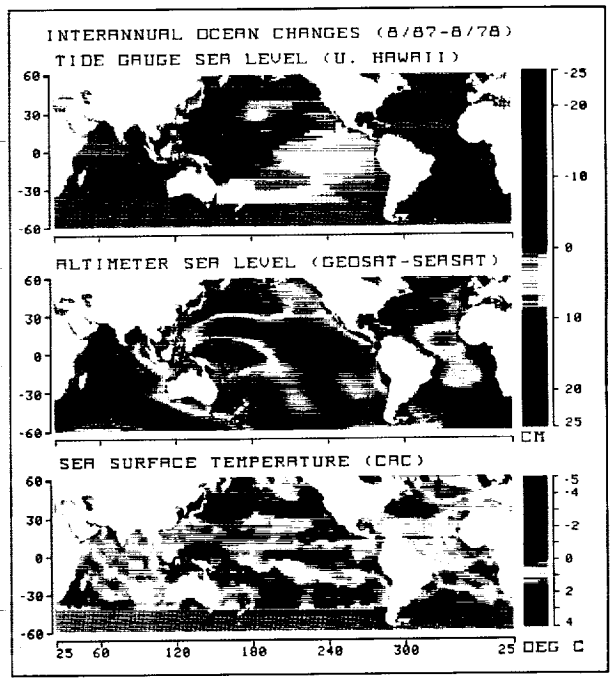

Interpolated sea level change derived from tide gauge observations (upper panel). Mean dynamic topography (annual cycle removed) for July-October 1978 and July-October 1987 from GEOSAT/SEASAT data (middle panel). Difference in sea-surface temperature between 1987 and 1978 from ship and satellite measurements (lower panel).

ORIGINAL PAGE
COLOR PHOTOGRAPH

observations is shown in the upper panel of the figure. While tide gauge measurements are admittedly sparse in the eastern tropical Pacific, the basic pattern of sea level change is apparent. The altimeter result is consistent with the tide gauge observations in the tropical Pacific. The lower panel in the figure shows the difference in sea-surface temperature between 1987 and 1978 derived from a combination of ship and satellite measurements. The evidence of the 1986-87 El Niño Southern Oscillation is clear in sea-surface temperature. The wind-forced planetary waves along the equatorial Pacific suppress upwelling of cold water in the eastern tropical Pacific, leading to a warmer sea-surface temperature in 1987. The longitudinal extent of the warmer sea-surface temperature is consistent with the sea-surface elevation change found in the tide gauge and altimeter observations.

Contact: Chester J. Koblinsky (Code 626)
(301) 286-2880

Sponsor: Office of Aeronautics & Space Technology (OAST), Ocean Topography Experiment Project, Ocean Processes Support Research and Technology, NASA Headquarters

Dr. Chester J. Koblinsky, a physical oceanographer, studies large-scale ocean circulation processes with satellite altimeters and scatterometers. He has a PhD in physical oceanography from Oregon State University.

PREDICTABILITY OF OCEAN FLOW

Numerical forecasts of ocean circulation are initial boundary value problems, which require knowledge of the governing physics, the initial state, and the external forcing of the system being simulated. Yet given precise knowledge of all boundary forcings and an exact knowledge of the governing physics for ocean flow, it is not possible to produce a numerical forecast that is accurate for an indefinite time. Small errors in the initial state, due to either observational error or imprecise knowledge of the small scale structure, will amplify in numerical simulations due to nonlinear interactions. Thus, there is an inherent time limit on the usefulness of a numerical forecast. This limit is sometimes called the predictability time scale.

Atmospheric scientists have been aware of the predictability limits of their numerical forecast models for the past 25 years. In the atmosphere, errors in the initial conditions double about every 2.5 days so that after about 14 days, numerical forecasts have very little skill. The relative sparsity of observations in the ocean compared to the atmosphere makes it difficult to determine accurately the initial conditions for a numerical ocean forecast. However, ocean-observing satellites are now returning high-resolution global data sets of the ocean's surface thermal structure and sea surface topography and estimates of atmospheric forcing so that adequate knowledge of an initial condition and surface forcing for ocean forecasts may soon be a reality. Thus, it is important to know how quickly any initial errors will grow in an ocean model.

A midlatitude quasi-geostrophic ocean model has been used to estimate the predictability time scale of an ocean flow with characteristics similar to the Gulf Stream. A rendering of the surface flow during one such simulation is shown in the upper panel of the accompanying figure. An intense Gulf Stream-like eastward flow extends out from the western boundary near the central latitude of the domain. The flow is rotating anticyclonically (clockwise) in the southern half of the domain and cyclonically (counterclockwise) in the northern half. By adding small errors to simulated fields and then integrating the model forward, it is possible to determine how quickly those errors grow by comparing two simulations: one where small errors are present in the initial conditions and the other where no errors are present in the initial conditions. For this flow, small errors double (on average) every 16 days, and the simulation displays forecast skill out to approximately 150 days.

Improvements in forecast fields can be made if more information on the observed conditions becomes available and can be incorporated into the model forecast. The process of incorporating newly observed data into a running forecast model is termed "data assimilation." With the knowledge of how quickly errors grow in a numerical forecast, it is possible to estimate how often observational data must be assimilated into a numerical forecast to keep that forecast on track with the observations. A linear stability analysis of the flow fields can be used to anticipate not only time scales but also spatial scales, which are likely to be relevant to the growth of errors in numerical simulations.

A linear stability analysis was performed for the Gulf Stream-like flow. The spatial structure of the fastest growing errors for this flow is shown in the lower panel of the accompanying figure. The fastest growing errors occur for an internal mode of the ocean; i.e., the magnitude of the errors will change with depth as opposed to

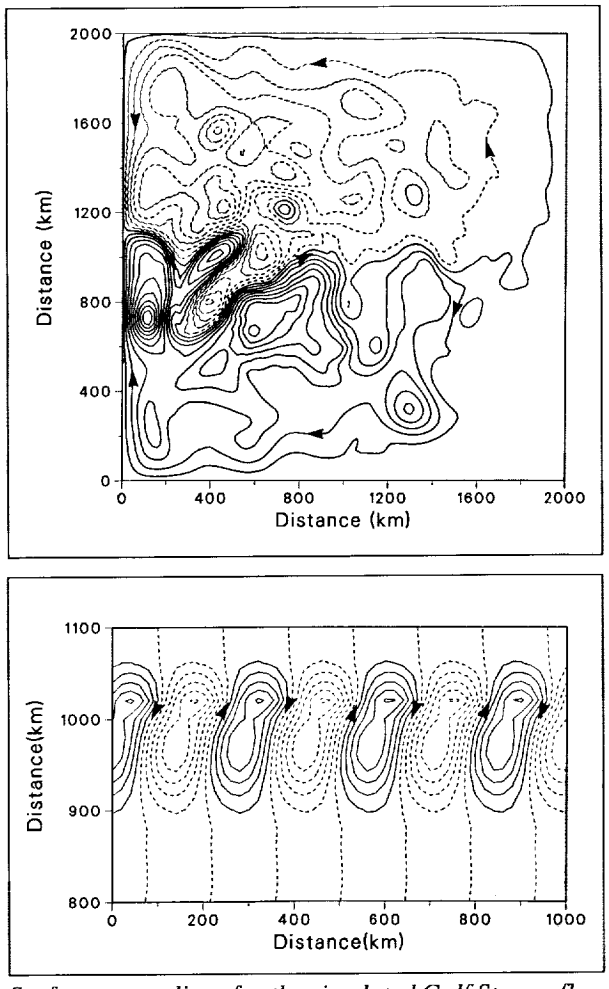

Surface streamlines for the simulated Gulf Stream flow for the entire domain (upper panel) and surface streamlines for the structure of the fastest growing errors in a predictability experiment (lower panel). Water particles flow along streamlines, and more densely packed streamlines are indicative of faster flow.

being constant with depth. The fastest error growth is confined to the area in the immediate vicinity of the Gulf Stream-like flow. The east-west scale is 290 km, and the error doubling time is about 2.5 days. Thus, it is important that data to be assimilated resolve features of length scale 290 km for an ocean forecast model to reflect accurately the evolution of an observed flow similar to the one discussed here.

The 290-km scale for largest error growth is commensurate with satellite orbit separation such as that of GEOSAT. However, the frequency with which data must be supplied for ocean forecasts may be higher than is currently available. Nevertheless, the 150-day predictability limit in a regime as active as this simulated Gulf Stream shows promise for assimilation of satellite data into ocean forecast models.

Contact: David Adamec (Code 671)
(301) 286-8513

Sponsor: Laboratory for Oceans

Dr. David Adamec earned his degrees in meteorology, receiving his BS and MS from Florida State University and his PhD from Naval Postgraduate School. As a research oceanographer in the Ocean Processes Program, Dr. Adamec currently conducts numerical simulations of mid-latitude ocean circulation and water mass transformation in the Gulf Stream and East Australia current systems.

NEW SURFACE CONTOUR RADAR ANTENNA DESIGN TO PERMIT HURRICANE FLIGHTS ON NATIONAL OCEANIC AND ATMOSPHERIC ADMINISTRATION (NOAA) P-3 AIRCRAFT

The oceanographic community looks on Goddard's Surface Contour Radar (SCR) as a standard in the measurement of ocean directional wave spectra. SCR has documented the sea state for major experiments and provided new insights into the manner in which waves are generated by wind. But despite a void of quantitative information on the directional wave spectrum of hurricanes, safety considerations have preempted acquisition of these important data. The Goddard P-3 aircraft lacks the special reinforcing and design features of the NOAA P-3 hurricane hunters.

The new design for the SCR's scanning antenna system greatly reduces the assembly's size, weight, and vibration over the present system. This reduction will permit installation of the new SCR (one of the modes of the new Goddard Multimode Airborne Radar Altimeters) on the NOAA P-3 to document the directional wave spectrum variation in hurricanes.

The figure is drawn to scale to contrast the old and new designs of the antenna assembly. In the old design shown at the top of the figure, a feed horn illuminates a lens whose axis is horizontal. The collimated beam is reflected downward by an external mirror (seen on edge) which is mounted at 45° on an oscillating shaft. As the

shaft oscillates, the beam is scanned in and out of the plane of the paper. The mirror, a 46- × 65-cm ellipse, is 2.5 cm thick, and the forces required to reverse the scan direction at a 20-Hz rate cause considerable vibration.

The new design, shown at the lower left in the figure, is based on the locus of the lens focal points for scanning the beam left and right lying very nearly on the dotted circle. The lens axis is vertical, and a much smaller mirror is shown horizontal at the center of the circle. A feed horn is on the lens axis at the bottom of the circle, pointing up to illuminate the mirror. Because the feed horn occupies the mirror image position of the nadir focal point at the top of the circle, the radiation is reflected back by the mirror to properly illuminate the lens.

The line joining the feed horn and some other focal point for scanning the beam off-nadir will always be a chord of the circle, since both lie on the circle. If the mirror is rotated about an axis through the center of the circle, it will be a radius of the circle. Because the perpendicular bisector of any chord of a circle is a radius, the mirror can always be rotated so that the feed horn is the mirror-image point of the actual focal point for scanning the beam off-nadir. In the new design, the mirror will rotate continuously in one direction to scan the beam, alternately using front and back surfaces, instead of oscillating back and forth.

Compared to the existing SCR antenna system, the new design is compact and vibration free. The new assembly is being fabricated and has tentatively been approved for installation on the NOAA P-3 aircraft for the 1990 hurricane season.

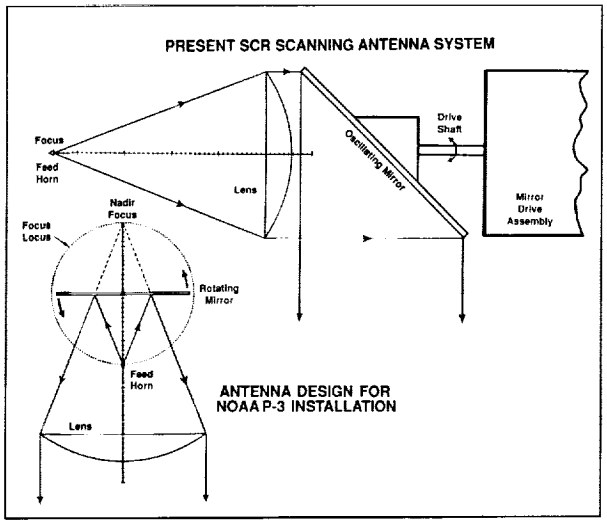

Old (upper) and new (lower left) designs for SCR.

Contact: Edward J. Walsh (Code 672)
(804) 320-6357

Sponsor: Office of Space Science and Applications

Dr. Edward J. Walsh presently assists the Observational Science Branch in the design of an improved SCR. Dr. Walsh has been at Goddard for 9 years and with NASA for 22 years. He received the NASA Medal for Exceptional Scientific Achievement and earned his PhD in electrical engineering from Northeastern University.

WAVELET ANALYSIS: A NEW ANALYTICAL TOOL

An innovative analysis technique, wavelet transformation, can be used to generate high-resolution spectral time series from time-series data. This tool provides enhanced resolution of high-frequency components as well as lower frequency components. In fact, all scales have optimum resolution in both time and frequency. This article presents a limited introduction to wavelet analysis using some examples related to findings on microwave scattering from the sea surface.

Researchers cannot predict when various events occur by using classic Fourier transformation techniques because entire time series of data are depicted in a single power spectral density (PSD) distribution. A window can be used with the Fourier transform to help isolate events. The window duration is often chosen to correspond to the spectral peak frequency and so time series of PSD are developed by stepping the window along in time. However, because the window duration is constant, averaging smears time resolution of higher frequency components, and consequently, multiple-scale processes cannot be resolved.

Obviously, the duration of the window must change to match each feature scale. This requirement is the essence of wavelet analysis, which employs window functions that have similar shape but variable duration. Duration is controlled by a scale parameter that contracts for high frequency and dilates for low frequency. Thus, multiple-scale resolution is possible at each instant of time by convolving the appropriate wavelet with the data time series. Grossman and Morlet (1984), Meyer (1986), Daubechies (1986, 1988), and others

have pioneered wavelet transformation theory by employing rigorous mathematical formulation to establish it as a super-set of sampling theory.

To illustrate an application of wavelet transform techniques, Goddard researchers conducted experiments in the $20 \times 1 \times 1.5$-m wind-wave tank at Wallops. Waves are generated by using a paddle and by recirculating air. Surface elevation is measured by capacitance probes, and wind friction velocities are estimated from wind speed profiles. During the experiments, analog signals were digitized at 100 Hz for later processing.

Two cases will be discussed: (1) regular, low-level paddle waves, and (2) combined high wind waves ($u^* = 82$ cm/s) plus high paddle waves. First, conditions will be described in terms of traditional time series; then examples of time-frequency image interpretation will be presented. All of these are shown in the accompanying figure.

The elevation time series for the paddle-only case is periodic due to the small-amplitude, sinusoidal paddle-generated waves. There is no evidence of wave groups (amplitude modulation) development because wave steepness is small. This case contrasts with the surface elevation time series of the combined wind-plus-paddle wave case. For these conditions, wave steepness is large, so the elevation time series is both amplitude and frequency modulated. The vertical scale has been increased by a factor of 10.

To conduct a wavelet analysis of these elevation time series, Goddard researchers employed the famous wavelet that was proposed by Morlet (1982). The wavelet looks like a modulated Gaussian. It is almost periodic and regular and is similar to the fundamental shape of smooth waves. The distinctive characteristic of the Morlet wavelet is that the Gaussian envelope achieves optimum resolution in time and frequency spaces.

Color-coded, water PSD time-series images were obtained by performing convolution of the elevation time series with Morlet wavelets, which are appropriately scaled in magnitude and duration. In the general format of these images, the horizontal axis represents time and the vertical axis represents frequency. PSD magnitude is represented by 24-level color coding and is normalized by the maximum value. Finally, the integral of PSD for all frequencies at a particular time (vertical section) is proportional to the wave energy (variance) at each particular instant.

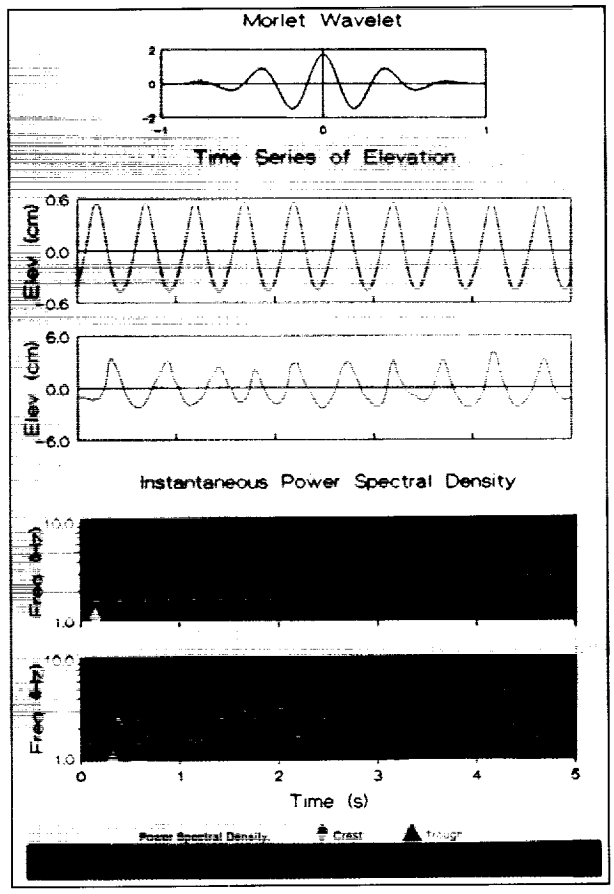

Regular waves and erratic waves presented in terms of traditional time-series format and the time-frequency format.

Further examination of the images shows that the prominent feature of the paddle-generated wave case is virtually uniform peaks at regular 0.25-s intervals due to the 2-Hz paddle-generated waves. In time-domain format, there is a maximum for each crest and each trough. Although it may be difficult to see, there also is a second series of periodic peaks (at 0.125-s intervals) for the 4-Hz components. These are the dominant wave's first harmonic and are traditionally modeled by a Stokes-wave representation (sinusoidal components, primary plus harmonics). The image also reveals that the total energy of wave crests is greater than that for troughs. Indeed, measurements from the elevation time series indicate that the average crest and trough amplitudes are to be 0.56 and 0.45 cm respectively. No organized pattern emerges for frequency components greater than 4 Hz. The wavelet image for the high-wind plus paddle-generated waves provides a wealth of information. It shows frequency

modulation of PSD peaks as perturbations from the 2-Hz average. The frequency modulation in this image corresponds to an accordion effect in the elevation time series. Additionally, the results show that the wave height variability (associated with wave group structure) can clearly be identified by variations of PSD magnitude. At higher frequencies, components are enhanced due to wind-wave generation. Finally, there is large asymmetry of higher frequency components with respect to the dominant 2-Hz waves, revealing that crest fronts and backs are very different. Wavelet analysis provides the means to resolve all spectral components for each time increment.

In summary, wavelet analysis is an exciting new mathematical technique that provides multiple-scale information. The theory is established on a firm mathematical basis that relates it to traditional sampling theory, and yet it provides a new way to investigate physical processes. While this article only touches upon its utility, its potential uses are broad for both theoretical and practical applications: extensions to higher dimensions (Mallat, 1989; Murenzi, 1988); measure of fractal objects (Holshneider, 1988); and data compression. Wavelet analysis development has been mainly theoretical; it needs to be implemented to further the understanding of physical processes.

In the future, Goddard researchers will employ wavelet analysis to further evaluate and formulate sea-surface microwave scattering models. Wavelet computations have been extended to two dimensions in order to characterize slope images of the water surface to quantify shorter Bragg wavelengths being tilted by long waves. This is the only technique which is capable of permitting the microwave-radiative-transfer function to be investigated in a time-series format instead of the usual comparison of time-averaged quantities. Thus Goddard researchers hope to gain a much-needed, better understanding of the underlying physical processes.

Contact: Larry F. Bliven (Code 672)
(804) 824-1057

Sponsor: Space Science and Applications, Office of Naval Resources

Dr. Larry F. Bliven develops improved active microwave algorithms for satellite systems. He is also interested in the physics of air-sea interaction as well as the remote sensing of atmospheres and oceans. Dr. Bliven, who has a PhD in marine sciences from North Carolina State University, belongs to the American Meteorological Society and the American Geophysical Union. He has 4 years' experience at Goddard.

THE USE OF SPECIAL SENSOR MICROWAVE/IMAGER (SSM/I) DATA IN ESTIMATING PRECIPITATION

Data from SSM/I on board the recently launched Defense Meteorological Satellite are proving to be a rich source of information for both operations and research. For example, the Department of Defense and NOAA are using the data to calculate cloud water content, precipitation rate, and sea ice concentration. NASA researchers are examining the data to better understand a wide spectrum of atmospheric, oceanographic, and land-surface phenomena such as vegetation cover, soil moisture, and precipitation.

The SSM/I views the Earth's surface over a swath 1,400 km wide and measures polarized microwave emission at 19.35, 22.24, 37.0, and 85.5 GHz. Particularly important are the 85.5-GHz channels, which expand the range of microwave frequencies observed from space. Because the current SSM/I is the first in a series of identical instruments to be flown on the defense meteorological satellites, a potential exists for a long record of observation for climate studies.

Microwave data from the SSM/I are displayed on a color monitor through the red, green, and blue guns as false-color images. Brightness temperatures observed at 85.5 GHz (vertical and horizontal polarizations) and at 37 GHz (vertical polarization) are displayed simultaneously. The images highlight geophysical parameters important to a wide range of disciplines.

Brightness temperatures in the SSM/I wavelengths (19 to 86 GHz) have been observed to be between 80 °K and 320 °K. To drive each "gun" on NASA's Atmospheric and Oceanographic Information Processing System, the data must be an integer between 0 and 255. This is accomplished by choosing $C = 305 - T_B$ where C is the digital count and T_B is the brightness temperature. Brightness temperatures less than 50 °K (not yet observed) would be set to a count of 255, and those greater than 305 °K are set to a count of zero.

The first figure presents hemispheric projections of SSM/I radiances observed on August 29, 1987, using this false-color algorithm. The images are displayed at 25-km

resolution in all channels, and the ascending (6 a.m.) and descending (6 p.m.) orbits have been combined. Note that global coverage is not quite complete in 24 h. Note also that when two orbits view the same area, the later orbit (in time) is displayed. The small dot like holes in the data near the Equator are due to the remapping algorithm; the size of each "dot" represents the pixel area of 25 km. The Inter-Tropical Convergence Zone is clearly apparent in the Northern Hemisphere image due to scattering (yellow), as is Typhoon Dinah off the east coast of China. At high latitudes, the atmospheric dryness is evident as the pale blue shades (dry air overlaying the low brightness temperature of the ocean surface). Over Greenland and the polar regions, snow cover and first- and multiyear ice are apparent, as are the Himalayas (whitish-grey area). The desert regions of Africa and Saudi Arabia stand out as lighter shades of green. This phenomenon is due to the polarization of 86-GHz radiation by the smooth desert surface and is known as caliche. Observations of the Saudi Arabian desert from the SSM/I at 85.5 GHz show polarization differences of 15 °K, compared to small polarization differences in central Europe.

In the Southern Hemisphere, Antarctica (white) and the surrounding sea ice (greenish-yellow) are readily discernible, as is the overall atmospheric dryness (light blue) of the winter hemisphere. Fronts and cyclones in the westerlies are seen as the darker shades of blue due to the warming by emission over the cold ocean surface. Very little scattering by precipitation ice (i.e., convective processes) is apparent in this hemisphere. The snow cover in the Andes might be interpreted as convection without prior knowledge of the geography and physics. Lake Titicaca and other high-altitude lakes in the Andes are visible as pale blue areas along the South American coast.

Atmospheric constituents such as water vapor, cloud water, and rain radiate power at their equilibrium temperature. The difference between a cold ocean background (150 °K) and the relatively warm emission from these constituents is ideal for their detection and quantification. Over the usually "warm" land background, the thermal emission characteristics of atmospheric constituents are difficult to detect.

Large raindrops and ice particles such as graupel or hail scatter microwave radiation, effectively lowering the background brightness temperature by scattering emitted radiation away from the satellite. This effect is most pronounced at high frequencies at which the particle size becomes comparable to the wavelength. This lowering of the brightness temperature due to scattering by precipitation-sized hydrometers is equally effective over water and land. The relationship between this scattering process and surface rainrate, though indirect, enables the 85.5-GHz observations to play a key role in identifying precipitation.

A combined cloud model/radiative transfer model has been developed to simulate the upwelling brightness temperatures observed over tropical convection. An algorithm developed for the 86-GHz frequencies (horizontal and vertical polarizations) has the form: ($R = 36.65 - 0.1398\,\hat{T}$ where $\hat{T} = 1.422T_v - 0.422T_h$). R is the rainrate in mm/h and T_v and T_h are the brightness temperatures in °K.

As a test of this approach, the model-based algorithm was applied to SSM/I data on August 5, 1987, coinciding with ground-based radar data from the NASA

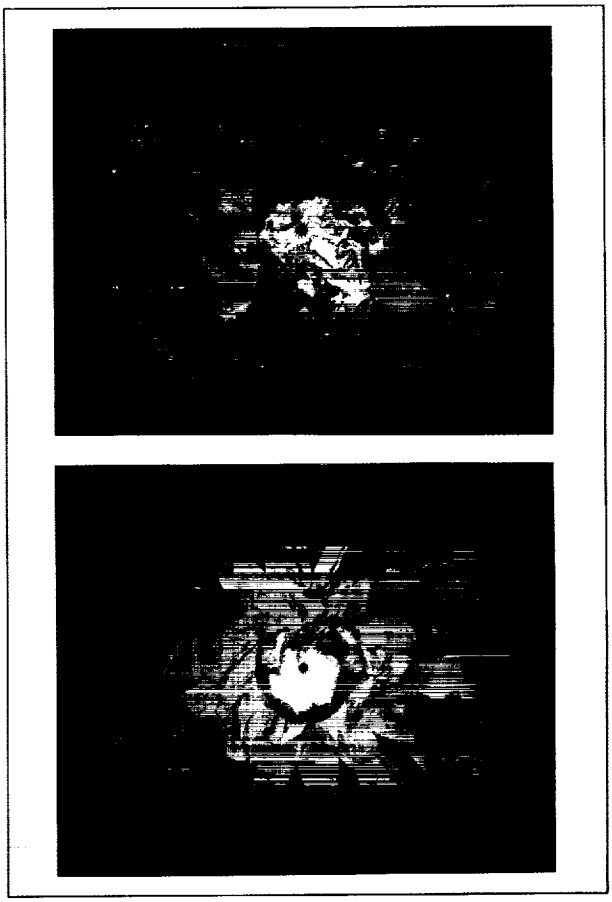

Hemisphere projection of SSM/I radiances observed on August 29, 1987.

ORIGINAL PAGE
COLOR PHOTOGRAPH

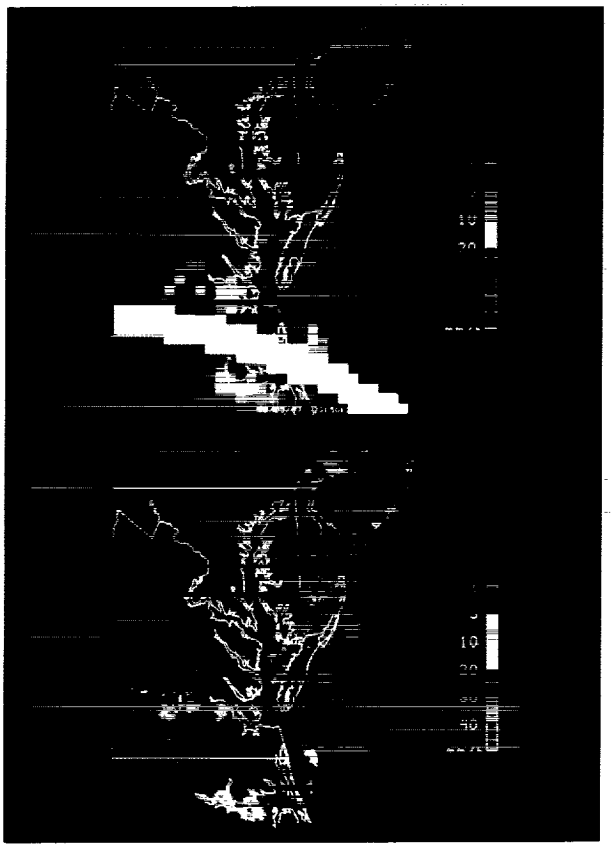

Rainrate maps for August 5, 1987, derived from a model-based algorithm applied to SSM/I data (upper) or ground-based radar (lower).

10-cm radar at Wallops Island, Virginia. The resultant rainrate maps are shown in the second figure. The patterns are quite similar, particularly in the areal extent of the rainfall and in the location of convective cores. The technique works equally well over land or water. Other cases are currently being evaluated.

Contact: Andrew J. Negri (Code 612)
(301) 286-9179

Sponsor: Severe Storms Branch, Laboratory for Atmospheres

Mr. Andrew J. Negri, of the Severe Storms Branch, is developing an infrared technique to estimate convective and stratiform rainfall and working on image processing techniques. He has an MS from Colorado State University and recently received the Laboratory for Atmospheres General Recognition Award and Group Achievement Award.

A 5-CM RESOLUTION PROFILING LASER ALTIMETER

Geoscience Airborne Laser Altimeter is a high-resolution laser altimeter designed for an airborne platform. It was designed as a small, dedicated altimeter that combines 5-cm vertical resolution, 1.5-m-diameter eye-safe laser footprints, and contiguous horizontal sampling. Geoscience Airborne Laser Altimeter also incorporates a high-resolution video camera which is boresighted to the laser spot and permits imaging of the surface track profiled by the altimeter.

Geoscience Airborne Laser Altimeter was designed to measure accurately and register the height profiles of small geological features on terrestrial targets to permit quantitative small-scale terrain studies. Such high-resolution profiles have not been previously obtainable and are essential to understanding many important dynamic geological processes, including lava flows, rock fields, glaciers, and barrier island dune evolution. The system's initial science targets are those involved in dynamic geology, such as boulder fields and areas of sand and beach erosion. Such data also are important for interpreting SAR images, which are sensitive to surface roughness at the 10-cm scale. Due to its horizontal and vertical resolution, Geoscience Airborne Laser Altimeter also will probably be useful for biomass surveys (e.g., tree heights) and airborne surveying applications.

The altimeter's transmitter is a small nitrogen laser which emits 500-ps-wide pulses at 337 nm. The transmitted laser energy is 20 μJ/pulse. The 35-cm-diameter Schmidt-Cassegr ain receiver telescope is mounted in a nadir-viewing configuration bistatic with the transmitted beam. A 500-ps response time microchannel plate photomultiplier is the stop detector. The ranging electronics preserve this response time and use cm-level time walk constant-fraction discriminators and a 100-ps (1.5-cm) accuracy time interval unit to perform the ranging measurement. The transmit and receive pulse energies are also measured on every laser firing by gated charge digitizers.

For horizontal position measurement, Geoscience Airborne Laser Altimeter incorporates a high-resolution video imagery system with 1-ms exposure time. It is boresighted to nadir within a fraction of the transmitted laser beam width. A vertical accelerometer and a sub-millibar accuracy atmospheric pressure sensor are used

ORIGINAL PAGE
COLOR PHOTOGRAPH

for measurement of aircraft vertical motion. All nonvideo Geoscience Airborne Laser Altimeter data are stored in the system's Compaq 386 computer.

This instrument has been installed and demonstrated on the Wallops Skyvan aircraft. For these flights, the aircraft was nominally 500 m, with ground speed 65 m/s. The data collection rate was 50 Hz, resulting in contiguous laser terrain profiling with 1.3-m laser spot spacing. A photograph of the altimeter installed in the rear of the aircraft is shown in the first figure.

Initial targets were selected to determine the system performance. Transitions from ground to building roofs and causeway roads to marsh areas near Wallops were used to simulate rough targets. Some profiles of Fishing Point Spit at the southern end of Assateague Island were also taken for preliminary science assessment. Fifteen data sets, with approximately 3,000 altimeter measurements per set, were collected during the 1-h test flight. The altimeter profiles show root mean square ranging precision over a smooth aircraft runway is 4 to 8 cm. The recorded video imagery shows that 20-cm features on the ground are resolvable.

Sample terrain profiles from Geoscience Airborne Laser Altimeter are shown in the second and third figures. Data from one traverse above the Wallops base are shown in the second figure. The double-peaked rooftop of the cafeteria is clearly shown, as well as the heights of cars in the parking lot, drainage dishes around a hangar, the extension of the hangar building, and a raised air-conditioning pipe on the rooftop. Data from a traverse above the southern end of Assateague Island (Fishing Point Spit) are shown in the third figure. The smooth water in Tom's Cove, sand dunes and vegetation, the beach on the ocean-facing side, and swells in the Atlantic Ocean also are illustrated.

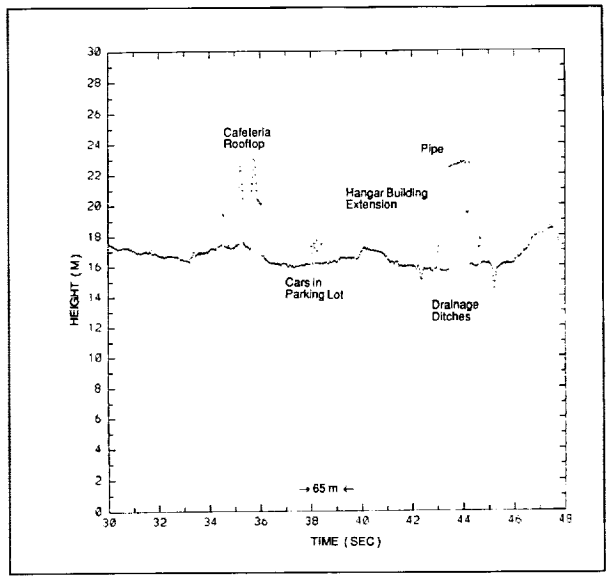

Sample terrain profiles collected from above the Wallops main base.

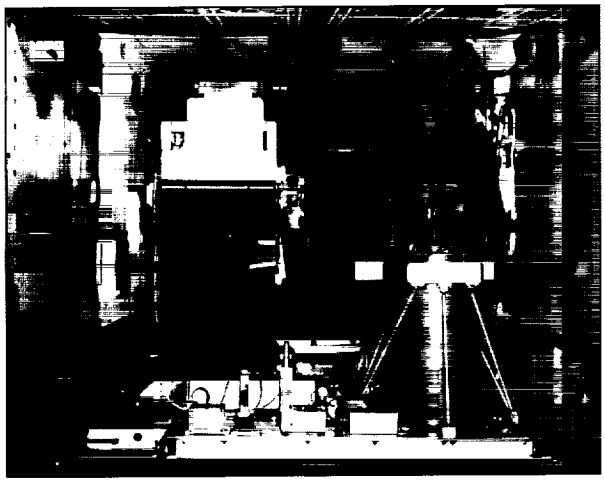

Geoscience Airborne Laser Altimeter provided contiguous laser terrain profiling and was installed in the rear of Skyvan aircraft.

ORIGINAL PAGE
COLOR PHOTOGRAPH

Contact: James B. Abshire (Code 674)
(301) 286-2611
William H. Schaefer (Code 723)
(301) 286-9751
Jan L.F. McGarry (Code 723)
(301) 286-5020
James B. Garvin (Code 620)
(301) 286-6565
Maria T. Zuber (Code 620)
(301) 286-2129

Sponsor: Goddard Director's Discretionary Fund

Dr. James B. Abshire led the technical development of the Geoscience Airborne Laser Altimeter and is interested in the development of new laser instruments for science applications. Dr. Abshire earned his PhD in electrical engineering at the University of Maryland and has been with Goddard for 15 years. He has received several awards for his work at Goddard, including being named Goddard's Inventor of the Year in 1986.

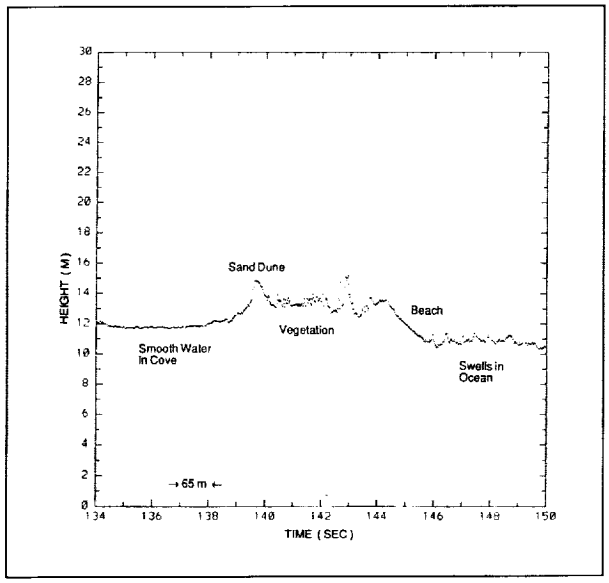

Sample terrain profiles collected from a traverse above the southern end of Assateague Island, Virginia.

Mr. William H. Schaefer designs data systems for laser instruments in the Instrument Electro-Optics Branch. His technical interests are in the areas of high-resolution terrain topology with short-pulse, high repetition rate lasers and reduction of aircraft motion errors in altimetry systems. Mr. Schaefer has 20 years' experience at Goddard.

Mrs. Jan L.F. McGarry, a mathematician and systems analyst in the Instrument Electro-Optics Branch, performs modeling and simulation of laser systems and components. She also develops real-time control software for laser systems. Mrs. McGarry won two NASA Special Achievement Awards, has 15 years' experience at Goddard, and earned an MA from the University of Maryland.

Dr. James B. Garvin is Staff Geophysicist at the Geodynamics Branch in the Laboratory for Terrestrial Physics. He is Co-Investigator on the Mars Observer Laser Altimeter experiment and Principal Investigator on the Iceland volcanoes project as well as the Lunar Observer Laser Altimeter study. He is also Project Leader on a NASA study of remote-sensing signatures of impact craters on Earth. Among his honors, Dr. Garvin has received the Sigma Xi Award for Excellence in Research and a NASA Group Achievement Award for work on Sally Ride's Task Group 1A project. He has earned a PhD in geological sciences from Brown University and has worked at Goddard for 5 years.

Dr. Maria T. Zuber is a geophysicist in the Geodynamics Branch and works on the theoretical modeling of solid planet deformation. She has 4 years' experience at Goddard and earned her PhD in geophysics from Brown University.

LAND PROCESSES

FIRST INTERNATIONAL SATELLITE LAND SURFACE CLIMATOLOGY PROJECT (ISLSCP) FIELD EXPERIMENT (FIFE)

FIFE was conducted on the Konza Prairie in Kansas, initially during the summer of 1987. A follow-up experiment at the same location took place in 1989. As well as being a key component of ISLSCP, the FIFE experiments are the central element in NASA's plan to develop a physically-based approach to the use of satellite remote-sensing systems.

FIFE has three general objectives: (1) to understand the biophysical processes controlling the fluxes in exchanges of radiation, moisture, and carbon dioxide between the land surface and the atmosphere; (2) to develop and test remote-sensing methodologies for observing these processes at a pixel-level; and (3) to understand how to scale the pixel-level information to regional scales commensurate with modeling of global processes.

Both the 1987 and 1989 experiments were executed at and around the Konza Prairie Reserve near Manhattan, Kansas, using the sites shown in the first figure. The FIFE site is a 15- × 15-km area of grassland, most of which is under private management for grazing. About one-third of the area is managed as a long-term ecological reserve (the Konza Prairie) for the study of grassland ecosystem dynamics.

The data acquisition effort of FIFE can be divided into two broad categories: the monitoring effort and the Intensive Field Campaigns (IFC's).

The monitoring effort, which operated more or less continuously through 1987, 1988, and 1989, covered several activities: acquisition of Advanced Very-High-Resolution Radiometer (AVHRR), LANDSAT, France's Satellite Pour L'Observation de la Terre, and Geostationary Operational Environmental Satellite (GOES) data; continuous acquisition of relevant meteorological data from 16 automated meteorological stations within the site; collection of gravimetric soil moisture surveys, streamflow data, and biometric measurements; and finally, observations of relevant atmospheric optical properties to study the effects of atmosphere on satellite remote-sensing images.

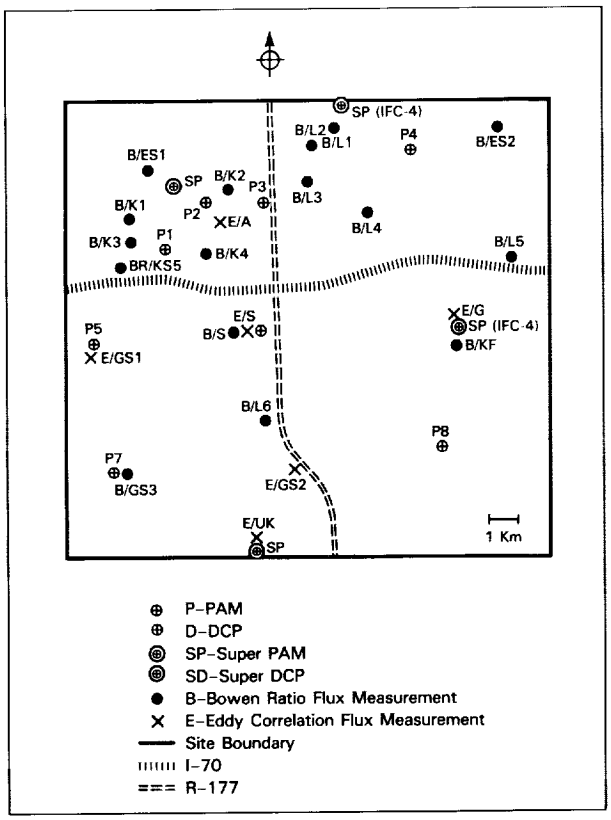

Map of FIFE site showing locations of flux stations and automated meteorological stations during the 1987 field phase. The automated meteorological stations were put in place in April and May 1987 and are still in operation. During 1987, the flux stations were moved into the site for the four IFC's. Both kinds of instruments were distributed around the site by means of a stratified sampling scheme.

The IFC's had the specific objective of acquiring surface airborne data in conjunction with the satellite overpasses to study the biophysical and energetic processes over spatial scales from millimeters to kilometers and temporal scales from seconds to an entire season. The IFC's required a large commitment of manpower and resources; thus, their combined duration during 1987 was only 57 days, as the second figure shows. The IFC campaign periods targeted the critical phases of vegetative development: (1) greenup, (2) peak greenness, (3) dry-down, (4) senescence. In the 1987 periods, as the third figure shows, unusual weather conditions produced very similar conditions during the first three IFC periods (wet soils and green vegetation) followed by a totally senescent vegetation cover and dry soil in the fourth period. During 1989, a 20-day period was instituted from July 24 to August 2 to obtain the "dry-down" missed during IFC's in the third period.

Roughly 100 science investigators and support staff were working at the FIFE site during the IFC's. In addition to the selected investigators working in FIFE, there were two large groups of scientists and support staff conducting measurements on site. The group based at Kansas State University carried out a wide range of measurements for the monitoring program and during the campaigns. The Goddard group supported experiment design, developed and operated the FIFE Information System, and provided administrative support.

As part of the experiment, three aircraft (a NASA C-130, a NASA helicopter, and a NOAA Aerocommander) took radiometric measurements using a variety of scanners, radiometers, and scatterometers operating over the visible, near-infrared, thermal, and microwave wavelength intervals. Three other aircraft [a Canadian Twin Otter, a National Center for Atmospheric Research (NCAR) KingAir, and a University of Wyoming KingAir] took flux measurements of heat, moisture, momentum, and (with the Twin Otter only) carbon dioxide (CO_2) fluxes over the site. These activities were closely coordinated with each other and with satellite overpasses. In total, some 180 missions and over 400 h of aircraft flight time were dedicated to data acquisition during FIFE.

The FIFE Information System, developed and operated by the FIFE science staff, uses an Oracle data base management system implemented on the Laboratory for Terrestrial Physics VAX 11-780 facility at Goddard. The Information System is linked to all the FIFE investigators via Telenet, INTERnet, and Space Physics

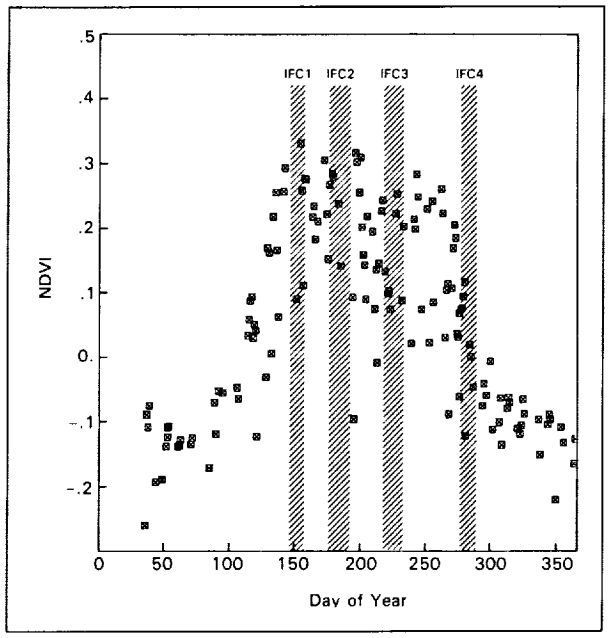

Timing of IFC's during 1987. Also shown are the NOAA-9 normalized difference vegetation index values for the year; high values indicate greener vegetation. Data from Goddard and Kansas State University researchers.

Analysis Network (SPAN). Data, accessible through a well-documented menu system, include the nearly 36,000 satellite and aircraft images acquired for FIFE as well as the surface meteorological and biophysical data. In all, FIFE contains roughly 100 Gbytes of data. The major components of the FIFE data were available to FIFE investigators within 2 to 3 months of data acquisition.

The components of the surface energy balance, all amenable to measurement by remote sensing, are

$$R_n = H + LE + G. \quad (1)$$

R_n is the net solar energy absorbed by the Earth's surface (incident - reflected + emitted); LE, the latent heat, is the energy returned to the atmosphere via turbulent transport to water vapor; H, the sensible heat, is the energy returned by the atmospheric heating; and G, the ground heat flux, is the energy going into heating the soil.

Theory suggests that the components in equation (1) can be expressed in terms of variables observable with remotely sensed data. For example, first order solutions to turbulent transport equations suggest that the difference between the air temperature above the canopy and the temperature within the canopy air space (T_{aero}) is proportional to sensible heat flux H. In FIFE, researchers were able to evaluate the ability to remotely infer T_{aero} by measuring canopy radiometric temperature T_{rad}. The fourth figure shows a plot of T_{aero} versus T_{rad}. A helicopter-mounted, nadir-looking radiometer operating in the 10.4- to 12.3-μm band measured T_{rad} from a height of 200 m above ground level. The slight overestimate of T_{aero} by T_{rad} and the scatter in the data probably result from the fact that the radiometer views somewhat different canopy elements than those that heat the air for sensible heat release. It is possible, however, that there are fundamental problems with using first order solutions to parameterize turbulent transfer of heat from the canopy.

For latent heat transfer from the surface, first order solutions to equations describing turbulent transport of water vapor suggest that the LE flux may be directly proportional to the air-canopy vapor pressure difference multiplied by canopy conductance, a term that parameterizes the bulk leaf stomatal conductance of water vapor from the canopy. Other research suggests that the maximum canopy conductance (g_c*) is related to total leaf area available for evaportranspiration and linearly related to the ratio of the canopy reflectance in the near-infrared to the visible spectral band. Again, FIFE was able to test this hypothesis.

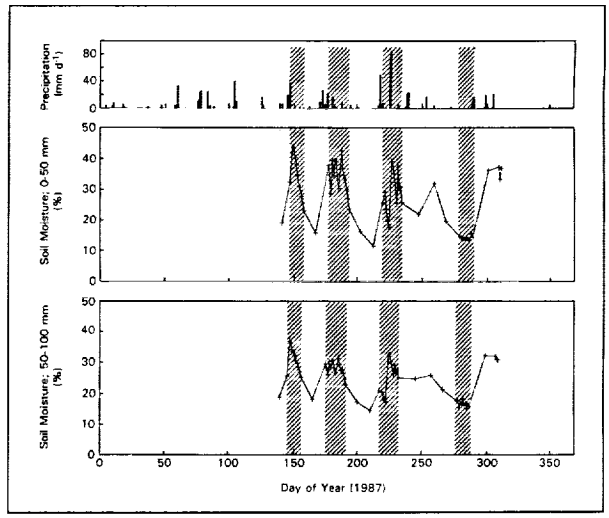

Precipitation and soil moisture conditions as measured at the FIFE site at or near the automated meteorological stations during 1987. Note wet soil moisture conditions during the first three campaigns. Data from the Kansas State group.

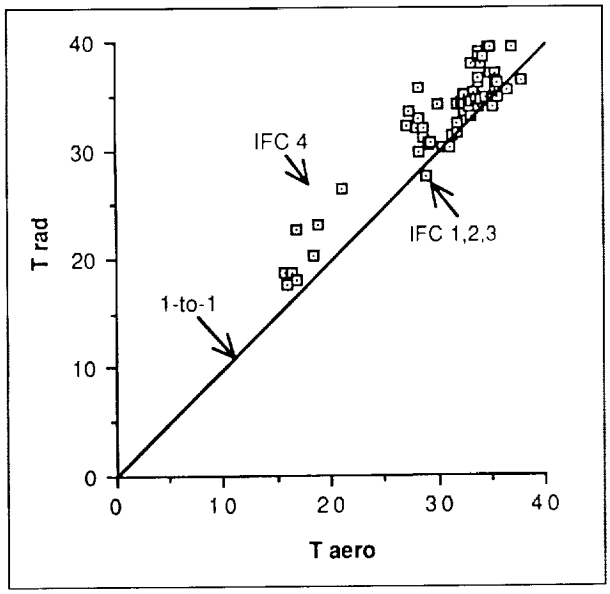

Plot of surface radiometric temperature, T_{rad}, as measured by a helicopter-mounted radiometer, and surface aerodynamic temperature, T_{aero}, as derived from surface-flux data for different flux stations during different IFC's in FIFE-1987.

The fifth figure shows a comparison between the maximum canopy conductance calculated from the surface *LE* measurements for an insolation of 600 Wm^{-2} for different campaigns, with corresponding simple ratio vegetation index data from the helicopter-mounted Barnes Modular Multichannel Radiometer. There appears to be a linear relationship between the two quantities, albeit with a large scatter; r^2=0.5111. Investigators have yet to determine whether the scatter is due to data-quality problems or other biophysical factors not considered in the analysis.

Future research will center on adjustment of g_c* for insolation, vapor pressure deficit, and temperature to yield an estimate of the actual surface conductance that may be used directly in the Penman-Monteith equation to calculate *LE*.

CO_2 flux and water-vapor flux from a plant canopy should be strongly related. In essence, when leaf stomata open to admit atmospheric CO_2 by diffusion (for photosynthesis), they necessarily lose water by the same process. The sixth figure shows net CO_2-flux data plotted against simple ratio vegetation index data collected by helicopter for a single site over several campaigns. The data exhibit a near-linear relationship and surprisingly little scatter.

These results indicate that the hypotheses relating spectral radiances or emittances to the energy balance components appear to be borne out by the data, although much work needs to be done to refine the quality of the data set.

A number of heat and moisture flux data sets were collected at difference spatial scales. The seventh figure shows the midday evaporation ratio, $LE/(LE+H)$, as measured by airborne and surface eddy correlation techniques and as calculated from radiosonde data for one day in each campaign. Also shown are the NOAA-9 maximum normalized difference vegetation index values for the corresponding campaigns. The flux measurement techniques appear to agree fairly well, and all capture the large drop in the evaporation ratio between the third and fourth campaigns.

These and other results indicate that the FIFE data set should be adequate for testing satellite data algorithms; that is, surface fluxes on large spatial scales can be computed from the field measurements and then compared with the output of surface energy balance models driven by satellite data.

During the summer of 1987, above average precipitation during FIFE created wet soil conditions, which prevented

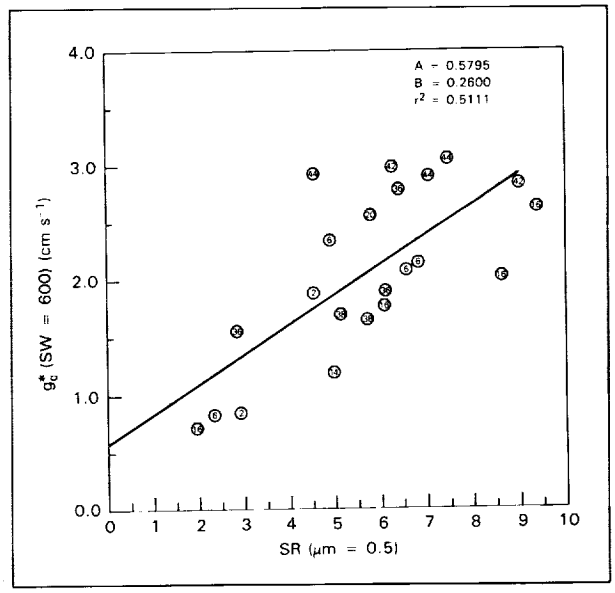

Plot of unstressed canopy conductance calculated for an insolation of 600 Wm^{-2} (g_c;short wave=600), plotted against (helicopter) simple ratio vegetation index data adjusted to a solar zenith angle of 30° (simple ratio vegetation index = 0.5), for several flux station sites during different IFC's.*

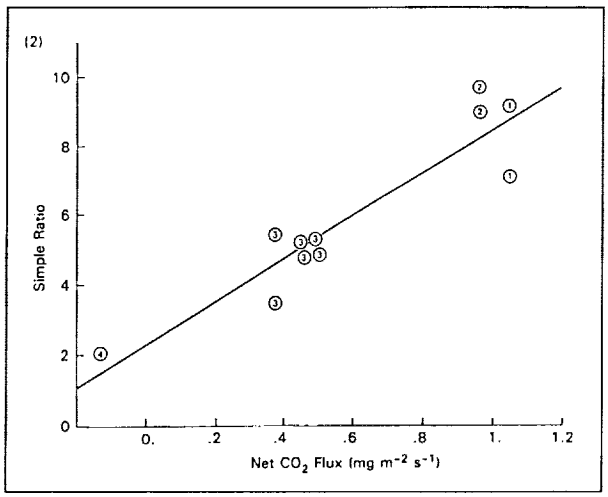

Plot of midday net CO_2 flux, as measured at site 16 using an eddy correlation technique, against helicopter simple ratio vegetation index data. Numbered points denote campaign.

observations where the strongest biological control would have been exerted on the energy balance components. FIFE-1989 was conceived and designed to address this issue and, in addition, a number of experiment design issues uncovered by the analysis of FIFE-1987 data, such as splitting the CO_2 flux into vegetative and soil contributions, measuring soil and vegetative contributions to evaporation independently, and obtaining improved in situ estimates of biophysical parameters relevant to the study of energy balance.

During the beginning of the 1989 campaign, the science team was able to observe the vegetated surface in a freely evaporating state with stress-free photosynthesis. Then an extended period of dry weather and clear skies permitted investigators to study the transition of vegetation from an unstressed to a stressed state, both in spectral terms and in terms of declining evapotranspiration and carbon exchange rates. The intercomparison of sites with similar vegetation but different environmental parameters (soil moisture, evaporative demand, etc.), will provide additional understanding to how biological and physical processes affect surface energy balance.

FIFE was conducted in conjunction with the National Science Foundation, the U.S. Department of Agriculture, the U.S. Geological Survey, and NOAA. FIFE-1989 included nine Soviet scientists. Among other instruments, the Soviets used an instrument with very high spectral resolution that had been flown on the Soviet's Mir space station. Late in the year, the Soviets also began contributing satellite data from a conical scanner on Cosmos 1939, which has spectral bands similar to the AVHRR on the U.S. operational satellites. As part of this U.S./U.S.S.R. exchange agreement, U.S. scientists are expected to visit Kursk in the Soviet steppes in 1991.

Investigators continue to analyze FIFE data, particularly from the 4 "golden days" when experimenters had the advantages of a satellite overpass (either LANDSAT or France's Satellite Pour L'Observation de la Terre), the weather was exceptionally clear, and the aircraft sensors were operated throughout a full diurnal cycle.

A major symposium on FIFE results is being held in February 1990 at the American Meteorological Society meeting in Anaheim, California. Toward the end of the year, a joint symposium is planned with the French-led Hydrological Atmospheric Pilot Experiment at the American Geophysical Union meeting.

Contact: Forrest G. Hall (Code 623)
(301) 286-2974
Piers J. Sellers, University of Maryland
(Code 624)
(301) 286-4173

Sponsor: Land Processing Branch,
NASA Headquarters

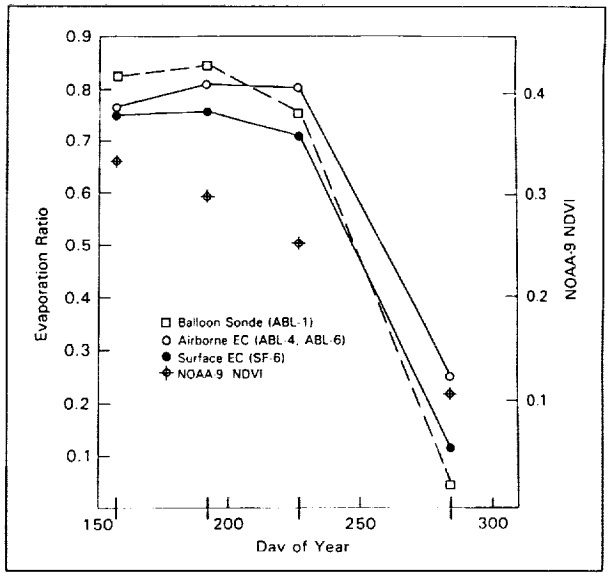

Midday evaporation ratio as estimated from airborne and surface eddy correlation, flux measurements, and radiosonde data.

Dr. Forrest G. Hall is the Science Coordinator of the FIFE. As Staff Scientist with the Laboratory for Terrestrial Physics, he researches forested ecosystems. Dr. Hall, who holds a PhD in physics from the University of Houston, has 4 years' experience with Goddard. He has received the NASA Medal for Exceptional Scientific Achievement as well as several NASA Achievement Awards.

Dr. Piers J. Sellers is Associate Research Scientist at the Center for Ocean and Atmosphere Interactions at the University of Maryland. Dr. Sellers works on simulation modeling of atmosphere-biosphere interactions, remote sensing of biospheric functioning, and experiment design and execution. He holds a PhD in atmospheric science and has 7 years' experience at Goddard.

A KNOWLEDGE-BASED EXPERT SYSTEM FOR INFERRING VEGETATION CHARACTERISTICS

The overall goal of this research is to develop a robust extraction technique for inferring physical and biological surface properties using nadir and/or directional reflectance data as input. A prototype expert system has been developed that concentrates on extracting spectral hemispherical reflectance using any combination of nadir and/or directional reflectance data as input. This system is designed to facilitate expansion to handle any other inferences of vegetation properties such as total hemispherical reflectance, percent ground cover, leaf area index, biomass, and photosynthetic capacity. The expert system accepts spectral data of an unknown target as input, determines the best strategies for inferring hemispherical reflectance, applies the strategies to the target data, and provides a rigorous estimate of the accuracy of the inference. The knowledge-based expert system uses methods based on remote sensing and artificial intelligence. The system integrates input spectral measurements with diverse knowledge bases available from the literature, data sets of directional reflectance measurements, and information from private experts into an intelligent and efficient system for making vegetation inferences.

Traditionally, the remote-sensing community has relied totally on spectral nadir reflectance to extract surface properties. Future sensors will be capable of collecting multispectral strings of data as shown in the first figure. The type of available data (e.g., number of off-nadir angles and their orientations) is highly variable from site to site,

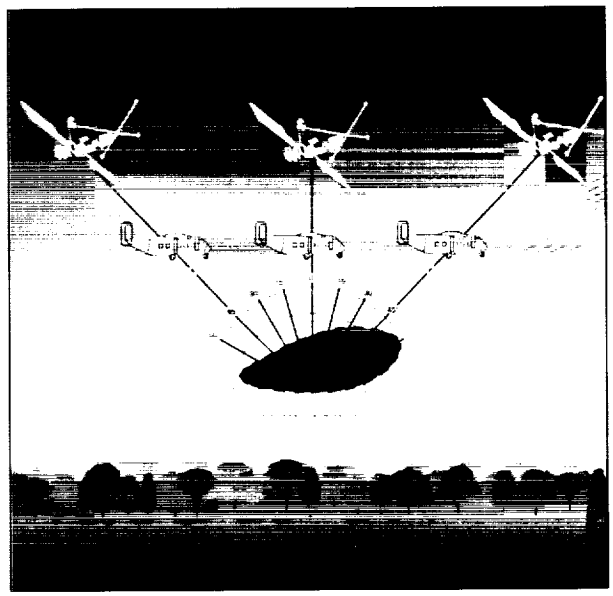

Sensors collecting a string of data. A string of data is a series of off-nadir view angles that occur in one azimuthal plane. The sensor views fore and aft along track as the sensor flies over the target. A full string occurs when a series of view angles is collected on both sides of nadir such as shown in the figure. A half string occurs when a series of view angles is collected from just one side of nadir.

due to the way satellites collect data and the problem cloud cover presents. After atmospheric correction procedures, the directional sensor data have variable levels of reliability. Thus, systems need to be developed that are flexible enough to handle many decisions at the expert level.

The system is written in the language LISP. It begins with an inference engine, as diagrammed in the second figure, that has the structure and knowledge necessary to decide how and when to apply the various knowledge bases and problem-solving techniques to meet any specific goal the user chooses. The inference engine uses a rule-based system implemented as a backward chaining program. The root goal described here is to extract the spectral hemispherical reflectance and the associated error bound from any combination of nadir and/or directional reflectance values of a target.

The system sets up several structures and tools that are used repeatedly. A blackboard structure is used as a dynamic base for current knowledge. Also defined is a simple rule-based system using forward and backward chaining. The system queries the user for the input

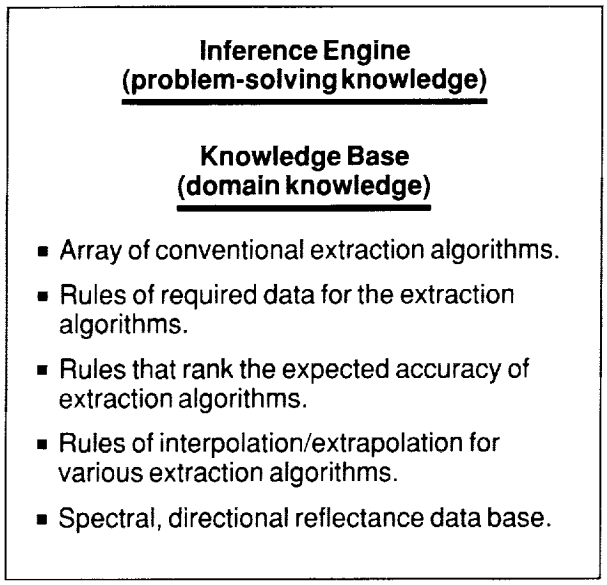

The structure of the knowledge-based expert system showing various types of domain knowledge used in the system.

spectral data. The system characterizes the input data by making assertions. For example, a list of assertions in LISP code for one data set might be: 8 off-nadir view angles are available, incomplete full string data is in the plane 90° to principal plane of Sun, etc.

Once the input data are characterized, the system begins to characterize the target. Some minimal knowledge about the target's characteristics can improve the accuracy of the system's estimate of hemispherical reflectance. The system can make inferences about the target using a variety of extraction techniques. For example, one technique uses a linear regression where the normalized difference is the independent variable and the percent ground cover is the dependent variable.

Next the system generates a ranked list of conventional techniques for extracting hemispherical reflectance that can be applied to the input data set. A knowledge base contains information (rules) on the type of input data required before each conventional technique can be applied and the expected accuracy after considering the conditions (Sun angle, number of view angles, orientation of view angles, etc.). Finally, the best or a few best techniques are applied to the appropriate spectral input data to calculate the estimated spectral hemispherical reflectance.

The system uses a generate-and-test technique in conjunction with a data base of field data to provide a rigorous estimate of hemispherical reflectance. The prototype system first generates a restricted data set to test the generated techniques on. The restricted data set consists of all of the directional reflectance distributions of cover types in the knowledge base that match closely the wavelength, Sun angle, and percent cover of the target. The restricted data set also contains the true hemispherical reflectance for each reflectance distribution. The system then applies the chosen conventional extraction techniques to each cover type in the restricted data set. The error (true hemispherical reflectance minus inferred hemispherical reflectance) is calculated for each cover type. These errors are used to calculate an error bound for each technique.

To illustrate what the expert system can do, data similar to what the High Resolution Imaging Spectrometer (HIRIS) could collect for an unknown target were used as input to the system. A string of off-nadir data occurring in an azimuthal plane was used as input, as the first figure indicates. The input data were for a near infrared band centered at 0.91 μm and a solar zenith angle of 42°. The data were actually taken from ground data of a dense green grass canopy. The true hemispherical reflectance of the target was 0.42.

It is common practice to use the nadir reflectance directly as hemispherical reflectance. This poor technique had an inferred hemispherical reflectance of 0.31 and a percent error of 26.2. In contrast, three physical-based techniques that use the entire string of data were applied by the expert system. The best technique had a 1.8-percent error, and the proportional error bound for the inference was 4 percent. Essentially all inferred hemispherical reflectances will lie plus or minus two times the error bound of the true hemispherical reflectances, as is the case in this example.

The inferences of the expert system are significantly more accurate and robust than conventional extraction techniques alone. The unique contribution of the expert system is its integration of traditional spectral measurements with diverse knowledge bases available from the literature, data sets of directional reflectance measurements, and information of private experts into an intelligent and efficient system for making vegetation inferences. The prototype expert system and anticipated system expansions may provide a valuable tool for intense study of sites using spectral data acquired from pointable sensors such as Advanced Solid State

Array Spectrometer, Moderate-Resolution Imaging Spectrometer (MODIS), and HIRIS.

Contact: Daniel S. Kimes (Code 623)
(301) 286-4927

Sponsor: Office of Space Science and Applications, Land Processes Branch

Dr. Daniel S. Kimes, with 10 years' experience at Goddard, works in the Laboratory for Terrestrial Physics in the Biospheric Sciences Branch. He develops mathematical models for visible, near-infrared, and thermal infrared radiation interactions with vegetation. Dr. Kimes received his PhD in Earth resources from Colorado State University.

THE UTILITY OF CLIMATIC STATION DATA IN MAKING HOURLY POTENTIAL EVAPOTRANSPIRATION ESTIMATES

Accurate and timely surface moisture estimates are valuable input parameters to a variety of hydrometeorologically related models, such as those for crop growth, river basin flood potential, and general circulation. The representativeness of regional soil moisture estimates is often suspect or even doubtful, primarily due to the high spatial variability associated with point measurements. The usefulness of these estimates made by conventional means is therefore somewhat limited. Climatic data are far more representative of an area than point measurements of soil moisture and may therefore yield more accurate regional soil moisture estimates when used in evapotranspiration models.

Satellite remote-sensing techniques have provided an opportunity to make large-area observations of such surface phenomena and have been used to infer a variety of areally representative surface fluxes and physical parameters, e.g., soil moisture and evapotranspiration. Since those measurements reflect the average surface conditions integrated over an entire instantaneous field of view or footprint, they may be a more accurate indicator of large-area surface condition than areally averaged point measurements. Unfortunately, to derive the proper relationships, a variety of surface data must be acquired to validate these models.

Even though micrometeorological measurements may not have been made at a study site or within the region of interest, climate station data are often available and are generally adequate for daily regional applications and may even be sufficiently representative for more local, hourly applications. Because radiation is a major driver of the evapotranspiration process, reasonable estimates of this

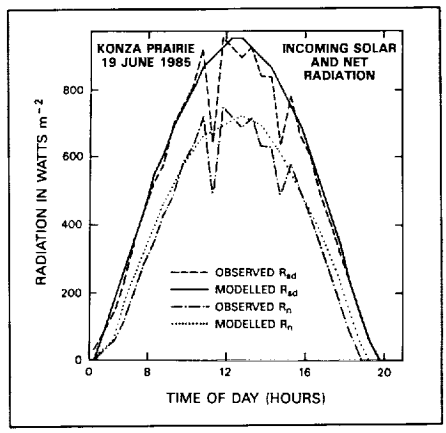

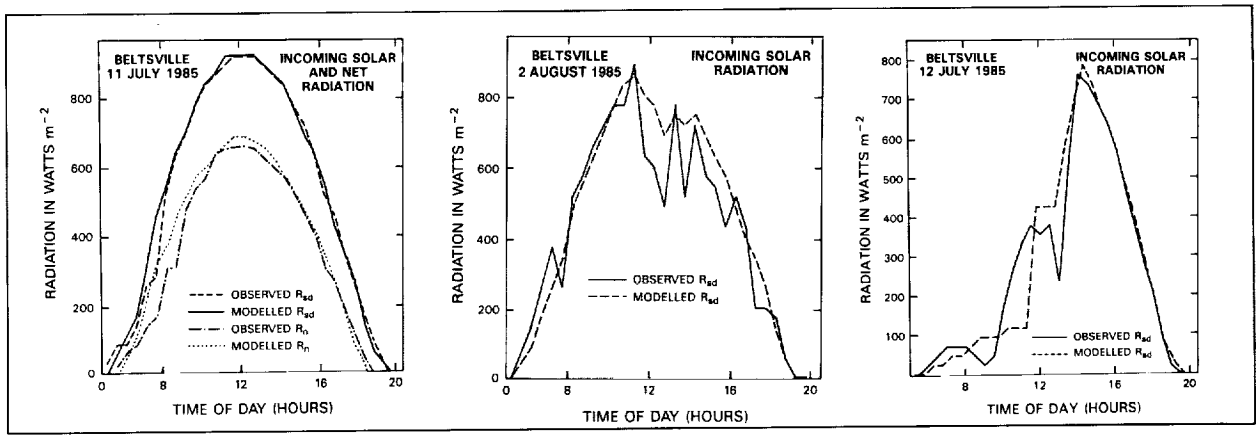

Comparisons between modeled downward solar and net radiation.

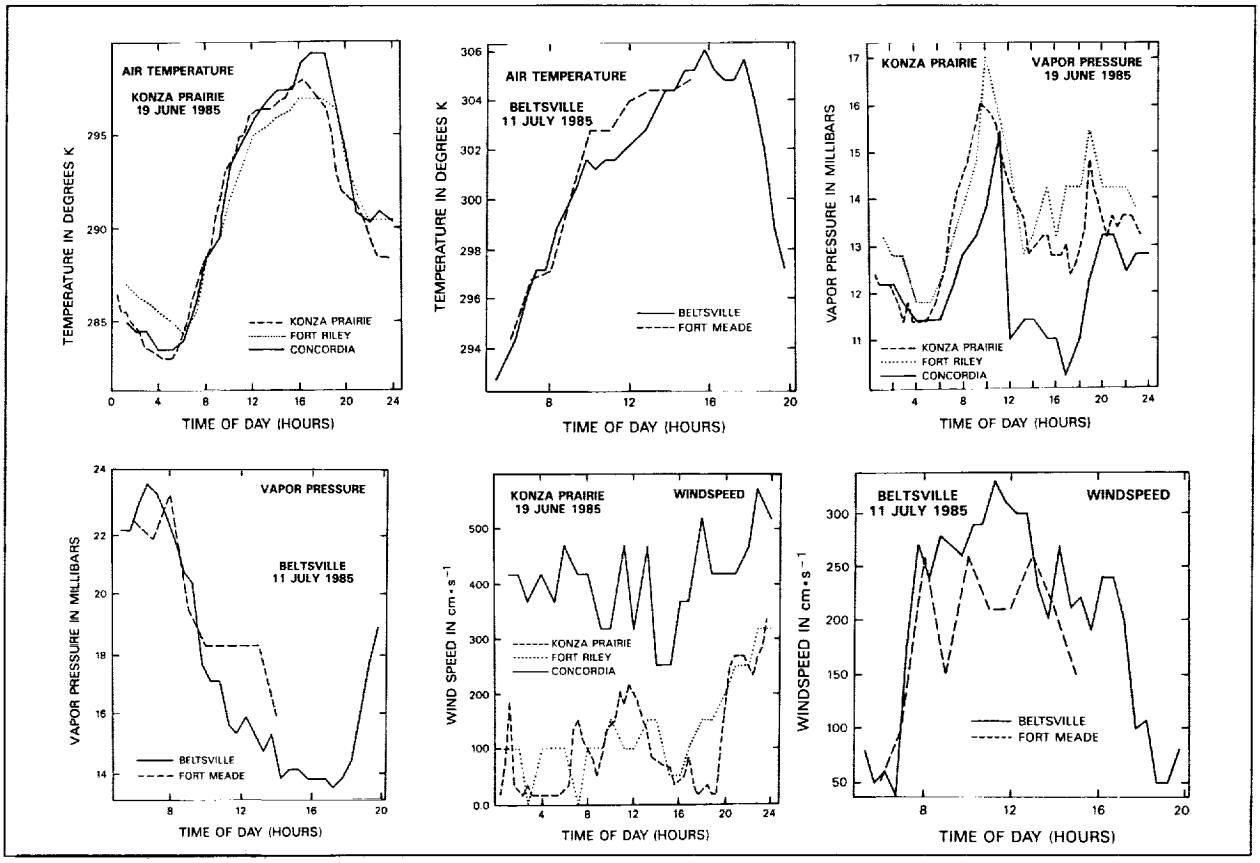

Comparisons between climatic parameters.

parameter should account for much of the variability affecting the moisture transfer process. Data are presented demonstrating that radiation data synthesized with routine weather station observations may be used to yield reasonable estimates of hourly potential evapotranspiration.

Micrometeorological data for several 24-h periods from two different climatic regimes, the Konza Prairie near Manhattan, Kansas, and the Beltsville Agricultural Research Center in Maryland, were used as a baseline. Potential evapotranspiration was calculated by using these data in a modified Penman approach. The mass transfer term, which was determined empirically by Penman (1948) from the Dalton equation, was replaced by a physically based expression describing the turbulent transfer of water vapor between a vegetated surface and the atmosphere (Van Bavel, 1966).

Atmospheric parameters then were replaced by measurements obtained from nearby climatic stations. Radiation values were synthesized in a manner similar to Eagleson (1970), but with the addition of a percentage of cloud cover and an air turbidity index, which was described as a function of the vapor pressure. Hourly climatic measurements taken at Concordia, Kansas, and Marshall Army Airfield, Fort Riley, Kansas, were used to replace the data from the Konza Prairie study site while measurements from Tipton Army Airfield, Fort Meade, Maryland, were used to replace the Beltsville observations. The climatic stations are approximately 100, 20, and 10 km respectively from the two original field sites.

The graphs in the first figure compare the observed and modeled downward solar and net radiation. The second figure shows comparisons between the climatic parameters measured at the various stations. While data from the micrometeorological stations are 30-min averages, climatic stations report hourly instantaneous observations.

Hourly estimates of potential evapotranspiration were made using the various data sets and are also shown in the third figure. The greatest deviations occurred during

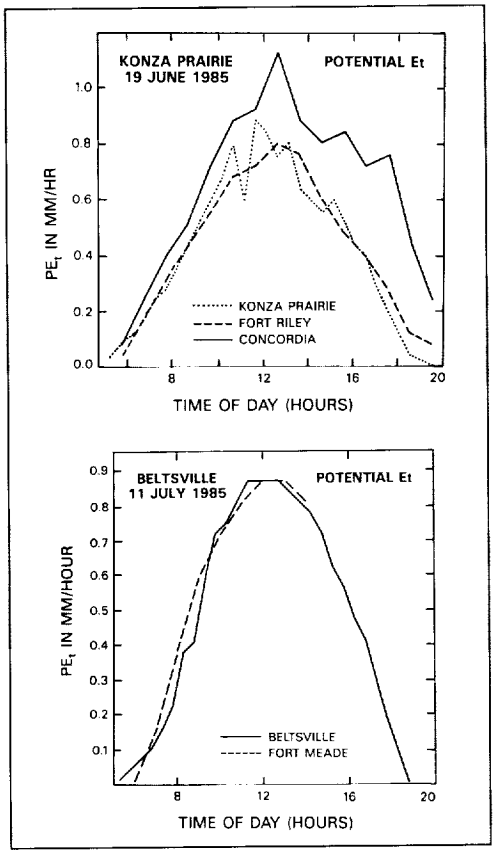

Hourly estimates of potential evapotranspiration.

periods of highly variable cloud cover although daily averages were affected less. The comparatively high potential evapotranspiration noticed in the June 19 Konza Prairie graph was caused by high wind speed.

Modeled radiation and commonly available hourly climatic station observations may be used in place of energy flux and micrometeorological measurements, even if taken at considerable distances, and have been shown to yield comparable estimates of potential evapotranspiration. The representativeness of the area surrounding the climatic station relative to the entire region of interest must be considered. If more than one station exists in the area, then areal estimates would most likely be improved by using all available data in a partial area approach.

Contact: Manfred Owe (Code 624)
(301) 286-5173

Sponsor: Office of Space Science and Applications, Land Processes Branch

Dr. Manfred Owe is Co-Investigator of the Water and Energy Balance Modeling study in Botswana. He develops remote-sensing applications in hydrology, models of regional evapotranspiration and soil moisture, and satellite microwave sensing of soil moisture for the Hydrological Sciences Branch. Dr. Owe, who has 9 years' experience with Goddard, holds a Goddard Special Achievement Award and received his PhD in environmental chemistry from the State University of New York.

AIRCRAFT AND SURFACE REMOTE-SENSING INSTRUMENTATION RADIOMETRIC CALIBRATION: THE FIRST INTERNATIONAL SATELLITE LAND SURFACE CLIMATOLOGY PROJECT (ISLSCP) FIELD EXPERIMENT (FIFE) EXPERIENCE

The relationship between a remote-sensing instrument's response and the brightness or radiance of the viewed target is its radiometric calibration. Knowledge of this relationship is necessary to begin the process of inferring Earth-surface parameters using data from these instruments. Maintaining absolute radiometric calibrations of many instruments—field, aircraft, or satellite—operating in the reflected solar portion of the electromagnetic spectrum is difficult. The design of the instruments, the standards currently available, and the need to consider many factors in the calibration transfer process contribute to the difficulties.

FIFE is one of the early large-scale attempts to relate remotely sensed radiances to land-surface parameters. Data from a number of platforms from the surface to satellites were collected simultaneously during five IFC's during the growing seasons of 1987 and 1989 at the Konza Prairie in Kansas. A goal in FIFE for instruments operating in the solar reflective spectrum was to provide radiometric consistency between the instruments at better than 5 percent and absolute accuracy at the 5- to 10-percent level. This accuracy is being achieved using a three-pronged approach: (1) consistent pre- and postseason calibrations, (2) calibration checks during the field campaigns, and (3) comparisons of the instrument responses from data taken during routine field measurements.

National Institute of Standards and Technology (NIST), formerly National Bureau of Standards, provides the standard for irradiance calibrations in the form of a 1,000-W quartz halogen lamp, which when operated at a

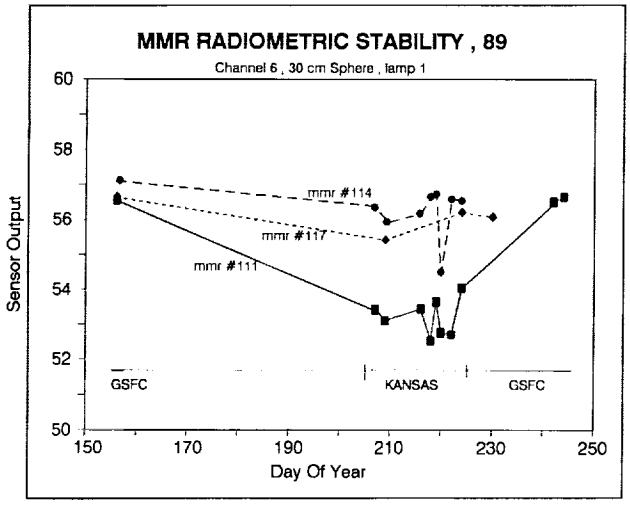

Radiometric stability of modular multiband radiometer channel 6 over the 1989 field season using 30-cm sphere with one lamp.

specified current, provides a known irradiance at a standard distance. This type of standard is not particularly useful for directly calibrating many instruments, partly because of the small area over which a uniform irradiance is available. Therefore, the calibration of this type of standard is usually transferred to a source that provides a more uniform irradiance distribution such as an internally illuminated integrating sphere. The process of transferring the calibration of the lamp (typically through several intermediary lamps, due to the cost of the NIST-supplied lamps) to the integrating sphere source is difficult to perform accurately, and when performed by different organizations, the process frequently leads to results differing by 10 percent or more. Also, calibrations by the same organizations of different sources using the same lamps and procedures are likely to produce less consistent results than those using one source. Thus, for FIFE one of the prime requirements was to use the same source for calibrating all the instruments wherever possible and, when not feasible, to use calibrations of different sources all performed by the same organization. The organization that provided the principal source and all the source calibrations for the experiment was the Goddard Standards and Calibration Office.

The calibration of field and aircraft instruments may degrade with time or vary with operating conditions. Therefore, to improve confidence in the calibration, field calibration checks were performed during FIFE. The field calibration source used was similar in design to the laboratory sources, though smaller and thus more portable. Field instruments were exposed to this uncalibrated 30-cm integrating sphere source shortly after their laboratory calibration at Goddard, periodically during the field experiment in Kansas, and then again at Goddard after the experiment at the time of the postseason laboratory calibration. The first figure illustrates the value of performing these checks because radiometer 111 showed a similar response to the source in one of its channels before and after the experiment, but an approximately 7-percent degraded response during the experiment.

Cross-calibrations of these radiometers, e.g., 111 and 117, using sunlight reflected off a white (Halon) panel, confirmed the field differences of radiometer 111. Artificial

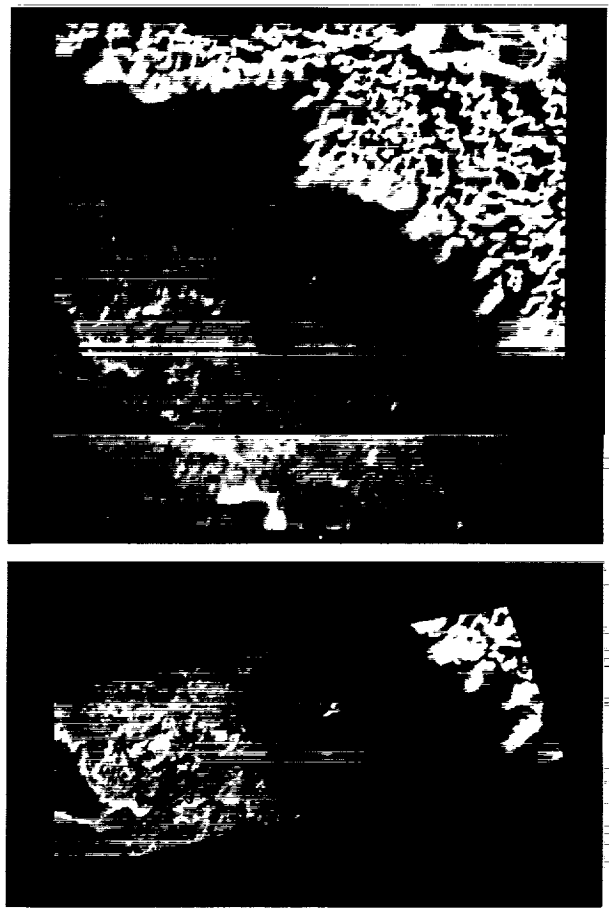

The panchromatic band from the high resolution sensor on France's Satellite Pour L'Observation de la Terre (upper panel) and Advanced Solid State Array Spectrometer images (lower panel) of White Sands, NM, test site acquired November 21, 1988.

source light, as from an integrating sphere, allows easily repeatable calibrations at any time, but does not simulate field conditions well. The combination of solar-illuminated and artificially illuminated calibration provides better understanding of the calibration. It allows researchers to adjust with confidence this instrument's radiometer measurements made in the field by 7 percent to bring them into better agreement with the other instruments.

An additional check on the calibrations of different instruments is provided by data collected simultaneously over the same target using the instruments in their normal operating modes. Because the different instruments operate from different platforms, the intervening atmosphere complicates the comparisons. Atmosphere effects are less important with brighter targets. Thus bright targets, like White Sands, New Mexico, are useful for comparing sensors. The second figure illustrates near simultaneous data taken on November 21, 1988, from the Advanced Solid State Array Spectrometer sensor flown on the NASA/Ames C130 and data from France's high resolution sensor on the Satellite Pour L'Observation de la Terre, both of which were used in FIFE. Because the satellite sensors are not available for retrieval and field checking, this method of intercomparison is one of the few available for checking satellite sensors. Similar comparisons are being done between surface and aircraft instruments.

Contact: Brian L. Markham (Code 623)
(301) 286-5240

Sponsor: Land Processes Branch, NASA Headquarters

Mr. Brian L. Markham, of the Biospheric Sciences Branch of the Laboratory for Terrestrial Physics, is interested in sensor radiometry and calibration and atmospheric characterization and correction. A 1981 William Fischer Award winner, Mr. Markham has 11 years' experience at Goddard and earned his MS from Cornell University.

NORMALIZED SATELLITE IMAGERY

Even though nearly 2 decades have elapsed since the initiation of NASA's LANDSAT program, satellite data are still distributed in raw radiance form consisting of the combined upwelling light emanating from atmospheric and surface reflectances. What the discipline needs is a reliable method to subtract the atmospheric radiance and to describe the reflection characteristics of the surface. The radiative transfer process in the atmosphere is rather complex in that it is difficult to provide a method of subtracting the atmospheric albedos from visible imagery taken from space.

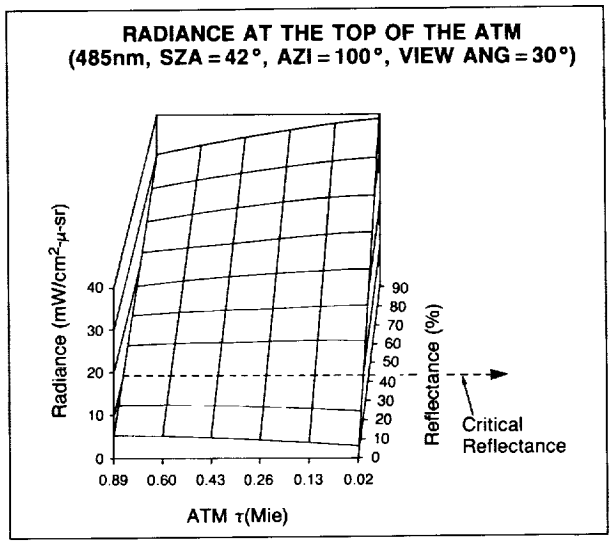

Atmospheric model describing the extent of Rayleigh and aerosol scattering and absorption on the total radiance for each scene.

In this study, sets of TM imagery taken over the Washington, DC, metropolitan area during the months of November, March, and May were converted into ground reflectance imagery. This was done, first, by selecting a model of the atmosphere that describes quantitatively the extent of Rayleigh and aerosol scattering and absorption on the total radiance for each scene, as shown in the first figure. Then the model is stored in a 3×3 matrix using a second-order, best-fit approximation. The approach is, in essence, an inversion method where a modeled atmosphere that best fits the scene is being sought by trial and error. The measured data, available in the form of pixel digital counts, are matched with the numerical results obtained from atmospheric modeling. When an atmosphere that best fits empirical data is found, a radiance model of the atmosphere is applied pixel by pixel to form a ground reflectance image.

In the set comprising the second figure (a, b, and c), derived ground reflectance images of the Washington, DC, area in fall and early and late spring are shown. The false color composite was created by assigning customary blue, green, and red guns to TM bands 1, 3, and 4 respectively. The images presented differ from other false-color TM images in that the values from each scene can be read directly to

describe quantitative information of the targets. The grey scale depicts variations in surface reflectance, and tonal signature of multiband color imagery can be directly interpreted for quantitative information of the target. In the table, the reflectances of various urban targets, retrieved directly from the corrected imagery, are listed.

An examination of the table reveals interesting facets of changing surface reflectance in a metropolitan area. First, the overall landscape varies seasonally due to the changes associated with the presence of vegetative areas. Also transient changes, such as the Potomac's high sediment load during spring, account for the high albedo of the Anacostia River in 1984.

Anomalous changes caused by human activities can be spotted easily from the imagery acquired in time series. There was a sudden change in the reflectances of the Pentagon South Parking Lot in the 1985 data, a drop from 12.3 to 8.5 percent in Band-4. This was first spotted as the May 26, 1985, image was superimposed on the March 23, 1984, image after geometrical and

Retrieved Refectances of Various Urban Targets from Corrected Imagery

		Reflectance (%)			
Data Source	**Year**	**TN/Band-1**	**Band-2**	**Band-3**	**Band-4**
Chesapeake Bay (Averaged)	82	2.2	2.6	2.4	2.1
	84	4.3	2.1	0.7	0.3
	85	2.9	2.0	1.1	0.9
Potomac River	82	1.4	4.1	0.9	2.4
	84	5.9	8.4	5.2	2.9
	85	4.5	5.0	1.9	3.2
Tidal Basin	82	1.4	3.1	0.2	2.4
	84	4.8	6.3	1.5	1.9
	85	4.3	4.8	3.8	3.1
Golf Course (E. Potomac River Park)	82	2.9	5.5	2.8	33.7
	84	4.7	6.3	2.3	32.4
	85	4.8	6.7	2.5	46.7
City Blocks (Averaged)	82	4.6	6.5	4.1	11.0
	84	7.8	9.0	6.2	12.4
	85	8.8	9.9	8.9	17.9
Concrete Roof (Kennedy Center for Performing Arts)	82	16.8	19.4	15.1	26.7
	84	23.4	24.9	20.3	32.4
	85	21.3	22.5	22.1	33.6
Asphalt Surface (1) (Pentagon N. Parking Lot, Northern Half)	82	6.1	6.9	5.6	10.5
	84	8.7	9.0	5.2	10.1
	85	9.0	8.8	7.1	11.2
Asphalt Surface (2) (Southern Half)	82	9.2	10.8	8.3	1.6
	84	8.9	9.7	6.2	12.3
	85	7.2	6.7	5.0	8.5

ORIGINAL PAGE
COLOR PHOTOGRAPH

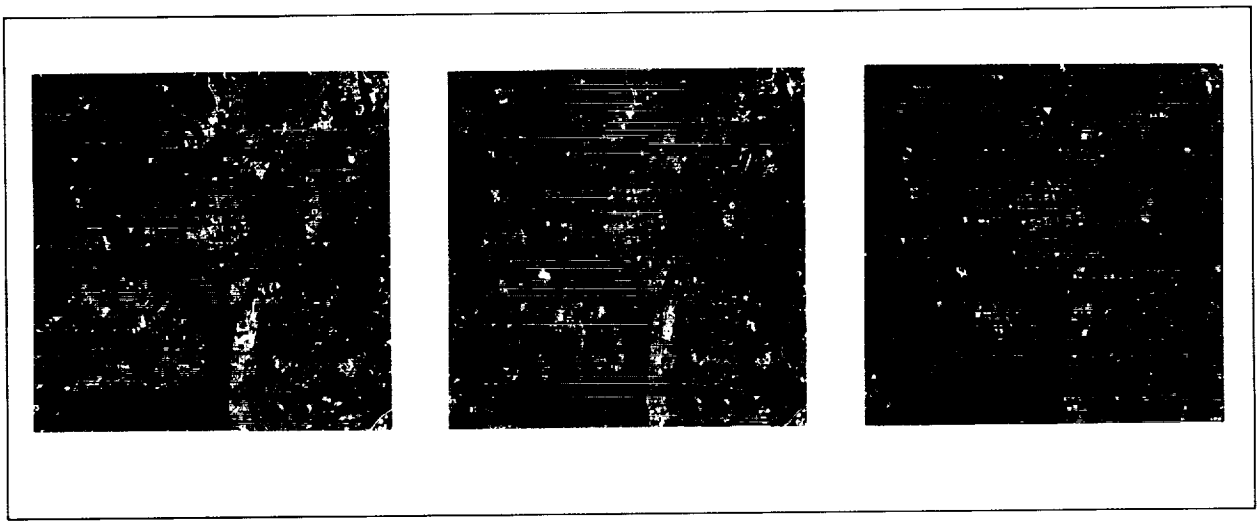

Ground reflectance images of Washington, DC: a) fall; b) early spring; c) summer.

atmospheric corrections. Most urban targets are relatively immune to seasonal alterations because features such as asphalt and concrete are not expected to change seasonally. Investigation revealed that the observed change was caused by repaving of the southern half of the Pentagon North Parking Lot during the winter of 1984-1985. Repavings and large excavations are man-made changes that are frequently sighted by overlaying two time-lapsed reflectance images of the same area.

The table also demonstrates the angular reflective properties of terrestrial targets. Even though concrete buildings are not expected to change reflectance seasonally, less than perfect Lambertian reflectance of the buildings introduces bidirectionality resulting in increasingly large reflectance as the incident sunlight angles increase. The Kennedy Center for Performing Arts and downtown Washington city blocks show such behavior. For instance, the average reflectances of downtown city blocks increased as much as 60 percent as the Sun elevation angle changed from 30° to 60°. Such bidirectional reflectance behavior is thought to be related to the size of building shadows.

In summary, the technical goal of this study was to develop a practical methodology to derive surface reflectance corrected for atmospheric scattering and absorption so that a time series of normalized TM data can be directly compared. This method should improve the prospects of applying satellite data to a much wider set of scientific problems. For instance, standardized crop imagery, provided monthly, would be much more useful in assessing the status of crops.

Contact: Hongsuk H. Kim (Code 625)
(301) 286-6465

Sponsor: MODIS-Nadir Project, Laboratory for Terrestrial Physics

Mr. Hongsuk H. Kim is the inventor of the Airborne Oceanographic Lidar System, lidar bathymetry, iodine laser, and multichannel photo-ionization chamber. He was one of the first shuttle-borne Earth observation experiment investigators of the Ocean Color Experiment for the Office of Science and Technology Assessment. Mr. Kim currently models atmospheric radiative transfer processes and their application to surface observation in the Sensor Concepts and Development Branch of the Laboratory for Terrestrial Physics. He also works on simulation of satellite data. He has been with Goddard for 11 years and NASA for 23 years.

AIRBORNE LASER ALTIMETER CHARACTERIZATION OF GEOLOGIC SURFACES

Geologic surfaces are frequently difficult to describe in a quantitative manner on the basis of their spatial and topographic complexity at various wavelengths. As local topographic slope properties are most diagnostic of the formation and modification of geologic processes that control landscape evolution, characterization of the high spatial- and vertical-resolution topographic properties of various fundamental geologic terrain types is a pressing

objective in the Earth sciences. Over the past several years a team of Goddard scientists and engineers have worked together to facilitate the measurement of the 1- to 10-m scale terrain properties of a broad suite of dynamic landscape types including volcanic areas, zone of active coastal erosion, and glaciers.

The method of choice for rapidly surveying the high-frequency topographic characteristics of complex landscapes is airborne laser altimetry. This technique can be used to efficiently acquire topographic profiles of geologic terrains with submeter vertical control over appreciable baselines (i.e., tens of km). With the advent of Global Positioning System tracking techniques, high-storage-capacity flight-worthy digital computers, and high-pulse-repetition-rate laser transmitters, airborne laser altimetry techniques can now produce topographic profiles with footprints as small as 15 cm and with vertical precision levels that approach 5 cm. High-altitude airborne laser altimetry systems can be used to profile extremely mountainous terrains or even the Grand Canyon. Since the advent of the program in late 1986, Goddard airborne laser altimetry systems have acquired hundreds of topographic profiles of diverse landscapes and their component landforms. Researchers have profiled the Grand Canyon, Mount Saint Helens, Meteor Crater, the Cape Cod Barrier Island system (Monomoy Island), the volcanic island of Surtsey, outlet glaciers in Iceland, stratovolcanoes (Mount Humphreys in Arizona), giant dune fields, and several volcanic lava-flow fields in the western United States and in Iceland. While there have been several objectives in this measurement program, particularly interesting results occurred in two areas. First, researchers identified systematic variations in the microtopographics of basic lava-flow types. Second, researchers examining the topography of explosion landforms observed some heretofore-unrecognized patterns. This report focuses on volcanic and impact explosion landforms.

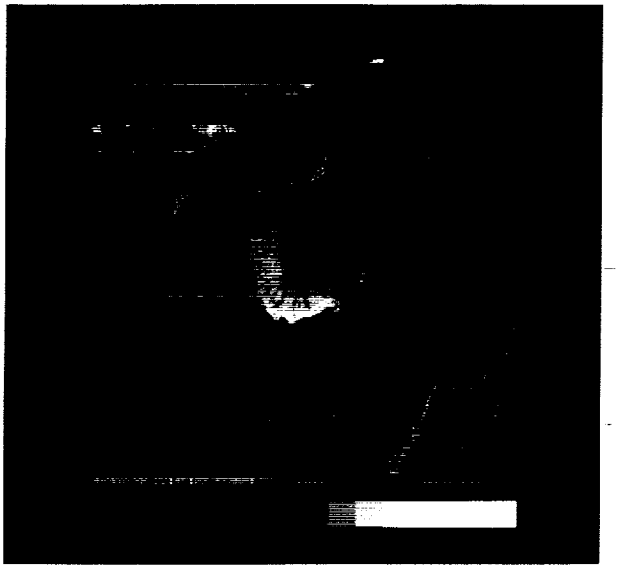

Airborne thermal infrared false-color image of the 1.2-km-diameter meteor crater impact landform in Arizona. The NASA Thermal Infrared Multispectral Scanner (TIMS) instrument obtained this image of Meteor Crater in September 1987. The colors reflect relative degrees of variation between thermophysical parameters of the surface deposits, many of which are related to the explosion event. The crater is somewhat polygonal in shape, and the ejecta deposit has been slightly modified by eolian drift deposits caused by prevailing southwesterly winds. The innermost portion of the crater depression has been infilled with lacustrine sediments and late-stage inner-rim wall slumping.

Explosion landforms are among the most abundant in the solar system, yet are often overlooked when basic terrestrial landforms are discussed. This is largely the result of rapid terrestrial erosion processes—many explosion landforms are obliterated almost as rapidly as they are formed. The first figure shows a false-color thermal infrared image of the well-known Meteor Crater landform in north-central Arizona. This relatively uneroded explosion landform was formed approximately 49,000 years ago as a result of the hypervelocity impact of an iron meteor, whose effective kinetic energy equaled that of nearly 20 Mtons of TNT, approximately 20 hydrogen bombs. Landforms similar in appearance are produced when volatiles such as water come in contact with magma near the surface to generate gas-driven explosions; such features are known as maar, and they resemble simple-impact craters in many respects. Less explosive volcanic eruptions often generate tephra, or tuff rings. In these cases, a continuous fire-fountain of volcanic ash from a confined vent produces a craterlike landform without a depressed floor or a true ejecta blanket. Summit craters of cinder or scoria cones are also produced by mildly explosive activity followed by subsidence; the vents at Surtsey (Iceland) and at the SP Cone (Arizona) are of this type. Large-scale explosive phenomena produce complex craterlike landforms, many of which evolve into a multiringed "sombrero" shape.

Volcanic- and impact-explosive landforms experience rapid release of energy during the course of their formation.

ORIGINAL PAGE
COLOR PHOTOGRAPH

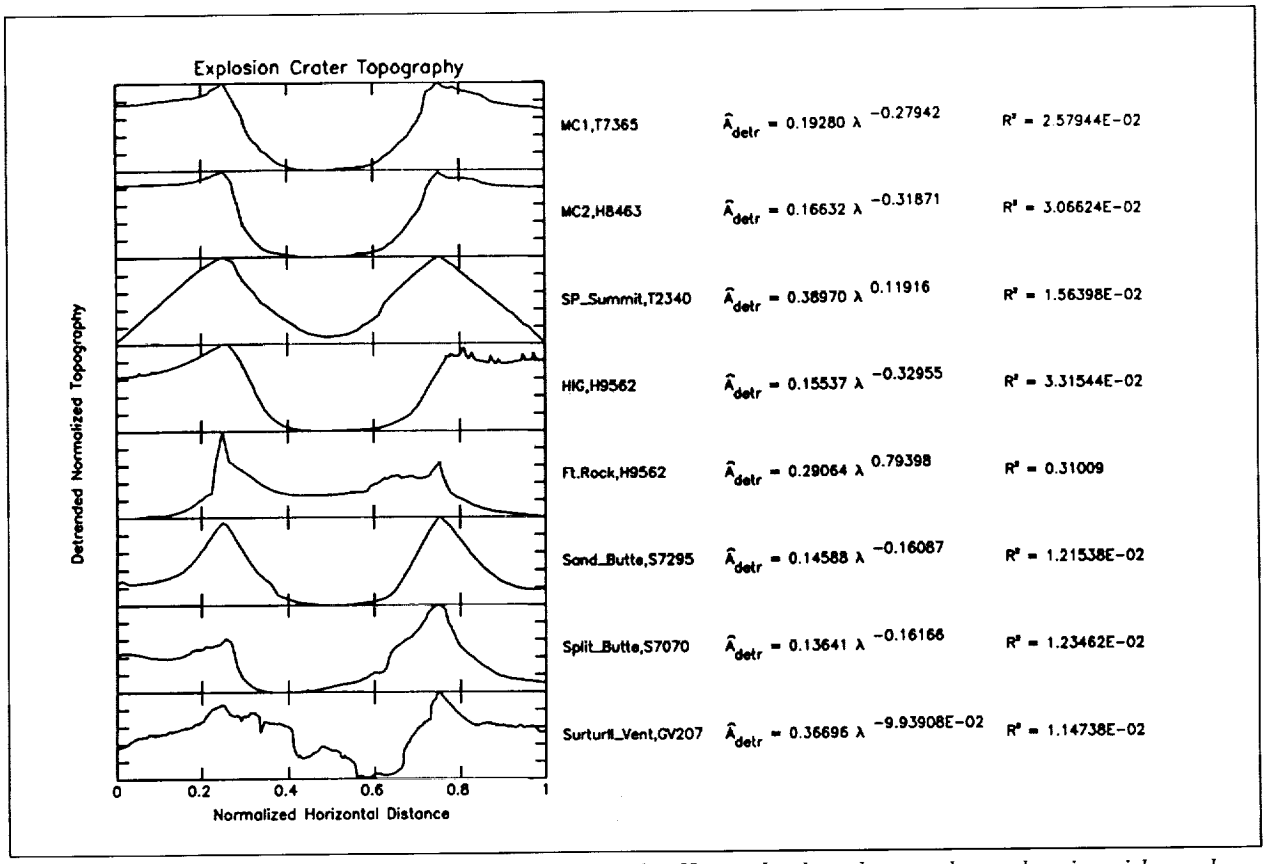

Array of topographic cross-sections of a suite of explosion landforms that have been under study using airborne laser altimetry techniques. In this figure, all of the profiles have been normalized so that the vertical scale at left is relative to the maximum relief for each independent landform. The horizontal scale is normalized to the total length of the profile. Thus, the shapes of the various landforms can be compared in this figure, independent of scale in either direction. The equations at right are power-law regressions fitted to the shapes of the craters in terms of detrended relative topography ($\hat{A}_{detr}$) and horizontal wavelength (λ). The exponent on the λterm is a useful single-parameter descriptor of the topographic cross-section of crater landform. The abbreviations are as follows: MC = Meteor Crater (AZ); SP Summit = SP Cone summit crater (AZ) ; HIG = Hole-in-the-Ground maar (OR); Ft. Rock = Fort Rock tephra ring (OR); Sand Butte = Sand Butte tephra ring in the Snake River Plain of Idaho; Split Butte is a combination tephra ring/maar crater in the Snake River Plain; and Surtur II = Surtur II vent crater on Surtsey Island, Iceland, formed during the 1963-67 eruptive sequences that generated the island. The same abbreviations apply to the third figure.

Typically, they display circular symmetry and a crater-like appearance. Researchers must understand the subtleties of explosive landform cross-sections (i.e., their topographic profiles) in order to separate those formed by impact from those of endogenic origin when Magellan radar images of crater form features on Venus are obtained in late 1990 at ~100-m resolution. For this reason, researchers have explored the extremely detailed microtopography of a suite of explosive landforms on Earth using both high- and low-altitude airborne laser altimetry techniques. The second figure is a comparison of the topographic cross-sections of a set of well-known explosion landforms; each of the profiles is normalized to the maximum relative relief and to the horizontal extent of the cross-section to permit comparison of shapes. The two uppermost profiles are for Meteor Crater (as shown in the preceding figure) and represent east-to-west and northwest-to-southeast cross-sections. In contrast, the third profile from the top is the summit collapse crater of the SP scoria cone, which was formed by fire fountaining and subsequent collapse and therefore has a very low index of explosivity relative to the Meteor Crater event.

However, the fourth profile is a cross-section of the Hole-in-the-Ground maar in the Newberry Volcanic Field of Oregon. This crater is very similar in its detailed topographic profile to Meteor Crater. Indeed, the Hole-in-the-Ground explosion may have been the result of a violent, gas-driven eruption as silicic magma came in contact with groundwater; the explosive energy could have reached a level of 5 Mtons. The power-law equations at the right-hand side of the profiles provide a quick means of comparing normalized profiles. These equations are cast in terms of normalized topography $\hat{A}_{detr}$ versus horizontal wavelength λ. The power-law exponent is a reasonable index of similarity for the landform shapes. For example, researchers have observed that the more explosive crater structures such as Meteor and Hole-in-the-Ground have exponents approaching -0.30, while the least explosive have values between 0.00 and 1.0 (see SP Cone, Fort Rock, and Surtur II at the bottom). The R2 parameter is merely an indicator of the quality of the power-law fit to the normalized topographic data. The topographic cross-sections of Sand Butte and Split Butte tephra rings in the Snake River Plain volcanic field of Idaho are very similar, although the Split Butte was the more explosive of the two. The Fort Rock tephra ring is a highly eroded or relic explosion feature; hence, its irregular topographic cross-section. The most youthful feature in the series is the lowermost, that of the Surtur II vent crater of the main lava shield on Surtsey. This crater developed between 1963 and 1967 during the construction of Surtsey. It is the result of mild fire fountaining and the collapse of a small lava pond at the summit of a subaerial lava shield. Evidently, the irregular topography reflects the "trapdoorlike" collapse or foundering episode that resulted in crater formation. Based on the topographic cross-sections shown in the second figure, researchers believe that the detailed topography of explosion

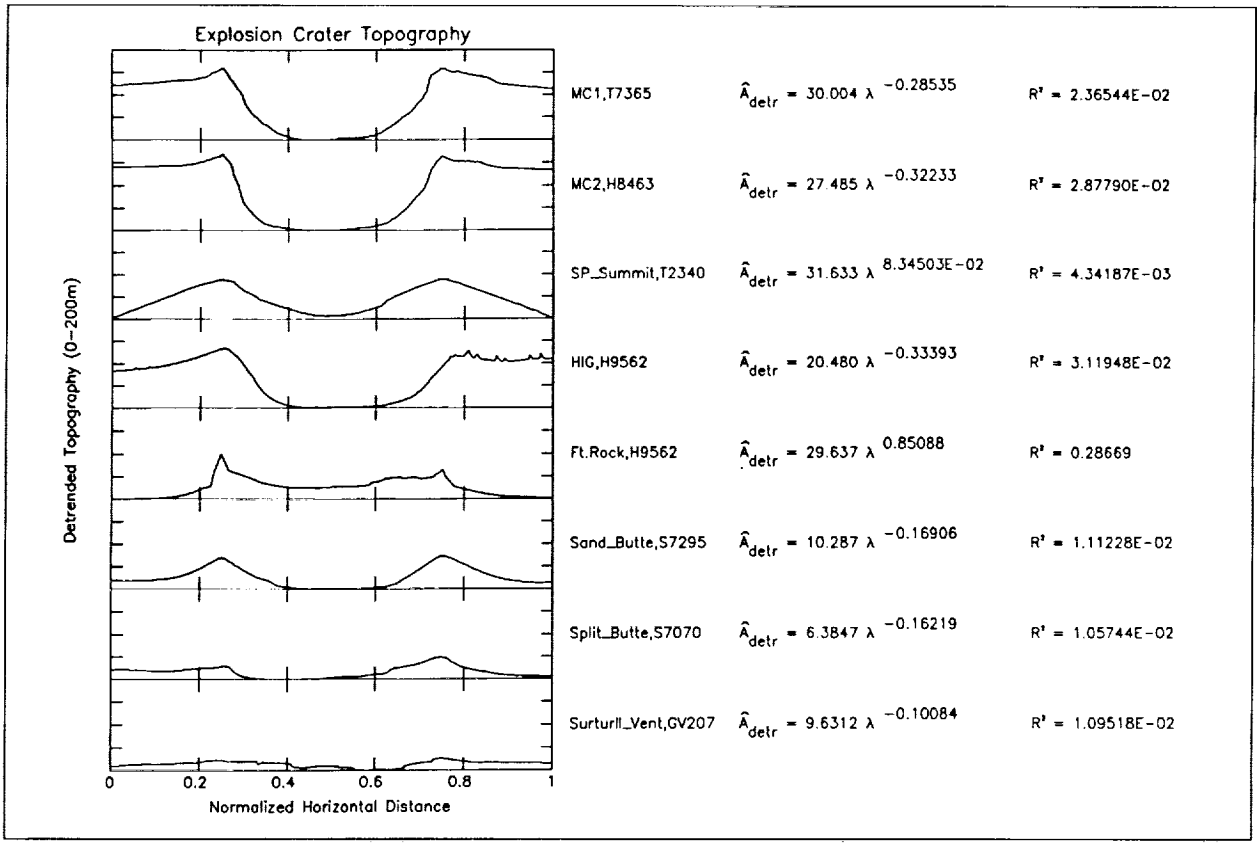

This figure follows the same format as the preceding one, except that the vertical axis at left is not normalized; it represents a scale from 0 to 200 m of relative relief. This format permits comparison of the magnitude of local relief associated with each explosion landform and illustrates the differences in explosive energies involved in the formation of impact craters (such as Meteor Craters) and simple-collapse craters such as Surtur II on Surtsey.

forms in this size class (from 300 m to 1.5 km in diameter) directly reflects the explosive energy involved in the formation of each landform.

In order to analyze more realistically the topographic shapes of distinctive explosion landforms such as those shown in the second figure, researchers often display relative relief at a fixed scale against normalized horizontal distance. The third figure shows the data from the second figure replotted with a vertical relief scale from 0 to 200 m. Using this comparison, it is easy to classify the various explosion landforms in terms of the intensity of the explosive event at the time of their formation. For example, the deepest craters with the most well-defined rim regions are the result of the most intense explosions (Meteor Crater and Hole-in-the-Ground maar), whereas the least explosive have the most subdued topography (Surtur II, Split Butte, and the highly eroded Fort Rock). Again, the power-law equations for the topographic profiles allow analysts to compare the different landforms in terms of a single parameter; the exponent on λ suggests that more explosive craters have values approximating -0.30, while the least explosive have values near to or larger than 0.00. These simple patterns give researchers confidence that the high-resolution topographic cross-sections of a diverse array of both endogenic and exogenic explosive landforms do indeed provide diagnostic information about landform formation and subsequent degradation. Thus, high-resolution radar images of explosion landforms on Venus and Earth should permit reliable discrimination between volcanic and impact varieties. However, one major ambiguity could arise, as with Meteor Crater versus Hole-in-the-Ground maar, when extremely high-energy volcanic maar craters are formed that closely resemble their impact cousins. However, the discovery of maar craters on Venus would be extremely provocative, as it would strongly suggest the presence of near-surface reservoirs of volatiles such as water, carbon dioxide, sulfur dioxide, or halogen gases (or even carbonates), volatiles that facilitate the intensive, gas-driven explosions required to produce such features.

The laser altimeter survey of the topographic cross-sections of a representative suite of terrestrial explosive landforms shown in the second and third figures is only one example of how airborne laser altimetry data can be used to study significant geologic processes on the Earth and nearby planets. The Mars Observer Laser Altimeter instrument currently under development at Goddard is an outgrowth of researchers' experience with airborne laser altimetry surveys of significant planetary analog landforms. Analysts expect to study thousands of explosive landforms on Mars using this technique to assess their modes of origin and subsequent erosional histories. The airborne laser altimetry surveys of additional varieties of explosion landforms under way in late 1989 and 1990 are a part of NASA's first Geologic Remote-Sensing Field Experiment in the western United States. As part of this project, the Ubehebe maar craters will be studied using a Goddard airborne laser altimetry system.

Airborne laser altimetry topographic surveys of distinctive terrestrial terrain types provide information on a human scale. These surveys bridge the gap between orbital data sets (with tens to hundreds of kilometers of resolution) and ground-truth studies (at meter scales). With the advent of flexible airborne laser altimetry systems, landscapes can now be quantified, at least in terms of cross-sectional topography, at meter and even submeter scales. Using these systems, microtopography can be assessed in terms of rates and styles of landscape development. Goddard researchers are confident that airborne laser altimetry techniques can be used to study coastal erosion and even to predict landslides in the future.*

**Key engineers who have been instrumental in the development of airborne laser altimeter instruments include Jack L. Bufton, James B. Abshire, and the Airborne Lidar Team at Wallops (W. Krabill, R. Swift, J. Youngel, W. Wright, and E. Frederick). Without the assistance of the Wallops T-39 and P-3 pilots, none of the data displayed in this report could have been collected; we are grateful to pilots V. Rabine, J. Riley, R. Gidge, G. Pottrell, C. Allen, and D. Roberts for their outstanding accommodation of our difficult flight requirements. Data analyst M. Ford [Remote Manipulator Systems (RMS) Technologies] has contributed in an outstanding fashion to the successful reduction of hundreds of laser profiles since 1987.*

Contact: James B. Garvin (Code 621)
(301) 286-6565

Sponsor: Land Processes Geology Program, Research and Technology Operating Plan, and Director's Discretionary Fund

Dr. James B. Garvin is Staff Geophysicist at the Geodynamics Branch in the Laboratory for Terrestrial Physics. He is Co-Investigator on the Mars Observer Laser Altimeter experiment and Principal Investigator on the Iceland volcanoes project as well as the Lunar Observer Laser

Altimeter study. He is also Project Leader on a NASA study of remote sensing signatures of impact craters on Earth. Among his honors, Dr. Garvin has received the Sigma Xi Award for Excellence in Research and a NASA Group Achievement Award for work on Sally Ride's Task Group 1A project. He earned a PhD in geological sciences from Brown University and has worked at Goddard for 5 years.

A SATELLITE SURVEY OF SULFUR DIOXIDE EMISSIONS FROM VOLCANOES

A correlation between volcanic eruptions and climate was suspected over 200 years ago when Benjamin Franklin related a year of cold weather in Western Europe to the 1783 emission of dust from the Laki (Iceland) volcano. More recently, it has become clear that the effect of enhanced volcanic sulfur dioxide (SO_2) is more important than that of volcanic dust in climate modification. Analysts have generally assumed that human contribution of SO_2 to the atmosphere, primarily through the burning of fossil fuels, far outweighs the contribution of volcanoes. However, volcanic input is poorly known, and semiquantitative estimates of the amount of volcanic SO_2 have risen by almost two orders of magnitude over the past 17 years. Only that portion of atmospheric SO_2 in the stratosphere is important to global climate modification; within the stratosphere, only the contributions of explosive volcanic eruptions are important, as anthropogenic SO_2 is removed in the troposphere.

Goddard researchers are currently engaged in an interlaboratory study to measure the emission of SO_2 from volcanoes using the 10-year Total Ozone Mapping Spectrometer (TOMS) data base. The objectives of the study are to improve current knowledge of the role of volcanic SO_2 in the geochemical cycle of sulfur, to determine the spatial variation of volcanic SO_2, and to quantify the SO_2 contribution that volcanoes make to the atmosphere.

TOMS was launched aboard the Nimbus spacecraft in late 1978 and is still operational. As the full name implies, this instrument was designed to measure atmospheric ozone. However, researchers discovered during the El Chichon eruption in 1982 that the instrument's six bands in the ultraviolet were so placed that they could measure the SO_2 emitted during large volcanic eruptions. TOMS' swath width of 2,800 km provides contiguous coverage of the Earth on a daily basis, with a noon local time overpass. Spatial resolution is 50 km at nadir, whereas at the edge of the swath, the pixel size is 150 by 300 km; the average resolution is 66 km. The theoretical sensitivity of the instrument is approximately 1 kton of SO_2 within a resolution element; background levels of SO_2 in the atmosphere are well below this level. In actuality, however, various factors affect sensitivity and precision, including background albedo, Sun angle, view angle, height of the SO_2 cloud, concentration of ozone, and instrument noise. The figure shows images of SO_2 emission from one volcanic explosion tracked over time.

In order to understand the volcano-climate relationship, researchers must first understand why certain volcanoes emit large quantities of SO_2 into the stratosphere, whereas others do not. The size of a volcanic eruption is measured by the volcanic explosivity index (VEI), which uses the height of the eruption plume and the volume of products to give a value on an open-ended scale from 0 (nonexplosive) to 7 (the largest volcanic explosion on record). About 400 volcanic eruptions during the period 1979 to 1989 have been examined for SO_2 emission. Researchers have observed SO_2 clouds from eruptions of all VEI values. Although analysts are still examining the basic data, several generalizations can be made at this time. As expected, the lower VEI eruptions have a much lower frequency of detectable SO_2 clouds than the higher VEI eruptions. About 50 percent of the VEI>3 eruptions have measurable SO_2 emission, as compared to about 10 percent of the VEI<3 eruptions. Observers are particularly interested in the VEI>3 eruptions, as these are the ones whose columns may reach into the stratosphere, where the gases can be widely distributed.

The largest SO2 emission during the decade of TOMS observation was from the March 1982 eruptions of El Chichon, Mexico (VEI=4), when approximately 3 to 4 million tons of SO2 were deposited into the stratosphere. The cloud circled the globe and was observable for more than 2 months. The next largest SO2 eruption was from Nyamuragira, Zaire, in December 1981, when about 1 million tons of SO2 were emitted. The third largest emission of SO2 was from Nevado del Ruiz, Colombia, in November 1985, when over 600 ktons were emitted, although little went into the stratosphere. The largest eruption during the decade, with a VEI of 5, was the St. Helens, Washington, eruption of May 1980, but it produced about an order of magnitude less SO2 than El Chichon. Also, most of the gas was deposited into the troposphere, not the stratosphere, and thus could have only a local effect. These TOMS-based observations are in relative agreement with

ORIGINAL PAGE
COLOR PHOTOGRAPH

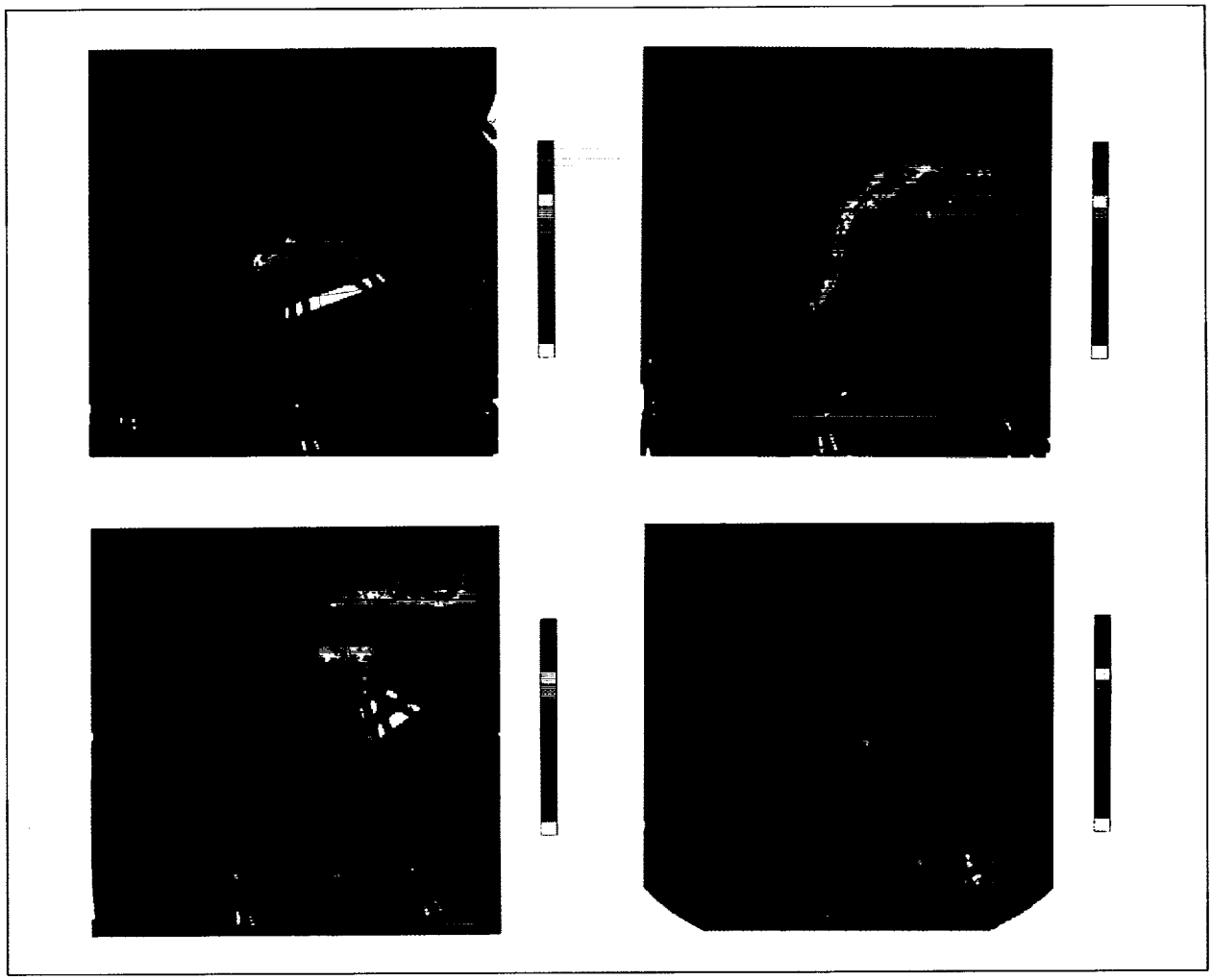

SO_2 emission from Alaid volcano, Kuril Islands, immediately south of the tip of the Kamchatka peninsula. a) This image shows the SO_2 plume on April 27, 1981, the day of a VEI-3 eruption. The plume has moved northeast and then east, but is still "attached" to the source (i.e., the volcano is still emitting SO_2). b) The plume on April 28 is no longer attached to the source and is spreading out. Most of the cloud is near the stratosphere and is drifting to the north and east, while a smaller, lower cloud is drifting to the south and east. c) The area on April 29 shows the smaller cloud has largely dissipated in the central Pacific, and the main cloud has become quite sinuous over Alaska, the Bering Sea, and Siberia. d) The remains of the April 27 eruption cloud on May 3, now over Hudson Bay and Labrador, with a secondary cloud off the mid-Atlantic States.

lidar measurements of aerosols in the stratosphere over Hawaii. Those measurements show that, for this period, El Chichon accounts for most of the aerosols, with the effects of Nyamuragira and Ruiz being less pronounced. St. Helens produced only a small, transitory effect.

Observers have also noted a great deal of variation in SO_2 emission by volcanoes from different chains. For example, researchers have yet to observe SO_2 from eruptions in the middle or southern Andes, but some even small-VEI Icelandic eruptions have produced detectable SO_2. It appears from these data that the amount of SO_2 a volcano emits is not closely linked with its explosivity and perhaps is more closely related to fundamental chemical differences among volcanoes or volcanic chains. Analysts hope to use these data to study the peterogenic and tectonic factors related to SO_2 emission.

Goddard researchers are currently defining spectral bands and algorithms used to derive the SO_2 data, so as to

improve the information received from future TOMS instruments. The importance of ozone measurements to pressing global environmental questions makes it very likely that another TOMS instrument will be launched within the next few years. Presently, several governments have made active proposals to fly such instruments. Although the 10-year TOMS data base is long in terms of satellite measurements, it must be extended if researchers are to fully understand what these data reveal about how volcanic SO_2 varies with time and place.

Contact: Charles C. Schnetzler (Code 622)
(301) 286-7496

Louis S. Walter (Code 620)
(301) 286-2538

Arlin J. Krueger (Code 616)
(301) 286-2538

Scott D. Doiron (Code 616)
(301) 286-4526

Sponsor: Land Processes Branch, NASA Headquarters

Dr. Charles C. Schnetzler works in the Geology and Geomagnetism Branch and researches the gaseous emissions from volcanoes and their impact on Earth. He has worked at Goddard for 26 years. He received a BS in geology from Kansas University and a PhD in geochemistry from Massachusetts Institute of Technology.

Dr. Louis S. Walter performs research on gaseous emissions from volcanoes in the Laboratory for Terrestrial Physics. Currently, he is writing a book on the use of space technology in disaster management. In the past, he has published analysis of the first lunar samples. Dr. Walter has 26 years' experience at Goddard and holds a PhD from The Pennsylvania State University.

Dr. Arlin J. Krueger is an atmospheric physicist studying the Antarctic ozone hole. He has worked as a sensor scientist on Nimbus 7 TOMS, as an Instrument Scientist on the Meteor-3/TOMS and Earth Probe TOMS, and as Principal Investigator on Advanced Eos TOMS. He has received an Exceptional Achievement Award and a Goddard Workstudy Fellowship for his work. Dr. Krueger has 20 years' experience at Goddard.

Mr. Scott D. Doiron surveys Nimbus 7 TOMS SO_2 data to find and examine detectable volcanic events as well as amounts and distribution of SO_2. His primary technical interest is observing volcanic eruptions using satellite data. He has received a NASA Group Achievement Award and has 4 years' experience at Goddard. He earned a BS in geology and another in computer science from Michigan Technological University.

FLOOD BASALTS, MASS EXTINCTIONS, AND IMPACTS

Flood basalts comprise vast extrusions of mafic lavas that were erupted episodically in the geologic past. Dating of these lavas, however, has been a problem owing to various sources of radiometric age scatter. Very recently, by using accurate argon-40/argon-39 dates and paleomagnetic measurements, researchers have discovered that these episodes lasted, at most, a few million years. Therefore, it is feasible now to use the much larger number of less reliable potassium-40/argon-40 dates to estimate statistically (in a suitably calibrated way) the ages of other flood basalt episodes for which argon-40/argon-39 dates are either not available or not of good quality.

Nearly all of the known flood basalt provinces are located on or near continental margins and have been dated as being less than 250 million years old. There are three reasons for this apparent bias in space and time: flood basalts are physically associated with continental rifting, most of the present seafloor is still unexplored for specific evidence of past flood basalt volcanism, and essentially all newly created seafloor becomes subducted into the mantle after about 200 million years. Eleven examples of post-Paleozoic continental flood basalt volcanism have been identified, and it is very likely that this tally is complete for the time period under consideration. The dates of initiation of the eruptions are indicated on the accompanying graph.

Furthermore, independent research has shown that some major extinctions of biological species have occurred, likewise, in brief episodes during the course of geologic history. Although the magnitude and precise duration of these extinction events are in some dispute, the major events and their approximate stratigraphic ages are accepted as known by most researchers. The mass biotic extinctions that occurred during Cenozoic and Mesozoic times are found to correlate closely with the initiation phases of major continental flood basalts, as the accompanying graph illustrates. In addition, there appears to have been a quasi-periodic lapse of roughly 32 million years between major events (or occasionally between clusters of major events).

How is all this to be accounted for? It is possible, and even likely, that the massive eruption of roughly a million cubic kilometers of basaltic lava also released to the atmosphere thousands of megatons of sulfur dioxide and other gases. Whether or not these gases reached the stratosphere may be irrelevant, as the eruptions probably continued off and on for many years. Damage to the local environment was undoubtedly severe, and extinctions of some species were almost inevitable. It remains to be proven, however, whether global effects resulted.

Triggering of such colossal eruptions is not an easy matter to explain. Possibly, internal forces caused the formation of deep mantle plumes, and the plumes penetrated upward into the crust to create hot spots. Yet it is difficult to account for the quasi-periodicity of 32 million years between eruptive episodes. An older suggestion has held that impacts of large extraterrestrial bodies—comets or asteroids—might have caused flood basalts by direct heating or pressure-release melting of the crustal rocks. Recent studies suggest that nonlocal effects could also have been significant, and perhaps new mantle plumes were created at depth. Two pieces of evidence support such an external mechanism: the known occurrence of an age cluster of large crater-forming impactors around the time of the Deccan Traps eruption in India (near the end of the Cretaceous Period) and the known episodic nature of impact cratering throughout Cenozoic and Mesozoic times.

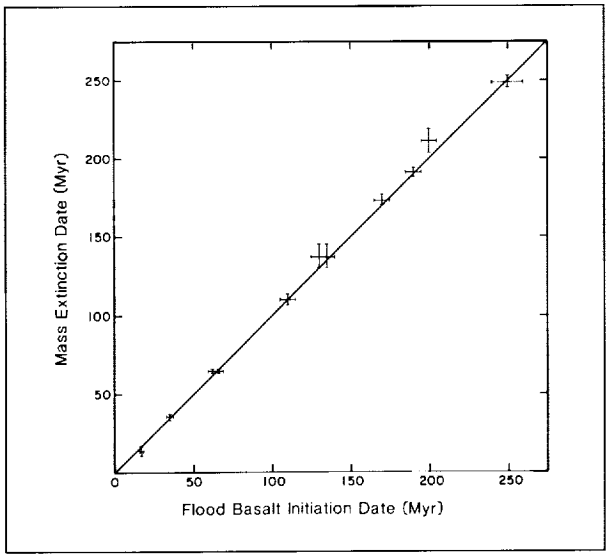

Correlation between the dates (in millions of years before the present) of flood basalt eruptions and of biological mass extinctions.

Whether or not these episodes of cratering were quasi-periodic has not been proven, but the mean cycle time between episodes was apparently about 32 million years.

Contact: Richard B. Stothers (Code 640)
(212) 678-5605

Sponsor: Office of Space Science and Applications

Dr. Richard B. Stothers, with 28 years' experience at Goddard, works in climatology, geophysics, astronomy, and the history of science at Goddard Institute for Space Studies. He received his PhD from Harvard University.

THE EAST AFRICAN RIFT SYSTEM: ITS MAJOR GEOLOGICAL FEATURES

The East African Rift is one of the most dramatically active areas of the Earth's surface. The Rift extends from the Middle East through the Red Sea, Ethiopia, and various countries of East Africa, as far south as Mozambique (see the first figure). This great linear feature is generally characterized by a central valley, or Rift, surrounded by steep cliffs whose walls recede in opposite directions away from the axis of the central valley. In some places the valley is offset by major fractures. In Ethiopia, the East African Rift is joined by an oceanic rift coming from the Gulf of Aden, south of Arabia; in northern Kenya, the East African Rift bifurcates to the east and to the west around Lake Victoria, with long, linear lakes marking the two branches of the Rift valley floor. The principal surface geologic features of the East African Rift are well suited for study by satellite remote-sensing techniques. Some of the earliest handheld photos by astronauts were of the Red Sea, but LANDSAT, AVHRR, large-format camera, and imagery from France's Satellite Pour L'Observation de la Terre are even more useful in studying the Rift.

The East African Rift is considered to be part of the worldwide rift system, which is found mostly under the oceans. Like its midocean extension, the Rift in East Africa is noted for its central valley, its surrounding mountains, volcanos, thermal springs, and earthquakes. Unlike the activity along the midocean extension, however, the motion of the Earth's crust away from the central valley is not steady or coherent, but fragmented and jerky on a geologic time scale. Understanding the evolution of this part of the Earth is a challenge to Earth scientists that can lead to an understanding of why the Earth's surface changes as it does.

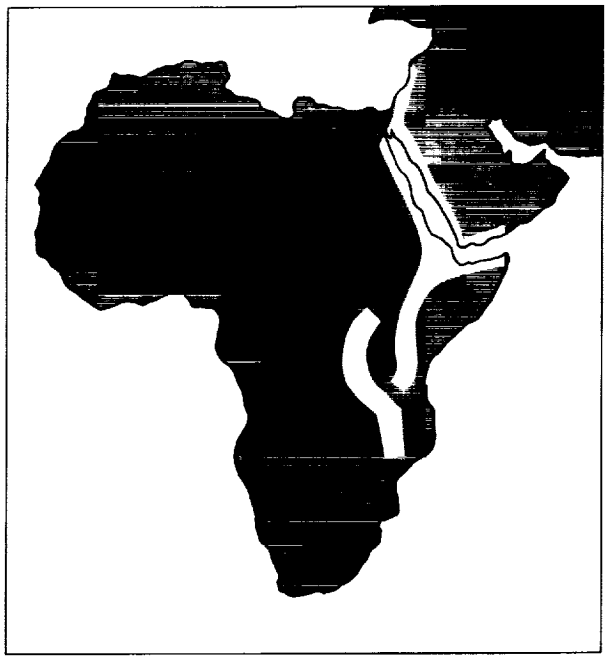

Location of the East African Rift system.

For some time the northern extension of this Rift has been known to follow the axis of the Red Sea, the Gulf of Aquaba, through the Dead Sea, the Sea of Galilee, and the valley of the Jordan River, continuing in an ill-defined manner to Turkey. Recent TM imagery of southern Lebanon and northern Israel, taken with LANDSAT, shows a fault that turns out to sea just south of Beirut toward Cyprus, redefining the boundary between the Sinai and Arabia tectonic plates (see the second figure). This is very similar to the San Andreas Fault, which turns into the Pacific off California.

Using TM imagery from opposite sides of the Red Sea and general knowledge of the land geology, it is possible to show precisely how Egypt and the Sudan on the west once fitted with Saudi Arabia on the east before the Red Sea opened, some 20 million years ago.

In the Afar region of Ethiopia, the Red Sea, Gulf of Aden, and East African portions of the Rift come together to form a complex "triple junction." Geologic mapping in this rugged area is difficult; remote-sensing imagery offers a convenient way to study the tectonic patterns. TM imagery has recently been used to guide University of California anthropologists to sites where the remains of early humans are found. Much of this area, adjacent to the Gulf of Tadjoura, is thought to have been seafloor in the recent geologic past and is today below sea level.

Near the Equator, Africa is covered with vegetation, and a study was made of vegetation cover, as expressed by the satellite-derived vegetation index, which is a function of topographic relief, latitude, and longitude. A relatively simple, first-order analytical expression can be written relating these variables. This provides analysts with guidance in knowing where the vegetation is likely to obscure local geology. There are some anomalous areas to which this analytic expression does not apply, where unusual meteorological conditions or coastal effects exist. A test study for western Kenya revealed that when vegetation is accounted for, satellite imagery reveals many times more faults than are shown on modern geologic maps.

While it is not easy to derive the age of volcanic centers from satellite imagery, it is sometimes possible to determine whether volcanic flows are "fresh." The Menengai caldera in western Kenya (see the third figure) has been used for such a study; evergreen bushes were found on younger flows, and grasses on the older flows.

Some types of satellite imagery show volcanic centers and lineations quite well. Many of the lineations are faults. A comprehensive evaluation of these centers and

TM imagery of the coast of Lebanon and Israel, showing faults running through Lake Tiberias (Sea of Galilee) separating the Sinai Plate to the left from the Arabian Plate to the right (after Girdler, in press). Beirut is on the coast at the upper edge of this image.

ORIGINAL PAGE
COLOR PHOTOGRAPH

ORIGINAL PAGE
COLOR PHOTOGRAPH

The Rift valley of western Kenya revealed by LANDSAT Matrix Switch System (MSS) imagery. This scene measures about 200 km on each side. The Menengai crater is identified by the letter "M," and the opposite-facing Rift valley walls by the toothed dashed lines. Lake Baringo is in the upper part of the Rift valley floor. Image copyrighted by Earth Satellite Corporation.

faults for the entire East African Rift has begun. TM imagery, with its 30-m resolution, would provide the best type of data for this, but its high cost since the commercialization of LANDSAT makes its use prohibitively expensive. AVHRR imagery, with 1-km resolution, must be used instead; a mosaic of these scenes will provide the first geologic image of this major structure.

Contact: James R. Heirtzler (Code 622)
(301) 286-5213

Sponsor: Office of Space Science and Applications, Earth Resources Branch

Dr. James R. Heirtzler, Head of the Geology and Geomagnetism Branch, supervises several Earth scientists who study major tectonic and volcanic structures, coastal erosion, and other aspects of the geomagnetic field. He has received a Goddard Special Service Award and has been recognized as a pioneer for work in geomagnetism and plate tectonics in Antarctica. Dr. Heirtzler has worked at Goddard for 3 years.

CRUSTAL DEFORMATION IN SOUTHERN ALASKA

Most of the Pacific/North American plate boundary along the southern coast of Alaska has been ruptured by large earthquakes in this century, the most well-known being the 1964 earthquake that devastated Anchorage and Kodiak. Relatively little is known, however, about the cyclic pattern of crustal deformation associated with these earthquakes. Recent advances in the geodetic application of very long baseline interferometry (VLBI) allows for precise measurements of deformation over regional and global spatial scales. VLBI is a technique derived from radio astronomy in which widely separated radio telescopes simultaneously observe quasars. For measurements in Alaska, one of the telescopes is a large (26-m) permanent dish antenna originally used to track satellites at Fairbanks (shown in the first figure). The other telescope is a small (3-m) mobile instrument built from a military surplus radar system and a backyard television dish (also shown in the first figure). VLBI development over the past 20 years has enabled scientists to measure in 1 day a baseline between two such telescopes to better than 1 cm. Site motions can be determined to a few millimeters/year by making repeated measurements over several years.

Since 1984, scientists have made measurements each summer at six mobile sites in Alaska and Canada, working with Fairbanks and other VLBI stations in North America. From this data, the researchers have been able to measure the motions of all the sites. The sites located in interior Alaska, away from the Pacific/North American plate boundary, show only a few millimeters/year of motion. However, the sites on the seacoast near the plate boundary are moving 7 to 35 mm/yr, reflecting a significant amount of deformation. This deformation presumably is indicative of strain buildup which will be released eventually in major earthquakes. The second figure shows a plot of horizontal motions measured with VLBI at each of the sites, along with the motion predicted by a global plate motion model called NUVEL. Near Alaska, the Pacific plate is predicted to move north-northwest at 50 to 60 mm/yr with respect to North America. The second figure also shows the Pacific/North American plate boundary. From Kodiak Island westward through the Aleutian Islands, the Pacific plate subducts under the North American plate along the Aleutian megathrust. Further east, strike-slip motions along the Fairweather fault accommodate most of

the relative motion between the two plates (similar to what happens on the San Andreas fault in California). The second figure shows the major faults, most of which closely parallel the arc-shaped coast. These arcuate structures bound a series of ancient geological blocks, called terranes, which have been plastered onto interior Alaska in a process known as terrane accretion.

Of particular interest is the VLBI site at Cape Yakataga located on a terrane which has been accreting to the southern coast of Alaska for more than 5 million years. From 1984 through the summer of 1987, researchers observed the site to be moving north-northwest at ~35 mm/yr. Although Cape Yakataga is already attached to the Alaska mainland, it shows motions of about two-thirds the Pacific plate rate. The trace of the Cape Yakataga site motions is shown in the third figure.

During the winter of 1987-88, two major earthquakes (magnitude 7.6) occurred in the Gulf of Alaska, about 100 km south of Cape Yakataga. When the mobile VLBI system returned the following summer, the resulting measurements showed the site position to be displaced ~80 mm to the west. No local ground disturbances were found, so it appeared that the entire region around the Cape Yakataga site deformed in response to the remote earthquakes. This interpretation is confirmed by data obtained by the U.S. Geological Survey in two nearby trilateration networks and by geodetic measurements made using the Global Positioning System satellites. The 1989 measurements verify the 1988 results and show that the site has resumed its original ~35-mm/yr northwestward motion.

These measurements were made as one element of the NASA Crustal Dynamics Project. The project staff have now been able to measure constant motions of most of the Earth's tectonic plates. The Cape Yakataga results are the first convincing evidence for episodic motions associated with earthquakes measured using a space-based geodetic

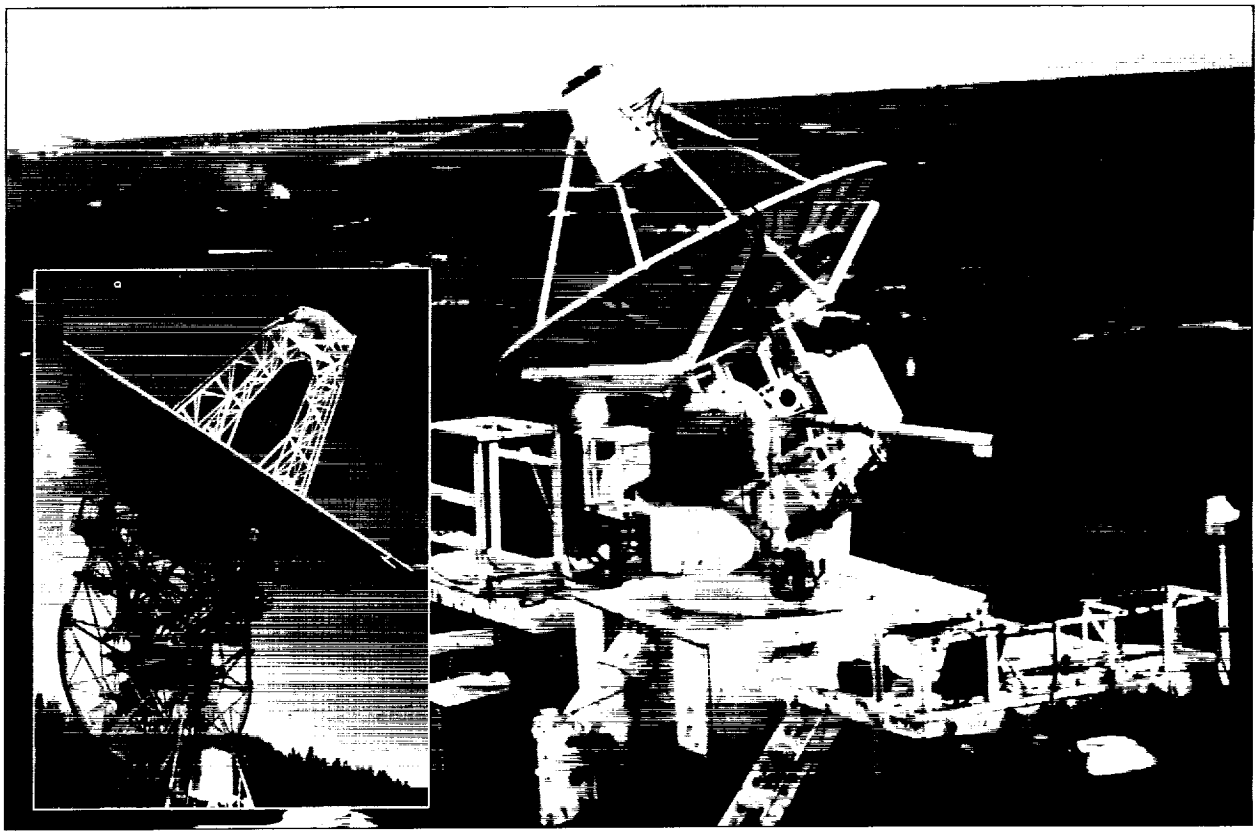

Two VLBI antennas operating in Alaska: the 26-m Gilmore Creek antenna located near Fairbanks (Inset) and the 3-m MV-2 mobile VLBI antenna.

ORIGINAL PAGE
BLACK AND WHITE PHOTOGRAPH

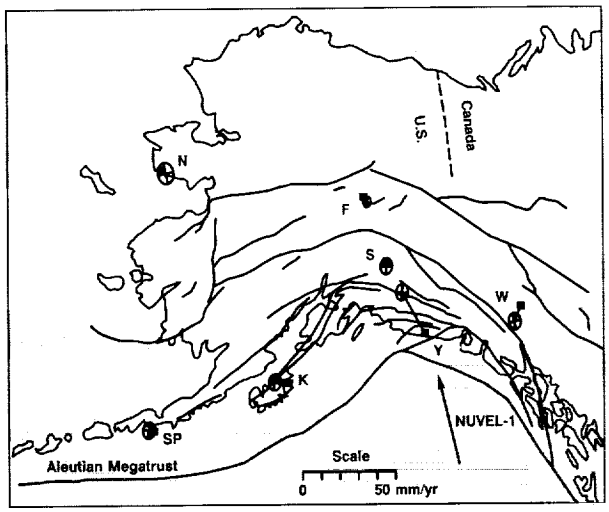

VLBI sites in Alaska and the Yukon Territory. F = Fairbanks, K = Kodiak Island, N = Nome, SP = Sand Point, S = Sourdough, W = Whitehorse, and Y = Cape Yakataga. The individual site velocities relative to stable North America are shown with their 3-sigma error ellipses. The major faults in Alaska are also shown.

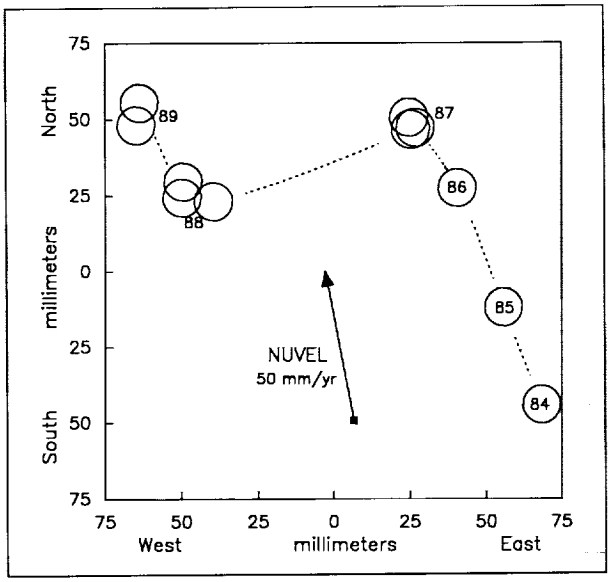

Cape Yakataga site motions relative to Fairbanks. Also shown is the NUVEL model prediction for 1 year's motion if the site were on the Pacific plate.

technique. By observing the response of an individual site relative to a region unaffected by the earthquake, researchers learn about the dynamical response of the Earth's crust to a discrete event.

Contact: Thomas A. Clark (Code 626)
(301) 286-5957
Jeanne M. Sauber (Code 621)
(301) 286-8586
Lynda J. Bell, University of Maryland
(Code 626)
(301) 286-9838

Sponsor: Crustal Dynamics Project

Dr. Thomas A. Clark is the VLBI Systems Manager in the Space Geodesy Branch working on the Crustal Dynamics Project. His special technical interests focus on the development of instrumentation and techniques for astronomical and geophysical measurements. He has received an Exceptional Performance Award, a NASA Medal for Exceptional Engineering Achievement, and several NASA Group Achievement Awards. Dr. Clark earned his PhD from the University of Colorado and has 22 years' experience with Goddard and a total of 24 with NASA.

Dr. Jeanne M. Sauber, geophysicist in the Laboratory for Terrestrial Physics, earned her PhD in geophysics from the Massachusetts Institute of Technology and holds a NASA Graduate Student Fellowship. Her technical interests center on numerical modeling of crustal deformation geodesy and neotectonics as well as the mechanics of the Earthquake Source.

Ms. Lynda J. Bell is a Research Assistant in the Geodynamics Branch and has worked at Goddard for 2 years. Her technical interests focus on geophysical modeling and interpretation of deformation data near active subduction zones. She earned her BS in geophysics from the University of Maryland.

GLOBAL MAPPING AND IMAGE PROCESSING

The global mapping and image processing software package written at Goddard is used to study land processes on global and continental scales. The AVHRR instrument aboard the NOAA satellites provides excellent coverage of the Earth with its 4-km, global-area coverage data stream. The software focuses on the use of these data. The package is being used at Goddard for the production of a multiyear temporal global data set from the AVHRR data and as a research tool for AVHRR calibration, cloud-masking techniques, and atmospheric correction. The software has also been installed at the University of Maryland's geography department computer laboratory and at the Food

and Agriculture Organization in Rome. The University of Maryland is using the system for FIFE and Coastal Zone Color Scanning data processing, as well as NOAA data. The Food and Agriculture Organization is using the system as a basis for its early warning research on locusts and for its range land studies.

The software is written in FORTRAN 77 on the Hewlett-Packard 1000 A-series computer interfaced to multiple Ramtek 9465 graphics/imaging subsystems. The image processing code is tightly bound to the Ramtek subsystem, which is configured to a 1,280 × 1,024 resolution, 10 data bits per pixel, and 6 bits of graphics overlay per pixel. This configuration accommodates AVHRR's 10-bit data without loss of information. This is especially important when resampling or otherwise manipulating the data.

The software is optimized for high throughput of massive amounts of data and is routinely used to map multiple orbits of data to a single output image. Both single-channel and vegetation-index products are normally produced. The philosophy behind the software is to register the data to a user-defined map as opposed to the more common scene technique. The choice of mapping parameters and map projection is made at run time, and a vector overlay with optional grid lines with marks and labels can be mapped simultaneously to provide a frame of reference. The software is designed to run unattended, allowing jobs to be run in a batch mode with all user input read from an answer file and echoed with running status to a log file. The software can also be run in an interactive menu mode for the non-routine job. Many data sources have been mapped, including but not limited to elevation data, climate modeling output, and data from other instruments. Data from various dates and sources can be registered by selecting the same mapping parameters and then can be analyzed with the image processing section of the package.

The image processing component is a simple geographical information system in that the geographical location of every pixel is not lost after the mapping process. The mapping is done analytically from derived equations (not curve-fitting) to convert a latitude, longitude pair to x,y coordinates. The advantage of this method is that the equations are easily passed to the analysis programs and can be inverted so that the researcher can frame the analysis in terms of geographical coordinates instead of pixel locations that will vary depending on the map projection and area of interest. Software tools exist for studying the spatial and temporal variability of entire images or at user-selected sites. While most of the software is interactive and menu driven (using a touch screen interface), multiyear data set preparation and analysis require much repetitive highly machine-intensive computation. A suite of programs addresses this issue by operating unattended on an unlimited number of input images and writing the output to computer disk for later retrieval. For example, these programs can produce histograms and statistics from user-defined regions or compute a mean and standard deviation image from multiple input images.

Although the software has various plotting routines, the general philosophy is to create disk files that can be fed into commercial software either on the Hewlett-Packard or personal computers to generate the report-formatted statistics and graphs. The graphics capability of the Ramtek is exercised by using draw-and-fill commands driven by the track ball interface to selected regions of an image for analysis by other programs.

The user interface is through a hierarchical menu structure for the novice user, or the expert can type in command acronyms (with options) without traversing the menu trees. Online help is available for every function. The functions are implemented as individual programs that are scheduled by the user interface. New modules are easily added to the system, and users with some competence in FORTRAN can add their own code through a shell program, which links to a user-written subroutine. There are two such shell programs. One allows pixel-by-pixel operations on multiple images, and another hands the user a line of data at a time for multiple images. The user fills in the blanks to a skeleton subroutine that takes care of the formal arguments. This feature allows the researcher to test algorithms before requesting new program development.

With data from various Earth Observing System (Eos) instruments forthcoming, it is important that research projects like this explore alternate methods of dealing with remotely sensed global data sets merged into a geographical information system context and examine realistic ways of monitoring global change.

Contact: Virginia L. Kalb (Code 623)
(301) 286-2605

Sponsor: Earth Resources Branch

Ms. Virginia L. Kalb, with 13 years' experience at Goddard, works in the Earth Resources Branch, Laboratory for Terrestrial Physics. She earned her BA and MA in mathematics, and her technical interests include image processing in geographic information systems.

ATMOSPHERES

UPPER ATMOSPHERIC RESEARCH SATELLITE (UARS)

UARS is an important upcoming NASA mission aimed at improving knowledge of the stratosphere, mesosphere, and lower thermosphere and emphasizing those levels that are known to be particularly susceptible to change by external agents. Using a combination of measurements and theoretical studies, UARS will provide a focus for the resolution of scientific questions relating to the chemistry, dynamics, and overall energy balance of this region.

Scientists have become increasingly concerned in recent years about the sensitivity of the Earth's atmosphere to changes caused indirectly by various human activities. Long-standing curiosity about atmospheric evolution and the factors influencing climate and weather has been sharpened and refocused by the discovery of technologically related threats that introduce the possibility of inadvertent atmospheric modification. The famous Antarctic ozone hole is probably the most visible manifestation of such effects, and researchers are now examining the possibility of a similar phenomenon in the Northern Hemisphere. Such changes, occurring in both the troposphere and the upper atmosphere, have far-reaching consequences and may eventually set constraints for life on Earth. These potential threats highlight the need for a program of scientific research directed toward improving knowledge of the physical and chemical processes occurring in the Earth's upper atmosphere.

The need to study the upper atmosphere as a tightly coupled system, using highly coordinated and complementary data, has led to the concept of the UARS observatory as "the instrument," with the individual sensors providing portions of the data required. The instrument complement was selected to make three general types of measurements: energy input to the atmosphere, temperature and important trace chemical species, and winds. The first two tables identify the UARS Investigators, and the first figure shows the remotely sensed atmospheric parameters, the instruments making the measurements, and the appropriate altitude ranges. The group composed of the Instrument, Theoretical, and Collaborative Principal Investigators forms the UARS Science Team, which is ultimately responsible for the scientific usefulness and success of the UARS mission.

The UARS is scheduled for launch in the fall of 1991 by the space shuttle from the Kennedy Space Center. The shuttle will deliver the spacecraft directly to the operational circular orbit at 600 km inclined 57° to the Equator. At this altitude and inclination, the remote sensors "looking" 90° to the spacecraft velocity can see to 80° latitude, providing nearly global coverage. This inclination also produces a precession of the orbit plane relative to the Earth-Sun line so that all local solar times are covered in about 36 days, thus providing resolution of diurnal atmospheric effects in a short period relative to seasonal effects. The design lifetime for the observatory is at least 36 months, although one of the cooled infrared instruments will be limited to about 18 months by the depletion of its stored cryogen. The fall launch, combined with the 18-month lifetime of the full instrument complement, will provide comprehensive coverage of two Northern Hemisphere winters, times and locations for particularly interesting atmospheric phenomena. The observatory, shown in the second figure,

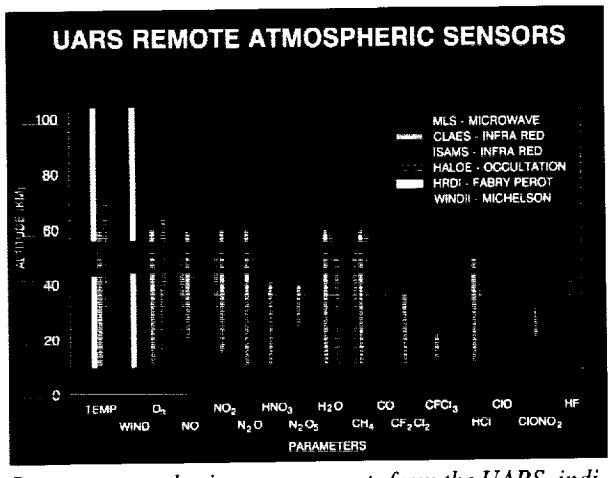

Remote atmospheric measurements from the UARS, indicating the pertinent sensors and appropriate altitude ranges. In addition to these instruments, there are three others that measure the solar energy incident on the atmosphere.

ORIGINAL PAGE
COLOR PHOTOGRAPH

Measurements

Energy Input

Instrument	Description	Investigator
SOLSTICE—Solar-Stellar Intercomparison Experiment	Full-disk solar irradiance spectrometer incorporating stellar comparison	G. J. Rottman, University of Colorado
SUSIM—Solar Ultraviolet Spectral Irradiance Monitor	Full-disk solar irradiance spectrometer incorporating onboard calibration	G. E. Brueckner Naval Research Laboratory
ACRIM—Active Cavity Radiometer Irradiance Monitor*	Full-disk solar irradiance radiometer	R. C. Willson, Jet Propulsion Laboratory
PEM—Particle Enviornment Monitor	X-ray, proton, and electron spectrometers	J. D. Winningham, Southwest Research Institute

**ACRIM is using the spacecraft as a "flight of opportunity" and is not part of the basic UARS scientific mission.*

Species and Temperature

Instrument	Description	Investigator
CLAES—Cryogenic Limb Array Etalon Spectrometer	Solid-cryogen cooled interferometer sensing atmospheric infrared emissions	A. E. Roche, Lockheed Palo Alto Reseach Laboratory
ISAMS—Improved Stratospheric and Mesospheric Sounder	Mechanically cooled radiometer sensing atmospheric infrared emissions	F. W. Taylor, Oxford University
MLS—Microwave Limb Sounder	Microwave radiometer sensing atomospheric emissions	J. W. Waters, Jet Propulsion Laboratory
HALOE—Halogen Occultation Experiment	Gas filter/ radiometer sensing atmospheric absorption of sunlight	J.M. Russell, Langley Research Center

Measurements (continued)

Wind

Instrument	Description	Investigator
HRDI—High-Resolution Doppler Interferometer	Fabry-Perot spectrometer sensing atmospheric emission, scattering, and absorption	P. B. Hays, University of Michigan
WINDII—Wind Imaging Interferometer	Michelson interferometer sensing atmospheric airglow emission	G. G. Shepherd, York University, Canada

is 35 ft long with a weight of approximately 14,000 lb, including 5,300 lb of instruments. The UARS telemetry data rate is 32 kbps with a tape recorder playback rate of 512 kbps. The solar array will provide 1,600 W for the instruments and other spacecraft functions.

The UARS data system is based on the following concepts:

- All UARS data will be processed as quickly as is feasible to the level of geophysically useful data (e.g., atmospheric temperatures and gas species concentrations).
- The Instrument Principal Investigators are responsible for developing the algorithms and for implementing and maintaining the programs used for processing data from their instruments.
- All scientific data will be available on line to all UARS Investigators.
- To reduce contention for computational resources, there will be functional separation between the computers used for data processing and storage and the computers used for the Investigators' scientific analyses.

The data system consists of a dedicated Central Data Handling Facility (CDHF) at Goddard, minicomputer-based Remote Analysis Computers (RAC's) at the investigators' sites, and a dedicated electronic communications system to connect the RAC's with the CDHF. Playback telemetry data from the observatory

Theoretical and Collaborative Investigations

Investigator	Institution
D. M. Cunnold	Georgia Institute of Technology
M. A. Geller	State University of New York, Stony Brook
J. C. Gille*	NCAR
W. L. Grose	Langley Research Center
J. R. Holton	University of Washington
J. London	University of Colorado
A. J. Miller	NOAA
C. A. Reber	Goddard
J. M. Russell**	Langley Research Center
P. White	United Kingdom Meterological Office
D. Wuebbles	Lawrence Livermore National Laboratory
R. W. Zurek	Jet Propulsion Laboratory

**Collaborating on the CLAES investigation*
***Collaborating on the ISAMS investigation*

are relayed through the Tracking and Data Relay Satellite System (TDRSS) where they are transmitted to the CDHF. Programs developed by the Investigators at their RAC's and transferred to the CDHF will be used to convert telemetry data (referred to as level 0 data) to several levels of processed data. The CDHF will be used primarily for production processing of all scientific data received from the spacecraft and for maintenance of the UARS data base. These data will be stored on line to facilitate quick access by users. A catalog of data maintained in a data base management system will permit searches on characteristics such as measurement parameter, time, instrument, and data level.

Level 1 data are the physical parameters measured by the sensors (e.g., atmospheric radiances in the case of the limb-sounding instruments). Level 2 data are the geophysical parameters calculated from level 1 data such as atmospheric temperature profiles, gas specie concentrations, winds, or solar spectral irradiances. Atmospheric data at level 2 are related directly to the instrument measurement "footprint"; for example, the character of the altitude scan is determined by a given instrument's scan rate, integration time, and viewing direction, as well as the spacecraft's orbital velocity. Level 3A atmospheric data, on the other hand, reflect the geophysical information of level 2 transformed into a common format and equally spaced along the measurement trajectory in time ("level 3AT," at 65-s centers) or latitude ("level 3AL," on 4° centers). Level 3B atmospheric data will provide daily latitude-longitude cross-sections at approximately one-half scale height altitude intervals. The definitions of the data at level 3 are different from the above for the energy input measurements and are appropriate to the specific measurements being performed.

The RAC's at the Investigators' sites will be used to access data in the CDHF for geophysical analysis of these data and, in some cases, for linking with larger computers for more complicated scientific analyses and modeling. For the Instrument Investigators, the RAC's are also used to develop the software for processing data to levels 1, 2, and 3 in the CDHF. After launch, these investigators will use their RAC's for data validation and refinement of their processing software. The high-speed communications between the CDHF and the RAC's create, in effect, a distributed data system for the UARS and facilitate connection with other scientific data networks such as the existing SPAN and the network to be used on the International Solar-Terrestrial Physics Project (ISTP).

Flight instruments were delivered for integration on the spacecraft in the fall of 1989. The first phase of the CDHF was in place, and the Instrument Investigators

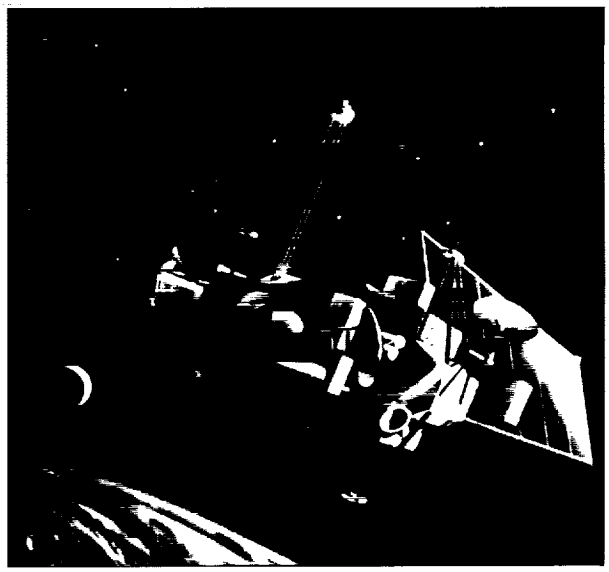

Artist's concept of the UARS in orbit.

had delivered the first version of their data processing software, which was undergoing test on the CDHF1.

Contact: Carl A. Reber (Code 610)
(301) 286-6534

Sponsor: Office of Space Science and Applications

Dr. Carl A. Reber, UARS Project Scientist in the Laboratory for Atmospheres, is responsible for the scientific integrity and usefulness of the mission. Among his achievements, Dr. Reber made the first direct measurements of upper atmospheric composition from a satellite on Explorer-17. He has also won several Special Achievement Awards and earned a PhD in atmospheric and oceanic sciences from the University of Michigan. Dr. Reber has 30 years' experience at Goddard.

MODEL PREDICTIONS OF FUTURE OZONE AMOUNTS

Ozone, the Earth's shield from harmful ultraviolet radiation, has been studied intensely since the early 1970's. Since finding the Antarctic ozone hole, researchers have discovered that mankind is capable of affecting the ozone layer. Complicated atmospheric models have been developed in the past 2 decades to help in understanding atmospheric phenomena as well as to make predictions of future changes in ozone caused by mankind. Two-dimensional (latitude and altitude) atmospheric models, which include detailed photochemistry and a zonally averaged dynamical scheme, are used most frequently in making these predictions.

Goddard researchers have developed a two-dimensional atmospheric model that can be used for assessments of future ozone amounts. This model includes 50 atmospheric constituents, about 130 photochemical reactions, and winds and mixing which simulate the transport in the atmosphere. In 1989, 11 atmospheric modeling groups from 7 different countries took part in assessment studies of ozone for the United Nations Environmental Program and the World Meteorological Organization. Eight different scenarios were proposed for the assessment studies, representing possible future atmospheric composition of chlorofluorocarbons ($CFC1_3$,CF_2C1_2,$C_2C1_3F_3$, $C_2C1_2F_4$, and C_2C1F_5), halons ($CBrC1F_2$ and $CBrF_3$), hydrochlorofluorocarbon-22 or CFC-22 ($CHC1F_2$), methyl chloroform (CH_3CC1_3), carbon tetrachloride ($CC1_4$), methane (CH_4), nitrous oxide (N_2O), and carbon dioxide (CO_2). Goddard researchers have completed a modeling computation for all eight scenarios and have model predictions of ozone for the 80-year time period from 1980 to 2060. The results are presented for only the two extreme scenarios, A1 and D3. Scenario A1 assumes that the increase of the chlorofluorocarbons, halons, CFC-22, CH_3CC1_3, $CC1_4$, CH_4, N_2O, and CO_2 continues at the present rate. Scenario D3 assumes that the production of

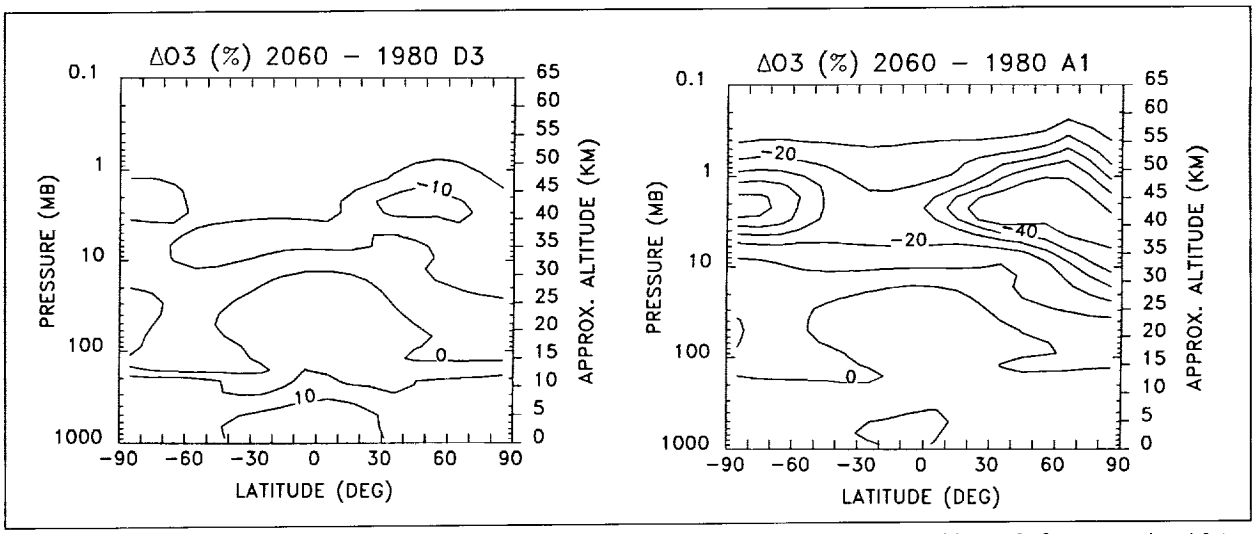

Model predicted percentage ozone change from 1980 to 2060 as a function of altitude and latitude for scenarios A1 (no change in production of CFC's) and D3 (reduce CFC production by 95 percent). Contours plotted for scenario A1 are -50, -40, -30, -20, -10, 0, and +10 percent. Contours plotted for scenario D3 are -10, -5, 0, +5, and +10 percent.

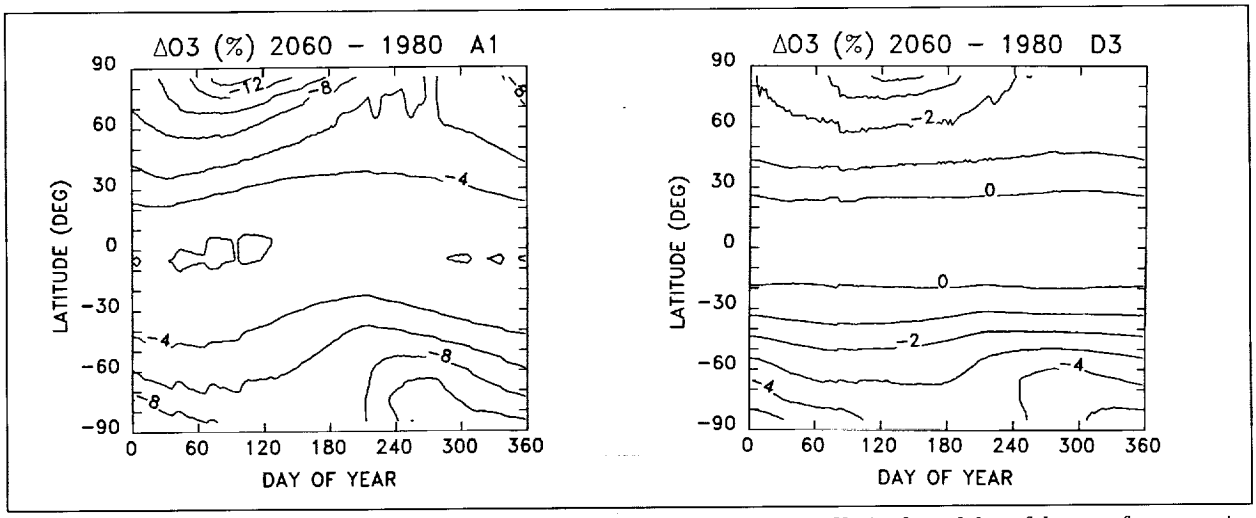

Model predicted percentage total ozone change from 1980 to 2060 as a function of latitude and day of the year for scenarios A1 (no change in production of CFC's) and D3 (reduce CFC production by 95 percent). Contours plotted for scenario A1 are -14, -12, -10, -8, -6, -4, and -2 percent. Contours plotted for scenario D3 are -5, -4, -3, -2, -1, and 0 percent.

the chlorofluorocarbons and halons is decreased by 95 percent over the time period 1990-1995, the CH_3CCl_3 and CCl_4 are fixed at their 1985 levels, and the increase in CFC-22, CH_4, N_2O, and CO_2 continues at the present rate.

The first pair of figures presents the percentage change in ozone from 1980 to 2060 as a function of altitude and latitude for the month of January for scenarios A1 and D3. The largest ozone decreases (over 50 percent) occur at high latitudes in the winter hemisphere near 40 to 45 km, the altitude range at which the Cl_x is most important in causingan ozone decrease. The troposphere indicates a positive change in ozone caused both by the self-healing of ozone in the atmosphere as well as a photochemical change brought about by the increase of CH_4 in the troposphere. Scenario D3 shows that the decrease of ozone in the upper stratosphere could be lessened significantly with regulation of the chlorofluorocarbons and the halons. The largest ozone decrease is only 10 percent at winter high latitudes for the year 2060 compared with 1980. Both scenarios A1 and D3 show the large tropospheric increase in ozone.

Changes in total ozone as a function of latitude and day of the year are given for scenarios A1 and D3 in the two other figures. Both figures indicate the largest ozone decreases at the highest latitudes in early spring with a large latitudinal gradient. Scenario D3 even shows a sizable region in the tropics from about -20° to +20° of positive ozone change. Most of this increase in ozone reflects the tropospheric ozone increase, also observed in scenario A1. Although tropospheric ozone helps to protect the world's organisms from ultraviolet radiation, it is a harmful oxidant that damages living organisms.

Goddard researchers' predicted stratospheric levels of ozone agreed with the other various modeling groups; however, there were substantial differences among the modeling groups in predictions of future levels of tropospheric ozone. The causes of these differences need to be investigated to determine the reliability of model forecasts for tropospheric and total ozone.

Contact: Charles H. Jackman (Code 616)
(301) 286-8399
Anne R. Douglass (Code 616)
(301) 286-2337

Sponsor: Office of Science and Applications and Upper Atmosphere Theory and Data Analysis Program

Dr. Charles H. Jackman researches the Earth's stratosphere and mesosphere using a two-dimensional photochemical model. His special interests include using photochemical atmospheric models to understand natural changes in the middle atmosphere and using satellite data to test theories of photochemical and dynamic processes of the atmosphere. He has received the Peer Scientific

ORIGINAL PAGE
COLOR PHOTOGRAPH

Achievement Award from the Laboratory for Atmospheres and a Certificate of Outstanding Performance. Dr. Jackman earned his PhD in atmospheric physics from the University of Florida and has 9 years of service at Goddard.

Dr. Anne R. Douglass works in the Laboratory for Atmospheres in the Atmospheric Chemistry and Dynamics Branch. Her major interest is modeling photochemistry and the transport of stratospheric constituents. With Dr. Charles Jackman, she has developed a two-dimensional chemistry and transport model to facilitate multiyear calculations and sensitivity studies. Dr. Douglass earned her PhD at Iowa State University and has worked at Goddard for 8 years.

BREAKUP OF THE ANTARCTIC OZONE HOLE SIMULATED WITH A THREE-DIMENSIONAL CHEMICAL TRANSPORT MODEL

A study of the Antarctic ozone hole has been made with a three-dimensional chemical transport model using a linearized photochemistry for ozone. The tracer model uses the winds and convection from the Goddard Institute for Space Studies general circulation model (8° × 10° × 23 layers). The general circulation model develops an Antarctic circumpolar vortex in early winter with strong westerlies that reverse in austral spring; the circulation compares favorably with the observed climatologies. A 4-year control run of the chemical transport model with annually repeating winds produces ozone distributions that compare reasonably with the observed annual cycle of ozone.

The linearization of the ozone photochemistry is developed from the current observed climatology of ozone and trace gases. In the control run, researchers found that the total ozone column is sensitive to the chemical time constants, and in particular, a large amount of ozone is chemically destroyed in the lower stratosphere in spite of relatively slow photochemistry. A budget analysis for the southern midlatitude stratosphere (10-350 mbar × 31-90° S) indicated the dominant source of ozone to be transported from the tropical stratosphere with the loss split equally between in situ chemistry and transport into the troposphere where atmospheric and surface reactions destroy ozone. The time constant to replace ozone in this stratospheric box is about 1.2 years.

An Antarctic ozone hole is induced mechanistically on October 1, and the chemical transport model is integrated for 1 year. The initial depletion, assumed to be 90 percent of the ozone poleward of 70° S between 22 and 200 mbar, amounts to about 5 percent of the total ozone in the Southern Hemisphere. A polar map of column ozone on October 2 for the control run and the ozone hole simulation are shown in the first figure. As the vortex breaks down and the ozone hole is dispersed, significant depletions to column ozone, on the order of 10 Dobson units (3 percent), occur as far north as 40° S during austral summer. The second figure shows this process in a 7-day sequence beginning October 8.

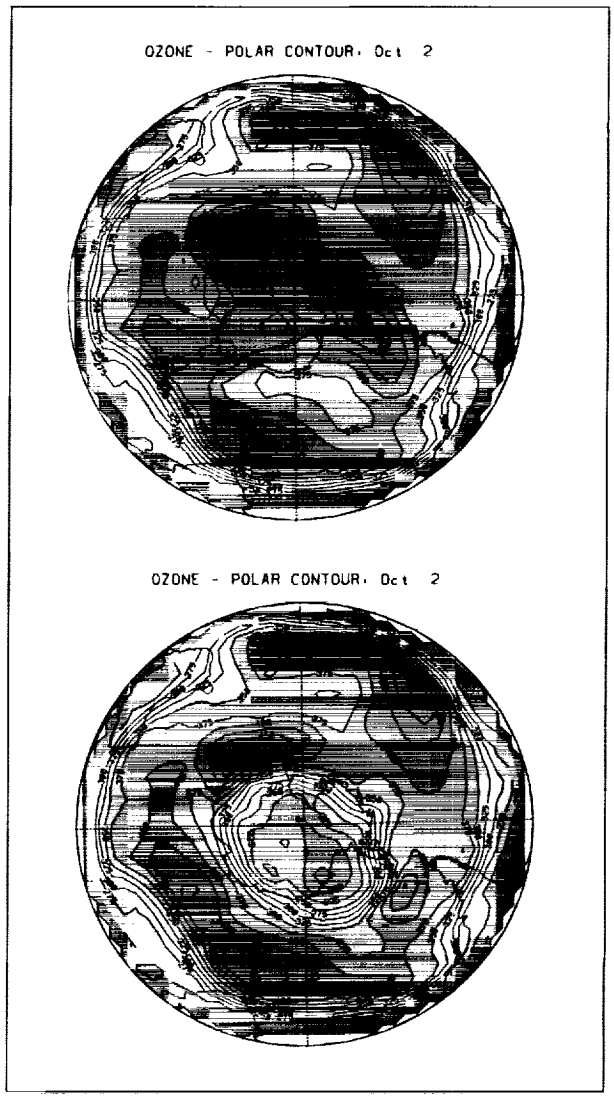

Column ozone (Dobson units) on October 2.

One year later, only 30 percent of the original depletion remains, mostly below 100 mb and poleward of 30° S.

ORIGINAL PAGE
COLOR PHOTOGRAPH

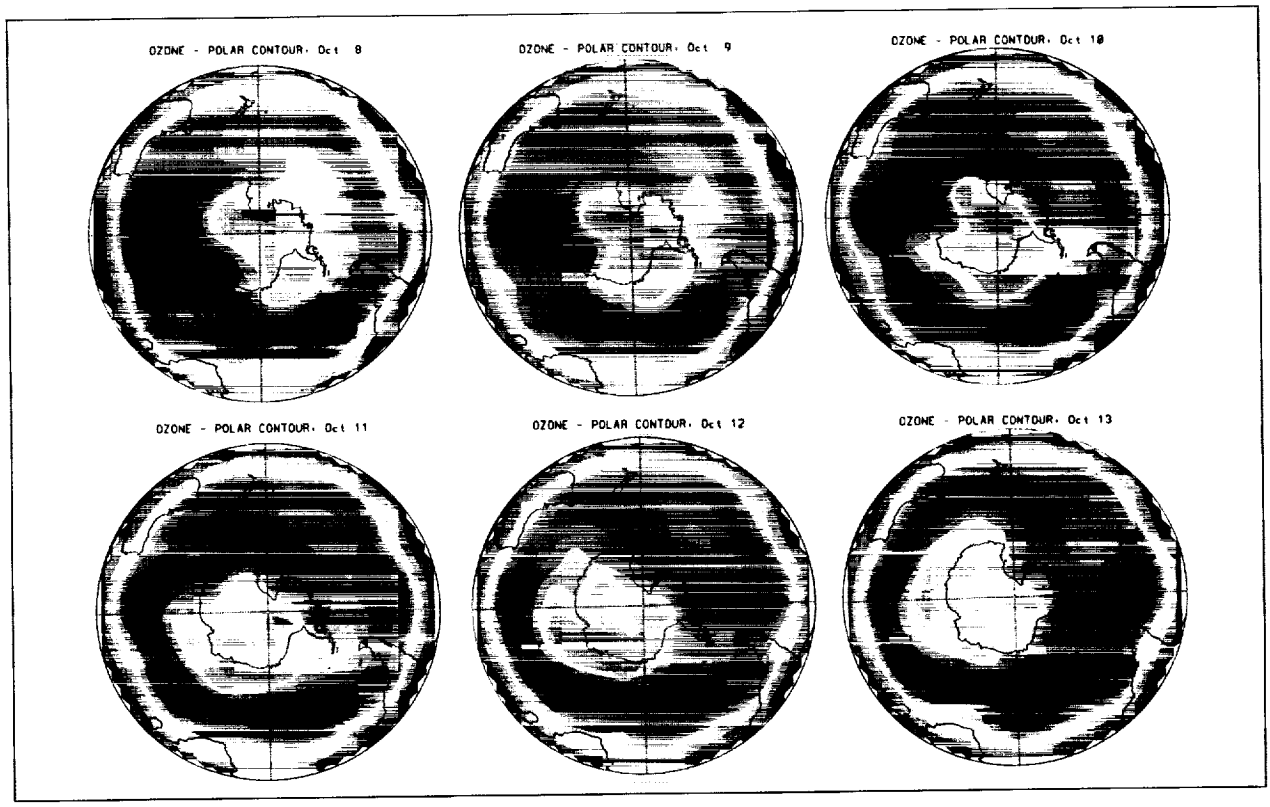

Ozone hole simulation (Column Ozone Dobson units).

The October 1 initialization is continued for a second year, reinducing the ozone hole for the second year. The cumulative effects from the year before are noticeable, but add only 20 percent to the depletion. The budget analysis for the southern midlatitude stratosphere (10-350 mbar × 31-90° S) indicates that the ozone hole is replenished equally by photochemical regeneration and by reduced transport of ozone into the troposphere.

Contact: Michael J. Prather (Code 640)
(212) 678-5625

Sponsor: Upper Atmosphere Theory and Data Analysis Program, Earth Science and Applications Division, Office of Space Science and Applications

Dr. Michael J. Prather is an atmospheric scientist involved in the three-dimensional modeling of atmospheric chemistry at the Goddard Institute for Space Studies. His work has emphasized atmospheric composition, identification of sources for trace gases, and perturbations to the stratospheric ozone. Dr. Prather has been with Goddard for 4 years and received his PhD from Yale University.

LIDAR MEASUREMENTS OF STRATOSPHERIC OZONE AND TEMPERATURE

In the past year, the Goddard Stratospheric Ozone Lidar Trailer Experiment has made two highly successful intercomparisons with several other ozone-measuring instruments. These were the first field tests of the Goddard instrument, which has been under development for several years. The instrument makes use of the differential absorption lidar technique in which two laser wavelengths are transmitted into the atmosphere: one that is strongly absorbed by ozone and another that is only weakly absorbed. The weakly absorbed wavelength thus serves as an atmospheric reference, and ozone can be extracted from the differences between the two lidar returns. In addition to extracting ozone from the two lidar returns, temperature can also be retrieved between 20 and 65 km, using the reference wavelength. The instrument has been installed in a trailer, enabling it to be taken to remote sites. The lidar has been built to be used as a transfer calibration standard among sites currently being considered to become part of a

worldwide network for the detection of stratospheric change. An artist's concept of the lidar within the trailer is shown in the first figure.

Examples of the data retrieved are given in the second and third figures. The second figure displays the ozone profiles obtained during the last stages of the first ozone intercomparison in November 1988. The agreement at the higher altitudes is good and the differences apparent at the ozone maximum appear to be due to atmospheric transport phenomenon. The anomalies in the November 6 data are due to aerosols, and subsequent treatment of the data has been able to extract reliable ozone from these regions.

The third figure displays a lidar measurement of temperature from the night of November 5-6 and compares it with the temperatures retrieved from an electrochemical cell sonde, a Rocket Ozone Sonde datasonde, and a nearby Stratospheric Aerosol and Gas Experiment II overflight. The agreement is good, particularly with the datasonde.

A second intercomparison was held in July, and a large body of data now exists comparing Goddard results with the results of all the major ozone-measuring instruments. Differential absorption lidar has proven to be an accurate ground-based instrument for the long-term measurement of ozone and temperature.

Contact: Thomas J. McGee (Code 617)
(301) 286-5645

Sponsor: Upper Atmospheric Research Program

Dr. Thomas J. McGee is currently the Principal Investigator of the ground-based lidar measurements of

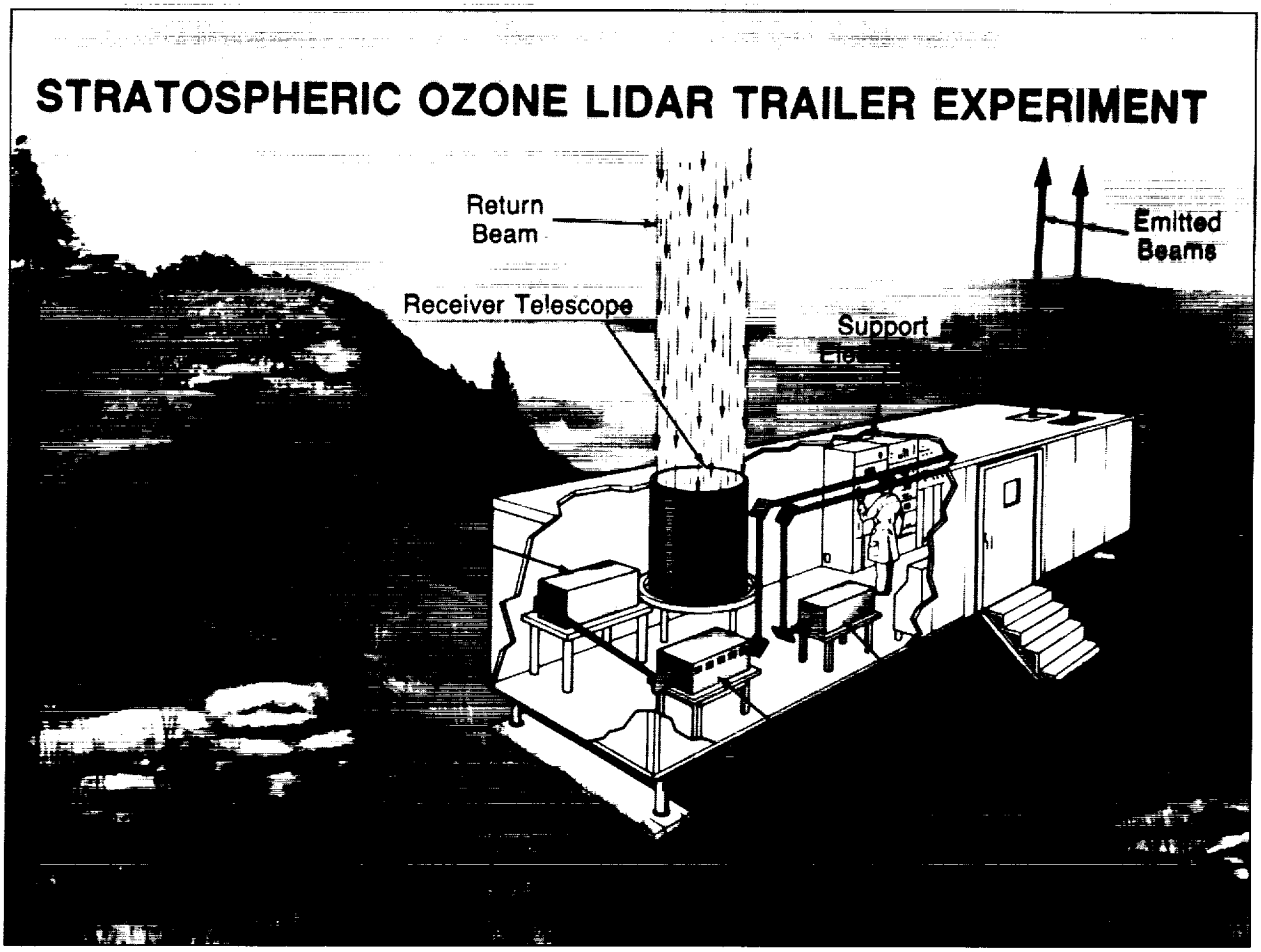

Stratospheric Ozone Lidar Trailer Experiment.

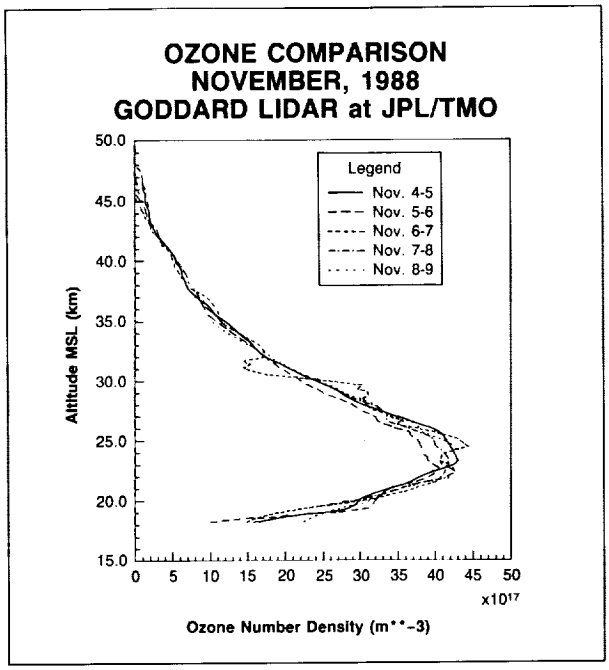

Ozone profiles during the last stages of the first ozone intercomparison (November 1988).

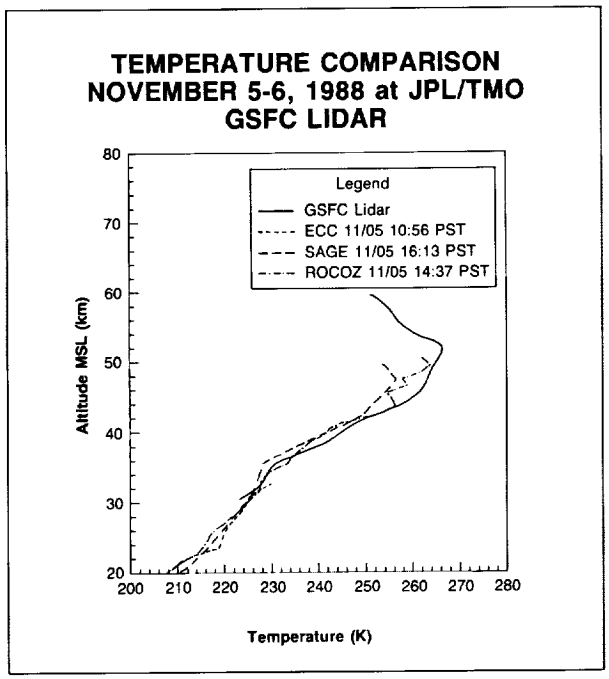

Temperature November 5-6, 1988, measured with Goddard lidar at Jet Propulsion Laboratory compared with measurements from other sources [Electrochemical Cell (EEC), Stratospheric Aerosol and Gas Experiment (SAGE), and Rocket Ozone Sonde (ROCOZ)].

stratosperic ozone and temperature and also Principal Investigator for laboratory studies on molecules of atmospheric interest. A member of the Optical Society of America, Dr. McGee has 10 years' experience at Goddard and received a PhD in physical chemistry from the University of Notre Dame.

BALLOON- AND ROCKET-BORNE MEASUREMENTS OF TEMPERATURE: IMPROVEMENT AND APPLICATION

Global satellite measurements of atmospheric temperature are providing useful information for synoptic meteorologists: the new lidar techniques allow researchers to develop detailed vertical profiles of temperature. Nevertheless, operational satellites and research instruments are not "stand-alone" means of obtaining atmospheric information. In situ temperature measurements from radiosondes and rocketsondes are still required for the calibration and verification of data from satellite measurement systems. The accuracy and precision of these in situ measurements are of unquestionable importance.

Early in the application of rocketsonde data, researchers recognized that temperature measurements were seriously influenced by a number of external factors. Among these factors were aerodynamic heating of the sensor, radiation, thermal lag, and sensor emissivity. The most serious of these influences were aerodynamic heating and radiation, which together accounted for about 90 percent of the measurement error. Temperature corrections were developed and applied. Recent investigations of global temperature trends established the fact that the corrections, although optimal for a uniform launch time (assumed to be 1200 noon local time at all the ranges), are deficient at most other times during the day. Recently, temperature correction studies of the balloon-borne radiosonde have shown that the temperature sensor is affected differently at different latitudes. The magnitude of the corrections varies; investigations suggest that this is due to actual temperature structure, which varies with latitude as well as season. Nighttime corrections appear to be adequate, although they too are apparently affected by the geographical location of the observation site.

Rather than undertake a costly and lengthy study to improve the corrections for the rocketsonde instrument, the inflatable falling sphere system is being considered as an alternate method of obtaining temperature

measurements. The inflatable sphere technique is already launched from many launch ranges. Spheres apparently have an intrinsic property of providing rather accurate temperature data. Vertical winds present in the atmosphere appear in the data as perturbations in density, meaning that temperature measurements contain nonhydrostatic variations; while these variations are not serious, they cause noisy temperature profiles that must then undergo further editing. Comparison between sphere-derived temperatures and in situ temperature sensor measurements reveal that the rocketsonde and sphere temperatures are in excellent agreement for distances up to 55-km altitude. Between 55 and 70 km (the upper limit of the in situ sensor), the direct sensing technique provides temperatures that may be too warm by 12 to 15 °C relative to the sphere-derived temperatures. Theoretical analysis and computer simulation have indicated that the sphere-derived temperatures are correct up to 90 km.

Although corrections for rocketsonde measurements were of major concern to researchers during the 1960's and 1970's, little or no effort was made to isolate radiosonde errors known to exist. Now, however, differences between radiosonde and remote measurements of 1 to 3 °C made it imperative to obtain accurate radiosonde temperatures. Radiosondes equipped with multiple thermistors coated to respond differently to long- and short-wave radiation were developed. This technique allows researchers to determine the radiation error of the thermistor. Since three coatings (thermistors) are used, three heat-transfer equations are solved simultaneously to derive the actual, or ambient, temperature. The difference between the thermistor temperature and the ambient temperature represents the radiosonde's temperature measurement error, or the correction that needs to be applied.

Results from approximately 100 radiosonde observations indicate that the daytime thermistor measurement error reached 1.0 °C at about 30 hPa for solar elevation angles of 30° to 60° and decreased to 0.5 °C at 10 hPa. On the other hand, the nighttime error was found to be negative from the surface to levels above 10 hPa, being 0.2 °C at 100 hPa and -1.4 °C at 10 hPa. Apparently, the decrease in daytime error at levels above 30 hPa results from the influence of the dominant and increasingly larger longwave influence with altitude and with the actual temperature structure present. The magnitude of the error also appears to be influenced by the temperature lapse rate and the underlying surface or cloud-top temperature. The corrections derived, although preliminary, were satisfactorily tested by meteorologists of the European Center for Medium Range Weather Forecasts. The National Weather Service analysts also tested the corrections; National Weather Service analysts are waiting for recently acquired data to be incorporated into the correction analysis before making a final decision on whether to use the corrections operationally.

There recently has been a proliferation of instruments from different manufacturers that operate on different principles and use different sensors. Unless data are adjusted to a known standard (not currently possible), the upper air data base will continue to be biased in as many ways as there are instruments flown and will contain large variances. Development of a reference standard will ensure that adjustments of the various radiosonde temperatures and geopotentials can be accomplished. The multiple-thermistor radiosonde has the potential to provide this reference standard. Periodic comparisons will still be necessary to guard against drift of the various sensors and to ensure that the occurrence of differences between the instruments is minimized.

Although the rocketsonde is an accepted technique for temperature measurement, very few measurements are now available for ground truth. (The number of rocketsonde launchings fell from approximately 55 per week in 1974 from about 18 launch sites to approximately 10 per week in 1989 from 9 launch sites.) Measurements that are currently available provide highly reliable temperatures to 50 km and, if falling-sphere data are included, to about 90 km. In order to monitor rocketsonde reliability, comparisons with radiosonde data are required. Also, satellite measurements depend on the worldwide data base of radiosondes to update regression coefficients used to retrieve temperatures. Thus, radiosondes continue to be the basic measuring tool of the atmospheric research community and promise to be widely used for many of NASA's present and future programs.

Contact: Francis J. Schmidlin (Code 672)
(804) 824-1212

Sponsor: Office of Space Science and Applications

Mr. Francis J. Schmidlin handles investigations of instrumental compatibility, accuracy, and precision for the Observational Science Branch. He received a BS in meteorology from The Pennsylvania State University.

ASSIMILATION OF SATELLITE SURFACE WIND SPEED DATA IN ATMOSPHERIC GENERAL CIRCULATION MODELS

Accurate observations of surface wind velocity over the oceans are required for the determination of surface heat, moisture, and momentum fluxes and for the study of a wide range of atmospheric and oceanic phenomena. Current conventional observations of surface wind are often of poor accuracy, cover only very limited regions of the world's oceans, and occur at irregular intervals in time and space. As a result, analyses of surface wind often misrepresent atmospheric flow over large regions of the global oceans, and this contributes to the poor calculation of wind stress and sensible and latent heat fluxes in these regions.

The SEASAT satellite scatterometer provided a new source of surface wind velocity data, with vastly improved coverage in time and space, for a 96-day period in 1978. In addition to the brief period of SEASAT data, surface wind speed measurements from space are also available from a number of satellites (e.g., Nimbus-7, GEOSAT, and the Defense Meteorological Satellite Program). These data have day-to-day widespread global coverage, in contrast to ship and buoy reports. However, neither operational nor research models are in general designed to use scalar wind observations, and these data have not been routinely used.

At the Goddard Laboratory for Atmospheres, a number of different methods for assimilating space-based wind-speed data to produce vector wind data sets have been developed recently. These include the following directional assignment methods: (1) assignment of model "first guess" wind directions to observed wind speeds and incorporation of resultant wind vectors into a standard analysis; (2) a multipass procedure in which all conventional and other satellite data are analyzed in a first pass to form a "first guess" direction for speed observations; (3) a multipass method in which analyzed surface pressures and winds are combined with the satellite speed observations in a momentum balance relation to assign directions; (4) a "hybrid" approach combining the relative strengths of the two preceding methods; and (5) a variational analysis method in which constraints on smoothness, closeness of fit to a first guess, and dynamical balance are used.

The accompanying table presents a summary of the relative accuracy of the directional assignment methods using simulated data (where the correct solution is known). Overall, and particularly at moderate to high wind speeds, the hybrid procedure (method 4) gives the best results.

As a further evaluation of the accuracy of the directional assignment methods, researchers have applied them to "real" SEASAT and SSM/I data. In the case of the SEASAT data, the objectively determined SEASAT wind directions were withheld and new directions (disregarding the SEASAT directional information) were assigned. In general, the new directions and the original SEASAT directions differed by less than 30°. In addition, as shown in the first figure, directionally assigned wind fields agreed very well with SEASAT fields.

With SSM/I data, a limited 5-day assimilation experiment was performed to evaluate the directional assignment (using method 2) and the impact of the resultant SSM/I winds on the gridded global analyses. The accuracy of the directional assignment was evaluated by comparing assigned SSM/I directions with an independent set of collocated buoys. During the 5-day period, 296 collocations were made in both the tropics and extratropics. These showed an average error of less than 30°, in good agreement with the simulation results for method 2.

The impact of SSM/I winds on global gridded wind fields was assessed by comparing analyses that were

Global Directional Error (in degrees)

Method	0-5 m/s	5-10 m/s	10-15 m/s	15-20 m/s	All Speeds
1	41.8	18.8	18.0	24.9	27.2
2	35.0	16.1	17.3	23.1	23.3
3	62.3	30.8	17.4	9.0	40.1
4	35.0	14.9	12.2	6.3	21.8
5	33.8	15.0	14.4	20.4	21.9

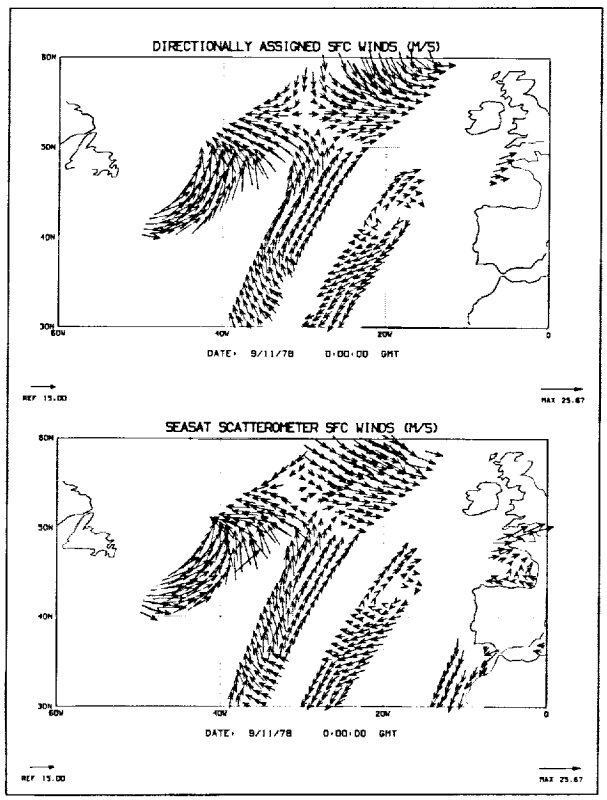

Comparison of directionally assigned winds with SEASAT scatterometer wind vectors.

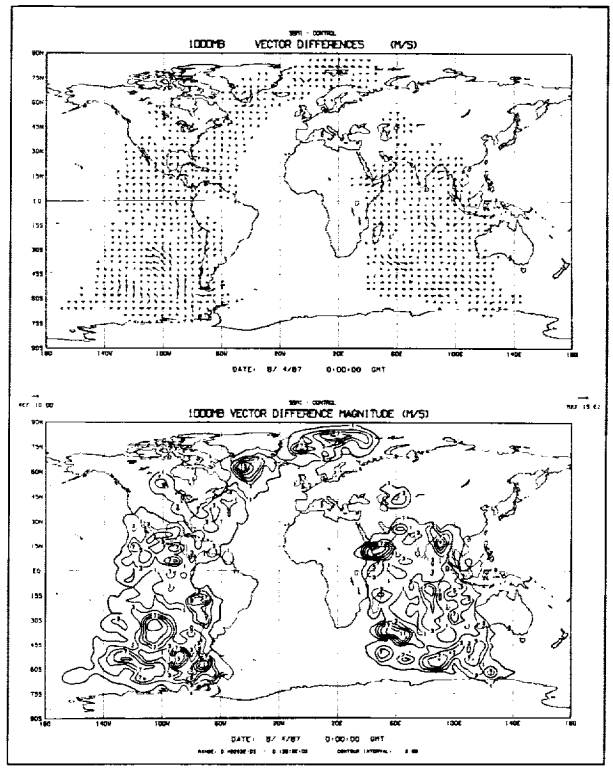

Impact of SSM/I speed data on the 1,000-mbar wind analysis computed by Goddard Laboratory for Atmospheres for August 4, 1987.

generated with and without the SSM/I data. As can be seen from the second figure, large coherent differences result from the inclusion of SSM/I winds, particularly in the Southern Hemisphere.

These results show the potential usefulness of satellite surface wind-speed data and indicate that the direction assignment methodology is sufficiently accurate to allow for the routine assimilation of such data in global atmospheric models.

Contact: Robert M. Atlas (Code 611)
(301) 286-3604

Sponsor: Earth Observation Division, Ocean Processes Branch and Global Scale Atmospheric Processes Branch

Dr. Robert M. Atlas works in the Global Modeling and Simulation Branch of the Laboratory for Atmospheres. Currently, he investigates the use of satellite data in atmospheric models to improve weather prediction and to further the understanding of atmospheric and oceanic phenomena. He has won several NASA awards, including the Laboratory for Atmospheres Science Achievement Award and Outstanding Paper Award. He has 11 years' experience at Goddard and has earned a PhD in meteorology and oceanography from New York University.

THE INTERACTION OF CONVECTIVE CLOUDS AND CHEMISTRY IN THE GLOBAL TROSPOSPHERIC EXPERIMENT/AMAZON BOUNDARY LAYER EXPERIMENT (GTE/ABLE)

Goddard researchers are using photochemical and cloud dynamical models to interpret data from field experiments such as the GTE/ABLE. Simulating key episodes or events offers a unique opportunity to test scientific understanding of tropospheric chemical mechanisms, biogeochemical cycles, and the interaction of chemistry and dynamics.

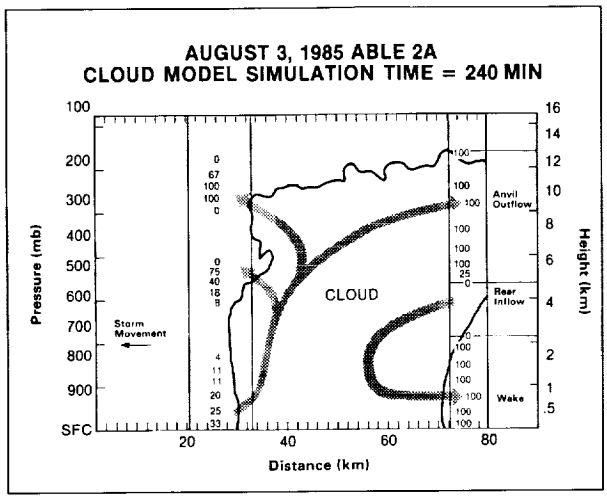

Summary of back trajectories produced by the cloud model for the August 3, 1985, ABLE 2A case. Numbers in the vertical columns ahead and behind the cloud indicate the percentage of the air at that altitude that is outflow from the cloud. Most of the air pumped out of the boundary layer exits from the anvil (8 to 12 km), and air in the wake below 5 km has also been "processed." The air in the boundary layer ahead of the storm is unperturbed. Arrows indicate main flowpaths.

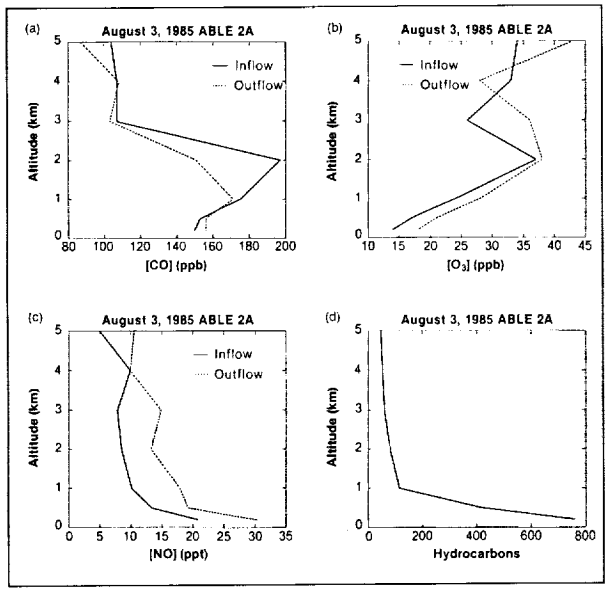

Profiles of observed trace gas data in cloud inflow and outflow air in the August 3, 1985, case. Cloud outflow air is elevated in NO, but CO in the outflow air has been diluted compared with inflow. The hydrocarbons, shown scaled to the concentration and reactivity of methane, are nearly all in the form of isoprene emitted from vegetation.

The specific problem Goddard researchers have investigated is the role of convection in photochemical ozone formation. It is well known that convective clouds are major mechanisms in transporting trace gases from the boundary layer to the free troposphere, and published studies have evaluated the transient effects of mass transport. The focus instead is on the aftereffects of transport and redistribution of reactive gases, e.g., carbon monoxide (CO), oxides of nitrogen (NO_x), and hydrocarbons, that can be pumped up to the mid- and upper troposphere before reacting to form ozone. Ozone (O_3) production has been calculated for convective episodes during the GTE/ABLE 1985 and 1987 expeditions to Brazil, and the effects of reactive trace gas redistribution have been assessed.

Analysis of observations is done in two steps. First, measurements of moisture, temperature, and winds are used to initialize the Severe Storms Branch cloud model that simulates the dynamics and microphysics of convective squall lines typically observed in the tropics. The first figure shows detailed trajectory studies that define regions of cloud inflow and outflow. Profiles of NO, CO, O_3, water vapor (H_2O), hydrocarbons, and temperature are selected to distinguish air that passes through the cloud and exits in cloud outflow from air that is essentially undisturbed by convection. The example shown in the first figure is from a squall line event from the latter part of ABLE 2A on August 3, 1985. Profiles of trace gases measured on the NASA Electra are given in the second figure.

The second part of the analysis is computation of ozone production by a one-dimensional photochemical model initialized with the observations given in the second figure. The calculation is made at intervals over the 24 h following convection, and a diurnally averaged O_3 production rate is shown in the third figure. Throughout the lower troposphere, the rate of ozone production is doubled in the cloud outflow air relative to undisturbed air. Integrating over the entire boundary layer shows O_3 production doubled in the presence of convection. This means that convection is not merely redistributing ozone, but causes ozone to form in greater amounts than if convection were absent.

To date six events have been analyzed: one ABLE 2A case, one ABLE 2B case, and four midlatitude cases (Oklahoma Prestorm, June 1985). These represent nonurban environments with moderately low levels of O_3 and NO and occasional incursions of polluted air, from biomass burning in ABLE 2A and from small cities in the U.S. data. In all cases, O_3 production correlated with NO_x

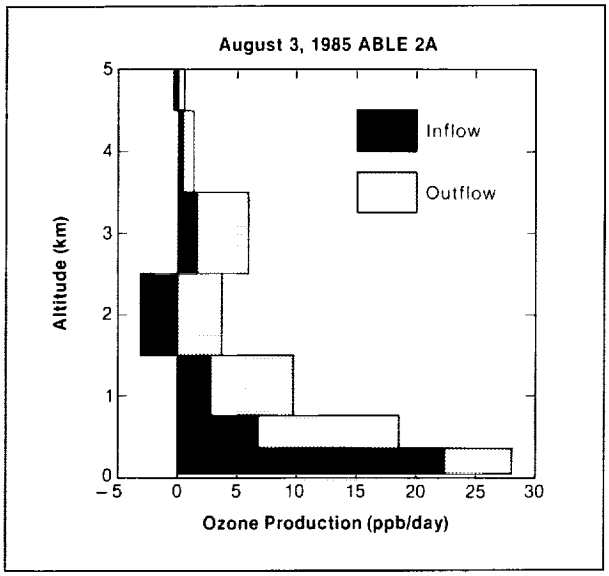

Profiles of diurnally averaged O_3 production in the inflow and outflow air. (Note the free troposphere O_3 production enhancement.) The increase in outflow air is about a factor of two.

levels, showing that these situations were NO_x limited in producing O_3. The distribution of O_3 production in convection can vary widely. Ozone enhancements may be restricted to air just above the boundary layer or far downwind from sources. In the ABLE 2B case, O_3 production was negligible (NO < 10 pptv) and O_3 distributions were dominated by convection.

This analysis illustrates the value of the high-density meteorological and chemical measurements made in GTE/ABLE. In the case of O_3 production, the calculation of convective enhancement requires high-frequency trace gas measurements. The chemical contribution cannot be evaluated, however, without knowledge of cloud dynamics and history. Researchers are continuing to use dynamical and photochemical modeling to develop a climatology of O_3 production in convective events and to evaluate the importance of this process in global ozone budgets.

Contact: Anne M. Thompson (Code 616)
(301) 286-2629
Kenneth E. Pickering (Code 616)
(301) 286-2097

Sponsor: Tropospheric Chemistry Program, NASA Headquarters

Dr. Anne M. Thompson is Principal Investigator on the Tropospheric Chemistry program to model trace gas distributions as sampled in NASA field programs. She is also Co-Investigator on Eos interdisciplinary investigations on biogeochemical fluxes at the atmosphere-ocean interface and chemical and dynamical changes in the stratosphere. Dr. Thompson has 5 years' experience at Goddard, and she earned her PhD in physical chemistry from Bryn Mawr College.

Dr. Kenneth E. Pickering received his PhD in meteorology from the University of Maryland. He currently conducts modeling and data analysis on tropospheric chemistry in the Atmospheric Chemistry and Dynamics Branch.

FRACTAL CLOUDS

There is a growing body of observational evidence on inhomogeneous cloud structure, most recently from the International Satellite Cloud Climatology Project (ISCCP) First ISCPP Regional Experiment (FIRE). Knowledge of cloud structure is important because it strongly influences the cloud radiative properties, one of the major factors in determining the global energy balance. Current atmospheric circulation models use plane-parallel radiation, so that the liquid water in each gridbox is asked to be uniform, which gives an unrealistically large albedo, forcing the models to divide the liquid water by a "fudge factor" to get the albedo right. In reality, cloud liquid water occupies only a subset of each gridbox, greatly reducing the mean albedo. If future climate models are to treat the hydrological cycle in a manner consistent with energy balance, a better treatment of cloud liquid water will be needed.

FIRE concentrated upon two cloud types of special interest: cirrus and marine stratocumulus. Cirrus tend to be high and optically thin, thus reducing the effective radiative temperature without increasing the albedo significantly, leading to an enhanced greenhouse heating. In contrast, marine stratocumulus are low and optically thick, thus producing a large increase in reflected radiation with a small change in emitted radiation, giving a net cooling which could potentially mitigate the expected greenhouse warming. Measurements in California stratocumulus during the FIRE field program in 1987 show variations in cloud liquid water on all scales (Cahalan and Snider, 1989). Such variations arise from inhomogeneous entrainment, in which entrained dry

air, rather than mixing uniformly with cloudy air, remains intact in blobs of all sizes, which decay only slowly by invasion of cloudy air. The following paragraphs describe two important stratocumulus observations, then describe a simple fractal model which reproduces these properties, and conclude by briefly discussing the model radiative properties.

Vertically integrated liquid water was measured at 10 Hz and averaged over 1-min intervals during a 3-week period on San Nicolas Island. The histogram of this data is shown in the figure on the left on a log-linear scale, with a lognormal fit plotted for comparison. The lognormal roughly follows the dates, while differing in detail. The "shoulders" seen to each side of the observed central peak are a reminder that individual days often show a bimodal distribution.

The liquid water wavenumber spectrum shown in the figure on the right was estimated from the frequency spectra computed from several 1-day time series from the same 19-day data set used for the histogram. Results were translated from frequency to wavenumber assuming frozen turbulence with a 5 m/s mean advection. The least-squares fit over the mesoscale regime from about 400 km down to about 400 m gives $S(k) \sim k^{-5/3}$.

This is the classic Kolmogorov result for the wavenumber spectrum of any component of the velocity field and is also the spectrum expected for a "passive scalar" (i.e., a scalar field whose variations in space and time are due only to advection). This suggests that the total integrated liquid water in stratocumulus clouds fluctuates with the vertical velocity, being large in updrafts and small in downdrafts. This kind of behavior has been observed by MacVean and Nicholls (1988) in fine-resolution numerical simulations, though they do not reproduce the highly irregular fractal structure described above. Higher resolution data show a steeper spectral falloff at scales smaller than the cloud thickness (200 m)—a regime still poorly understood.

To simulate mesoscale variations in stratocumulus liquid water, a procedure is needed to generate a random function having the probability and spectrum shown above. Consider a stratocumulus cloud forming an infinitely long slab of horizontal width $L \sim 100$ km and a typical optical depth of, say, $\tau_0 = 10$. Divide this into two slabs of width $L/2$, and transfer a fraction f_1 of the

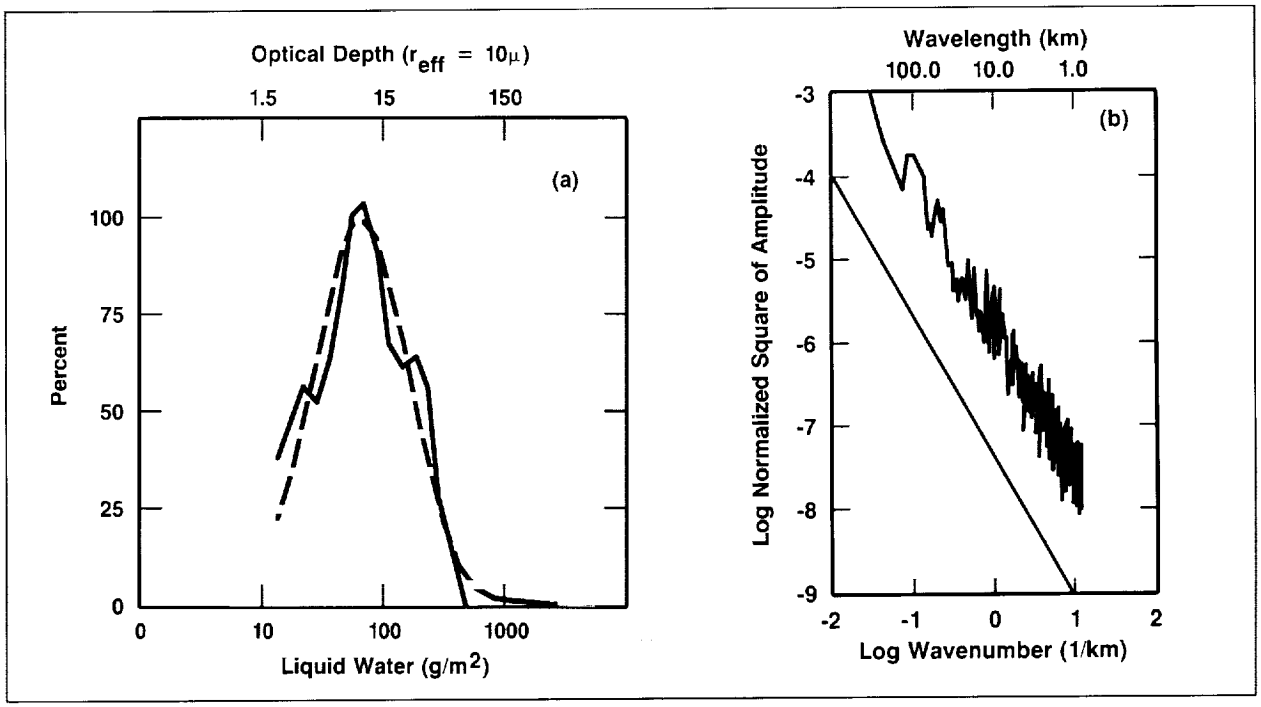

On the left, histogram of logarithm of vertically integrated stratocumulus liquid water in mm along with a lognormal fit. The equivalent optical depth scale shown at the top assumes a 10 μ effective radius. On the right, wavenumber spectrum of integrated liquid water computed from time series assuming 5 m/s frozen turbulence.

liquid water from one half to the other, with the direction chosen at random. The optical depth in one half is then increased (by increasing the densitythickness is assumed unchanged), and the other half is correspondingly thinned. This may be written $\tau^{(\pm)} = (1 \pm f_1)\tau_0$, where the superscript on the left indicates whether the brighter or darker half is being considered.

To continue the process, each half is itself divided in half, and a fraction of liquid water, f_2, is transferred, again in a random direction. After iterating for n cascade steps, there are 2^n segments, each with an optical depth of the form

$$\tau_n^{(\pm \ldots \pm)} = \prod_{k=1}^{n} (1 \pm f_k)\, \tau_0 , \qquad (1)$$

where $0 < f_k < 1$. Any of the possible combinations of signs in (1) may be found somewhere among the 2_n segments. An upper bound on the optical depth of the optically thickest segment may be found from

$$\tau_{max} = \prod_{k=1}^{n} (1 + f_k) < \prod_{k=1}^{n} \exp(f_k) = \exp\left(\sum_{k=1}^{n} f_k\right) \qquad (2)$$

Consider two cases: a "singular model" in which the fraction does not change with k (i.e., $f_k = f$), and a "bounded model" in which the fraction decreases (i.e, $f_k = fc^k$, where f and c are both constants between 0 and 1). The upper bound given by (2) diverges for the singular model, and one can show that the liquid water becomes concentrated on a fractal set of singularities as $n \rightarrow \infty$. The upper bound for the bounded model is $\exp(fc/(1-c))\tau o$ and is close to τ_{max}. It is possible to show that both models have a wavenumber spectrum of the form $S(k) \sim k^{-\alpha}$, where

$$\alpha = \begin{cases} 1 - \dfrac{\ln(1+f^2)}{\ln 2} \\ 1 - 2\dfrac{\ln c}{\ln c 2} \end{cases} \qquad (3)$$

Note that as $f \rightarrow 1$, the exponent of the singular model approaches zero, giving a flat spectrum, while as $f \rightarrow 0$ the spectrum steepens to k^{-1}. No value of f allows the singular model to fit the observed $k^{-5/3}$ spectrum. The exponent of the bounded model, on the other hand, gives $\alpha = 5/3$ if we choose $c = 1/2^{1/3}$. The probability density is sensitive to c and often shows considerable structure, but when $c = 1/2^{1/3}$, it is close to lognormal and similar to the first figure.

These simple models of one-dimensional fractal cloud streets can be generalized to allow variations in three dimensions and tuned to simulate other cloud types. The albedo and other radiation properties are computed by Monte Carlo techniques, and results are parameterized to provide alternatives to plane-parallel theory. For the stratocumulus models the redistribution of liquid water at each iteration decreases the mean albedo from the plane-parallel case, since the albedo of optically thick regions saturates for large optical depths, so that realistic cloud liquid water amounts lead to realistic albedos.

Contact: Robert F. Cahalan (Code 613)
(301) 286-4276

Sponsor: Office of Space Science and Applications

Dr. Robert F. Cahalan is a physical scientist in the Climate and Radiation Branch of the Laboratory for Atmospheres. He earned his PhD in theoretical physics from the University of Illinois. His current work includes empirical and theoretical studies of cloud fractal properties and the discovery of large-scale sea ice variations due to atmospheric forcing. His has won a Senior Fellow Award from the National Center for Atmospheric Research and a NASA Quality Increase Award. He has 10 years' experience with Goddard.

RECENT RESULTS OF EARTH-ATMOSPHERE INTERACTION STUDIES AT GODDARD LABORATORY FOR ATMOSPHERES

Over the last decade, controlled simulation experiments using numerical models of the general circulation of the atmosphere have helped scientists understand the effects of Earth-atmosphere interactions on extended-range weather and climate. Studies at the Goddard Laboratory for Atmospheres have shown that the slowly varying boundary conditions at the surface of the Earth significantly influence the boundary layer humidity, temperature, and winds, which in turn affect cloudiness, rainfall, atmospheric circulation, and net heating. Specifically, analysts have made significant advances in understanding the importance of vegetation-dependent land surface processes and sea-surface temperatures, both of which influences surface fluxes of heat, moisture, and momentum.

On land, the presence of vegetation increases the surface absorption of solar energy, evapotranspiration, and

ORIGINAL PAGE
COLOR PHOTOGRAPH

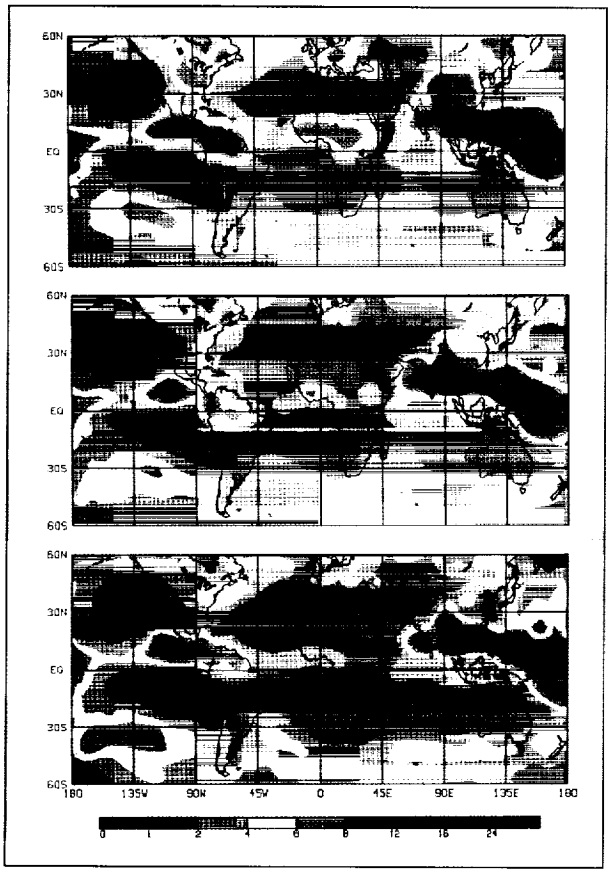

Model-simulated rainfall (mm/day) for the ensemble mean July: a) without the simple biosphere model (top); b) with the simple biosphere model (middle); and c) a single July with improved radiative and cloud radiative forcings. A key to the colors is below the maps.

momentum exchange with the atmosphere. Using computer models, scientists have also investigated these aspects of land-atmosphere interactions for different regions of the world. Consequently, it is now generally recognized that the presence of tall natural vegetation (forests) increases local rainfall during the rainy seasons of the year. Indeed, the same studies have also shown that the influence of vegetation in a specific situation can be quite complex and that a realistic vegetation model is essential for a better understanding of the influence of Earth-atmosphere interactions on weather and climate. For this reason, the simple biosphere model, which defines parameters for biophysical processes of vegetation-radiation-atmosphere interactions, has been developed and included in the Goddard atmospheric model. Simulations with the simple biosphere model have clearly demonstrated that the surface radiation balance, as well as surface energy fluxes, can be significantly altered by the biosphere. In the model, even with adequate soil moisture at the vegetation root-zone, evapotranspiration is largely controlled by the incoming photosynthetically active shortwave radiation, humidity gradients between the stomates of leaves and the surrounding air, and ambient temperature itself. Consequently, simple biosphere simulations produce much smaller changes in evapotranspiration in response to changes in soil-moisture, compared to the previous mechanical model(s) of evapotranspiration (often referred to as bucket/sponge models). Therefore these simulations do not show a strong rainfall response to the local soil moisture and thus the antecedent rainfall. This finding does not imply that the biosphere plays an insignificant role. On the contrary, the biosphere has a large impact on the rainfall climatology of the Earth, as can be seen in the rainfall simulations made with and without the simple biosphere model, shown in the first figure.

On another front, Goddard scientists have conducted several simulations of the role of sea surface temperature anomalies on circulation and rainfall anomalies. The Goddard model has successfully reproduced the tropical circulation anomalies in response to the observed sea surface temperatures anomalies of the strong El Niño of 1982-83. Additionally, Goddard studies have shown that the choice of cumulus convection scheme can make a significant difference in the simulated rainfall anomaly, as well as the vertical distribution of latent heat release, both of which clearly affect the accuracy of the simulated circulation. Modelers have achieved better distribution of the incoming solar radiation over land and ocean by modifying the cloudiness and cloud-radiation interaction calculations. As a result, the rainfall patterns show large changes in many regions. A comparison (b and c) in the first figure shows that in the improved simulation (bottom panel) the rainfall over Sahel in North Africa suffered a reduction, and the rainfall over the southern part of Saudi Arabia was completely eliminated; the rainfall over the tropical western Pacific (maritime islands) was also reduced. Most importantly, the strong monsoon circulation that was previously simulated over the coastal regions of large continents changed to a much more realistic pattern, thus agreeing with observations. Not only does this demonstrate the importance of an accurate simulation of surface radiation for the circulation (not shown) and rainfall climatology of the Earth, but it also suggests some of the institutions of model simulation experiments. Clearly, despite many recent advances, modelers still have a long

way to go. It is hoped that the Eos program will provide vital data for this progress.

To help understand the natural variability of the model's simulated circulation and rainfall in the month of July, a 365-day model integration was made. In the integration, the sea surface temperature and the position of the Sun were kept fixed in order to perpetuate solar and sea surface temperature forcings for mid-July. The soil-moisture was interactive, however. The large variability seen in the consecutive 30-day means was very surprising. If the model simulation is viewed as a set of 12 July integrations, the rainfall variability of monthly means is about half as much as the mean rainfall, as shown in the second figure. While the baroclinically active extra-tropics are known to possess a large natural variability, such a strong variability in the tropics was quite unexpected. Even the rainfall for the last 4 months, 9 through 12, continues to exhibit low-frequency oscillations, shown in the second figure. The results, though preliminary, suggests that seasonal climate prediction as a boundary-forced problem might suffer from severe limitations unless models can successfully forecast the low-frequency behavior of the atmosphere. The mechanisms for the unforced, low-frequency oscillation of the model simulations and its relationship with the observations needs to be investigated further. Goddard scientists are planning future experiments to determine the roles of interactive soil moisture and other physical processes such as cumulus convection on the maintenance of these oscillations.

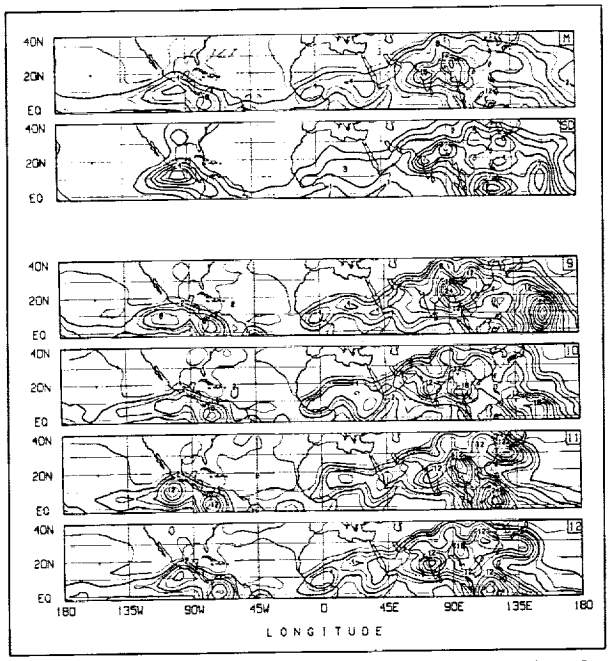

a) Mean and standard deviations of rainfall (mm/day) for the entire 12-month period, after allowing 1 month for the intitial adjustment (top two panels). b) Monthly rainfall (mm/day) for the consecutive 4 months of a perpetual July simulation, after 8 months of integrations with the model (bottom four panels).

Contact: Yogesh C. Sud (Code 611)
(301) 286-7840

Sponsor: Land Program and Climate Program, NASA Headquarters

Dr. Yogesh C. Sud studies Earth atmosphere interactions using the general circulation model developed in the Laboratory for Atmospheres. He investigates the influence of the biosphere on weather and climate cumulus convection and cloud radiation interaction using general circulation model simulation experiments. Dr. Sud has recieved a Peer Award, a Performance Award, and two Quality Increase Awards during his 9 years with Goddard.

AN ALGORITHM TO ESTIMATE THE HEATING BUDGET FROM HYDROMETEOR DISTRIBUTIONS

The importance of cumulus convection to the heat and moisture balance of the tropical trough zone is well recognized. A recent study also indicates that the pattern of latent heat release by cumulus clouds in the tropics has made a significant impact on midlatitude climatic events such as the 1988 North American drought. Because these cumulonimbus clouds are much smaller than circulations resolvable from large-scale numerical weather prediction or climate models, the incorporation of the collective effects of convective clouds into a large-scale prediction model is needed. It is also difficult to measure temperature and humidity as well as microphysical processes within and around clouds. Reliable information on the latent heat release by deep cumulus clouds is still not available. Alternatively, a numerical cloud model with parameterized microphysical processes can be used to estimate the cloud heating effects. The cloud microphysics are included through a two-category water scheme (cloud water and rain) and a three-category ice-phase scheme (cloud ice, snow, and graupel). The phase change of water substance is evaluated on the basis of the assumption that 100-percent humidity is maintained within the

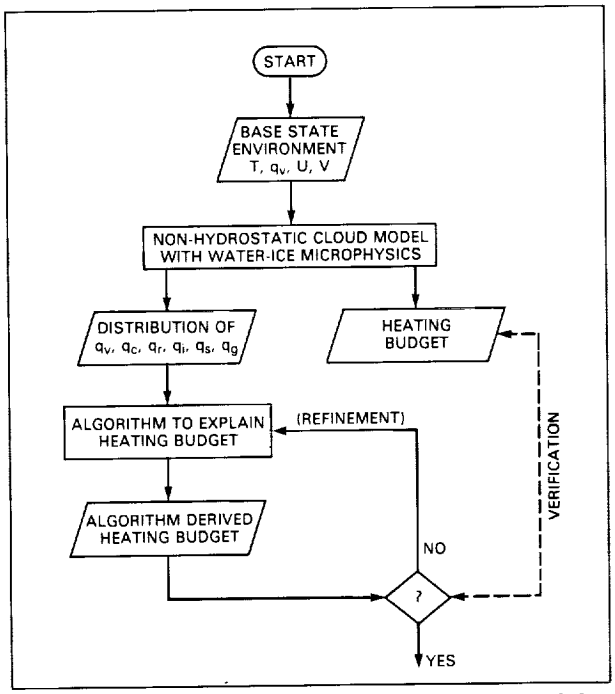

Flowchart showing the procedure for deriving and validating the heating budget estimation algorithm.

cloud. About 30 different microphysical processes are included in association with the growth and transfer rates among the hydrometeors.

A simple algorithm to estimate the latent heating of cloud systems from their hydrometeor distributions is proposed. The input to the proposed algorithm can be obtained from either a rain retrieval technique based on information from multichannel passive microwave signals or a kinematic cloud model based on information from Doppler radar wind fields and radar reflectivity patterns. Such an application would have significant implications for spaceborne remote sensing and the large-scale weather prediction data assimilation problem, which affect the Tropical Rainfall Measurement Mission and Eos, for example.

The first figure is a flowchart showing the procedure for deriving and validating a heating budget estimation algorithm. An environmental condition associated with a specific cloud system is used as the initial condition for the numerical cloud model. The model, in turn, can estimate the heating budget caused by convective transport and microphysical processes. The model would also provide the distribution of different hydrometeor types that correspond to the associated model-predicted heating budget. These hydrometeor distributions are used as the input for the proposed algorithm. Verification with the model-predicted heating budget is then needed to assess algorithm performance.

The mature stage of a tropical squall-type convective system has been tested. The heating budget profiles in the convective and anvil regions of the simulated cloud system are shown in the second figure. The third figure shows the model-generated vertical distribution of hydrometeors associated with the convective and stratiform regions. These profiles correspond to the model-generated heating profile shown in the second figure. Features in the second and third figures are obviously related. For example, the rain distribution is almost constant with height in the convective region, but it increases with height in the stratiform region in the lower troposphere. This implies that low-level evaporation is significant in the stratiform region, but not in the convective region. A relatively large amount of cloud ice, snow, and graupel above the melting layer in the stratiform region may relate to the latent heating shown in the second figure.

The fourth figure is a process diagram associated with cloud microphysics and was constructed in the convective and stratiform regions to help derive the proposed algorithm. This process diagram identifies the most important processes associated with transfer rates between

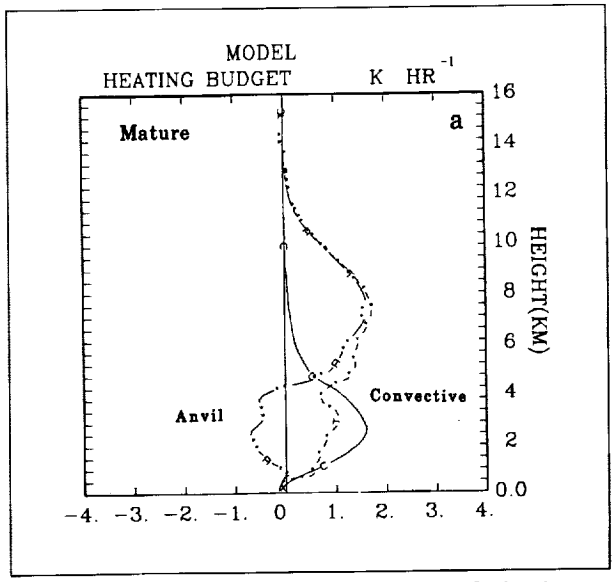

Heating budget for a tropical squall system during its mature stage. These curves represent an average over a period of 2-h simulation time.

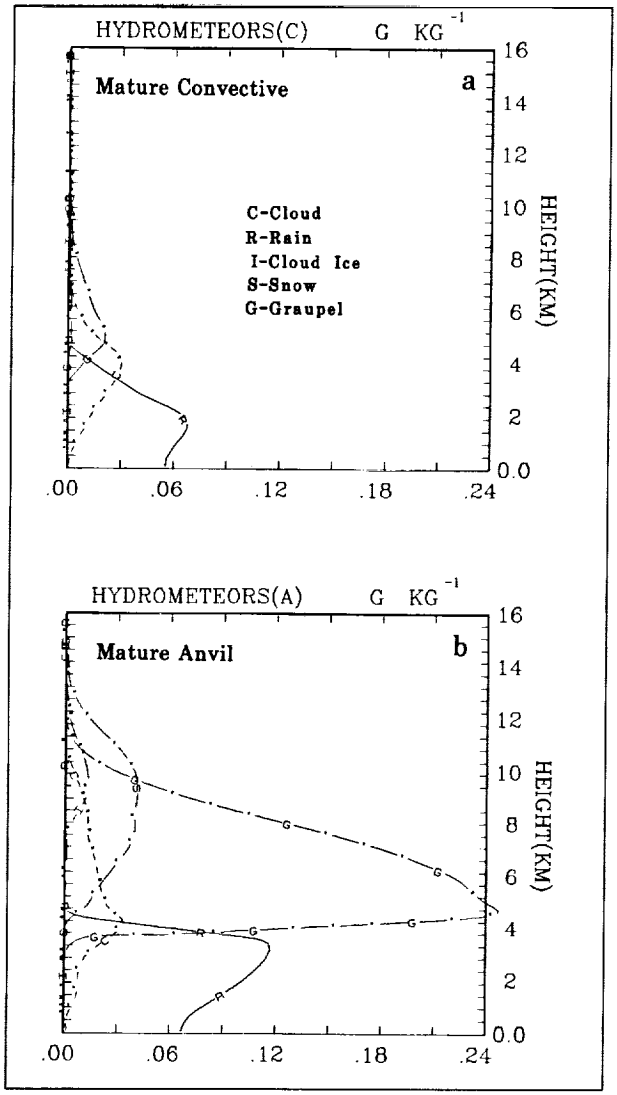

Vertical hydrometeor distribution for (a) convective and (b) stratiform regions during the mature stage.

each category of hydrometeor. The diagram also shows the region (layer) where each process takes place. The heat released (condensation/deposition) or absorbed (evaporation/melting) that is associated with phase changes of water is used for algorithm derivation. The results of the algorithm are shown in the fifth figure. Overall, the major characteristics of the model heating budget in the convective and stratiform regions as shown in the second figure are well captured by the algorithm.

The derivation of the algorithm depends on parameterized cloud microphysical processes. It is only a first order approximation based on the process diagram. The coefficient used in estimating condensation heat release is quite different in the convective and stratiform regions due to important differences in microphysical processes between these two regions. The relative importance of selected microphysical processes may also be quite different in tropical and extratropical locations. These differences may imply that some tuning of the algorithm may be needed when it is applied to cloud systems other than those of tropics. Testing of this algorithm for mesoscale convective systems in other geographic locations is underway. In addition, multichannel microwave rainfall retrieval using SSM/I and geosynchronous data sets in combination with the cloud model simulation results will be considered.

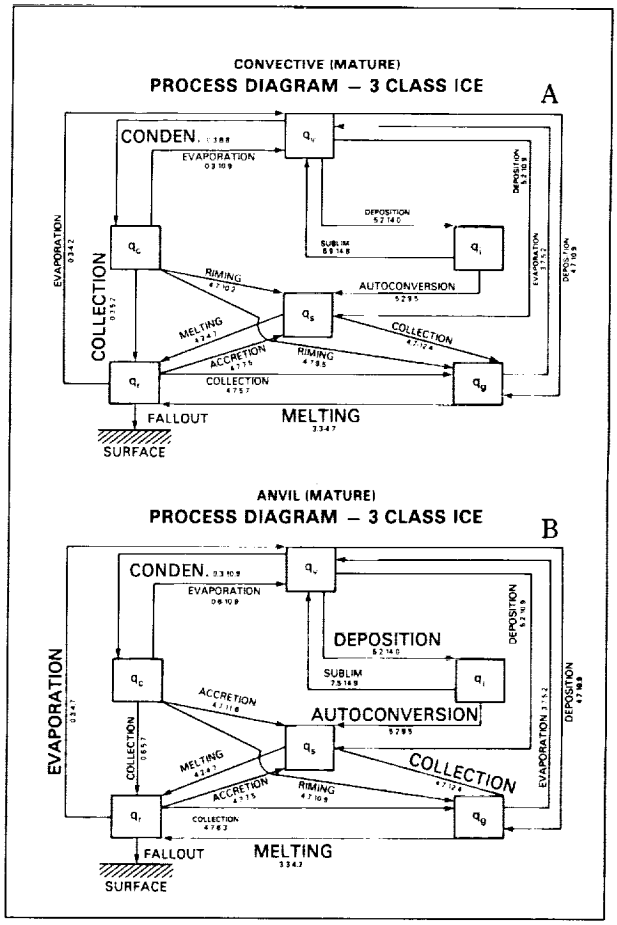

Process diagram for (a) convective and (b) stratiform region during its mature stage of simulated systems. Size of letters indicates the order of importance for each microphysical process. (Larger is more important.)

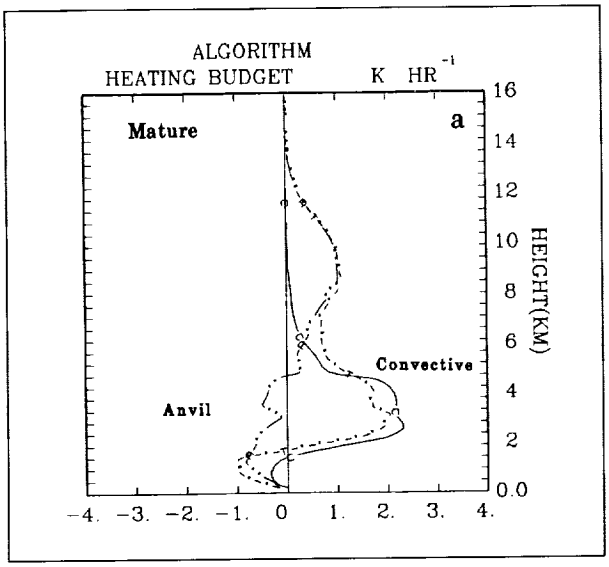

As in second figure except algorithm-derived heating profile.

Contact: Wei-Kuo Tao (Code 612)
(301) 286-4035

Sponsor: Severe Storms Branch

Dr. Wei-Kuo Tao studies numerical modeling of clouds and precipitation processes to improve understanding of their relationship to weather and climate. He works to combine dynamic, microphysical cloud models with radiative transfer models to simulate and interpret satellite, radar, and other conventional weather data. Dr. Tao has 7 years' experience at Goddard. He earned his PhD in atmospheric sciences from the University of Illinois.

MEASUREMENTS OF NATURAL RAINFALL FOR EVALUATING HEAVY RAIN CHARACTERISTICS

The effect of rain on the aerodynamic performance of an airplane is being addressed by both Goddard/Wallops and Langley. Tests have shown that heavy rain produces a degrading influence on wing performance and is a potential hazard to airplanes during the landing and takeoff phases. These tests have also shown that the transition from a steady-state dry condition to a steady-state wet condition takes place in a matter of seconds. This short transitional period led to a need for understanding short-duration, high-intensity natural rainfall. The current data base of the National Weather Service for rainfall is averaged over relatively long time constants. This averaging tends to mask the short-duration, high-intensity rainfall characteristics. Also, most conventional rain gauges produce errors when measuring heavy rainfall.

A weight-measuring rain gauge system with a 1-s sample rate was developed by Goddard/Wallops to measure high-intensity naturally occurring rainfall at ground level. The system has been tested under a rain simulation system to a maximum rain rate of 1,000 mm/h. The weight-measuring gauge has a 1-ft^2 rain collector from which rain water is funneled to a container mounted on a platform scale load cell (see the first figure). A computer samples the measured weight on the load cell, stores the weight data, and calculates the rain rate based on the rate of change in the weight of the accumulated rainwater. Other forces exerted on the load cell due to the downward momentum of the rain and the forces of the wind are minimized by the use of baffles and screens. Currently, these gauges are located at Goddard/Wallops, Langley, and Kennedy Space Center. Data have been collected since February 1989 from Goddard/Wallops and since June 1989 from the other two sites.

Researchers are evaluating the high-intensity natural rainfall data collected from the weight-measuring rain gauge at high sample rates. Instead of averaging the rain rate in minutes, hours, and sometimes days as normally performed, the rain rate data collected are examined in seconds. The results are compiled for defined heavy rain rate levels exceeded, as well as the time of the duration. Hence, the frequency of heavy rainfall rate events exceeding 100

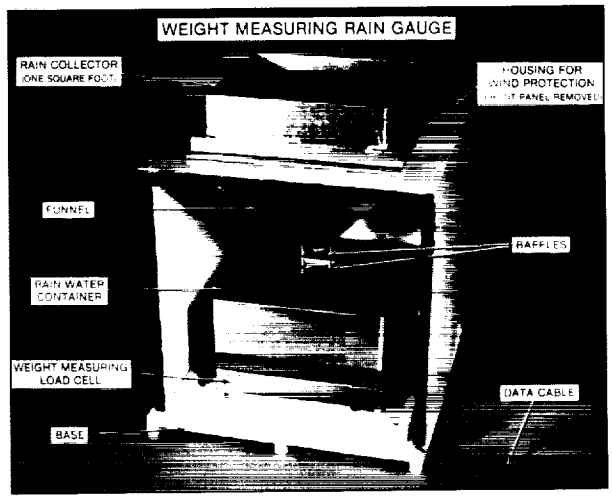

The weight-measuring rain gauge.

ORIGINAL PAGE
BLACK AND WHITE PHOTOGRAPH

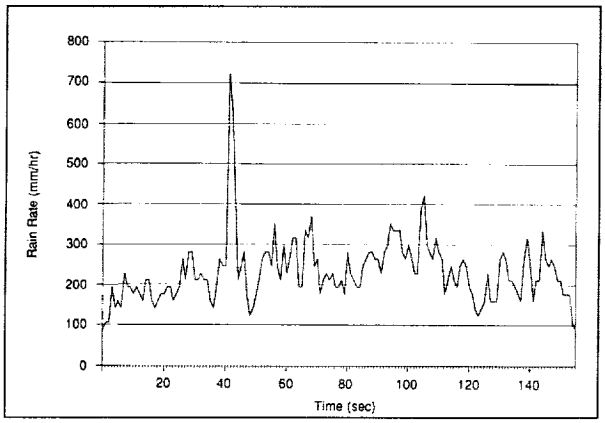

Heavy rainfall events with durations measured in seconds.

mm/h, 200 mm/h, 300 mm/h, etc., and the duration for each event exceeding its defined level are described, as shown in the second figure. By the end of August 1989, the number of events exceeding 100 mm/h was 1,718 and, of those events, 121 lasted longer than 10 s and 5 lasted longer than 1 min. The number of events exceeding 200 mm/h was 453, which included 13 events greater than 10 s. Events exceeding 300 mm/h were 132 and showed only durations of 10 s or less. These results show that the highest rainfall rate exceeding 10 s occurred between the levels of 200 and 300 mm/h. This observation is based on a small sample size at only three locations. More rainfall measurements are being taken and data are being compiled to establish a statistical base which will further describe the short-duration, heavy-rainfall characteristics.

Contact: W. Edward Melson, Jr. (Code 824.2)
(804) 824-1306

Sponsor: Langley Research Center Director's Discretionary Fund

Mr. W. Edward Melson, Jr., is a researcher investigating the effects of heavy rain on aerodynamics and is Head of the Systems Assurance Section. He holds an ME in aerospace engineering and has worked at NASA for 25 years.

LIDAR MEASUREMENTS OF THE ATMOSPHERIC PRESSURE FIELD AND GRAVITY WAVES

Goddard researchers are developing high-vertical-resolution lidar techniques for the accurate measurement of atmospheric temperature and pressure profiles (and surface pressure) from ground-based and aircraft platforms for NASA's Global Scale Atmospheric Research program. The application of these experiments from satellite platforms will provide a vastly improved vertical resolution (as high as 0.5 km) and accuracy (1 °K for temperature measurements) and a totally new capability for the remote measurement of the pressure profile and surface pressure, with 0.1- to 0.3-percent accuracy. This article summarizes the development of high-accuracy aircraft measurements of the two-dimensional pressure field, which may open up a new way of observing atmospheric gravity waves.

Pressure is one of the most fundamental atmospheric descriptors. The vertical and horizontal structure of the static pressure field characterizes the spatial distribution of mass in the atmosphere. Horizontal gradients of pressure represent the primary physical force leading to all scales of atmospheric circulations in the horizontal dimension, including the large-scale general circulation, extratropical and tropical cyclones and anticyclones, and mesoscale phenomena such as sea-land breezes.

The advantages of an active satellite-based lidar temperature and pressure sounding system over any passive alternative are substantial. For example, in a numerical simulation of the performance of a scanning, space-station-based lidar system, the vertical weighting function has a half-width of 0.5 km in the lower troposphere and a corresponding root-mean-square uncertainty of ±1 °C in temperature and 0.3 percent in pressure over 250-km areas. In comparison, passive infrared temperature

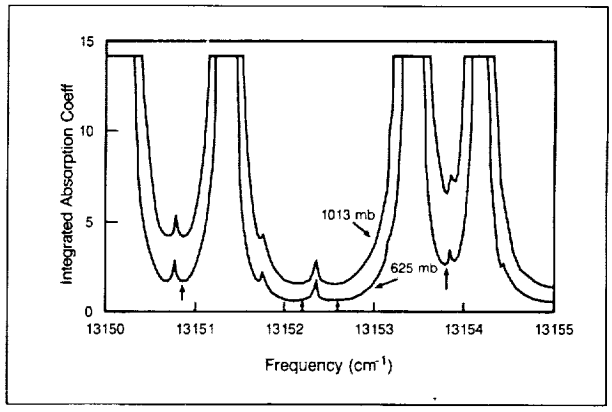

Calculated atmospheric absorption spectra of oxygen from space to the surface and from space to the 625-mbar level. The vertical arrows indicate the trough frequencies at which a laser may be turned to measure the pressure profile.

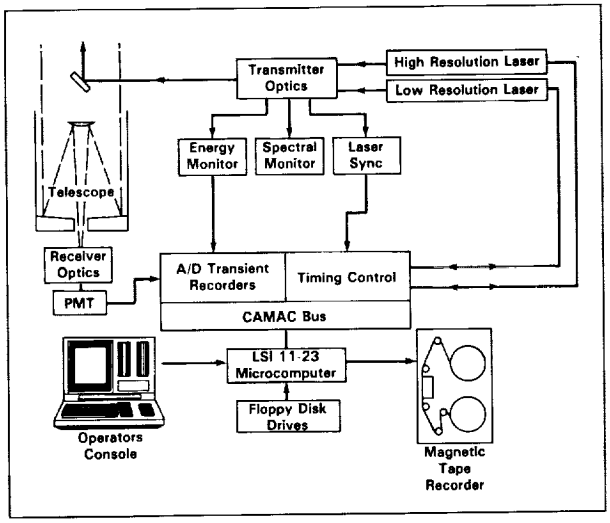

Block diagram of the lidar system used to make ground-based and airborne measurements of the atmospheric pressure field.

measurements have a limiting half-width of about 8 km and a root-mean-square uncertainty of nearly ±2 °C. There are no passive techniques for measuring atmospheric pressure. Other than lidar measurements of pressure profiles, accurate direct measurements of the vertical distribution of pressure have only been made using precision radar tracking of rawinsondes. Only the lidar technique has the potential to be developed as a satellite-based global pressure-observing system.

A differential absorption lidar technique forms the basis for the pressure measurements. It uses two tunable pulsed lasers, one with high spectral resolution tuned to a frequency in a trough of minimum absorption between two strongly absorbing oxygen lines and a second tuned to a nearby nonabsorbing reference frequency. The total absorption between the laser and each range is the log of the ratio of the laser energy backscattered by molecules and aerosols in the atmosphere at each frequency. Since the pressures at various heights in the atmosphere are related by the hydrostatic equation, the measured extinction is directly proportional to the difference in the squares of the pressures at the measurement altitude and the laser, respectively. The oxygen *A* band region near 760 nm has lines of appropriate strength and energy levels for the measurement of pressure, and this region has minimal interference from other species. An example of trough regions in the oxygen *A* band near 760 nm is shown in the first figure, which shows integrated absorption versus frequency calculated by a satellite-measuring laser backscatter from ground-level and 4-km altitude. Extremely high vertical resolution, better than 50 m for ground-based and aircraft profile measurements or 0.5 km for satellite measurements, can be obtained. With these measurements, one is also able to detect and account for effects such as the presence of subvisible cirrus, aerosols, and thin clouds with no significant loss in accuracy. For satellite measurements in the presence of low-lying clouds with large optical depths, profiles of pressure can be obtained above the clouds, and the cloud top pressure-height can also be determined.

The second figure shows the lidar system block diagram. The major components of the system are: (1) a transmitter, which has two narrowband-pulsed alexandrite lasers with associated diagnostic instrumentation and beam-steering optics; (2) a receiver, which has a large-aperture, narrow field-of-view telescope with photomultiplier detectors and low-noise amplifiers; and (3) a microcomputer-controlled data acquisition system. Each laser fires a 100-ns pulse at a 10-Hz repetition rate. A 200-μs time delay between the paired laser pulses is introduced to separate the absorption and reference signals. The laser energy backscattered from the atmosphere is collected with a 40-cm-diameter telescope and detected with a multialkali photomultiplier tube. The receiver optics include a

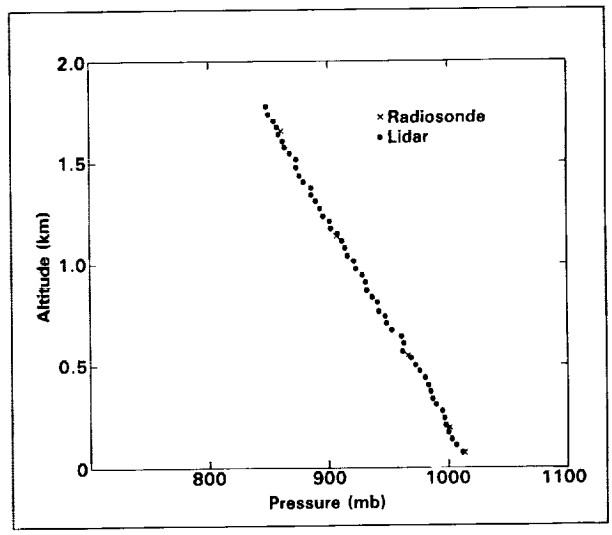

Comparison of lidar-measured pressure versus altitude (dots) and radiosonde pressure altitudes (x's) calculated from measured pressure and temperature. The average deviation of the lidar data to a best linear fit to the radiosonde profile is 1.5 mbar.

spectral filter for removing background light. The signals from the photomultiplier are digitized with a 12-bit transient digitizer at a 5-MHz sampling rate. A microprocessor controls system functions, monitors the operators' inputs, displays system status and absorption data in real time, and records the raw data on a nine-track tape recorder. The only remote measurements of the atmospheric pressure field have been made with this system.

Goddard researchers have made a series of ground-based and airborne measurements of the atmospheric pressure profile. Airborne data were taken in November 1985 and in May and June 1989 using the Goddard lidar facility on the NASA/Wallops Lockheed Electra aircraft. The third figure shows a comparison of the lidar-measured pressure profile 115 km southeast of Sea Isle, New Jersey, to radiosonde data taken 2 h earlier at Wallops Island, Virginia, during the 1985 campaign. The average deviation of the lidar pressure profile data from the radiosonde data is 1.5 mbar.

The two-dimensional pressure field observed by the lidar system between 140 and 90 km off the coast of southern New Jersey on November 21, 1985, is shown in the fourth figure. The data consist of 23 contiguous pressure profile measurements. The horizontal resolution of the data is 2 km and the vertical sampling interval is 30 m. The data are displayed as the altitude of constant pressure levels at intervals of 15 mbar. Gravity wave structure is apparent in the pressure data. A gravity wave is a vertical transverse wave where the air particles move in the vertical as the wave propagates horizontally.

To examine the wave structure in more detail, the corresponding perturbation pressure field was calculated. When the mean pressure is removed at each altitude, a coherent wave structure is apparent at a wavelength of approximately 60 km. In addition, a wavelength of approximately 20 km is more evident if the linear trend (average horizontal gradient) is removed in the pressure at each altitude as well as the mean pressure to filter out the longer wave features. Goddard researchers have also performed PSD analysis of the pressure structure in this data. This analysis shows strong evidence of Fourier components at 60- and 20-km wavelengths, shown in the fifth figure.

The meteorological conditions at the time of these measurements were very favorable for the formation and propagation of mesoscale gravity waves. These included a strong jet stream (65 m/s) and deep convection along an advancing cold front. Smaller scale Kelvin-Helmholtz wave activity was also favored by a complex vertical structure in the boundary layer—an intruding layer of continental origin with high-wind shear (Richardson number of 0.1) at its lower boundary near 400 m.

This capability represents a new and exciting tool for remotely probing the atmosphere. It could be used for quantitative analysis of various atmospheric phenomena such as the fine-scale structure in the pressure field or gravity wave structure and propagation. The

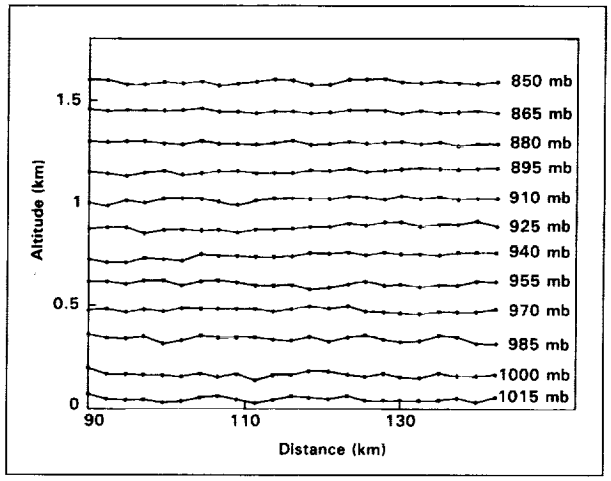

The two-dimensional pressure field measured southeast of Sea Isle, New Jersey, the night of November 21, 1985.

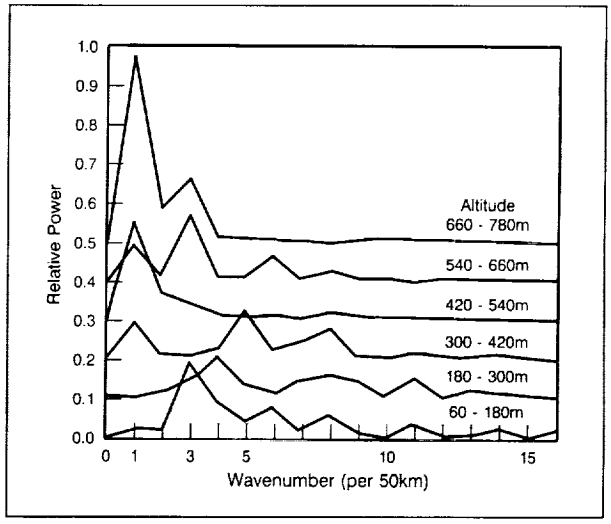

PSD of horizontal spatial structure in the two-dimensional pressure field of the fourth figure. Pressure data were averaged over 120-m altitude intervals before computing the spectrum.

technique may be extended to high-altitude research aircraft platforms and to low Earth-orbit or polar-orbiting satellites for large-area coverage.

Contacts: Geary K. Schwemmer (Code 617)
(301) 286-5768
C. Laurence Korb (Code 617)
(301) 286-6233

Sponsor: Office of Space Science and Applications

Mr. Geary K. Schwemmer is Project Manager and Lead System Design Engineer of the pressure-temperature lidar program and Co-Investigator on the Laser Atmospheric Sensing Equipment II Project. He has developed techniques for analyzing molecular absorption spectra to obtain accurate line strengths and pressure-broadening coefficients. He has published work in theoretical and technical aspects of lidar programs, numerical modeling of atmospheric lidar, and water vapor spectroscopy. Mr. Schwemmer has 12 years of experience with Goddard and 14 years with NASA. He has earned a Quality Increase Award and the Tech Brief Award, and he holds a BSEE from the University of Maryland.

Dr. C. Laurence Korb is a Senior Scientist in the Laboratory for Atmospheres and is the Principal Investigator for the pressure/temperature lidar program. Among his accomplishments at Goddard, Dr. Korb has developed and published the measurement of absolute line strengths at low pressures and the first experimental proof of the Doppler lineshape in absorption spectroscopy. He has served as a member of the International Lidar Working Group and of the Lidar Atmospheric Sounder and Altimeter panel. Dr. Korb received a PhD in physics from Florida State University.

OBSERVATION OF ATMOSPHERIC FRONTS USING RAMAN LIDAR MOISTURE MEASUREMENTS

Water vapor is one of the meteorological variables needed to fully define the state of the atmosphere. It is an important source of the heat that drives circulations and acts to modify atmospheric radiative properties through direct absorption of infrared radiation and by the formation of clouds. When expressed as a mixing ratio, water vapor is a conserved parameter under all meteorological processes except condensation and evaporation. Thus, moisture-mixing ratio serves as a good tracer to visualize dynamic features of the atmosphere. One research area in which moisture plays an important role and where the moisture structure can be used to visualize dynamic processes is the study of atmospheric fronts. Fronts are three-dimensional sloping surfaces that separate different air masses. They extend from the surface into the troposphere and are identifiable as regions across which occur rather abrupt changes in temperature, moisture, and winds.

Detailed studies of frontal characteristics such as slopes, frontal zone thickness, turbulent mixing, entrainment across the frontal zone, and shape of the front as it impinges on the surface require continuous high-vertical-resolution measurements of atmospheric parameters in the vicinity of the front. A recent study using data from the Boulder Atmospheric Observatory Meteorological Tower has clearly shown the importance of continuous measurements to observe the detailed structure associated with an intense cold front as it passed over the tower site. Meteorological towers are ideal for these detailed studies but are limited in height to a few hundred meters; thus, they frequently miss important frontal features aloft. This article describes continuous high-vertical-resolution water vapor mixing-ratio measurements acquired as a cold front passed over Goddard at Greenbelt, Maryland, on June 9, 1987. The measurements, which extend from near the surface to nearly 7 km, were made using a ground-based Raman lidar. The lidar, as it is presently configured, operates only during darkness.

The lidar consists of an Nd:YAG laser operating at the tripled wavelength of 355 nm. The laser beam is pointed vertically with its optical axis aligned parallel to the optical axis of a 30-in.-diameter Dall-Kirkham telescope. The scattered laser light is collected by the telescope as the laser pulse propagates through the atmosphere. The output of the telescope is divided by beamsplitters into three channels, one sensitive to Raman scattering by water vapor molecules at 408 nm, a second sensitive to Raman scattering by nitrogen molecules at 387 nm, and the third sensitive to scattering by molecules and aerosols at the laser wavelength (355 nm). The output of each of the three photomultipliers is applied to both an analog-to-digital converter and a photon counter. Analog-to-digital converter data are generally used from near the surface to an altitude of approximately 2 km, with photon counter data used above. Photon counter data tend to be of higher quality but cannot be used below 2 km because the high atmospheric backscatter intensity from short ranges leads to photon counter saturation.

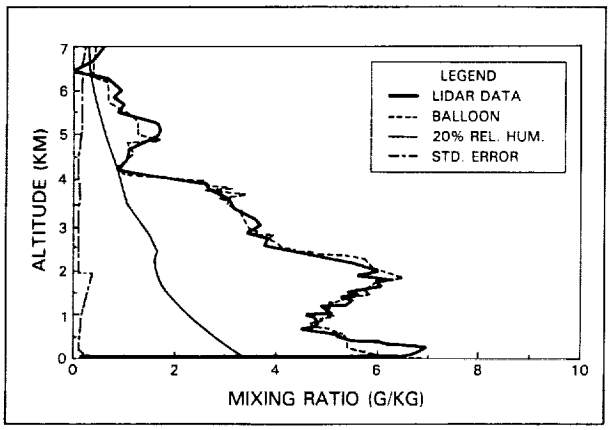

A comparison of Raman lidar-derived water vapor mixing-ratio profile acquired at 2156 EDT on June 6, 1987, with a balloon-sonde-measured profile. The sonde was launched at the experiment site at 2146 EDT on the same night.

Raman backscatter in the atmosphere is a very weak phenomenon; thus, signals from a number of laser shots are accumulated to improve measurements statistics. Generally, the laser is fired approximately 1,000 times, after which the accumulated signals acquired by the analog-to-digital converters and photon counters are stored on magnetic disk.

The ratio of Raman scattering by water vapor to that by nitrogen is proportional, to a very good first approximation, to the value of atmospheric water vapor mixing ratio. A small correction to the calculated ratio is made which takes into account differential atmospheric attenuation at the two Raman wavelengths. Under clear atmospheric conditions, this correction is less than 5 percent at an altitude of 7 km and is less at lower altitudes.

An example of a lidar-derived water vapor mixing-ratio profile obtained at Greenbelt, Maryland, on the night of June 6, 1987, is shown in the first figure. The lidar data were calibrated by performing a least-squares fit between the lidar-derived mixing ratio and an independent measurement of water vapor mixing ratio from a balloon-sonde launched concurrently from the experimental site. The balloon-sonde data are shown in the first figure for comparison. Also shown is the estimated standard error (estimated random noise) for the lidar data. The detailed agreement as a function of altitude between the lidar and the balloon-sonde measurements of moisture mixing ratio is excellent, having a correlation coefficient of 0.99, with all major moisture features revealed by both techniques. The estimated standard error shown in the first figure indicates a random uncertainty for the lidar measurements of less than ±10 percent or ±0.5 g/kg from near the surface to 7- km altitude.

During an operating period, moisture profiles like those shown in the first figure are acquired continuously once every 2 min. All profiles from a single period of operation then are combined together to form an image which provides a visual indication of the time/height variation of moisture mixing ratio during that period. Water vapor mixing-ratio measurements displayed as a time/height image and obtained during the night of June 9-10 are shown in the second figure. In this image, time increases from left to right starting at about 2200 EDT and extending to nearly 0500 EDT the next morning, and altitude extends vertically from the surface to nearly 7 km. Regions of the atmosphere of similar concentrations of moisture in the time/height display have been color coded the same, with the lowest concentration near 0 g/kg being black extending through shades of blue, green, yellow, red, and violet representing 12 g/kg. The color bar on the figure shows the relationship between color and moisture mixing ratio. The image is constructed from approximately 240 independent moisture profiles, each taken 2 min apart.

On the afternoon of Tuesday, June 9, 1987, a low-pressure region was centered over Maine. A cold front extended from the low toward the southwest over central Pennsylvania and West Virginia. During the late afternoon and into the evening, the cold front moved southeastward at a speed of approximately 7.5 m/s. The surface cold front which was oriented along a west-southwest, east-northeast axis, moved over Greenbelt, Maryland, at approximately 2245 EDT. Throughout the night of June 9-10, the front continued to move southeastward at a nearly constant speed. There were no clouds or precipitation associated with the passage of the front. The image shows the moisture structure of the cold front as it passed over the experiment site. The two curves overlaid on the image indicate the most probable location of the front and back of the front and, as such, delineate the frontal zone which lies between the curves.

The shape of the frontal zone has an interesting character. There appears to be a "nose" within the frontal zone, extending from 2245 to 0100 EDT, which serves to elevate the front and steepen its slope as it impinges on the surface. The "wall" of moisture in advance of the front around 2200 EDT extending to an altitude of nearly 3 km is indicative of an elevated front, a feature which has been

observed to be associated with cold fronts over England. After 0130 EDT, the frontal zone slopes from lower left to upper right as expected for a cold front when displayed with time increasing from left to right as in the figure. The slope has been estimated to be 4h/km, or about 110 to 1, using a front speed of 7.5 m/s. Generally, cold fronts are expected to have slopes around 100 to 1.

Never before has the moisture structure of a cold front been observed in such detail. The high vertical and temporal resolution of the lidar, as demonstrated in the image, has proven invaluable in understanding the detailed structure of this dynamic feature. Standard balloon-sondes proved incapable of capturing the changes. With this new observational capability Goddard expects to increase scientific understanding of several important atmospheric processes such as gravity waves, gust fronts, and the dry line.

Contact: Samuel H. Melfi (Code 617)
(301) 286-6348

David N. Whiteman (Code 674)
(301) 286-3115

Richard A. Ferrare, Universities Space Science Research Association (Code 613)
(301) 286-9089

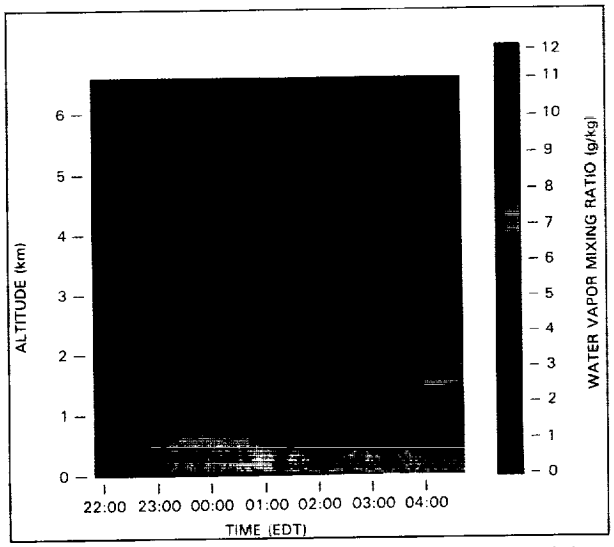

A color-coded time/height image of water vapor mixing-ratio acquired with the ground-based Raman lidar on June 9-10, 1987. The two curves overlaid on the image indicate the most probable position of the frontal zone associated with a cold front which passed over the experiment site.

Sponsor: Office of Space Science and Applications

Dr. Samuel H. Melfi is Head of the Environment Sensors Branch in the Laboratory for Atmospheres. He has been at Goddard for 10 years in a variety of research and management positions. Dr. Melfi, who holds a PhD in physics from William and Mary College, conducted the first remote measurements of high-resolution atmospheric moisture profiles.

Mr. David N. Whiteman is in the Experimental Instrumentation Branch in the Laboratory for Oceans. Since joining Goddard 10 years ago, he has worked in all phases of lidar system design, implementation, and management. He holds a BA in physics from Williams College in Massachusetts.

Mr. Richard A. Ferrare, who is a research scientist with the Universities Space Research Association, holds an MS in meteorology from the University of Wisconsin-Madison. He has developed the algorithms for the analyses of the Raman water vapor lidar data and the Differential Absorption Lidar stratospheric ozone lidar data.

THERMOSPHERIC CIRCULATION AND DYNAMO INTERACTION

The absorption of extreme ultraviolet (EUV) radiation dominates the energetics and dynamics of the Earth's upper atmosphere or thermosphere and is responsible primarily for the formation of the ionospheric plasma. The photons in this part of the solar spectrum are relatively energetic so that, typically, the neutral temperatures are 1,000 °K and the wind velocities are 100 m/s as observed from the Dynamics Explorer-2 satellite. The much larger wind velocities of the polar vortices are driven mainly by plasma drift due to convection electric fields of magnetospheric origin.

At low latitudes, the observations show specifically that the solar-driven diurnal tide dominates the circulation of the neutral atmosphere, with winds blowing across the terminators from the sunlit hemisphere into the night side. In addition, the observations show, as illustrated in the accompanying figure, that the ionospheric plasma drifts with somewhat smaller velocities that tend to track the winds of the neutral atmosphere.

In the presence of the Earth's magnetic field, the atmospheric circulation generates electric fields through the dynamo interaction, and these electric fields accelerate

ORIGINAL PAGE
COLOR PHOTOGRAPH

the ions. The current system from the atmospheric dynamo causes variations in the magnetic field. Studies of these variations have contributed significantly to understanding of atmospheric tides. However, models have largely been confined to generating the dynamo electric field from a given wind field without accounting for the feedback due to the drag the ions exert on the neutrals—a process known to dominate the circulation of the polar region. This correlation between neutral and ion velocities is not yet fully understood. It raises questions about the extent to which the internal dynamo interaction affects the thermospheric circulation and the location in the ionosphere where this interaction occurs.

To address these questions, Goddard researchers have developed a multiconstituent model [including the major species atomic oxygen (O), molecular nitrogen (N_2), and molecular oxygen (O_2)], which describes in self-consistent form the interactions between the neutral winds driven by solar radiation, the associated dynamo electric fields and ion drifts, and their feedback due to drag. In the thermosphere, a large tidal component is generated in situ, but there is also a smaller component due to tides propagating from the lower atmosphere. These propagating tides have large amplitudes in the E-region of the ionosphere (around 120 km) where the conditions are favorable for generating dynamo electric fields. Thus, the model must account for tides generated throughout the entire atmosphere, from the ground up to the exobase.

Tidal theory has shown that below 100 km the inertial and Coriolis accelerations primarily balance the horizontal pressure gradients, while at higher altitudes the viscous and ion drag accelerations are more important. Accordingly, two classes of basis functions have been introduced to describe atmospheric tides: Hough modes at lower altitudes and spherical harmonics at higher altitudes. These basis functions represent the approximate eigenfunctions for the two altitude regimes. These describe, respectively, the horizontal variations of the diurnal tides in the lower atmosphere (below 100 km) and in the thermosphere at higher altitudes, with the transition region occurring somewhere between 100 and 150 km. Using these basis functions, researchers have adopted a two-step solution procedure. (1) Hough modes are used to provide a good first-order description of the tides that are generated in the lower atmosphere and propagate into the thermosphere. (2) Given these Hough modes (expressed in terms of spherical harmonics), spherical harmonics are then used to describe the

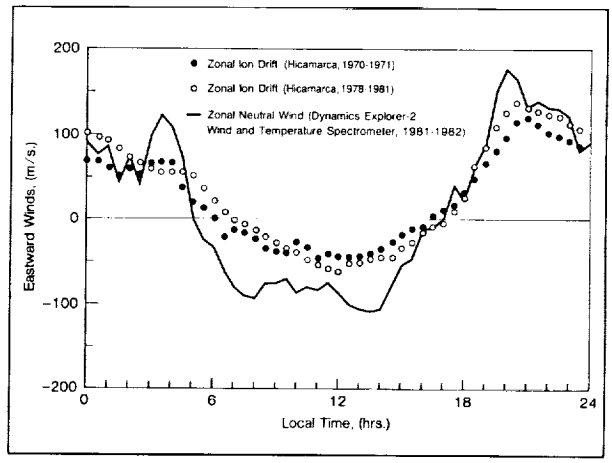

Zonal velocities near the Equator. The solid line represents the average of the neutral wind data measured on the Dynamics Explorer-2 satellite between 300 and 450 km (Wharton and others, 1984). The circles and dots represent ion drift data taken by the radar at Hicamarca (Fejer and others, 1981).

tides generated by the EUV source within the thermosphere and account iteratively for corrections due to the dissipative and electrodynamic processes not fully described by the individual Hough modes. In both steps of this solution procedure, the complete set of conservation equations (including viscous dissipation, Coriolis force, and dynamo interaction) are solved from the ground up to the exobase.

The model study leads to the following conclusions. The largest component of the thermospheric circulation is generated in situ by the absorption of EUV radiation. These winds also produce the largest contribution to the dynamo electric field which originates primarily at F-region altitudes above 150 km. Tides originating in the lower atmosphere generate dynamo electric fields in the E-region of the ionosphere where the electrodynamic conditions are most favorable. However, the vertical wavelengths of these tides are relatively short so that cancellations take place, preventing the buildup of a significant dynamo electric field. The model results are compared with amplitude and phase of the dominant Fourier components in the observed winds and ion drift velocities (as shown in the table) and show generally good agreement. The table also presents a solution for the neutral winds in which the dynamo electric field is forced to zero. This solution demonstrates that the dynamo-induced ion drift is very important in accelerating the neutral

Computer Temperature Amplitudes and Phases in Comparison with Observations

Diurnal Component (24-hour period)

		Amplitude (m/s)	Phase (h)
Zonal Winds:	Observations	119	22.7
	Model with dynamo	126	22.2
	Model without dynamo	61	20.9
Zonal Ion Drift:	Observations	85	23.0
	Model	80	23.0
		Ratio	**Phase Difference (h)**
Wind/Drift:	Observations	1.40	0.3
	Models	1.57	0.8

The measured neutral winds are taken from Wharton and others, 1984, and the ion drift from Fejer and others, 1981.

atmosphere at higher altitudes. Due to the internal dynamo interaction, the wind velocities increase by about 50 percent. However, the dynamo affects primarily the curl component of the circulation, which is not involved in the redistribution of mass and energy. Thus, the effects on the temperature and density variations are negligible.

Contact: Hans G. Mayr (Code 614)
(301) 286-7505

Isadore Harris (Code 614)
(301) 286-8560

Fred A. Herrero (Code 692)
(301) 286-5660

Sponsor: Laboratory for Atmospheres and Laboratory for Extraterrestrial Physics

Dr. Hans G. Mayr is an atmospheric scientist with the Dynamics Explorer and Pioneer Venus projects. Dr. Mayr, who holds a PhD from the University of Graz in Austria, has 21 years' experience with Goddard.

Dr. Isadore Harris, who received a PhD from Northwestern University, is a planetary aeronomist with 29 years' service at Goddard.

Dr. Fred A. Herrero has been with Goddard for 6 years and works in thermosphere dynamics. His interests include charged-particle spectroscopy and its application to space plasmas and neutral atmospheres.

MAXIMUM ENTROPY SPECTRAL ENHANCEMENT OF PROPANE

The uncertainty principle says that if a time series contains most of its information in the time span t, then its Fourier transform contains most of its energy in the bandwidth $\Delta f \geq 1/\Delta t$. This is not the same as saying that if one has a sample of stationary time series of length Δt, the best frequency resolution one can hope to attain will be $\Delta f = 1/\Delta t$. The difference lies in assuming that a function is zero outside the interval Δt in which it is given, rather than assuming that it continues in a natural way outside the given interval. If the data sample can be continued in a natural fashion some distance beyond the interval in which it is given, then the frequency resolution Δf may be considerably finer that $1/\Delta t$. The frequency resolution will depend upon the predictability of the data off the ends of the sample. If one has a sequence of a stationary series which is short compared to the autocorrelation of the stationary series, then the maximum entropy estimation of the corresponding spectrum will be radically better than a truncated Fourier transform result. The Maximum Entropy Principle, which was pioneered by E.T. Jaynes, has its roots in the work of L. Boltzman and J.W. Gibbs in the latter part of the 19th century and by C.E. Shannon in the 1940's. It involves drawing inferences from incomplete information and states, fundamentally, that any inferences made concerning the outcome of any natural process should be based upon the probability distribution, which has the maximum entropy permitted by the data taken during the observation of the process.

For a given time series consisting of measured values of an autocorrelation function, J. Burg chose the spectrum that corresponded to the most random time series whose autocovariance coincides with the given set of values. Alternately, for a series of known lags of an autocorrelation function, Burg showed how to extrapolate the autocorrelation function through the entropy maximization approach. Therefore, unlike conventional methods, this result does not consider the time series information to be zero outside the interval in which it was taken. Instead, it is continued according to the Maximum Entropy Principle so that the given autocorrelations are extrapolated to the point where the observed process can be uniquely identified in the Kolmogorov sense. In all cases, this estimation will be consistently better than a direct Fourier transform result, except for the Fourier transform of an

infinitely extended autocorrelation function. In this case, the power spectra are equivalent.

The Burg Maximum Entropy spectral density is given by

$$P(f) = \frac{P_{n+1}/f_n}{2|1 + \sum_{j=1}^{n} a_{nj} \exp(-2\pi i f j \Delta t)|^2} \quad (1)$$

where f_n is the Nyquist frequency and specifies the bandwidth for a sampling interval of Δt

$$f_n = \frac{1}{2\Delta t} \quad (2)$$

The a_{nj} and P_{n+1} are the n^{th} order prediction error filter and prediction error power respectively.

The Nicolet 8000 Fourier transform spectrophotometer was used to measure the propane transmittance spectrum. This instrument is a Michelson interferometer that operates in vacuum to eliminate atmospheric absorption and noise caused by beamsplitter vibrations. The optical path difference between the two interfering beams is produced by a movable mirror mounting on dual air bearings with a maximum mirror travel of 8.3 cm. The distance limits the maximum resolution of the spectrometer to 0.06 cm^{-1} for unapodized, single-sided interferograms. With three sources, five beamsplitters, and four detectors, the instrument covers a very broad wavelength range from 1 m to approximately 2 mm (10,000 cm^{-1} to 5 cm^{-1}).

For this measurement, a global source at approximately 900 °K and a mercury-cadmium-telluride detector operating at 77 °K were used. The beamsplitter was a 5-cm-diameter potassium bromide crystal coated with a thin file of germanium. A 10-cm-long gas cell with caesium-idodide windows beveled to eliminate multiple reflections was placed in the infrared beam. The pressure of propane in the cell was 103.6 T at room temperature, and 1,000 scans at maximum resolution were averaged to produce this interfogram. The cell was evacuated to a pressure of less than 10^{-6} T, and the measurement was repeated to produce the interferogram for the background spectrum, or instrument profile. Each interferogram contains 2^{18} data points between which the mirror moved a distance of 316.4 nm, resulting in a Nyquist frequency of 7,899 cm^{-1}. A low-pass filter ensured that there was no signal above this frequency.

Before applying the Fast Fourier transform route, the size of each interferogram was doubled by adding an equal number of zero data points onto the end, giving a total of 524,288 data points. The Happ-Genzel function was used to apodize the interferograms because it gives the best compromise between removing the false sidelobes caused by the finite optical path difference and minimizing the degradation of the resolution. The ith data point of each interferogram as multiplied by the function

$$.54 + .46 \cos\left[\pi \frac{i - i_o}{N - i_o}\right] \quad (3)$$

where i_o is the number of the peak data point, and N is the total number of data points. A low-resolution Fast Fourier

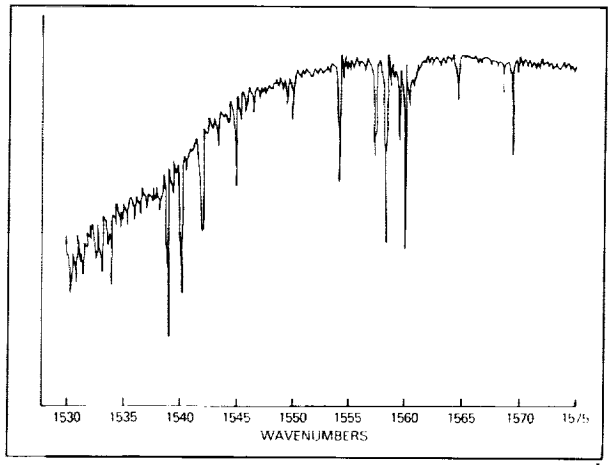

Fast Fourier transform spectral estimate in a 45-cm^{-1} band from 1,530 cm^{-1} to 1,575 cm^{-1}, using a full 2^{18} data samples.

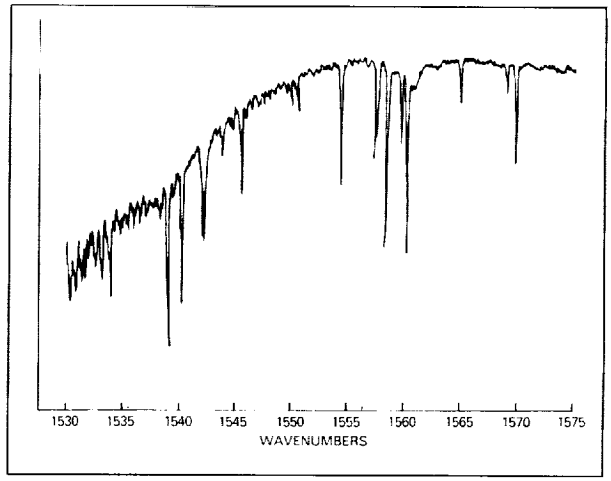

Burg/maximum entropy spectral estimate in this same 45-cm^{-1} band from 1,530 cm^{-1} to 1,575 cm^{-1}, using the first 2^{16} data samples.

transform was done on 100 data points on each side of the zero path difference peak of the interferogram to correct for any phase errors in the single-sided high-resolution interferogram. The sample and background interferograms were then transformed, and the ratio of the two spectra reduced the transmittance spectrum of propane.

The first figure shows the result of Fast Fourier transform power spectral calculation for propane using 2^{18} interferogram data samples and concentrated on a 45-cm^{-1} region (1,530 cm^{-1} to 1,575 cm^{-1}) out of a total spectrum from 400 cm^{-1} to 4,900-cm^{-1}. The resolution in this case is 0.06 cm^{-1}. The second figure is the Burg/maximum entropy spectral estimate for this same 45-cm^{-1} region, but was calculated using only the first 2^{16} data samples and a filter order value of 0.56 times the number of data samples. The latter is required to determine the prediction error filter coefficients. The Burg results were produced on the CYBER 205, and they agree well with the Fast Fourier transform results, both in location and relative dynamic range for the major resonances, as well as for the number of minor absorption peaks.

If resolution gain is to be measured by the number of sequential data samples employed in the calculation from some arbitrary origin prior to the zero path difference of the interferogram, then the resolution increase achieved by the Burg spectral estimate for propane is exactly a factor of 4. Although an inspection of the computer results of the Burg estimate reveals additional lines at 1,558.5 cm^{-1} and 1,560.25 cm^{-1} respectively, these cannot be confirmed by the interferometer measurements.

Since the correlations are not given exactly as required by Burg, but instead are derived from a time series, then, as suggested by Jaynes, the filter order is estimated by examining the Z-transform version of equation (1) and then counting the number of poles far enough away from the origin of the unit circle so as to make an appreciable contribution to the structure of the spectral estimate and the predictability of the time series. In this sense, the maximum entropy method provides a test of the model order in that the sequence is terminated whenever the poles begin to accumulate near the origin. In this case, the filter coefficients did not necessarily follow the expected near neighbor-high correlation relationship. Instead, intermittent peaks appeared out to an appreciable fraction of data samples. This result indicates the presence of long-range order in propane. It also indicates that, on a selective basis, the filter-order to data-sample ratio can be much lower than 0.56 for the same resolution.

Resolution enhancement, or superresolution, is of considerable interest to NASA, especially in systems such as Eos. Fourier transform spectrometers are ideally suited to this environment due to their compactness and efficiency. Since there is a direct correlation between the length of mirror travel and the degree of resolution in Fourier transform spectroscopy, then the ability to extrapolate a finite length interferogram beyond the measured record would allow the use of a short mirror-travel interferometer with the resolution capability of a more sophisticated instrument but at considerably less expense.

Contact: N.L. Bonavito (Code 636)
(301) 286-4079

Sponsor: Office of Space Science and Application

Dr. N.L. Bonavito is a physicist with the Information Systems Development Facility. Dr. Bonavito, who earned a PhD in physics from The Catholic University of America, is interested in statistical physics, stochastic processes, neural networks, and information theory. He is a member of the American Physical Society and the Society of Sigma Xi and has been with Goddard for 27 years. During his military tour of duty, he served as a first lieutenant at the U.S. Army's Guided Missile Center at Fort Bliss, Texas.

Space Sciences

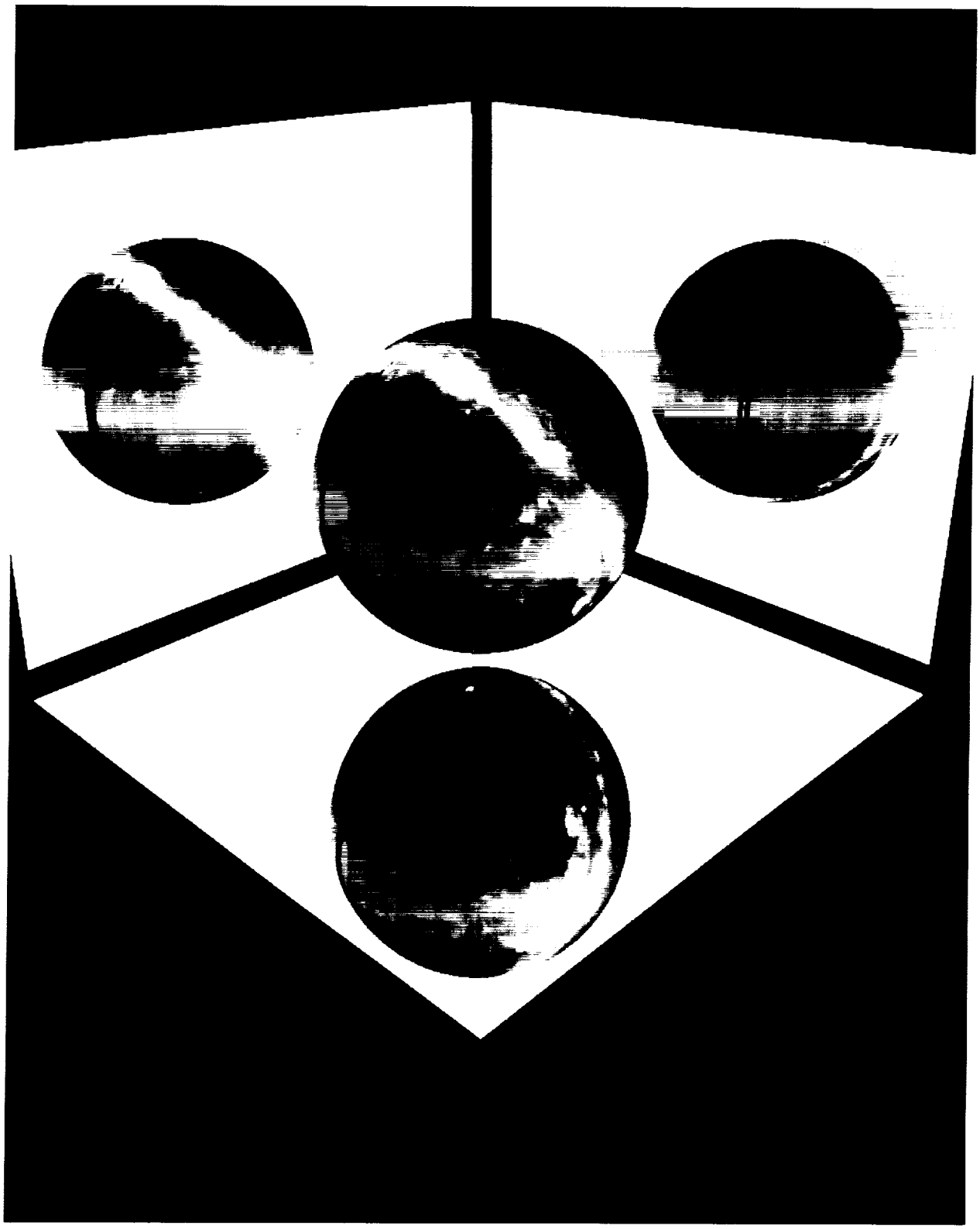

ORIGINAL PAGE
BLACK AND WHITE PHOTOGRAPH

Goddard's analog model of the magnetosphere is a generalization of Shaw's dripping-faucet model.

PLANETOLOGY

A LAYER THERMOCLINE MODEL FOR THE SATURN ATMOSPHERIC CIRCULATION

The observed cloudtop motions of Jupiter and Saturn continue to defy any comprehensive explanation. Both planets exhibit superrotating equatorial currents and, at higher latitudes, an alternating, axisymmetric pattern of counterflowing jet streams. As revealed by Voyager imaging measurements, Saturn has an equatorial velocity exceeding 400 ms^{-1} and at least three alternating jet pairs with speeds of about 100 ms^{-1}. The horizontal scale of the motion on both planets appears to be diagnostic of two-dimensional vorticity-conserving motion as exhibited, for example, by oceanic gyres. It still is not known how the appropriate stratification, typically associated with shallow, quasi-barotropic dynamics, is supported within a deep, internally convective atmosphere without a rigid lower bottom. Some isolated features of the Jovian dynamics have been simulated with elaborate numerical models that dramatically illustrate the importance of eddy-mean flow exchanges. However, given the present ignorance of the deep atmospheric structure, these models necessarily require the specification of artificial lower boundary conditions and forcing as well as the experimental adjustment of several parameters.

To further elucidate the possible physical mechanisms, a new conceptual theory for the Saturn (and Jupiter) atmospheric circulation has been investigated, emphasizing dynamic processes analogous to the inertial control of oceanic boundary currents such as the Gulf Stream. The theory is based on the hypothesis that the Saturn zonal circulation is controlled by the global homogenization of the potential vorticity for a shallow wind layer with a convectively stratified lower interface or "thermocline" overlying a static interior envelope. The potential vorticity for the assumed configuration is the ratio of the relative plus planetary vorticity to the effective variable depth. With a sufficiently uniform eddy stirring, this ratio is constant with latitude. On the global scale of latitudinal variation, the absolute vorticity is dominated by the local normal projection of the planetary rotation (the Coriolis parameter), so that the effective thickness must vary from its polar value to nearly zero close to the Equator. A second constraint on the variation of the flow depth is provided by the geostrophic balance of the Coriolis acceleration of the motion, measured against its buoyantly adjusted gravity, in proportion to the thermocline slope. The combined application of the two constraints, together with imposed boundary conditions, provides a simple but powerful relationship between the current velocity, its characteristic deformation scale, and the vertical stratification of the system.

The development of the Saturn circulation model requires a consideration of the metrical variation with latitude of the potential vorticity on a sphere and the buoyant

The center globe is a map of the sky in three of the infrared wavelengths that DIRBE will see. Three reflecting mirrors show the parts of the globe that are hidden from view.

stratification of the no-motion level in the upper convection zone. The decrease in the planetary vorticity and thermocline depth toward low latitudes is then consistently correlated with an increase in the equatorial flow velocity that is dynamically analogous to the westward intensification of the Gulf Stream. Over latitudinal intervals comparable to the internal deformation scale of the system, the gradient of the absolute vorticity is dominated by the mean flow curvature, in balance with the depth variation. When coupled with the geostrophic balance for the assumed convective thermocline, a correlation results between prograde motion and the latitudinal steepening of cyclonic (negative) flow shear, implying a periodic reversal in vorticity and depth variations, in step with the alternation of the jets.

The mathematical statement of these ideas leads to a simple governing equation that, with the imposition of appropriate latitudinal boundary conditions, admits approximate analytic solutions containing a single free parameter corresponding to the number of high-latitude jets or, equivalently, their horizontal deformation scale. With n=3 for Saturn, corresponding to an inverse meridional wavenumber $L \approx$2,900 km, the model indicates an equatorial flow velocity of $2\Omega\ a(L/a)^{4/3} \approx 340\ m\,s^{-1}$, with a minimum latitude for the cyclonic shear of $(L/a)^{2/3} \approx 8°$ and a polar jet speed of $\Omega a(L/a)^{5/3} \approx 62\ m\,s^{-1}$. (Here Ω is the rotation frequency and a the radius of the planet.) The accompanying figure displays the depth and velocity profiles obtained from the approximate solutions appropriate to Saturn and Jupiter. These bear a remarkable resemblance to the shape and amplitude of profiles assembled from Voyager cloud-tracked wind measurements. Further work must be devoted to understanding the way in which convective or diabatic processes, perhaps in conjunction with layered condensation and ortho-para hydrogen disequilibration, might provide the assumed stirring and stratification (or forcing) for the proposed model. High-resolution microwave observations at 10-cm wavelengths from the proposed Cassini mission to Saturn will provide an important test of the proposed deep atmospheric structure.*

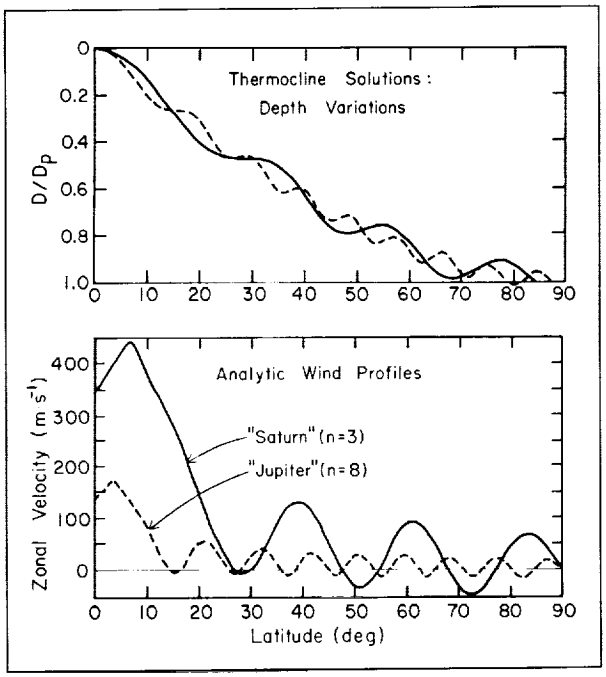

The approximate analytic solution to the convectively layered, potential vorticity conserving thermocline model for the zonal circulation of Saturn and Jupiter.

**This research was performed in collaboration with graduate student James T. Lumetta of the Department of Physics at Columbia University.*

Contact: Michael D. Allison (Code 640)
(212) 664-5554

Sponsor: Planetary Atmospheres Program

Dr. Michael D. Allison earned his PhD at Rice University and has worked at Goddard for 5 years. Currently, he works in the Goddard Institute for Space Studies and performs theoretical studies on the dynamics of planetary atmospheres. In the recent past, he has provided research and planning support for the Institute's Photopolarimeter Radiometer experiment on the Galileo mission to Jupiter. Dr. Allison also served on the joint European Space Agency/NASA Science Working Group for the proposed Cassini mission to Saturn and Titan, a Saturn moon.

TURBULENCE MODELING OF THE PLANETARY BOUNDARY LAYER

The climate group at the Goddard Institute for Space Studies has continued the development of their global climate model to further refine predictions concerning the future climate of the Earth. These predictions depend on the reliability of the many ingredients involved, such as the modeling of the oceanic circulation and the planetary boundary layer. The credibility of these predictions

depends heavily on whether the parameters of the various ingredients have been defined correctly and the physics correctly understood. It has been known for many years that one of the most critical ingredients of any global climate model is the heat flux through the planetary boundary layer. The major difficulty in the physical modeling of the heat flux is that the transport of thermal energy occurs not through diffusion but through the action of turbulence. In recent years some progress has been made in understanding turbulence and in applying this understanding to the development of better turbulence models. The most fundamental modeling, however, has been for the idealized case of homogeneous, isotropic turbulence, whereas the planetary boundary layer turbulence is dominated by effects that are essentially inhomogeneous and anisotropic.

Lacking a satisfactory physical model of turbulence, climate researchers have had to rely on purely empirical relations in modeling the turbulent heat flux. These empirical relations contain free parameters that are fixed to yield reasonable results for a limited data set. Thus, it is not possible to make theoretical predictions that are sensitive to the values of these parameters. These free parameters should be fixed by a model of turbulence.

Goddard researchers have developed and refined a pragmatic turbulence model that has been tested against a wide variety of laboratory and astrophysical turbulent flows, yielding good results. This turbulence model is now being applied to the needs of climate researchers. In particular, the turbulent transport of heat in the planetary boundary layer can be better modeled by the use of this physical turbulence model.

The essential ingredient of the turbulence model is the instability function, which defines the rate at which energy is supplied to turbulence. First, the instability problem associated with the planetary boundary layer must be solved. It is known that a linear instability model is deficient. Rather, a secondary instability model must be adopted that can accurately predict the critical Reynolds number at which channel flow undergoes transition from laminarity to turbulence (the linear instability model predicts a value five times too large). Due to the complexity of the secondary instability, the Reynolds number has been computed only for a limited number of flows. It has not yet been computed for the type of flow that interests climate researchers, i.e., a planetary boundary layer flow involving a mean velocity, temperature gradients, rotation, and buoyancy.

The growth rate of the secondary instability requires calculation of the primary flow field. The primary flow is that of a narrow-gap Ekman flow driven by a constant mean pressure gradient. The standard Ekman velocity profile results from the assumption that the angular velocity vector is transverse to the surface of the Earth. Since the effect of latitude variation must be included, the equations for the velocity profile have been generalized to include an oblique component of rotation. At the Equator, where the deviation from the standard Ekman profile is greatest, the mean flow becomes a Poiseuille flow, whereas at the pole the mean flow becomes the standard Ekman spiral.

Knowing the primary flow, researchers can calculate the secondary flow. The primary flow is one-dimensional in the sense that the velocity field depends on only one spatial variable, altitude. A secondary flow, which is two-dimensional, is added to the primary flow. The composite flow field is substituted into the Navier-Stokes equations resulting in a set of nonlinear partial differential equations to be solved exactly for the secondary field. The two-dimensional field is assumed to be periodic with a certain wavelength and steady in a Galilean frame comoving with a certain phase velocity. The secondary flow field is expanded in a truncated Fourier-Chebychev series yielding a set of nonlinear algebraic equations for the expansion coefficients. It is known that neutrally stable, finite amplitude, two-dimensional modes exist: for a given Reynolds number, Ekman number, Richardson number, latitude, and direction of the geostrophic wind, solutions of this set of equations satisfy a nonlinear dispersion relation between the energy, the wavelength, and the phase speed of the secondary flow. These equations are solved numerically using a Newton-Raphson method.

The two-dimensional secondary flow is perturbed by small three-dimensional disturbances. The resulting equations are then linearized in the perturbed quantities. This results in an eigenvalue equation for the growth rate of the secondary instability.

This growth rate is the instability function required for the Goddard model of turbulence. Application of this model then yields values for the turbulent viscosity and turbulent conductivity. These transport coefficients are then parameterized as functions of a given Reynolds number, Ekman number, Richardson number, latitude, and direction of the geostrophic wind. The results will be utilized in developing Goddard's global climate model.

Contact: Vittorio M. Canuto (Code 640)
(212) 678-5571
Gregory J. Hartke (Code 640)
(212) 678-5573

Sponsor: Research and Technology Operating Plan, NASA Headquarters

Dr. Vittorio M. Canuto's technical interests lie in the theory of turbulence with applications to Earth and planetary sciences. He has 21 years' experience at Goddard and currently works with the Goddard Institute for Space Studies. Dr. Canuto holds a PhD in physics from the University of Turin in Italy.

Dr. Gregory J. Hartke works at Goddard Institute for Space Studies. He investigates turbulence theory and its applications to geophysical and astrophysical phenomena. Dr. Hartke received his PhD in astronomy from the University of Massachusetts and has 5 years' experience at Goddard.

SOLAR PHYSICS AND ASTRONOMY

MULTISPECTRAL IMAGING OF THE SOLAR CORONA

The Sun, a star so close to the Earth that researchers can study its atmosphere in great detail, provides a unique laboratory where theories of plasma physics on astrophysical scales can be evaluated with actual observations of its outer atmosphere, the tenuous corona. As this corona expands into interplanetary space, it interacts with the Earth through the propagation of high-speed wind streams that can result in geomagnetic disturbances. Furthermore, during large solar flares, energetic particles that can constitute a hazard to orbiting astronauts also originate in the low corona. Discovering how the corona is propelled outward at high velocity would provide a significant advance in understanding the outer atmospheres of stars in general as well as the origin of the interplanetary plasma of our own solar system.

To attempt to identify the characteristics of energy sources and driving forces in the corona, Goddard scientists and technicians have prepared and flown an extreme ultraviolet (EUV) imaging spectrograph called the Solar EUV Rocket Telescope and Spectrograph. This instrument for the first time displays the complexity of the lower corona in image form and provides detailed spectroscopic measurements of the corona's physical state. By observing the rich EUV spectrum between 240Å and 450Å , a region with numerous emission lines of highly ionized magnesium, silicon, and iron, each produced over a relatively narrow band of plasma temperature, researchers can characterize the corona over the solar disk without interference from the 6,000-°K blackbody radiation from the Sun's photosphere. The instrument flew on a Nike-Black Brant rocket in May 1989 and recorded successfully both images and spectra of a strong region of solar magnetic activity.

The accompanying illustration presents two of many coronal images recorded during the flight. The two images, taken over the same field of view of about 200,000 × 320,000 km on the Sun, represent emission from coronal plasmas in two different temperature ranges: frame (a), recorded in the light of fifteen-times ionized iron at 335.4 Å, is from plasma at about 3×10^6 °K, while (b), recorded in the light of eight-times ionized magnesium at a wavelength of 368.1 Å (36.81 nm), is emission from plasma at about 1×10^6 °K. A schematic representation of the complex photospheric magnetic fields underlying this region of the corona is shown in the third frame. The EUV images, by their strikingly different appearances, demonstrate that tightly confined individual loops at widely differing temperatures can exist in close proximity to one another. Such differences in temperature most probably result from differing levels of localized coronal heating and may be related to the strength of the underlying magnetic field. The most tightly confined emission [observed as the brightest feature in the central portion of the high temperature image, shown in (a) of the figure] probably represents particularly intense coronal heating associated with strong chromospheric activity and could be the beginning of a small flare. Spectral signatures of all EUV-emitting features along the center lines of the images were also recorded. These data will be used to derive information on

ORIGINAL PAGE
BLACK AND WHITE PHOTOGRAPH

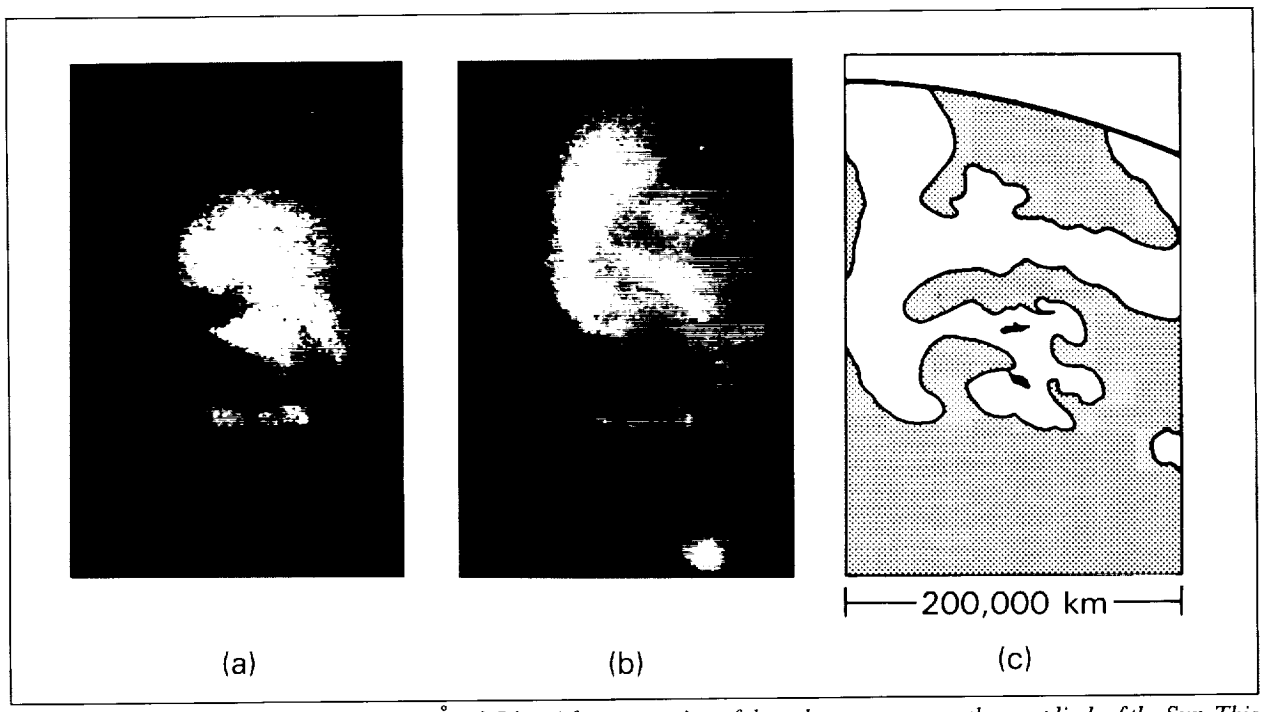

(a) Extreme ultraviolet emission at 335.4 Å (33.54 nm) from a portion of the solar corona near the west limb of the Sun. This radiation is produced by 15-times ionized iron atoms (Fe XVI) at temperatures in the range of 2.5-3.5 × 10^6 °K. (b) Emission from the same portion of the corona in the radiation of 8-times ionized magnesium (Mg IX) at 368.1 Å, at about 1 × 10^6 °K. (c) A schematic representation of the distribution of magnetic polarities of the Sun's longitudinal (line of sight) magnetic field [courtesy of Dave Speich, National Oceanic and Atmospheric Administration (NOAA)] within the data frame of the EUV photographs. Positive magnetic polarity is indicated by the clear areas and negative magnetic polarity by the shaded areas. Sunspots are shown in black. Strongly enhanced coronal emission is associated with the particularly complex field distribution in the center of the data frame. A portion of the Sun's limb is indicated by the arc in the upper region of this data frame.

the density, temperature, and dynamic states of the plasmas (plasma turbulence and mass flows). Combining the images and spectral data will provide new insight into the mechanisms that produce and sustain highly confined loops of plasma, which must also be present in the coronae of many other stars as well as on the Sun.

Contact: Werner M. Neupert (Code 680)
(301) 286-3756
Roger J. Thomas (Code 682.1)
(301) 286-7921
Gabriel L. Epstein (Code 460)
(301) 344-4869

Sponsor: Supporting Research and Technology Program, NASA Headquarters

Dr. Werner M. Neupert is Principal Investigator of the Solar EUV Rocket Telescope and Spectrometer, Co-Investigator on the EUV Imaging Telescope for Solar Heliosphere Observatory, and Project Scientist for NASA sounding rockets. Dr. Neupert received a PhD from Cornell University and has 28 years' experience at Goddard. He currently works in the Laboratory for Astronomy and Solar Physics.

Dr. Roger J. Thomas is Principal Investigator for the development of Solar EUV Optics in the Laboratory for Astronomy and Solar Physics. He is also Co-Investigator for Solar EUV Rocket Telescope Spectrometer, for the Coronal Diagnostic Spectrometer for the Solar Helioscope Observatory, and for solar ultraviolet measurements of emitted radiation for the helioscope project. Dr. Thomas received his PhD from the University of Michigan and has 19 years' experience with Goddard.

Dr. Gabriel L. Epstein was Instrument Manager for the last flight of the Solar EUV Rocket Telescope and Spectrograph. He is currently Instrument Manager of

the Orbiting Solar Laboratory (OSL) Project. Dr. Epstein earned his PhD in atomic physics from the University of California at Berkeley and has 19 years' experience at Goddard. He has received the NASA Special Achievement Award for Exceptional Service in the Performance of Official Duties.

DEVELOPMENT OF THE RED GIANT BRANCH (RGB) IN STELLAR SYSTEMS

Astronomers have long recognized that stellar systems, such as the globular clusters in the Milky Way and in the Magellanic Clouds, hold the key to many important astrophysical problems. For this reason, extensive observations have been made, both of the individual stars and of the integrated properties of many stellar systems. In order to interpret these and similar observations to be obtained with the Hubble Space Telescope (HST), it is necessary to understand how the stars in a stellar system evolve.

The figure shows the evolution from the main sequence to the RGB for five stars of intermediate to low mass. Most of the evolutionary lifetime of these stars is spent on the main sequence, where hydrogen is slowly burned into helium at the center. Once the central hydrogen supply is exhausted, all of the nuclear burning shifts outward to a thin, hydrogen-burning shell surrounding the newly formed and presently inert helium core. In response, the stars in the figure rapidly evolve to the RGB. Their subsequent evolution up this branch continues until the temperatures within the helium core reach the value of 10^8 °K needed for the next set of nuclear reactions—namely, the burning of helium into carbon.

There is a fundamental dichotomy in the evolutionary properties of the RGB between intermediate- and low-mass stars. In intermediate-mass stars, the temperatures within the helium core are relatively high, and as a result these stars ignite helium at rather low luminosities shortly after reaching the RGB (see the figure). In low-mass stars, however, the core temperatures are significantly lower, and consequently the core must then grow much larger in mass before helium burning can begin. Low-mass stars can therefore reach luminosities along the RGB that greatly exceed the maximum luminosities of the intermediate-mass stars. In addition, the densities within the core of a low-mass star reach such high values that the core becomes electron degenerate. Under these conditions, helium ignition leads to a helium flash during which the core's energy output is briefly comparable to the luminosity of an entire galaxy.

This dichotomy in the RGB evolution of intermediate- and low-mass stars is so important for the observable properties of a stellar system that it is generally termed the RGB "phase transition." During this transition there is a change not only in the luminosity, but also in the amount of time that a star spends on the RGB. Thus, the phase transition is accompanied by the appearance of many bright RGB stars that, in turn, greatly increase the RGB contribution to the integrated light of a stellar system.

Extensive calculations have been carried out at Goddard in collaboration with the University of Bologna to investigate the RGB phase transition in detail. Evolutionary sequences consisting of approximately 90,000 stellar models have been computed for 100 intermediate- to low-mass stars over a range of compositions. Using these results, researchers have been able to quantify the properties of the RGB phase transition much more precisely than was previously possible. In particular, researchers

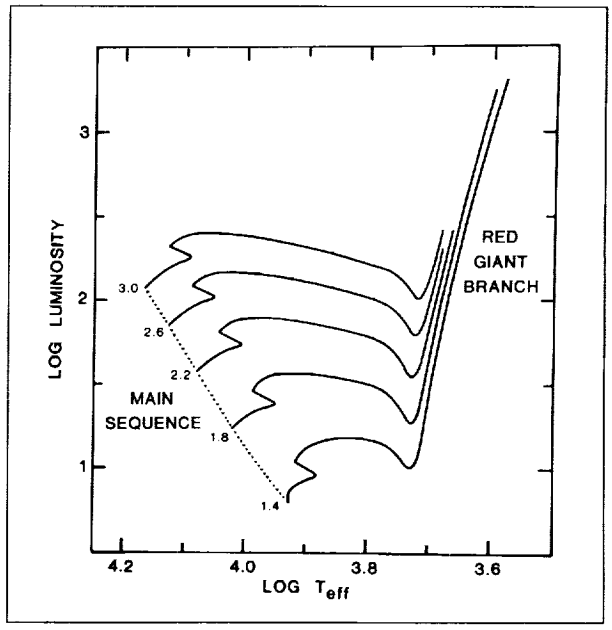

Variation in the luminosity in solar units and the effective (or surface) temperature in °K for five stars of approximately solar composition during the evolution from the zero-age main sequence (dotted line) to the onset of helium burning at the tip of the RGB. Each evolutionary track is labeled by its mass in solar units.

have found that the phase transition occurs quite abruptly with decreasing stellar mass and is therefore a sudden event in the life of a stellar system. Most surprisingly, researchers have found that the age at which a stellar system undergoes the phase transition—close to 600 million years—is virtually independent of the system's composition, providing astronomers with a useful tool for estimating the age of many stellar systems. Researchers have also been able to predict the number of bright RGB stars that should be observable in various stellar systems.

The present investigation of the RGB phase transition provides a good example of the strong interaction between stellar evolution theory and observation.*

**Italian astronomers Alvio Renzini and Laura Greggio of the University of Bologna carried out extensive calculations for this work.*

Contact: Allen V. Sweigart (Code 681)
(301) 286-6274

Sponsor: Office of Space Sciences, Laboratory for Astronomy and Solar Physics, Research and Technology Operating Plan

Dr. Allen V. Sweigart applies numerical models to understanding stellar evolution and interpreting space observations in the Laboratory for Astronomy and Solar Physics. Dr. Sweigart has 9 years' experience at Goddard and has won a Certificate for Outstanding Performance. He holds a PhD in astrophysics from Princeton University.

RESEARCH AMPLIFYING IMAGING DETECTOR

The Research Amplifying Imaging Detector is an intensified charge-coupled device (CCD) camera developed and tested at Goddard's Laboratory for Astronomy and Solar Physics for solar observations at EUV wavelengths, in the range 200 to 400 Å. This detector was developed for use in the Solar Extreme-Ultraviolet Rocket Telescope and Spectrometer sounding rocket program. Current plans call for flight in the autumn of 1991. A modified version of this camera has been chosen as the detector for the normal incidence spectrograph part of the coronal diagnostics spectrometer on the European Solar Heliospheric Observatory satellite.

The camera's basic design consists of a Varo 25-mm sealed microchannel-plate image intensifier tube coupled

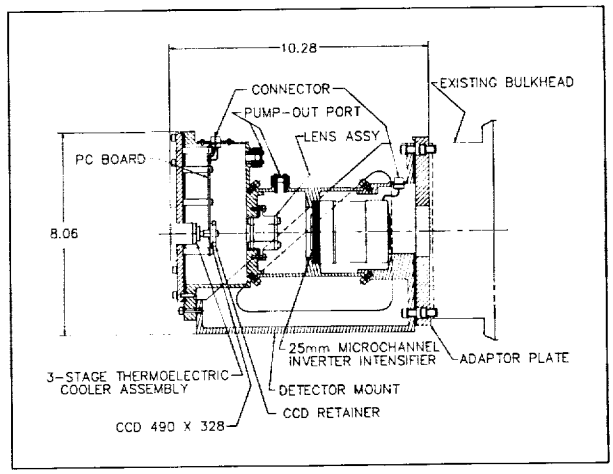

Diagram of the Research Amplifying Imaging Detector.

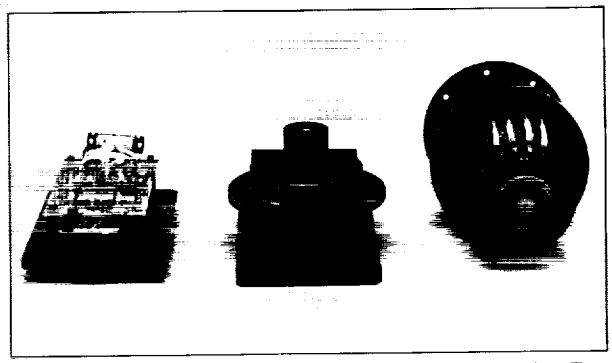

The components of the Research Amplifying Imaging Detector camera showing the microchannel-plate intensifier on the right, the lens assembly in the center, and the CCD camera with cooler and electronics on the left.

with a focusing lens onto a CCD detector (see the first and second figures). The front input window of the microchannel-plate tube, a fiberoptic faceplate, is covered with a thin coating of the phosphor tetraphenyl-butadiene, which converts EUV radiation into visible light. Optionally, there can also be a thin coating of aluminum that allows the EUV radiation through to the phosphor tetraphenyl-butadiene but keeps out any stray visible light. The visible light produced by the phosphor tetraphenyl-butadiene is carried down the fiberoptic channels to an S-20 photocathode inside the microchannel-plate tube; this process produces electrons. The electrons are focused and accelerated by electrostatic fields onto a microchannel-plate wafer. A potential field across the channels produces amplifications, so that for every electron entering one of the microchannel-plate channels, several thousand electrons exit at the other end.

ORIGINAL PAGE
BLACK AND WHITE PHOTOGRAPH

These electrons are then accelerated onto a P-20 phosphor coated on the inside face of the fiberoptic output window of the microchannel-plate tube, which reconverts the electrons into visible radiation. The image brightness is amplified by a factor of 7,000.

An f/2 lens is used to focus the image from the microchannel-plate tube onto a CCD detector. Using a lens to couple the image intensifier tube to the CCD has several advantages. First, the mechanical design is simplified because there is no physical contact between the two. Also, the lens allows one to magnify or demagnify the image to best match the pixel size of the CCD. The CCD used is a virtual-phase CCD with 490 × 328 pixels, each 24.4 μm on a side. To reduce the dark current and readout noise, the CCD is mounted on a thermoelectric cooler that maintains a temperature in the CCD of -30 °C. Electronics designed and built at Goddard control the CCD and convert the analog signal into digital format, which can be stored and displayed on a MicroVAX II computer. The third figure shows the camera assembled.

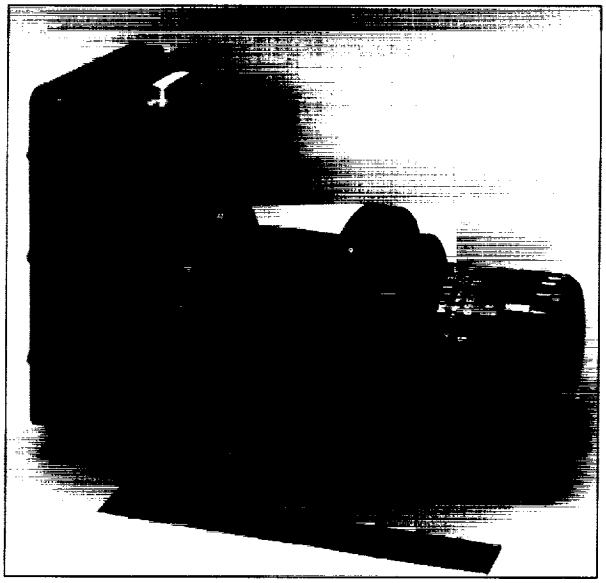

The assembled Research Amplifying Imaging Detector.

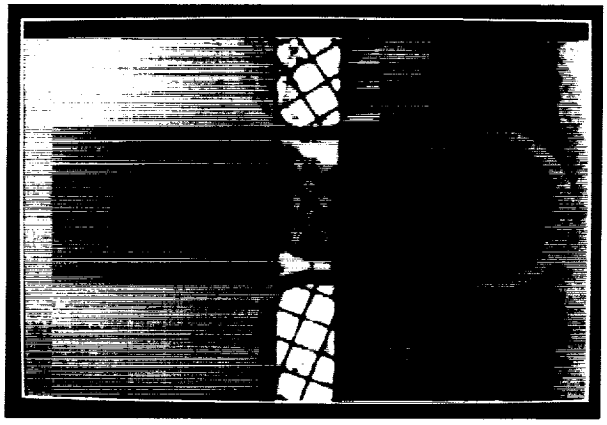

Image taken with the Research Amplifying Imaging Detector camera of the test grids used to determine system modular transfer function. The HeII λ304-Å line is in the center, and the HeII λ256-Å line is on the right.

The Research Amplifying Imaging Detector camera has been tested at Goddard at both visible and EUV wavelengths. The fourth, fifth, and sixth figures illustrate the results. The tests were designed to measure EUV spectral sensitivity, spatial resolution (both of components and of the system as a whole), noise, linearity, and dynamic range. To test the camera at these wavelengths, a vacuum tank was used, with a helium flow lamp and a grating to separate the λ304-Å line of helium. The λ256-Å and λ243-Å lines were also visible. Included in the dynamic range tests were measurements of the camera's ability to observe faint objects in the presence of saturated bright objects (the "multiple exposures" entry in the table). The results in the test program appear in the table.

The camera to be provided by Goddard for the coronal diagnostic spectrometer on Solar Heliospheric Observatory will be modified in several aspects. The electrostatically focused microchannel-plate tube will be placed with a proximity-focused tube. Also, the current CCD chip will be replaced by a chip with a larger format, 1,024 pixels on a side. Between the microchannel-plate tube and the lens

Research Amplifying Imaging Detector Camera (Multiple Exposures)

Sensitivity	photons/s/pixel
	8 photons/count
Resolution	5-percent modular transfer function
	Function at 20 lp/mm
Noise (background)	5 counts
Noise (image)	1-2.5 percent
Dynamic range (single exposure)	700
Dynamic range (multiple exposures)	22,000

ORIGINAL PAGE
BLACK AND WHITE PHOTOGRAPH

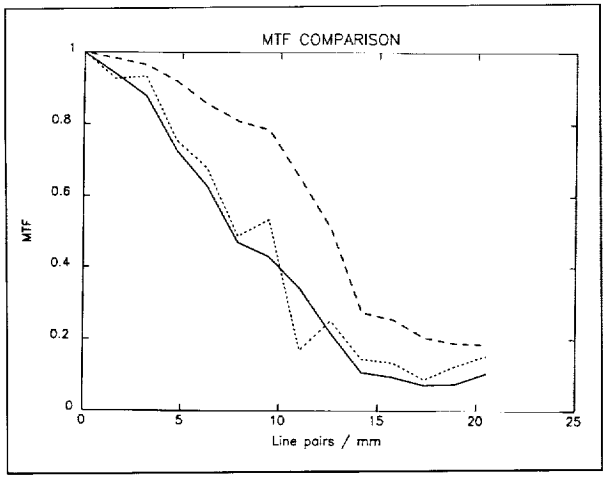

Measured modular transfer function curves for the lens and CCD alone (top curve), total system in visible light (solid line), and total system in the EUV range (lower dashed line).

will be a fiberoptic formatter, which will take a rectangular image with 2,048 × 512 pixels, move to the left half over the right half, and produce an image with 1,024 × 1,024 pixels to match the CCD format. The lens coupler will magnify the image onto the CCD so that the effective pixel size at the entrance window of the image intensifier tube will be 12.5 μm, even though the CCD pixel size will be greater. Using a faster lens is currently being considered. Improvements in the electronics should lead to lower noise characteristics and greater sensitivity.

Contact: William T. Thompson, Applied Research Corporation (Code 682)
(301) 286-2040

Marvin Swartz (Code 682)
(301) 286-5616

Sponsor: Laboratory for Astronomy and Solar Physics, Solar EUV Rocket Telescope and Spectrometer Project

Dr. William T. Thompson implements computer programs and conducts data analysis for solar research in the Laboratory for Astronomy and Solar Physics. He has worked at Goddard for 5 years and earned his PhD in astronomy from the University of Massachusetts.

Mr. Marvin Swartz is an aerospace technologist in the Solar Physics Branch. He works on the development of the EUV imaging detector and on calibration of spectrometers and detectors for flight on the Solar Heliospheric Observatory and for rockets. Mr. Swartz received a Superior Accomplishment Award for developing an imaging detector for use in the EUV wavelengths region. He has 23 years' experience at Goddard and holds a BS in physics from Wake Forest University.

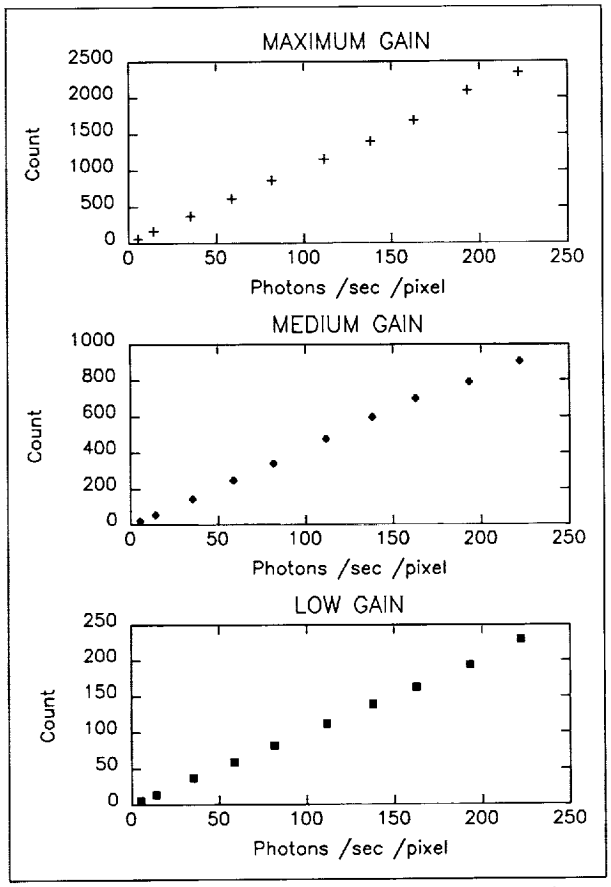

Plots of detector counts as a function of input HeII λ304 Å light. Each curve is for a different microchannel-plate setting.

ARE SOLAR FACULAE MOUNTAINS?

Faculae have puzzled solar physicists since their discovery. Latin for "torches," these bright features are even more important than sunspots for providing variations in the solar constant. Their primary energetic importance is indicated by their appearance in the photospheric continuum radiation, unlike other solar features, such as flares, coronal eruptions, prominences, and mass ejections.

Thermal, one-dimensional models of facular structures have been proposed but have failed to provide a self-consistent description. The so-called well model, used primarily for sunspots, fails to describe the contrast behavior of faculae. This is not surprising because sunspots have a contrast behavior opposite to that of faculae. Sunspots appear most prominently at disk center and disappear near the limb, whereas faculae are invisible at disk center but bright near the limb. Additionally, the features have different colors, with sunspots appearing red and faculae, blue. These differences suggest that faculae may have a geometric structure significantly different from that of sunspots. A few years ago, a theoretical investigation led the authors to conclude that faculae may be hillocks, rather than the wells suggested for the sunspot geometry. To shed light on such differences in geometry, these researchers have recently examined some relevant observational evidence.

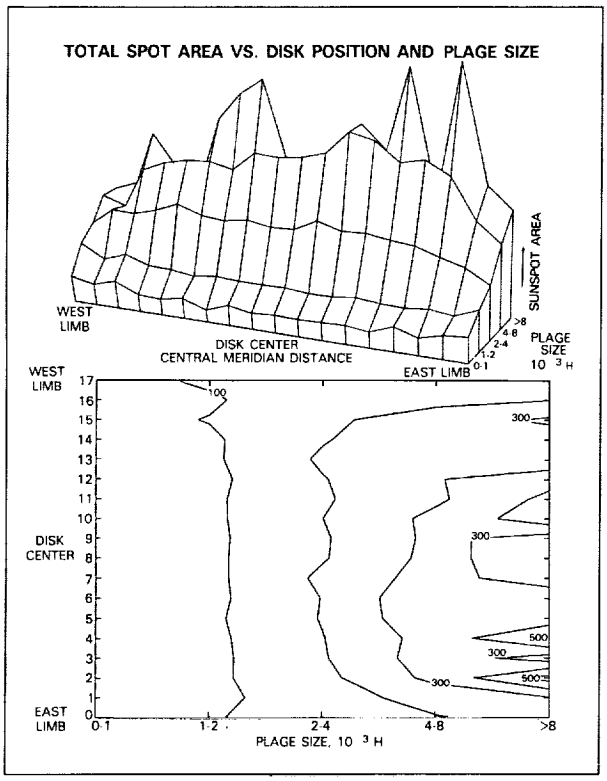

Shown in two different formats is the average sunspot group area (given in millionths of a solar hemisphere) as a function of facular (plage) size and disk position. The top format is a three-dimensional view, and the lower format is a conventional contour map. Large plage correspond to large spot areas. For most groups, the total sunspot area decreases when the limbs of the Sun are approached (even though they are corrected for foreshortening). The effect, however, virtually disappears when the faculae (plage) are small, suggesting that the effect is facular related. This impression is further strengthened when one notices that for the western groups, the effect dominates even more, supporting the view that the following plage (which are larger than the preceding ones) are responsible for blocking the sunspot areas there.

In view of the proposed hillock geometry for faculae, they asked whether faculae can "blanket" sunspots—i.e., whether faculae can obscure features, such as sunspots, which are behind them, when both features are near the Sun's limbs. To address this question, they have graphed average sunspot areas and counted numbers per McMath plage region versus disk position and plage size (used as a proxy for facular areas), using the solar activity data published by NOAA. The data cover almost two whole solar cycles, a period from 1966 through 1982, containing information on roughly 8,000 active regions.

The figure dramatically illustrates the blanketing effect. Total sunspot areas (umbra plus penumbra—to avoid the Wilson effect) are presented, corrected for foreshortening, so that, if unobscured, they should have a constant area as they rotate across the solar disk. Large sunspot areas are generally associated with large facular areas. As the features approach the Sun's limb, however, the sunspot areas decrease, particularly for large facular sizes. On the other hand, when the faculae are small, the sunspot areas are generally constant across the solar disk. The decrease in total area observed is not the Wilson effect, since this influences only the relative sizes of penumbral areas due to geometric foreshortening and does not affect the projected total area. The data are inexplicable except by allowing that the faculae are blocking the appearance of the sunspots behind them. Facular hillocks could do this, but facular wells could not!

This blanketing effect by the faculae is further substantiated by the slight east-west asymmetry in the figure. For large faculae, the sunspot areas are reduced more on the west limb than on the east limb. It is well known that plage and faculae tend to trail sunspots as they rotate across the solar disk, with larger areas following the active region. This means that when the active region is on the west limb of the Sun, the larger facular areas are in front of the main centrally located spot areas and thus are in a better position to shield them

from view. Interestingly, the sunspot areal decreases occur in amounts directly related to the surrounding facular (plage) size. These reductions also occur for the number of sunspots per McMath plage region, further supporting the facular shielding view (as opposed to some sort of sunspot geometry explanation). A computer-based geometric model for faculae in a hillock form of roughly 200-km height is consistent with the observational findings obtained. The findings indicate that these features are truly mountainous (dwarfing Everest by a factor of 25), particularly considering that the solar gravity is 27 times the Earth's.

If faculae are indeed mountains and can obscure sunspots, model studies are needed to understand the physics shaping them. A number of questions need be addressed. If these features stick up above the photosphere, they require support from below. How does this occur? The facular gases will not be in hydrostatic equilibrium with their surroundings, but must expand into the relative vacuum of the neighboring solar atmosphere. Does this cause the enhanced chromospheric densities above faculae? If so, what controls the rate of expansion? And what is the role of the magnetic field?

Contact: Kenneth H. Schatten (Code 610.1)
(301) 286-3831
Hans G. Mayr (Code 614)
(301) 286-7505

Sponsor: Laboratory for Atmospheres

Dr. Kenneth H. Schatten, who received his PhD from the University of California at Berkeley, is a solar physicist with the Solar Radiation Office of the Laboratory for Atmospheres. Dr. Schatten has been with Goddard since 1969 and has received several awards for his scientific achievements.

Dr. Hans G. Mayr is an atmospheric scientist with the Dynamics Explorer and Pioneer Venus projects. Dr. Mayr, who holds a PhD from the University of Graz in Austria, has 21 years' experience with Goddard.

SOLAR WIND TURBULENCE AND ACCELERATION

The Sun produces a continuously flowing wind of ionized particles that has an average speed of 400 km/s but that can reach 800 km/s or more in high-speed streams. The average wind is widely believed to be produced by the thermal pressure gradients that exist naturally in the gravitationally stratified, hot solar corona, but this mechanism has long been known to be inadequate to explain the high-speed flows. One possible resolution to the problem of generating fast wind is that the Sun generates hydromagnetic waves of sufficient flux to provide the extra needed momentum. Such fluctuations are difficult to observe near the Sun, and thus it is of interest to try to extrapolate scientific knowledge of the interplanetary fluctuations as observed, for example, by Helios, International Sun/Earth Explorer, and Voyager spacecraft back to regions within the closest approach—60 solar radii—of any solar wind probes. This extrapolation requires knowing the detailed characteristics of the magnetic and plasma measurements and understanding the dynamics of the fluctuations well enough to have confidence in an extrapolation procedure. In collaboration with Bartol Research Institute, Goddard researchers have recently made considerable progress in these areas.

This research has shown that the interplanetary fluctuations do not behave as simple, noninteracting linear waves, but that nonlinear interactions are important at all heliocentric distances so far observed. Both the spectrum of the waves and the correlation between the velocity and magnetic field fluctuations change as the wind moves outward, and neither effect would be expected in linear theory. The velocity-magnetic field correlation is initially characteristic of waves propagating outward from the Sun, as might be expected for Alfvén waves generated in the solar corona, but with increasing distance there are progressively more fluctuations present that are not outward propagating (in the frame of the wind) and, therefore, must be generated locally as the wind moves outward. The research staff have studied the evolution in this correlation using a compressible magnetohydrodynamic simulation code. The results for the evolution of the velocity-magnetic field correlation in the case of a shear layer between high- and low-speed flows in the presence of a mean magnetic field (directed from left to right) are shown in the accompanying figure. Red represents the initial outward traveling waves. As time goes on, one first sees the appearance of locally generated fluctuations (yellow through blue) in the shear layer, and at later times the whole region has become well mixed in propagation directions with alternating red and violet ("inward") regions. These pictures are in good qualitative agreement with the observed evolution

ORIGINAL PAGE
COLOR PHOTOGRAPH

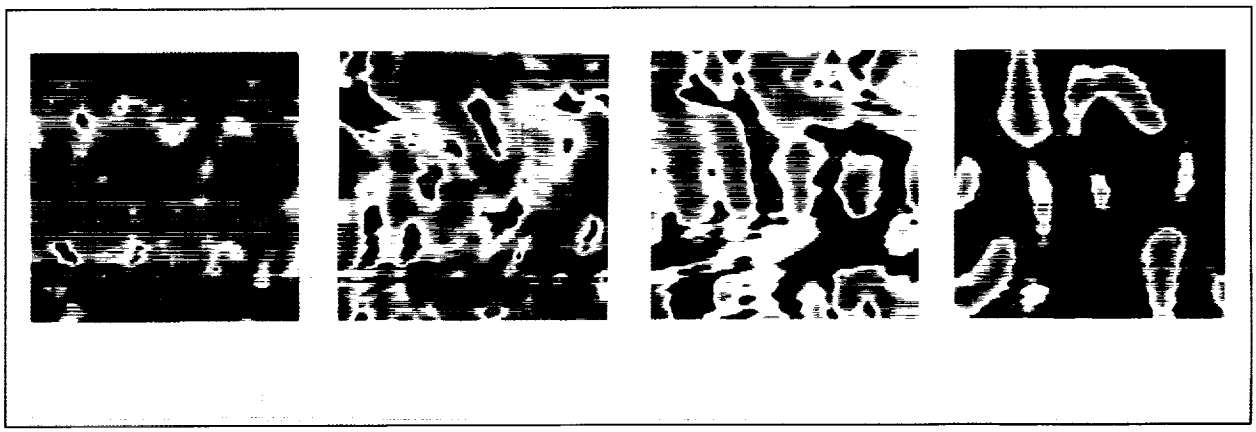

Figure showing the evolution of small-scale, initially purely "outward" propagating waves (red) to more mixed and "inward" propagation (violet) within and near a shear layer. There is a flow left to right through the middle of the box and the reverse at the edges. At T = 1 eddy-turnover time (a), the pure red has begun to be eroded away in the shear regions, and as time progresses (T = 2, b; T = 4, c), the influence of the flow is felt farther from the shear layer, finally (T = 25, d) resulting in an essentially random distribution of propagation directions.

in the solar wind, and this agreement increases confidence in a magnetohydrodynamic turbulence description of many interplanetary phenomena.

Simulations such as those illustrated here may help explain processes closer to the Sun. In particular, as aids, along with detailed data analysis, in extrapolating the level of magnetic and velocity fluctuations back to the Sun, they help researchers determine the role of waves in accelerating high-speed streams. At the larger scales in the solar wind, it has often been suggested that the level of fluctuations "saturates" when the fluctuations in the magnetic field become comparable to the mean magnetic field, but this relationship is not borne out by observations. If saturation did occur, then a high level of fluctuations, sufficient to accelerate the wind, could exist close to the Sun without a correspondingly high level of fluctuations near the Earth. From the slow evolution of the large scales seen in the simulations, researchers may infer that these scales probably evolve nearly as in a simple noninteracting wave case, which gives a way of extrapolating the large-scale wave power to the Sun. The evolution of the smaller scales involves a dissipation of waves to heat that, from both theory and simulation, should be slower as the mean field increases and thus should be slower nearer the Sun. This line of reasoning leads to the conclusion that the wave levels predicted near the Sun by a simple theory of noninteracting waves will not be wrong by more than a factor of two or so and, thus, that the fluctuations will not have enough power to accelerate high-speed streams. If correct, this result forces scientists to look elsewhere for the source of the acceleration, perhaps to nonthermal electron distributions in the solar corona.*

**The compressible magnetohydrodynamic simulation code cited in the article was developed for the study of nonlinear turbulent evolution by S. Ghosh, a postdoctoral associate in Goddard's Visiting Scientist Program, and W. Matthews of Bartol.*

Contact: D. Aaron Roberts (Code 692)
(301) 286-5606

Sponsor: Space Physics Division

Dr. D. Aaron Roberts studies the dynamics and evolution of the interplanetary medium using data analysis, numerical simulation, and analysis methods. Dr. Roberts has established many properties of interplanetary fluctuations in magnetic fields, velocity, and density and found strong evidence that the solar wind is a dynamically evolving turbulent medium. He was Co-Investigator on two NASA Research and Analysis grants to Goddard and on a Director's Discretionary Fund grant. He has 4 years' experience at Goddard and holds a PhD in physics from the Massachusetts Institute of Technology.

EXTRATERRESTRIAL PHYSICS

A DYNAMICAL ANALOG MODEL OF GEOMAGNETIC ACTIVITY

Geomagnetic activity is a direct manifestation of solar wind-magnetosphere coupling. An outstanding issue in solar-terrestrial physics is understanding how the linked physical processes within the magnetosphere evolve as the system goes from weak to strong geomagnetic activity levels. Early studies of solar wind coupling concentrated on the method of cross-correlation analysis. These kinds of studies revealed that relatively modest, isolated substorms were closely related to the amount of southward interplanetary magnetic field carried up to the dayside magnetopause by the solar wind during the hour preceding substorm onset. Later analyses have extended this work and have attempted to find the "best" combinations of solar wind parameters to describe and predict both moderate and strong magnetospheric activity. However, it is probably fair to say that these solar wind-magnetosphere coupling studies, using traditionally available statistical techniques, have come nearly to the useful limit of the methods. Past work has demonstrated that geomagnetic activity results from nonlinearly coupled physical processes. Moreover, the strength and nature of the coupling changes dramatically as the magnetosphere is driven harder and harder by increasing energy input. Thus, the authors have recently suggested that, in fact, the magnetospheric system evolves to an essentially chaotic state in which the traditional statistical approaches no longer shed much light. Nevertheless, the authors believe that through the use of the tools of deterministic chaos theory, they can gain considerable insight into the nature of energy transfer processes from the solar wind to the magnetosphere.

Goddard scientists have constructed an elementary dynamical analog model of the magnetosphere to study its possible transition into a chaotic state with increasing energy input. The model has its conceptual origin in the dripping-faucet analogy discussed by Hones. Hones noted that substorms represent the catastrophic release of energy in the sense that, at intervals, the magnetotail releases large amounts of stored energy. He likened this occurrence to the detachment of a droplet of water from a dripping faucet. In this picture, a blob or bubble of magnetized plasma (a plasmoid) pinches off within the magnetotail during the substorm expansion phase and is rapidly carried away into the downstream solar wind. The detachment of the plasmoid is accomplished by magnetic reconnection in the plasma sheet at ~20 R_E from the Earth. On the Earthward side of the neutral line, the magnetic field lines snap back, due to magnetic tension, into a much more dipolar configuration after the severance of the plasmoid. This reaction causes intense plasma injection events near synchronous orbit and causes major auroral disturbances.

In Hones' dripping-faucet analogy, the flow of energy into the magnetosphere is similar to the flow of water out of the faucet. The formation of the plasmoid is analogous to the formation of the water droplet. In the magnetotail case, the magnetic tensional forces are similar to surface tension in the water droplet. The expulsion of the plasmoid from the magnetotail is thought to be caused by open magnetic field lines extending out into the solar wind and enveloping the plasmoid like a slingshot. This expulsion force acts in analogy to gravity in the case of the dripping faucet. The sequence of energy storage in the magnetotail, plasmoid formation, and then release has been named the loading-unloading energy release mechanism.

The rather superficial analogy suggested by Hones may be much more profound than previously assumed. In fact, the dripping faucet is an example of a system capable of a chaotic transition; the system can change from periodic and predictable to aperiodic and quasi-random behavior as a single parameter, the flow rate, is varied. Shaw and coworkers have carried out an extensive experimental study of the dripping faucet. They found that for low flow rates, the faucet drips with a steady, clocklike pattern, but for high flow rates, while the drops may be separate and distinct, they fall in an irregular, nonrepeating pattern. According to Shaw, "As the flow rate is varied, many features of the phenomenology of nonlinear systems can be seen, including chaotic transitions, familiar and unfamiliar bifurcation sequences, hysteresis, and multiple basins of attraction."

Further, Shaw devised a simple mechanical analog model of the dripping faucet. The model consists of a variable mass hanging on a spring. The mass always increases with time at a constant rate except when the spring

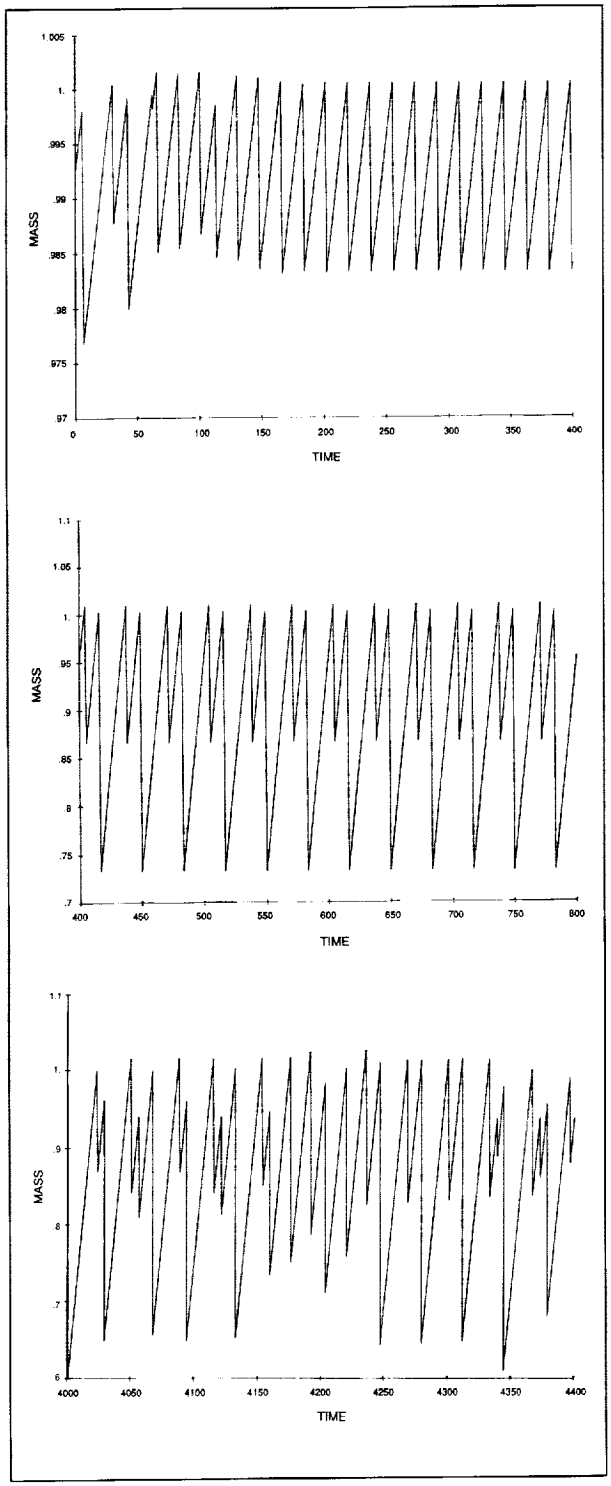

Evolution of mass with time for (a) a low mass loading rate, (b) an intermediate mass loading rate, and (c) a high mass loading rate.

becomes extended to a critical length. At the time of critical extension, a portion of the mass is dropped off. The portion of the mass that is dropped is set proportional to the downward velocity that the mass has when the critical spring extension is reached. Surprisingly, this model, which has only three degrees of freedom (viz., position, velocity, and mass) is capable of reproducing many features of the dripping-faucet data including much of the phenomenology of nonlinear systems described above.

Thus, a fluid containing an uncountable number of degrees of freedom often evolves with only a few of those degrees of freedom excited, and yet, a chaotic, unpredictable evolution is still possible.

Goddard's analog model of the magnetosphere is a generalization of Shaw's dripping-faucet model. The authors consider the energy loading-unloading cycle a central issue in the response of the magnetosphere to energy input from the solar wind. The authors hold the premise that magnetic flux and plasma can be transferred from the dayside of the magnetosphere into the magnetotail where it can be stored and then released as a plasmoid. Thus, the total quantity of plasma contained in the tail can vary upward and then downward as the loading and unloading portions of this cycle proceed. The analog model contains a variable mass (representing the total plasma in the tail) that increases and decreases in time according to the dynamic evolution of the system. In the analog model, the mass hangs on a spring which represents the resistance to the stretching and thinning that is provided by closed field line tension and plasma sheet pressure. Motion of the mass on the spring represents dynamic adjustment of the magnetosphere either in the form of natural modes of oscillation or in response to external driving forces such as solar wind energy loading. Goddard researchers have included friction in the analog model to represent the dissipation that results when the magnetosphere adjusts dynamically to loading.

The figure shows an example of the evolution of the mass with time in the Goddard analog model. Until $t \approx 150$, the system is in a transient phase. Following that time, the system is effectively in a limit cycle, and the mass evolves in a simple periodic fashion. This is a case in which the loading rate is small in the sense that it leads dynamically to simple one-period, periodic evolution.

In the low loading-rate regime, the general behavior that emerges is that the frequency of the periodic loading-unloading cycle remains constant as the loading rate is varied, but the amplitude of the loading-unloading cycle is

proportional to the loading rate. Goddard staff have traced this characteristic behavior with the loading rate varying over almost a factor of ten. For a somewhat higher loading rate, the character of the solution changes suddenly. The second panel shows the evolution of the mass with time for this case. The transient is long lived and has, therefore, been eliminated from the plot. The loading-unloading cycle for this loading rate is still periodic but there are now two periods instead of one. The system appears to have gone through a bifurcation in its evolution.

To be sure that the system has passed through a bifurcation with increasing loading rate will require further study. If this is a bifurcation, then it may be the first of a sequence of bifurcations that lead to chaotic evolution of the system. This interpretation of the system evolution with increasing loading rate is supported by the results shown in the third panel. Here the researchers have increased the mass loading rate even further. In this case, the system never settles down to a periodic behavior. The quasi-random behavior of the system for these high loading rates is suggestive of chaotic behavior for the system when it is driven hard.

Based on these initial results obtained from the model, the authors believe that a chaotic transition takes place in the analog system as the loading rate is increased beyond a critical value. This suggests that beyond the analogous transition, the loading-unloading cycle of the magnetosphere would be chaotic. Thus, the tools of nonlinear dynamics and deterministic chaos theory may allow us to gain substantial new insight into the behavior of the magnetosphere during substorms and during geomagnetic storms. This work may bring solar wind coupling research into the realm of fluid dynamics, meteorology, and other areas where powerful methods are being developed for studying chaotic development of systems. The authors look forward to the conversion of Goddard's mechanical analog to a more plasma-physical character to test the rudimentary ideas presented here. The authors also look forward to devising empirical tests of the magnetospheric system to see if the paradigm presented here is, indeed, valid in the complex natural system.

Contact: Alexander J. Klimas (Code 690)
(301) 286-3682
Daniel N. Baker (Code 690)
(301) 286-8112

Sponsor: NASA Headquarters, Magnetospheric Physics Division, Space Physics Division

Dr. Alexander J. Klimas, who holds a PhD in physics and mathematics from the Massachusetts Institute of Technology, has served 14 years as an astrophysicist at Goddard. His scientific interests include numerical plasma simulation, plasma kinetic theory, and the theory of deterministic chaos.

Dr. Daniel N. Baker is currently Chief of the Laboratory for Extraterrestrial Physics. His research interests include solar-planetary relations, magnetospheric physics, plasma astrophysics, cosmic particle acceleration, and magnetosphere-atmosphere coupling. Dr. Baker holds a PhD from the University of Iowa.

MAGNETIC STRUCTURE OF THE CONTINENTAL LITHOSPHERE

The NASA MAGSAT mission and the follow-on research proved that researchers could handle global magnetometer records and further that they could separate the contributions due to sources in the magnetic lithosphere from the background of the main field and external sources. Unfortunately, the MAGSAT elevation was too high for adequate spatial and amplitude resolution, but the results still demonstrated the enormous potential of a MAGSAT-type mission at a lower elevation. One of the most important outcomes of the MAGSAT mission was the development of a global perspective for considering the origins and spatial distribution of magnetization contrast in the crust of the Earth. This was timely because it preceded the current intense interest in the deeper reaches of the continental crust. A low-level satellite magnetometer mission would have the spatial and amplitude resolution adequate to global mapping of the magnetic structural elements of the lithosphere, thereby providing the geoscience community with a powerful new tool.

The pioneering work on the magnetic structure of the continental lithosphere was accomplished at Goddard. Xenoliths, tectonically exposed crustal sections, and various types of high-grade metamorphic terrain were studied in order to determine how magnetization was distributed in the continental lithosphere and how geologic processes might contribute to the creation and destruction of magnetization over geologic time.

Achieving a reasonable level of understanding of the magnetic structure of the continental lithosphere would appear, at first glance, to be an impossible task. For example, it would appear to be technologically and

C-2

financially impossible to drill to the bottom of the crust; researchers would need hundreds of holes to be able to obtain the data base required. Fortunately, investigators have access to xenoliths which are found worldwide in all types of tectonic settings. A xenolith (from the Greek meaning "strange") is a block of rock picked up by ascending magma from different levels in the upper mantle and crust and deposited at the surface as part of the eruptive event. The xenoliths, therefore, provide the only source of information about the in situ aspects of lithologies, including magnetic properties, at the time the eruption took place. The conceptualization of the moho, the boundary between crust and mantle, as a magnetic bottom was developed at Goddard as a result of xenolith studies. The transit time is relatively short, as verified by various types of petrologic studies indicating that the pressure and temperature at which the xenolith precursor last equilibrated (at depth) is preserved. There are sources of magnetic contamination, such as the filling of cracks by the eruptive magma and the reduction associated with adiabatic decompression melting, but these are easily verified with thin-section petrography. For example, researchers may assume that the magma source is the upper mantle and the magma will pick up blocks of rock in the lower to upper crust. Once the magma captures the block, heating commences, and in the ideal case, the rock is thermally demagnetized because temperature *(T)* exceeds the Curie temperature *(Tc)* of the magnetic minerals. Once at the surface, the magma and included xenolith cool together in the magnetic field of the Earth *(H)*, and both acquire thermoremanent magnetization which is directionally coincident.

What information is contained in this xenolith? The in situ remanence is demagnetized, and therefore, the remanence measured is a thermoremanence induced by the ambient field present when it cools. By evaluating this remanence and other properties of the magnetic minerals, researchers can model the in situ remanence. They measure the Curie point, magnetic hysteresis loops, and initial susceptibility. They identify the magnetic minerals and the quantity present, estimate the size distribution of the magnetic minerals, and determine the induced magnetization. They therefore have access in the xenolith record to information about crustal magnetization from regions of the crust and upper mantle that would otherwise be inaccessible. Xenolith records from different tectonic settings in different regions of the world are providing an increasingly

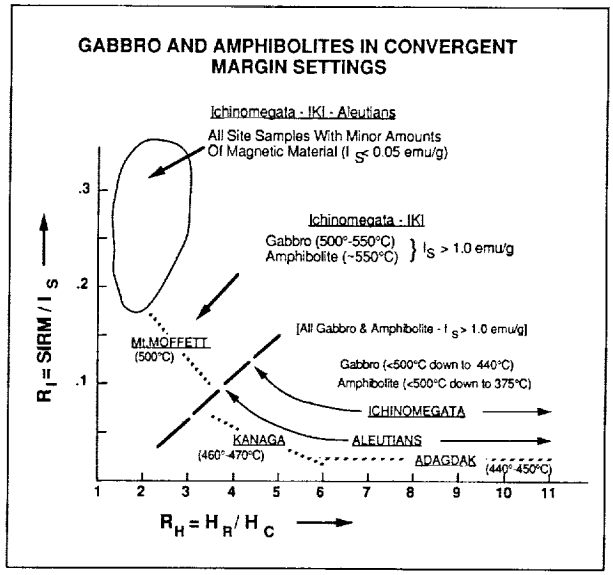

The R_I-R_H plot essentially characterizes the magnetic-domain structure of the convergent margin lower crustal rocks. The temperatures in parentheses are the Curie points, and the I_S values are saturation magnetization values proportional to the amount of magnetic material present. With this information, researchers can begin to model the total magnetization of the lower crust of the arcs. (R_I is the ratio of saturation remanence to saturation magnetization and R_H is the ratio of remanent coercive force. All underlined names are localities.)

sophisticated view of the magnetic structure of the continental lithosphere.

At any temperature above the Curie point of a magnetic mineral, the remanent magnetization and ferromagnetic susceptibility is zero. Therefore, remanent and induced magnetization are replaced by the much lower level paramagnetic character of iron-bearing minerals. Considering a possible array of temperature-depth curves (geotherm) for the continental crust, it is clear that a specific mineral—for example, magnetite, with minor impurities, having a 550 °C Curie point—can remain magnetic over a depth range of tens of kilometers. If magnetite were the only mineral in the crust and were uniformly distributed, then researchers could construct the topology of the 550-°C isothermal surface from long-wavelength magnetic anomalies. Suppose that geodynamic regimes with geotherms different from other regimes provided circumstances whereby different magnetic minerals would dominate—iron with a 780-°C Curie point in one case and a titanomagnetite with a 200-°C Curie point in

another. Given the same geotherm, the magnetic thickness of the crust can vary considerably, depending on whether the 200-°C titanomagnetite, the magnetite at 550 °C, or iron with a 780-°C Curie point happens to be the dominant magnetic mineral. The Curie point distribution in the lithosphere is therefore important if researchers are to address crustal magnetization realistically.

If researchers attempt to model long-wavelength magnetic anomalies, it is critical to constrain the magnetic bottom. Goddard analysts assumed that the moho was a magnetic mineralogy discontinuity. This concept was developed from measuring the magnetic properties of xenoliths from the upper mantle and the lower crust and from further reading in the literature about the opaque mineral chemistry in upper mantle rocks and lower crustal granulites. Peridotites should be essentially nonmagnetic unless subject to crustal alteration or metamorphism. In general, mantle spinels have little oxidized iron and titanium, in contrast to the more oxidized lower crustal granulites. Xenolith peridotites may contain the primary spinels which are unaltered in transit and are therefore essentially nonmagnetic, reflecting on the nonmagnetic character of the upper mantle. Ilmenites in xenoliths or in nodules are magnetic, contain lamellae of magnesian titanomagnetite with variable amounts of oxidized iron, and have a broad range of Curie points.

The Colorado Plateau is a distinct structural element of the western United States. Xenoliths from the plateau regardless of the lithology have magnetite Curie points (Tc~550° to 570°C). In contrast, the Rio Grande Rift, which is a high-heat-flow area bordering the plateau, is relatively hot and anhydrous, and the mineralogies are reduced, thereby allowing ilmenite with some oxidized iron to dominate. The metapelitic rocks (those derived by metamorphism of sediments) are weakly magnetic, and the iron is mostly in a reduced state and is contained in paramagnetic silicates. The metabasic rocks (derived from metamorphism of basic magma) have reasonable magnetization but, in the examples studied, have dominant Curie points near 200 °C. These samples show textural evidence of reduction. The high heat flow in the rift, which translates to a steep geothermal gradient, ensures that at present only about 15 km of the 30-km thick Rio Grande Rift crust is magnetic. When the rift cools down, as it must eventually, the lower crust will remain nonmagnetic because any regional geotherm will ensure that the low Curie point metabasic rocks remain demagnetized.

Convergent margins such as the Aleutian and Japanese arcs are regions where active magmatism contributes to the growth of continental fragments. This contribution occurs in three ways. First, the subducting plate contributes to the generation of magma that finds conduits to the surface and manifests itself as volcanoes. Second, this magma underplates and thickens the crust. Third, the heating generated by the intruding magma melts preexisting crust, thereby producing granitic magma that rises to shallower levels. The xenolith record allows researchers to evaluate the magnetic properties of these constructional elements of the convergent margin crust. Different episodes of magma production give rise to magma with different degrees of hydration, and as the magma becomes more reducing, nonmagnetic ilmenite becomes a dominant mineral. The Aleutian arc contains gabbroic rocks that are highly magnetic and have subtle indications of magma-site to magma-site variation. The xenolith record offers additional insight into the creation, destruction, and modification of rock magnetization. The Colorado Plateau and Rio Grande Rift granulites—metamorphic rocks last equilibrated at high pressure and relatively high temperature—are rocks that have been transported from higher levels in the crust to the lower crust and, as a consequence, have been recrystallized, meaning that the original material has been completely modified. The Japanese and Aleutian arc rocks, in contrast, have crystallized at granulite-grade conditions. Therefore, the magnetic properties are a consequence of the crystallization history and subsequent subsolidus modification of titanomagnetite. These differences are implied in the Curie-point contrasts.

Magnetic hysteresis loops provide information about the amount of magnetic material present and the particle-size microstructural characteristics of the magnetic materials. R_I and R_H are called the magnetic hysteresis loop and provide evidence for the bulk magnetic structure of rocks. The ratios are defined in the figure. For example, a single-domain grain of magnetite would have an R_I of about 0.5 and R_H <1.5. As the particle size increases, R_I is lowered and R_H increases. There are of course additional interpretive complications due to exsolution- and oxidation-induced microstructures when researchers consider real rocks. In some gabbros and amphibolites from convergent margin settings, small amounts of magnetic material—Is is the saturation magnetization and is proportional to the amount of magnetic material—are always present as very fine particles. Crystallization conditions are such that most of the iron is bound up in silicates or ilmenite, conditions are relatively reducing, and the

small amounts of oxidized iron are crystallized with magnetite late in the crystallization sequence. The predominant mafic rocks in the lower crust contain 1- to 10-percent magnetite with large values of remanent and induced magnetization. In the figure, the numbers in parentheses are the Curie points measured for the gabbros and amphibolites. The Aleutian data are particularly interesting. Trending from Adagdak (with 440- to 450-°C Curie points) to Kanga (460- to 470-°C Curie points) to Mt. Moffett (500-°C Curie points), the R_H value decreases and the R_I value increases. Adagdak, Kanga, and Mt. Moffett are three distinct volcanoes. The Curie-point variations reflect the development of microstructure indicating distinct evolutionary contrasts for each site. The same general trend is noted for the Japanese arc samples.

Upper mantle xenoliths from the Aleutians, Antarctica, Japan, Eastern Australia, southern Africa, Hawaii, and numerous sites in the western United States have magnetic susceptibility values less than 0.13 americium $(Am)^{-1}$. Mafic lower crustal granulites from eastern Australia, Antarctica, southern Africa, Japan, the Aleutians, and western United States have magnetic susceptibility values ranging from 0.5 to 10 Am^{-1}, with most between about 1 and 5 Am^{-1}.

Goddard researchers have abundant information suggesting the moho is a magnetic discontinuity. Over the last decade much new information has come to bear on the nature of the moho (or, more appropriately, the crust-mantle boundary). The transition appears to be gradational in detailed seismic records. One explanation is the mix of mafic and ultramafic rocks. Goddard analysts have evaluated eclogites and pyroxenites, two additional candidate lithologies that together with the peridotites are logical in reconstructed sections. Both the eclogites and pyroxenites are relatively nonmagnetic. The effect of mixing the ultramafics and eclogites together with mafic granulites is to dilute the magnetization across the crust-mantle boundary.

A unique and provocative data set became available because of MAGSAT. The perspective, a global view of the magnetic signature of the magnetic crust, immediately demonstrated that conventional approaches to magnetic anomaly interpretation were entirely unrealistic. Block models average the magnetization of a craton and neglect the implications of billions of years of Earth history.

It is apparent that a new framework, a new direction, is required, one that determines how to relate hand samples, i.e., laboratory-scale results, to the resolution of the lateral variation of the vertical integral of magnetization in the continental lithosphere. Following the Goddard vanguard, other researchers are now actively pursuing the many unanswered questions about the distribution of crustal magnetization.

Contact: Peter J. Wasilewski (Code 691)
(301) 286-8317

Sponsor: Office of Space Science and Applications, Land Processes Branch

Dr. Peter J. Wasilewski studies the magnetic structure of the continental lithosphere and the magnetic history of meteorites in the Astrochemistry Branch of the Laboratory for Extraterrestrial Physics. Dr. Wasilewski has been at Goddard for 15 years and received his PhD in science from the University of Tokyo.

GLOBAL CONFIGURATION OF A MAGNETIC CLOUD

Magnetic clouds are plasma and magnetic field structures observed in the solar wind between the Sun and the orbit of Saturn. They have relatively strong magnetic fields and low temperatures, so that the magnetic pressure is much greater than the thermal pressure in a magnetic cloud. At the orbit of Earth (1 au), the size of the cross-section of a magnetic cloud is approximately 1/4 au. Previous studies have shown that magnetic clouds are produced by solar flares and eruptive prominences, and some magnetic clouds are manifestations of coronal mass ejections. Major geomagnetic storms are caused by those magnetic clouds with a strong and sustained southward magnetic field component. Many magnetic clouds, particularly those that are interacting with other flows and shocks, have such a component. Magnetic clouds also produce disturbances in the flux of galactic cosmic rays.

Burlaga has shown that the local structure of a magnetic cloud can be described by the solution for a cylindrically symmetric "constant-alpha force-free magnetic field." This means that the pressure of the magnetic field is balanced by the tension in the magnetic field lines and that the current flows along the magnetic field lines. The large-scale structure of a magnetic cloud is a matter of considerable interest to researchers, but it has been a mystery.

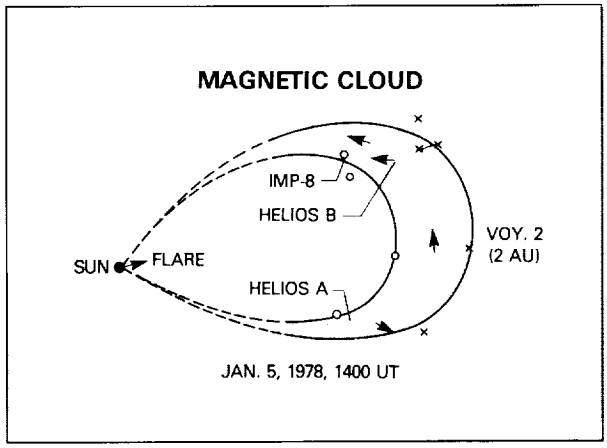

A magnetic cloud (shaded area) was observed by four spacecraft, all located in or near the ecliptic plane. The local positions of the front and rear boundaries, shown by "x" and "o" respectively, were determined from the arrival times at each of the spacecraft and the measured speeds of the boundaries. The solid arrows indicate the local directions of the axis of the magnetic cloud, determined using the fitting procedure developed by the authors. The average of the local inclinations of the axis with respect to the plane of the figure (the ecliptic) for the four sightings was 11°.

The authors developed a procedure for determining an optimal fit of the constant-alpha force-free solution to the data for a magnetic cloud (*Research and Technology 1988*). This procedure allows researchers to determine the local orientation of the axis of a magnetic cloud observed by a single spacecraft. By applying this procedure to the observations of a magnetic cloud made by four spacecraft at different positions in the solar wind, it was possible to determine the large-scale structure of the magnetic cloud.

The magnetic cloud was observed in January 1978 by Interplanetary Monitoring Platform (IMP)-8, Helios-A, Helios-B, and Voyager-2. The positions of the spacecraft are shown in the first figure. Note that IMP-8 was at Earth and Voyager-2 was at 2 au, which is to the right of the figure. The direction of the axis of the magnetic cloud, determined by analyzing the magnetic field data using the procedure developed by the authors, is shown as a solid arrow in the figure. One arrow is obtained from each of the four spacecraft, providing widely spaced estimates of the cloud's axis. The figure shows that the axis bends around in an arc. The local positions of the front boundary of the magnetic cloud, shown by an "x" in the figure, were determined from the time that the boundary arrived at the spacecraft and the observed speed of the boundary. The figure shows the local positions of the front boundary at a particular instant, 1400 UT on January 5, 1978. The local positions of the rear boundary were determined in the same way, and they are shown by the "o" in the figure. Drawing smooth curves through the local boundary positions gives the shape of the magnetic cloud boundaries. The curves corresponding to the boundaries are consistent with the estimated local orientations of the axis of the magnetic cloud in the figure. Since the magnetic cloud was associated with a solar flare, the figure shows the boundaries of the magnetic cloud extending to the flare site. The boundaries near the Sun are drawn as dashed curves to emphasize that there are no measurements in that region.

The global configuration of the magnetic field lines in a magnetic cloud is illustrated in the second figure. The inner and outer boundaries of the magnetic cloud in this figure are reproduced from the previous figure. Since the magnetic field in a magnetic cloud is locally a force-free field, the local form of the magnetic field lines is known (Lepping and others, 1988). The magnetic field line in the middle of a magnetic cloud is coincident with the axis of the magnetic cloud. The

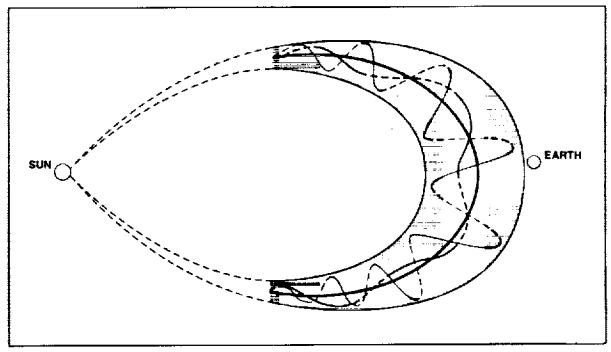

The global configuration and average magnetic field structure of a magnetic cloud. The shape of the magnetic cloud is taken from the results in the previous figure. The magnetic field lines in the magnetic cloud are determined by the fact that the field was found to be force free. At the center of the magnetic cloud, the field line is coincident with the axis of the cloud. Moving away from the axis, the magnetic field lines are helices wrapped around the axis and progressively changing in pitch angle and magnetic field strength. The magnetic field strength is strongest at the axis and weakest at the boundary.

magnetic field lines off the axis are helices that wind about the axis. The magnetic field lines farther from the axis are wound more tightly than those near the axis. The magnetic field is stronger near the axis of the magnetic cloud; this fact is illustrated in the second figure by the varying thickness of the magnetic field lines.

In summary, Goddard researchers determined the global configuration of a magnetic cloud shown in the first figure using some rather old (1978) magnetic field and plasma data from four widely separated spacecraft, a mathematical model, and a special fitting procedure. They also successfully applied the fitting procedure developed by the authors to single spacecraft sightings of many magnetic clouds at 1 au, in order to determine their properties. In some cases, the axis of the magnetic cloud was highly inclined to the ecliptic, in contrast to the example given above.

Contacts: Leonard F. Burlaga (Code 692)
(301) 286-5956
Ronald P. Lepping (Code 695)
(301) 286-5413
Jeffrey A. Jones (Code 694)
(301) 286-4912

Sponsor: Office of Space Science and Applications

Dr. Leonard F. Burlaga, of the Interplanetary Physics Branch in the Laboratory for Extraterrestrial Physics, studies dynamic processes in the outer heliosphere. He has been at Goddard for 20 years and has received a Senior Fellow Award, the Lindsay Award, an Award of Merit, and an Exceptional Scientific Achievement Medal.

Dr. Ronald P. Lepping specializes in plasma physics and magnetospheric and interplanetary physics at the Laboratory for Extraterrestrial Physics. He performs magnetometer experiments on IMP-8 (Principal Investigator), Voyagers 1 and 2 (Co-Investigator), and International Solar-Terrestrial Physics Project (ISTP)-GEOTAIL and WIND (Principal Investigator). Dr. Lepping holds a PhD in physics from Rensselaer Polytechnic Institute. He has 20 years' experience at Goddard and has earned several Special Achievement Awards for his work.

Mr. Jeffrey A. Jones handles analysis and programming in the Laboratory for Extraterrestrial Physics and the Laboratory for Oceans. His interests include mathematical modeling, numerical analysis, and radiative transfer. Mr. Jones has a BS in physics.

A HIGH-SPEED PITCH-ANGLE SORTER

As spacecraft instrumentation becomes faster and more sophisticated, limitations in the rate at which data can be transmitted to ground become increasingly important. Often the central processing unit (CPU) is unable to perform the data compression needed to conform to the allotted telemetry fast enough while concurrently handling the normal command and control functions required of it. Thus the use of either microprocessors or digital logic dedicated to specific processing tasks is often necessary. Goddard researchers have developed a pitch-angle sorter board which is to be used in conjunction with a fast plasma analyzer being developed for use on the upcoming Global Geospace Science-Polar spacecraft mission. The board is able to sort the direction of incoming particles detected by the analyzer according to the polar angle of the particle with respect to the ambient magnetic field direction. This compression is justified when the electron distribution has gyrotropic symmetry about the magnetic field vector, usually when the motion is strongly coupled to the magnetic field, and when the bulk flow velocity of the plasma in the spacecraft frame is much less than the velocity of the electrons. The pitch-angle sorter can handle particle counts at rates up to 2 MHz, and it is designed to accommodate the high angular resolution of the plasma analyzer of nearly 1°. This is accomplished with minimal assistance from the CPU, which needs only to secure the reduced data presented to it by the pitch-angle sorter.

The researchers who developed the pitch-angle sorter have also developed a parallel plate analyzer constructed to act much like a camera with a 32° × 32° field of view segmented into 32 × 32 pixels along lines of constant polar and azimuthal angles. When a particle is detected on the plasma analyzer, the particle's angular direction is recorded and presented to the pitch-angle sorter. The pitch angle, Ψ, is derived simply by taking the inverse cosine of the inner product (dot product) between the magnetic field, M, and the particle direction, P,

$$\Psi = Cos^{-1}\,[M(\theta_1,\phi_1) \cdot P(\theta_2,\phi_2)] \qquad (1)$$

where the magnetic field is obtained from the magnetometer measurements on board the spacecraft. The problem is illustrated schematically in the first figure.

The strategy employed in the design of the pitch-angle sorter is to eliminate any arithmetic operation in the

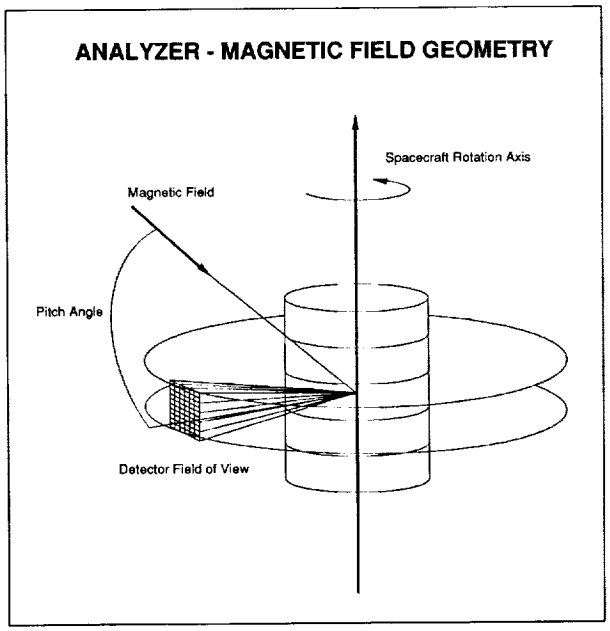

The field of view of the analyzer is fixed to the rotating spacecraft. Thus, the pitch angle of a detected particle must be evaluated promptly.

evaluation of equation (1) and instead use lookup tables coded into random access memory (RAM) to achieve the speed needed to handle the high rates of the analyzer. Instead of integrating on each detector pixel, counts received by the analyzer are promptly evaluated by the board, and an accumulator assigned to the appropriate pitch angle is incremented by one.

The use of lookup tables rather than the CPU to perform the calculations is a commonly used technique, particularly when transcendental functions must be evaluated. The primary limitation is the amount of memory needed. For example, if researchers were unable to use the high symmetry found in equation (1), the number of memory addresses required would be given by the product of the number of pixels on the analyzer and the minimum number of magnetic field directions on the unit sphere needed to maintain the required angular degree resolution. For example, if researchers desire an angular resolution of one digital degree, where a digital degree is defined by $2\pi/2^8$, then the amount of memory required is given by the product $32 \times 32 \times 4\,\pi/(\pi/128)^2 = 2.1 \times 10^7$ addresses.

This amount is simply too large, given the expense of radiation-hardened memory. Fortunately, by employing a few simple symmetry operations on the coordinate system researchers can reduce the domain over which they must store the inner products in the lookup table. These operations lead to a reduction in the amount of memory required by over a factor of 150. Goddard researchers take advantage of the fact that any rotation of

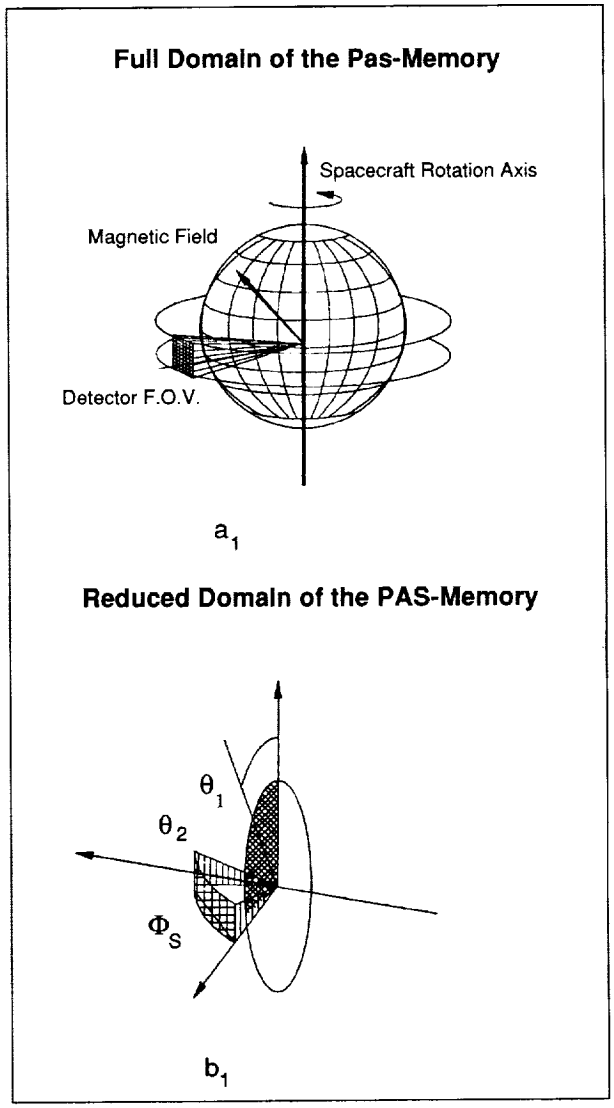

(a) Without compaction, memory must be stored over four dimensions which include the full unit sphere for all possible magnetic field directions and the 32 °× 32 °field of view of the analyzer. (b) After compaction the domain has been reduced to three dimensions over the angular limits

$$0 < \theta_1 < \frac{\pi}{2},\ \frac{\pi}{2} - \frac{\Delta}{2} < \theta_2 < \frac{\pi}{2} + \frac{\Delta}{2},\ 0 < \phi_2 < \frac{\pi}{2}$$

where ϕ_s is given by ϕ_2 - ϕ_1 and Δ is the angular limit of the detector given here by 32 °.

the coordinate system or any reflection through a plane does not change the value of the inner product in equation (1) while inversion through the origin of one of the two vectors changes only the sign. Inner products outside this domain can be brought into it by a suitable choice of transformations.

The advantage of this approach is the achievement of high rates in evaluating equation (1) by simply accessing memory and by foregoing any intermediate integration time on the individual detector pixels. These rates are needed to prevent angular blurring caused by the rotating spacecraft. The rotation will degrade the near-1° angular resolution that researchers are attempting to recover.

As illustrated in the second figure, the domain over which memory must be assigned is reduced by these transformations from four to three dimensions, and the extent of the dimensions is reduced as well. If the domain is segmented into digital degrees, the number of elements in the lookup table (addresses in memory) is reduced to $2^{17} = 1.3 \times 10^3$, a decrease of over a factor of 150.

The third figure shows a block diagram of the pitch-angle sorter board. A 15-bit word corresponding to the magnetic field direction and a 10-bit word corresponding to the pixel location of one of two plasma instruments are latched onto the board. After the symmetry operations are performed, the pitch angle is recalled from memory and the accumulator assigned to the pitch angle is incremented by one.

The board handles two identical plasma analyzers which are mounted antiparallel to each other. With this geometry, corresponding pixels on the two analyzers lead to a sign change in inner product. This sign change is equivalent to another symmetry operation and is handled in the same way.

Finally, the board can pass the data through from the analyzers directly, accumulating counts on each pixel for a given period of time. This allows for calibration of the detectors and makes it possible to recover the unsorted two-dimensional picture that is acquired by the analyzer. Due to the high overhead in CPU time, this mode can only be run infrequently.

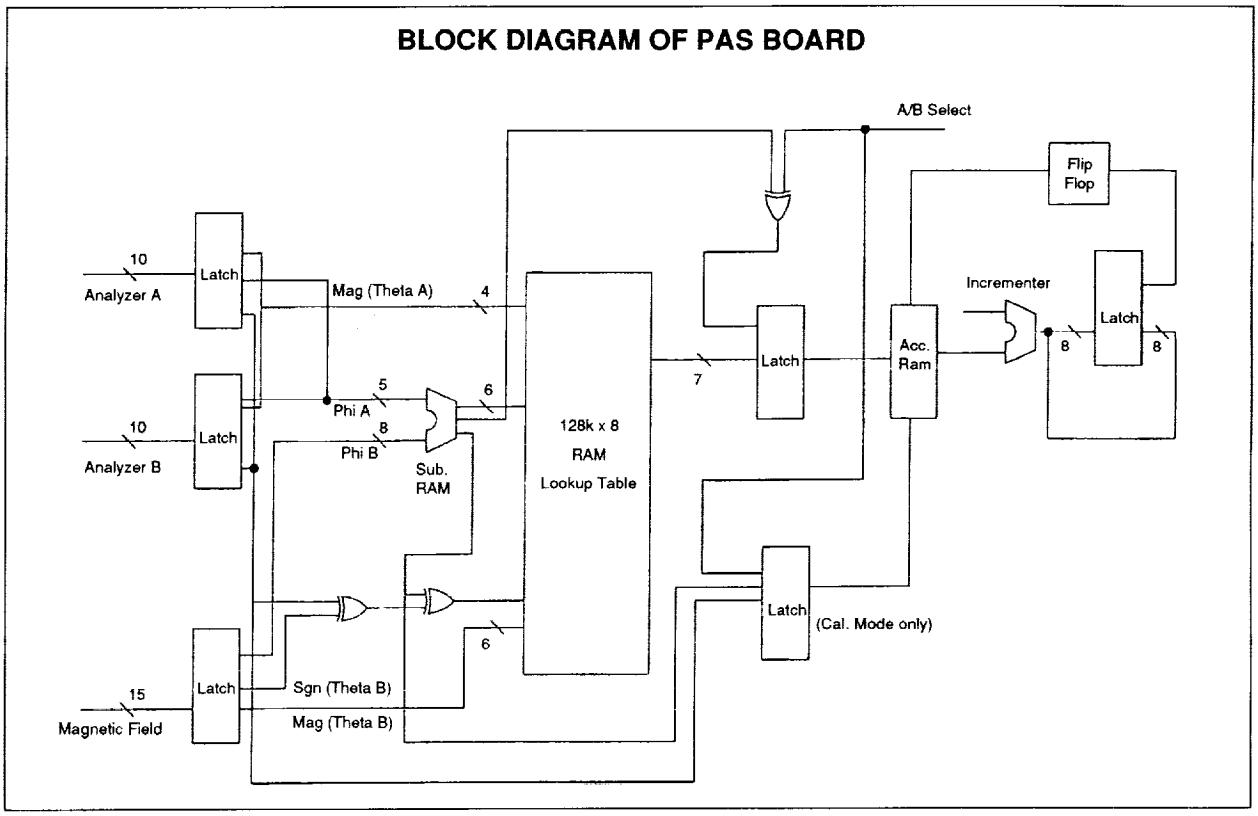

Block diagram of the pitch-angle sorter board.

When the conditions of gyrotropic symmetry in the two-dimensional distribution of particle velocities can be met, projection onto the one-dimensional pitch-angle distribution without loss of information is possible. This projection results in a tremendous compaction of the data with the challenge being the rapid evaluation of the projection. The pitch-angle sorter board described here will be used in conjunction with a space plasma physics experiment on the Global Geospace Science Polar spacecraft. The board uses a random-access memory lookup table to eliminate arithmetic operations and invokes the high degree of symmetry in the evaluation of inner products to reduce the amount of radiation-hardened memory to reasonable levels. The board can handle particle count rates at up to 2 MHz, and it is designed to accommodate the high angular resolution of the plasma analyzer of nearly 1°. This accommodation is accomplished with minimal assistance from the CPU, freeing it for its other tasks.*

**The work described in this article is part of a collaboration between John Keller and Jack Scudder at Goddard and Roy Torbert and Jim Vandiver at the University of New Hampshire.*

Contact: John W. Keller (Code 692)
(301) 286-3871

Sponsor: ISTP

Dr. John W. Keller conducts laboratory experiments on atomic and molecular systems and contributes to the design and testing of spacecraft-based particle analyzers. Dr. Keller has been with Goddard for 3 years. He works in the Space Physics Branch of the Laboratory for Extraterrestrial Physics. He earned a PhD in physical chemistry at the University of Maryland.

A PARALLEL-PLATE ELECTROSTATIC ENERGY ANALYZER WITH 1° ANGULAR RESOLUTION WITHIN A FIELD OF VIEW OF 30° × 30°

A new spectrometer has been developed to measure angular distributions of magnetospheric electrons with an angular resolution of about 1° and within a field of view of 30° × 30°. The spectrometer also scans electron energy to provide both angular distributions and energy spectra. The energy bandwidth is between 0.01 percent and 0.20 percent of the mean electron energy; the specific bandwidth chosen is determined by the dimensions of internal apertures (slits) of the spectrometer.

The first figure shows the spectrometer is located somewhere beneath the spacecraft skin. It consists of a parallel-plate electrostatic energy analyzer, which deflects the incident electrons onto a position-sensitive detector. The aperture on the spacecraft skin (plus additional baffles) serves to limit the field of view of the position-sensitive detector. This view of the parallel-plate analyzer shows the entrance and exit aperture slits *i* and *o*, respectively, as seen from the side. However, it does not show that the entrance slit *i* is, in fact, circular and that the exit slit has the shape of a circular arc with center at *i*. That arc spans a 30° angle. The parallel plates produce a constant electrostatic field that makes the electrons move in parabolic trajectories so that the incident angle θ_i is equal to the exit angle θ_o. This condition is true for all trajectories, independent of the incident angle θ_i. Trajectories with a component of velocity perpendicular to the paper preserve that component of velocity because no electric field is present in that direction. Therefore, all trajectories with the same angle of incidence θ will span a 30° total angle in a plane perpendicular to the paper. That arc is projected onto the position-sensitive detector. In practice, it is possible to vary θ between 30° to 60° to scan a 30° range in θ. Thus, a two-dimensional field of view of 30° × 30° made up of all arcs with angles of incidence from 30° to 60° can be obtained with this device.

The transmission of electrons with a fixed energy as a function of the angle of incidence varies as shown in

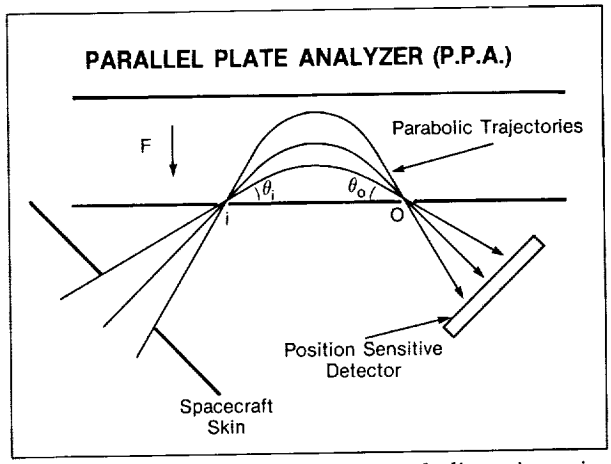

Parallel-plate analyzer showing parabolic trajectories followed by electrons entering the spacecraft skin from the ambient plasma. Angle of incidence θ_i equals exit angle θ_o for all trajectories.

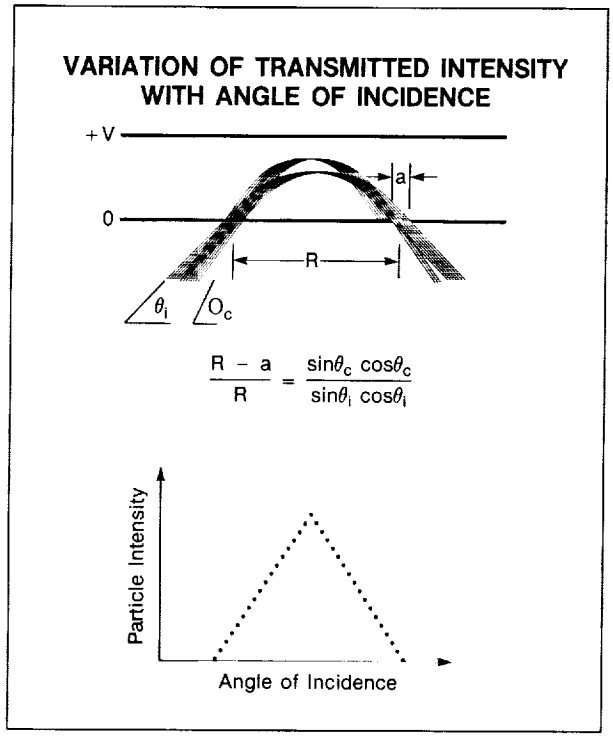

Effect of angle of incidence on the transmission of a parallel bundle of trajectories.

the second figure, where two bundles of parallel trajectories are shown incident at two different angles. The masking effect of the exit aperture on the transmitted energy is shown in the plot at the bottom. The slit width a, which is the same as the diameter of the entrance slit, and the distance between the slits R determine the angle θc at which the transmitted intensity is cut off completely. The angle θc may be obtained from the relation shown in the second figure. The simplicity of this relation and of most analyses associated with the parallel-plate analyzer represents one of the advantages of operating this device.

Because the conducting surfaces of the parallel plates have constant electrostatic potentials, apertures in the plate generate small electric fields which distort the trajectories of the electrons. Such distortions broaden the angle of divergence of an initially parallel bundle of trajectories, spreading the electrons over several pixels of the position-sensitive detector. In the position-sensitive detector, a pixel size corresponding to angular resolution of 1° × 1° is determined by the width of the parallel bundles. So, two bundles differing by 1° must land on two adjacent pixels with little or no overlap in order to be resolved adequately. This requirement determines the distance between the position-sensitive detector and the exit slit. This distance may become very large unless the slit width a is very small. For example, for a slit width $a = 0.1$ in., the position-sensitive detector must be placed at a distance of about 6 in. beyond the exit slit in order to separate two bundles differing by 1°. This distance may be reduced by focusing, as discussed below.

The angular resolution of the parallel-plate analyzer is determined by two factors: (a) the spatial resolution of the position-sensitive detector, and (b) the ability of the analyzer to gather the electron trajectories onto a single pixel of the position-sensitive detector. The approach adopted in this application is to achieve a small degree of convergence on the parallel bundles by the small electric field of an electrode placed within the analyzer. This additional electric field is strongest near the electrode. Therefore, the trajectories coming closest to the electrode are deflected the most. This is illustrated in the third figure, where the solid curves show the actual parabolic trajectories corresponding to a perturbation potential of 0 volts on the electrode P. The dashed curves represent the effective parabolic trajectories produced by a nonzero perturbation potential on P. Note that these trajectories appear to pass through the plate near the entrance slit i, though the actual trajectories there resemble the solid curves. Near and beyond the exit slit, however, the dashed trajectories are representative of the actual ones, and convergence occurs at some point Q beyond the exit

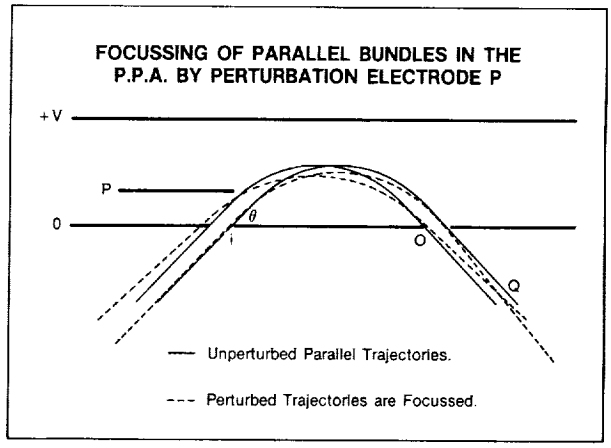

The potential on the perturbation electrode may be adjusted to achieve focusing of parallel incident rays onto a point Q.

slit. The focusing occurs because the trajectory coming closest to P is deflected the most; thus, its effective parabola is inclined at an incident angle that is smaller than the equivalent angles for all the other trajectories in the bundle. In the operation of the device, the perturbation potential P is chosen to place Q on the surface of the position-sensitive detector.

The fourth figure shows four distributions obtained over a position-sensitive detector for three values of the electrode potential. The position-sensitive detector used was a microchannel-plate electron multiplier equipped with a CODACON anode with 1,024 pixels laid out in a square 32 × 32 array. This detector was developed by George Lawrence at the University of Colorado. Its dimensions are 1.1 × 1.1 in^2, and for the data shown in the fourth figure, it was placed 3.8 in. beyond an exit slit 0.10 in. wide. The focusing effect of the perturbation potential P is seen in the surface plots of the electron distribution. The top plot shows the electron angular distribution under normal operating potentials for the parallel-plate analyzer. That is P = 0 volts. The distribution has a width of about 7° in θ. As P is increased to 50, 100, and finally 125, the distribution narrows gradually to within a width of about 1° in θ in the plot at the bottom.

These results are preliminary, and work is continuing to achieve an optimum size for the parallel-plate analyzer and a proper configuration for the pixel array of the position-sensitive detector. The parallel-plate electrostatic energy analyzer is to be used in measuring the loss cone distribution of electrons as part of the Hydra instrument on the Polar spacecraft of the coming ISTP mission to be launched in 1992.

Contacts: Fred A. Herrero (Code 692)
(301) 286-5660
George N. Miller (Code 692)
(301) 286-7307
John W. Keller (Code 692)
(301) 286-3871

Sponsor: Office of Space Science and Applications

Dr. Fred A. Herrero has been with Goddard for 6 years and works in thermosphere dynamics. His interests include charged-particle spectroscopy and its application to space plasmas and neutral atmospheres.

Mr. George N. Miller is an electronic and vacuum technician with 15 years' experience at Goddard. He currently

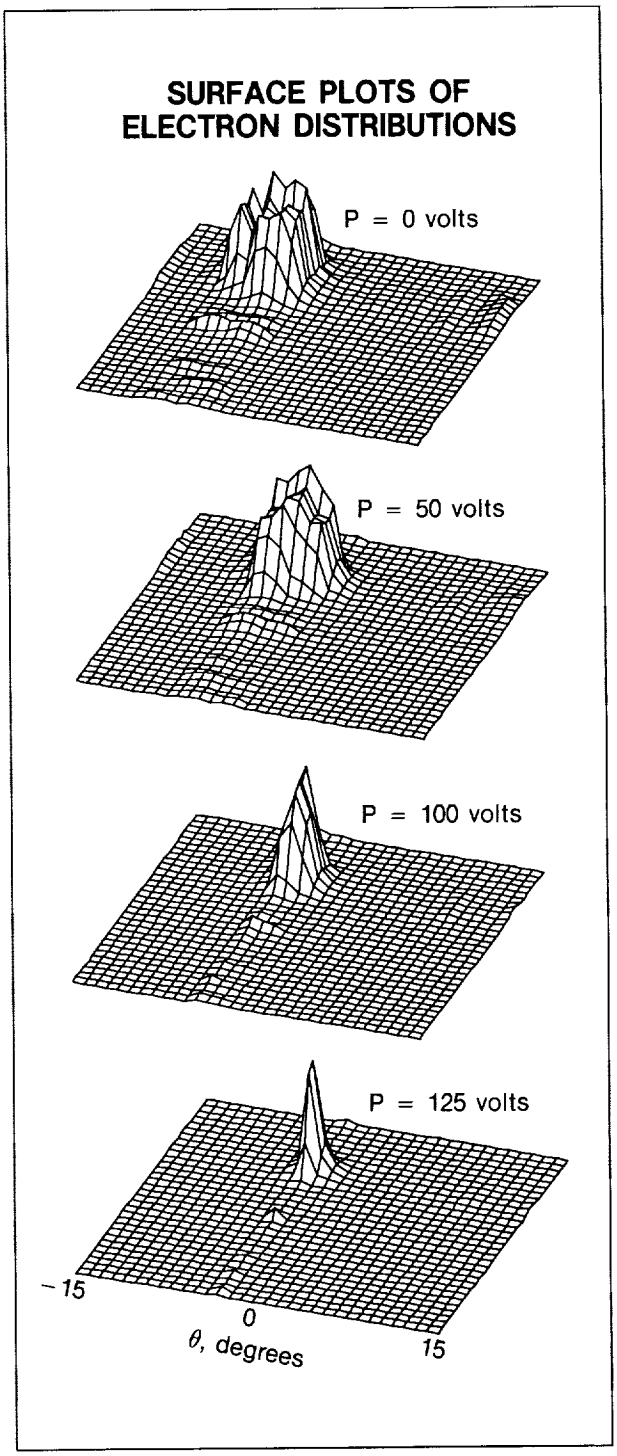

Actual tests of the performance of the analyzer with the perturbation electrode. Perturbation electrode potential P = 125 V produces focusing within 1° of a beam spanning about 7° without focusing (P = 0 V).

assembles and develops ground-support equipment for the WIND and Polar projects.

Dr. John W. Keller conducts laboratory experiments on atomic and molecular systems and contributes to the design and testing of spacecraft-based particle analyzers. Dr. Keller has been with Goddard for 3 years. He works in the Space Physics Branch of the Laboratory for Extraterrestrial Physics. He earned a PhD in physical chemistry at the University of Maryland.

INTERPLANETARY MONITORING PLATFORM (IMP)-8 TRAVELING COMPRESSION REGION OBSERVATIONS: LOBE SIGNATURES OF PLASMOIDS AND NEUTRAL LINES

The understanding of the plasma processes that produce magnetic substorms is one of the primary objectives of magnetospheric physics. Visible from the ground only as 10- to 100-min intensifications and movements of auroral arcs and horizontal electrical currents in the ionosphere, substorms are known to involve magnetosphere-wide disruptions of quiet-time magnetic fields, plasma convection, and energetic particle motion. During the expansion phase of large substorms, more than 1 million MW of power can go into accelerating energetic particles, heating the plasma sheet, and driving the ionospheric electrojets.

While no single theory of substorms is accepted by the space physics community at large, the cislunar magnetotail plays a critical role in many of the leading formulations. The IMP-8 spacecraft with its 30- to 40-Earth radii moderate-inclination orbit is ideal for probing this region of space. The accompanying figure displays 15.36-s averages of the magnetometer observations in geocentric solar magnetospheric coordinates for a substorm lasting from 1900 to 2030 UT on August 22, 1983. The IMP-8 spacecraft was in the magnetotail at a downstream distance of 35 Earth radii. Also displayed are 30- to 200-keV energetic electron fluxes from a geosynchronous spacecraft and the AL auroral index based on data supplied by the Los Alamos National Laboratory and the Geophysical Institute/Kyoto University, respectively.

The large-scale features of the IMP-8 magnetic field observations all follow closely the predictions of the near-Earth neutral line model formulated in the early 1970's. Between 1825 and 1900 UT the lobe field intensity increases by approximately 10 percent. This corresponds to the "growth" phase of the substorm where the tail stores energy extracted from the solar wind. The tail begins to dissipate this energy around 1854 UT when an "injection" of energetic electrons into the inner magnetosphere marks the onset of the "expansion" phase of the substorm. The strength of the tail field then remains high through additional injections at 1927 and 1950 UT before recovering to presubstorm levels around 2028 UT.

The new features reported here are the 5- to 10-min, 3- to 5-nT field increases which occur at 1932 and 2009 UT in conjunction with correlated changes in the north-south (i.e., B_Z) component of the field. Similar field variations have been studied in the International Sun/Earth Explorer-3 section of distant tail measurements and termed traveling compression regions. These lobe field compression events are believed to be due to the rapid tailward movement of large magnetic islands or plasmoids. Their discovery in the IMP-8 data is of great significance in two respects. First, the IMP-8 traveling compression regions provide strong indirect evidence that plasmoids and, hence, multiple neutral lines do form in the near tail as predicted by certain substorm models. Second, the IMP-8

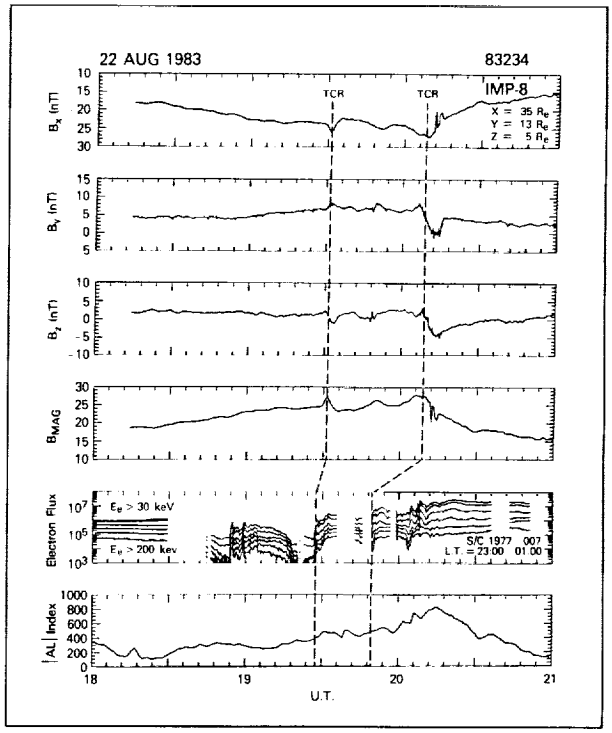

IMP-8 magnetic field and geosynchronous energetic electron observations are displayed for 1800 to 2100 UT on August 22, 1983.

observations can be correlated closely with near-Earth substorm measurements. The results suggest that plasmoids are not only formed early in the expansion phase, an important prediction of the near-Earth neutral line model, but also during later phases of substorms as the inner neutral line retreats tailward.

Contact: James A. Slavin (Code 696)
(301) 286-5839
Ronald P. Lepping (Code 695)
(301) 286-5413
Daniel N. Baker (Code 690)
(301) 286-8112

Sponsor: Office of Space Science and Applications, Space Physics Division

Dr. James A. Slavin, who received his PhD from the University of California at Los Angeles, currently works in Goddard's Laboratory for Extraterrestrial Physics. Dr. Slavin is the Lead Investigator for the Dynamics Explorer Magnetometer investigation and Co-Investigator for several other magnetometer efforts. He is also the ISTP Deputy Project Scientist for Polar and Study Scientist for the Mercury Orbiter.

Dr. Ronald P. Lepping specializes in plasma physics and magnetospheric and interplanetary physics at the Laboratory for Extraterrestrial Physics. He performs magnetometer experiments on IMP-8 (Principal Investigator), Voyagers 1 and 2 (Co-Investigator), and ISTP-GEOTAIL and WIND (Principal Investigator). Dr. Lepping holds a PhD in physics from Rensselaer Polytechnic Institute. He has 20 years' experience at Goddard and has earned several Special Achievement Awards for his work.

Dr. Daniel N. Baker is currently Chief of the Laboratory for Extraterrestrial Physics. His research interests include solar-planetary relations, magnetospheric physics, plasma astrophysics, cosmic particle acceleration, and magnetosphere-atmosphere coupling. Dr. Baker holds a PhD from the University of Iowa.

REACTION RATE KINETICS OF Br + C_2H_4: EFFECTS OF MOLECULAR OXYGEN AND IMPLICATIONS FOR ATMOSPHERIC MODELING

Recently reported observations have shown the occurrence of ozone destruction in the lower atmospheric regions of the Arctic. A chemical link with bromine chemistry of the natural and anthropogenic bromine species present in the Arctic atmosphere has been suggested to explain this depletion of ozone. In particular, renewed interest regarding the role of bromine species in atmospheric reactions concerns catalytic reactions of bromine compounds and the photochemistry of bromoform ($CHBr_3$) derived from biological sources in the Arctic Ocean. One type of atmospheric reaction, which may serve as a potential bromine loss process to interrupt the catalytic ozone destruction cycle initiated by reaction of atomic bromine (Br) with ozone (O_3),

$$\begin{aligned} Br + O_3 &\rightarrow BrO + O_2 \\ BrO + O &\rightarrow Br + O_2 \\ \text{NET: } O_3 + O &\rightarrow 2O_2 \end{aligned}$$

is formation of reservoir molecules produced by reaction of bromine atoms with hydrocarbon compounds:

$$Br + \text{Hydrocarbons} \rightarrow \text{Br-containing products}$$

Laboratory measurements of chemical kinetic reaction rates of gaseous species present in the atmosphere provide some of the information needed to understand and model accurately the Earth's ozone system. Previously, the authors have studied reactions of atomic bromine with ozone and with molecules such as formaldehyde (H_2CO) and acetylene (C_2H_2). To further ascertain the effect of potential bromine atom reaction sinks upon catalytic destruction of atmospheric ozone by bromine species, the authors have continued investigating chemical kinetic reaction rates of bromine atoms by performing a direct study to determine the temperature dependence of the reaction rate of atomic bromine with ethylene (C_2H_4):

$$Br + C_2H_4 \rightarrow \text{Products}.$$

The kinetic experiments were performed by the laboratory technique of flash photolysis production of bromine atoms, followed by time-resolved measurement of resonance fluorescence signal of the bromine atoms as they decayed by reaction with ethylene molecules. Two different series of experiments were conducted, one in the absence of oxygen and the other in the presence of low concentrations of molecular oxygen (O_2) in the argon diluent gas. Experiments in the absence of O_2 determined the reaction rate constant, k, as a function of temperature and pressure over the temperature interval of 268 to 423 °K and a range of total pressure of 15 to 400 Torr (argon).

Reaction rate data results obtained at each of the five temperatures studies show that, within experimental uncertainty, the reaction rate is independent of both total pressure and temperature. The overall result yields the reaction rate constant, $k = (1.65 \pm 0.51) \times 10^{-15}$ cm^3 s^{-1} (1σ). Experiments to measure the reaction rate constant in the present of O_2 were made at 298 °K to determine the effect of oxygen concentration and the effect of total pressure at fixed oxygen concentration. Results of the experiments performed as a function of O_2 concentration in the argon diluent reaction system show a significant enhancement (factor of 12) in the reaction rate constant within the small range of increasing O_2 concentrations used in this study (0 to 2 Torr O_2). Limitations of the flash photolysis-resonance fluorescence technique, due to absorption of bromine atom fluorescence signal by O_2, precluded experiments at higher concentrations of O_2. In addition, the rate constant exhibits a noticeable increase (factor of 2.5) with increase in total pressure [10 to 800 Torr (argon)] at fixed O_2 concentration.

The positive dependence of the reaction rate constant on the partial pressure of O_2 in the reaction system and on the total pressure is consistent with results obtained by other researchers at higher O_2 concentrations, including those with synthetic air at atmospheric pressures. Results from the authors' present study demonstrate that the magnitude of the rate constant, even in the presence of O_2, is still that of a relatively slow reaction.

Thus, the Br + C_2H_4 reaction probably could not serve as a sink or loss process for bromine atom removal from catalytic ozone destruction cycles. This conclusion helps to better define pertinent input parameters for more valid predictive atmospheric models. In addition, the present study suggests that rate-constant measurements of other atmospheric reactions not yet made in the presence of O_2 need to be performed.

Contact: David F. Nava (Code 691)
(301) 286-6007
Walter A. Payne, Jr. (Code 691)
(301) 286-5483

Sponsor: Office of Space Science and Applications

Dr. David F. Nava is an astrophysicist with the Laboratory for Extraterrestrial Physics. He is Co-Investigator for the Upper Atmosphere Research Program and for the Planetary Atmospheres Program, and he was Principal Investigator for NASA's Returned Lunar Sample Program. He also served on the editorial board of Chemical Geology. *Dr. Nava, who received a PhD in chemistry from Arizona State University, has worked at Goddard for 21 years and has received two NASA Special Achievement Awards and a NASA Exceptional Performance Award.*

Dr. Walter A. Payne, Jr., an astrophysicist in the Astrochemistry Branch, is a Co-Investigator in the NASA Upper Atmosphere Program and in the NASA Planetary Atmospheres Program. His professional interests include chemical kinetics, photochemistry of small molecules, and laser-induced fluorescence. Dr. Payne, who earned a PhD in physical chemistry from Howard University, has been at Goddard for 20 years.

HIGH ENERGY ASTROPHYSICS

ELECTRON-TRAPPING MATERIALS AS PARTICLE-TRACKING DETECTORS

The microelectronics revolution of the past 2 decades has led the push toward "perfect" semiconductor materials—that is, materials with nothing to impede the smooth flow of electrons. A place where the electron flow in a material is disrupted is referred to as a trap. Typically, traps are caused by impurity atoms in the silicon or lattice dislocations and lead to decreased performance in standard silicon devices. It is possible, however, to exploit the traps caused by impurity atoms to "image" or localize sites of energy deposition. By a careful doping process, impurity states can be created that are well isolated from each other and well below the excitation energy to the conduction band at room temperatures. The accompanying figure illustrates the

band structure of such a material. The excitation energy from the impurity level to the conduction band is in the infrared range, between 800 and 1,600 nm.

The free electrons produced when a cosmic ray traverses such materials have a high probability of becoming trapped in these impurity states. These electrons are markers that indicate the passage of the cosmic ray nuclei through the detector. They remain trapped for long periods of time, on the order of hours. The surface of the material can then be probed with a laser (tuned to the appropriate energy) to release the trapped electrons. Their release produces an emission of visible light that can be detected with either a photomultiplier tube, CCD camera, or photodiode. By correlating the emission of the light pulse with the position of the probing laser, the location of the original ionizing particle can be determined. A series of such detectors can be used to follow a particle's trajectory through an instrument. To date, typical large-area tracking detectors have been able to attain position resolutions on the order of 100 μ at best. The major advantages of these new electron-trapping materials are that they can be made into large-area pieces at costs much lower than other position-sensitive silicon detectors and have a resolution approximately equal to their thickness, which can be as little as 8 μ.

Goddard researchers are exploring the use of these materials in a balloon-borne magnet spectrometer system. Planes of electron-trapping material about 40 × 40 cm in size will be stacked in the high magnetic-field region of the instrument. Above the magnet will be timing and charge-measuring paddles and energy-measuring Cherenkov detectors. The electron-trapping planes will provide a measurement of the particle rigidity—that is, its momentum per unit charge. The combined rigidity and energy measurements permit determination of the isotopic composition of the cosmic ray beam. The higher spatial resolution of the electron-trapping material will allow scientists to extend present measurements to higher energies than currently possible. The only other way to reach these energies would require a larger and heavier magnet—a severe constraint on either a balloon-launched or space-based experiment.

Currently, Goddard staff are working toward a rugged, flight-ready readout system. The current design is to have a coarse positioning system, perhaps composed of optical fibers, which will localize the cosmic ray nuclei to within a few square centimeters. This smaller region will then be scanned with an array of laser diodes to provide the high-resolution position information. A set of fiducial marks built into the material or its substrate will correlate the coarse- and fine-coordinate measurements.

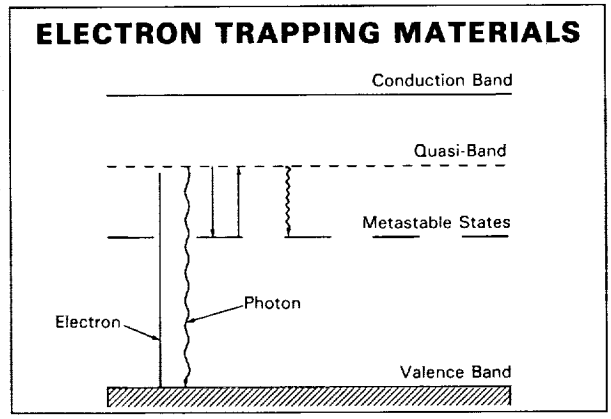

Schematic energy band structure of a typical electron-trapping semiconductor. The metastable states are produced by doping with impurity atoms. Electrons are stored in the metastable states until read out by a laser scanned across the material surface.

Contact: Louis M. Barbier
National Academy of Sciences/
National Research Council (Code 661)
(301) 286-4054
Jonathan F. Ormes (Code 660)
(301) 286-6811

Sponsor: National Academy of Sciences/National Research Council

Dr. Louis M. Barbier conducts research on cosmic-ray astrophysics and designs new instruments for studying the cosmic-ray composition and spectra, including scintillating fiberoptic detectors, electron-trapping semiconductors, silicon strip detectors, and Cherenkov detectors. Dr. Barbier holds an MS and a PhD from Louisiana State University.

Dr. Jonathan F. Ormes is Associate Chief of the Laboratory for High Energy Astrophysics and Acting Chief of the Nuclear Astrophysics Branch. He is currently Project Scientist for Astromag and Principal Investigator for the Large Isotope Spectrometer for Astromag. He received the NASA Exceptional Service Medal in 1986 and earned his PhD in physics.

SUPERNOVA 1987A: THE GAMMA-RAY IMAGING SPECTROMETER (GRIS) GAMMA-RAY LINE PROFILES

GRIS is one of a new generation of powerful spectrometers designed to achieve the combination of high sensitivity and high resolution necessary to measure the shape of gamma-ray lines from astrophysical sources. Virtually all scientific knowledge of the atomic processes that dominate the surface of stars is based on the spectroscopy of optical lines. This breakthrough in technology promises the same type of sensitive probe for the high energy physics of nuclear processes in hot, violent astrophysical sites such as supernova explosions and black hole accretion systems. It is an extraordinary coincidence that Supernova 1987A (which happens once in 400 years) occurred just as this new instrument was ready. GRIS was rushed to completion, and in two highly successful balloon flights (spring and fall of 1988 in Alice Springs, Australia) it measured the shape of the gamma-ray lines from the radioactive decay of the freshly synthesized element ^{56}Cobalt (Co). There were 1.5×10^{26} metric tons (25,000 times the mass of the Earth) of this radioactive material created in the supernova explosion. The decay of this element is the dominant source of energy in the supernova after the first week, and it directly produces the gamma-ray lines Goddard researchers observed. The final product of this decay is ^{56}Iron isotope mass, and

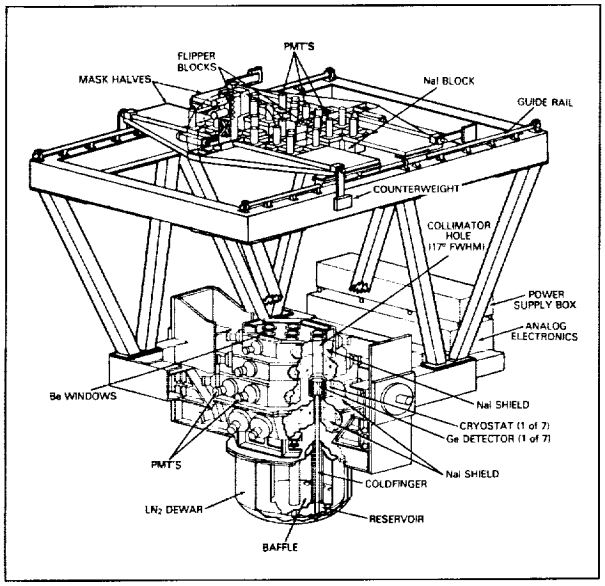

The Gamma-Ray Imaging Spectrometer.

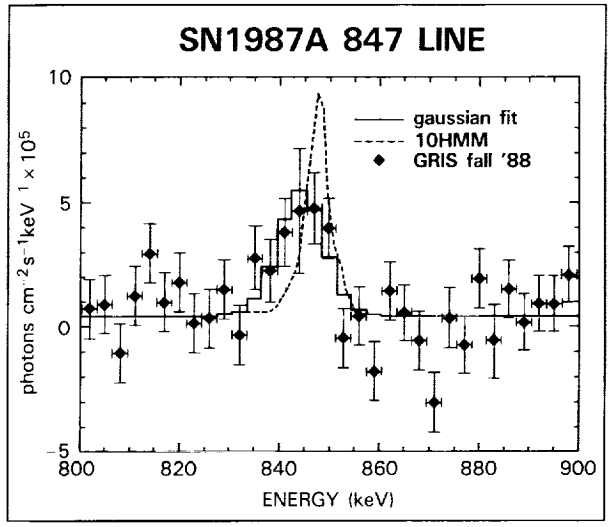

The GRIS data for the 847-keV line in the fall flight; the best-fit Gaussian line profile; and the line profile predicted by the 10HMM model of Pinto and Woosley.

supernovae are the dominant source of the iron in our galaxy, including the core of the Earth.

The initial discovery of gamma-ray lines from Supernova 1987A was made by the gamma-ray spectrometer on the Solar Maximum Mission (SMM) and confirmed by balloon-borne experiments. The direct confirmation of core collapse theory by the observation of lines from the decay of ^{56}Co rivals in scientific significance the confirmation of core collapse theory by the observation of the neutrino burst from Supernova 1987A. Theories of the development of the early supernova remnant were not as successful. The surprisingly early turnon of the gamma-ray lines and the flat gamma-ray light curve after turnon were inconsistent with early models. The introduction of mixing allowed the escape of gamma rays at a time when the remnant was still optically thick. These spherically symmetric mixed models were adjusted to fix the early gamma-ray line light curves and the ~0.075 solar masses ($M_\odot$) of ^{56}Co determined from the bolometric light curve. Although different in detail, the predictions of these models for the gamma-ray line profiles were similar: the lines would be blueshifted as the gamma-rays escaped from the approaching surface while most of the redshifted material was still hidden by the optically thick remnant. Since scintillation spectrometers like SMM do not have sufficient energy resolution to measure the supernova line profiles, these measurements could not be made by the balloon-borne

germanium spectrometer experiments. GRIS (see the first figure) was the largest and most sensitive of the instruments available in time to observe the supernova lines. The GRIS measurements of the gamma-ray line profiles are crucial to understanding the dynamics of the expanding supernova remnant and will require significant changes in the existing theoretical models.

GRIS uses many techniques to achieve a dramatic improvement over the previous generation of instruments. The improved resolution provided by germanium detectors is six times more sensitive than an equivalent sodium iodide (NaI) detector for narrow lines at 1 MeV. GRIS uses an array of seven very large detectors, a very heavy active shield (≥=15-cm NaI), and custom-designed low-mass cryostats and shield housings to achieve sensitivity three to eight times greater than the Center's previous germanium balloon experiment, the Low Energy Gamma Ray Spectrometer. This achieved sensitivity for a single transit of the source is about twice as good as the High Energy Astrophysics Observatory-3 satellite achieved in its all-sky survey and is nearly the same as the predicted sensitivity of the Oriented Scintillation Spectrometer Experiment on Gamma-Ray Observatory (GRO) for equivalent observing times.

The gamma-ray lines from the decay of ^{56}Co produced by Supernova 1987A were observed during both flights of GRIS. Gaussian profiles yield acceptable least-squares fits to the lines, and the resulting parameters are summarized in the accompanying tables. On day 433 after the initial optical sighting (spring flight), the 847- and 1,238-keV lines were observed at 2.3 and 4.3 sigma significance. On day 613 (fall flight), the lines at 847, 1,238, and 2,599 keV were observed at 4.6, 3.4, and 1.9 sigma respectively. The combined significance for the three-line complex in both flights is 7.8 sigma. The second figure shows the GRIS data for the 847-keV line in the fall flight and the best-fit Gaussian line profile. The line profiles are centered on the red side of the rest energy with typical velocity dispersions of ~3,500 km s^{-1} full width half maximum (FWHM).

Gris Supernova 1987A Gamma-Ray Line Fluxes

Day No. (After Explosion)	Line Rest Energy (keV)	Flux (ph cm^{-2} s^{-1})	Fraction of Mission From 0.75 M. of ^{56}Co
433	846.8	(21 + 12.,-9) 10^{-4}	20 + 11,-8 %
433	1238.3	(9.1 2,1) 10^{-4}	13 3%
613	846.8	(6.5 1.4) 10^{-4}	31 7%
613	1238.3	(3.1 0.9) 10^{-4}	22 6 %
613	2598.6	(1.3 + 1.1, - 0.7) 10^{-4}	37 + 31, - 19%

Gris Supernova 1987A Gamma-Ray Line Profiles

Day No.	Peak Energy (keV) Doppler Shift (km s^{-1})			FWHM [keV and (km s^{-1})]	
	Measured	LMC[a]	Model (10HMM)[b]	Measured	Model (10HMM)
433	844.6 1.2[c] (500 425)	846.0	848.7 (-950)	8.7 + 4.9,-3.3[b] (3100 1700)	5.4 (1900)
433	1235.5 2.2 (400 525)	1237.2	1240.1 (-700)	14.8 5.2 (3600 1300)	7.3 (1800)
613	844.2 1.3 (650 450)	846.0	848.0 (-700)	10.8 + 2.9,-2.4 (3800 1000)	5.5 (1900)
613	1233.5 1.8 (900 425)	1237.2	1239.6 (-575)	11.0 + 3.7,-3.1 (2700 900)	6.5 (1600)
613	2589 + 16,-6 (825 + 700,-1850)	2596.2		20.2 + 23.6,-9.9 (2300 + 1100,-2700)	

[a] *Rest energy of line corrected for Large Magellanic Cloud redshift.*
[b] *Corrected for Large Magellanic Cloud redshift.*
[c] *Statistical errors only (systematic background subtraction effects may be significant).*

The line fluxes derived from these fits are consistent with spherically symmetric mixed models of the supernova shell, but the line profiles are not. The line profile predicted by the 10HMM model of Pinto and Woosley is shown by the dashed line in the second figure for comparison with the GRIS data. The peak energies of all the lines are consistently lower and the line widths are consistently greater than predicted. The combined significance of the differences between the data and the 10HMM model is 4.9 sigma for the line centroids and 3.0 sigma for the widths (spring flight 847- and fall flight 2,599-keV lines not included). The large widths associated with the lines imply high velocities for the ^{56}Co, which must have been mixed or accelerated into higher velocity layers of the expanding supernova shell. Unmixed models produce line widths that are <6 keV full width. The observed line profiles shown in the lower table are consistent with a transparent source, but the line flux values, also shown in the first table, require a significant optical depth to explain the bolometric light curve, which is primarily powered by radioactive decay. This apparent paradox may be resolved by dropping assumptions of spherical symmetry or homogeneity. An example of a possible model is one containing dense knots or filaments, which are optically thick, with ample space between them to see the receding back side of the remnant. Another possible model is a flattened disk where one can see over the top of the disk to the receding material. The general conclusion is that the gamma-ray line profiles, shown in the smaller table, indicate the need for further changes in the geometry of the models of the expanding remnant.

Significant advances are planned for future flights of GRIS, including detector segmentation, which will reject localized background to double the detector's sensitivity by a factor of two; a coded aperture imaging system to position point sources; and a new shield of bismuth germanate scintillator to reduce background and payload weight. GRIS is more than just a testbed for new technology. High sensitivity and high resolution will make GRIS one of the premier instruments for gamma-ray astronomy until it is superseded by a satellite instrument of similar capabilities such as the Nuclear Astrophysics Explorer (NAE) described elsewhere in this report. Goddard researchers are hopeful that new discoveries by the gamma-ray astronomy satellites GRO and Gamma 1, both to be launched within a year, will provide a growing list of new targets for high-resolution spectroscopy and keep this instrument active for many years to come. The Supernova 1987A results clearly illustrate the power of high-resolution spectroscopy to extract from the spectra of astrophysical sources significant new information not available to NaI detectors.

Contact: Jack Tueller (Code 661)
(301) 286-4678
Sponsor: Laboratory for High Energy Astrophysics

Dr. Jack Tueller, working with the Low Energy Gamma Ray Spectrometer group of the Cosmic Ray Branch, serves as Co-Investigator on both the GRIS balloon experiment and the NAE.

COSMIC RAYS AND DYNAMIC BALANCE IN THE MAGELLANIC CLOUDS

In the near future, high-energy gamma-ray astronomy offers the promise of a new means of examining the closest galaxies. The Small and Large Magellanic Clouds should be visible to the high-energy gamma-ray telescope on the GRO and Gamma-1. Goddard researchers expect the telescopes to be able to examine the intensity and structure of the Magellanic Clouds enough to study the cosmic ray density and its variation at least on a coarse scale and, thereby, determine several aspects of the nature of the dynamic balance.

The already existing radio synchrotron data provide information on the high-energy cosmic ray electrons interacting with the magnetic fields. A study of this information on the Large Magellanic Clouds suggests that the cosmic ray electron energy density in the central region is similar to that in the local region of our galaxy. If the ratios of cosmic ray electrons to cosmic ray nucleons are the same in each galaxy, then the cosmic ray nucleon energy density would be similar. Goddard researchers reached the same conclusion on the basis of the Large Magellanic Clouds matter density and the assumption of the same ratio for the cosmic ray pressure density to the magnetic field pressure density. Hence, within the uncertainties, the synchrotron radiation supports the concepts of similar cosmic ray spectra in the Large Magellanic Clouds and dynamic balance.

If the appropriate gamma-ray measurements can be made with sufficient accuracy, it should also be possible to obtain a better estimate of the molecular hydrogen content in the Magellanic Clouds, or more specifically the normalizing factor. This is true because,

by using the high-energy gamma-ray data from both galaxies and the variations within the galaxies, the cosmic ray energy density should be understood reasonably well. By varying the molecular hydrogen normalization, the factor most consistent with the data can be determined because of the significant difference in the average molecular hydrogen density in the two galaxies and the highly concentrated nature of the molecular hydrogen relative to the atomic hydrogen in the Large Magellanic Clouds. The molecular hydrogen normalization factor should be determined to within a factor of two or better on the basis of the number of photons expected to be observed, thereby permitting a reduction in the uncertainty for the normalization of the molecular hydrogen content. The factor of two or better comes principally from the fact that the molecular hydrogen is highly concentrated in a few small regions at and to the south of the 30 Doradus region in the Large Magellanic Clouds.

Detectable photons from the Magellanic Clouds should be sufficient in number to measure the energy spectrum adequately to determine if it is markedly different from the energy spectrum in our own galaxy. For example, it should be possible to see if the cosmic ray electrons are playing a greater or lesser role than the nucleons in the production of gamma rays.

Contact: Carl E. Fichtel (Code 660)
(301) 286-6281

Sponsor: Gamma Ray Astrophysics Branch

Dr. Carl E. Fichtel is Chief Scientist at the Laboratory for High Energy Astrophysics and Acting Chief of the Gamma Ray Astrophysics Branch. His efforts include work on sounding rocket, balloon, and small astronomy satellite projects. He has received several Special Achievement Awards during his 29 years at Goddard and holds a PhD from Washington University in St. Louis.

GAMMA RAYS FROM THE GALACTIC CENTER

The galactic center source of gamma-ray line emission at 511 keV has reappeared after being in a quiescent state since the early 1980's. The line was observed by the GRIS, a new-generation balloon instrument developed by Goddard's Low Energy Gamma-Ray group in the Laboratory for High Energy Astrophysics.

The 511-KeV line is thought to be the signature of positron annihilation in the galactic center region. Positrons are produced in astrophysical sites by energetic processes such as the interaction of two gamma rays or the decay of radioactive nuclei. They then annihilate with electrons in the region, producing either two 511-keV gamma rays (energy equal to the positron rest mass) or three gamma rays with energies between 0 and 511 keV. The spectrum from such a source is therefore expected to have a sharp line at 511 keV, with a width that depends on the temperature of the annihilation region, plus a continuum below the line.

In 1970, a line near 511 keV was discovered in the spectrum of the galactic center region. The identification of the line as positron annihilation radiation was not unambiguous, however, due to the limited resolving power of the sodium iodide detectors used at that time. In 1977 the line was observed for the first time with a high-resolution germanium detector and found to be a narrow line at exactly 511 keV, accompanied by a continuum below the line indicative of the 3-photon annihilation. The strength of the line was impressive at about 10^{-3} photons $cm^{-2}s^{-1}$, which translates into a luminosity of about 10^{37} ergs s^{-1} assuming a source at the galactic center distance emitting isotopically. This remarkable energy is equal to several thousand solar luminosities in a single spectral line! Both of these observations were made with balloon-borne spectrometers.

The next critical gamma-ray measurement of the galactic center was made from space by the spectrometer on High Energy Astrophysics Observatory-3. With germanium detectors, the spectrometer observed the line in the fall of 1979 at about the same strength as the earlier detections. However, when the instrument scanned the region again in the spring of 1980, the line intensity was significantly reduced. The source was turning off. These were important observations, because they gave the first information on the source size. The fact that the source changed intensity in half a year implied to researchers that the source had a spatial extent of less than one-half of a light-year.

In 1981 and again in 1984, balloon-borne spectrometers failed to detect the positron annihilation line, confirming that the source at the galactic center had turned off. However, throughout this time period the gamma-ray instrument on the SMM did detect a line at 511 keV. Since that instrument has a larger field of view than the balloon spectrometers (130° versus 15°), researchers

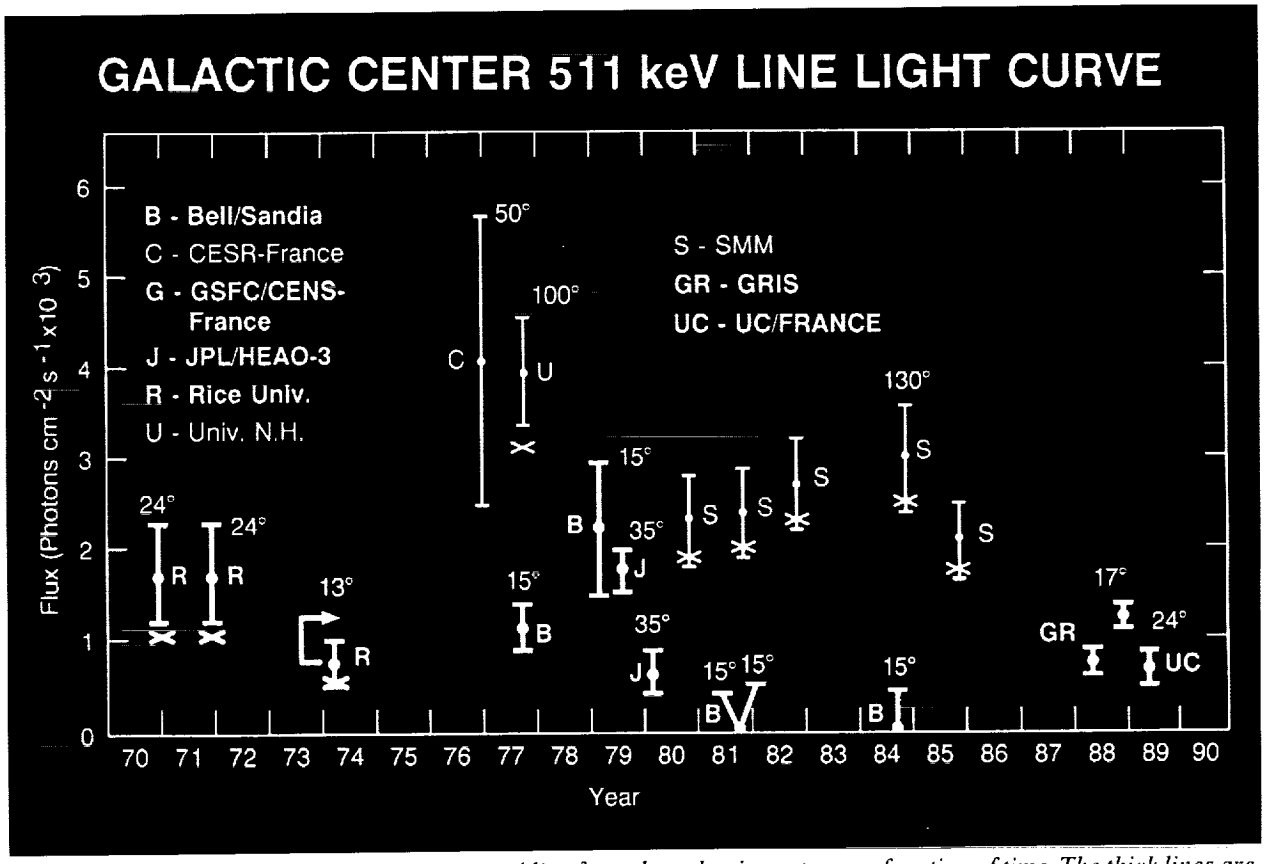

Measurements of the flux in the 511-keV spectral line from the galactic center as a function of time. The thick lines are for instruments with field of view less than 40°, and the thin lines are for greater than 40°. Fluxes measured by moderate-resolution sodium iodide detectors must be corrected for the contribution of the 3-photon continuum to the line. Corrected fluxes are indicated by the arrow, because the measurement was 4.2° off the galactic center.

believe that it was detecting a diffuse positron annihilation emission from the galactic plane.

By the mid-1980's researchers had concluded that there were two components to the 511- keV line emission from the galactic center region, a pointlike source near the galactic center and a distributed source along the galactic plane. The pointlike source was "on" in the 1970's and then turned off in 1979 to 1980. The first figure shows the sequence of measurements from 1970 through the present. Since all instruments involved in these observations have relatively wide fields of view (>15°) by astronomical standards and no imaging capabilities, the exact location of the pointlike source was not known, and its spatial extent was only indirectly surmised from the High Energy Astrophysics Observatory-3 time measurement.

In 1988 two new observations of the galactic center were made by the powerful new GRIS balloon instrument. The instrument was developed by scientists, engineers, technicians, and students in the Low Energy Gamma-Ray group in collaboration with groups at a private laboratory and at Sandia National Laboratories. A schematic of GRIS is shown in the second figure. It consists of seven large germanium detectors surrounded by a thick sodium iodide anticoincidence shield. The detectors are cooled to ~90 °K by liquid nitrogen. The field of view is 17° FWHM defined by aperture holes in the shield. The detector-effective area at 511-keV is 85 cm^2, and the energy resolution is 1.8 keV FWHM. The payload launch weight is 1,680 kg. The GRIS instrument has a major portion of the world's largest germanium detectors and is the most sensitive astrophysical gamma-ray spectrometer in existence.

The GRIS observations of the galactic center were performed in May 1988 and October 1988. The balloon flights were made from Alice Springs, Australia, in the middle of the great central desert. This remote location was chosen because of its good view of the galactic center in the southern skies, its low population density, and its long distance from the ocean. The May flight lasted 23 hours. Eleven hours were spent observing the galactic center and 12 hours were spent observing Supernova 1987A. The October flight lasted 44 hours, which allowed two separate, approximately 10-hour observations of the galactic center region. The quality of the data was so good from the first observation that a real-time decision was made during the flight to point the instrument 25° west of the galactic center (but still in the galactic plane) for the second observation. The purpose of this pointing was to exclude the galactic center from the GRIS field of view and thereby obtain the first direct measurement of the spatial distribution of the 511-keV line along the galactic plane.

The spectra between 350 and 700 keV for the May and October galactic center observations and for the October galactic plane observation are shown in the third figure. An intense line at 511 keV is seen in both galactic center spectra, but is virtually absent from the galactic plane spectrum. GRIS scientists have analyzed these spectra in detail and have achieved several new and exciting results by fitting each spectrum with a Gaussian line plus a continuum with a step at 511 keV (for the 3-photon annihilation).

The major discovery from these observations is that the galactic center source had turned back "on" again. The line flux observed was close to the 10^{-3} photons $cm^{-2}s^{-1}$ level (1.0×10^{-3} May; 1.2×10^{-3} October) that had been seen in the 1970's. The second important result was that the line flux was much lower ($\sim 0.2 \times 10^{-3}$ photons $cm^{-2}s^{-1}$) for the galactic plane observation. Since that pointing just excluded the galactic center, the implication is that the intense source of positron annihilation radiation is narrowly confined (to within a few degrees) to the actual galactic center region of the sky.

The third result is that the width of the galactic center line (October data) was 3.5 keV. This was the first time the line width had been measured; the findings suggest a temperature in the annihilation region of $<10^5$ °K.

There are several candidates for the positron source in the galactic center region. The most promising hypothesis is a black hole at the dynamic center of the galaxy. Positrons could be produced in sufficient quantities in the hot, violent region near the black hole where material and possibly whole stars swirl inward. Some fraction of the positrons might then escape to cooler regions where they annihilate. The on and off states of the 511-keV line would correspond to times of more and less material infall. Other possibilities for the positron source include the binary x-ray sources in the galactic center region, such as GX1+4. The GRIS team hopes to solve the mystery of which source is producing the positron annihilation radiation in the next flight. A coded-aperture imaging system will be added for that flight that will allow a point source of 511-keV line emission to be located to better than 1°.

Contact: Neil A. Gehrels (Code 661)
(301) 286-6546

Sponsor: High Energy Astrophysics Branch, Supporting Research and Technology Program

Dr. Neil A. Gehrels is the Instrument Scientist for the Nuclear Astrophysics Explorer and the WIND

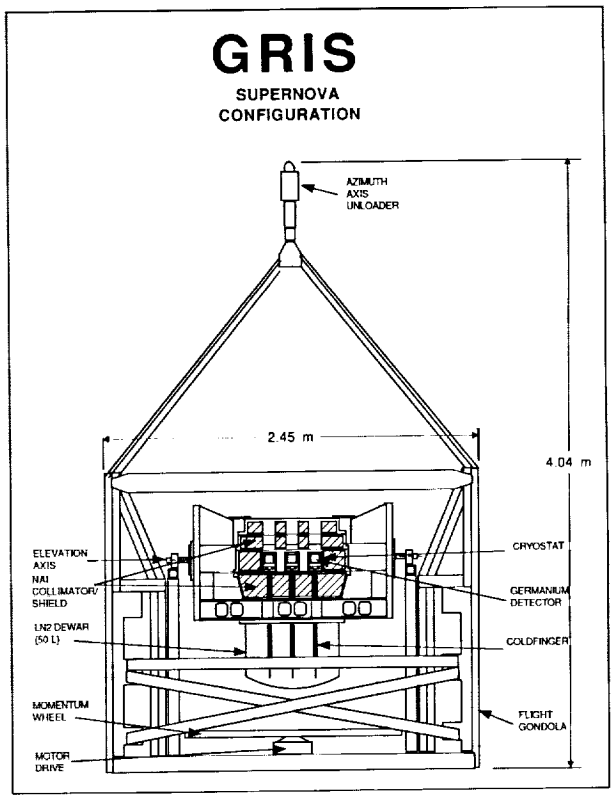

Schematic of the GRIS instrument, without the coded-aperture imaging system.

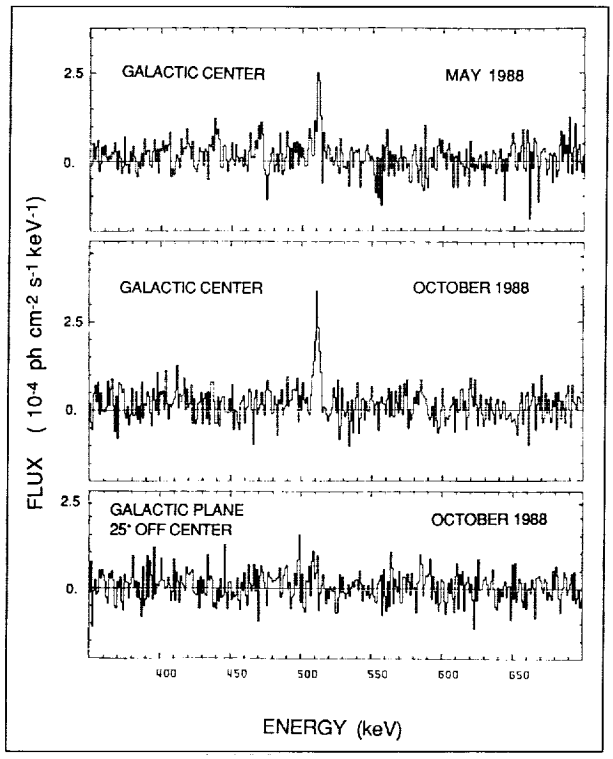

Gamma-ray spectrum between 350 and 700 keV of the galactic center in May and October 1988 and of the galactic plane 25 °away from the center in October 1988. The 511-keV positron annihilation line is strong in the galactic center spectra, but almost nonexistent in the galactic plane spectrum.

Transient Gamma-Ray Spectrometer and is an Investigator on the GRIS and the Galileo Heavy Ion Counter. Dr. Gehrels has 7 years' experience at Goddard and has earned a PhD in physics from the California Institute of Technology.

GAMMA-RAY ASTRONOMY AND THE SEARCH FOR THE MISSING MASS

More and more, cosmologists, particle physicists, and astronomers are reaching the opinion that nine-tenths of the mass of the galaxy, and perhaps even a greater fraction of the mass of the universe, may be in an entirely different form than the ordinary stars, gas, and plasma with which astronomers have long been familiar. This matter, manifested by its gravitational effects within and between galaxies and clusters of galaxies, is in a form as yet unseen, not only in visible radiation, but also in radiation in all other wavelength ranges opened up by the advent of the space age.

The past decade has seen the dawn of a new era of partnership for particle physicists and astrophysicists. An excellent example of this new symbiosis involves the question of the nature of the unseen dark matter or "missing mass." The missing mass problem is an old one in astronomy, having first been framed by Fritz Zwicky in the 1930's. Zwicky noticed that clusters of galaxies did not appear to have enough total mass in their stars to gravitationally bind the galaxies into clusters. It is known now from studies of the motion of stars in the outer regions of galaxies that there must be nonluminous matter in the galaxies themselves which far outweighs their stellar mass. This mass appears to be in the form of halos of gravitating matter which probably extend far beyond the visible stellar disks of galaxies. There are various reasons for believing that the dark matter is not ordinary matter made up of protons, neutrons, and electrons, but may be in the form of exotic new particles predicted by theoretical physicists.

Many cosmologists and particle physicists would like to have enough dark matter around to close the universe gravitationally. Additionally, cosmologists have found that an abundance of dark matter with primordial density fluctuations appears to be necessary to condense and form galaxies gravitationally without conflicting with measurements of the uniformity of the universal microwave background radiation from the big bang. In order to form galaxies and quasars early enough in the history of the universe, it appears necessary that the dark matter in galaxies should be "cold"; i.e., it should not have had large thermal velocities at the time in the early universe when it became gravitationally dominant. One way of ensuring this would be for the dark matter to be made of neutral particles left over from the early stages of the big bang, which would have masses much larger than the proton mass.

Such particles, which theorists calculate would be left over from the big bang in the required quantities, are actually predicted by a particle theory called "supersymmetry," a theory which may play a crucial role in understanding the unification of all the known forces. The heavy, weakly interacting particles predicted by supersymmetry theory are counterparts of known particles, such as photons, and postulated particles, such as the

so-called Higgs bosons, that play a crucial role in unifying the electromagnetic and weak interactions. The supersymmetric partners of these particles are known as "photinos" and "higgsinos."

Particles like photinos and higgsinos have an interesting property; they are their own antiparticles. They can annihilate with others of their own kind. This suicidal tendency is a lucky break for high-energy astrophysicists, because when such particles annihilate, they produce "ordinary" things which are observable, including cosmic gamma rays. Such radiation will have calculable spectral characteristics for which astrophysicists can search with gamma-ray telescopes as the signature of dark-matter annihilation.

Recently, researchers at Goddard and the U.S. Naval Research Laboratory have been able to calculate in great detail exactly what these annihilation spectra should look like. To perform this calculation, they employed an elaborate computer program developed originally by particle physicists to help determine the nature of annihilation products produced in high-energy electron-positron accelerators. The program is based on the theory of strong interactions known as quantum chromodynamics or QCD. The researchers adapted this program to predict spectra of the annihilation products of supersymmetric particles.

In a recent journal article, they reported the following important characteristics of the predicted cosmic gamma-ray spectrum: (1) a high-energy cutoff at an energy of about Mc^2, where M is the mass of the exotic dark-matter particles; (2) a peak in the energy spectrum at an energy of approximately 100 MeV; (3) a spectrum that is much harder than that from competing sources in the 100-MeV energy range; and (4) in some cases, a possibly observable monochromatic line at energy Mc^2. By calculating their fluxes and energy spectra, these researchers have shown that annihilation gamma rays, although of measurable numbers, may be difficult to study. The difficulty lies in distinguishing them from those expected to be produced in similar quantities by cosmic-ray collisions. However, the galaxy may have a dense core of dark-matter particles at its center that may show up as an observable hard gamma-ray source around 100-MeV energy, which could be detected by the Energetic Gamma Ray Experiment Telescope (EGRET) spark chamber telescope on GRO. It may also be possible to detect annihilation gamma rays from a halo of dark matter surrounding the galaxy if one looks perpendicular to the disk of the galaxy in regions of low gas density. In such patches of the sky, competing gamma radiation from cosmic-ray collisions would be minimized.

Future gamma-ray telescopes using technology just now being developed, such as liquid argon drift chambers, may have a chance of making the definitive "smoking gun" test of exotic dark-matter particles. In principle, their energy resolution and sensitivity could be good enough to look for characteristic high-energy gamma-ray spectral lines produced by dark-matter annihilation. These lines would be at an energy several thousand times that of ordinary nuclear gamma-ray lines. Lines at such energies could be produced only by very heavy dark-matter particles.*

**Allan Tylka of the U.S. Naval Research Laboratory is Dr. Stecker's partner in this research.*

Contact: Floyd W. Stecker (Code 665)
(301) 286-6057

Sponsor: Office of Space Science and Applications, Laboratory for High Energy Physics

Dr. Floyd W. Stecker, a theoretical astrophysicist, pursues interests in many fields: high-energy astrophysics; infrared, gamma-ray, and neutrino astronomy; galactic structure and formation theory; cosmology and particle physics. He has published articles in major journals, and he wrote the first book on gamma-ray astronomy, Cosmic Gamma Rays. *He earned a PhD at Harvard University, has 22 years' experience at Goddard, and has received the NASA Medal for Exceptional Scientific Achievement.*

NEW DRIFT CHAMBER TECHNOLOGY FOR HIGH-ENERGY GAMMA-RAY TELESCOPES

High-energy (10-MeV to >20-GeV) gamma-ray astronomy permits the direct study of the largest transfers of energy occurring in astrophysical processes, including rapid expansion processes, explosions, high-energy particle acceleration and interactions, high-energy emission from superdense objects, and nucleon-antinucleon annihilations. In the era of gamma-ray astronomy following the results from the EGRET experiment on the GRO, additional improvements in angular resolution, sensitivity, and possibly energy resolution will be required to continue the

study of gamma-ray processes in the universe. To date, gamma ray telescopes—Small Astronomy Satellite-2, COS-B, Gamma-1, and EGRET—have used an assembly of high-voltage spark chambers interleaved with high-Z metal foils, which provide the pair production medium, to record a picture of the two electron and positron tracks produced when a high-energy gamma ray undergoes electron-positron pair production. The picture of the "A" formed by the electron and positron gives a unique signature to identify a gamma-ray event and a means to determine its direction and energy. To achieve the angular resolution, energy determination, and sensitivity goals that will permit continued advances in gamma-ray astronomy, the next generation of gamma-ray telescope is envisioned as a 2-m-class instrument, a picture-type detector with an aperture of approximately 2 × 2 m and a depth of about 4 m. A new technology approach, using alternatives to spark chambers, will be needed to construct such an instrument.

Orthogonal wire grid spark chambers have been the detector of choice for space use because of their low power requirements, high efficiency, simplicity, and suitability for space. The track resolution of spark chambers is limited, however, by their inherent digital nature and by scattering of the electrons in the high-Z foils. Both of these effects reduce the accuracy to which the direction of the incident gamma ray can be determined. Also, the long, ~0.1-s recharge time of the high-voltage pulsers becomes a significant contributor to the deadtime of spark chamber instruments as they are made larger. For this and other reasons, the use of high-efficiency spark chambers with apertures of 2 × 2 m is probably not feasible. Large-area drift chambers are an attractive alternative for a picture-type detector. They have long been used at accelerators, but have not been viable for use in space because of the power required by their high-speed amplifiers and discriminators and the need to find appropriate materials and mechanical approaches for their fabrication. Goddard researchers have been working toward finding solutions to these problems.

Drift chambers have many advantageous properties such as high spatial track resolution of approximately 0.1 mm. Xenon gas can be used as the main component of the drift gas where it can also double as the pair production medium. Thus, the large-area high-Z metal foils, which are difficult to make, are not needed. This reduces the electron scattering and some of the mechanical design constraints. The high track resolution and reduced electron scattering combine to improve the instrument angular resolution. The drift chamber readout time for a gamma-ray event can be reduced to less than 20 μs, which reduces the instrument deadtime and increases the instrument sensitivity.

The material from which the drift chamber frame is made must be strong, lightweight, nonconducting, and low outgassing. Additional desirable properties include fracture resistance, machinability, and bondability. Various plastic and composite materials have been considered in an extensive study of new materials. The 0.5- × 0.5-m drift chamber frames were made from G-10, a glass/epoxy material, because of its nonconductivity, availability, machinability, and low cost. S-2/PEEK, a material similar to G-10, but stronger and lighter, has been identified as the best material currently available for construction of large 2-m-class frames. Goddard staff are currently working on the mechanical design of an instrument using 2-m-class drift chambers. This instrument will be used for mechanical and electrical tests of space-qualifiable large-area drift chambers.

Modern electronics has made it possible to design an amplifier and discriminator with power reduced to a level suitable for use in space. The amplifier and discriminator design will be tested on a gamma-ray telescope built with 0.5- × 0.5-m drift chambers. The amplifier is a discrete four-transistor surface-mount design with a gain of 30, 20-ns risetime, and 20-mW power. The discriminator is a discrete 10-transistor surface-mount design with a variable threshold and 135-mW power. The power of typical commercial designs is 65 mW for the amplifier and 375 mW for the discriminator.

In addition to the amplifier and discriminator, Goddard scientists have developed a 12-channel quad time-to-amplitude converter (TAC). Each TAC is a two-field-effect transistor constant-voltage circuit with operational amplifier buffer output. The constant-voltage design was chosen because it is simpler and more stable than a constant-current design. The quad TAC circuit of each channel allows four separate timing measurements to be made for each anode: the electron, the positron, a random cosmic ray, and one for redundancy.

In summary, xenon gas drift chambers, modern composite materials, and low-power electronics offer technological advantages that now make it possible to pursue the

construction of a next-generation high-energy gamma-ray telescope with exceptional capabilities.

Contact: Stanley D. Hunter (Code 662)
(301) 286-7280

Sponsor: Supporting Research and Technology

Dr. Stanley D. Hunter, Co-Investigator on EGRET, earned his PhD at Louisiana State University. During his 4 years at Goddard, he has constructed and flown a solid-state star camera aspect system for use on balloon experiments. Dr. Hunter has also won a Special Achievement Award, a Certificate for Outstanding Performance, and a Quality Increase Award.

MICROCALORIMETRY USING KINETIC INDUCTANCE THERMOMETERS

Thermal x-ray detectors, or microcalorimeters, were first proposed by Moseley, Mather, and McCammon (1984) as a way of simultaneously achieving high-energy resolution (comparable to dispersive spectrometers) and high-quantum efficiency. Adapted from infrared bolometers, microcalorimeters measure the energy of individual x-ray photons by converting them into heat and sensing the resulting temperature increase as a change in voltage across a thermistor implanted into the device.

Researchers at Goddard and the University of Wisconsin are among several groups developing these devices, primarily for use in x-ray astronomy, although microcalorimeters have interesting applications in atomic and nuclear physics as well. An energy resolution of about 12 eV (FWHM at 6 keV) has been achieved using a low heat-capacity monolithic silicon design with mercury telluride (HgTe) as the x-ray absorber. The high spectral resolution of these monolithic devices is due largely to their low thermal conductance and optimized thermistor geometry. This optimization minimizes excess current noise ("1/f noise") and a known thermistor nonlinearity that decreases signal responsivity. Present work on these devices is centered on studying the thermalization properties of various materials, including superconductors, and producing a spaceflight-qualified microcalorimeter assembly for the Advanced X-Ray Astrophysics Facility mission.

Despite the substantial progress that has been made with the thermistor-type thermometers, it is useful to consider whether other types of temperature sensors offer advantages for improved spectral resolution or ease of fabrication. For example, in addition to the current noise and nonlinearity, resistive thermometers have Johnson noise as a fundamental noise component. On the engineering side, the electrical resistance of the thermistor at cryogenic temperatures depends strongly on the implant dose, thus placing very tight tolerances on the implantation and fabrication processes. One alternative which may avoid these problems is a capacitive thermometer being investigated by a group at Lawrence Livermore National Laboratory and the Lawrence Berkeley Laboratory; another alternative is an inductive thermometer, suggested by D.G. McDonald of National Institute of Standards and Technology (NIST) in 1987. The thermometer has a three-layer structure, as seen in the first figure. The meander strip (a 5- μm-wide line 70 mm long) and the ground

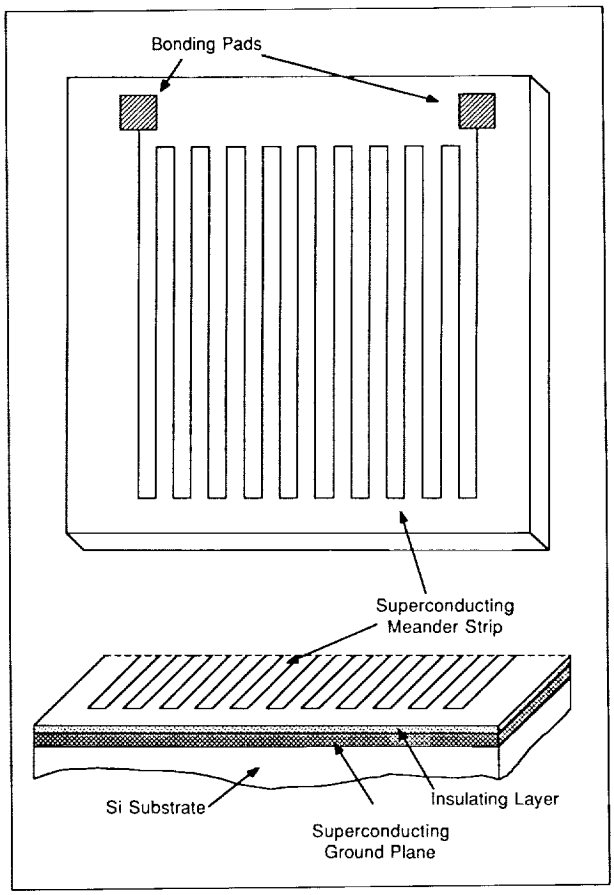

Top and section schematic views of prototype inductive thermometer.

plane are both superconductors. The inductance of a device with this geometry is due mainly to the inertia of the free electrons and thus depends on the magnetic penetration depth (the characteristic decay length into the superconductor of an external magnetic field). In this case, the inductance is termed kinetic inductance. Penetration depth depends on temperature, and the greatest temperature sensitivity occurs near the critical temperature of the superconductor.

There are two main advantages to the kinetic inductance approach: first, because there is no ohmic dissipation involved, there is no Johnson noise, and second, a low-noise, low-impedance superconducting quantum interference device amplifier can be used for the first stage of amplification. Because the inductor remains superconducting, the electronic component of the heat capacity is very low, giving a detectable temperature increase for small energy depositions. For maximum sensitivity, four inductors are configured into a bridge, and the signal is detected as a deviation from bridge balance. This design, shown in the second figure, requires two of the inductors to be thermally isolated, with one to set bridge balance and the other to act as the detector. Sauvageau and McDonald (1989) have constructed such an inductance bridge thermometer and demonstrated its operation near 8 °K for use in the infrared.

X-ray detectors have more stringent design constraints than the infrared detector. The heat capacity of the device must be minimized to allow detection of individual x-ray photons. This implies the use of very small substrates at cryogenic temperatures, as well as a careful consideration of the low-temperature properties of the materials used for the inductors and the supports. Because the electron contribution to the specific heat of a superconductor is large above the critical temperature, one of the layers should be well below the critical temperature to reduce the heat capacity. In addition, the thermal time constant of an ideal nondissipative detector is given by $\tau = C/G$, where C is the heat capacity and G is the thermal conductance to the heat sink. The thermal conductance must be chosen to give a small enough time constant to prevent pulse pileup.

Goddard researchers have designed a prototype device for operation at 1.5 °K. It has an aluminum ground plane and tin meander strip, both of which are easily deposited by thermal evaporation. Patterning of each of these layers is done using a liftoff technique, in which photoresist is patterned before metal deposition; the photoresist is then removed, leaving the metal pattern behind. The insulating layer between the strip and the ground plane is chemically deposited silicon oxide.

Goddard's early tests will use single inductors rather than a bridge of four. For this configuration, an oscillator readout has been developed whose frequency depends on the inductance of the thermometer. The expected energy resolution for a bridge of inductors like the prototype, using a commercial direct current superconducting quantum interference device readout, is 9.9 keV. While this is not sufficient to detect x-rays, scientists will be able to verify that the device is working using alpha particles with typical energy deposits of 5 MeV. Future plans call for operation at a lower temperature, giving lower thermal noise, and for the development of a low-noise superconducting quantum interference device readout. By reducing the readout noise below the level of the noise due to thermal fluctuations, researchers should be able to achieve a resolution of approximately 1 eV operating at a temperature of 0.1 °K.

Contact: Gayle L. Rawley,
National Academy of Sciences/
National Research Council (Code 666)
(301) 286-8100

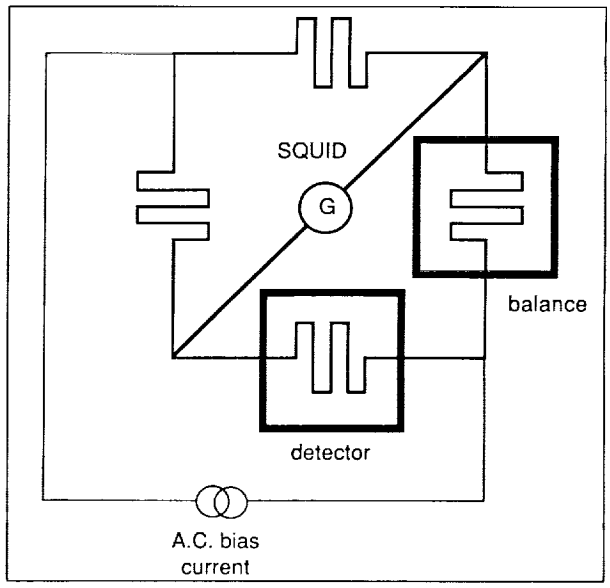

Schematic of inductance bridge.

Richard L. Kelley (Code 666)
(301) 286-7266

Sponsor: Goddard Director's Discretionary Fund, National Academy of Sciences/National Research Council Research Associateship Program

Dr. Gayle L. Rawley is a Resident Research Associate for the National Academy of Sciences/National Research Council. She is developing a new temperature sensor for high-resolution, high-throughput microcalorimeters (cryogenic x-ray detectors). Dr. Rawley received her PhD in physics from Princeton University.

Dr. Richard L. Kelley works with the calorimeter x-ray spectrometer for the Advanced X-Ray Astrophysics Facility, as well as with several other x-ray astronomy investigations being planned or developed in the Laboratory for High Energy Astrophysics. Dr. Kelley, who holds a PhD from the Massachusetts Institute of Technology, is interested in x-ray-emitting binary systems and the use of nondispersive x-ray spectrometers in astrophysics. He has been at Goddard for 7 years.

Data and Information

ORIGINAL PAGE
COLOR PHOTOGRAPH

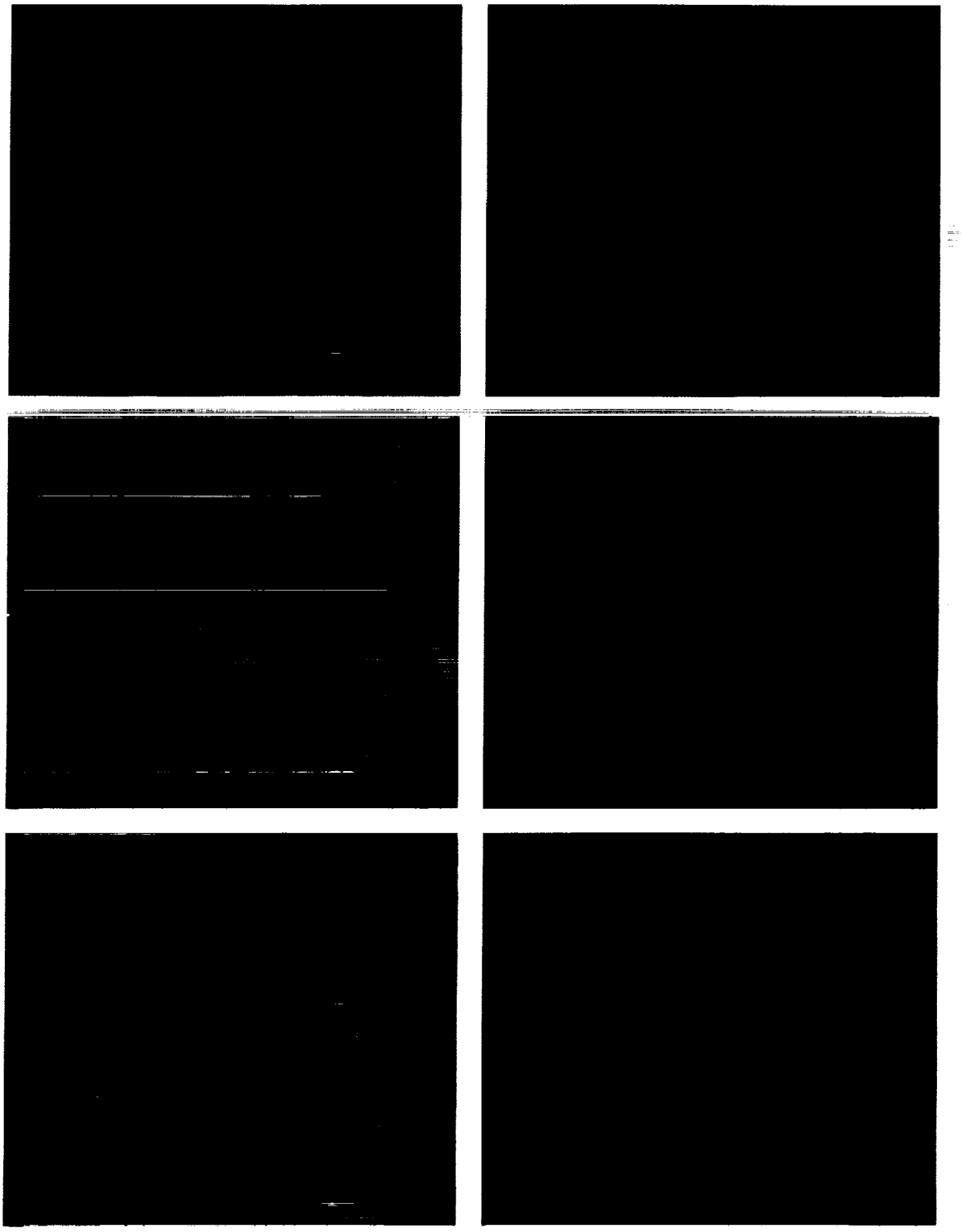

The scientist can manipulate the orientation of the sphere with a mouse. In this way, the entire sky can be viewed at once and without spatial or photometric distortion.

DATA AND INFORMATION

COSMIC BACKGROUND EXPLORER (COBE) ANALYSIS CENTER DEVELOPMENT

The COBE satellite, launched into a polar orbit in November 1989, observes the remnants of the big bang explosion that formed our universe and searches for data on the formation of the first galaxies. COBE, an entirely in-house Goddard project, carries three scientific experiments. The Differential Microwave Radiometer (DMR) measures the isotropy of the 2.7-K cosmic background radiation to the highest accuracy yet attempted. The Far Infrared Absolute Spectrophotometer (FIRAS) examines the spectrum of the cosmic background radiation over the whole sky, searching for deviations from the thermal character predicted by theories of the big bang. The Diffuse Infrared Background Experiment (DIRBE) observes the sky at 10 infrared wavelengths short of the cosmic background radiation. Its goal is to look for evidence of the earliest galaxy formation. Because the Earth is imbedded in the interplanetary dust cloud of our solar system, which glows brightly at many wavelengths, scientists must model the distribution, composition, and emission characteristics of this zodiacal dust to separate its effects from data of extragalactic origin.

The COBE data are very much oriented to all-sky analysis and require a great deal of careful global modeling to allow achievement of the science goals. The data analysis is an extremely complex task. The Space Data and Computing Division is supporting the COBE project through the development and operation of the COBE Analysis Center. The analysis center supports algorithmic and operational validation of the project pipeline (level 0 to level 1 processing) and scientific validation of the level 1 data products (data stripped of the instrumental and environmental signatures); development of the science pipeline (level 1 to level 2) software and production of the level 2 data sets (scientific models and model-corrected maps of the sky); and development of tools and techniques for science data modeling, display, and analysis. The accompanying figure illustrates one such data visualization tool Goddard scientists have developed. The center globe is a map of the sky in three of the infrared wavelengths COBE will observe. Three reflecting mirrors show the parts of the globe that are hidden from direct view. The scientist can manipulate the orientation of the sphere with a mouse. In this way, the entire sky can be viewed at once and without spatial or photometric distortion. This particular image uses false color to display the temperature of the radiation. Data from the 25-μ band are coded in blue; that is, the brightness of blue light in the picture is proportional to the brightness of the sky at 25-μ. Similarly, 60-μ and 100-μ data are coded with green and red, respectively. The resulting visible colors therefore represent the infrared colors or temperatures of the emitting material. The greenish-blue bands around the Equator of the globe arise from the interplanetary dust. (The Equator of the globe is the ecliptic plane of the solar system.) The ring of reddish-yellow material is the plane of the Milky Way galaxy. As the colors indicate, the dust from which the zodiacal light originates is hotter (bluer) than the dust in the galaxy. One goal of COBE is to model and subtract the light of the zodiacal dust to high accuracy

Iterative parallel region growing is being studied as a method for segmenting imagery. On the left is a Ridgely, Maryland TM image and segmentations to 64 and 49 regions, respectively. On the right is a Menengai Crater TM image and segmentation to 30 and 20 regions, respectively.

ORIGINAL PAGE
COLOR PHOTOGRAPH

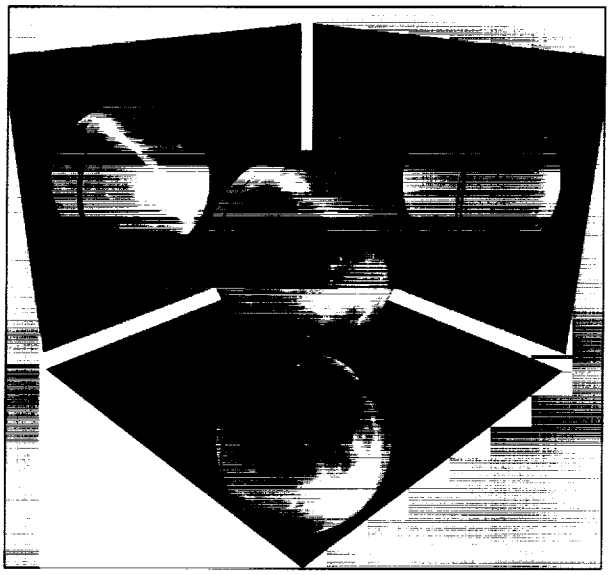

The sky reflected in three mirrors as COBE sees it.

to allow scientists to peer out to the galaxy and extragalactic space. This type of display helps to evaluate the success of such models and guides their improvement.

The COBE Analysis Center staff support approximately 75 full-time users, about half of whom are members of the Science Working Group, their graduate students and postdoctoral fellows, and guest observers. The remainder are contractors to the Science Working Group. In addition, Code 630 is providing civil service manpower with expertise in computer modeling, visualization, and COBE science. The analysis center hardware will include a VAX 6440 and approximately 20 imaging work stations in a single cluster. Each node will share access to at least 40 Gbytes of online storage and an optical disk jukebox with a capacity of about 300 Gbytes. Additional high-resolution image processors and image hard-copy devices will be available on the cluster.

The COBE level 0 to level 1 and level 1 to level 2 software is VMS dependent and COBE specific. The various display and analysis tools being developed are based on artificial intelligence Astronomical Image Processing System (AIPS) and Interactive Data Language (IDL), each of which has both VMS and Unix versions and will reside on a variety of work stations. The portability of these tools will be an important development goal, and the staff expect them to be useful to other scientific projects at Goddard and to the community at large.*

**The accompanying image was produced by David Hon of ST Systems, Inc., and William Spiesman of Applied Research Corporation.*

Contact: Richard A. White (Code 636)
(301) 286-7802

Sponsor: COBE Project

Dr. Richard A. White is Science Manager at the COBE Analysis Center. His technical interests are in science data modeling and visualization and in clusters of galaxies. He earned his PhD in astronomy and astrophysics from the University of Chicago. Dr. White has 9 years' experience at Goddard and currently works in the Space Data and Computing Division.

THE ROENTGEN SATELLITE (ROSAT) STANDARD DATA PROCESSING SYSTEM

ROSAT is an x-ray observatory that will be used for both an all-sky survey and for pointed observations of celestial x-ray sources. ROSAT is an international cooperative program among NASA, the Bundes Ministerium Forschung und Technologie of the Federal Republic of Germany, and the British Science and Engineering Council. Germany has provided the spacecraft, the x-ray telescope, and two redundant position-sensitive proportional counters located at the focal plane. The United Kingdom's contribution is the wide-field camera, which is coaligned with the optical axis of the telescope and is sensitive to extreme ultraviolet (EUV) light. NASA has provided another focal-plane instrument, the High-Resolution Imager, and will provide a Delta-2 launch in May 1990.

The ROSAT mission will support a guest observer program that will enable the astrophysical community to obtain high-resolution data on selected objects observed during previous missions (Einstein and EXOSAT, the European Satellite for X-Ray Astronomy, etc.) and objects identified from the all-sky survey. ROSAT will allow the logical and timely continuation of data gathering along the directions indicated by Einstein and provide new inputs for the observation program of the Advanced X-Ray Astrophysical Facility. The pointed data will be processed and distributed by both the Max Planck Institut fuer Extraterrestrisch Physik in Germany and the ROSAT Science Data Center at Goddard's Space Data and Computing Division.

The data will be processed at both centers using the Standard Data Processing System software package. This system is under strict configuration control to ensure data integrity on both sides of the Atlantic.

The Standard Data Processing System software will be used to produce scientifically useful results from the satellite data. This will be accomplished by applying the aspect solution, instrument corrections, and calibrations to the raw data. The Standard Data Processing System software consists of three integrated packages: the steering system, which provides interactive control and monitoring of the processing packages; the position-sensitive proportional counters instrument package; and the high-resolution imagers instrument package. This software will be run on a high-performance system, the main component of which is a VAX 8820 computer. The system has two central processing units providing multiprocessing capabilities, 128 Mbytes of memory, fast transfers of data by way of state-of-the-art tape and disk drive technology, exceptional graphics tools, and a dedicated 56-Kbyte line (high transfer rate) for data verification. An investigation is currently under way to explore the utilization of optical disk storage, a practical, new mechanism that is quickly replacing less efficient forms of data storage.

The output from this system will consist of contour maps, relevant housekeeping data, source spectral information, and a list of detected sources identified by celestial and detector coordinates. The output products will be checked for scientific validity by the ROSAT Science Data Center staff of the Space Data and Computing Division working in conjunction with the Smithsonian Astrophysical Observatory, a partner in the ROSAT Science Data Center.

An important result of the ROSAT mission will be identifying new x-ray sources discovered with the satellite. Spurious sources will also be detected due to statistical fluctuations in the background counts. It will be crucial to eliminate as many of these false sources as possible, in order to detect genuine new sources that have count rates only slightly above the background. The detection method involves determining the background precisely. Then, given a background value, a threshold is set that yields the maximum allowable number of spurious sources per field (e.g., less than 1.0 or 0.1). The logical flow of the algorithm is shown in the first figure. Module 4.2 generates a map of background values per pixel, and the values are used to compute a signal-to-noise ratio. A sliding cell (composed of a predetermined number of pixels) is moved across the field in each direction, with a set step size, and based on the total counts and background from the map, a signal-to-noise ratio within the cell is computed. A tentative source detection occurs whenever this ratio exceeds the established threshold obtained from the threshold map (modules 4.3 and 4.4). Subsequent processing involves consolidating adjacent, or contiguous, cell positions into a single source position (module 4.5) and generating a list of sources and their respective positions.

The Space Data and Computing Division has been running part of the High-Resolution Imager instrument software in a stand-alone mode shown in the first figure in order to establish these thresholds. Part of the work involves generating simulated fields with no sources present. The fields are generated by running a Monte Carlo simulation of the expected background which includes

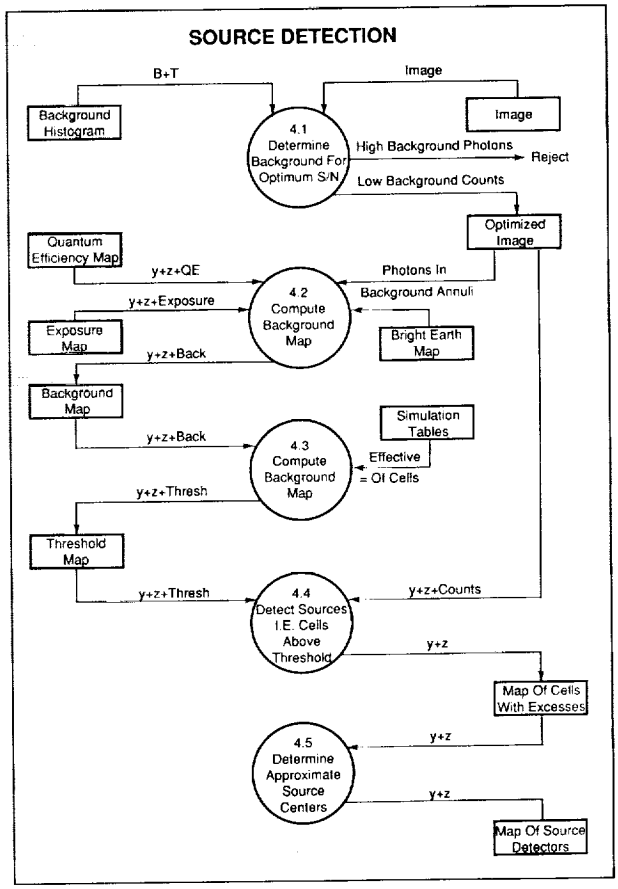

Portion of the High-Resolution Imager software that is used for source detection. These modules are operated in stand-alone mode in order to establish the thresholds needed for accurate source detection.

ORIGINAL PAGE
COLOR PHOTOGRAPH

Simulated ROSAT data set of a 10,000-s exposure. The left-hand side shows background counts only. These data are used to establish thresholds. The right-hand side has both 2 point sources [full width half maximum (FWHM) = 5 arc-sec] and an extended reddish source with faint "nebulosity" above it. The logarithm of the data is displayed to bring out the faint counts.

Poisson distributed interphoton arrival times. A typical data set is shown in the left half of the second figure. All the counts are due to the background; no sources are present. Data sets corresponding to different exposure times are generated and analyzed using the stand-alone software. Therefore, the Space Data and Computing Division can generate a table of thresholds versus exposure time that will be used to differentiate the spurious sources from the real ones. The simulation program can also generate point sources with the correct ROSAT point-spread function, as is illustrated in the lower right-hand side of the second figure. The upper right-hand side of the figure shows an extended source (red core) with corresponding "nebulosity." These simulations will be used further to tune the parameters of the Space Data Processing System software to obtain accurate source detections.

Contact: Ryszard L. Pisarski (Code 636)
(301) 286-9392
Laura A. Potler (Code 635)
(301) 286-9420

Sponsor: ROSAT Project

Dr. Ryszard L. Pisarski earned a PhD in astrophysics from Columbia University and has been at Goddard for 5 years. He currently works in the Space Data and Computing Division, verifying the scientific validity of data reduction software used by the ROSAT project. His technical interests center on image processing and data analysis of x-ray emission from Supernova remnants.

Ms. Laura A. Potler is Senior Computer Engineer on the ROSAT standard data processing system in the Computer Science Research Facility of the Space Data and Computing Division. She has completed benchmarks, defined specifications, and installed and tested systems and components to prepare them for the production phase (launch readiness). Ms. Potler has been with Goddard for 4 years and holds a BS in computer science.

CRUSTAL DYNAMICS DATA INFORMATION SYSTEM (CDDIS)

The Crustal Dynamics project was formed by NASA to apply space methods and technology to advance the scientific understanding of Earth dynamics, tectonophysics, and earthquake mechanisms. The project uses two principal types of space-age techniques in this study: laser ranging to an artificial satellite or the Moon and very long baseline interferometry (VLBI). As part of its data management, the project has designed and implemented a centralized CDDIS (shown in the accompanying figure). The system has been fully operational since September 1982. Its main purpose is to store all geodetic data products acquired by the project in a central data bank, to maintain information about the archiving of all project-related data, and to disseminate selected data sets to authorized project investigators and analysis centers. It operates on a dedicated MicroVAX II computer. All authorized project investigators, staff, and cooperating institutions have access to the system through Space Physics Analysis Network (SPAN), INTERnet, BITnet, and Global Tropospheric Experiment (GTE) Telenet facilities as well as dialup telephone lines. The menu-driven system provides the user with access to the different parts of the system, and data retrievals or queries are possible with user-friendly interfaces.

The archives of preprocessed laser and raw, correlated VLBI data are retained off line in the system tape library. All other information can be accessed through a data base using the Oracle data base management

system. The laser and VLBI data sets accessible through the CDDIS fall into four major categories.

Preprocessed Data: These include catalogs of preprocessed satellite laser ranging data from 1976 through the present, lunar laser ranging normal and mininormal point data from 1969 through the present, and VLBI data from 1976 through the present. Summaries of satellite laser ranging data from the Laser Geodynamic Satellite, Beacon Explorer-C, Starlette, and the Experimental Geodetic satellites are stored on line in a data base; the actual data are archived off line on magnetic tape. The VLBI data consists of online experiment listings in the data base and magnetic tape archives of the actual experiment data.

Analyzed Data: These include satellite and lunar laser ranging, VLBI, and combined analyzed results supplied by the project's science support groups and other analysis centers and project investigators at Goddard, Jet Propulsion Laboratory, National Geodetic Survey, the University of Texas, and many other global institutions. These analyzed results currently span different periods from 1976 through the present and are accessible through the data base management system. They include precision baseline distances, Earth-rotation and polar-motion determinations, length-of-day values, and calculated station positions.

Ancillary Data: This information includes descriptions of Crustal Dynamics project site locations, a priori

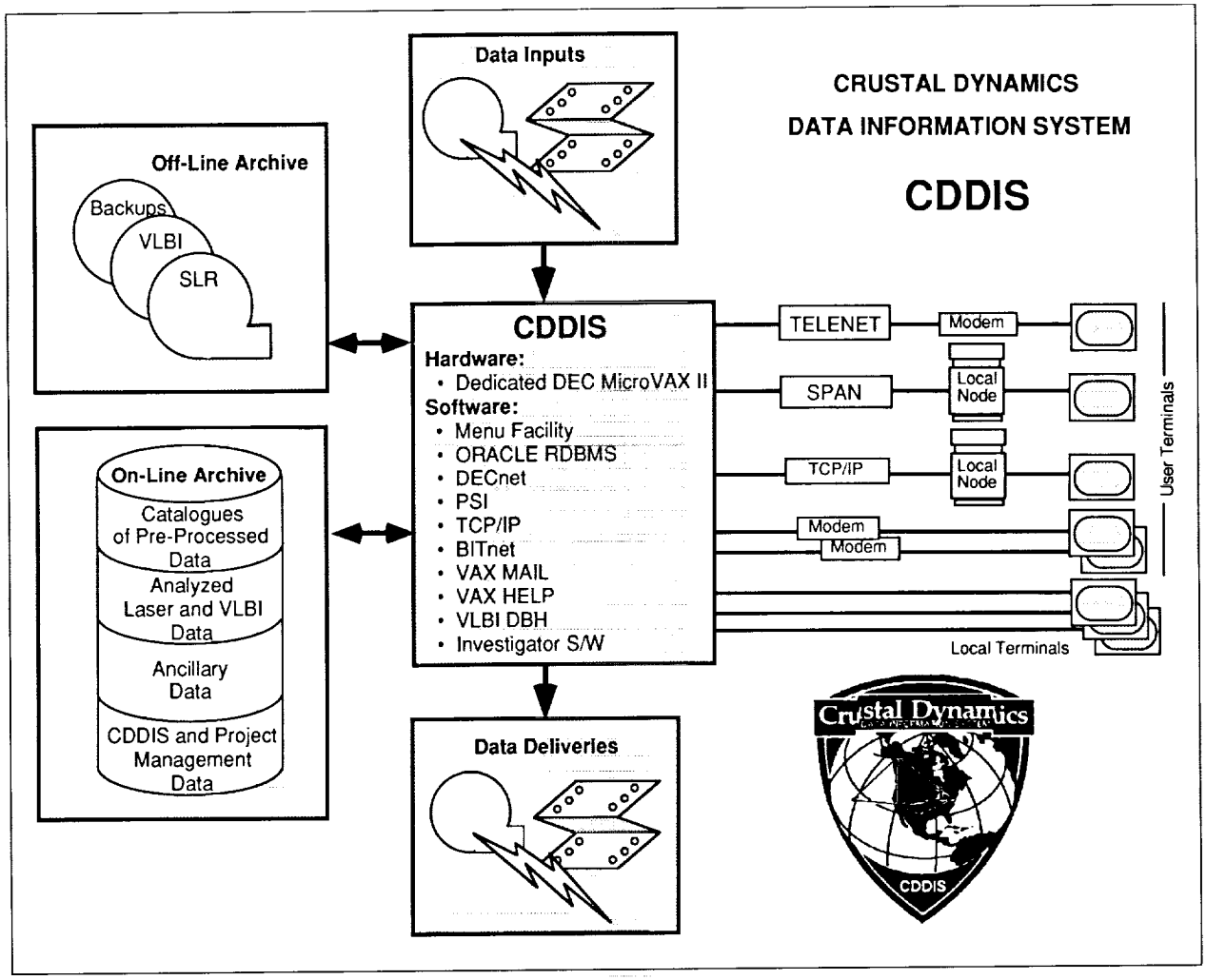

C-. Crustal Dynamics Data Information System flowchart.

monument coordinates and calibration data, and a priori star coordinates. These data sets are often used in the analysis of the preprocessed data sets and are contained in the online data base.

Project Management Information: This category is accessible through the CDDIS data base to authorized project personnel only and includes mobile system schedules, occupation information, and configuration control information. In addition, system operational information is kept in the data base and is accessible to CDDIS staff only. These data include logs of all lasers and VLBI tapes received from the many global sources and all tapes created by the CDDIS for outside users, and listings of CDDIS backup tapes.

In addition to the online, menu-driven user view, the CDDIS is tasked to assist the investigator community with its data requirements. These data services consist primarily of receiving and archiving crustal dynamics-related data on magnetic tape and cataloging this data in the CDDIS data base. All data received from the many contributing global sites must be verified and often reformatted before its distribution. The CDDIS is then responsible for the dissemination of this data to authorized investigators of the Crustal Dynamics project located in the United States and various institutions worldwide. Data can be made available in the form of printout listings, magnetic tape or floppy disk, or network files.

Most efforts during 1989 concentrated on enhancing the CDDIS and its computer environment. The CDDIS MicroVAX became directly accessible to users through the GTE Telenet system. The computer also became a node on the store-and-forward mail and file transfer network, BITnet. CDDIS' connection to the major worldwide networks (SPAN, INTERnet, BITnet, and Telenet) greatly benefits the Crustal Dynamics project. Users located all over the world can access the system through networks connected to their home institutions and can transfer analyzed data files for inclusion in the CDDIS. The computer system has become a cost-effective mechanism for the exchange of data and information within the project. Users can log into the computer in the least expensive manner to forward messages and data to other interested parties. Thus, telephone, telex, and other costly forms of communication can be avoided. The CDDIS computer facility also permits users in different time zones to communicate more efficiently.

Several new data sets were received from project affiliates and loaded into the CDDIS data base. These projects include revised Goddard fixed and mobile VLBI analysis results, National Geodetic Survey mobile VLBI analysis results, Goddard satellite lunar ranging baseline and station position solutions, and monthly sets of International Earth Rotation Service polar motion determinations from a variety of sources.

A brochure was designed to provide information about the Crustal Dynamics project and the CDDIS. The brochure, which details access methods and contact information, was distributed to a worldwide group of project personnel, investigators, and affiliates.

The latest version of the document *Crustal Dynamics Project: Catalogue of Site Information* was completed and distributed to a worldwide group of the project's Principal Investigators and cooperating institutions. The catalog is designed to provide descriptions of the observing sites utilized by NASA's Crustal Dynamics project. The information contained in the catalog is also available on line through the CDDIS. The *DIS Bulletin* continued publication on a regular, bimonthly basis, and the latest version of the *Crustal Dynamics Project Personnel and Networking Directory* was completed and distributed to the user community. The document has greatly benefited the project by promoting electronic communication between the project office and cooperating institutions and scientific investigators.

Over 25 accounts were established on the CDDIS computer in support of the project's VLBI science support group. These accounts are accessed by users located worldwide for the exchange of VLBI data, system schedules, experiment log files, and general messages. This facility has greatly benefited the VLBI group by using electronic means to decrease transmission time and costs.

Future plans include the establishment of more extensive archives of Global Positioning System data. The user interface of the interactive Data Information System will be redesigned to take advantage of advances in data base management system technology. Optical disk hardware will be evaluated, procured, and used to store the archives of the project's laser and VLBI data.

Contact: Carey E. Noll (Code 634)
(301) 286-9283

Sponsor: Crustal Dynamics Project and NASA Headquarters

Ms. Carey E. Noll is Data Manager for the Crustal Dynamics Project, overseeing the CDDIS and the management of its MicroVAX computer. Ms. Noll, who received a BA in mathematics from Western Maryland College, has 9 years' experience at Goddard.

THE 9-YEAR NIMBUS-7 EARTH RADIATION BUDGET (ERB) DATA SET

A 9-year (November 1978-October 1987) Nimbus-7 ERB data set was recently completed and is now being analyzed by climate scientists. The concurrent 6-year Nimbus-7 cloud data set is often used in these studies. Both data sets were produced by the Nimbus project in the Space Data and Computing Division, in cooperation with the ERB Nimbus-7 Experiment Team.

Life on Earth and our weather system derive their necessary energy from the Sun. After it is used, this energy is reradiated to space at low temperatures. The incident solar radiant energy is absorbed principally in the equatorial regions. Then the excess energy is moved to the high latitudes by ocean and atmospheric currents. The first figure shows the Earth's annual radiation energy budget for the year July 1983-June 1984. The other 8 years recorded by the Earth Radiation Budget Experiment (ERBE) showed very similar patterns. The bright central band indicates the positive tropical energy budget regions where more energy is received from the Sun than is radiated back to space. Energy-deficit regions are indicated in blue. The green bands near latitudes 30° N and 30° S indicate an annual budget near zero.

The complex tropical patterns show large differences in the tropical net radiation budget. The deep red spot off India has a positive balance greater than 90 W/m^2, while the outer red-brown ring indicates values greater than 70 W/m^2. These high net radiation regions lie chiefly in the oceans. The black-and-yellow bands

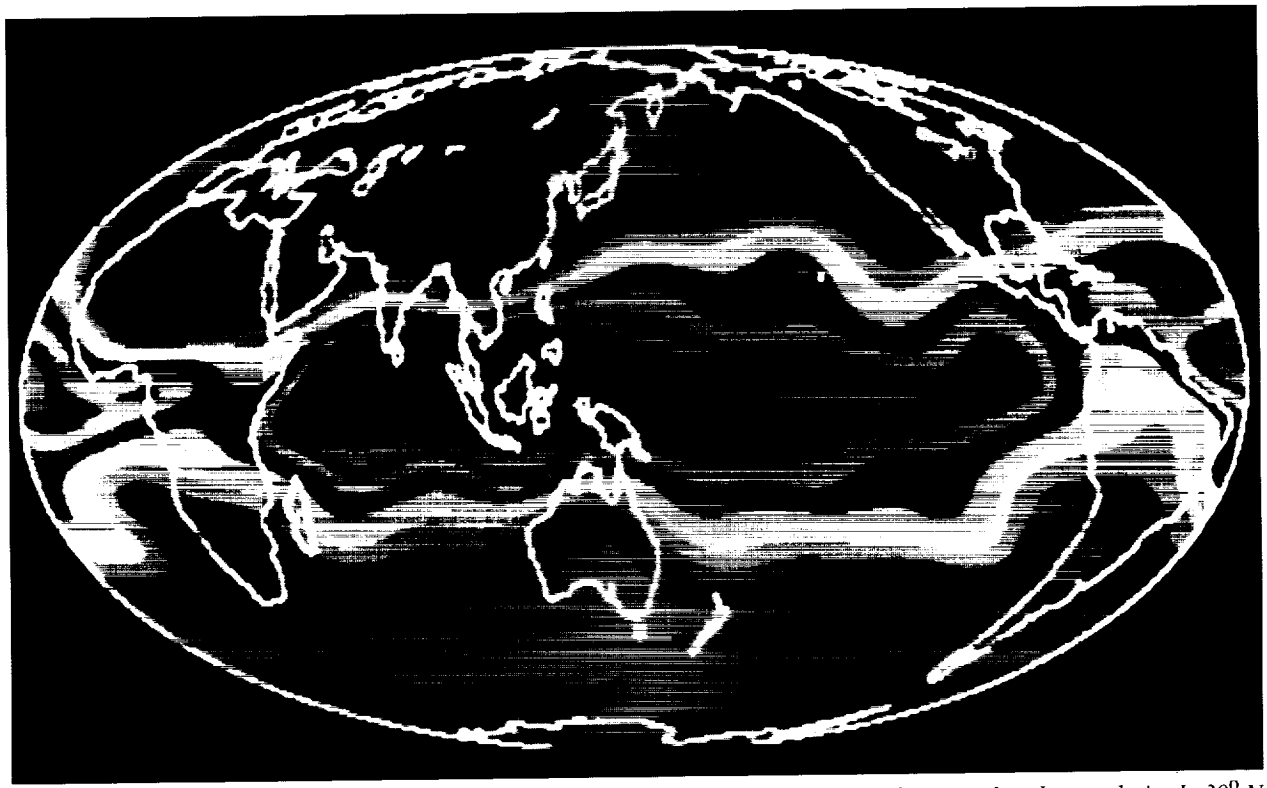

The Earth's annual net radiation energy budget for the year July 1983-June 1984. The green bands near latitude 30° N and 30° S indicate an annual budget near zero. Here, as much energy is absorbed from the Sun as is radiated back to space at low temperatures. The deep red circle below India indicates a positive balance greater than 90 W/m^2. The outer red-brown ring indicates values greater than 70 W/m^2. The blue regions indicate a net loss. The dark blue polar regions have a negative loss algebraically less than -100 W/m^2.

ORIGINAL PAGE
COLOR PHOTOGRAPH

ORIGINAL PAGE
COLOR PHOTOGRAPH

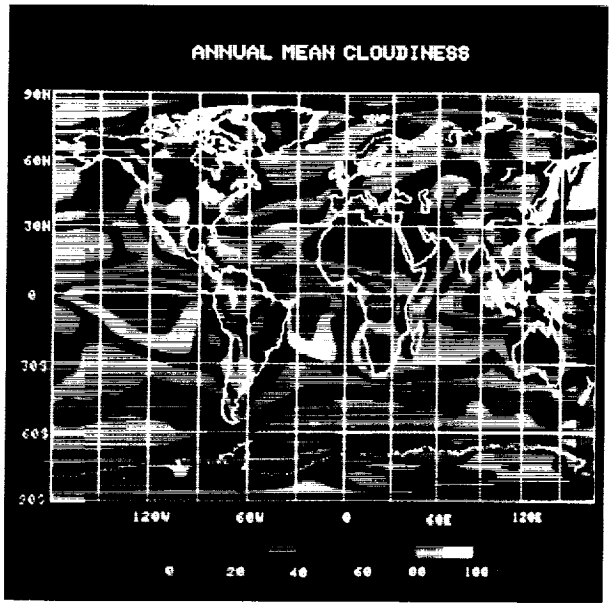

Annual mean cloudiness. This is a 6-year mean for the period from April 1979 to March 1985.

prominent in central Africa indicate net radiation between 50 and 60 W/m^2.

The equatorial land areas are not efficient energy absorbers. In fact, the Sahara and Saudi Deserts are in the mean energy sinks with the zero net radiation line dropping to about 20° N latitude across much of North Africa. Deserts have a low net radiation because their surfaces are relatively both bright and hot. This decreases the absorbed solar radiation but increases the emitted longwave radiation.

The annual mean global cloud cover is shown in the second figure, which indicates a 6-year mean for the period April 1979-March 1985. Three great global cloud belts are evident. The first lies in the southern ocean and circles the Antarctic continent. A similar cloud shield appears in the high northern oceans. The equatorial rainbelt forms the third belt. Overall, the tropical regions, where most of the solar energy is absorbed, are less cloudy than the energy-deficient higher latitudes. Note, however, that Indonesia has both high net radiation and high cloud cover. In fact, the tropical regions, which have the highest net radiation, tend to have a cloud cover of 50 percent or greater. On the other hand, recent studies have shown that the bright high-latitude cloud belts sharply reduce the net radiant energy absorbed during the polar summers.

Both net radiation and cloud maps change markedly with the seasons. The zero net radiation lines move up to 15° S and 70° N latitude from June to August. However, the Sahara shows some negative net radiation regions even in the summer. From December to February, they move down to about 15° N and 65° S latitude. The southern deserts are, in general, darker than the Sahara and Saudi Deserts and, therefore, have a somewhat higher net radiation. Similarly, the tropical rainbelt moves up to 8° to 10° N latitude from June to August and about the same distance south from December to February.*

**The Nimbus-7 ERB and cloud data sets are available from National Space Science Data Center (NSSDC), Code 633.4, Goddard Space Flight Center, Greenbelt, MD 20771 (301) 286-6695.*

Contact: H. Lee Kyle (Code 636)
(301) 286-9415

Sponsor: Office of Space Science and Applications

Dr. H. Lee Kyle is Manager of Nimbus-7 Cloud and ERB data sets preparation. Dr. Kyle, who received a PhD in atomic physics from the University of North Carolina, has worked at Goddard for 30 years. He has received a Certificate of Outstanding Performance and a Group Achievement Award for his work.

A VIDEO ATLAS OF TOTAL OZONE MAPPING SPECTROMETER (TOMS) DATA, 1978-1988

NASA's daily satellite observations of ozone over the Earth for the past 10 years have been transferred onto ordinary videocassette tape. Originally intended as a browsing tool for Goddard scientists, the video is a vivid presentation of the Earth's atmospheric dynamics and chemistry with broad appeal for scientists, educators, policy makers, and citizens concerned about the global environment. The rapid and complex ozone variations presented in the animation are a clear demonstration of the difficulty in distinguishing man-induced climate changes from natural variability.

TOMS on NASA's Nimbus-7 weather satellite has been observing ozone over the Earth once per day since 1978. The Nimbus data processing team collates the daily TOMS observations onto a regular grid with a resolution of 1° in latitude and 1.25° in longitude. These gridded

TOMS data are a public-domain data base available in digital format. Because a decade-long, Gbyte digital data set is difficult to browse for transient weather-related phenomena, the numerical files were converted first to digital images in byte/pixel format and then to television pictures in analog National Television Standards Committee format, one frame per day for 3,440 days. Each image represents the digital data archive, including day-to-day variability, climatological trends, dramatic highs and lows, and occasional regions of missing data and data processing errors. Total ozone is measured in Dobson units, the height of a column of molecules, defined so that 100 Dobson units are equal to 1 mm of ozone at standard atmospheric pressure and temperature. Over the United States, ozone amounts commonly range from 250 to 500 Dobson units.

The accompanying figure presents a sample TOMS image, containing Cartesian and polar projection maps of the Earth at approximately 100-km resolution. Ozone amounts and ultraviolet reflectivity are illustrated using the color bar located below the Cartesian images on the lower left side of the figure. Ozone is illustrated with a change in hue every 50 Dobson units. Over the globe, ozone values are normally 250 Dobson units above the tropics (colored blue) and 400 Dobson units above mid-latitude storms (colored red). In the video, values as low as 150 Dobson units and as high as 650 Dobson units can be found by a watchful viewer. In the figure, the Southern Hemispheric storm track can be located easily by the enhanced ozone above the "roaring 40's," while the 1986 Antarctic "ozone hole" that surrounds the waning polar night is just developing, with a 200-Dobson unit minimum (colored white) south of the Indian Ocean.

If TOMS data are missing at a grid point, the corresponding pixel is colored blue-black. Because TOMS uses reflected sunlight, ozone measurements are unavailable during polar night (e.g., over the South Pole in the figure). TOMS data are also missing where an orbital swath is not well processed (often when an orbit crosses the international dateline) and where the orbital swaths slightly underlap near the Equator.

TOMS ultraviolet reflectivity is visualized using shades of grey. The bright cloud fields in the reflectivity image help to locate corresponding storms. The ice sheets over Greenland and Antarctica are also prominent, with reflectivities approaching 100 percent. In the animation, the annual growth and melting of the sea ice surrounding Antarctica and variations in snow cover on the northern land masses are quite apparent.

The TOMS videotape presents a 2-min introduction to the image format, followed by the entire decade of data, which is presented twice: first in 4 min (at 15 frames per s to show the climatology) and then in 30 min (at 2 frames per s to show synoptic scale events). Individual days can be studied using the slow-motion and freeze-frame features available on most videotape players.

The most noticeable climatological feature in the TOMS imagery is the distinct division of the ozone into tropical, midlatitude, and polar regimes. Each regime has different photochemical, dynamic, and seasonal mechanisms, many of which are poorly understood and are currently the subject of research into the behavior of the rare gases that interact with the weather and control climate change.

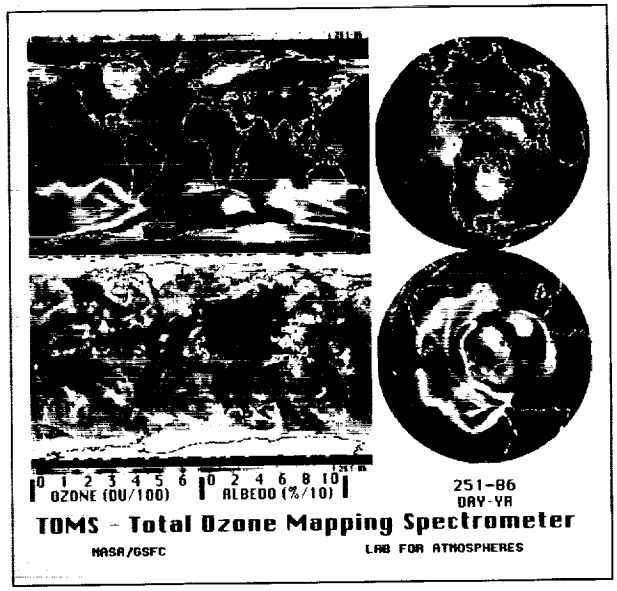

A sample frame from the animated atlas of TOMS ozone data for Julian date 251-86 (September 8, 1986). Ozone is presented with color changes at 50-Dobson unit (0.5-mm) intervals with warmer colors for larger ozone amounts, while ultraviolet reflectivity is presented in shades of grey, as indicated in the colorbar below the two Cartesian maps. North and south polar views are presented at the right. Missing data at grid points in the digital data base are colored dark blue, such as for polar night over the South Pole and for a missing orbital swath across the international dateline. On the time-lapse videotape, this frame is presented in just 1/15 s, so that a decade can be presented in 4 min.

ORIGINAL PAGE
COLOR PHOTOGRAPH

Over the equatorial regions, ozone amounts are low (200 to 250 Dobson units) because there is approximately 50 percent less stratospheric air above the high tropical tropopause than at higher latitudes. It is an irony of nature that the equatorial latitudes are less protected by the ozone layer even though they experience the most intense solar ultraviolet radiation.

At midlatitudes, ozone amounts are approximately 50 percent larger (300 to 400 Dobson units) and much more variable than at low latitudes. The larger total column ozone values at midlatitudes are due mainly to the lower tropopause and hence thicker stratosphere, and localized ozone maxima are well correlated with midtropospheric low-pressure fields. Land-induced effects are also significant. Large values of ozone frequently occur over northeastern Asia and northeastern North America, while smaller values frequently occur over the Tibetan plateau, northwestern North America, the midnorthern Atlantic Ocean, and Scandinavia.

At high latitudes, ozone values are extremely variable as a result of complex photochemistry and dynamics. Over Antarctica, low values of ozone occur each year around polar night, covering the continent for 4 to 8 weeks during austral spring and then vanishing as the circumpolar vortex breaks down. During the 1980's, the Antarctic ozone holes became significantly deeper each year. In the north, short-lived arctic ozone minima occur around the edges of the Arctic Ocean, often east of Greenland and above Scandinavia, but rarely near the North Pole. The frequent occurrence of large values of ozone at high latitudes in the Northern Hemisphere, especially above spring storms, must be due to efficient stratospheric transport mechanisms that are still poorly understood.

Although videotape lacks the bandwidth to resolve every single pixel in the TOMS data base, the low cost and widespread ownership of tape players make this format the best choice for browsing and educational purposes. With ordinary desktop computers, it is now possible to create high-resolution, animated digital imagery and then videotape recordings from other climatologically interesting satellite data products such as global cloud cover, sea ice, and rainfall. In the future, the "Mission to Planet Earth" being discussed for the 1990's may collect Tbytes/day—a mass storage, visualization, and information-extraction effort that will challenge the limits of future technology.*

**VHS videotape copies of the* Animated Atlas of TOMS Ozone Data, 1978-1988 *can be ordered for the cost of shipping and handling ($20.00) from National Space Science Data Center, Request Coordination Office, NASA/GSFC/Code 633.4, Greenbelt, MD 20771. The National Space Science Data Center Request Office can also be reached by telephone at (301) 286-6695 or by electronic mail at SPAN::REQUEST. Requests for a studio-quality videotape for use by the media can be obtained from the Office of Public Affairs at Goddard, (301) 286-5565.*

Contact: Dennis Chesters (Code 613)
(301) 286-9007

Sponsor: NASA Mesoscale Processes Program

Dr. Dennis Chesters investigates the relationship between weather and patterns in upper-air water vapor and ozone at the Laboratory for Atmospheres, where he has developed techniques for visualizing satellite-observed radiances. In his 11 years at Goddard, he has earned four performance awards.

NASA CLIMATE DATA SYSTEM (NCDS)

NCDS is an integrated scientific data and information system that supports researchers in the atmospheric, ocean, and Earth sciences by allowing them to locate, access, manipulate, and display climate-related data interactively. NCDS enables researchers to find and learn about data of interest by accessing a comprehensive catalog of data descriptions and an inventory of temporal and volume information, to access subsets of online or offline data, and to view and manipulate these data. After many years of development with limited operations as the Pilot Climate Data System, the system has now reached a state of operational maturity. It is available on the NSSDC VAXCluster (VAX/VMS) to the international user community over a wide variety of networks, including SPAN and INTERnet.

NCDS continues to build upon off-the-shelf software packages in both commercial and public domain. The Oracle data base management system serves catalog, inventory, and data access subsystems, IDL supports the data manipulation subsystem, and the graphics subsystem uses Template. Transportable Applications Environment (TAE) Classic provides the basic structural framework for the user interface. Common Data Format (CDF) is

ORIGINAL PAGE
COLOR PHOTOGRAPH

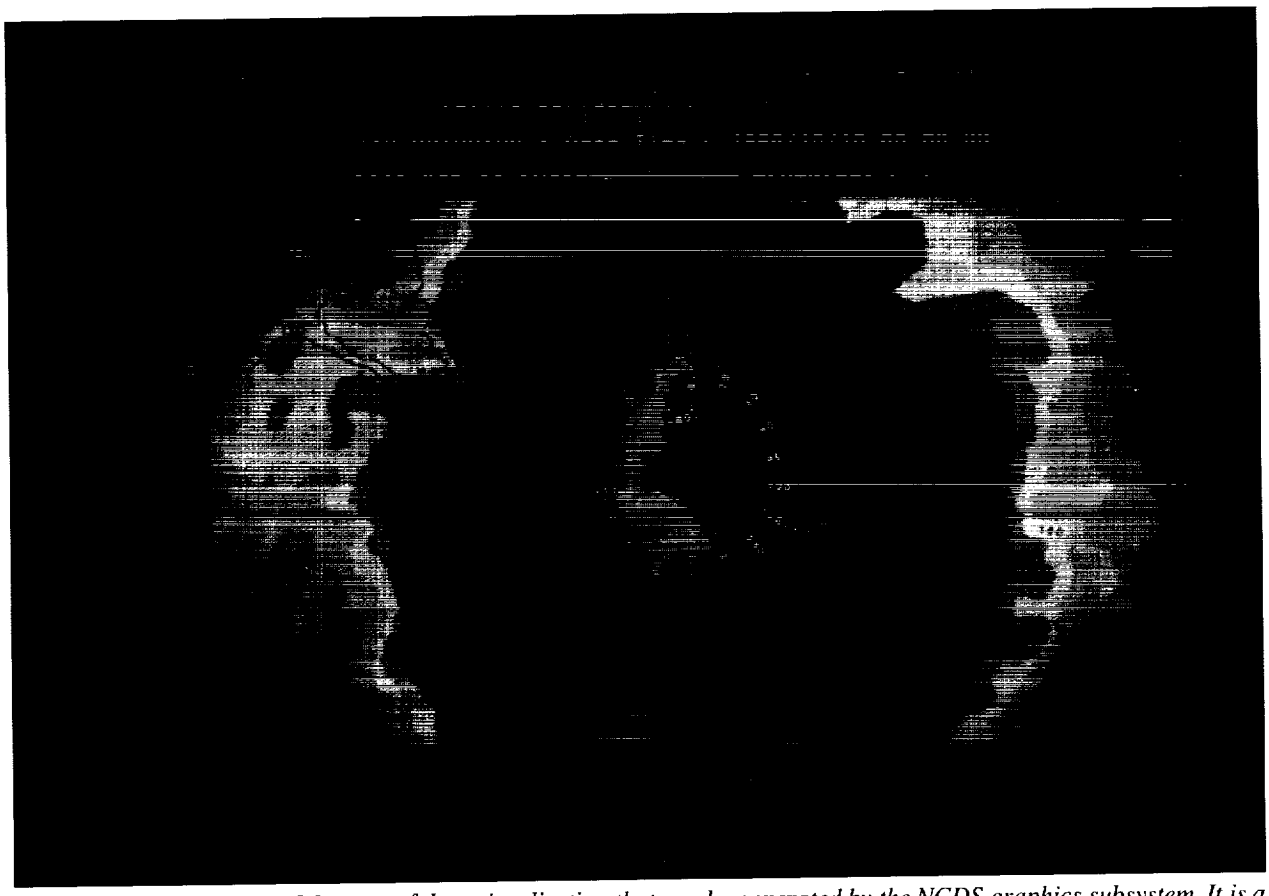

The figure is an example of the type of data visualization that can be generated by the NCDS graphics subsystem. It is a pseudocolor image of the temperature of the Earth's surface as viewed on an azimuthal equidistant map projection showing approximately the southern two-thirds of the Southern Hemisphere. This map is derived from a data set developed by the U.S. Navy Fleet Numerical Oceanography Center based upon 12-h forecasts by the Navy's Operation Global Atmospheric Prediction System. The full support of the Fleet Numerical Oceanography Center data set was added to the NCDS in fiscal year 1989. The Fleet Numerical Oceanography Center has been accumulating the results of these numerical models, which include many meteorological parameters, since the early 1960's. The scope of this data set has expanded in recent years to include, for example, global coverage every 12 h since 1983. A nominal grid of 200 × 200 cells has been derived from the model-based global surface temperatures for October 10, 1986, at 0000 GMT and displayed in the figure.

used by the data access, data manipulation, and graphics subsystems for direct utilization of online data stored on magnetic and optical disks.

NCDS provides access to approximately 500 Gbytes of data, mostly off line, spanning about 46 distinct data sets. A portion of the data sets held by the system resides on line, along with samples of offline data (about 2 Gbytes total). The majority of these data sets fall into four primary subdisciplines, the first of which is solar activity-irradiance. The Nimbus-7 ERB instrument, Solar Maximum Mission (SMM), Active Cavity Radiometer Irradiance Monitor, the ERBE scanners, and the Solar Mesospheric Explorer (SME) ultraviolet spectrometer provide the bulk of the data.

A second subdiscipline is clouds and radiation. ERBE, International Satellite Cloud Climatology Project (ISCCP), and the First ISCCP Regional Experiment (FIRE) program are three primary projects supported by NCDS. The Nimbus-7 ERB and the National Oceanic and Atmospheric Administration (NOAA) satellite series' Advanced Very-High-Resolution Radiometer (AVHRR) instruments also offer valuable data for analysis.

A third grouping of NCDS data is the general category of global climatologies and oceanographic data sets. In this category, users find sea-surface temperature data from the Climate Analysis Center, Fleet Numerical Oceanography Center, NOAA's Satellite Data Services Division, and the Comprehensive Ocean Atmosphere Data Set. Several of these same data sets, along with the National Meteorological Center's analyses, provide winds, humidity, fluxes, and other meteorological parameters. The First Global Atmospheric Research Program Experiment data still remain popular, especially since their recent reanalysis. The Angell and Jones temperature deviation data sets are also available. The World Monthly Surface Station Climatology [National Climate Data Center (NCDC) and National Center for Atmospheric Research (NCAR)] data set, which spans the period from 1731 through the present, represents the longest period of record of any data set held by NCDS.

The fourth category is that of atmospheric constituents. Ozone, aerosols, nitrogen dioxide, and water vapor are the major species derived from the Nimbus instruments Backscatter Ultraviolet Radiometer, Solar Backscatter Ultraviolet Radiometer, Limb Infrared Monitor of the Stratosphere, TOMS, and Stratospheric and Mesospheric Sounder II, Stratospheric Aerosol and Gas Experiment (SAGE) I on the Atomic Explorer Mission, and SAGE II on Earth Radiation Budget Satellite (ERBS) have collected data on the same four species.

In addition to the expansion of its comprehensive data holdings, the NCDS software services have improved the user interface, performance, and use of new versions of the off-the-shelf software packages employed. Software development activities occur in parallel with the user support and data management efforts. Implementation is focused on the seamless integration of the off-the-shelf software and custom software. For example, NCDS must accommodate a variety of often obscure data formats for the data sets that it supports for both inventory and access purposes. New tools for easy listing and subsetting have been developed based on common data formats to expedite the transfer of data from the NSSDC to users' computer systems. An experimental data base for online data has been installed and will free the user and developer from user interface overhead. NCDS provides access to 46 data sets, which are further subdivided into 115 data types for efficient storage in common data format. The functionality of the manipulation and visualization tools available for data sets in CDF has also been improved. (See the accompanying figure.)

The major accomplishment by the NCDS in 1989 was expanding significantly the scope of its operational services by providing timely access to a wide range of data. These efforts culminated in the first NCDS workshop, which brought more than 200 interested users from around the world to Goddard to evaluate and experiment with the system. Data producers (for data sets held by the NCDS), data center representatives, scientists, and data system specialists had an opportunity to use NCDS and to discuss their applications of data holdings. This workshop brought the concept of a truly integrated, data-independent system into reality for many participants and demonstrated its potential for supporting scientific research.

The figure is an example of the type of data visualization that can be generated by the NCDS graphics subsystem. It is a pseudocolor image of the temperature of the Earth's surface as viewed on an azimuthal equidistant map projection showing approximately the southern two-thirds of the Southern Hemisphere. This map is derived from a data set developed by the U.S. Navy Fleet Numerical Oceanography Center based upon 12-h forecasts by the Navy's Operation Global Atmospheric Prediction System. The full support of the Navy data set was added to the system in 1989. The Navy center has been accumulating the results of these numerical models, which include many meteorological parameters, since the early 1960's. The scope of this data set has expanded in recent years to include, for example, global coverage every 12 h since 1983. A nominal grid of 200×200 cells has been derived from the model-based global surface temperatures for October 10, 1986, from midnight to noon GMT and is displayed in the figure.

Contact: Lola M. Olsen (Code 634)
(301) 286-9760
Lloyd A. Treinish (Code 634)
(301) 286-9884

Sponsor: Office of Space Science and Applications

Ms. Lola M. Olsen oversees the implementation of data sets in NCDS, supports NCDS system users, and writes data set information catalogs. Ms. Olsen has an MA from the University of North Carolina in Charlotte and has completed course work for her PhD. She has 4 years' experience at Goddard.

Mr. Lloyd A. Treinish is a computer scientist at the NSSDC with 10 years' experience at Goddard. He develops advanced data systems to support scientific applications and studies space and atmospheric phenomena. Mr. Treinish was the chief designer and developer of the Pilot Climate Data System, and he originated the CDF, the first self-describing data abstraction for the storage and manipulation of multidimensional data. He has an SM in physics from the Massachusetts Institute of Technology and has received several professional awards including four NASA Certificates of Outstanding Performance.

PILOT LAND DATA SYSTEM (PLDS)

PLDS is a distributed information system that provides information about and access to land science data for NASA land scientists. This prototype system has nodes at three NASA centers: Ames Research Center, Goddard, and Jet Propulsion Laboratory. The PLDS was conceived as a distributed data system, the one feature that sets it apart from the other NASA Earth science pilot data systems for climate and ocean. Integration of this concept into the overall design and architecture is a fundamental part of the data system.

The focus of PLDS over the past year has been twofold: first, to develop, document, and then test the software required to provide the basic functionality needed in a land data information system and, second, to develop a strategy and the procedures and policies that would facilitate conversion to a small-scale operational system that supports long-term growth and expansion of the data system. To meet the first objective, the Goddard node of PLDS released a β-test version of the data system software and the *PLDS User's Guide*. This software was available at the Goddard node for 6 months during which four groups of land scientists from NASA, U.S. Geological Survey, and academia evaluated and reviewed the software and the documentation. The evaluators' reports were very favorable and are available in the document *Verification and Validation of PLDS-88*. In response to the evaluation, the PLDS development team modified and enhanced the β-test software and the documentation and then released them in a production mode in March 1989.

Further software enhancements and user documentation that could not be incorporated into the production release are currently under way. They will provide added functionality suggested by the evaluators and by the members of the PLDS Science Working Group. In addition, the Jet Propulsion Laboratory node of PLDS has been enhancing and improving the functionality of the spectral analysis package, a tool to display and manipulate spectral data.

To meet the second objective, the PLDS team has developed a strategy to facilitate conversion to a small-scale operational system that permits long-term growth and expansion. This strategy is outlined in last year's PLDS project plan, which details the short-term and intermediate-term objectives of the project. The strategy describes a method that gives the data system the flexibility to evolve as the needs of the scientific community change. This strategy enables the data system to use a variety of hardware and software platforms, to incorporate new functionality and new technologies as they are needed, and to provide a level of compatibility across all PLDS nodes while allowing individual nodes the flexibility to respond to the needs of the scientists at that node.

To support this strategy, the PLDS is developing policies and procedures that guide its implementation. The strategy states that an operational data system must have three major components: software functionality, data in the data system, and a responsive system. Software functionality includes user capabilities provided by the software, such as finding and ordering data and the portability of the software itself, i.e., its ability to run under different operating systems.

The new strategy identifies the required and optional functions and the software that provides the required functions. The figure shows the three levels of functions: core, intermediate, and site-specific. The core functions

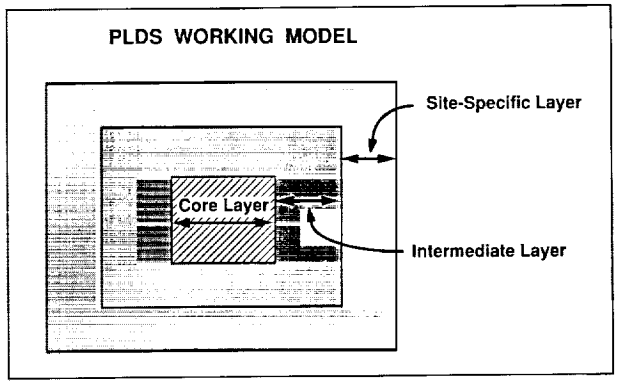

The PLDS development strategy differentiates among core functions required at all sites, intermediate functions useful at several sites, and functions specific to one site.

Data Sets Currently Available through PLDS

Data Set	Images/ Granules	PLDS Node
Aerial Photograph	12,576	Ames
Aerial Photograph	5,260	Jet Propulsion
AMS	99	Goddard
AVHRR-LAC	806	Goddard
AVIRIS	564	Jet Propulsion
Botanical Sample	1,219	Jet Propulsion
DEM	54	Jet Propulsion
Earthquake Epicenter	983	Jet Propulsion
Geological Sample	4,800	Jet Propulsion
LSAT-TMPT	1	Goddard
Thematic Mapper	168	Jet Propulsion
SMMR-PDVI	12	Goddard
SMMR-Snow	106	Goddard
TIMS	922	Ames
TIMS	594	Goddard
TIMS	845	Jet Propulsion
NS001-TMS	1,215	Ames
TMS-NS001	539	Goddard
NS001	1,037	Jet Propulsion
Daedalus-TMS	4,350	Ames
TMS	3,706	Jet Propulsion
Topographical Map	361	Jet Propulsion

are required at all PLDS nodes and are provided by the same software tools throughout the data system. These functions provide compatibility and continuity between the nodes. They must help the user to find data, communicate with other nodes, or interface with the data system. The software that provides these functions must also meet coding and implementation standards because it must run on the various computer systems that exist at the different PLDS nodes. One of the main activities this year has been to establish the coding and implementation standards and to bring all core software up to those standards. The intermediate and site-specific level functions are the optional functions; they are not essential elements of the PLDS but may be present at a node if needed by the local users. Intermediate-level functions differ from site-specific ones in that they must satisfy specific functional requirements that are deemed generally useful to many PLDS nodes. The software must meet the same standards as the core software. Intermediate functions that have received attention this year are the spectral analysis package and ingest software for several data sets. The site-specific software need not meet any functional requirements or software standards.

Another element of the strategy, the extent of the data described in the data system, has also been addressed. The project has been active in expanding the temporal and spatial coverage for specific data sets and in adding new data sets. The table shows data sets currently available via the PLDS. The expansion of existing data sets and the addition of new ones is an ongoing activity. In the last year, the Goddard node provided access to two new data sets, Thermal Infrared Multispectral Scanner (TIMS) and Thematic Mapper (TM) Simulator data from the International Satellite Land Surface Climatology Project (ISLSCP) in the First ISLSCP Field Experiment (FIFE) project, and to two global data sets, snow cover and depth derived from the Scanning Multichannel Microwave Radiometer (SMMR) instrument, and a vegetation index data set derived from SMMR data. Goddard also expanded the inventory of available AVHRR Local Area Coverage (LAC) data. The Ames Research Center node did not add any new data sets but expanded its information about TIMS, TM Simulator (NS001 and Daedalus), and aerial photographs (visible and infrared). Lastly, the Jet Propulsion Laboratory node added three new data sets (AVHRR, Airborne Visible/Infrared Imaging Spectrometer, and TM) while expanding holdings of visible and infrared spectra from planet rock samples.

The project also addressed the responsiveness of the system. Responsiveness includes both the performance of the computers used to access the data system and the speed with which personnel can add new data to the data system, fill requests for data, or provide user assistance. This year, the staff addressed the computer performance aspect. The node at Ames Research Center was expanded so that it now has its own computing resources, and the Goddard node acquired a computing environment for software development so that the scientific users and the development staff do not vie for the same computing resources. Lastly, the Jet Propulsion Laboratory and Goddard nodes began an upgrade of the computing resources accessible to their scientific users. That upgrade will be completed in 1990.

The project made substantial progress toward the two principal objectives for this fiscal year: providing basic functionality and developing a framework for future growth and expansion. Activities in all these areas will continue into this year. Late in 1990, the data system will be converted to a fully operational mode running for 6 to 9 months, providing services and data to a limited group of scientific users.

Contact: Blanche W. Meeson (Code 634)
(301) 286-9282

Sponsor: Office of Space Science and Applications, Communications Division and Earth Science and Applications Division, Land Processes Branch

Dr. Blanche W. Meeson is Project Manager for the PLDS in the Data Management Systems Facility at the NSSDC. With a research team, she is responsible for the evolution of PLDS. Her technical interests focus on the integration of commercially available software into a coherent system for describing and presenting scientific data. Dr. Meeson has worked at Goddard for 3 years.

COLLABORATIVE DATA ANALYSIS IN THE COORDINATED DATA ANALYSIS WORKSHOP (CDAW)

The CDAW program of the NSSDC is a unique experiment in enhancing a traditional workshop format of presentations and discussions by allowing the participants simultaneously to access and display relevant data interactively. The first in the new CDAW-9 series of workshops took place at Goddard May 12-16, 1989. This meeting was attended by more than 60 solar-terrestrial scientists including participants from the United States, Canada, Japan, and Europe.

The program began as a part of the International Magnetospheric Study in the late 1970's as a testbed for an approach to dealing with space-science problems of global scale and complexity. The goal of the CDAW program has been to develop and use tools and techniques for the assembly and use of data from a multitude of sources to involve a wide cross section of the interested scientific community to attack these problems. Collaborative data analysis of this general nature is planned as an essential part of many of the new NASA programs for the 1990's. A prime example is the joint U.S.-Japanese-European International Solar-Terrestrial Physics (ISTP) program, where numerous spacecraft are to be simultaneously deployed in a concerted attempt to unravel the continuing puzzle of dynamic processes and energy-plasma flow in the Earth's magnetosphere. Such a system includes tightly intertwined spatial and temporal dependencies that scientists can attack only with access to simultaneous data from many instruments at many dispersed locations.

CDAW-9 is directed at the analysis of data collected during the Polar Regions Outer Magnetosphere International Study (PROMIS) campaign. During this period (March-June 1986), the various international space agencies and numerous ground-based observers made a coordinated effort to gather simultaneous observations on a wide range of solar-terrestrial phenomena, with the goal of improving understanding of the relation between polar phenomena (such as aurora) and physical processes taking place in the outer magnetosphere of the Earth. The lack of such widespread and simultaneous data has been a recurrent problem in understanding the physics and dynamic structure of the Earth's magnetosphere. In many ways, the study's focus and data base are prototypical of the observations that the ISTP program will generate routinely.

The CDAW format is unique in its effort to blend a traditional scientific workshop with access to a large digital data base assembled from relevant observations. The collected data (contributed by the interested science community in response to a call for such data) are converted into a common format with appropriate software and workshop computer facilities to allow the participants direct interactive access to that data base during workshop meetings. Between workshops, NSSDC maintains the data base on line to allow an ongoing analysis by access to electronic networks such as SPAN.

The CDAW-9 analyses benefit greatly from the wealth of simultaneous data collected during the PROMIS campaign. A sampling of that data has been distributed by NSSDC in a six-volume PROMIS series of data source books. Five specific event periods from within the PROMIS interval were selected by Dr. Robert H. Manka, CDAW-9 scientific convener, and an international steering committee as the initial focus of the workshop, based on a combination of a preliminary assessment of the physics taking place and the availability of relevant spacecraft and ground-based data. To date, data from instruments on 14 spacecraft and numerous ground instruments, for a total of more than 60 distinct data sets (most

including data from all five analysis periods), have been received and integrated into the online data base. Requirements for some further data were defined during this first workshop and are now being solicited.

CDAW 9.1, as the first meeting in the CDAW-9 series has been termed, followed the spring American Geophysical Union meeting in Baltimore. The 5-day workshop agenda was composed of a mix of software system training and data access sessions, plenary presentations, and subgroup discussions. During the workshop, participants made 1,300 interactive plots of data using 22 high-resolution, color-graphics terminals and personal computers with color-graphics terminal emulators. More than 300 plots subsequently were directed to hard-copy devices. NSSDC staff created 1,700 interactive plots in the weeks preceding the start of CDAW 9.1 to prepare and validate the data base and to produce summary plots to help the participants in their initial analysis efforts.

Participants were uniformly enthusiastic about their reception at the workshop, the data base-supporting software, and the work they accomplished. As a whole, the workshop made the transition successfully from the initial phase of laying out consistent time lines for all the events to focusing on specific aspects of events with scientific promise. Participants continue to access the data base remotely to pursue their analyses. The second full workshop (CDAW 9.2) was held at Stanford University, after the fall American Geophysical Union meeting and in conjunction with the U.S.-Finnish Auroral Workshop. NSSDC facilities supported data access entirely over electronic network links.

Several key elements in the CDAW program anticipate ISTP science analysis:

- An emphasis on the coordinated analysis of simultaneous data from widely separated sites and diverse instruments, including both observations and models.
- The use of a common format as the foundation for a common mode of access to these diverse data sets.
- The development of powerful graphics and data manipulation software (the Network Assisted Coordinated Science system) keyed to this common format, for interactive access to and display of the assembled data base.
- The use of widely accessible electronic networks to allow remote access to the central data base and to facilitate data exchange.

The combination of these technical elements allows CDAW participants to examine and correlate data interactively as ideas occur during the workshop discussions. The participants can continue and extend these analyses from their home institutions between formal meetings of the workshop by using SPAN.

The common format used for the data base includes self-description of data set contents and the natural accommodation of multidimensional and gridded data. The analysis software allows a full range of selection, averaging, and computation on variables in the data base as well as device-independent graphics including histograms, two-dimensional x-y plots, three-panel plots with multiple traces/plots, mapped contour plots, spectrograms, and pseudocolor image plots. The executive/user interface is built on the Goddard-developed TAE. Commercial software packages manipulate and display data. Some recent software enhancements have improved the interface to alphanumeric/graphics terminals available in these packages.

Before the CDAW-9 series of workshops, substantial effort had gone toward further CDAW-specific system developments. These developments include new software to better support "data ingest," which consists primarily of the conversion of data received to the common format, and improvements in the basic user interface for data set selection and graphics specification and in the functionality of the graphics subsystem.

From a systems perspective, the workshop was highly successful. The ingest process was much smoother for CDAW-9 than its predecessor (CDAW-8), and users found the interface and graphics generally much better. To the extent that resources permit, further software improvements now focus on performance-related software analysis and enhancements and on modest enhancements to the interfaces and graphics subsystem.

The NSSDC has placed a high priority on extending the CDAW concept beyond a traditional focus on solar-terrestrial physics into new and broader discipline areas, for example, atmospheric sciences and astrophysics. Possible topics include the general problem of the Antarctic ozone, global cloud cover data collected

under FIRE, and a coordinated analysis of data related to Supernova 1987A.

Contact: Robert E. McGuire (Code 633)
(301) 286-7794

Sponsor: The Communications Division and the Space Physics Division, Office of Space Science and Applications.

Dr. Robert E. McGuire directs the NSSDC Digital Data Restoration Program and serves as liaison to the ISTP project. He is also Principal Investigator and Acting Deputy Project Scientist on the Interplanetary Monitoring Platform (IMP)-8 Goddard Medium Energy Experiment. He has received a NASA Group Achievement Award and two Outstanding Performance Awards. Dr. McGuire earned his PhD in physics from the University of California at Berkeley.

DISCIPLINE-INDEPENDENT STORAGE AND MANIPULATION OF DATA

NSSDC's CDF is a self-describing data abstraction for the storage and manipulation of multidimensional data in a discipline-independent fashion. The development of CDF arose out of NSSDC's recognition of the need for a class of data models that matches the structure of scientific data as well as to how such data may be used. Applications served by an appropriate data model include analysis by statistical and numerical methods, visualization, and management. For large, complex data sets, particularly visualization applications, traditional methods of handling scientific data such as flat sequential files are generally inefficient in storage, access, or ease of use. Modern, commercial relational data management systems do not offer an effective solution because they are oriented toward business applications. The relational model does not accommodate multidimensional or hierarchical structures often found in scientific data sets. In addition, relational systems do not provide adequate performance for the size, complexity, and type of access dictated by current and future data sets and their potential usage. In contrast, relational data base management systems have been quite viable for managing a large class of nonspatial metadata (i.e., information about data) within a number of NSSDC data systems.

A data (base) model is needed that possesses elements of a modern data base management system but is oriented toward scientific data sets and applications. This intermediate approach should offer ease of use, support large disk-based data sets, and accommodate scientific data structures. CDF is one implementation of such a data model. It is based upon the concept of providing abstract support for a class of scientific data that can be described by a multidimensional block structure. Although not all data fit within this framework, a large variety of scientific data does. For example, the type of data used in the NASA space and Earth science research community can be easily characterized by its dimensionality (e.g., 0 for point data, 1 for vector data, 2 for imagery, etc.). Since CDF is designed to support many scientific applications in a discipline-independent fashion, it is a powerful tool for the development of systems that can archive, manage, manipulate, display, or analyze data. This abstraction, which consists of a software package and a self-describing data structure, results from some of NSSDC's applied computer science work.

CDF Version 1, which was completed in early 1986, consists of FORTRAN language bindings and operates on VAX/VMS systems. More than 100 organizations outside of the NSSDC—including various NASA laboratories, research groups, current and future flight projects, as well as other Government agencies, universities, corporations, and foreign institutions—are currently using or have requested this software package. As a result, the CDF development efforts have become a standard method for storing space and Earth science data for a variety of applications. Language bindings for IDL, a commercial data analysis software package on VMS systems, are also available.

Version 1 has been critical to the success of the NSSDC's CDAWs 8 and 9 and the NCDS activities. CDF has enabled workshop participants to produce scientific results via data interpretation and analysis at an unprecedented rate. CDF was used to manage a diverse solar-terrestrial physics data base (more than 50 different data sets for each workshop) that was a driver for various generic (i.e., CDF-based) data analysis and display tools. CDF is a key element in the NCDS, by providing a mechanism for climate researchers to easily work with data on line in association with information about climate data (i.e., catalogs and inventories) and an extensive data archive. In addition, a CDF Support Office has been established in conjunction with the NSSDC Standards Office, to help disseminate information about the CDF and to distribute CDF software and documentation.

NSSDC has recently completed version 2 of CDF. A summary of the bindings is listed in the accompanying table. Version 2 software is a completely new implementation in the C language with separate C bindings. It offers significantly enhanced performance and flexibility over version 1 and is upwardly compatible with it. The FORTRAN bindings will be maintained as a veneer on top of C, which provides a transparent interface to the new software for current CDF users and handles incompatibilities between the C and FORTRAN programming languages. A key feature of version 2 is its ability to operate on a wide range of different computer systems (e.g., DEC VMS, Sun and Silicon Graphics Unix, Apple Macintosh, IBM MVS, and VM). Currently, the FORTRAN veneer layer will be supported only on a subset of those systems where FORTRAN bindings will continue to be required (e.g., VMS, Sun). Version 2 language bindings will also be implemented for IDL, which currently operates only on DEC VAX/VMS and Sun Unix systems.

Operations of the CDF Software Package (Language Bindings for the CDF Data Abstraction)

Name/Operation	Function
Global	The entire CDF
▪ CDF_create	Create a CDF
▪ CDF_open	Open a CDF
▪ CDF_close	Close a CDF
▪ CDF_delete	Delete a CDF
▪ CDF_inquire	Inquire about a CDF
Attribute	Global or variable-specific information
▪ CDF_attr_create	Create a CDF attribute
▪ CDF_attr_inquire	Inquire about a CDF attribute
▪ CDF_attr_put	Enter a value for a CDF attribute
▪ CDF_attr_get	Extract a value for a CDF attribute
Variable	The actual data
▪ CDF_var_create	Create a CDF variable
▪ CDF_var_inquire	Inquire about a CDF variable
▪ CDF_var_put	Enter a value for a CDF variable
▪ CDF_var_get	Extract a value for a CDF variable
▪ CDF_hyper_put	Enter a multidimensional block for a CDF variable
▪ CDF_hyper_get	Extract a multidimensional block for a CDF variable

The performance improvements in version 2 come from the inherently greater efficiency of C over FORTRAN, including restructuring of the software to take advantage of C functionality, optimization of internal disk caching, and new access methods. While version 1 provides random access to all elements within a data set stored as a CDF, version 2 extends the bindings to provide hyperplane access. The hyperplane technique provides random, aggregate access to subdimensional blocks within a multidimensional variable. In other words, a single call can access a vector, plane, parallelepiped, etc., out of an equal or higher dimensional structure. The subdimensional structure can span the full extent of the multidimensional block, or it may be smaller.

In addition to portability, version 2 gives a user-programmer the ability to select a run-time binding to a physical data format layer. The physical layer may be either the native format of the computer system being used or a machine-independent layer built upon the Institute of Electrical and Electronics Engineers (IEEE) standard via the External Data Representation protocol developed by Sun Microsystems and placed in the public domain. Many computer manufacturers (typically of Unix-based systems) have adopted External Data Representation as their native protocol. On other systems (e.g., VMS), External Data Representation services are available via software. However, for applications where data portability is not critical and absolute performance is of greater importance, the optional run-time binding to the native physical format offers significant flexibility. In addition, the upward compatibility of the software will apply to the data as well; version 2 will provide read access to version 1 on VMS systems.

NSSDC has started the planning for version 3, which will enhance version 2 with machine- and media-independent distribution and network services. Part of this activity is currently focusing on testing the NCS. Initially, NCS would be used to provide a network shell to provide transparent access to CDF data bases distributed over a network. In this scenario, an application running on a Sun work station could have transparent access to a large data set stored in CDF on a VMS system via an optical disk, for example, at the applications programmer's level. For environments where task-to-task networking

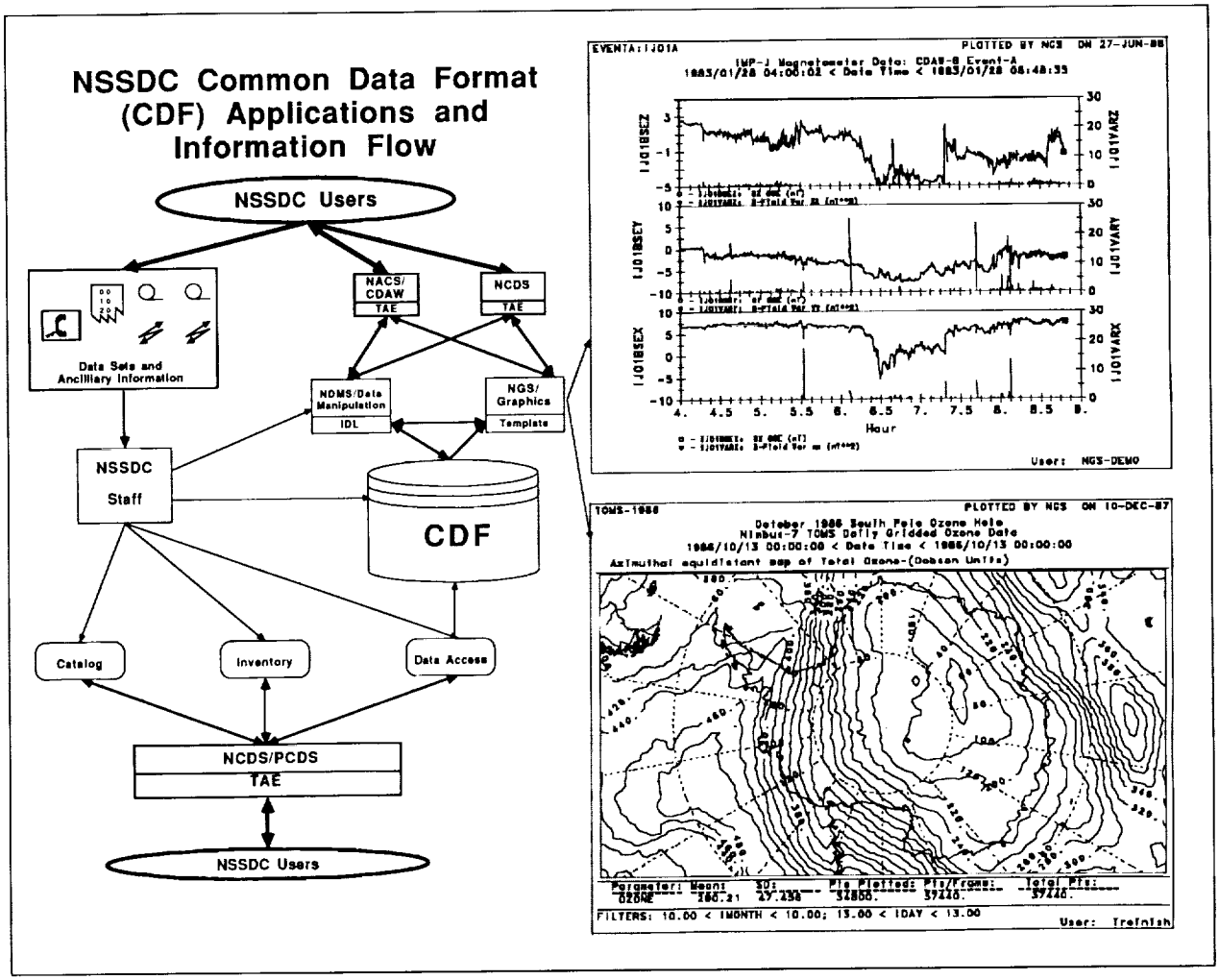

The role of CDF in data systems supporting CDAW and NCDS.

is neither available or feasible, transport distribution services would be developed to provide computer-independent mechanisms for "shipping" of CDFs through a variety of media. This software—truly interoperable over heterogeneous environments—is expected to become available in 1990.

Other future work will concentrate on additional access methods and alternative (e.g., hierarchical) data structures, which will be particularly relevant for large volumes of spatial data. Since the implementation of the CDF data abstraction really implies an extension of a conventional programming language for the support of multidimensional data objects, a recasting of CDF into an object-oriented environment such as C++ will be pursued.

The CDF design effort involves the integration of various physical science disciplines and the computational sciences with an emphasis on developing capabilities for researchers to concentrate on scientific research, freeing them from the mechanism of working with specialized data structures or formats. What is important is not the technical details, but the benefit the technology can easily and inexpensively provide to promote science. Such technical developments will further the use of heterogeneous computer systems to support the management, analysis, and display of scientific data separate from a centralized computer system.

The accompanying figure illustrates the role of CDF in the data systems that support two NSSDC programs, the

CDAW and NCDS. In addition, the sample plots show the diversity of the data sets that can be supported.

The top plot on the right illustrates data about the Earth's magnetic field derived from the IMP-J spacecraft. These data were among the ensemble of data sets that formed the CDAW-8 database. This plot is divided into three panels, one each for the x, y, and z components of the magnetic field. Each of the traces represents approximately 5 hours of in situ observations by the IMP-J magnetometer on January 28, 1983. The right-hand series of three traces is for the magnetic field components in GSE coordinates in units of 10^{-9} T, which are marked by a circle. The left-hand traces are for the variance of the components in units of 10^{-18} T^2.

The bottom plot on the right illustrates data from the TOMS on board the Nimbus-7 spacecraft. The data are available as daily world grids (37,440 cells per grid) from late 1978 through the present at the NSSDC and are supported by the NCDS. These data have become increasingly valuable as they indicate the presence of the so-called ozone hole over the South Pole. This plot shows the internal structure of the ozone hole for October 13, 1986, projected in an azimuthal equidistant map centered over the South Pole so that Antarctica fills the viewing window. The contour lines of total ozone are incremented every 20 Dobson units.

Contact: Lloyd A. Treinish (Code 634)
(301) 286-9884
Gregory W. Goucher (Code 634)
(301) 286-2341

Sponsor: NSSDC

Mr. Lloyd A. Treinish is a computer scientist at the NSSDC with 10 years' experience at Goddard. He develops advanced data systems to support scientific applications and studies space and atmospheric phenomena. Mr. Treinish was the chief designer and developer of the Pilot Climate Data System, and he originated the CDF, the first self-describing data abstraction for the storage and manipulation of multidimensional data. He has an SM in physics from the Massachusetts Institute of Technology and has received several professional awards including four NASA Certificates of Outstanding Performance.

Mr. Gregory W. Goucher, senior programmer analyst at NSSDC, provides technical support for the development and implementation of advanced scientific software applications. He has 6 years' experience at Goddard and is currently pursuing an MS in computer science at Johns Hopkins University.

INTELLIGENT DATA MANAGEMENT

The objective of the Intelligent Data Management project is to develop intelligent information fusion systems that integrate emerging software technologies using three-dimensional graphics, communications, object-oriented data bases, natural language query processing, connectionist models, artificial neural networks, artificial intelligence techniques, and expert systems. The research into the utilization of these technologies will provide the basic information environment for NASA's planned space missions through the foreseeable future. The following technical areas are being addressed in this research:

- Intelligent user interface development.
- Automatic data labeling, characterization, and cataloging.
- Knowledge-based geographic information systems.
- Object-oriented data base development.
- Knowledge acquisition tools.
- Intelligent domain-specific resource planning and scheduling.

This end-to-end information fusion system will remove from the user the burden of learning the system architecture, data content, available resources, and system language. The user can easily input his/her domain-specific information into the system, which automatically encodes the input into a knowledge base.

The intelligent user interface work has created a large-scale domain-independent spatial data management expert system that serves as a front end to data bases containing spatial data. This system uses spatial search techniques to generate a list of all the primary keys that fall within a user's spatial constraints before invoking the data base management system, an approach that substantially decreases the amount of time required to answer a user's query. This system also uses a domain-independent query expert system that preprocesses the user's English query and maps a broad class of queries into a smaller subset that can be handled by a commercial natural language

processing system. This system was applied to data from the International Ultraviolet Explorer satellite as proof of concept. This work was presented at the 1989 Goddard Conference on Space Applications of Artificial Intelligence and received an honorable mention award. The first figure illustrates this prototype.

The concept of using artificial neural networks for automatic labeling and characterization of data objects stems from the enormous data-generating capabilities in the next generation of satellite remote sensors. Current data management technologies cannot cope effectively with the data complexity and magnitude. Therefore, an innovative approach is needed to create object-oriented data bases that characterize, label, and catalog remotely sensed data on the fly; that are manageable in a domain-specific context; and whose contents are available interactively and in near real time to the user community. Goddard researchers have recently completed a prototype system using a back propagation supervised learning procedure for training layered networks of neuronlike nodes to recognized objects or features within a satellite data stream.

Values of four spectral bands from LANDSAT-4 TM imagery were used as input to the network. Results showed that information is available in the raw spectral values concerning the ground truth classes into which individual pixels can be categorized. The limited training set precludes any conclusions about how accurate a neural network could become with this data; however, the results look very promising. In the future, project designers hope

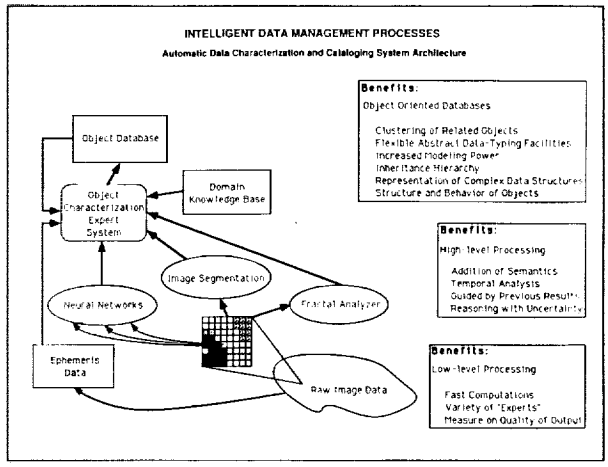

Expert data management system.

to extend this paradigm to work on multiple images taken of different locations and from different instruments. The decision on when and how to apply different kinds of networks could eventually be implemented by an expert system which would also procedurally place the appropriate metainformation into an object-oriented data base for interaction by the user in near real time with an intelligent interface described above. This work was also presented at the 1989 Goddard Conference on Space Applications of Artificial Intelligence and received the Best Paper award. The second figure illustrates this work.

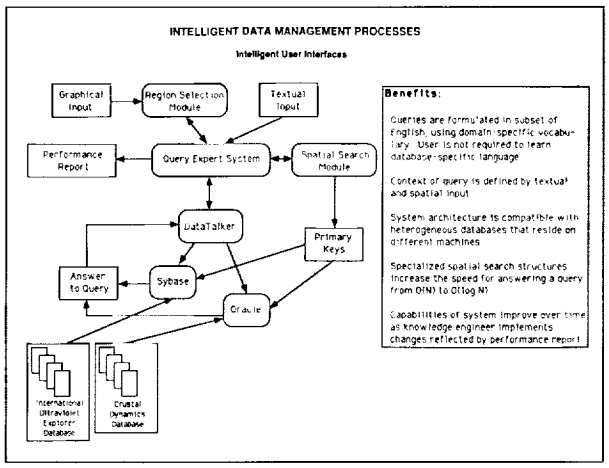

The large-scale domain-independent spatial data management expert system resulting from work on intelligent user interfaces.

Goddard researchers have been working on the development of an intelligent interface for adding spatial objects into a geographic information system. The research team is building on a prototype system, Knowledge-Based Geographic Information Systems, currently being developed by the University of California at Santa Barbara. This system can accommodate high-level expert system rules and heuristics and efficient spatial data-search techniques through the use of new data structures. It also develops a learning capability through interaction with the user. Its basic differences from traditional systems are its ability to embody the user's point of view about the data layers and the manipulation procedures that can be implemented on those layers. The immediate goal is to transform it into a portable system by converting the VAX dependencies to a standard Unix system. Goddard staff are also adding the capability to import Land System Analysis (LSA) imagery easily into the prototype. Once this work is completed, the staff will evaluate the feasibility of linking and customizing a natural language query

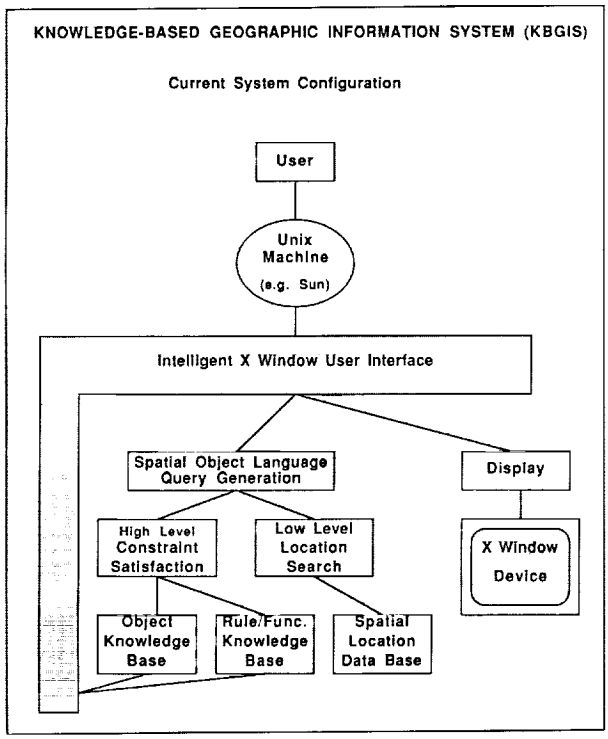

Current development of the Knowledge-Based Geographic Information System.

processor and a high-level expert system that will deal with the pragmatic translation between the natural language query processor and the knowledge-based geographic information systems. The third figure illustrates the research team's current progress.*

**Contributors to this work include Robert Cramp, Scott Hill, and Craig Goetsche of Science Application Research, Inc.*

Contact: William J. Campbell (Code 634)
(301) 286-8785

Sponsor: Office of Aeronautics and Space Technology (OAST) and Director's Discretionary Fund

Mr. William J. Campbell is the Principal Investigator in the Intelligent Data Management project of the NSSDC. He is also Head of the Advanced Technology Development task for the Data Information System serving Earth Observing System (Eos). During his 11 years at Goddard, Mr. Campbell has managed the training program in the Eastern Regional Remote Sensing Application Center and served as leader of the Geographic Information Systems. He has also received several awards including three Outstanding Achievement Awards. He earned his MS in physical geography from Southern Illinois University.

IMAGE SERVER

The Image Server software module is intended to alleviate contention among Goddard scientists for shared image analysis displays such as the IIS. Because of the large number of Macintosh IIs already available and the number expected, it seemed to analysts that this color-capable member of the Macintosh family would be an appropriate substitute for the IIS terminal, especially for basic uses such as displaying an image and using simple color lookup tables with an image. However, to use the Mac as an IIS required adding some functions. Image Server was developed to meet this need.

Image Server itself is an application running on the Macintosh (see figure). It is written in the C language, contains about 5,000 lines of code, and takes up 110 kbytes of memory when running. To start it, one merely double clicks on the icon. The only other necessary components are a software package, called CommUnity Mac, and an Ethernet board. This combination permits the Macintosh to pose as a DECNet node on the Ethernet and allows it to act as a server. The Image Server waits for a request from a process on any DECNet node (typically, the node is closeby, usually in the same building, but any reachable DECNet node could serve), opens the logical connection, and starts processing commands from the remote processor. These commands can include sending an image, coloring an image, or even scaling it. Once the image is on the Macintosh, the user has various display options, including window sizing, scrolling, scaling, and color. If the image data needs to be kept on the Macintosh, it can be easily saved to disk.

In a typical-use scenario, a user of a supercomputer such as the Massively Parallel Processor (MPP) starts up the Image Server on the Macintosh and then runs a favorite terminal program (Image Server will run in the background) to log onto the MPP's host VAX. Once on the VAX, the user runs a program that has previously been modified to use the VAX-side Image Server routines. The routines provide a quick and easy way to send images, look up tables, and perform similar tasks on the Macintosh. While using this program, the user interacts exactly as if he/she were using the IIS graphics terminal. The only

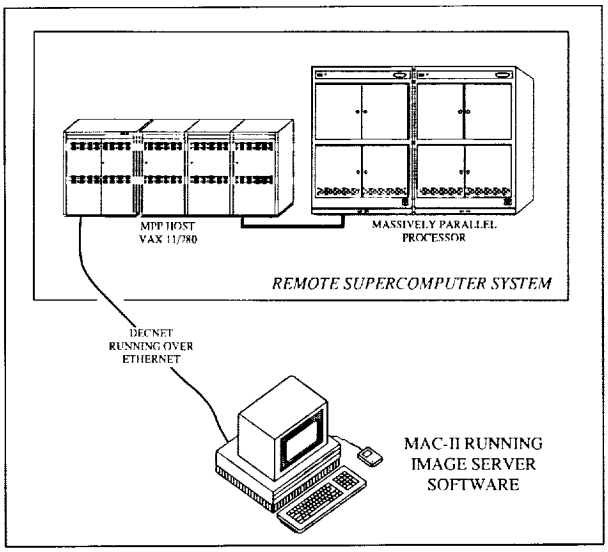

Image Server allows Mac-II user to easily view and store color images from remote supercomputer system.

difference is that the user has the convenience of the Macintosh and the comfort of knowing that no one else is waiting to use the display device.*

**The entire Image Server software package was implemented by Peter Duniho, an intern from Virginia Polytechnic Institute and State University.*

Contact: John E. Dorband (Code 635)
(301) 286-9419

Sponsor: OAST

Dr. John E. Dorband is a computer scientist with 4 years' experience at Goddard. He holds a PhD in computer science from The Pennsylvania State University and is interested in concurrent processing, computer language, and artificial intelligence processing. Dr. Dorband has received a Group Achievement Award.

IMAGE SEGMENTATION BY ITERATIVE PARALLEL REGION GROWING

Image segmentation is the process of partitioning an image into constituent parts, called "regions," using image features such as pixel intensity, spectral values, and/or textural properties. Several approaches have been used for image segmentation, including characteristic-feature thresholding or clustering, boundary detection, and region growing. The approach explored here is region growing, implemented as an iterative parallel process.

Image segmentation is a key step in many approaches to data compression and image analysis. For example, an encoding of an image segmentation, such as through a region-label map and region-feature file, can be used for data compression. Also, image analysis can be performed on an image segmentation by using the shape, texture, spectrum, etc., of the regions, found by the image segmentation, and/or interrelationships between the regions. This region-based analysis of imagery is usually more effective than analyzing an image one pixel at a time, because region-based analysis exploits spatial information, whereas pixel-based analysis does not. It also can be more effective than spatial analysis based on analyzing pixels in areas defined by a fixed grid. Grid-based analysis essentially uses an arbitrarily imposed segmentation of the image, whereas region-based analysis uses a segmentation that is derived from characteristics of the image data.

Other researchers have studied iterative region growing in which the single most similar pair of spatially adjacent regions is merged at each iteration. Goddard analysts suggest, however, that it is more efficient to perform parallel merges of a set of region pairs per iteration, rather than just one merge per iteration. When implemented on a massively parallel computer, such as the MPP at Goddard, as many as several thousand region pairs can be merged simultaneously in a parallel implementation.

The set of region pairs for merging can be chosen for each iteration by selecting the best merges from within

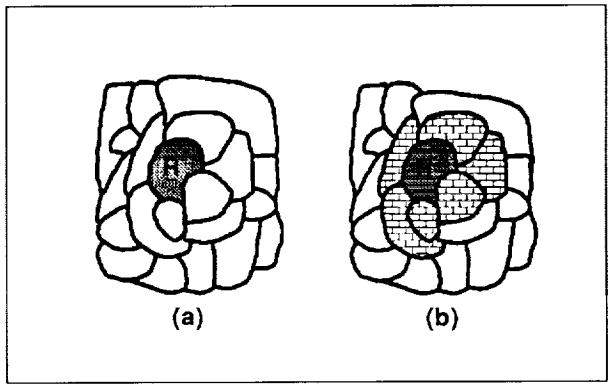

(a) Level 1 subimage for region R, and (b) level 2 subimage for region R.

ORIGINAL PAGE
COLOR PHOTOGRAPH

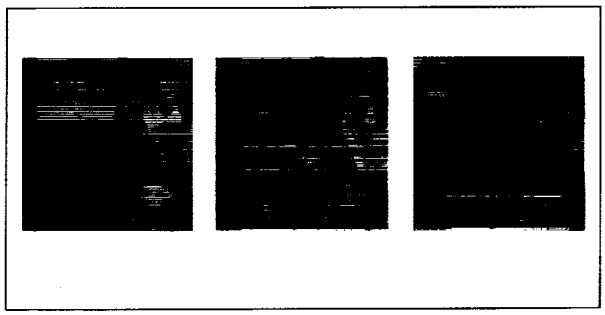

Segmentation of Ridgely, Maryland, TM image with merge constraint level 2.0 and band average mean-square error similarity criterion. (a) Original image . (b) Iteration 153 with 64 regions and mean-square error 0.14 . (c) Iteration 161 with 49 regions and mean-square error 0.15 .

different areas of the image. When the maximum region size is small compared to the image size, and if the region pairs are sufficiently distant from each other, whether or not a pair of regions is merged in one part of the image should not affect whether or not a pair of regions is merged in another part of the image.

The current iterative parallel region-growing algorithm initially labels each image pixel as a separate region. Then it selects the set of region pairs to be merged at each iteration by choosing the best merge within overlapping subimages centered on each region, or on each pair of spatially adjacent regions, subject to a global threshold. Iterations continue until the process converges to a prespecified number of regions or error threshold.

The subimages used by the iterative region-growing algorithm can be defined recursively as follows: A level 0 subimage with respect to any region is the empty set. A level 1 subimage with respect to a region is the region itself. A level 2 subimage with respect to a region is the level 1 subimage with respect to that region, plus all regions that are spatially adjacent to the level 1 subimage. Finally, a level n subimage with respect to a region is the level n-1 subimage with respect to that region, plus all regions that are spatially adjacent to the n^{th} level subimage. The first figure shows examples of this definition. For merge constraint level n, a pair of regions are merged in a particular iteration if and only if that pair of regions is the most similar pair of regions within the union of the level n subimages with respect to each of the regions.

Similarity criteria are used to measure how similar one region is to another region. In general, choice of the best similarity criterion to use depends on the application for the segmentated image and on the characteristics of the image data. A limited number of general-purpose similarity criteria have been developed and used to test the iterative parallel region-growing algorithm. Two of the criteria are based on minimizing the increase in mean-space error between the original image data and the region-mean image. The region-mean image is created by replacing each pixel with the value of the mean of the region it belongs to at a given iteration. Another criterion is based on minimizing the change in image entropy.

The second and third figures show the results of segmenting two different Landsat TM images with the iterative parallel region-growing algorithm. The image processed on the left above is from the area near Ridgely, Maryland, while the image processed below is from the eastern edge of the Menengai volcano crater in the East African Rift area.

The segmentations depicted in the second and third figures outline various image spatial features at different levels of detail. In both (b) and (c) of the second figure, dark blue bodies of water are outlined very nicely in the upper right portion of the image. In (b), forest areas in two different shades of green are delineated in the lower left portion of the image, while in (c), these forested areas are joined together in one large region. Pinkish agricultural fields are outlined clearly in both (b) and (c), with (b) showing slightly more detail, particularly in the upper right corner. Pinkish agricultural fields are also outlined

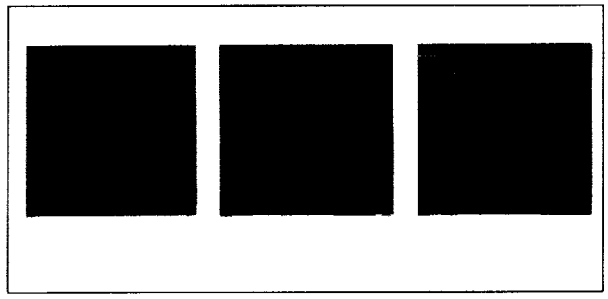

Segmentation of Menengai Crater TM image with merge constraint level 2.0 and band average mean-square error similarity criterion. (a) Original image. (b) Iteration 217 with 33 regions and mean-square error 0.11. (c) Iteration 230 with 20 regions and mean-square error 0.13.

clearly in (b) and (c) of the third figure, with (b) showing more detail particularly in the lower right corner. In the third figure, (c) outlines two main shades of lava flow that appear in the lower left corner and continue up to the top of the image. A lighter area of lava surrounds a smaller, darker flow. In (b), the lighter lava flow is broken up into three separate regions that are probably not significantly different from each other.

Goddard researchers are continuing to study the use of image segmentation in image compression and analysis.

Contact: James C. Tilton (Code 636)
(301) 286-9510

Sponsor: OAST

Dr. James C. Tilton focuses on the analysis of spatial and hyperspectral information in remotely sensed imagery data and the development of high compression ratio image techniques. He has won a Group Achievement Award and an Outstanding Performance Award during his 8 years with Goddard. Dr. Tilton received his PhD in electrical engineering from Purdue University.

A PERSONAL COMPUTER MAP PROJECTION TOOL

MAPPER is a set of software tools designed to let users create and manipulate map projections on a personal computer. During 1987, a small program was written to create maps for an airborne Unix microcomputer. In addition to creating the maps, the program projected current position data onto the maps in real time. However, due to an upcoming NASA mission over the North Pole, further effort was needed to ensure map integrity for the entire globe. The current projection (sinusoidal) was inadequate, particularly with regard to the polar regions.

Research showed that many map projections and derivatives of map projections are used today. Five common projections were studied and incorporated into MAPPER. Of the five, three projections are of the cylindrical type (cylindrical to equal area, Mercator, and pseudocylindrical to sinusoidal), one projection is conical (Lambert Conformal), and one is azimuthal (azimuthal equidistant). Of the five, the azimuthal equidistant is most useful for aircraft work, because it can be used anywhere on the globe.

Data used to create MAPPER projections come from a scaled-down version of a Central Intelligence Agency map data base. High- and low-resolution versions of this data base are included. The entire world is contained at low resolution, while the U.S. East Coast alone is contained at high resolution. Both versions show State boundaries and coastal outlines, with rivers and lakes included in the East Coast version.

Since this project was written entirely in the C programming language, exporting the source code to the personal computer platform was relatively easy. Further enhancements were made that provide the user with a friendlier environment than the familiar Unix command line. A simple screen shell was written to hide the keystrokes needed to create and plot maps. Also, a feature was added to allow a user to import MAPPER projections into an inexpensive computer-assisted design program. From the program, the user can manipulate the map in any way, including adding text and symbols. Also, many printers and plotters are supported for hard-copy output.

For quick and easy creation on maps of the personal computer, MAPPER has proven quite useful. Although the final product is no longer part of an airborne data acquisition system, it can create maps with flight line data, either preflight or postflight. The accompanying figure demonstrates this capability.

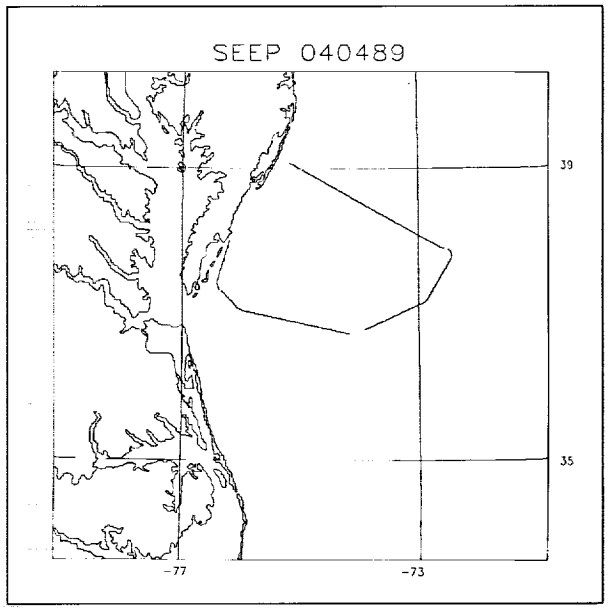

Example of postflight map using aircraft position for flight lines.

Contact: Steven A. Bailey (Code 672)
(804) 824-1429
Sponsor: Airborne Oceanographic Lidar Program

Mr. Steven A. Bailey works on software engineering for several remote sensing projects in the Observational Science Branch of the Laboratory for Oceans. His technical interests include working on software tools and applications for data acquisition systems using personal computers. Mr. Bailey received a BA in geology from Slippery Rock State University and a BS in computer science from the University of Maryland. He has 5 years' experience at Goddard.

GEOMETRIC CORRECTION OF OFF-NADIR IMAGERY FROM SPACE

The Monocular Electro-Optical Stereo Scanner, which was to have flown in July 1988, was designed to provide three different views (two off-nadir) of the same area on the ground that could have been used in stereo analyses to determine elevations. The off-nadir views were to point in the forward and backward directions relative to the orbit of the spacecraft. Because all images would be obtained within a few seconds of each other, the relative position of the spacecraft for each image would be accurately known, thus providing the best chance for obtaining correct elevation measurements. The Science Information Systems Center was to automatically perform the stereo analysis on the three images to determine elevations and incorporate these elevations into the geometric correction process, generating a universal transverse Mercator map. A stereo matching algorithm developed for Goddard's MPP was to be used for the stereo analysis. When the spacecraft failed to achieve orbit, Goddard analysts decided to test the geometric correction algorithm using simulated imagery. This report summarizes the geometric correction algorithm and the results of the simulation experiment.

The object of the experiment was to start out with a universal transverse Mercator-projected image along with a known elevation function. From these, a scanner nadir image and forward looking off-nadir image were simulated. The Mercator image is shown in the first figure. If the geometric correction is accurate, the output Mercator-projected image should be the same as the original. The results described are from the geometric correction of the forward off-nadir image, which had a considerable amount of distortion from elevation.

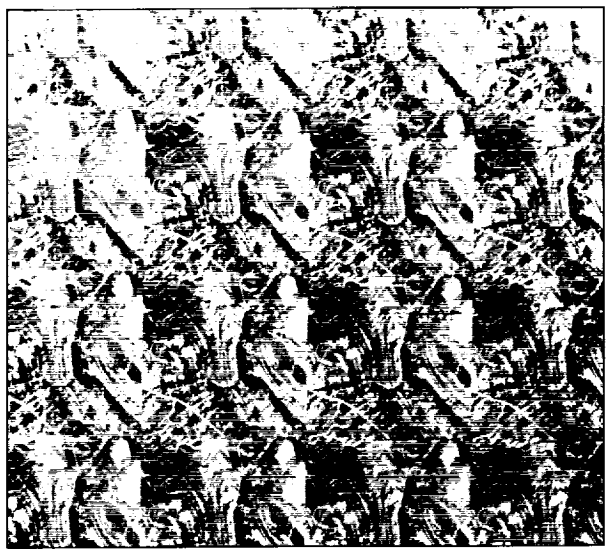

Universal transverse Mercator image generated as a mosaic of a 512 × 512 portion of a LANDSAT image.

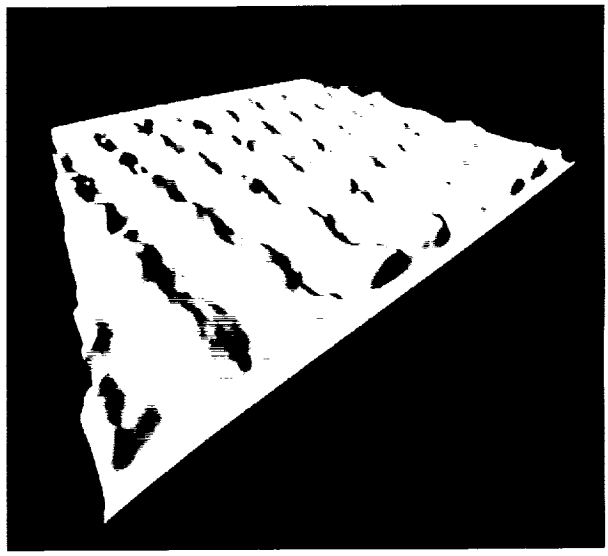

Elevation function derived from automated stereo analysis on the MPP.

The first step of the process was to perform an initial geometric correction on the forward and nadir images to remove spacecraft roll, pitch, and yaw errors and to align the images for stereo analysis. This step included dividing the images into 512 × 512 overlapping subimages for

ORIGINAL PAGE
BLACK AND WHITE PHOTOGRAPH

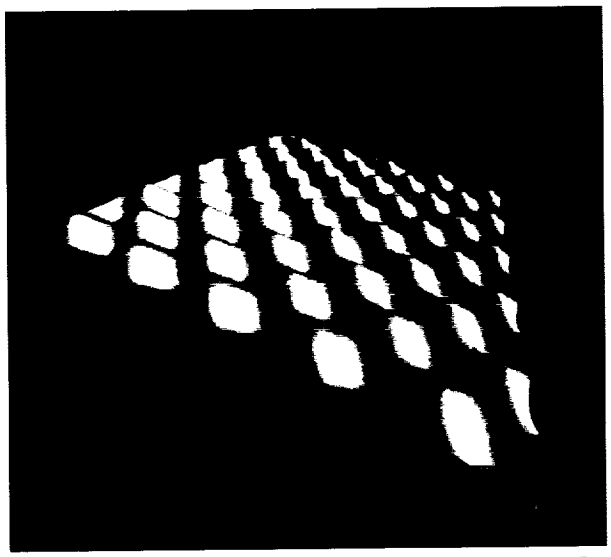

Sinusoidal "egg crate" function used as elevation for simulation of Monocular Electro-Optical Stereo Scanner.

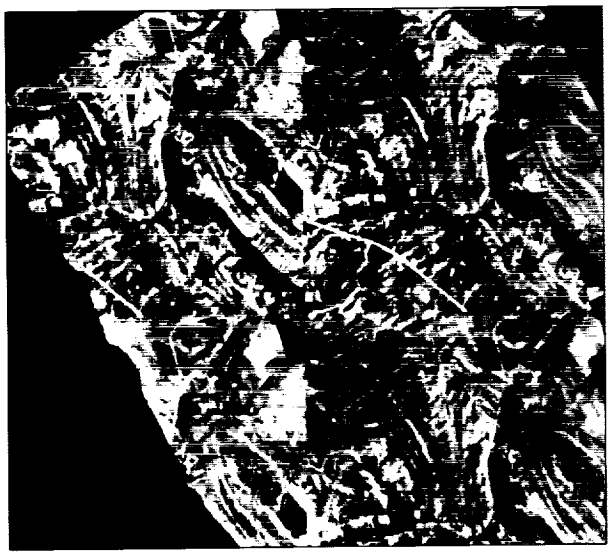

Superposition of a portion of the original Mercator image and the geometrically corrected forward image.

input to the MPP stereo matching program. The elevation function chosen for the simulation was the "egg crate" function shown in the second figure. The elevation derived from the stereo analysis is shown in the third figure. The flat areas in the third figure correspond to areas in the stereo analysis pair where there was no overlap between the images. Once the elevations were computed, they had to be incorporated into the geometric correction process. To accomplish this, for each pixel in the forward image, a ray or vector was projected toward the Earth from the sensor detector at the orbit position corresponding to that pixel. The three-dimensional coordinate where that ray intersected a sphere of radius $R_e + H$ was then computed where R_e was the Earth's radius and H was the elevation at that pixel. The projection of this three-dimensional coordinate onto the Mercator map projection was then computed to finish the geometric correction task. The fourth figure shows a portion of the original Mercator image in red and the corresponding portion of the output Mercator projection overlayed in cyan (blue-green). Where there is accurate registration between the two, the resulting image appears gray. A position error analysis showed that the two images were accurate to within ± 2 pixel locations in the grey area. In one area of the overlay, the two images are obviously not in registration. This is the area corresponding to the flat region in the elevation function where there was no overlap in the stereo pairs. The results in this region are equivalent to assuming zero elevation or not including elevation into the geometric correction process. Thus one can see that in off-nadir views where there is some degree of elevation variation, it is essential to include the elevation in the geometric correction process.

The software developed for this task can handle large-format (over 3,000 × 3,000 pixel) images. It is the first to include the MPP into an operational type of task.

Contact: Dr. James P. Strong (Code 636)
(301) 286-9535

Sponsor: Monocular Electro-Optical Stero Scanner Project

Dr. James P. Strong holds a PhD in electrical engineering and computer science from the University of Maryland. Dr. Strong is currently developing algorithms for image analysis and signal processing on the MPP.

COMPACT DISK DEVELOPMENTS AND PREMASTERING AT NSSDC/ASTRONOMICAL DATA CENTER

Compact disk-read only memory (CD-ROM) constitutes a low-cost, long-lived, high-capacity (600-Mbyte) data storage medium which is especially appropriate to the dissemination of multiple copies of data to scientific owners of personal computers, Unix work stations, and microVAX's. In the past year, the

NSSDC has made major steps forward in developing and exploiting this technology.

The disks are mass produced at a vendor's site by duplicating a master disk and are also produced by the vendor from user-supplied data on magnetic tapes or other media. The process of organizing data on these media and casting them in the International Standards Organization (ISO)-9660 standard format is called premastering. The Data Center's recent acquisition of a premastering work station enables it and other NASA groups to perform premastering at the Data Center rather than at a vendor site. This acquisition not only saves money but allows the simulation of final compact disks before shipping data to a mastering house.

Two disks were premastered at the Data Center and subsequently mastered, replicated, and widely distributed in the first half of 1989. The first was a disk holding approximately 30 of the most often requested astronomical source catalogs of the Astronomical Data Center. The second was a disk holding multiple data types related to Comet Giacobini Zinner, including imagery data associated with the pilot phase of the International Halley Watch as well as in situ magnetic field and plasma data obtained by the International Cometary Explorer spacecraft in 1985.

The creation of these disks required several key decisions. They would be of interest to both the astronomical community, which is oriented to the Flexible Image Transport System format, and to the planetary community, oriented to Planetary Data System labels. Thus, both systems' header records were written to the disks, with each pointing to the data files. This strategy enabled the data files to be addressed by software expecting one format or the other. Also, files were written for personal computer users whose software expected neither Flexible Image Transport System nor Planetary Data System format. Data Center researchers made key judgments about organizing overall data into user-natural and efficient directories and subdirectories to facilitate users' access to data.

The principal software package used for image display of compact disk data on personal computers is IMDISP, created and upgraded primarily at the Jet Propulsion Laboratory Planetary Data System. In its CD-ROM development work, the NSSDC suggested a number of IMDISP upgrades and developed a SHELL software package. The package allowed the user to call for IMDISP for image display and also for other retrieval/display software modules (including the FITS Table Browser software developed in association with the Astronomical Data Center CD-ROM discussed above) for data types other than bit-mapped images.

A workshop held at the Data Center in June 1989 reviewed the experience gained from the creation and use of the disks created at the Center and elsewhere at NASA and developed standards at a higher level than the ISO-9660. These higher standards specify a unique identification approach, Standard Formatted Data Unit usage, format, and content of metadata files describing the formats and contents of the actual data files, disk surface labeling, etc. The Data Center staff intend the premastering work station to be available to other NASA groups on a capacity-available basis and, after that, to other NASA-relevant Government groups. Guidelines for such use, and the support levels available from the Data Center, were also discussed at the workshop.

Contact: Joseph H. King (Code 633)
(301) 286-7355

Sponsors: Information Systems Branch, Communications Division, Office of Space Science and Applications, with support from the International Halley Watch Program and the Ultraviolet and Visible Astrophysics Branch, Astrophysics Division

Dr. Joseph H. King is Head of the Central Data Services Facility of the NSSDC and has been at Goddard since 1967. He holds a PhD in space plasma physics from Boston College, pursues a range of data management activities, and serves as Project Scientist for IMP-8.

GENERIC VISUALIZATION OF SCIENTIFIC PHENOMENA

Critical to the understanding of data is the ability to provide pictorial or visual representations of those data, particularly in support of correlative data analysis. Hence, a researcher must employ tools to visualize data as one important mechanism in the exploratory data analysis-interpretation process. An explosion of technology has occurred over the last few years in methods of computing that take advantage of the huge bandwidth and

processing power of the human visual system to help comprehend large volumes of complex data by giving visual form using graphics and imaging technology. This concept of data visualization has the power to bring an unprecedented capability to the scientific community. Despite the advancement of this visualization technology, there are still significant problems in bringing today's hardware and software into the hands of the typical scientist. For example, other computer science domains outside of computer graphics are required to make visualization effective. Data management and intuitive human computer ergonomics are needed to build systems that have appropriate, easy-to-use interfaces for use with data of interest. In addition, there are specific rendering algorithms, data transformations, etc., that, as part of a visualization pipeline, can be cast into a generic framework. NSSDC has an ongoing research and development program to implement such effective visualization tools using generic (i.e., data-independent) techniques for the display of multidimensional data. These efforts are designed to bring visualization to the space and Earth sciences research community in a discipline-independent fashion. The results of this research are available to the scientific user community for browsing of data sets as an adjunct to metadata management as well as for data analysis. This research will be of critical importance for the interpretation of information from current and planned large-scale data generators, such as supercomputer-based models and simulations, and spacecraft-based instruments like those of NASA's Eos.

The figure uses data from the Infrared Astronomical Satellite to represent the celestial sphere in galactic coordinates.

Visualization of scientific data in a discipline-independent fashion implies two basic tenets. First, to support correlative data analysis, it is necessary to be able to look at multiple sets of data in exactly the same fashion (i.e., visual correlation within a common framework). This may be as simple as placing two different parameters from different data sets in an x-y plot along a common time line. On the other hand, displaying different sets of point data, mapped grids, or images in some arbitrary geographic window, which is independent of the specific data sets in question, must also be accommodated. Second, a variety of different visualization techniques must be available to examine either a single set of parameters from one source or a number of different parameters from disparate sources. Specific representation techniques illustrate different aspects of data. A visual understanding of data at appropriate levels of qualitative and quantative detail and at appropriate microscopic and macroscopic levels can be achieved by using a variety of tools. Of course, not all techniques for representing data are useful for all data sets. Hence, a wide variety of representations schemes is necessary to accommodate a disparate collection of data.

Therefore, discipline-independent visualization implies the development of software that can manage arbitrary data sets and possesses different tools for displaying data. In other words, data management is as important a component of a data visualization system as underlying graphics and imaging technology. To implement a system that can provide these features in a practical fashion, the management of and access to the data must be decoupled from the visualization software. Within such a system, there must be a clean interface between the data and the display of the data, so that arbitrary data can be accessed by the visualization software. Hence, the visualization software needs only some basic descriptions of the data that it will display, but must be supported by a uniform data storage format. In addition, a common user interface for the selection of the techniques for representing data and associated options and a common design for the actual displays are required. Therefore, a software system of this design has an open framework. It can ingest arbitrary data objects for visualization, and other visualization techniques can be added independent of the application. This approach implies that a significant reduction in long-term software development

ORIGINAL PAGE
COLOR PHOTOGRAPH

costs can be realized because new data sets do not require new display software, and new display techniques do not require new data access software.

To implement these concepts for the space and Earth science research community, the NSSDC has developed the NSSDC Graphics System (NGS), an interactive discipline-independent toolbox for nonprogrammers to support the visualization of data, on the NSSDC Computer Facility's VAXCluster. Parts of the NGS are being recast or ported to powerful Unix work stations to provide highly interactive visualization tools. The NGS can access arbitrary data through the NSSDC CDF, which serves as a uniform interface between the visualization tools and the data. The NGS supports displays of any arbitrary multidimensional subset of any CDF-based data set by providing a large variety of different representation schemes, all of which are supported by implicit animation (i.e., slicing of a data set into sequences).

The NGS design provides an open-ended framework for discipline-independent data visualization so that new capabilities can be added. New tools that have been implemented as a result of NSSDC's research in several areas of computer science include novel computer graphics rendering techniques and data structures. These approaches include rendering and manipulation algorithms with portable implementations that can operate on any data object for *n*-dimensional gridding, geometric (spherical and Cartesian) data modeling, and ray-tracing via recursive spherical triangle subdivision.

The NGS is designed to be portable so that it eventually can be made available on computer systems outside of the NSSDC Computer Facility to promote the exchange of both software and data. The NGS is already being β-tested at several VAX/VMS sites on SPAN to evaluate it for potential use in future flight projects and to support specific scientific investigations. It is expected that the NGS implementation for Unix work stations will be made widely accessible in the future. In addition, the NGS is currently available operationally to the users of NSSDC's Network Assisted Coordinated Science system on SPAN in support of its CDAW activities and to users of NCDS.

The NSSDC is currently helping a number of scientists in a variety of disciplines to solve their problems in scientific data visualization through the tools available in the NGS. This research support is in addition to the aforementioned β-testing and evaluation of the NGS for future NASA flight missions. Because space for this article is limited, the following example is offered as a basic sample of the capabilities of the NGS and, hence, as proof of the concepts outlined above. This example illustrates only one basic visualization technique and that it, as well as those not shown, can be applied to any data.

The figure illustrates data derived by Richard White of Goddard from an all-sky infrared image prepared from the zodiacal history file of data from the Infrared Astronomical Satellite. The data were provided to the NSSDC as a collection of pixels with associated intensities laid out in galactic coordinates. The figure is a representation of the celestial sphere in galactic coordinates derived from the Infrared Astronomical Satellite data. The sphere, which is modeled as a geodesic consisting of 81,920 triangles, is deformed from a nominal level according to the log of the infrared intensity from about 10^6 to 10^8 Janskys/Steradian. The color scale also corresponds to the log of the intensity. The center of view is along the galactic equator at 0° longitude. The intense band along the equator corresponds to the Milky Way. The height mapping dramatizes the spatial structure of the infrared intensity, while the color enhances this perception as terrain color would enhance a topographic map. Other visualization techniques (e.g., high-resolution pseudocolor imagery) might emphasize only the detailed, quantitative nature of the spatial structure. This technique emphasizes both qualitative and quantitative information about the infrared intensity.

Contact: Lloyd A. Treinish (Code 634)
(301) 286-9884

Sponsor: Office of Space Science and Applications, NSSDC

Mr. Lloyd A. Treinish is a computer scientist at the NSSDC with 10 years' experience at Goddard. He develops advanced data systems to support scientific applications and studies space and atmospheric phenomena. Mr. Treinish was the chief designer and developer of the Pilot Climate Data System, and he originated the CDF, the first self-describing data abstraction for the storage and manipulation of multidimensional data. He has an SM in physics from the Massachusetts Institute of Technology and has received several professional awards including four NASA Certificates of Outstanding Performance.

USER-FRIENDLY PHOTO PRODUCTS FACILITY

The photo products facility at Science Information Systems Center has implemented a new user-friendly interface that is available to the Goddard community and other scientific organizations. The facility can produce high-quality hard copy of scientific data, such as images taken by satellite or computer-generated scientific data models. In the past, obtaining a high-quality hard copy of raw or processed data required having the data files catalog under the LSA at the Science Information Systems Center computer facility. The effort was tedious and time consuming for individuals who did not use the local facility or the LSA system or were not familiar with LSA. Therefore, a user-friendly environment for processing the data to the hard-copy final product was created.

Currently, the hardware consists of a Colorfire 240 and a Dicomed D47. The Colorfire 240 is a high-speed film recorder capable of producing color or black-and-white photo products. It has the resolution of 8,192 samples per line and 8,192 lines per frame, which is approximately 8 $in.^2$ The Dicomed D47 is also capable of producing color or black-and-white photo products. It can use Polaroid or single-frame film. Its resolution is 4,096 samples per line and 4,096 lines per frame.

To create a user-friendly access to the Colorfire 240, software has been developed and implemented on the Science Information Systems Center computer facility, which is the interface between the user and the LSA system. The task of submitting image data for processing was partitioned into two parts. Under the first part, CATTAE, a single image is exposed onto a single frame of film, and under the second part, MOSAIC, multiple images are placed onto one frame of film. Both tasks can be executed interactively or in batch mode. A data preparation and verification program for each task, which can be executed interactively, was implemented to further facilitate the submission of the images. The data programs prompt for all the pertinent data, verify the existence of the input files, and create a command procedure file. The command procedure can be submitted to execute the respective program.

CATTAE processes one image per film frame, so the number of images on a submission is limited by the availability of computer time, disk space, film, and money. For each submission, CATTAE can process one-, two-, or three-band images, and each frame may be in black-and-white or color. Each image, whether single or multiple banded, can have its individual color table applied.

MOSAIC can access up to 89 image files concurrently. The 89 files may be for single- and multiple-banded images, as long as the total number of samples of 8,192 per line is not exceeded. Each image, whether single or multiple banded, can have its individual color table applied. MOSAIC also allows the images to be superimposed, so that a collage effect can be created.

CATTAE and MOSAIC copy VAX/VMS files with file attributes of unformatted, sequential access, fixed-record type, from the local VAX node, IAF, or a remote node. They catalog the new files under the LSA system for processing through the Colorfire 240 for photographic products. Both programs will process image files for color and black-and-white products in the same session. Basic input requirements for both programs consist of the name of file or image file to be processed, access to the image files, and parameters such as the initial image parameters and final photo product parameters. The programs will generate task-order and accounting files and send them via VAX/VMS mail to the operations office for processing and to the computer facility for accounting and billing. In addition, the person submitting the images for processing will get a copy of the task-order and accounting information file via VAX/VMS mail.

Contact: Raul Garza-Robles (Code 636)
(301) 286-9513

Sponsor: Division Enhancement Fund

Mr. Raul Garza-Robles is a mathematician and data analyst in the Information Systems Development Facility. He develops and implements computer software associated with application data analysis and image display techniques. He has won three NASA Special Achievement Awards and a Performance Award. He has 19 years' experience at Goddard and earned his BS from Florida State University.

ORIGINAL PAGE
BLACK AND WHITE PHOTOGRAPH

The three COBE instruments are pointed away from the Earth to survey the cosmos—FIRAS along the spin axis and the DMR and DIRBE 30° off the spin axis.

FLIGHT PROJECTS

COSMIC BACKGROUND EXPLORER (COBE) MISSION

COBE was designed specifically for studying the Big Bang, the primeval explosion that started the expansion of the Universe, and for measuring diffuse infrared and microwave background radiation, which includes the primary remnant of the explosion. In addition, COBE instruments determine the spectrum of the radiation and the variances between different points of the sky with far better sensitivities than can be achieved with other techniques. COBE was designed, integrated, and tested by engineers, scientists, and technicians at Goddard; certain major subsystems, such as the liquid-helium-cooled dewar, were procured from contractors.

The COBE Observatory carries three instruments: the Differential Microwave Radiometer (DMR), the Far Infrared Absolute Spectrophotometer (FIRAS), and the Diffuse Infrared Background Experiment (DIRBE). Using standard microwave receivers, the DMR measures the anisotropy of the cosmic background radiation at wavelengths of 3.3, 5.7, and 9.6 mm, with an angular resolution of 7°. The FIRAS measures the spectrum (the intensity as a function of wavelength) over a wavelength range of 100 μ to 1 cm, with a 5-percent spectral resolution and a 7° angular resolution; it is a cryogenically cooled polarizing Michelson interferometer. The DIRBE measures the brightness of the sky at wavelengths from 1 to 300 μ with a 1° angular resolution in 10 bands; it is a cryogenically cooled, off-axis, Gregorian telescope.

The three COBE instruments are pointed away from the Earth to survey the cosmos—FIRAS along the spin axis and the DMR and DIRBE 30° off the spin axis. These instruments are located inside a large deployable radiofrequency thermal shield to protect against thermal and electromagnetic radiation from the Sun, the Earth, and the observatory. Within the radiofrequency thermal shield is a liquid helium dewar, similar to that successfully flown on board the Infrared Astronomical Satellite. To satisfy the requirements of two of the COBE experiments, the observatory rotates at approximately 0.8 rpm.

Science and ancillary data are stored continuously on board one of the two observatory tape recorders, which are played back once per day to the ground system located at Wallops. The Tracking Data Relay Satellite System (TDRSS) is used to provide orbit tracking and telemetry and command for observatory safety and health monitoring.

The COBE Observatory was originally designed to be launched by the space shuttle from the Western Space and Missile Center. As a result of the *Challenger* shuttle accident, COBE was redesigned as shown in the figure for launch by a Delta 5920 expendable launch vehicle (ELV)

COBE was launched by a Delta 5920 on November 18, 1989, from the Western Space and Missile Center. COBE carries three instruments that study the Big Bang and measure the sky's background radiation.

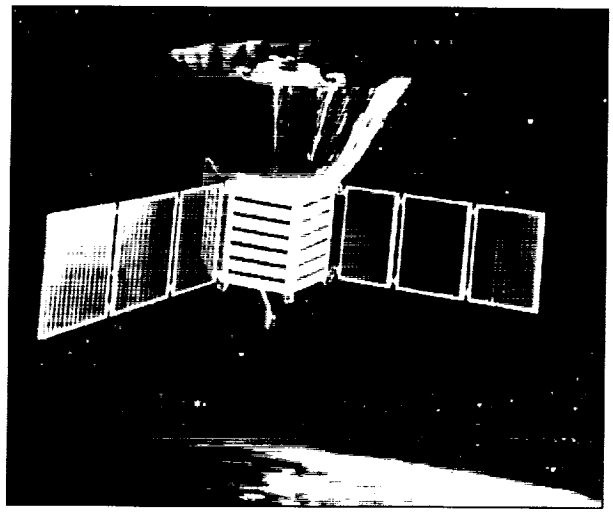

The COBE Observatory redesigned for launch by a Delta 5920 ELV.

from the Western Space and Missile Center. During the past year, the flight spacecraft subsystems and flight instruments were totally integrated, and the observatory was subjected to system-level testing, including vibration testing, acoustic testing, and thermal vacuum/thermal balance testing. In April 1989, as part of the system functional test plan, the observatory was placed in a horizontal position to better simulate the zero-gravity environment for the cryogenic instrument mechanisms. During this testing, it was found that the FIRAS external calibrator (XCAL) would not remain properly positioned in the sky horn for calibration purposes. As a result of this problem, a decision was made to fix the XCAL mechanism, requiring warmup of the dewar and removal of the dewar cover to gain access to the mechanism. The dewar was opened after successful completion of observatory thermal vacuum/thermal balance testing in July, and the FIRAS XCAL was fixed while it remained in place in the dewar. In addition to the repairs, additional heat strapping was added to the XCAL to increase its thermal efficiency, and a radiation shield was added to block stray light to the DIRBE instrument detectors. The dewar was pumped back down to cryogenic conditions, and system-level testing, which resumed in August, demonstrated that the planned solution for the problems had been effective. Testing of three observatory-deployable systems (solar array, radiofrequency thermal shield, and omni antenna) was completed successfully, and so were the final stages of system-level calibration. After system-level testing was completed in September, the observatory was shipped to the launch site in October and launched in November.

Contact: Roger A. Mattson (Code 401)
(301) 286-7751

Sponsor: Office of Space Science and Applications, NASA Headquarters

Mr. Roger A. Mattson, COBE Project Manager, has worked at Goddard for 25 years. Mr. Mattson, who holds a BS in chemical engineering, was Project Manager for the first successfully launched, commercially developed upper stage and the first NASA employee to attend the National War College.

GAMMA RAY OBSERVATORY (GRO)

GRO has now completed its final assembly and environmental testing and is undergoing prelaunch preparations at the Kennedy Space Center (see figure). The focus of activities is shifting to preparation for orbital activities. The Flight Operations Team is establishing the Payload Operations Control Center which will initiate operations procedures and train staff. A complete dress rehearsal of the operational elements, from end-to-end, has been completed. In addition, the instrument teams are in the final stages of the preparation of their data reduction and analysis software to allow adequate training time and are adding staff to handle the continuous routine data processing activities.

GRO has the following scientific objectives:

- To study discrete objects such as black holes, neutron stars, and objects emitting only at gamma-ray energies.
- To search for sites of nucleosynthesis—the fundamental process in nature and other gamma-ray lines emitted in astrophysical processes.
- To explore the galaxy in gamma rays in order to study the origin and dynamic pressure effects of the cosmic-ray gas and the structural features revealed through the interaction of the cosmic rays with the interstellar medium.
- To study the nature of other galaxies as seen at gamma-ray wavelengths, with special emphasis on radio galaxies, Seyfert galaxies, and quasi stellar objects.
- To search for cosmological effects, through observations of the diffuse gamma radiation, and for possible primordial black hole emission.

The first major goal of GRO is to complete a full-sky survey during the first 15 months of operations (phase 1). This survey will provide the first comprehensive, simultaneous view of the entire sky, covering over six orders of magnitude (.1 to 3×10^4 MeV) of energy range with over an order of magnitude improvement in sensitivity. The remainder of the mission will be devoted to detailed studies, including deep surveys, studies of time fluctuations, correlated observations, and other observations of special interest. The decision to extend the GRO mission well beyond its originally planned 2-year lifetime provides the opportunity to conduct a vigorous guest investigator program. Not only does this program provide for broader scientific participation, but it will enhance the scientific return.

In phase 1, the guest investigator program will offer limited opportunities to work with the Oriented Scintillation Spectrometer Experiment (1 to 10 MeV) and the Burst and Transient Source Experiment. Phase 1 will also provide for correlated observatories and related theoretical studies. In phase 2 and beyond, major portions of the observing time will be available to guest observers. In addition, archival data will be available beginning 1 year after the receipt of usable data by the instrument teams.

A Science Support Center is being established to provide information and assistance to guest investigators interested in the use of GRO data. Located at Goddard, the Science Support Center will provide assistance to potential users from the proposal stage to completion of the investigation. It will provide electronically accessible directories of available data and the tools required to access them.

Contact: Donald A. Kniffen (Code 662)
(301) 286-6617

Sponsor: NASA Headquarters, Astrophysics Division

Dr. Donald A. Kniffen is an astrophysicist in the Gamma Ray Astrophysics Branch, the Project Scientist of the GRO Branch, and a Co-Investigator for Energetic Gamma Ray Experiment Telescope (EGRET). Dr. Kniffen, whose early interests were in galactic and solar cosmic rays, has become a pioneer in the field of gamma-ray astronomy. He has 29 years' experience with Goddard.

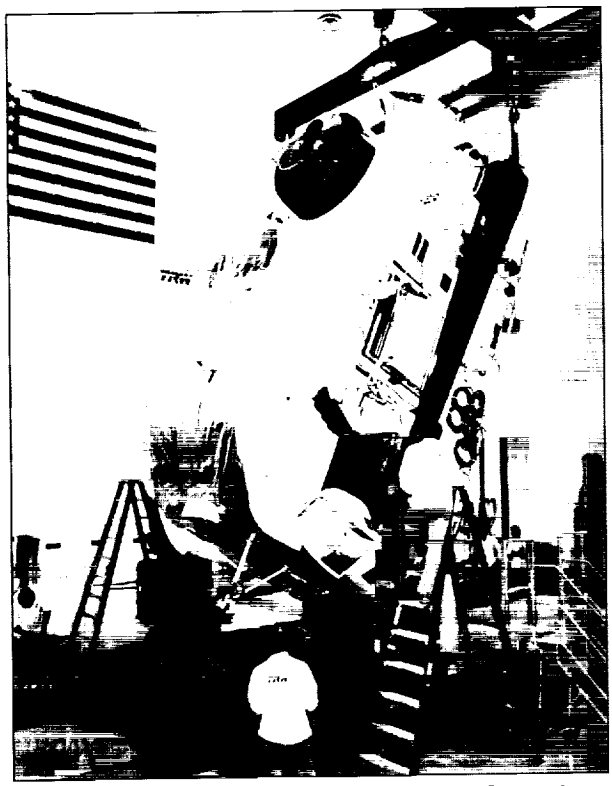

The 16,000-kg GRO begins its preparations for environmental testing.

EXTREME ULTRAVIOLET EXPLORER (EUVE) MISSION DESCRIPTION

EUVE is an Earth-orbiting, astronomical survey mission that will produce the first definitive sky map and catalog in the portion of the electromagnetic spectrum that extends from approximately 100 to 1,000 Å. It is the first NASA mission specifically designed for scientific payload retrieval while in orbit and for return to Earth upon conclusion of the mission.

Scientifically, the mission has three objectives: an all-sky survey, a deep survey, and spectroscopy observation of selected objects. The all-sky and deep surveys will be done concurrently during the first 6 months of the year-long mission. Spectroscopy will be added to the continuing survey studies in the second 6 months. At NASA's option, the mission can be extended at least 6 more months.

The major elements of the EUVE flight segment are the Explorer Platform and the Payload Module. The Explorer Platform is composed of a Multi-Mission Modular Spacecraft and a Platform Equipment Deck that supports various scientific payloads. (See the first figure.) The Multi-Mission Modular Spacecraft is a standard, reusable spacecraft

ORIGINAL PAGE
BLACK AND WHITE PHOTOGRAPH

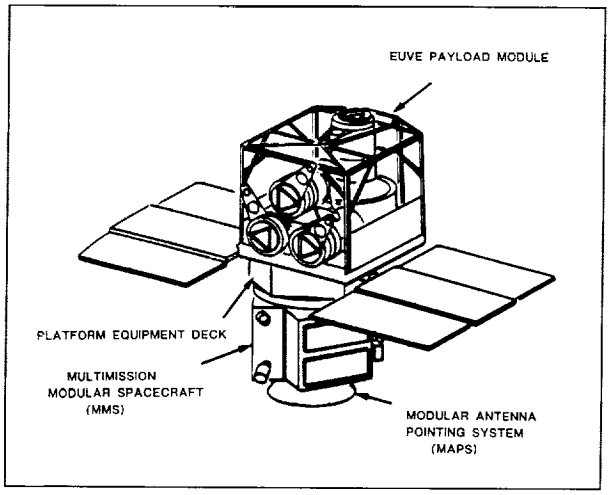

The Extreme Ultraviolet Explorer.

bus that supplies the Explorer Platform and its payload with all required services through the module support structure, a modular attitude control subsystem, a modular power subsystem, a communications and data handling subsystem, a modular antenna pointing system, and the signal conditioning and control unit. The newly designed Platform Equipment Deck provides mechanical and electrical interfaces between the Multi-Mission Modular Spacecraft and the Payload Module and accommodation for solar arrays, solar array drives, other mission-unique equipment, and secondary payloads. A payload attach plate, built with the Platform Equipment Deck, is used to ensure the mechanical and electrical interface between the Platform Equipment Deck and the Payload Module.

The EUVE Payload Module consists of the science payload, instrument support platform, support electronics, thermal radiators and control devices, the payload attach plate, and the support structure for restraining the solar arrays during launch. The Payload Module will be mated to the Explorer Platform, at the payload attach plate-Platform Equipment Deck interface, using motorized screws and floating connectors that will facilitate the Payload Module exchange with the X-ray Timing Explorer (XTE) at the conclusion of the EUVE mission.

The EUVE satellite will be launched aboard a Delta II ELV from Cape Canaveral, Florida. Its circular orbit will reach an altitude of ~550 km, with an inclination of 28.45°. The mission time line consists of launch, in-orbit checkout, all-sky survey, and spectroscopy phases before retrieval by the Space Transportation System (Shuttle) Study (STS). Mission characteristics for EUVE are given in the accompanying table.

After launch, a checkout phase that lasts for approximately 30 days is used to perform operational tests and to allow outgassing of volatile substances. The 6-month survey phase commences after analysts determine that the satellite is operating satisfactorily.

The primary mission objective of the EUVE is to gather enough data to map the entire sky in the extreme ultraviolet (EUV) spectrum. This will be accomplished

Extreme Ultraviolet Explorer (EUVE) Mission Characteristics

Item	Specification
Launch Date	1991
Mission Life	12-month mimimum (after 1 month in-orbit checkout)
Orbit	Circular 28.45° inclination, altitude 500-550 km
Launch Vehicle	Delta II ELV
Launch Site	Eastern Space & Missile Center
Observatory	
Classification	Scientific
Weight	Approximately 3,375 kg
Length/Diameter	4.59 × 2.79 m in diameter
Instruments	Three scanning telescopes, one deep-survey/ spectrometer telescope
Attitude Control	3-axis, inertially stabilized
Power	800 W, orbit average, minimum
Thermal	Passive, with heaters
Data Rates	32 kbps real time; 512 kbps, tape recorder playback
Ground System	
Forward Data Link	TDRSS Multiple Access
Return Data Link	TDRSS Multiple Access/S-Band Single Access real-time data and tape playback
Science Data Capture	Data Capture Facility
Science Data Processing	Science Data Room

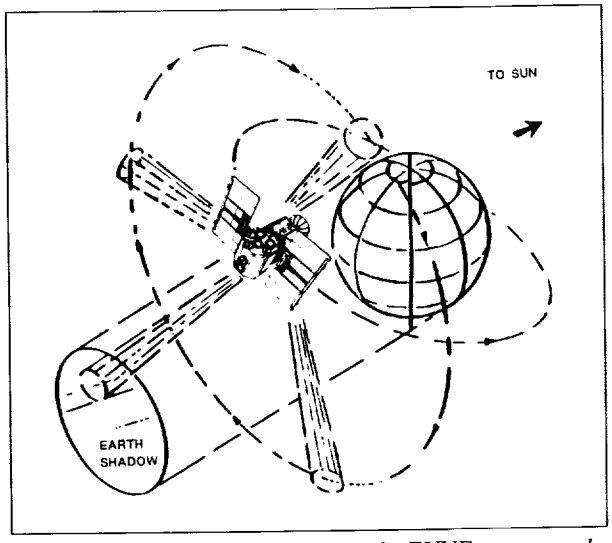

Scanning telescopes map the sky in the EUVE survey mode.

during the survey phase. The EUVE will be oriented so that the Payload Module points in the anti-Sun direction, with the Explorer Platform roll axis along the Earth-Sun line. The spacecraft will roll at approximately 3 revolutions per orbit and will be precessed by 1° per day using onboard magnetic torquer bars to keep the solar panels pointing directly at the Sun. The scanning telescopes each scan a great circle in the plane perpendicular to the Earth-Sun line as shown in the second figure. Orbital motion allows the telescopes to scan the entire sky in 6 months.

The deep survey part of the deep-survey/spectrometer telescope points into the shadow of the Earth during this survey phase and views a small area (2° by 180°) in the plane of the ecliptic. It is capable of operating with greater sensitivity than the scanning telescopes and therefore can look deeper into space.

The final, or guest observer, phase of the mission is devoted to spectroscopy. During this phase, the EUVE will be operated in an inertially stabilized mode while pointed at objects identified during the survey phase. Spectral data will be collected from sources located up to 30° to 45° from the Earth-Sun line.

Operations during this phase will permit the spectrometers to image at least 30 selected sources for periods of up to a week at a time. Concurrent operation of the scanning telescopes will allow additional survey data to be collected along with the spectroscopy data.

A 16-kbps data rate is shared by the science payload and Explorer Platform engineering data and is recorded at 32 kbps on a 10^9-bit capacity tape recorder. Subsequent transmission to the ground is via the TDRSS at 512 kbps.

At the conclusion of the last mission phase, the EUVE instruments will be turned off and the satellite retrieved by the STS. Using the Remote Manipulator System (RMS), the satellite will be placed on the Flight Support System, and the Payload Module will be removed and temporarily stowed. The Payload Module will be installed on the Explorer Platform, checked out, and released. The EUVE Payload Module attached to a payload carrier mounted on the Flight Support System will be returned to Earth.

The EUVE science payload, weighing approximately 1,650 lb, consists of four telescope assemblies and eight associated electronics boxes. Three of the telescopes are

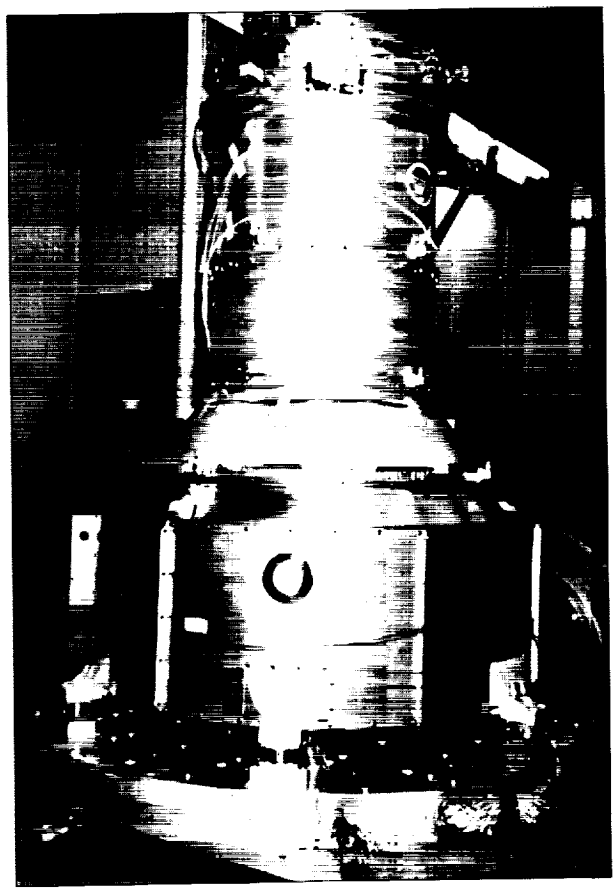

The EUVE scanning telescope.

ORIGINAL PAGE
BLACK AND WHITE PHOTOGRAPH

ORIGINAL PAGE
BLACK AND WHITE PHOTOGRAPH

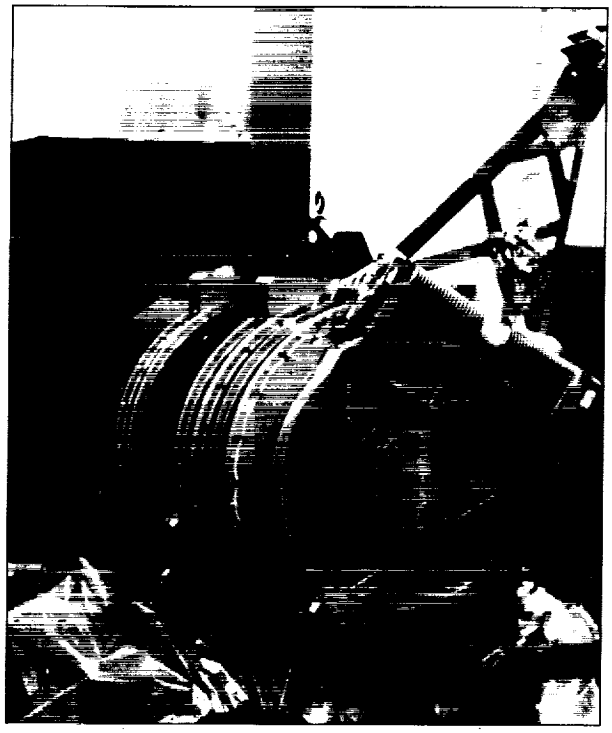

The deep-survey/spectrometer telescope

used to make the all-sky survey, and the fourth is the deep-survey/spectrometer.

The scanning telescopes are approximately 22 in. in diameter by 35 in. in length and weigh about 260 lb each. (See the third figure.) The grazing incidence mirrors and filter complements are identical in two of the telescopes, which will take data in the range of 100 to 500 Å. The third telescope uses a different type of mirror and associated filters and takes data in approximately the 500- to 1,000-Å range.

The deep-survey/spectrometer telescope is 64 in. in length and 44 in. in diameter at the base and weighs about 700 lb. (See the fourth figure.) It consists of a grazing incidence mirror and four separate channels, each having its own filter and detector system. The deep survey channel has its detector located along the boresight; photons of extreme ultraviolet light are permitted to impinge upon it after being reflected by the mirror. The spectroscopy channels, each having a separate diffraction grating, observe the light in different frequency bands.

Spacecraft telemetry data will be processed in the Payload Operations Control Center at Goddard and displayed for analysis by the Flight Operations Team. Stored and real-time commands will be formatted and generated by the Control Center and the Command Management System, respectively. All commands will be transmitted from the Control Center to the Explorer Platform by way of the NASA Communications Division and TDRSS. The Explorer Platform real-time and playback telemetry data will be decommutated in the control center and displayed for Explorer Platform health and safety monitoring.

The Payload Operations Control Center will support all the EUVE operational and control requirements. These requirements include processing real-time and playback telemetry to verify EUVE health and safety; displaying spacecraft and instrument housekeeping data; performing mission and trend analyses; performing mission planning, including TDRSS scheduling, and coordinating TDRSS-NASA ground terminal configuration by way of the network Control Center; and formatting and issuing all commands to the Explorer Platform.

The EUVE Science Operations Center, located at the University of California at Berkeley, will accomplish science planning and iteration of the time line with the Command Management System; evaluate real-time/quick-look data and payload health and safety; generate onboard microprocessor command loads and maintain onboard microprocessor software; build and maintain the science data bases; and analyze data. The Science Operations Center will be connected to the Payload Operations Control Center's Command Management System via the NASA Communications Division switching center and the Command Management System gateway. The Science Operations Center will receive the data stream through the data capture facility via the switching center.

Contact: Donald L. Margolies (Code 410)
(301) 286-8984

Sponsor: Office of Space Science and Applications

Mr. Donald L. Margolies is Deputy Project Manager of the Explorers and Attached Payloads Project and Project Manager for the EUVE mission. During his 26 years at Goddard, Mr. Margolies has been honored with the NASA Exceptional Service Medal and a Goddard Outstanding Performance Award. He holds a BSEE from Rensselaer Polytechnic Institute and an MSE and an MEA from George Washington University.

THE X-RAY TIMING EXPLORER (XTE) MISSION SUMMARY

The XTE will be the first science payload to be exchanged on orbit using the Explorer Platform concept. The XTE will study timing of compact objects, galactic and extragalactic, using a variety of x-ray sources: white dwarfs, accreting neuron stars, black holes, and active galactic nuclei. Measurements will be made over a wide range of photon energies from 2 to 200 keV.

The instrument payload module will be carried into space in late 1994. It will be mounted to the Explorer Platform Flight Support System located in the shuttle orbiter bay for its rendezvous with the EUVE satellite. After "capture," the EUVE satellite will be brought into the orbiter bay and attached to the Flight Support System's tilt table where the XTE science payload module will be exchanged with the EUVE payload module. The first figure illustrates this exchange. After any required maintenance to the Explorer Platform and a brief check-out in the orbiter bay, the XTE satellite will be placed in orbit using the shuttle remote manipulator arm, and the EUVE payload module will be stowed on the Flight Support System for its return to Earth.

Three instruments make up the XTE science payload: the Proportional Counter Array; the All-Sky Monitor; and the High Energy X-Ray Timing Experiment. An experimental data system provides onboard data processing for both the All-Sky Monitor and the Proportional Counter Array. An artist's concept of the satellite is shown in the second figure.

The Proportional Counter Array consists of five identical sealed propane and xenon methane proportional counters having a total effective area of about 6,250 cm^2 with a 1° field-of-view covering an energy range of 2 to 30 keV. Each detector element, which weighs about 230 lb and measures 13 × 32 × 47 in., also houses the analog processing electronics and high and low voltage supplies.

The All-Sky Monitor is a scanning shadow camera assembly with three one-dimensional detectors mounted on a boom to clear its 60° × 90° field-of-view and a resolution of 0.2°. The camera assembly will make a complete revolution during each orbit, surveying approximately 75 percent of the sky to monitor source activity and look for changes. The detector is a xenon-filled proportional counter with a sensitivity of 2 to 10 keV. The imaged data is deconvolved on the ground with Fast Fourier transform techniques to give source intensity and position. The All-Sky Monitor weighs 70 lb and measures 35 × 18 × 32 in. exclusive of the mounting boom.

The data processing system for both the Proportional Counter Array and the All-Sky Monitor is provided by the Experiment Data System. To achieve a required data compression of as high as 50:1, the system uses six identical microprocessor-driven event analyzers, which convert the event pulse height, time, and detector number to an energy, time, and bin address. The compressed data are transmitted on a common microprocessor data bus and transferred to the Explorer Platform communication and data handling system for onboard storage and transmission to the ground. The experiment data system weighs 45 lb and measures 20 × 10 × 12 in.

The High Energy X-Ray Experiment consists of two clusters of sodium-iodide/cesium-iodide (NaI/CsI) scintillation detectors with a total effective area of about 1,600 cm^2 and a spectral range of 15 to 200 keV. Each cluster is independently gimbaled so as to "chop" between source and background, thereby facilitating background calibration. The detector field-of-view is 1° and is coaligned with the Proportional Counter Array detectors so that

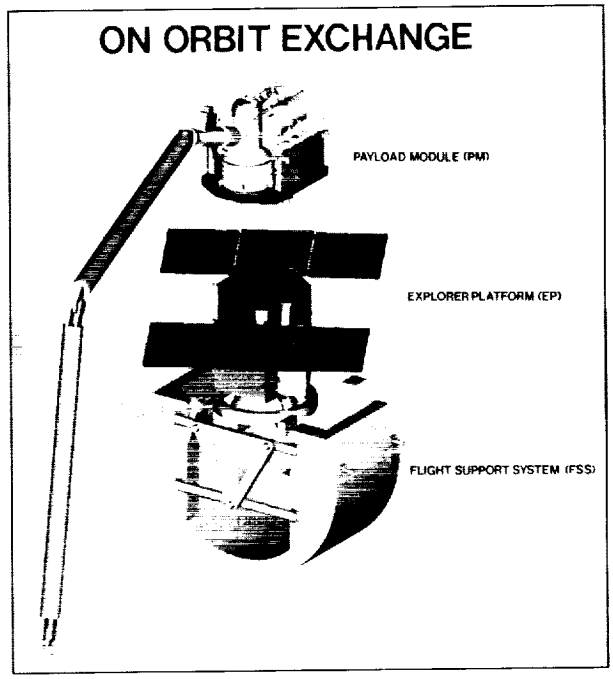

The EUVE payload module being removed from the Explorer Platform in the orbiter bay.

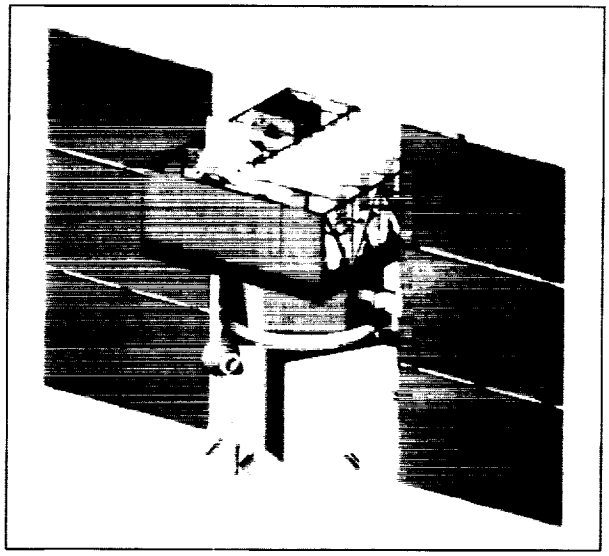

The XTE satellite after assembly and launch from the STS.

concurrent measurements from 2 to 200 keV can be made. Each high energy detector assembly weighs 325 lb and measures 24 × 24 × 27 in. It has its own data system for onboard analysis and data compression.

The studies using the XTE instrumentation will be done by scientists from all around the world. The Proportional Counter Array and High Energy X-Ray observing time will be a 100-percent guest-investigator program. Potential observers, including principal investigators, will compete for observing time in this process. Observing proposals will be selected by a peer group based on scientific merit and instrumentation capability.

Satellite telemetry data will be processed in the Explorer Platform Project Operations Control Center and displayed to the Flight Operations Team for health and safety monitoring. Stored and real-time commands will be formatted and generated by the control center's Command Management System. All commands will then be transmitted from the control center to the XTE satellite via NASA Communications Division's TDRSS network.

The control center will support all the XTE operational and control requirements. These requirements include the processing of real-time and playback telemetry to verify the XTE health and safety; display of satellite housekeeping data; performance of mission and trend analyses; performance of mission planning, including TDRSS scheduling and coordinating the TDRSS-NASA ground terminal configuration via the Network Control Center; and formatting and issuing of all commands to the XTE satellite.

The XTE Science Operations Center, located at Goddard with planning support and data analysis at the University of California at San Diego and the Massachusetts Institute of Technology, will perform the following functions:

- Science planning and iteration of the time line with the Command Management System.
- Evaluation of the real-time/quick-look data and payload health and safety.
- Generation of onboard microprocessor command loads and maintenance of onboard microprocessor software.
- Building and maintaining the science data bases.
- Data analysis.
- Management of the guest investigator program.

The Science Operation Center will be connected to the Command Management System via the NASA Communications Division switching center at Goddard. It will also be connected to the data capture facility.*

**Dr. Hale Bradt is Principal Investigator for both the All-Sky Monitor and the Experiment Data System, which are being built at the Massachusetts Institute of Technology.*

Contact: Dale F. Schulz (Code 410)
(301) 286-8417

Sponsor: NASA Headquarters, Astrophysics Divison

Mr. Dale F. Schulz, Associate Project Manager for the XTE, is responsible for the mission's development. He has received Quality Increase Awards, Group Achievement Awards, and a Service Award. Mr. Schulz earned his MS in electrical engineering and has 25 years' experience at Goddard.

THE LYMAN FAR ULTRAVIOLET SPECTROSCOPE EXPLORER (FUSE)

The Lyman FUSE Mission is a candidate for Explorer Next, a follow-on to the EUVE and XTE series.

The prime scientific goal of this mission is high-resolution spectroscopy from 1,200 Å to 912 Å and moderate-resolution spectroscopy to 100 Å. These requirements are

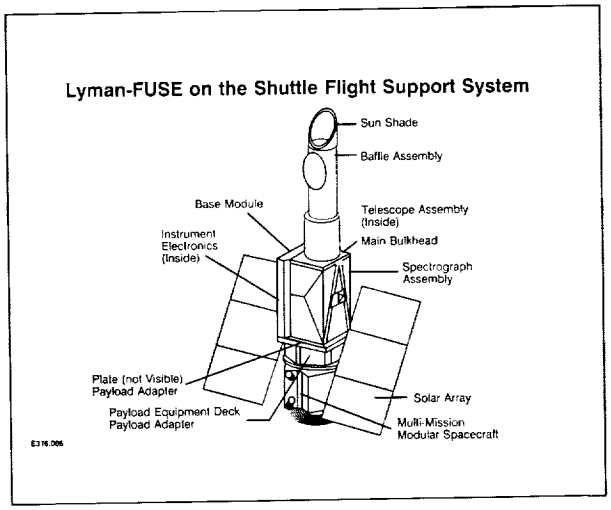

The instrument model for the Lyman FUSE.

met with a 70-cm-diameter glancing incidence telescope feeding a single spectrograph. Using gratings mounted on the Rowland circle and two-dimensional detectors to analyze the far ultraviolet achieves the necessary resolving power with excellent sensitivity. The extreme ultraviolet band is covered at lower resolution using a grating and detector based on EUVE technology. The instrument module is carried to orbital altitude by the STS, where it will replace the XTE instrument module on the Explorer Platform. The FUSE mission life, at the orbital altitude of 450 km, is 3 years. With minimal implementation changes, the mission can also use an ELV.

The instrument module for Lyman FUSE (shown in the figure) is relatively simple because the mission has only one instrument. The instrument consists of three assemblies: the baffle, the telescope, and the spectrograph. The baffle assembly consists of the fixed baffles inside the telescope, the baffle support cylinder which fits over the telescope, the baffle and the sunshade which are folded alongside the instrument at launch, the dust covers that cover the optics before the baffle is erected, and the associated drive and latch mechanisms. The telescope assembly consists of the primary mirror and the secondary mirror spaced by a Zerodur spider to form a single unit, the telescope support ring attached to the telescope mirror, and the metering truss structure which connects the support ring to the main bulkhead. The spectrograph assembly consists of the spectrograph structure (main bulkhead, truss structure, optics plate, and grating box) which serves as a bench for the optical systems mounted on it (spectrograph optics, detectors, fine error sensor, and slit wheel).

The base module is the base structure supporting the instrument, consisting of two plates and two aluminum bars forming an inverted V between the lower plate and the main bulkhead. Also included in the base module and mounted on the base structure are a grapple, mission-unique magnetic torquer bars, and two payload adapter plates for mounting to the Flight Support System in the STS and on the platform of the Explorer in orbit. Completing the base module assembly are the instrument electronics, memory, and remote interface units.

Present plans for Lyman FUSE are for a cooperative mission with Canada and the United Kingdom, each contributing significant hardware. Communications with Lyman FUSE will be through the TDRSS. Flight operations will use existing Goddard institutional support facilities. The Science Operations Center at Goddard will interface through existing telecommunications networks with the Principal Investigator, Co-Investigators, and Guest Observers.

Contract: John J. O'Brien (Code 402)
(301) 344-4875

Samuel E. Bergeson-Willis (Code 705)
(301) 286-5344

Sponsor: Explorers Office, NASA Headquarters

Mr. John J. O'Brien, Study Manager in the Advanced Missions Analysis Office, has served as technical officer for the Lyman FUSE Phase A study. During his 23 years at Goddard, Mr. O'Brien has received several NASA achievement awards. He holds a BS in physics.

Mr. Samuel E. Bergeson-Willis is currently the Study Manager for the Lyman FUSE project. During his 22 years at Goddard, he has contributed to the evolution of the space station, acted as Study Manager in the Advanced Missions Analysis Office, and directed thermal design efforts for NASA's Atmosphere Explorer and Multi-Mission Modular Spacecraft projects. He has earned 18 NASA and Goddard awards and has received a BS in applied mathematics from Johns Hopkins University.

EARTH OBSERVING SYSTEM (Eos)

Eos is to be the centerpiece of NASA's Mission to Planet Earth. NASA plans to launch a total of six major Earth-looking observatories starting in 1997, and these observatories are to be accompanied by still other

observatories provided by the European Space Agency and the Japanese National Space Development Agency. Once the program is fully under way, there will be two NASA observatories and one each from Europe and Japan in orbit at the same time. The goal is to provide a minimum of 10 years of simultaneous, continuous Earth observations.

The NASA observatories will be placed in Sun-synchronous polar orbits at 705 km and will have 1:30 p.m. Equator-crossing times. The second observatory is to be launched within 24 to 30 months of the first launch. The platforms are planned to be functionally identical.

As the instruments and the platforms to carry them are being developed, a major Eos Data and Information System (EosDIS) will be developed to provide access to the data from the instruments and to the scientific results of research using these data. EosDIS will serve both flight operations and science data requirements. EosDIS will provide for planning, scheduling, and command and control of both the overall mission and the individual Eos instruments; and it will provide for production of standard and specialized data products, computational facilities for support of research, data archiving and distribution, and communications.

EosDIS will be the most complex and advanced information system ever developed to meet scientific research needs. It will deal with an enormous data volume of 50,000 terabytes and have an extremely high data processing rate (up to 50 Mbps of raw telemetry input and 500 Mbps output of a great variety of high-level geophysical products), which will require considerable processing to achieve.

The overall goal of Eos is to advance scientific understanding of the entire Earth system on a global scale through developing a deeper understanding of the components of that system, the interactions among the components, and the changes taking place in this system. Three mission objectives have been defined for Eos:

- To create an integrated scientific observing system that will enable multidisciplinary study of the Earth's critical, life-enabling, interrelated processes involving the atmosphere, the oceans, the land surface, and the solid Earth.
- To develop a comprehensive data and information system including a data retrieval and processing system to serve the needs of scientists performing an integrated multidisciplinary study of planet Earth.
- To acquire and assemble a global data base emphasizing remote-sensing measurements over a decade or more to enable definitive and conclusive studies of aspects of Earth system science.

In pursuit of the third objective (developing a global data base), Eos is to make measurements related to the global distribution of energy input to and energy output from the Earth; atmospheric structure, composition, and dynamics from the ground to the mesopause; the physical and biological structure, composition, and dynamics of the land surface; key characteristics of the Earth's biogeochemical cycles; physical and biological characteristics of the oceans; characteristics and distribution of land and sea ice; the distribution of worldwide precipitation; and the dynamic motions of the Earth as a whole, including tectonic plate motions.

There have been three approaches to providing the instruments needed to carry out the Eos objectives. Six major instruments have been designated as U.S. research facility instruments and are being developed by the NASA centers. Twenty-four other instruments have been selected through the Announcement of Opportunity process to be developed under the leadership of Principal Investigators from universities, industry, and government. In addition, there are four mission-unique instruments: Advanced Microwave Sounding Unit (AMSU), supporting atmospheric corrections; Space Environment Monitor (SEM); and Wide-Band Data Collecting System and COMM (the direct broadcasting system used to preselect data in real-time transmission to the ground) supporting communications requirements. The accompanying table lists the Eos research facility and Principal Investigator instruments and indicates their contribution to Eos science.

A major new step toward ensuring in-depth analyses of the data that will flow from the many instruments has been the selection, also through the Announcement of Opportunity process, of 28 interdisciplinary investigators. The interdisciplinary investigators will be performing modeling studies in various areas that may be grouped into hydrological cycle studies, climatological process studies, biogeochemical cycles studies, and geophysical process studies. (Geophysical process studies include atmospheric, oceanic, and solid Earth studies.)

The NASA observatories, including both platforms and instruments, and the EosDIS are being managed by

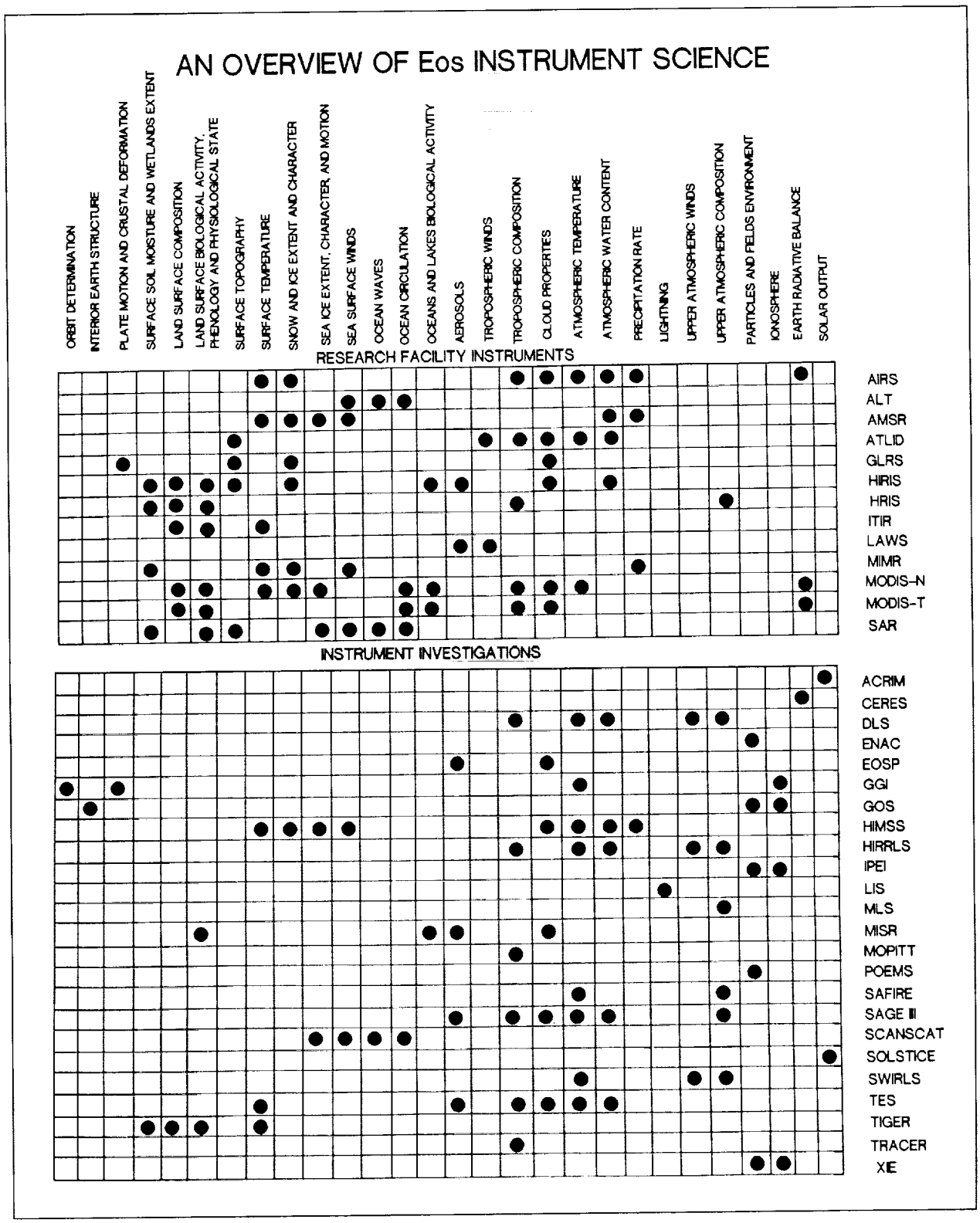
AN OVERVIEW OF Eos INSTRUMENT SCIENCE
ORBIT DETERMINATION
INTERIOR EARTH STRUCTURE
PLATE MOTION AND CRUSTAL DEFORMATION
SURFACE SOIL MOISTURE AND WETLANDS EXTENT
LAND SURFACE COMPOSITION
LAND SURFACE BIOLOGICAL ACTIVITY, PHENOLOGY AND PHYSIOLOGICAL STATE
SURFACE TOPOGRAPHY
SURFACE TEMPERATURE
SNOW AND ICE EXTENT AND CHARACTER
SEA ICE EXTENT, CHARACTER, AND MOTION
SEA SURFACE WINDS
OCEAN WAVES
OCEAN CIRCULATION
OCEANS AND LAKES BIOLOGICAL ACTIVITY
AEROSOLS
TROPOSPHERIC WINDS
TROPOSPHERIC COMPOSITION
CLOUD PROPERTIES
ATMOSPHERIC TEMPERATURE
ATMOSPHERIC WATER CONTENT
PRECIPITATION RATE
LIGHTNING
UPPER ATMOSPHERIC WINDS
UPPER ATMOSPHERIC COMPOSITION
PARTICLES AND FIELDS ENVIRONMENT
IONOSPHERE
EARTH RADIATIVE BALANCE
SOLAR OUTPUT
RESEARCH FACILITY INSTRUMENTS
AIRS
ALT
AMSR
ATLID
GLRS
HIRIS
HRIS
ITIR
LAWS
MIMR
MODIS-N
MODIS-T
SAR
INSTRUMENT INVESTIGATIONS
ACRIM
CERES
DLS
ENAC
EOSP
GGI
GOS
HIMSS
HIRRLS
IPEI
LIS
MLS
MISR
MOPITT
POEMS
SAFIRE
SAGE III
SCANSCAT
SOLSTICE
SWIRLS
TES
TIGER
TRACER
XIE

Goddard. An artist's rendering of the first (Eos A) platform is shown in the accompanying figure.

There are six designated U.S. research facility instruments. (1) The moderate-resolution imaging spectrometer consists of two embodiments: Moderate-Resolution Imaging Spectrometer (MODIS)-Tilt measures biological and physical processes when off nadir pointing is desired, and the MODIS-Nadir with greater spatial resolution is used when off nadir pointing is not required. (2) The High Resolution Imaging Spectrometer (HIRIS) serves as a very high-resolution companion to MODIS. (3) The Geoscience Laser Ranging System (GLRS) studies the Earth's crustal movements using arrays of retroreflective targets and performs high-resolution, precision profiling of ice sheets and of land and cloud-top surfaces. (4) The Laser Atmospheric Wind Sounder (LAWS) uses Doppler lidar to perform direct tropospheric wind measurements. (5) The Atmospheric Infrared Sounder (AIRS) measures atmospheric temperature and moisture. (6) The radar altimeter measures sea-surface elevation.

Eos will advance virtually every aspect of the study of Earth from space, including all of the traditional disciplines which make up Earth science. Eos will extend and build upon the Upper Atmospheric Research Satellite (UARS) and Ocean Topography Experiment programs by providing long-term continuity in measuring stratospheric composition and ocean circulation. It will improve meteorological observations to help extend the range of long-term weather forecasts. It will enhance measurements for biological oceanography and increase our ability to measure biogeochemical and hydrological processes on the land surface, particularly at large scales, and to determine motions at the edges of tectonic plates.

Eos is a cooperative international effort. NASA's contribution will be complemented by contributions from the European Space Agency and the Japanese National Space Development Agency. The Europeans and the Japanese will provide additional polar orbiting observatories and scientific instruments. Some U.S. instruments will fly on the platforms of the international partners, and some of their instruments will fly on the U.S. platforms. Eos scientific data will be made available to researchers from all the partners.

Contact: Charles M. MacKenzie (Code 415)
(301) 286-3249
Sponsor: Eos Project

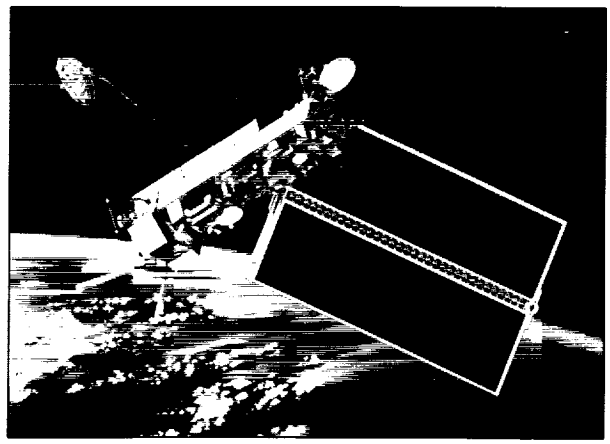

An artist's rendering of the first Eos platform.

Mr. Charles M. MacKenzie works on the Eos Project as Manager of Feasibility and Definition Studies for the initial global change science investigation program. He has won the Goddard Award of Merit and team awards for the European Space Research Organization-I and II, Azur, Helios, and Nimbus satellites. Mr. MacKenzie has 27 years' experience at Goddard and holds a BS in electrical engineering.

THE NUCLEAR ASTROPHYSICS EXPLORER (NAE) MISSION

NAE is a proposed Explorer mission that would be 100 times more sensitive to narrow gamma-ray lines than instruments flown to date. It would also be 10 times more sensitive to narrow gamma-ray lines than the Oriented Scintillation Spectrometer Experiment to be flown on GRO. This remarkable improvement is possible due to several advances in technology.

One of these advances is the availability of large-volume (290-cm^3) germanium solid-state detectors. NAE is intended to fly nine of these detectors. When a gamma ray stops in germanium, it creates electrons in proportion to the energy of the gamma ray. By measuring the size of the electron pulse, NAE can determine gamma-ray energy with high accuracy. The large volume ensures that a statistically significant number of gamma rays will be collected from weak sources in a reasonable amount of observing time.

A disadvantage limiting current use of germanium detectors is that they must be cooled to approximately 80

°K in order to keep noise to a low level. Fortunately, long-life mechanical coolers suitable for space use at these temperatures are also becoming available. A refrigerator of this type will fly for the first time on an instrument on the UARS.

Another technology improvement has been the development of shielding crystals made from bismuth germanium (BGO). These BGO crystals surround the germanium detectors except for the entrance aperture. They prevent background gamma rays from the Earth's atmosphere, the spacecraft, and the rest of the instrument from being counted. These crystals provide more shielding for their weight and volume than other materials and are free of many of the problems of the shield materials used in the past. Even with the very good shielding-to-weight ratio provided by BGO, only about half the mass of the NAE instrument will be devoted to the shield. Older shield materials would have weighed significantly more.

Another innovation will allow NAE to produce a low-resolution map of gamma-ray sky. Since gamma rays cannot be focused, images are very difficult to produce. One way is to use the entrance aperture in the BGO shield to restrict the view of the sky by the detector. If that were the only way to make a map, the NAE would be able to make an image with only 10°-sized pixels. The new technique alternately places a shadow mask and a shadow antimask in front of the nine-detector array. The mask/antimask produces two unique shadow patterns on the nine detectors for each gamma-ray source in view. This pattern can then be deconvolved in a computer to form an image of nine pixels, each 4° square. Moving the instrument so that it points in other directions adds additional pixels to the map. Strong sources can be located to better than 1°.

These gamma-ray advances will allow the investigation of scientific questions that could not be explored before. One of these is the understanding of nucleosynthesis and supernova dynamics. NAE sensitivity will offer a view of these processes in the Virgo cluster of galaxies, providing the opportunity to study a few supernova per year. A lower sensitivity instrument would not be able to see these supernova and would have to depend on supernovas' occurring in our own galaxy or other nearby galaxies. During the few years an instrument is in orbit, this is a most unlikely event.

NAE will also be able to locate, date, and determine the size of supernova events that have occurred in our galaxy during the past million years. These events have long since disappeared in the usual sense but will be visible to NAE. Each supernova generates an expanding spherical shell of matter. Some of that matter reduces gamma rays while undergoing radioactive decay. The three most important gamma-ray producing elements are ^{44}Titanium, ^{26}Aluminum, and ^{60}Iron. The NAE will locate these shells and, by using the "look-back effect," determine the approximate date of the explosion.

NAE will make extensive use of high-purity beryllium for instrument structure inside the BGO shield. Beryllium is the one structural metal that has little astronomical interest whereas the more conventional metals—aluminum, titanium, and iron—are of the highest interest. If these common metals were used, they would be activated by cosmic rays and Van Allen Belt radiation, and the resulting gamma-ray decays could not be distinguished from gamma rays of scientific interest. One recent finding was that beryllium can be obtained with adequate purity for the NAE instrument.

NAE is proposed as a payload aboard the Explorer Platform that will already be in orbit performing another mission. In this scenario, NAE will be launched on the shuttle, and after rendezvous with the Explorer Platform, astronauts will exchange the NAE with the instruments previously aboard. The old instruments will be returned to Earth by the shuttle. Alternatively, NAE may be launched on its own spacecraft by an ELV.

Contact: Ronald M. Muller (Code 402)
(301) 344-4878

Sponsor: Explorers Office, NASA Headquarters

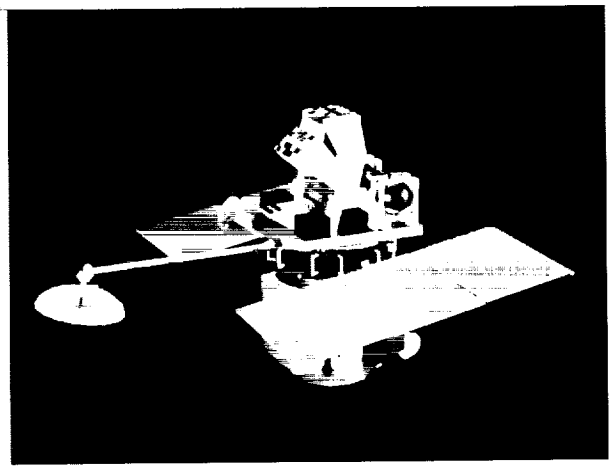

The NAE.

Mr. Ronald M. Muller, who has 30 years' experience at Goddard, was Technical Officer for the NAE Mission Phase A study. Among his accomplishments, Mr. Muller has received two Special Achievement Awards and three Certificates of Outstanding Performance. He earned his MS in electrical engineering at Thayer School of Engineering at Dartmouth College.

ORBITING SOLAR LABORATORY (OSL)

NASA's OSL is a free-flying spacecraft, which will carry several state-of-the-art instruments to observe the Sun across a wide spectral range. The first figure shows the Phase-A conceptual design. OSL will provide the highest-ever resolution images in the visible, ultraviolet, and extreme ultraviolet ranges and will also detect x-rays. A 1-m primary mirror will service a tunable filtergraph, a photometric filtergraph, and an Echelle spectrograph. It will provide them with solar images that have at least 0.15-arcsec resolution in the 220- to 600-nm wavelengths and that are diffraction limited from 600 to 1,000 nm. In addition, independent ultraviolet and extreme ultraviolet telescopes will be coaligned with some offset pointing capability for coordinated science and optimal limb coverage. Recent advances in charge-coupled devices have produced cameras with electronic film, which now has the necessary resolution in selected spectral bands. Unlike regular film, this film is reusable and does not require replacement on orbit. OSL will fly 20 charge-coupled-device cameras, generating 20 Mbps of real-time science data.

NASA's TDRSS is required for all OSL communications. OSL will schedule the high gain K-band single-access TDRSS service for real-time science telemetry or for playback of the onboard recorders at the 20-Mbps rate. Because of its orbit, OSL has visibility of at least one TDRSS satellite 97 percent of the time. This visibility time will permit almost continuous monitoring of OSL via the low-rate S-band multiple-access link, which does not require TDRSS to point its high-gain antennas at OSL. OSL will use this link routinely to send a full Sun image, which can be used for science planning and targeting, to the Science Operations Facility. Also, the OSL Project Operations Control Center at Goddard will maintain 24-hour command and housekeeping coverage via this link.

Because of its Sun-synchronous polar orbit, OSL will see the Sun without interruption for about 9 months each year. Hence, unprecedentedly long observation windows are baselined routinely. The mission features telescience, whereby scientists can control the observatory pointing and their instrument's operating modes from their work stations. OSL forecasts several operating modes depending on the science campaign and the communications link available. For example, whenever TDRSS can point its K-band single-access antenna at OSL for extended periods, coordinated science at 20 Mbps will be conducted in real time. Otherwise, OSL has a store-and-forward patrol mode, where 2 Mbps is recorded for up to 50 min and then played back during the next TDRSS contact. These operational capabilities, coupled with the highest resolution across a wide spectral range, will enable OSL to accomplish solar physics science never before possible.

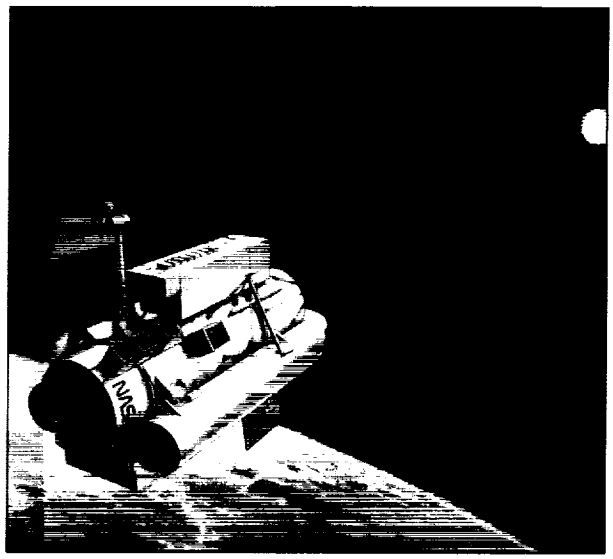

The OSL Phase-A conceptual design.

OSL is planning for a state-of-the-art, facility-class Science Data Operations Center to accommodate the plethora of data to be collected during its 3-year lifetime. This center, to be located at Goddard, will support both principal investigators and guest investigators, with real-time and offline data processing and analysis services. The Science Operations Facility will control the real-time science planning and operations. It will also receive observation request inputs from remote facilities and can return television-resolution image data, all via a high-speed network. With these near-real-time links, scientists can participate in the OSL flight operations from remote terminals. The Science Data Operations Center is set up to

give all investigators, including guests, all the facilities they need to conduct real-time science observation planning and offline data processing and analysis.

The second figure depicts the conceptual design for the center. Because all investigators will have access to level 0 data from all the flight instruments, the interactive, coordinated, multi-instrument operations that are essential to the OSL mission will be facilitated. In addition, the center includes a Data Analysis Facility with sufficient data analysis resources for guest investigators to completely analyze their OSL data sets on site. The guest investigators will automatically be provided with browse data, which are analog representations of their nonreal-time data, extensively annotated and processed to video resolution. These data will be in sequence with the information needed for scaling and aspect. The Science Data Operations Center will also provide magnetograms, Dopplergrams, and geometrically corrected spectra in the same format. Scientists will be able to overlay graphical display sequences from different instruments, such as the slit position of a spectrograph over the image from a filtergraph. With browse data and the Data Analysis Facility work stations, they can sift through their data and perform considerable analysis. Data processing costs are controlled because scientists can efficiently identify that small fraction of their total data that warrants further analysis at the full, original, digital resolution.

Proposals for a Phase B OSL study are currently being reviewed. A new start is expected in fiscal year 1992 and a launch in fiscal year 1997. OSL is designed to last at least 3 years, but is expected to last through the next Solar Maximum with tolerable degradation.

Contact: Michael A. Comberiate (Code 460)
(301) 344-4860
Sponsor: OSL Project

Figure 2. OSL Science Data Operations Center (SDOC)

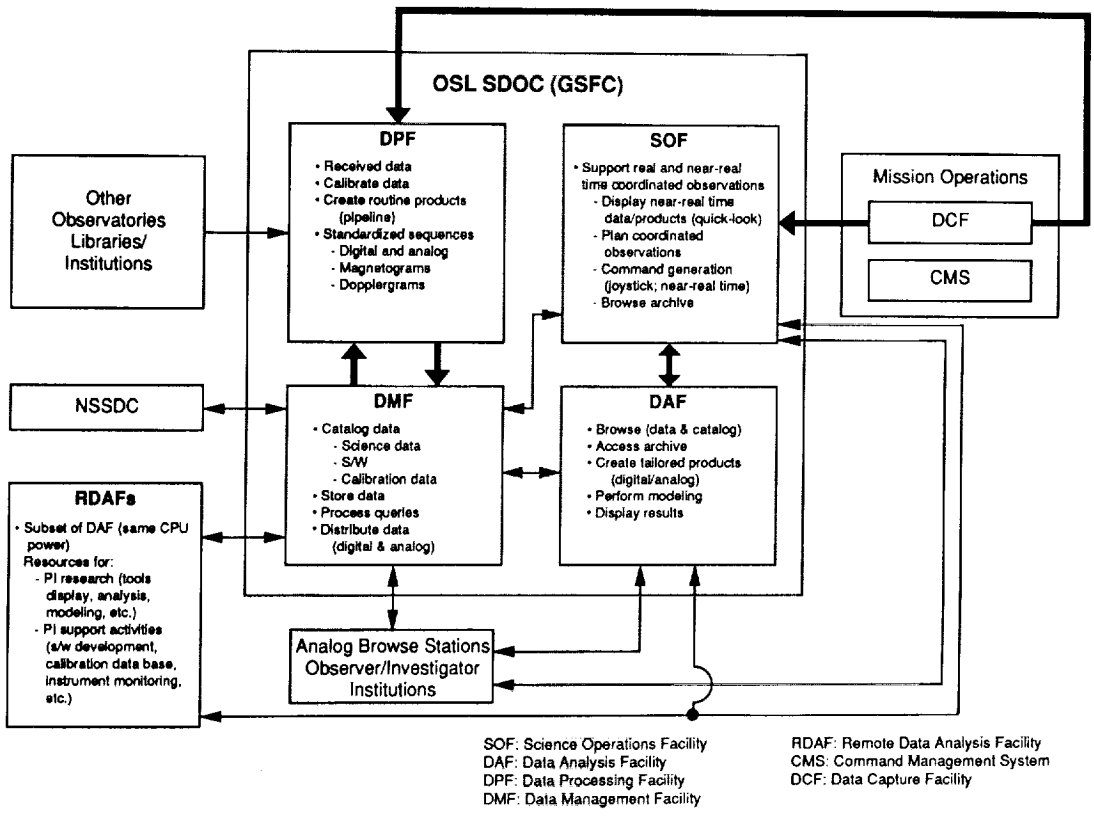

The OSL Science Data Operations Center design.

Mr. Michael A. Comberiate is OSL Observatory Manager and has been with NASA for 21 years. He holds an MS in electrical engineering and has designed flight and ground support electronics for several NASA missions. He also served as Electrical System Manager for COBE, Acting System Manager for Origin of Plasmas in Earth's Neighborhood/International Solar-Terrestrial Physics (ISTP), and the OSL Phase A Study Manager for the Advanced Missions Analysis Office.

ASTROMAG

The Astromag is a payload attached to Space Station Freedom, consisting of two instruments and a set of cryogenically cooled, superconducting electromagnetic coils capable of producing a long-duration, high-intensity magnetic field. The magnet-cryostat assembly together with other supporting subsystems (power, data, command, thermal heat rejection, structures, and mechanisms) form the Astromag Core Facility to which investigators may periodically attach a variety of instruments developed to support the general investigation of particle astrophysics.

Astromag's primary scientific goal is the study of cosmic rays, which consist of suprathermal gas from energetic charged particles still of unknown origin, which pervade the galaxy and perhaps the space beyond. Cosmic rays provide a unique sample of matter from far outside our solar system and an important means of studying the dynamics and evolution of the galaxy. Study of the origin, acceleration, and propagation of cosmic rays is certain to yield important new understandings of the ubiquitous phenomenon of relativistic plasmas in space.

The Astromag facility will permit flying a series of complementary long-duration, large cosmic-ray experiments, each tuned to explore different aspects of high-energy particle astrophysics. These experiments will be capable of measuring the composition and spectra of energetic charged particles with unprecedented accuracy and will address a wide range of fundamental questions.

During the past two decades the development of lightweight superconducting magnet technology together with the development of spaceflight-proven liquid helium cryogenic technology has made the development of Astromag technically feasible.

During the past year, an Astromag Technical Advisory Team appointed by NASA headquarters reviewed the Phase A study and concluded that an Astromag facility is feasible within state-of-the-art technology. NASA headquarters also released an Announcement of Opportunity for Space Station Freedom Attached Payloads and subsequently selected three Astromag-related experiments for further development:

- Large Isotope Spectrometer for Astromag (LISA), Principal Investigator Dr. J.F. Ormes, NASA/Goddard.
- Measurements of Cosmic Rays including Anti-Protons, Positrons, AntiNuclei and a Search for Primordial Antimatter (WiZard), Principal Investigator Dr. R.L. Golden, Particle Astrophysics Laboratory, New Mexico State University.
- Spectra, Composition, and Interactions of Nuclei above 10 TeV (SCINATT), Principal Investigator Dr. T.A. Parnell, NASA/Marshall.

The basic Astromag concept shown in the figure and summarized in the table consists of the core facility containing the three components: (1) magnet, cryostat, utility distribution and control system and structure and experiment interface latches; (2) the two in-orbit replaceable experiments; and (3) the Space Station Freedom support elements (a zenith-oriented outrigger extension, attached-payload accommodations equipment, and the full complement of assembly and servicing equipment).

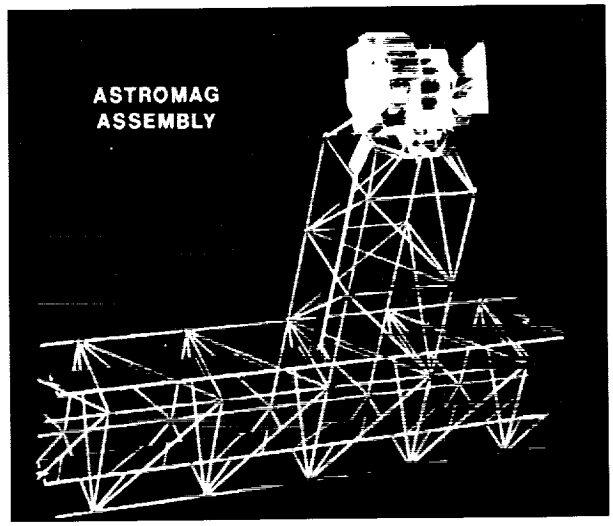

The Astromag assembly.

ASTROMAG SYSTEM PARAMETERS		
Magnet	Field Intensity	7.0 T
	Stored Energy	11.0 MJ
	Decay Rate	1 Percent Per Year at 4 °K
	Size	1.7 m dia. (650 kg)
Cryostat	Working Fluid	Liquid Helium
	Life Time	3 to 4 Years
	Tank Capacity	3,500 L
	Size	2.1 m dia. 2.6 m long (1,350 kg)
Utilities	Power	2 - 3 kW
	Data	150 kbps
	Command	1 kbps
Size	Core Facility	4.4 m dia. 2.7 m long (4,000 kg total)
	Experiments:	
	Lisa	4.4 m dia. 2.0 m long (2,400 kg)
	Wizard	4.4 m dia. 2.0 m long (3,400 kg)
	Scinatt	4.4 m dia. 2.2 m long (1,500 kg)
	Outrigger	5 m × 5 m × 10 m high

The support elements, which provide the structural, power, data, and command interfaces between Astromag and the Space Station Freedom utilities, will be installed prior to the STS launch of Astromag and the first set of experiments.

Astromag will be developed jointly by the Italian Space Agency and NASA. Astromag and the three selected instruments are currently undergoing Phase B studies as the next step leading toward a launch sometime late in the coming decade.

Contact: Jonathan F. Ormes (Code 660)
(301) 286-6811
James E. Phenix (Code 402)
(301) 344-4876

Sponsor: Flight Systems Division, Space Physics Division

Dr. Jonathan F. Ormes is Associate Chief of the Laboratory for High Energy Astrophysics and Acting Chief of the Nuclear Astrophysics Branch. He is currently Project Scientist for Astromag and Principal Investigator for LISA. He received the NASA Exceptional Service Medal in 1986 and earned his PhD in physics.

Mr. James E. Phenix, who has 23 years' experience at Goddard, is currently the Astromag Study Manager. He received his BSME from the University of Maryland.

SPACE STATION

ELEMENTS OF SPACE STATION FREEDOM: INTRODUCTION

The advent of an operational space station in the 1990's will usher NASA into a new and exciting era of space exploration. The new era will feature increased deployment of self-managing, semi-autonomous space systems, increased reliance on telerobotic techniques and principles to conduct routine on-orbit operations and maintenance activities, and manned participation in scientific research performed in microgravity environments. Responsibilities for conducting the research and technology needed to implement Space Station Freedom's elements are distributed among the various NASA centers. Goddard is responsible for the customer servicing and assembly facility, the attached payload accommodation equipment, the platforms, and the FTS. The following articles present some of these tasks in detail.

FLIGHT TELEROBOTIC SERVICER (FTS) FACILITY

The FTS Project is responsible for building a robotics laboratory to develop, test, and evaluate ground and flight systems to support NASA's robotics efforts, particularly for Space Station Freedom. The facility is housed in a high bay designed to accommodate development and test equipment and personnel.

In 1989, many important new pieces of equipment were installed in the facility:

- A 3-degree-of-freedom dual arm overhead gantry robot for the RMS simulator.
- A pair of robotic arms, mounted on a strongback attached to one of the gantry arms, simulating the telerobotic servicer on the RMS.
- A full-scale mockup of a space-station-attached payload, including interface adapter, payload interface adapter, orbital replacement unit, and a truss section.
- A prototype mockup of the STS aft flight deck with the telerobotic servicer operator work station.
- A pair of robotic arms with instrument alignment task mockup and operator work station.

Development and testing tasks are being evaluated and simulated. Meanwhile, the following activities are planned for the current year:

- Install the complete mockup of the STS aft flight deck and telerobotic services operator work station.
- Develop and install mockup of robot-serviceable Astromag experiment.
- Develop and install mockup of robot-serviceable radiator panels.
- Get approval for expansion of the telerobotic service facility's high bay.

The additions to the facility will enhance its value in developing and evaluating robotic hardware, software, and operations for Space Station Freedom, STS, and satellite servicing. Knowledge and experience gained in the laboratory will ensure smooth, reliable, and safe operations in space.

Contact: George E. Alcorn (Code 700)
(301) 286-2463

Sponsor: Space Station Freedom

Dr. George E. Alcorn holds a PhD in physics from Howard University and has worked at Goddard for 11 years. Dr. Alcorn is a noted pioneer in plasma semiconductor device fabrication and was twice recognized by IBM's Chairman of the Board for his creative contributions. In 1984 he was named NASA's Inventor of the Year. He currently serves as Deputy Project Manager for Space Station Freedom's advanced development activities.

SPACE STATION FREEDOM USER SERVICING CAPABILITY EVOLUTION

The Space Station Transition Definition Program has sponsored a study to analyze and evaluate the impacts of Space Station Freedom evolution on user servicing capabilities. Goddard works closely with users to provide them with a definition of the baseline and planned growth for user servicing capabilities available on Space Station Freedom (see figure). User servicing includes replacement, replenishment, retrieval, storage, assembly, and test and verification of user hardware residing outside the pressurized modules. Planned services extend from attached payloads to free flyers and coorbiting platforms.

The transition definition study objectives include impact assessments of evolutionary space station configurations on user servicing and identification of hook and scar requirements to support the customer servicing facility, which will provide major growth capability. The evolutionary space station configurations considered are the transportation node space station and the research and development space station.

An assessment of the research and development configuration identifies the proposed relocation of the customer servicing facility as a potential detriment to user services. Some of the problems identified include—

- Cargo transfer: the space shuttle cannot be unloaded in its current tail-down configuration.
- Thermal issues: the passive radiation capabilities of the customer servicing facility may be compromised due to thermal radiator panel proximity.

This work highlights the need to ensure that space station evolution not adversely affect user servicing capabilities.

The baseline user servicing system consists of Space Station Freedom elements available to support user hardware. This baseline comprises the National Space Transportation System, FTS and its accommodations, the crew and equipment translational aids, intravehicular and extravehicular crew activity, intravehicular servicing support, the logistics supply system, the mobile servicing center, and the special purpose dexterous manipulator. However, thorough analysis of the servicing capabilities for the baseline configuration does not satisfy all identified servicing requirements, such as —

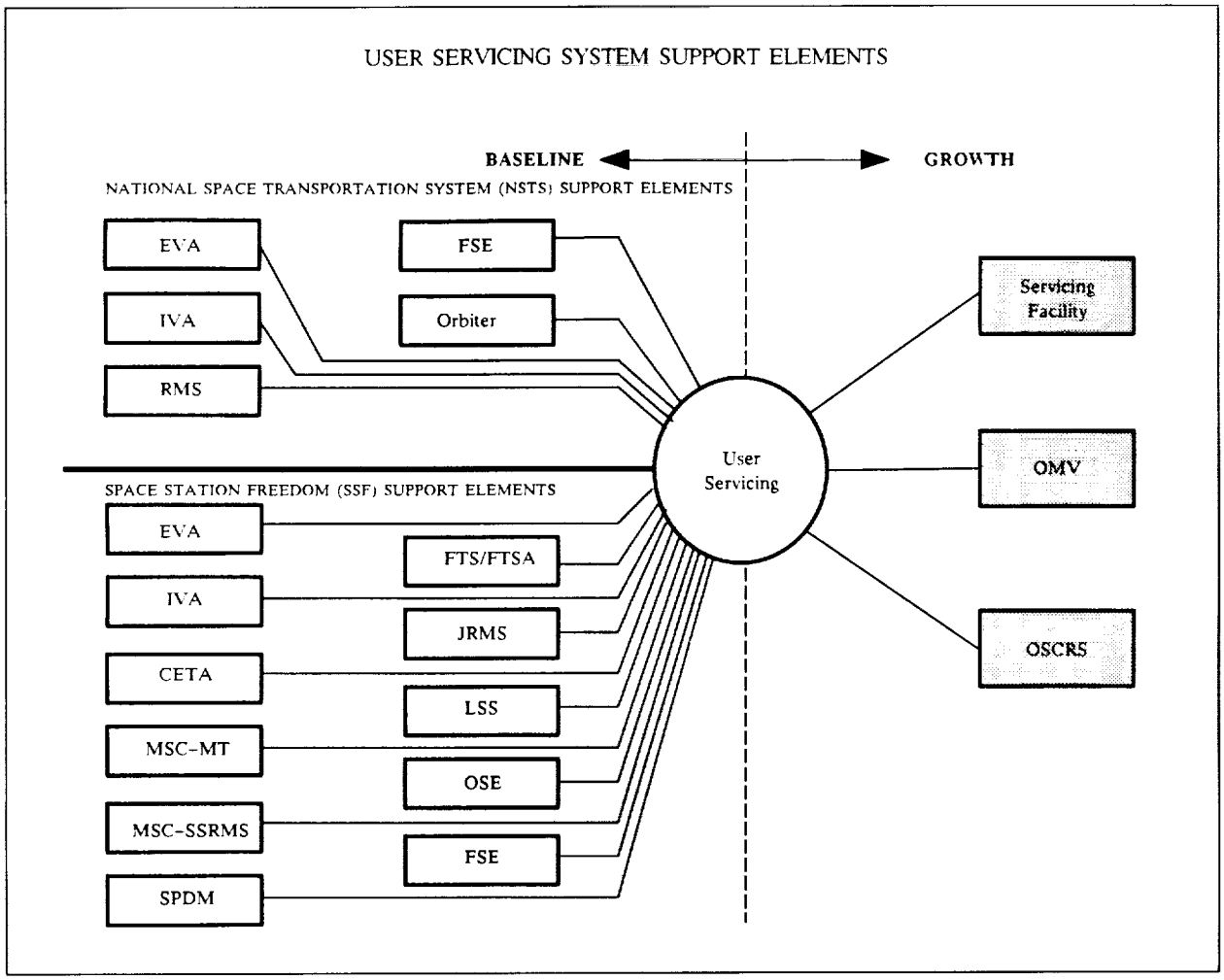

The diagram illustrates the overall Space Station Servicing System Architecture. The acronyms' definitions are as follows: CETA - Crew and Equipment Translation Aids; FTS - Flight Telerobotic Servicer; FTSA - Flight Telerobotic Servicer Accommodations; IVA - IntraVehicular Activity; EV - ExtraVehicular; MSC - Mobile Servicing Center; OMV - Orbital Maneuvering Vehicle; OSCRS - Orbital Spacecraft Consumables Replenishment System; SPDM - Special Purpose Dexterous Manipulator.

- Long-term unpressurized storage with either thermal control or contamination protection for spare equipment.
- Accommodations for storing and servicing the space-based orbital maneuvering vehicle.
- Replenishment of user fluids.

These capabilities will not exist until the completion of the planned-growth user servicing system.

The user servicing system continuously evolves in response to growth in users' requirements. A key component of this growth is the customer servicing facility. Other growth elements include the station-based orbital maneuvering vehicle and the orbital spacecraft consumables resupply system. Addition of these elements will completely satisfy currently identified user servicing requirements.

Hook and scar requirements to support planned growth in user servicing were identified. Hooks are the design accommodations to facilitate the addition or update of computer software, whereas scars are the accommodations to add or update the hardware. The customer servicing facility will be designed with all the hooks and scars necessary

to accommodate a station-based orbital maneuvering vehicle and the orbital spacecraft resupply system. Results of this task indicate that all major subsystems require hooks into the Space Station Freedom Operating Management System. The subsystems that require scarring include structural and mechanical, electrical power, fluid management, data management, and communication.

Studies of in situ servicing techniques, originally proposed for the Polar Orbiting Platform may be applicable to the space station-based free flyers. The results of these studies may enhance in situ user servicing capabilities. Continued analysis of the Space Station Freedom servicing system is necessary to ensure that the evolving servicing capabilities satisfy user requirements.

Contact: Edward F. Thomas, Jr. (Code 406)
(301) 286-8125

Sponsor: Space Station Program

Mr. Edward F. Thomas, Jr., is currently Simulations and Interface Manager of Work Package 3 in the space station program. His past experience includes work on the Hubble Space Telescope (HST), Solar Maximum Mission (SMM), and Multi-Mission Modular Spacecraft projects. He received a BS in electrical engineering from Northeastern University and joined Goddard in 1963.

SPACE STATION FREEDOM PLATFORM SCHEDULING ISSUES ANALYSIS

The Platform Management System will manage the operations of systems and payloads on board an unmanned Space Station Freedom platform. The system performs real-time and near-real-time management functions including management of short term plans and conflict recognition and resolution. Functions allocated to the system are split between the ground and space. The ground segment is designated the Platform Management Ground Application, and the space segment is the Platform Management Application.

Schedule generation is not performed by the Platform Management System but, as the figure shows, by a Platform Control Center scheduler which furnishes the short-term plan. The Platform Management System manages the short-term plan and performs rescheduling. Rescheduling, the system's conflict recognition and resolution function, is of particular interest because it can be initiated from three sources: the payload and the end user (both in response to a target of opportunity) and the platform itself (as an effect of transaction management).

The initial schedule is generated from mission requests for platform resources. These internally consistent and conflict-free mission requests are based upon requirements for platform resources to support users activities. The telescience concept—users directly interacting with platform instrument—raises a number of issues including the impact on allocation, scheduling, and rescheduling of platform resources. Operating from remote home institutions, users will require more support including access to information system services for planning and scheduling instrument activity. However, according to past experience and user comments, most users prefer not to become system (or multiple system) experts. Rather, a knowledge-based planning-scheduling application is needed that resides in the user's work station, provides the access to planning and scheduling information, assists the user in planning and scheduling instrument activity, and facilitates telescience interaction.

Two research and technology tasks, the Platform Management System Scheduler and the Instrument Scheduler/Control Expert System, address issues in the preceeding specific areas of Space Station Freedom platform scheduling. The platform scheduler task has developed requirements for automated Platform Management System scheduling and has implemented a prototype scheduler. The instrument scheduler task is extending the functionality of a user's work station

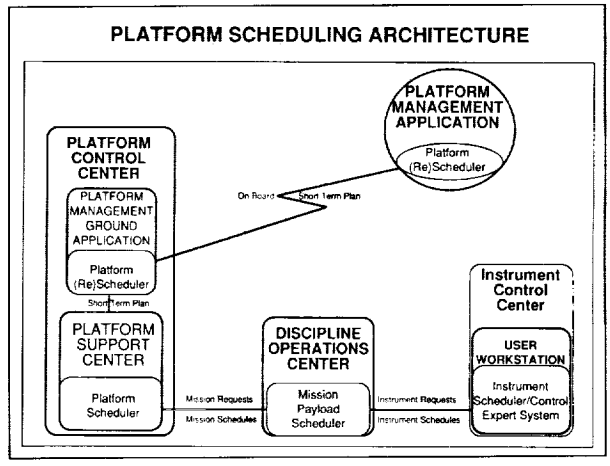

Platform scheduling architecture.

prototype and implementing a knowledge-based application to assist the user.

The platform scheduler task is integrating the prototype into two Goddard testbeds. In the testbed for Scheduling Concepts, Architectures, and Networks, it will manage the short-term plan as part of the ground application. In the testbed for the Platform Management System itself, the scheduler will manage the onboard portion of the short-term plan. Of specific interest are the interfaces between the platform control center scheduler and the ground application schedulers and between ground and spare platform schedulers. The task will investigate rescheduling issues, evaluate operational performance of the prototype, and assess the feasibility of pseudoscheduling, a scheme for efficient use of platform resources without a sophisticated Platform Management Application scheduler. Pseudoscheduling is considered either an alternative or an interim step in the development of automated Platform Management System scheduling capability.

The instrument scheduler task is enhancing a generic instrument planning and scheduling system which incorporates an instrument control work station prototype. The initial prototype provided experiment planning assistance for the Solar Mesospheric Explorer (SME). The present work supports both the University of Colorado SOLSTICE instrument on the UARS and their proposed Eos experiment. The task is presently building a knowledge-based application to support a targeting sequence of 60 stars based upon slew time, wave length characteristics, and past observations. Future work will provide additional functional capabilities including access to relevant planning and scheduling information from remote sources (transparent except for time delay) and ability to plan using "what if" instrument scheduling scenarios.

These tasks have been coordinated with the contractors designing and implementing the Platform Management System, and results will likewise be the contractors'. Results are also presented at relevant Space Station Freedom working group meetings.

Contact: Larry G. Hull (Code 522)
(301) 286-3009

Sponsor: Space Station Program

Mr. Larry G. Hull is a Senior Computer Engineer with 23 years' experience at Goddard in areas such as real-time operational support for manned and unmanned spaceflight missions, computer performance and capacity management, discrete event simulation of computer and communications systems, expert systems, activity scheduling, and project management. He received an engineering degree and an MEA from George Washington University and holds a Certificate of Data Processing. Mr. Hull's primary research interests focus on artificial intelligence and activity scheduling.

PLATFORM MANAGEMENT SYSTEM TESTBED

The Platform Management System performs seven real-time or near-real-time operations management functions for Space Station Freedom platforms. It manages the short-term plan, manages platform operations, monitors operations, supports onboard testing, recognizes and resolves resource conflicts, manages global faults, and checks transactions. The system comprises both a flight portion, the Platform Management Application, and a ground portion, the Platform Management Ground Application.

The system's approach to managing operations is based on resource allocation, usage monitoring, and control, rather than execution of an integrated and constraint-checked command time line. This new approach requires early efforts to demonstrate the feasibility of these concepts.

The testbed pilot is a prototype of the Platform Management System software implemented in the Ada programming language. This prototype has been integrated with existing testbed elements including a science user work station, a scheduler, and a payload simulator. The figure shows the testbed elements and their mapping to elements of the Space Station Information System (SSIS). The purpose of phase 1 of the testbed was to validate the current Platform Management System architecture, to explore the implications of telescience and transaction management for platform operations, to gain experience in the management and development of Ada software, and to explore platform planning and scheduling issues.

Development of phase 1 of the testbed started in October 1987, and the testbed was demonstrated in March 1989. The testbed accomplished much of what it set out to do. Parts of the system architecture were implemented in a

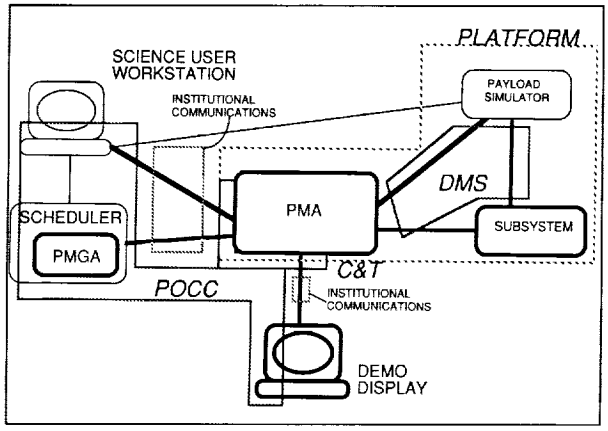

Phase 1 of the testbed for the space station Platform Management System is an implementation using computers and networks local to Goddard. A mapping of testbed elements to parts of the SSIS is shown.

moderate fidelity simulation of the real system, including aspects of both telescience and transaction management. No significant problems were found with the architecture or with the new operations management concepts. The Platform Management Application was coded in Ada, giving many team members valuable experience. Many planning and scheduling issues arose, leading to a better understanding of the requirements for planning and scheduling in a transaction management environment.

The testbed taught team researchers some valuable lessons. Although the testbed showed that the Platform Management System concept is sound, it also pointed out the need to support it with the platform's core systems and much of the ground system. These dependencies were not well understood prior to initiation of the testbed. The Platform Management System contains many interdependent time-critical functions, and great care must be taken during implementation to avoid timing problems. Formality in management of testbed and prototype software must be carefully considered. Although the desire for informality is great, a strong emphasis must be placed on interface control, configuration control, and individual element testing. Finally, Ada software development is unique. Because of the language's great expressive power, the use of language features must be controlled. It is recommended that all Ada projects create a set of Ada feature use guidelines which describe when and how it is appropriate to use language features such as tasking, generics, exception handling, and dynamic memory management.

Contact: Jonathan B. Hartley (Code 512.2)
(301) 286-8540

Sponsor: Space Station Program

Mr. Jonathan B. Hartley is Head of the Systems Development Engineering Section in the Flight Software Systems Branch. His background in software applications includes laboratory data acquisition and analysis, military command and control, and spacecraft flight software. His current interests focus on the engineering of real-time software and spacecraft operations.

PLATFORM MANAGEMENT SYSTEM EVOLUTION

In 1988 a study was begun to define the Platform Management System functions required for the mature platform operations era. The task has these objectives: 1) defining how to increase the operational productivity of the platform by providing enhanced capability for responding to changing events; 2) influencing the initial system design by identifying required hooks and scars; and 3) evaluating potential automation techniques that are appropriate given predicted onboard computing resources.

Initial platform operations scenarios were defined. The focus was on functions related to the Platform Management System where operations enhancements were likely to occur. Operations productivity was defined in terms of scientific productivity of the platform as well as the level of automation of the ground system. The *Platform Operations Productivity Enhancement Report* was completed early in 1989 documenting system enhancements to increase science productivity and ground system automation.

The *Platform Management System Definition Document* for the Platform Management System established the baseline, and the *Platform Management System Evolution Plan* set forth a series of enhancements that will provide progressively more sophisticated operations management capabilities. The plan includes enhancements to resource scheduling, resource modeling, system and payload anomaly management, and transaction sequence interpretation. A plan for migration of functions from the ground portion of the management system to the flight portion is also included. The impacts of this plan on the platform are being documented to ensure that the required hooks and scars are included in the baseline system.

Future plans include a prototype to determine whether some of the enhancements are feasible and how they can be implemented in the onboard computing environment.

Contact: Jonathan B. Hartley (Code 512.2)
(301) 286-8540

Sponsor: Space Station Program

Mr. Jonathan B. Hartley is Head of the Systems Development Engineering Section in the Flight Software Systems Branch. His background in software applications includes laboratory data acquisition and analysis, military command and control, and spacecraft flight software. His current interests focus on the engineering of real-time software and spacecraft operations.

PLATFORM EVOLUTION STUDIES

The Polar Orbiting Platform being developed by the Work Package 3 Project at Goddard will play a key role in the NASA Leadership Initiative, Mission to Planet Earth. It becomes, with the addition of payloads, an Eos observatory.

The Polar Orbiting Platform, a highly modular design with distributed systems packaged in Orbital Replacement Units (ORUs), is in the current baseline program. During phase B studies, the same ORU's, which are thermally independent, were also used in a configuration for an Astrophysics Coorbiting Platform. Other coorbiting platform configurations are also possible.

Mission to Planet Earth also has Geostationary Platforms as part of its global observational system. A study was begun in March 1988 to assess the applicability of the Polar Orbiting Platform ORU's for a geostationary Earth-observing mission. Two test cases, summarized in the first table and representative of Mission to Planet Earth payloads, were studied. Case A was used to emphasize the Geostationary Platform configuration and design; it used a Titan/Centaur to achieve orbit. Case B, considered to be much further in the future, included some assembly at the Space Station Freedom manned base and use of an Orbital Transfer Vehicle to achieve orbit; requirements on the manned base to support such a mission were emphasized.

The study found the Polar Orbiting Platform systems more than adequate to meet Geostationary Platform

Geoplatform Test Cases

Sensor Description	Mass (Kg)	Power (W)	Data (Mbps)	Case A	Case B
Microwave Imager/Sounder (20m Mesh + 10m Solid)	1,000	300	0.1		X
Microwave Imager/Sounder (4.4m Solid)	200	250	0.1	X	
Infrared Sounder (Michelson)	165	130	7.4	X	X
Lightening Mapper	30	100	0.1	X	X
Active Cavity Radiometer	30	25	<0.1	X	X
Solar Spectrometer	105	65	<0.1	X	X
Climate Radiation Radiometer	50	30	<0.1	X	X
Ozone Mapper	20	30	<0.1	X	X
Operational Imager/Sounder (GOES-Next Enhanced)	300	300	3.0	X	X
Space Environment Monitor	40	25	<0.1	X	X
Operational/Research Data Collection	25	40	<0.1	X	X
Search & Rescue	10	30	<0.1	?	X
Operational/Research Data Distribution	40	?	?	X	X
Moderate Resolution Imaging Spectrometer	110	100	20.0	X	
Visible/Infrared Imager (1.5 × 5m SEOS)	1,000	150	80.0		X
Payload Total Case A	1,200	1,200	40.0		
Payload Total Case B	3,000	1,500	100.0		

Weight Summary For Geoplatform Case A

	WT (LB)	Comments
Payload	2,645	Case A, 1,200 kg
Platform Bus	6,810	Core (dry) + 8 ORU'S
Total Spacecraft Dry	9,455	Payload + Subsystems
Propellant	3,610	Hydrazine
Launch Vehicle Infrared	110	Centaur-G Infrared
Launch Mass	13,175	Beginning of Life at Geostationary Orbit
Platform Bus Contingency	1,825	27 Percent of Dry Bus

Titan IV/Centaur Launch Capability

- Performance to geosynchronous orbit (0° inclination, 0.00° eccentricity, 19,323 nm)

1988[1]	1991[2]	Mid-1990s[3]
10,300 lb	13,500 lb (Goal)	15,000 lb (Goal)

- 86-ft long fairing allows 40-ft long geostationary platform

Notes:

[1]*Titan IV User's Handbook*, March 1988.
[2]Requires solid rocket motor upgrade.
[3]Requires further solid rocket motor upgrade and/or 3rd-stage upgrades.

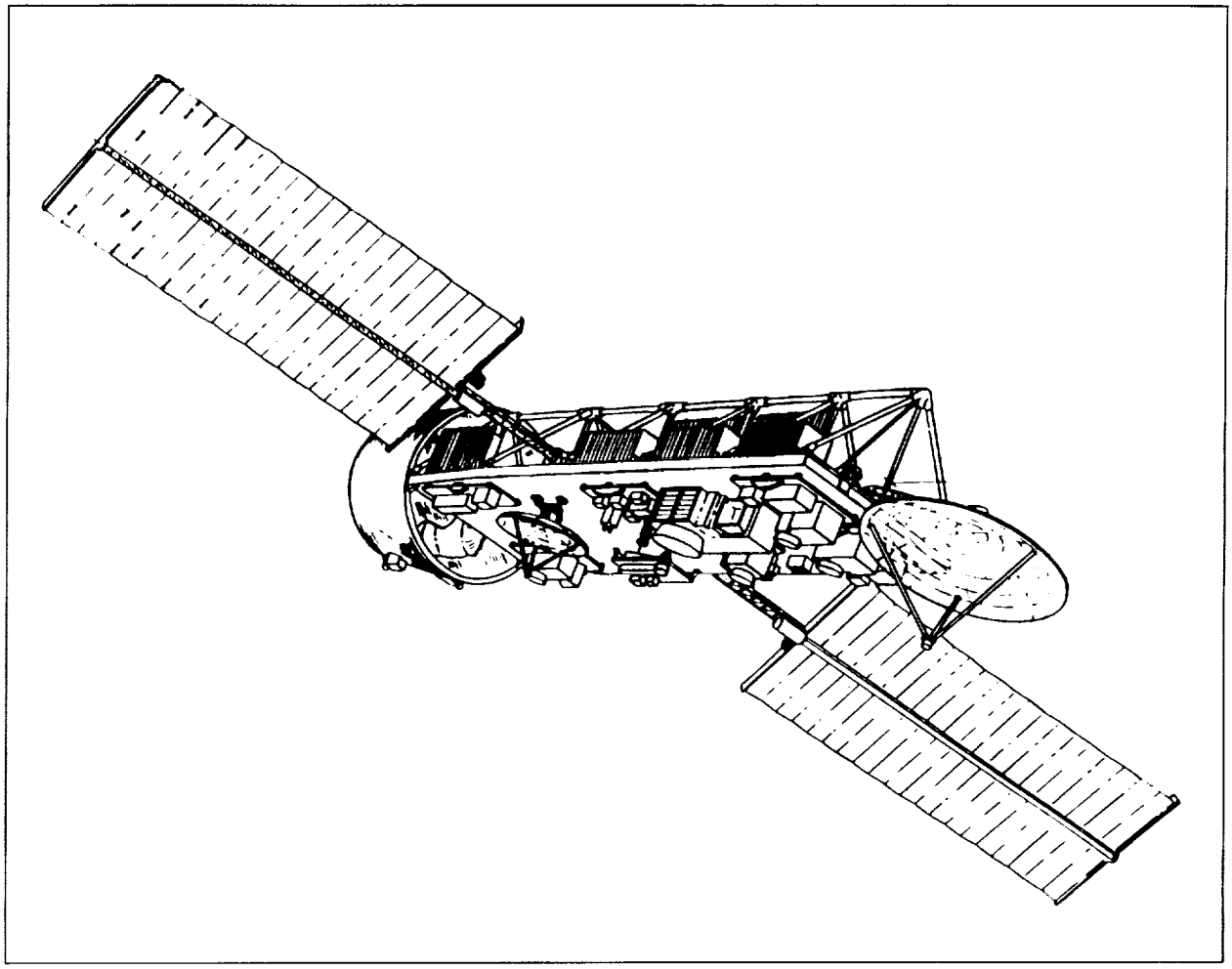

Geostationary Platform Case A configuration.

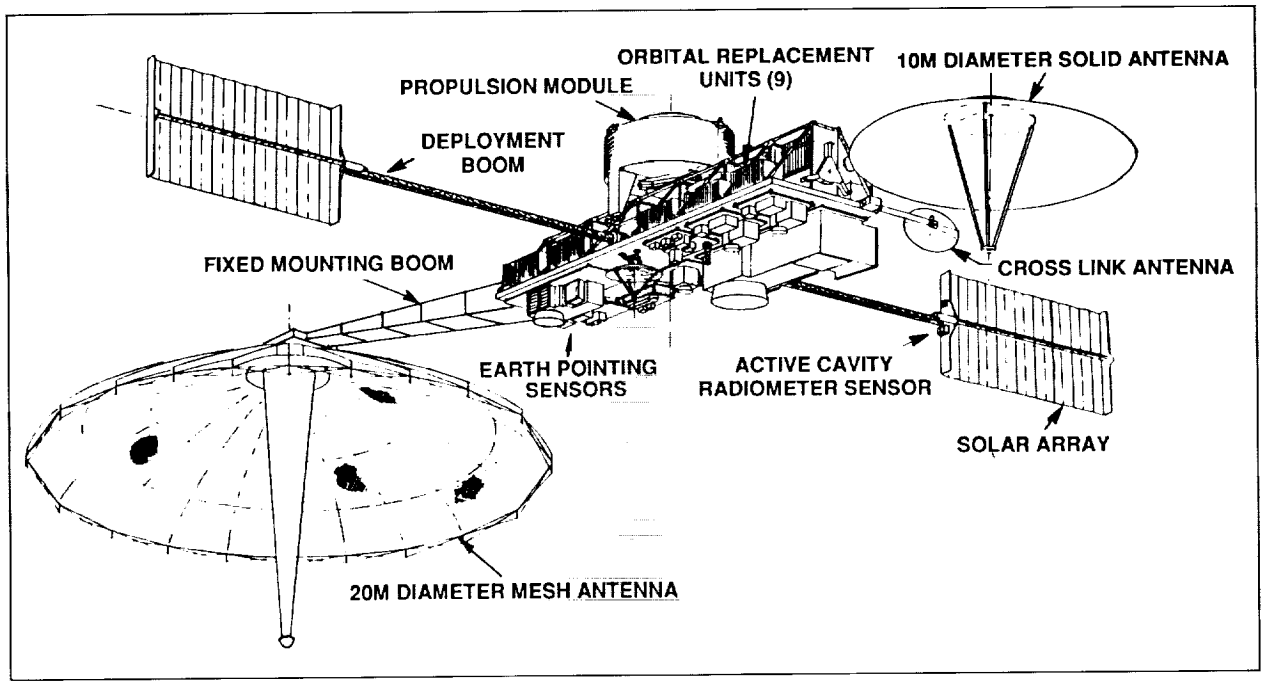

Geostationary Platform Case B configuration.

requirements. Two types of changes were required for the Polar Orbiting Platform ORU's:

(1) Modification to use only one surface for heat rejection; for the battery ORU, this modification meant "opening up" the ORU to retain the radiator area with a corresponding decrease in depth.

(2) Deletion of equipment not needed.

The first figure shows the Case A configuration. The second table summarizes the weight, which is within the planned capability of the Titan IV/Centaur for the end of the century as shown in the third table. The second and third figures show the Case B configuration, which is driven by the large microwave antennas of two of the payloads. These were presented at the final review on April 19, 1989.

Contact: Barbara A. Walton (Code 406)
(301) 286-6180

Sponsor: Space Station Program

Ms. Barbara A. Walton, the Platform Instrument Manager for Work Package 3, has been with Goddard for 23 years. She has a BS in chemical engineering from The Pennsylvania State University and a MChE from the University of Oklahoma.

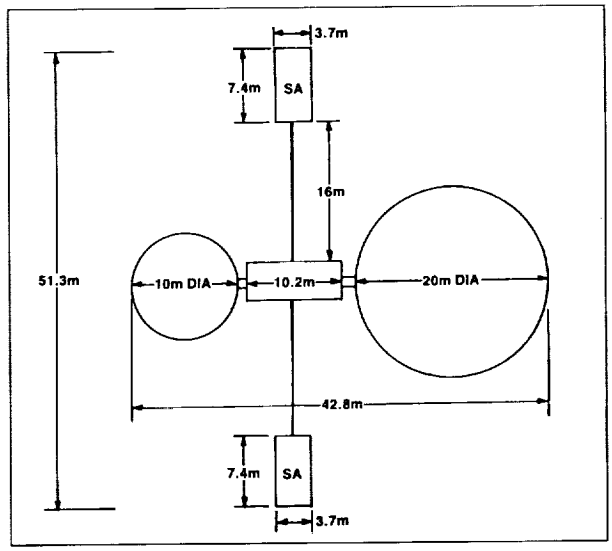

Geostationary Platform Case B dimensions.

SPACE STATION FREEDOM

Space Station Freedom sponsors research and technology in a number of areas including Thermal Systems and Robotics.

Included in the thermal systems activity are the Thermal Flight Experiments. Three experiments are being readied for flight. One is the Temp 2c, a flight experiment using a hybrid (capillary and mechanically pumped) two-phase loop which simulates the instrument bus. When combined with the Johnson Space Center portion (Temp 3c), the combined Space Station central bus and instrument bus is simulated.

Temp 2a-3 is planned to fly first of the three experiments. This flight will provide the first flight data on a two-phase, mechanically pumped loop. Capillary Pumped Loop Flight Experiment (CAPL) is a capillary pumped system with no moving parts having very low-level vibration. The CAPL system is ideally suited for the Polar platform and is planned for that use. An important two-phase thermal management system designated the High Power Spacecraft

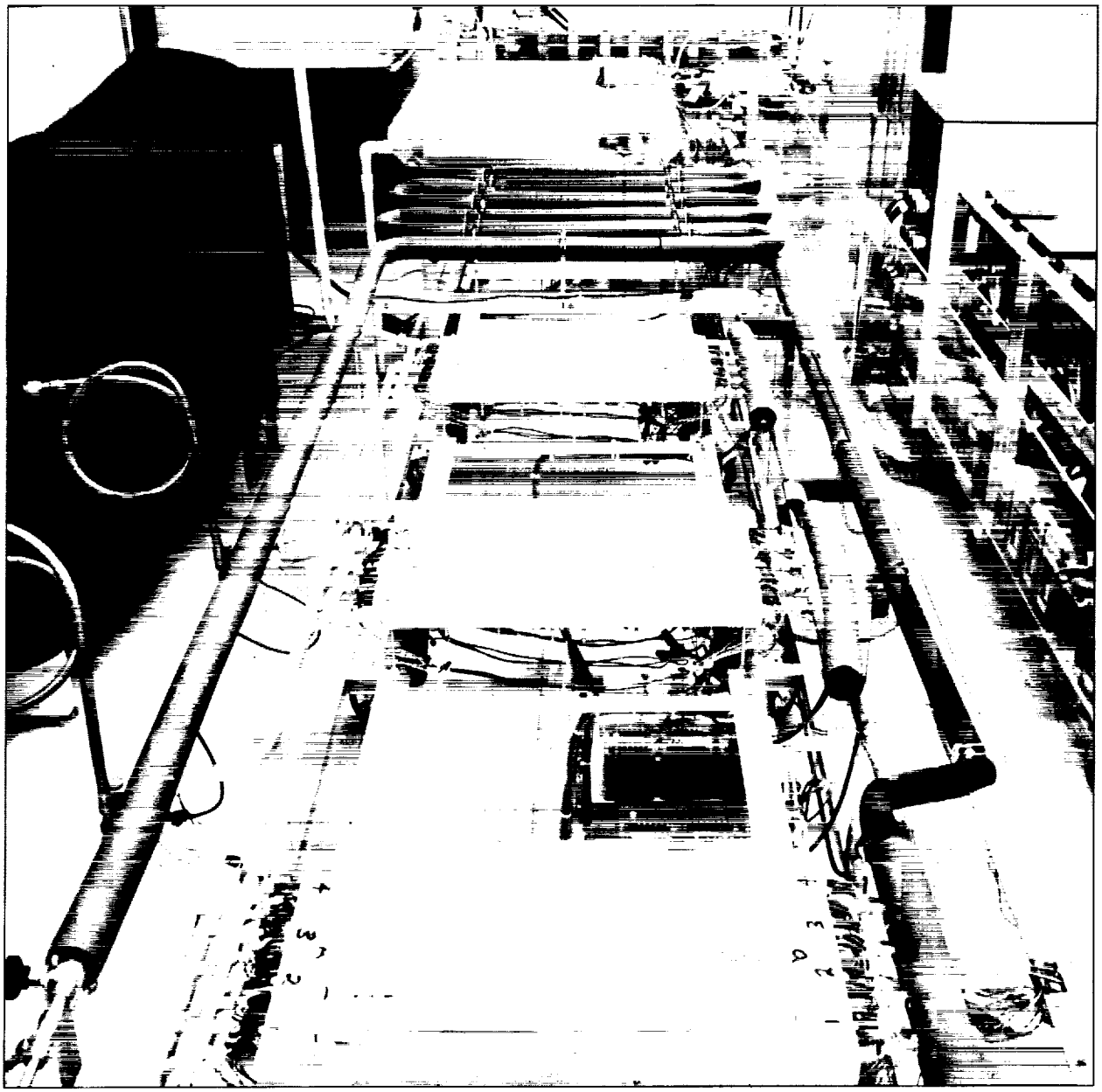

High Power Spacecraft Thermal Management System.

ORIGINAL PAGE
BLACK AND WHITE PHOTOGRAPH

Thermal Management System has been tested successfully. The system is essentially a Hybrid Capillary Pumped Loop (HCPL), which can be operated in either the capillary or mechanically pumped mode. The system has demonstrated exceptional heat loading managing capabilities, including an ability to manage 75 W.

The Space Station requires development of several different types of two-phase thermal systems, for example, capillary pumped systems as well as mechanically pumped systems. To support these diverse applications, a full-scale generic testbed has been designed and is currently being fabricated. This loop, designated as the Instrument Thermal Testbed, can be used to test a wide variety of system components, which can be operated in either a pure capillary, mechanically pumped, or hybrid capillary/mechanically pumped mode. The Instrumental Thermal Testbed is vacuum rated and is compatible with a variety of working fluids including ammonia. It is composed of five sections for ease for transportability. In its full configuration, the Instrumental Thermal Testbed occupies a 14- by 30-ft envelope.

Several fruitful areas of research in robotics have been pursued in the past year. A research area entitled Rolling Friction Fingers concerns a finger design for space robot grippers that will greatly improve the grasping and manipulating of objects by reducing the effects of friction. Using an arrangement of rollers on the gripper fingers that guide, align, and seat the object being grasped produces several substantial advantages over V-groove design. A research effort for the FTS, Controls and Analysis Capability for Flexible Robotic Systems, demonstrated that multibody software can be used to develop a robot dynamics simulation compatible with the needs of the FTS control system. Two simulation programs were developed, one for higher fidelity autonomous control and one for low fidelity control.

Another project is developing a two-finger gripper which mates with a standard handle to permit robot grasping operations. This two-finger gripper can readily perform a variety of tasks such as grasping Orbital Replacement Units or opening the doors on an Orbital Replacement Unit. Alignment is performed by means of a wrist camera.

Another robotics project centers on the dual-arm teleoperation of a pair of 7-DOF manipulators, each with its own 6-DOF mini-master hand controller. A control processor provides all of the coordinate transformations between the 6-DOF and 7-DOF space. The control scheme is designed with the NASA Standard Reference Model architecture developed by NIST. The control software is developed using the Ada language.

Two vital research and development facilities are being developed: the FTS Development, Integration and Test Facility and the Instrument Thermal Testbed. The Development, Integration and Test Facility and the Instrument Thermal Testbed supported by Space Station provide for the test, evaluation, and development of ground and flight systems to support NASA's robotics efforts.

New equipment in this facility includes several kinds of robotic arms and mockups of the Space Station attached payloads. These resources will facilitate developing and evaluating robotic hardware, software, and operations for the Space Station, STS, and satellite servicing. Knowledge and experience gained in the laboratory will ensure smooth, reliable, and safe operations in space.

Contact: George E. Alcorn (Code 700)
(301) 286-2463

Sponsor: Space Station Freedom

Dr. George E. Alcorn holds a PhD in physics from Howard University and has worked at Goddard for 11 years. Dr. Alcorn is a noted pioneer in plasma semiconductor device fabrication and was twice recognized by IBM's Chairman of the Board for his creative contributions. In 1984 he was named NASA's Inventor of the Year. He currently serves as Deputy Project Manager for Space Station Freedom's advanced development activities.

Communications Technology

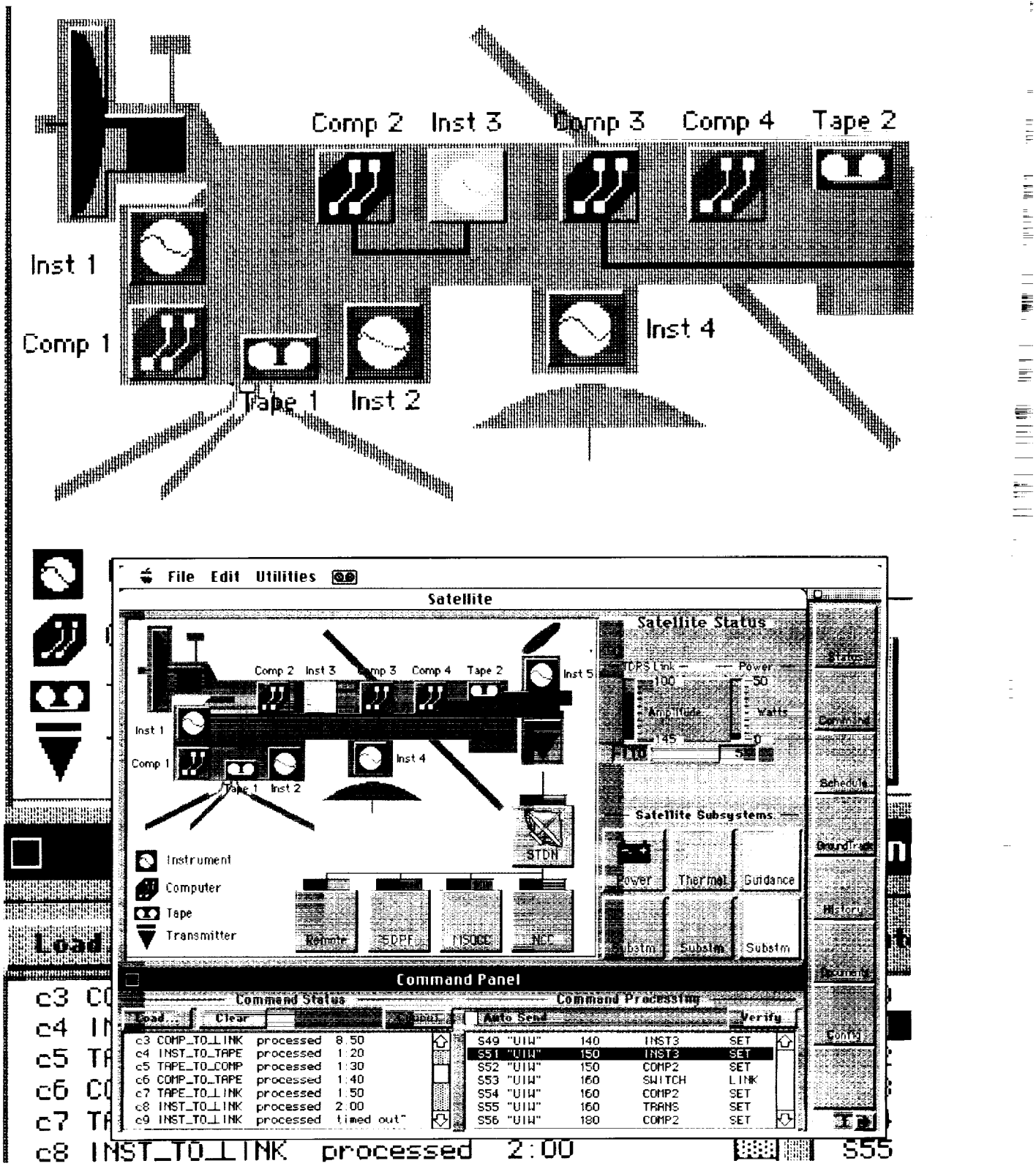

ORIGINAL PAGE
COLOR PHOTOGRAPH

Future end-to-end systems for spacecraft operations will involve more sophisticated uses of automation. This automation will provide enhanced operational and user interface/interaction capabilities.

SPACE COMMUNICATION SYSTEMS

HIGH-CAPACITY GENERIC MATRIX SWITCH SYSTEM (MSS)

Telemetry data systems of the 1990's will need to process an ever-increasing flow of data. As data transmission rates increase and the number and types of data devices proliferate, the systems that transmit and process these data will need to expand their functions and capabilities.

One such data system known as an MSS is used for switching the data paths of multiple devices to one another. Past MSS's have reached a capacity of 128 × 128 (the ability to switch 128 input devices to 128 output devices). However, the increased data needs of the 1990's will require switches of at least 256 × 256. To construct such a switch without increasing size, expense, or complexity, or trading off reliability and maintainability, modern design techniques and technologies must be used.

The Microelectronics Systems Branch, drawing on its expertise in building generic data systems based on very large-scale integration (VLSI) technology, is currently building a proof-of-concept prototype MSS, shown in the first figure. It will be capable of replacing older switches whose abilities have been outstripped by the needs of present facilities such as the Multi-Satellite Operations and Control Center and will fulfill the requirements of new facilities such as the Data Interface Facility.

The MSS is actually two switches in one: a 256 × 256 switch that handles data rates to 50 Mbps (the main switch) and a 32 × 32 switch that handles data rates to 300 Mbps (the high-speed switch). The main switch accepts serial, digital, differentially paired signals, such as those sent by the RS422 protocol, and may be synchronous or asynchronous. However, the high-speed switch uses a special data format that is compatible with emitter-coupled logic (ECL).

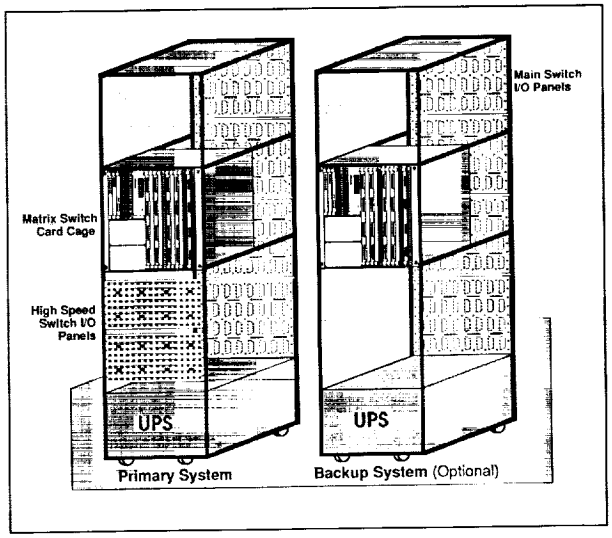

The MSS.

Sample of an information display associated with the distributed knowledge base testbed being used by the Data Systems Technology Division to prototype the intelligent control center of the future.

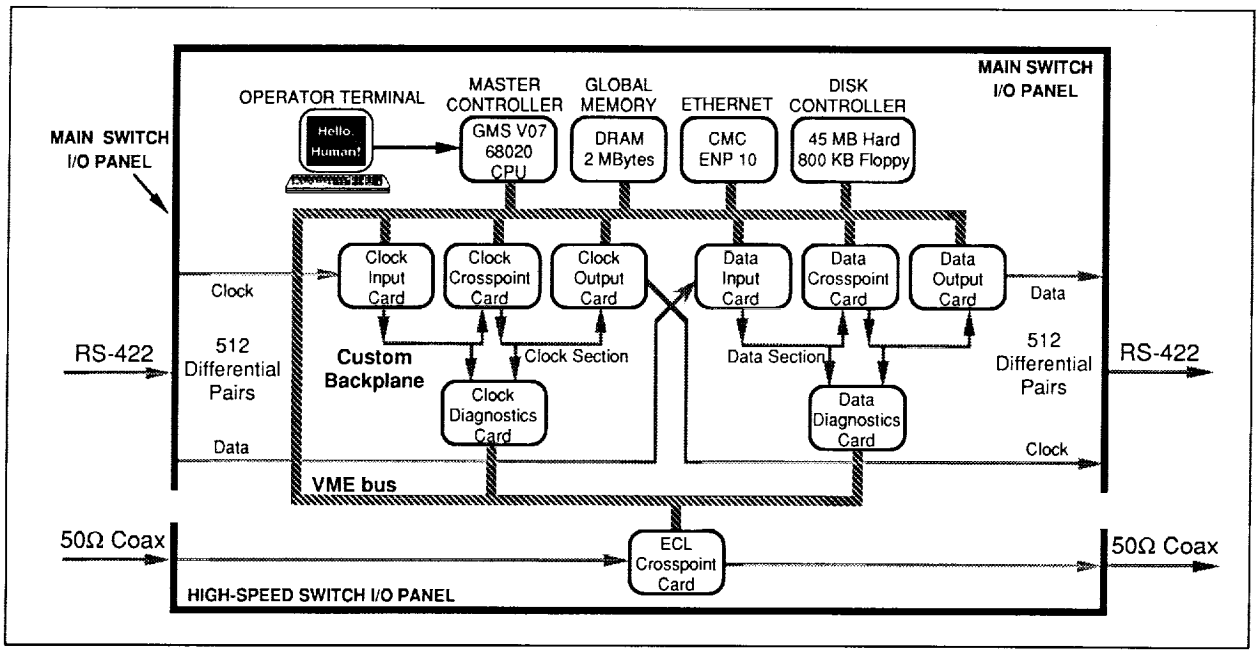

Functional block diagram of the MSS.

The MSS demonstrates flexibility during setup, operation, maintenance, and repair. For instance, any input may be switched to any one or multiple outputs, or it may be disconnected. In addition, the MSS may be interactively controlled through either dedicated terminals or high-resolution graphics work stations through an Ethernet interface. For simplicity, the MSS is entirely controllable by software. And finally, to simplify maintenance, repair, and system upgrade or modification, the MSS uses a modular set of cards that is easy to replace if necessary.

Error handling and diagnostics on the MSS are very powerful. Built-in diagnostics circuitry continuously monitors all signals entering and leaving the system for data discontinuities or irregularities (such as incorrect data rate). In addition, the MSS contains self-test circuitry capable of testing every switching line. An uninterruptible power supply keeps power to the MSS clean and stable even during transient power failures, and a fully redundant backup system is always kept on line in cases of hardware failure.

The MSS is a VMEbus-based system, capitalizing on previous experience in VMEbus data systems. A customized backplane contains the VMEbus and also transports the 512 signals between the cards.

The MSS hardware architecture contains two functional sections. The first section, located at the top of the second figure, consists of commercially available VME cards including the master controller, memory, Ethernet controller, and disk module cards. These cards do not interact directly with the signals, but rather perform control operations for the system.

The other section, located in the middle and bottom of the second figure, contains the custom cards, which directly manipulate the signals entering and leaving the MSS. The clock section and the data section are functionally identical. The input card is responsible for converting all signals from their RS422 differential format to single-level transistor-to-transistor logic (TTL) signals. The output card performs just the opposite function, converting the signals from TTL back to RS422. In the middle lies the 256×256 crosspoint card, which performs all the routing (switching) of the data paths. The diagnostics card, which taps off all input and output signals but does not alter them, counts logic-level transitions to ensure against discontinuities in the data.

On the bottom of the figure, completely separate from the rest of the MSS, lies the high-speed crosspoint card. This card contains all of the circuitry for the 32×32 high-speed switch and uses ECL technology to achieve its extremely

high-speed capabilities. The input/output panels for the high-speed switch perform functions analogous to the input and output cards for the main switch (i.e., the conversion of the data to the necessary logic levels).

The Microelectronics Systems Branch is currently developing a slightly scaled-down MSS prototype, which consists of only one rack but is fully functional. Prototype testing will soon be completed.

Contact: Howard M. Kram (Code 520)
(301) 286-3212
Luis G. Salichs (Code 521)
(301) 286-5782

Sponsor: Microelectronics Systems Branch, Data Systems Technology Division, Mission Operations and Data Systems Directorate

Mr. Howard M. Kram started as a cooperative student at Goddard in 1985. Since then, he has worked on a number of projects and has been involved with both hardware and software designs. He is currently working on his Professional Intern Program Level II work assignments which include the integration and testing of the MSS.

Mr. Luis G. Salichs has been at Goddard since 1986 and currently works in the Data Systems Technology Division of the Mission Operations and Data Systems Directorate. He concentrates on the hardware arena, specializing in the design of high-frequency devices. Mr. Salichs is working on an MS in electrical engineering at Johns Hopkins University.

VIRTUAL CHANNEL SORTER MULTIPLEXER (VCSM) SYSTEM

Goddard's Mission Operations and Data Systems Directorate is applying advanced technologies such as VLSI to the development of components and systems to meet NASA's data-handling needs well into the future. These systems will be needed to support space elements communicating through Tracking and Data Relay Satellite System (TDRSS) such as Space Station Freedom, Polar Orbiting Platform, and the Co-Orbiting Platform.

The Data Interface Facility is a key element in NASA's advanced communications systems. The Data Interface Facility will support communications among space elements and multiple ground facilities. The core element of the Data Interface Facility, the return link processor, will accept data streams from the ground terminals that comply with the framing format recommended by the Consultative Committee for Space Data Systems. This format is referred to as the Virtual Channel Data Unit (VCDU), which may be protected by a Reed-Solomon code. The Data Interface Facility return link processor will route the VCDU's to first-level destinations. The Microelectronics Branch and the Systems Engineering Branch are currently developing the VCSM prototype as a proof of concept for a VLSI-based solution to performing the basic data-handling functions needed in the Data Interface Facility's return link processor.

The multiplexer performs the functions of frame synchronization, Reed-Solomon decoding, virtual channel sorting, and frame multiplexing at rates up to 20 Mbps. Two composite data streams, each containing encoded and/or unencoded VCDU's, are input to the prototype. First, synchronization to the data units within each data stream is performed. Next, errors detected by the Reed-Solomon code are corrected if possible. VCDU's are then sorted by virtual channel, and all data units destined for the same first-level destination are multiplexed together into one composite output stream.

The VCSM is based on the commercially available, open-architecture VMEbus system. It is housed in one standard 19-in. VME rack containing both commercial cards and custom cards, as shown in the first figure. The commercial cards provide the overall system environment, which includes the setup of all custom cards, status monitoring,

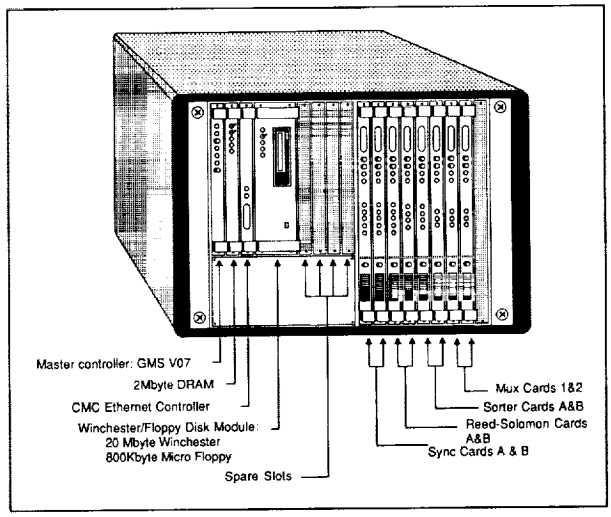

The VCSM card cage.

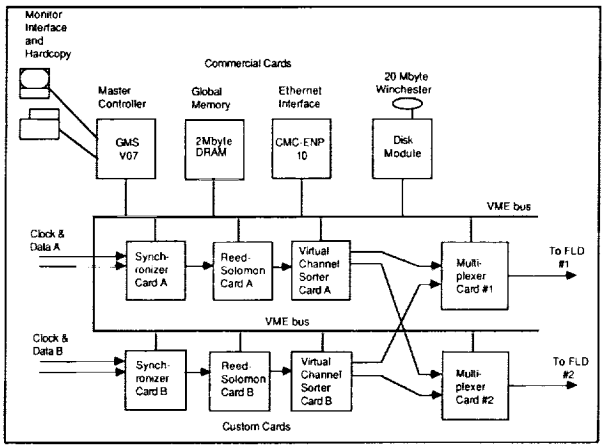

The VCSM bus-level architecture.

diagnostics, program and catalog storage, and communication with a local or remote monitoring bus system. The custom cards provide all of the system's specific data processing functions (i.e., synchronization, error correction, sorting, and multiplexing).

The VMEbus serves as the control path by which the commercial cards set up and control the system, as shown in the second figure. The movement of data units through the system is accomplished by the custom cards through the separate telemetry data path or data pipeline.

Each custom card is actually a commercial central processing unit (CPU) card with a unique side connector through which the custom card is connected. The CPU provides local control and interfaces with the commercial cards. The custom card provides the hardware to perform the card's unique function (synchronization, multiplexing, etc.). Two of the backplane connectors are used for interfacing with the VMEbus, and the third is the telemetry data path.

The VCSM accepts data on two independent channels (A and B), each of which consists of a synchronizer card, a Reed-Solomon card, and a virtual channel sorter card. (The Reed-Solomon chip set for the Reed-Solomon card was provided by the University of Idaho.) Each channel synchronizes to the incoming VCDU's, performs error correction, and sorts the data units by virtual channel. All data units destined for the same first-level destination are input to one multiplexer card, where they are combined into a single composite output stream. In addition to performing its particular data-handling function, each custom logic card performs setup and self-test and also maintains quality and accounting statistics.

The VCSM system components underwent individual testing and development. System integration took place in the fall of 1989, and the prototype was completed in January 1990.

Contact: Sarah L. Hand (Code 520)
(301) 288-3912

Sponsor: Mission Operations and Data Systems Directorate and University of Idaho

Ms. Sarah L. Hand, who received a BS in electrical engineering from the University of Maryland, has been a member of the Microelectronics Branch for 2 years. She is involved in the development of data-capture and processing systems. Ms. Hand is currently earning an MS in electrical engineering at Johns Hopkins University.

HIGH-RATE MULTIPROCESSING LEVEL ZERO PROCESSING (LZP)

In the Space Station Freedom era, telemetry data will be transported from payloads to the ground and distributed to customers by the Space Station Information System (SSIS). One primary goal of the system is to make the data transportation transparent to the customer so that the interaction with the payload takes place as if the payload were at the customer facility. This objective requires a process to remove from delivered data products all artifacts and disturbances introduced during data transport through the system. This type of processing is a key part of what is usually referred to as LZP. While the complete process of preparing telemetry data for delivery to NASA's customers requires a number of steps or levels (level 0, 1, 2... etc.), LZP poses a real technical challenge for NASA in the 1990's Space Station Freedom era. This challenge is the result of requirements to provide real-time or near-real-time LZP products at rates up to 150 Mbps. In addition, increased use of sophisticated data formats places even more demand on NASA's future ground telemetry data systems.

The main object of the LZP system is to restore the order of data for a given observation or collection period. Such a data set is called a data take and is delivered to the customer as an LZP product. Restoration of a data take requires performance of one or all of the following four basic functions: (1) reassembling user packets from VCDU's; (2) reversing "backward" playback data; (3) merging together real-time data and playback data with proper time

order; and (4) deleting redundant data due to the overlap between real-time and playback data.

Traditionally, such tedious LZP tasks are performed by software running on mainframe computers. To meet NASA's needs for drastically increased data speed and volume, the Data Systems Technology Division has proposed a new high-speed processing algorithm and architecture for the LZP system using VLSI technologies that will significantly reduce the complexity of data base management necessary for reconstructing payload data streams and offer potential processing rates up to 150 Mbps.

The new architecture is based on state-of-the-art distributed real-time processing and uses the generic functional component approach telemetry system platform to achieve a low cost/performance ratio while at the same time reducing design/development schedules and costs. The functional component approach is based on the industry-standard VMEbus and makes use of multiple commercial and custom VLSI hardware-based cards to provide standard off-the-shelf telemetry processing functions (frame synchronization, Reed-Solomon decoding, packet processing, etc.) for almost any telemetry data handling application.

The new LZP system, called a data take processor, will operate in three nonexclusive operational modes: real-time, quick-look, and production processing. In the real-time processing mode, customers' packets are transmitted as soon as each packet is received and reassembled. Also, the data are retained for normal production. In the quick-look processing mode, a higher priority subset of the data take will be made available to the customer. No redundancy deletion is performed. Again, the data are retained for normal production. The final and most important mode is the production processing mode. In this mode, data are processed and grouped into data takes specified by the customer through scheduling tables. The completed data take will be available to the customer within 90 min after data capture.

LZP is a two-stage process. In the first stage, a serial data stream is assembled into user packets and then stored in a mass storage buffer. The big ordering of playback data within each packet is corrected. In the second stage, packets are sorted according to their source identification numbers and time sequence and grouped together to form data takes.

With the data rate of 150 Mbps and average packet size of 8 kbit, a 15-percent duty cycle operation can generate 15 million packets each orbit. To trace every packet in the buffer would result in a huge data base in the magnitude of Gbytes. The management of such a large data base would be an extremely cumbersome and time-consuming task, even for a high-performance mainframe computer. Therefore, a new processing algorithm is employed that significantly reduces the size of the data base. One key is to define a new class of data unit called the data segment. A data segment is a group of user packets that have identical source identification numbers, data direction, and continuous time sequence. The other key is to presort packets from different sources in separate logical buffers. Accordingly, the disk farm storage system is partitioned into a number of logical buffers. Each buffer is dynamically sized to accommodate maximum data load generated by the source for up to three orbits.

User packets from various source identification numbers are saved in corresponding logical buffers as data segments. Any change in the data stream that results in a reversal of data direction or a break in the time sequence for a source will result in the closing of the current data segment, the opening of a new data segment, and an entry into the data segment's data base. Because this action occurs relatively infrequently, the size of data segment is significantly larger than that of packet. It is reasonable to assume there are at least 1,000 packets per segment. Thus, the data segment data base will be reduced to the level of megabytes and handled easily by microcomputers. Individual packets in a data segment are retrieved easily because the size of packets from the same source is a constant and the starting address of a packet is a known offset from the beginning of data segment. The offset is calculated from the packet sequence number in that segment and the packet size. All processes in the second-stage LZP are simplified greatly because they are performed on a data-segment basis rather than on individual packets.

The data take processor is based on a dual-bus multiprocessor architecture housed in a 19- × 24-in. rack, as shown in the first figure. The communication between microprocessors is through the VMEbus and the telemetry data flows through a custom data pipeline bus. As illustrated in the second figure, the configuration of the data take processor includes three processing units: the system base unit, the front end unit, and the back end unit.

The system base unit is responsible for overall system control and serves as the system master. Through the use

of BASE and Modular Environment for Data Systems (MEDS), both Goddard-developed software packages, the operator controls the LZP operations by sending commands and gathering status to and from other system components through the unit. In addition, the system base unit maintains the quality and accounting data files and production catalog files and the like in the operational data base. The system base unit also provides system disk and memory, as well as the Ethernet interface to remote terminals or work stations.

The front end unit is responsible for reassembling user packets from serial data in NASA Communications Division block format. It consists of the frame synchronizer, Reed-Solomon decoder, packet processor, and data simulator. The serial telemetry data is ingested to the frame synchronizer and synchronized to VCDU's. Reed-Solomon error decoding occurs when coded VCDU's are passed through the Reed-Solomon decoder card. At the next processing node, the packet processor strips off the headers and trailers, reassembles user packets, reverses "backward" data for playback packets, and sends them to the back end unit. The packet processor also generates quality and accounting data and annotates the packets. The data simulator simulates NASA Communications Division blocks and VCDU's used for system test and diagnostics.

The major function of the back end unit is to reassemble the specified data takes from user packets. The three processing modules in the unit are the segment processor,

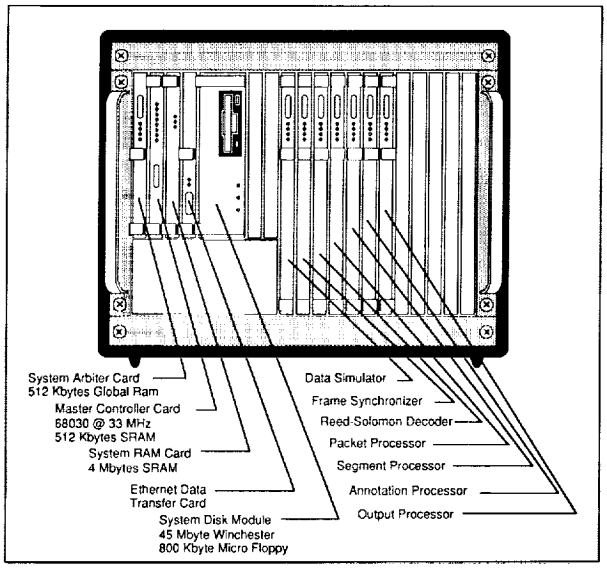

The data take processor.

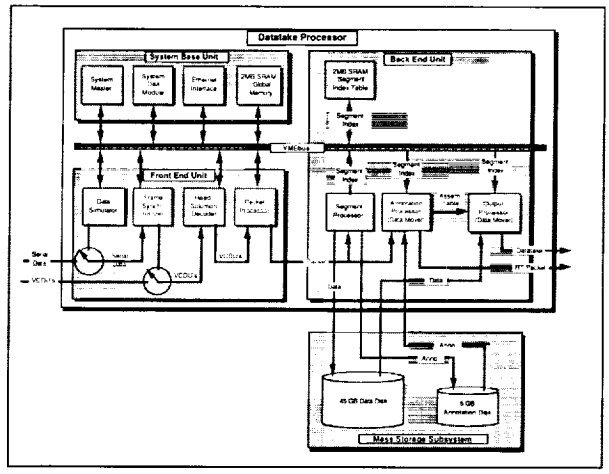

The configuration of the LZP processor.

annotation processor, and output processor. The segment processor separates the annotation data and user packets and sorts them according to their source identification numbers in a local memory buffer. When the data in any local memory buffer reaches a predetermined size, that buffer will be transferred to the disk farm storage system into a partition allocated for that source identification number. Meanwhile, the segment processor monitors the sequence numbers and space time of each packet to define data segments. If a change in data direction or a gap in space time is detected, the segment processor will terminate the current data segment, make a new entry in the segment index table, and start a new segment with the new packet.

The annotation processor reads any new entry in the segment index table and compares it with its current data take request table. If the new data segment is recognized as a part of a requested data take, then its index will be inserted into the corresponding data take assembly table following the algorithm previously described. When all data have been received for a data take, the processor deletes redundant packets from the assembly table. The complete data take assembly table is then passed to the output processor. The other function of the annotation processor is to sort source packets that are designated as real time from the packet processor and to pass them through for immediate output.

The output processor uses the data take assembly table and segment index table to assemble a data take. The first table specifies data pieces in the data take, and the

second table computes the addresses of these data pieces on the disk farm storage system. The data are transferred from the disk, block by block, to a local buffer, then from the local buffer to the output port. In this way, the data can be selectively output, e.g., to delete redundant data. If the data segment to be output contains playback data, i.e., all packets in that segment are in reversed time order, the output processor restores the order simply by transferring the last-received packet first and the first-received packet last. Furthermore, the output processor generates data take annotations and attaches them to the data takes as either headers or trailers. If requested, the packet annotations can also be output along with corresponding packets.

The mass storage requirements for the prototype data take processor include sustained transfer rates above 100 Mbps, random-access storage up to 45 Gbytes, and multi-read-write ports. These requirements are minimal, however, when compared to the potential expected rates of up to 300 Mbps and storage capacity beyond 100 Gbytes.

Only a few years ago, storage systems that could support these requirements were either not available or very expensive, one-of-a-kind, research tools. Today, a number of vendors offer systems which will (or soon will) meet these high-performance requirements. These systems use parallel disk arrays, "disk farms," to achieve various combinations of high speed, density, flexibility, and reliability. The third figure outlines the block diagram and some of the basic requirements and characteristics expected from state-of-the-art parallel disk controllers/systems and the type of functional and performance required for the prototype LZP system. The term kernel refers to a basic multiple-disk-farm configuration.

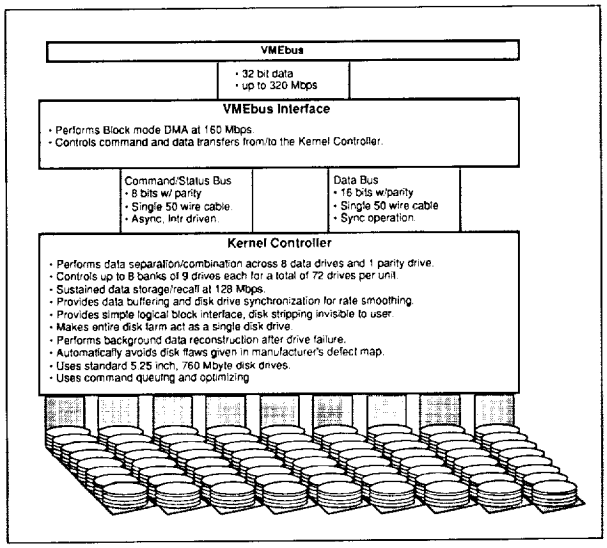

Basic storage kernel needed for the LZP system.

The single LZP system can handle up to 8 virtual channels and 24 sources with combined data volume of 15 Gbytes per orbit. For greater demands, multiple systems can be configured in parallel, each being called a processing channel and assigned a subset of virtual channels. The telemetry data stream can be steered into different processing channels in accordance of their virtual channel identification numbers. This super system can cope with a nearly unlimited number of virtual channels and sources.

The prototype architecture and implementation of a high-speed LZP system has been shown. Because of the new processing algorithm and VLSI technology, the prototype system features compact size, low cost, high processing throughput, easy maintainability, and increased reliability. Though extensive control functions have been done by hardware, the programmability of processing tasks makes it possible to adapt the system to different data formats and processing requirements.

Contact: Ward P. Horner (Code 521)
(301) 286-5804
Sponsor: Office of Space Operations

Mr. Ward P. Horner is Manager of the Data Storage Technology Division with 7 years' experience at Goddard. He earned a BSEET from Capitol College and received a NASA Group Achievement Award. Mr. Horner specializes in the design of multiprocessing hardware and software implementations. He manages, coordinates, and designs a variety of sophisticated hardware- and software-oriented projects.

A RULE-BASED SCHEDULING SYSTEM FOR INTERFERENCE MITIGATION IN SPACE COMMUNICATIONS

Projected increases in the number and data rates of user spacecraft supported by TDRSS in the S- and Ku-bands will result in congestion of the radiofrequency spectrum. Consequently, the space network must be concerned increasingly with the problem of mutual interference. While current techniques for interference

mitigation are adequate for scheduling under light loading scenarios, the concerns regarding mutual interference become more critical as the number of users increases and as their data rates exceed 150 Kbps.

Consideration of the effect of communications factors such as signal-to-interference ratio, link margins, and power received is beyond the scope of most current network scheduling systems. Usually, these schedulers preclude unacceptable mutual interference by avoiding overlapping communications contacts.

To avoid placing severe restrictions on network and user resources, scheduling systems must consider all relevant communications parameters. Therefore, a prototype rule-based interference mitigation schedule (IMS) is under development for the space network. IMS is designed to produce schedules that are free of unacceptable mutual interference and that satisfy both generic and specific communications requirements of user spacecraft while minimizing space network and user restrictions.

The scheduler is under development for mission planning and interference analysis purposes at Goddard within Communications Link Analysis Simulations System (CLASS), which is a software tool for the prediction and evaluation of TDRSS-user spacecraft communications link performance.

IMS addresses two problems: scheduling and interference mitigation. It uses an iterative algorithm that selects event start times from allowed start time intervals. An allowed start time interval consists of the times at which an event may start as specified by a given user communications requirement. Within each such interval only the points represented by successive divisions of the interval by halves are considered.

The scheduling algorithm is described in terms of contacts, events, event times lines, and candidate schedules. A contact is a time interval during which a user spacecraft communications link with Tracking and Data Relay Satellite (TDRS) is active. An event is a combination of contacts specified in a user requirement and, typically, includes a forward link used for sending commands to the user spacecraft and a return link used for telemetry data from the user spacecraft. An event time line is a series of events (for example, one event per user spacecraft orbit) that will completely satisfy a given user requirement for the entire scheduling period, which typically will be 2 weeks. Finally, a candidate schedule is a set of event time lines that will satisfy all user requirements, and if found to be free of unacceptable interference, the candidate schedule will be identified as the final solution.

When the algorithm creates a new contact, it builds all of the events, event time lines, and candidate schedules that are possible, tests the candidate schedules, and then starts the process over again by creating a further new contact. When creating new contacts, IMS gives priority to any allowed start time at which unacceptable interference is found to occur between two events.

Interference mitigation in the present implementation is concerned with interference between pairs of user spacecraft. The heuristics presented below are based on the consideration of frequency separation, polarization isolation, pseudonoise coding isolation, signal-to-interference ratio, separation angle, and bit-error-rate margin degradation. Since interference between two forward links or between a return and a forward link is never a problem, the heuristics concern only interference between two return links.

The accompanying figure illustrates the heuristics employed for interference mitigation in IMS. These heuristics are shown in the form of a decision tree in which frequency band and polarization are used as early decision factors. If the users employ different frequency bands (S- and Ku-bands), then the heuristics stipulate that there is no unacceptable interference. If the users have frequency separation greater than 10 MHz, or if both are S-band multiple-access users with the same polarization, then again there is no unacceptable interference. If both are using Ku-band with the same polarization and any desired user channel is unspread or both users have total data rate greater than or equal to 48 Mbps, then the heuristics stipulate that there is definitely unacceptable interference. In all other cases, IMS performs an additional test to determine whether there is the possibility of unacceptable interference. This test calculates the signal-to-interference ratio and compares the result to two threshold values, 8 dB and 12 dB. If signal-to-interference ratio is less than 8 dB, then interference is definitely unacceptable. If signal-to-interference is at least 12 dB, then interference is definitely acceptable.

In the acceptable case, the signal-to-interference calculation assumes the signal level for the desired user is the maximum power received at TDRS (minimum range from TDRS), and the signal level for the interferer is the minimum power received at TDRS

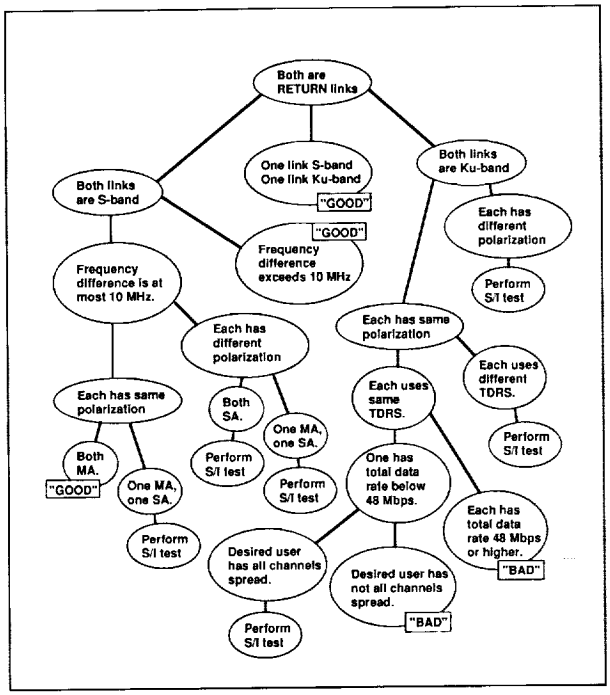

Interference mitigation heuristics.

(maximum range from TDRS). In the unacceptable case, the reverse is assumed.

IMS adjusts these signal-to-interference ratio values to account for additional factors, such as pseudonoise coding gain (if the desired user is pseudonoise spread) and polarization isolation (if different polarizations are used). An additional adjustment to the signal-to-interference ratio compensates for the loss of interfering signal strength at the desired user's TDRS when the interferer's antenna is pointing toward a different TDRS.

If the calculated signal-to-interference ratio falls between the two threshold values (8 dB and 12 dB), then IMS will compute the actual bit-error-rate margin degradation for the separation angle between the users as seen from TDRS. This computation represents the final basis for determination of interference at any point in time. The magnitude of the degradation allowed for acceptable interference is under study.

The above heuristics have been applied to the example case where the Hubble Space Telescope (HST) and the space shuttle compete for communications through TDRSS, each requiring 100-percent in-view coverage. Results show that one TDRS will not permit workable schedules to be generated due to interference on the shuttle S-band single-access 192-kbps return link from the HST's multiple-access 32-kbps return link. Future work with the IMS will be directed toward generating hypothetical schedules based on more than one TDRS with acceptable interference for these two users.

Contact: James L. Rash (Code 531)
(301) 286-3595
Yen F. Wong (Code 531)
(301) 286-7446

Sponsor: Telecommunication Systems Branch

Mr. James L. Rash is NASA's Principal Representative on the American National Standards Institute Accredited Standards Committee X3J14, which is developing a proposed standard for the computer language Forth. He also develops artificial intelligence applications in CLASS. Mr. Rash has been a planning committee member and editor for Goddard's annual conference on space applications of artificial intelligence for the past 2 years. He earned a Special Service Award in 1987 and received his MA in mathematics from the University of Texas.

Mr. Yen F. Wong is an electronics engineer working on CLASS in the Telecommunication Systems Branch. He is interested in signal processing, digital-data satellite communications, computer-aided modeling, and analysis of communications systems. Mr. Wong earned his MSEE from the City University of New York and has 5 years' experience at Goddard.

COMMUNICATIONS LINK ANALYSIS SIMULATIONS SYSTEM (CLASS) BIT-BY-BIT SIMULATION

An accurate simulation of a full communications link system through NASA's TDRSS has been designed and implemented in the CLASS environment. All impacts on the link are modeled in the system and considered in the analysis.

The system is operable in multiple configurations. Configuration is accomplished through the run control using either a full emulation modeling approach or the functional simulation approach. The essential concepts of the CLASS bit-by-bit simulation are illustrated in the accompanying diagram. The model is separated into three subsystems: (1) the Video Compression Unit and Video

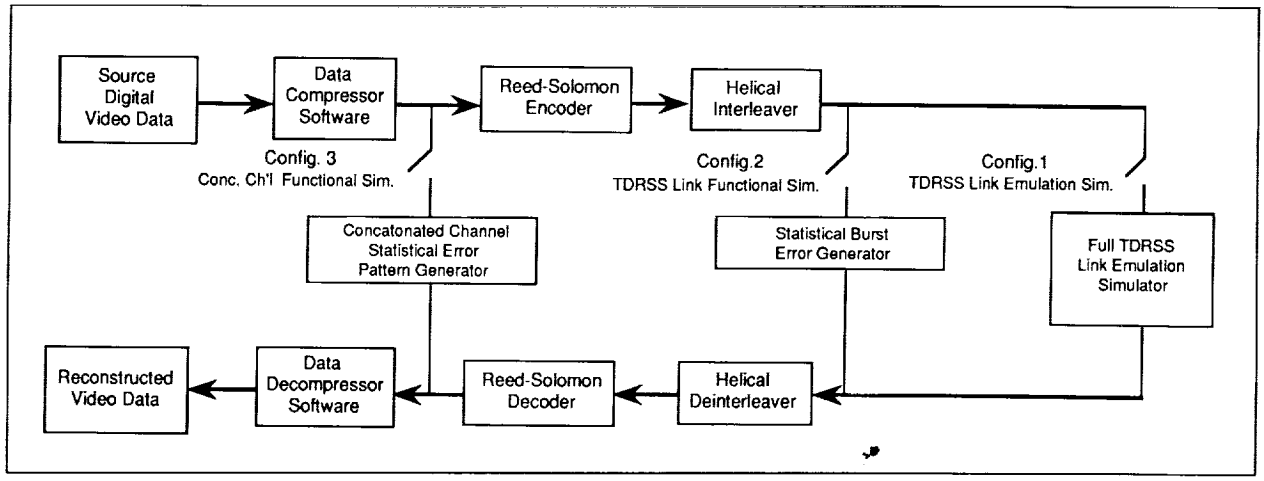

CLASS bit-by-bit simulator configuration diagram.

Reconstruction Unit; (2) the Reed-Solomon coder/encoder; (3) the TDRSS link.

Each subsystem is divided further into submodules where each of the hardware communications modules in the link is simulated separately and chained together to make the system extremely flexible. The data stream being analyzed is output at the completion of each module and used as input to the next to allow calculations of statistics at crucial points between submodules. These analytical statistics provide otherwise unobtainable information equivalent to hardware test results on the performance of each individually modeled hardware subsystem. Statistical data from each run are provided as plots, histograms, and tables. Statistics from different runs are plotted versus equivalent isotropically radiated power margin for each radiofrequency interference condition since radiofrequency interference is the major influencing factor on the link's performance.

The computational support for the CLASS bit-by-bit simulation is provided by software hosted on a Hewlett Packard 9000 computer, under a Unix operating system. The system includes a user-friendly interface provided by a Macintosh II.

At present this software is the first and only system available to NASA for processing representative user data bit-by-bit through the simulated TDRSS return link channel. This new capability allows prediction of channel performance through statistical characterizations of the data at the receiver, aiding in user communication system design. The Orbital Maneuvering Vehicle project at Marshall Space Flight Center is currently using this simulation system in designing its video communication system.

Contact: Nancy D. Smith (Code 531)
(301) 286-2218
Sponsor: Office of Space Operations

Ms. Nancy D. Smith, Deputy Project Manager of CLASS, is responsible for the design and configuration control of the project's operational system within the Telecommunications Systems Branch. She earned a BS in computer science from The Pennsylvania State University.

ATTITUDE HEADS-UP DISPLAY

Several operational graphics systems have been developed in the Flight Dynamics Division to present spacecraft attitude information in a more comprehensible and efficient manner. To date, the systems' displays have been in one of three formats: x-y plots, two-dimensional celestial projections, and three-dimensional spacecraft solid models. A new system, the Attitude Heads-Up Display, has been developed to present attitude data in a new format.

The system's concept is to present real-time spacecraft sensor and actuator data in a format similar to an aircraft instrument panel, as shown in the accompanying figure. An aircraft's instrument panel displays the current state of the plane's hardware and sensors, often with respect to safety ranges. This display system can be configured to display a spacecraft's hardware and sensor status with respect to its

Q-3

safety ranges. For instance, potentiometers provide a mechanism for displaying reaction wheel, gyro, magnetic torquer assembly, and three-axis magnetometer data in a manner that clearly states the correlation of data values to sensor or actuator limits. Color coding of the potentiometer bars as green (safe), yellow (caution), or red (unsafe) indicates the relationship of operation to possible hardware damage. Less complex instrumentation such as light-emitting diodes arranged in the same configuration as attitude control and orbit adjust thrusters provide a simple indication of thruster activity. Other instrumentation includes field-of-view windows to display celestial targets acquired by fixed-head star trackers and fine Sun sensors and an attitude-directional indicator to provide an overall feeling of spacecraft attitude and motion.

The heads-up display system is a distributed processing system. Real-time spacecraft data are retrieved, unpacked, and converted to engineering units on a National Advanced Systems 8063 mainframe computer executing the VM/MVS operating system. The data are then transmitted over an IBM 327x communications line to an IBM PC/AT compatible work station where it is displayed graphically.

Using the system's instrument displays, color coding, and additional text information, analysts can determine easily how a spacecraft, with its complement of sensor and actuators, is reacting during initial deployment, attitude maneuvers, sensor validation, and other day-to-day activities. The first heads-up display system has been developed to support the Gamma Ray Observatory (GRO) mission. The system is currently being upgraded to support additional spacecraft information.

Contact: James F. Jeletic (Code 552.2)
(301) 286-4244

Scott A. Greatorex (Code 554.1)
(301) 286-3082

Sponsor: Office of Space Operations

Mr. James F. Jeletic researches, develops, manages, and analyzes the flight dynamics computer graphics systems and other mission support software in the Advanced Technology Section. He holds a BSE in computer science and engineering from The University of Pennsylvania and has served at Goddard for 5 years.

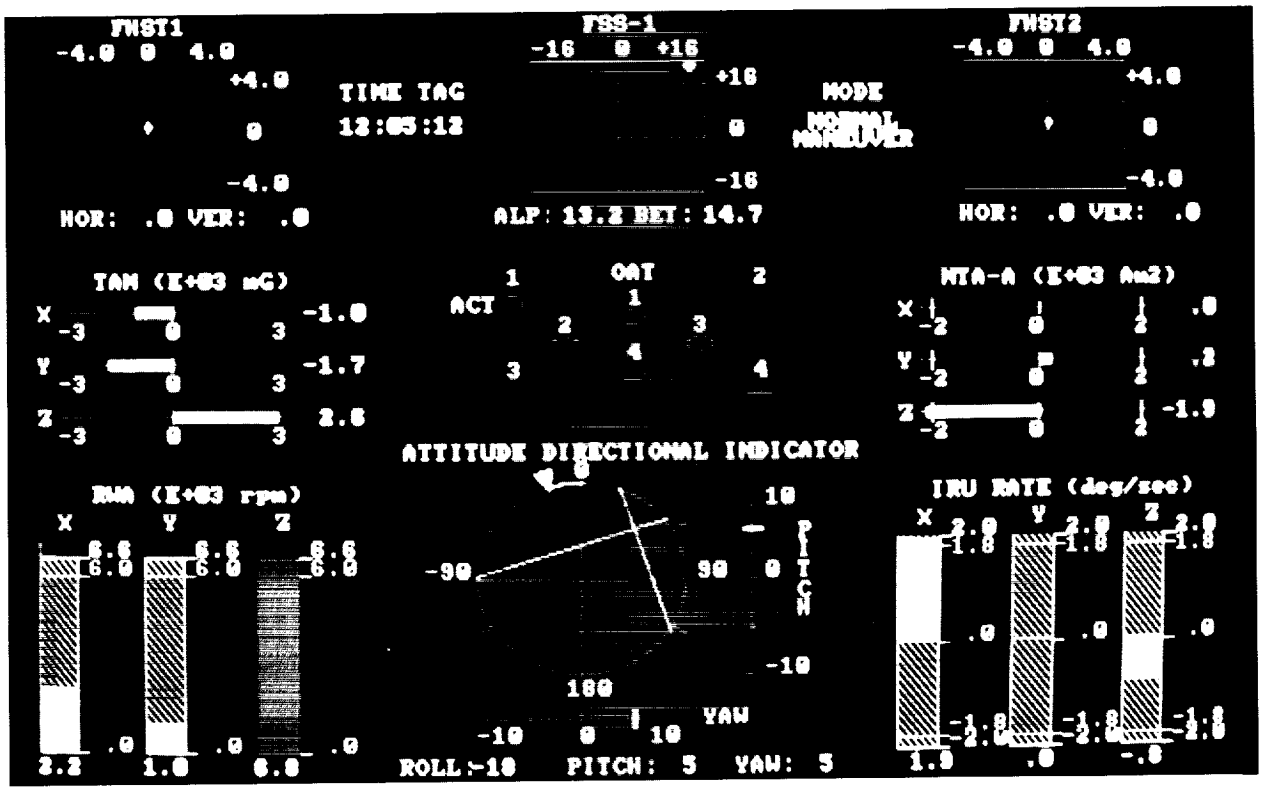

Attitude Heads-Up Display for GRO.

Mr. Scott A. Greatorex is the Attitude Computations Engineer for planning, coordinating, and implementing all Flight Dynamics Division mission-support activities for the GRO satellite. He holds a BS in aerospace engineering from the University of Maryland and has 9 years' experience at Goddard.

ADVANCED TELEMETRY PROCESSING TECHNOLOGY RESEARCH AND TECHNOLOGY OPERATING PLAN

The Advanced Telemetry Processing Technology Research and Technology Operating Plan will evaluate alternative approaches to high-data-rate packet telemetry processing for parallel and nonparallel computer architecture developments applicable to space-station-era data systems. This Research and Technology Operating Plan will study telemetry processing functions, higher levels of telemetry processing, and telemetry processing system architecture requirements. To evaluate alternative approaches to telemetry processing, computer architectures will be matched to high-data-rate telemetry processing requirements. Critical telemetry functions will be benchmarked, and computer architecture performance will be evaluated. Programming techniques, software conversion, and higher levels of telemetry processing will also be evaluated.

The accomplishments for fiscal year 1989 are the identification of telemetry processing functions for space-station-era data systems and the matching of computer architecture to high-data-rate telemetry processing requirements. The identification of telemetry processing functions was accomplished using requirements developed for LZP systems in the space station era. The development of system models, environmental and behavioral, and of a data dictionary for these processing requirements led to a system description independent of implementation considerations. The environmental model defines the external inputs and outputs to and from the system using a high-level context diagram. The behavioral model describes the transformations required to generate system outputs from external inputs using more detailed diagrams.

Three target space-station-era data systems ranging in throughput rates from 20 to 100 Mbps were defined to match processing functions to parallel and nonparallel computer architecture. These systems conform to the consultative committee for Space Data Systems Advanced Orbiting Systems Standards. Categories of parallel and nonparallel machines (e.g., von Neumann, Pipelined Vector Uniprocessor, Processor Array, Operand Driven, and Multiprocessor/Distributed) then were mapped to these data systems to determine the best types of computer architecture for the specific target telemetry processing system.

Contact: James A. Pritchard (Code 564)
(301) 286-7785

Sponsor: Office of Space Operations, NASA Headquarters

Mr. James A. Pritchard works on the development of the Customer Data and Operations System and the Advanced Orbiting System. He also directs research on the application of parallel processing techniques to telemetry processing systems. He earned a BSEE from the University of Tennessee and has won two Group Achievement Awards in his 23 years at Goddard.

SYSTEM AND SOFTWARE ENGINEERING

BACKUP CONTROL MODE ANALYSIS AND UTILITY SYSTEM (BCAUS): A SPACECRAFT DIAGNOSTIC SYSTEM USING EXPERT SYSTEMS AND NEURAL NETWORK TECHNOLOGY

BCAUS has been developed for use in the GRO control center to perform failure diagnosis for the Attitude Control and Determination (ACAD) subsystem. BCAUS combines a neural network component for telemetry trend analysis and an expert system component for diagnosis. Scheduled to become operational in early 1990, BCAUS is an expert system designed to assist flight operations personnel in diagnosing the cause of a spacecraft autonomous mode transition. The GRO spacecraft has been designed with onboard capability to autonomously make itself safe, transitioning from a primary operating mode to a backup control (safing) mode if

certain error conditions in the ACAD subsystem occur. Flight operations personnel need to understand what error condition triggered the onboard computer to order the mode transition and why that error condition occurred so that proper corrective action may be taken. While the number of mode transition triggers is small, potentially hundreds of underlying causes could affect these triggers. Thus, the task of diagnosing failures is not trivial and involves substantial expertise.

Since GRO will not be in contact with the ground for most of its orbit, it is expected that an autonomous mode transition, should one occur, would happen while the spacecraft is not in ground contact. Information relating to the transition, which would normally be telemetered in real time, will be recorded on one of the onboard tape recorders for playback later. Once received and processed, the tape-recorded telemetry is available through the Systems Test and Operations Language (STOL) interface, and BCAUS will access these data.

A combination of elements has been chosen to implement BCAUS: an expert system to encode the specific knowledge on ACAD failures and their causes, a neural network to perform trend analysis on the numerical output of the spacecraft sensors, and an executive to tie the two components together with processes to obtain telemetry data and provide a flexible user interface. The expert system was implemented using ART-IM, a commercially available software package, the neural network was built using another commercial package, NeuralWorks Professional II, and the remaining processes were written in C by a contractor.

The development of the operational version of BCAUS was preceded by extensive knowledge acquisition and construction of a prototype expert system. Experts from NASA and a contractor and operations personnel with several NASA contractors were interviewed about possible failures in the ACAD system and their manifestations in the spacecraft's telemetry output.

The flight operations user in the GRO Mission Operations Room will initiate BCAUS with parameters obtained from the real-time postmode-transition telemetry available from the spacecraft at contact. These parameters include the current ACAD operating mode, the type of mode transition, and the time of the mode transition. The BCAUS executive invokes the telemetry archive subsystem, which issues STOL and Recorder/Utility Processing System requests to obtain values of the specific telemetry mnemonics needed to make a diagnosis. The PC/386 microcomputer running BCAUS will use the control center work station terminal emulator functions to obtain and store required telemetry mnemonic values from the recorder/utility processing system through the STOL page interface.

The telemetry archiver stores all needed telemetry items (approximately 120 items) for the several-minute time period before and through mode transition. The number of samples to be processed for trending purposes depends on the selected duration and how often the data are expected to change for the particular telemetry item or type of item.

Once required telemetry data have been archived, the BCAUS executive initiates the trend-analysis subsystem of the BCAUS system. The trend-analysis subsystem characterizes the behavior of each required telemetry mnemonic by assigning a symbolic pattern classification to the individual mnemonics (e.g., a "rising" trend or a "falling" trend), using a neural network classifier.

To accomplish this, the trend-analysis subsystem reads the archived analog/digital telemetry values and provides these as input to a neural network. One neural network is expected for each type of analog-digital telemetry mnemonic to be analyzed. The neural network characterizes the input and produces output in the form of one or more behavior classifications, each with an associated probability.

The BCAUS trending-analysis subsystem uses a three-layer back-propagation neural network simulation with input, hidden, and output layers. Each layer has a number of simple processing elements, which accept one or more inputs and produce an output based on the application of a few simple arithmetic operations.

Each output layer processing element corresponds to a possible trend classification that may be output by the network. The number of possible trend classifications depends on how many behavior categories are judged by the diagnostic experts to be meaningful for that particular telemetry mnemonic.

Discrete bilevel telemetry values stored by the telemetry archive subsystem are read by the trend analysis subsystem, and any change in the state of the value is classified. The output of both the neural network-analyzed analog-digital values and the classified discrete

values are transformed to symbolic values acceptable to the diagnostic subsystem.

The symbolic values resulting from the trend analysis subsystem are input to the diagnostic subsystem. The BCAUS diagnostic subsystem reasons about possible spacecraft failures using an expert system. This component of the system compares the symptoms (symbolic values) to the known failure scenarios using stored knowledge to relate potential failures to specific symptoms. The diagnostic subsystem also receives as input from the operator any necessary supplementary information, such as the commanded state of the spacecraft. The diagnostic reasoning process results in the output of one or more possible failures that satisfactorily account for the observed symptoms, ranked from highest to lowest probability.

The expert system uses rules and schemas to perform the diagnostic reasoning. BCAUS uses schemas, which are framelike structures holding a collection of information, to encode the specific knowledge about GRO failures that may trigger autonomous mode transitions. Approximately 160 failure schemas are in the current BCAUS expert system knowledge base. Rules are used in the diagnostic knowledge base to direct how the system reasons about the information provided in the failure schemas. The rule base consists of approximately 20 rules, most of which provide options for user queries of system results.

The user interface subsystem obtains information from the user at the time of system initiation and, if necessary, during the diagnostic process. The user interface function also controls the format and display of system results and responds to user queries about system functioning. This interface is designed to be both graphical and textual in nature. At the present time, the user interface is restricted to textual output; graphical additions are planned as a future enhancement. These additions include graphs of the telemetry trend analysis and depictions of functional block diagrams of pertinent GRO subsystems labeled with telemetry mnemonics. Also shown are samples of the textual windows used by the current system for user communications.

Contact: Daniel J. Mandl (Code 511)
(301) 286-4323
Steven J. Weaver, Computer Sciences Corporation (Code 511)
(301) 497-2551
Joy L. Bush, Computer Sciences Corporation (Code 511)
(301) 497-2586
Douglas Carlton, Computer Sciences Corporation (Code 511)
(301) 497-2529

Sponsor: Office of Aeronautics & Space Technology (OAST)

Mr. Daniel J. Mandl works in the Control Center Systems Branch. He received a BS in electrical engineering from the University of Maryland and has 9 years' experience with Goddard.

Mr. Steven J. Weaver is a developer of the spacecraft diagnostic system. His technical interests include working with expert systems and neural networks. He holds a BS in information systems management.

Ms. Joy L. Bush develops and enhances the spacecraft diagnostic system described in this article. Her professional interests center on expert systems and neural networks. She holds one MS in anthropology and another in computer science.

Mr. Douglas Carlton is Department Manager of Research and Development for the Control Systems Technology Group at Computer Sciences Corporation. His primary technical interests lie in computer graphics and expert systems. He holds a BS in mechanical engineering and has 8 years' experience at Goddard.

WILDCARD DISPLAY CREATOR (WDC) PROTOTYPE

The Multi-Satellite Operations Control Center is a multimission facility that provides Payload Operations Control Center support functions for the launch and on-orbit operations of various scientific satellites. The Payload Operations Control Center contains the equipment, software, and personnel needed to evaluate and control the performance of spacecraft payloads. Its primary concern is the health and safety of the spacecraft.

The Multi-Satellite Operations Control Center provides hardware and software facilities for the operations of a variety of different satellites. A generic test and operations language forms the interface between the operator and the Multi-Satellite Operations Control Center software. Using this language, the user can obtain status information

and command the control center software and, indirectly, the satellite. Each mission that uses the control center develops its own specializations of the generic STOL. One of the capabilities provided is the ability to define a wild-card display page to be called up on an operator's console by the STOL FORMAT directive.

A wild-card display page definition consists of a series of directives in a STOL procedure. Only a few people possess the skill to use the FORMAT directive effectively; successful creation of a display page usually requires a trial-and-error approach. The present project, the WDC, provides a window-oriented editor to permit the easy generation of display page formats and the automatic generation of directives to define them. The project is an outgrowth of a previous project (the Jargon Interpreter), which investigated the feasibility of using natural language in the interface, and the WDC project uses tools that were generated for the earlier effort.

The WDC allows wild-card pages to be seen in their true format as they are designed. It is intended to lessen the user's need to use the display page creation portion of FORMAT directive. Building wild-card display pages requires minimal knowledge of the language and no knowledge of the directive. Pages built with the WDC are automatically translated into the STOL procedures containing FORMAT directives. Conversely, STOL procedures containing FORMAT directives are automatically translated into internal form.

The WDC is built on a Macintosh II using the Allegro Common Lisp or CL package. The prototype uses the Toolbox for low-level graphics and editing operations. Access to these low-level functions is a feature of Allegro CL. The programmers expended considerable effort on making the user interface compatible with standard Macintosh user interface guidelines. The conversion between the WDC's internal representation and STOL is performed by an inference engine written in CL during the prior Jargon Interpreter project. In this forward-chaining inference engine, rules can invoke Lisp functions to perform actions with side effects such as the creation and interpretation of the internal representation of display page text and mnemonics. This approach results in a very flexible separation of effort into those parts that are appropriate for a rule-based approach and those that are best performed procedurally. Rules are grouped into contexts so that the inference process does not need to consider irrelevant rules. The

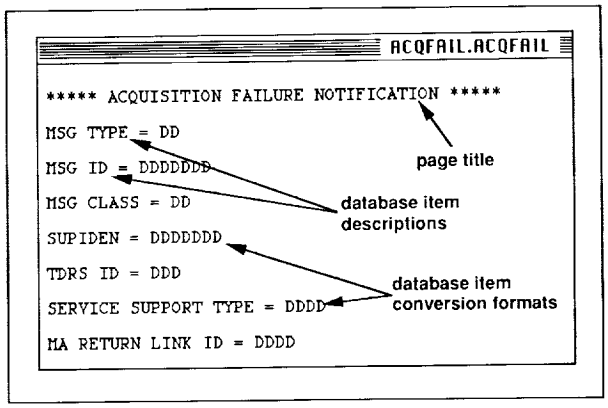

WDC edit window.

translation from STOL into internal form uses approximately 25 rules in 3 contexts and several Lisp functions that deal with the representation details. The inverse translation uses five rules in four contexts.

In the editing process, the user simply types in fixed text and mnemonic names at any positions desired within the window, whose size defaults to the exact number of lines and columns available on the screens. To specify a conversion format for a mnemonic, the user highlights the mnemonic's name in the window and selects the Change Mnemonic menu item. This selection presents the user with a Macintosh-style dialog box from which the desired conversion and format parameters can be selected. The selection is immediately reflected in the editing window. Once conversion parameters have been selected, they can be applied repeatedly without using the menu. Changes can be made to the window using the usual cut/copy/paste operations of any Macintosh application. The WDC constrains these operations so they do not disrupt a mnemonic's display fields. The flexible symbolic processing provided by Lisp allows the user to manipulate the screen while the WDC handles the semantic differences between text and mnemonics and controls their display using the Macintosh Toolbox as much as possible.

The first figure shows a sample editing window on the Macintosh (with annotation). Data base items are shown as a schematic representation of their display formats, uppercase "D" in this example. The format is represented on the screen in the same number of characters that will be displayed on the consoles, allowing the user to see exactly how the screen will appear and to move the text around for the most effective use of the screen area.

The second figure shows the corresponding STOL directives that define the window for interpretation on the applications processor, as created by the WDC translator. Although the user will usually not be concerned with this representation, it is shown as an example of the syntax of the FORMAT directive. It is also possible to start from this representation and translate it into the display page format shown in the first figure. Therefore, a user can start from a previously defined page and make changes to it (in a copy-and-edit style), rather than creating a new page each time. Because many displays are related and contain similar information, this facility can save a great deal of labor.

The third figure shows the layout of the page defined in the first and second figures as it would appear on the applications processor.

The WDC allows multiple procedures and display pages to be opened for editing to simplify cutting and pasting parts of one or more existing pages into a new page. The window control is based on the Object Lisp extensions to CL provided by the Allegro CL package. This object-oriented package simplifies the definition of the various interface elements that the user sees, such as dialog boxes and menus. Most of the dialog boxes are created as they are needed. Allegro CL provides many object classes for the buttons and text items that appear in the dialogs and handles their memory management. In addition, the editing windows that the WDC uses are defined as specializations of an Allegro-provided class. Thus, they inherit the standard Macintosh features of resizing, moving, zooming, and many others that are invisible to the user. Specialized features such as selecting mnemonics are added as new behavior on top of the inherited behavior of standard windows. This object-oriented approach vastly simplified the programming after the initial learning period. Another tremendously useful effect of using Lisp for the implementation was the automatic incremental compilation of individual functions. This process made prototype building very easy; several approaches could be tried and their merits evaluated in the time that more traditional languages would allow for only one approach to be designed, coded, and debugged. In the highly interactive area of user interface design, the value of this capability cannot be stressed too much.

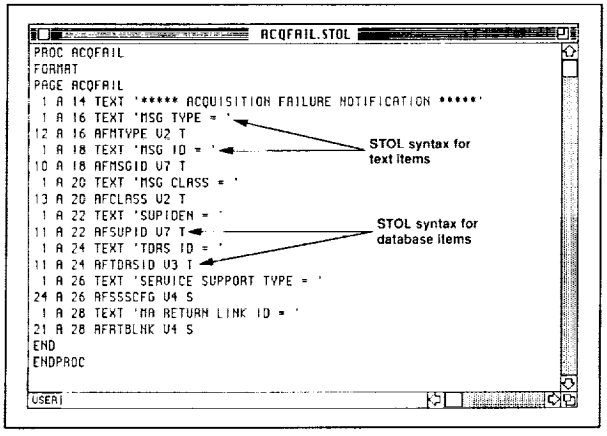

STOL procedure for WCD page "ACQFAIL."

The WDC is a functioning prototype and can be used to generate display pages as described above. It has not yet been integrated with the rest of the Multi-Satellite Operations Control Center installation. Currently it obtains the STOL version of existing pages by a cumbersome process of transferring floppy disks between the control center work stations and a single personal computer that is on a TOPS network with the Macintosh. The ultimate goals are to allow the Macintosh to transfer files more directly with the Multi-Satellite Operations Control Center applications processors and to use this capability on multiple platforms; at present it is available only on a single Macintosh, which must be shared by those who wish to use it. Nonetheless, the prototype has successfully demonstrated the merging of several different techniques in an integrated advanced user interface.*

**Brenda Page and Joe Maynard of UNISYS Corporation contributed to the development of WDC.*

Contact: Henry L. Murray (Code 511)
(301) 286-6149

Michael Blackstone, UNISYS
Corporation (Code 511)
(301) 731-0022

Sponsor: OAST

Mr. Henry L. Murray is Section Head for the Software Systems Section in the Central Center Systems Branch. He currently designs and implements spacecraft control centers. His main technical interests focus on computer graphics and artificial intelligence. He has 18 years' experience at Goddard and received an MS in engineering administration from George Washington University.

Mr. Michael Blackstone assists in the transition of the WDC to operational use in the Multi-Satellite Operations

```
PAGE    COMPLETE

GRO ;ACQFAIL ;G; 114/09/22/36.815;0 00123;S TDE;F 037;FMT I-SCI;SRC R/T;AP 7
***** ACQUISITION FAILURE NOTIFICATION *****
MSG TYPE = 92
MSG ID = 0000001
MSG CLASS = 63
SUPIDEN = A4625MS
TDRS ID = TDE
SERVICE SUPPORT TYPE = SSA1
MA RETURN LINK ID =
```

WCD page as it would appear on the applications processor.

Control Center and evaluates potential new applications in the Software Systems Section. He has worked at Goddard for 12 years and holds an MS in physics from the University of New Hampshire.

MODULAR ENVIRONMENT FOR DATA SYSTEMS (MEDS)

The systems designed, built, and programmed in Goddard's Data Systems Technology Division all have a similar pipelined, multiprocessor, dual bus hardware architecture as a platform on which to build applications-specific hardware. When application programmers design software for such a system, many questions need to be answered. What data and parameters will each processor need to accomplish its job? How will the processors communicate with each other and with the operator? How can the total job be subdivided into tasks? On which processors will they run? What data and parameters will each task need to accomplish its job? How will each task get data? MEDS was developed to help answer these questions and give an application programmer a starting point for designing a system based on the standard hardware platform.

MEDS is designed as a general-purpose software platform that is expanded and customized by application programmers to suit their particular requirements. It supports the basic software functions needed in all systems—namely, the ability to set up application-specific hardware and software, process the telemetry data based on the setup parameters, monitor the processing, and supply network support for remote operator interface and data transfer. This environment supplies an infrastructure to pass data between systems, processors, and tasks as well as to provide support for operator interface development. A complete system is built by adding custom to the general-purpose MEDS code. Therefore, MEDS spares the application developer the burden of creating an infrastructure for each new system and adds consistency in all system design, implementation, and maintenance.

A MEDS-based system unites and manages the data system's standard multiple-processor hardware platform. The processors are organized as a single master processor directing multiple subordinate application-specific custom cards. (See the accompanying figure.) The master processor is the single point of control within the system; it interfaces with the operator, on either a local terminal or a remote work station. Using a set of operator-defined setup files, the master processor will initialize the custom cards and monitor their processing on various status pages. Telemetry data may enter as well as exit the system via the remote interface. In any case, it is the pipeline of custom cards that actually processes the telemetry data.

The MEDS software resides mainly on the master processor with cooperating software running on each custom card. The basic functions include—

- Setting up the system and subsystems for processing (e.g., set up VLSI chip registers).
- Controlling the application-specific processing (e.g., enable, disable, reset a card).
- Monitoring the system and subsystems (e.g., gather and display card processing status).
- Streaming data transfer over the network (e.g., transfer telemetry data to/from a work station).

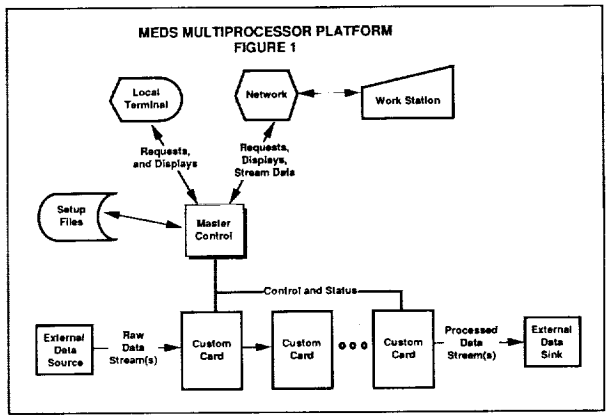

The MEDS multiprocessor platform provides a base on which to build application-specific software.

A MEDS-based system is a group of cooperating tasks built on these software packages. The tasks are spread across the processors of the system and are tightly coupled on the bus and loosely coupled on a network between the rack and remote work station. Some of the packages exist as linkable libraries that the programmer will use to build a task, such as a command handler. Other packages exist as customizable source code files, where the applications programmer will copy the source file, add in an application-specific code, and compile, for example, a status task. In all cases, the programmer does not need to know the details of the environment code; he needs only to interface to it. All processors in the system run in a real-time, multitasking operating system. MEDS software is written in C and assembler for interrupt handlers.

The need for this software platform was apparent from the outset in working with telemetry systems. Therefore, much effort was put into making every element of the first system general purpose. These elements are evolving constantly. Goddard researchers will attempt further to generalize and enhance the designs of the hardware and software platforms and make them more functional in each revision. The results are found in time, effort, and money saved on current and future system development and system modification. It took 3 years to develop the first system from the application specific integrated circuits to the operator interface. More complex systems, however, are being planned for next year. These systems could not be completed as scheduled without MEDS.

Contact: Stephen Sabia (Code 520)
(301) 286-7951

Sponsor: Flight Systems Division, Space Physics Division

Mr. Stephen Sabia, who started at Goddard as a cooperative student in 1983, works on real-time telemetry data capture systems software, usually done in the C programming language. Mr. Sabia is interested in hardware-software interface, and he is currently pursuing an MS through the Applied Physics Laboratory of Johns Hopkins University.

TRANSPORTABLE APPLICATIONS ENVIRONMENT (TAE)

TAE made significant technical advances in 1989. Several major new functions and enhancements were added to the TAE Plus software to improve its capabilities and utility as a user interface development tool.

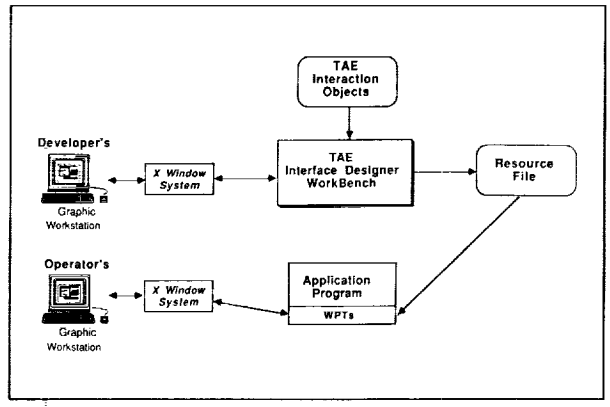

TAE Plus structure.

TAE Plus is a tool for designing, building, and tailoring an application's user interface and for controlling the designed user interface throughout the application's execution. The main component of TAE Plus is a what-you-see-is-what-you-get user interface designer's WorkBench that allows an application developer to interactively construct the look and feel of an application screen by arranging and manipulating interaction objects (radio buttons, menus, icons, gauges, dials, etc.). As a designer tool, it also provides the capability to define connections between interaction objects dynamically, rehearse the designed user interface, and generate fully annotated and operational code which will display and manage the entire WorkBench-designed user interface.

Once the application's screen has been designed, the WorkBench saves the user interface details in a resource file. TAE Plus includes runtime services, Window Programming Tools that are used by application programs to display and control the user interfaces designed with the WorkBench. Because the runtime services access the resource file during execution, the user interface details remain independent from the application code, allowing changes to be made easily to the look and feel of an application without recompiling or relinking the software. To change the user interface, the designer returns to the WorkBench and dynamically makes the modifications; the resource files are automatically updated. The next time the application is run, the modifications will be in effect. The first figure illustrates the TAE Plus structure.

In addition to providing the Window Programming Tool runtime subroutines, TAE Plus also offers control of interaction from the interpreted TAE Command Language. This capability provides an extremely powerful means to

quickly prototype an application's use of TAE Plus interaction objects and add programming logic without the requirement to compile or link.

During 1989, the following significant features were added to the TAE Plus software:

- The WorkBench was "human factored," giving it a new look and making it easier to use. The second and third figures show the WorkBench main menu and an item (i.e., interaction object) specification window.
- The software was upgraded to use the latest X Window System release (X11R3) and the X Toolkit layer with its "widget" architecture. This improvement included rewriting the Window Programming Tools in the C++ language.
- A new type of interaction object, a Data-Driven Object, was added to the WorkBench. This is a real-time graphic object that has been "connected" to an application data variable. Elements of the Data-Driven Object change as the application data value changes. The WorkBench provides a drawing tool to enable the designer to draw the static background and dynamic foreground of the Data-Driven Object. The types supported currently include rotators, stretchers, sliders, discretes, text, and strip charts.
- Ada and FORTRAN were added as options to the WorkBench's source code generation capability. (C and TAE Command Language were the original code generators supported.)

The WorkBench and the Window Programming Tools are written in the object-oriented C++ programming language and use the X Window System as the underlying windowing standard. Stanford University's drawing utility, *idraw*, which is a sophisticated direct manipulation C++ application, is integrated into the WorkBench to provide the tool for drawing the Data-Driven Object. The employment of these "state-of-the-art" technologies enables Goddard programmers to evaluate and understand the applicability of object-oriented programming to the user interface management environment and to analyze portability issues.

Each year the transportable element of TAE becomes more evident as the number of computers operating TAE continues to grow. TAE Classic [i.e., the original TAE developed for user interface support on American Standard Code for Information Interchange (ASCII) terminals] is currently available for VAX/VMS, VAXStation II/GPX/VMS; VAX/Ultrix; Sun/Unix; Gould/Unix; ISI/Unix; Jupiter/Unix; Apollo/Unix; CDC/Unix; HP9000/Unix; AT&T/Unix and Altos/Unix. In 1989, a port to the IBM VM/CMS environment was successfully completed.

The base development of the graphic-oriented TAE Plus software is being done on a Sun work station under Unix. TAE Plus is also operating on the Apollo/Unix, VAXStation II/Ultrix, DECStation 3100/Ultrix, Macintosh II under A/UX, HP/Unix, IBM PS/2 with AIX, Masscomp/Unix, and IBM RT/AIX. A port to the VAX/VMS environment was completed in fall 1989.

TAE Plus popularity continued to grow in 1989. Currently, there are over 470 TAE installations, of which 300 are TAE Plus sites. Applications cover a wide range of disciplines such as operations, simulation, production systems, network management, real-time command and control, planning and scheduling, data base management, image processing, science analysis/services, prototyping activities, and office automation. Users include NASA centers and contractors, the Department of Defense, other government agencies [e.g., National Library of Medicine, Earth Resources Observation System Data Center, National Institute of Standards and Technology (NIST)], universities (e.g., University of Colorado, Duke University, California Institute of Technology, Georgia Institute of Technology), and private companies. In 1989, two successful user workshops were held at Goddard, providing an excellent exchange of ideas between the end users and the TAE Plus developers.

The current TAE Plus provides a powerful and needed tool for the continuum of software engineering—from the initial design phases of a highly interactive prototype to the fully operational application package. However, a long list of enhancements and new capabilities will be

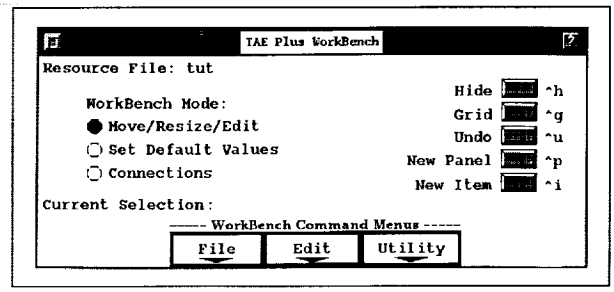

WorkBench main menu.

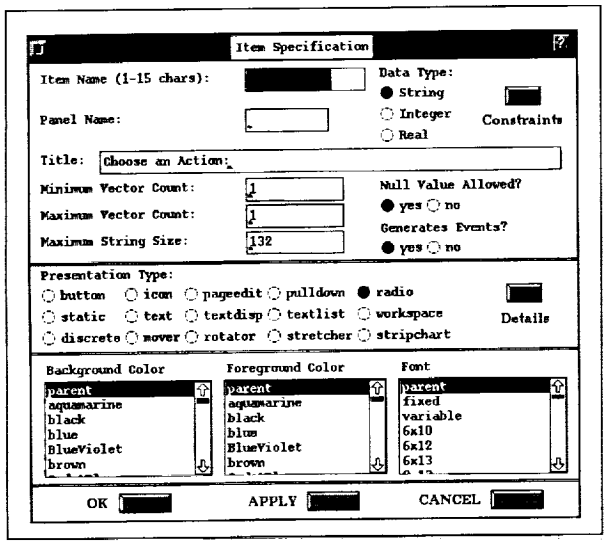

Item (interaction object) specification window.

added to TAE Plus in future releases. New features include extensions to the interaction objects, particularly in the data-driven object category; integration with the Open Software Foundation's Motif user interface style; ports to new work station platforms; on-line tutorial and training tools; introduction of hypermedia technology; integration of expert system technology to aid in making user interface design decisions; and implementation of additional user interface designer tools, such as a what-you-see-is-what-you-get graph builder.

TAE Plus is an evolving system and its development continues to be guided by user-defined requirements. To date, each phase of TAE Plus' evolution has taken into account advances in virtual operating systems, human factors research, command language design, standardization efforts, and software portability. With TAE Plus flexibility and functionality, Goddard designers believe it can contribute to more advances and more standardization in user interface development system technology.

Contact: Martha R. Szczur (Code 522)
(301) 286-8609

Sponsors: Office of Space Operations and Office of Space Science and Applications

Ms. Martha R. Szczur, who received a BS in mathematics from Converse College, is Manager of the TAE project. Her professional interests center on user interface issues, emphasizing human factors, designer support tools, and common, standardized interfaces.

SPACELAB OUTPUT PROCESSING SYSTEM (SOPS)

Recently Goddard's Data Systems Technology Division and Information Processing Division initiated a cooperative effort to build an expert system that can support the data-accounting and quality-assurance functions of the SOPS.

The objectives of this project were the following:

- To distribute domain expertise among less experienced quality assurance analysts.
- To automate routing aspects of the analyst's task.
- To support expert system technology transfer within the Mission Operations and Data Systems Directorate.
- To demonstrate the capabilities and limitations of an operational expert system in the SOPS environment.
- To establish the direction of future work to achieve a higher level of automation in the system environment.
- To have an operational expert system in place for the Astronomy-1 mission scheduled for 1990.

The extremely large volume of data from one mission to another and the short turnaround requirement for delivery to users make the data-accounting and quality-assurance task both demanding and tedious. A quality assurance analyst must combine information on various summary reports and processing logs to determine the quality of data. Based on this information, the analyst must then isolate problems and select the appropriate course of action: either to accept the data as the best possible or to request that the data be reprocessed. The expert system, acting as an advisor, will greatly decrease the physical demands upon operations personnel, without diminishing the high productivity and quality standards SOPS has consistently maintained. Another benefit provided by the expert system is utility as a training tool. The expert system allows a relatively inexperienced analyst to step through the logic of the expert system and obtain explanations for each decision made. The expertise of experienced staff members is captured within the expert system and available when needed.

The operational expert system runs on a Sun 3 work station in the SOPS environment. A network interface

exists between the data-processing computer, a UNIVAC 1100/82, and the Sun work station to transfer data quality information for the expert system analysis between system components.

The expert system tool, CLIPS—C Language Integrated Production System—a forward chaining rule language, was selected to develop the expert system. This language was developed by the Artificial Intelligence Section at NASA/Johnson Space Center. The commercially available object-oriented language Objective-C, was chosen for the interface software. Objective-C is the C language extended with a number of new syntactic features; it retains the compatibility of C, but provides the reusability and productivity of an object-oriented programming language.

During project development, developers have identified ways to further automate current procedures, to increase accessibility to data, to improve processing speed, and to decrease the monotony of repetitious tasks. The expert system project, in conjunction with other projects in the Spacelab Data Processing Facility, takes a first step toward Goddard's future data-processing challenges.

Contact: Angelita C. Kelly (Code 564)
(301) 286-3660
Lisa Basile (Code 564.2)
(301) 286-2771
Troy J. Ames (Code 522.3)
(301) 286-5673

Sponsor: Office of Space Operations

Ms. Angelita C. Kelly, Project Manager for the Spacelab Data Processing Facility, has 16 years' experience at Goddard. Her primary technical interests include development of a real-time data transmission system for the space station era. Ms. Kelly has won many NASA awards, including three Special Achievement Awards and an Exceptional Service Medal.

Ms. Lisa Basile is Technical Officer for several software development and maintenance tasks within the Space Lab Data Processing Facility, including the SOPS expert system. Ms. Basile has 5 years' experience at Goddard and holds a BA in computer science.

Mr. Troy J. Ames performs research and development in advanced technologies concerning artificial intelligence and human factors. He has been at Goddard for 5 years and currently works in the Automation Technology Section. He holds a BS in computer science and another in mathematics.

DISTRIBUTED ARTIFICIAL INTELLIGENCE CONTROL CENTER ENVIRONMENTS

Automation of control center operational systems is currently realized through application of single expert systems to support individual subsystem functions. State-of-the-art research in artificial intelligence and the cognitive sciences now considers that this one-to-one mapping between system function and automating agent is an extremely inappropriate paradigm, which will have limited usefulness as system complexities increase. What is needed to support higher levels of automation in such systems is the use of multiple autonomous agents cooperatively supporting desired system behaviors. This cooperation is the long-term solution to the problem of providing operational knowledge-based spacecraft control centers of the future. Goddard researchers have begun work in the areas of knowledge-base management and formal models of cooperation among knowledge-base agents to support this evaluation to an intelligent control center. Also, the researchers have established a testbed for demonstrating distributed knowledge-base technologies in a spacecraft command/control environment.

The basic drivers for the knowledge-base management system research are the expectations that future autonomous systems used in operational control centers will be both knowledge and data based, distributed yet cooperating and integrated, potentially large scale and long lived and needing to be maintained and updated regularly. A knowledge-base management system is intended to support these drivers. The first figure illustrates the current version of the system's reference model in development. The purpose of the model is to help identify the major concepts associated with knowledge-base management and to put these concepts in proper perspective.

The work on the formal modeling of autonomous agents is intended to assist in the planning, specification, development, and verification of control centers involving distributed cooperating knowledge-base systems. The current model describes a community of cooperating rule-based systems at four layers of increasing capability: (1) communication agents, with no assumption of intelligence or rule-based capability; (2) belief-sharing knowledge sources, where a knowledge source is an agent specializing in a specific domain and a belief is any data arrived at through an inference process; (3)

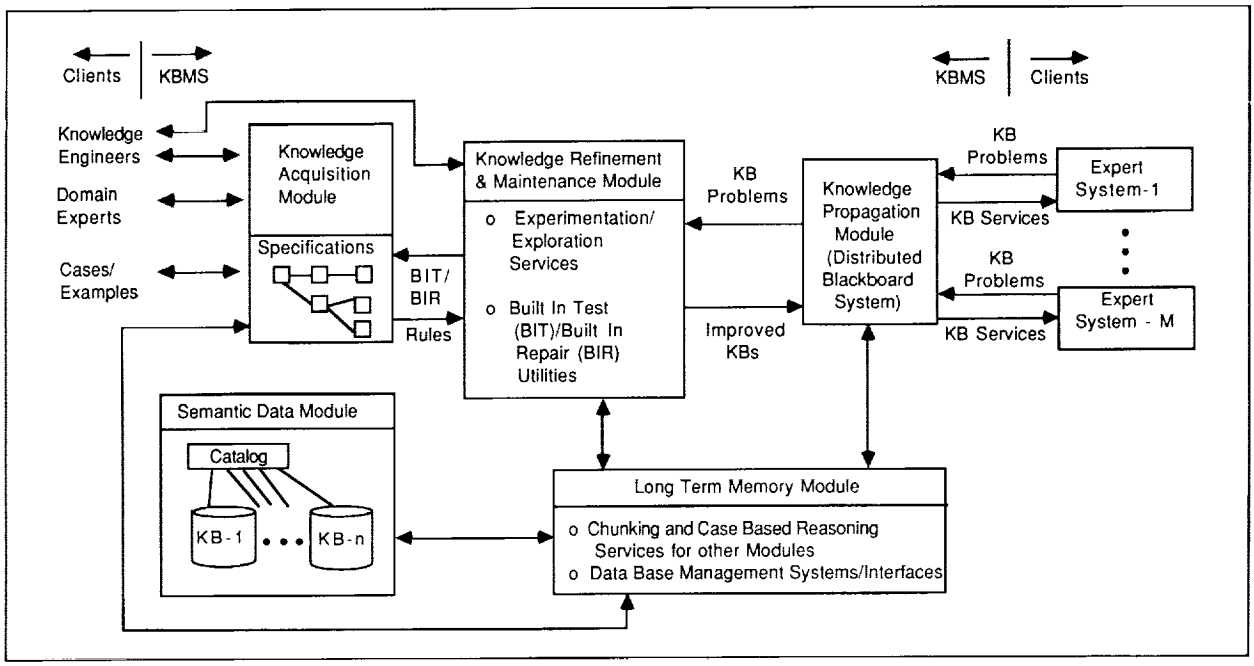

Overview of the reference model for the knowledge-base management system.

goal-sharing interest areas, where the first indications of goal-directed reasoning appear; and (4) task-sharing job roles, the fourth level of the model where overall system goals are decomposed into tasks which are allocated among various job roles. At this final level, cooperation is most fully achieved.

The results of these two research activities have been combined to support the development and operation of a distributed knowledge-base testbed. This testbed, depicted in the second figure, currently incorporates three expert systems, a spacecraft simulator, and a user interface module. This initial testbed is designed to demonstrate and test preliminary ideas and concepts that derive from the knowledge-base management system and modeling work and that are considered to be important for supporting advanced knowledge-base automation in future control centers. These concepts include communication among agents, information fusion, knowledge acquisition and refinement, information synthesis and presentation to external agents, model-based reasoning, and various levels of cooperative activity. This initial testbed is currently running in the Data Systems Technology Laboratory in Code 520. One of the major activities in the coming year will be to exercise operational scenarios to gain a quantitative insight into the behavior of multiple knowledge-base systems engaged in cooperative activity. The results from these experiments will be used to fine-tune the operational aspects of the emerging technologies. Additionally, the testbed will be refined to include more and higher levels of automation and realize a greater fidelity to operational control center functionality. Technology infusions from this testbed into truly operational environments will be accomplished as soon as possible.

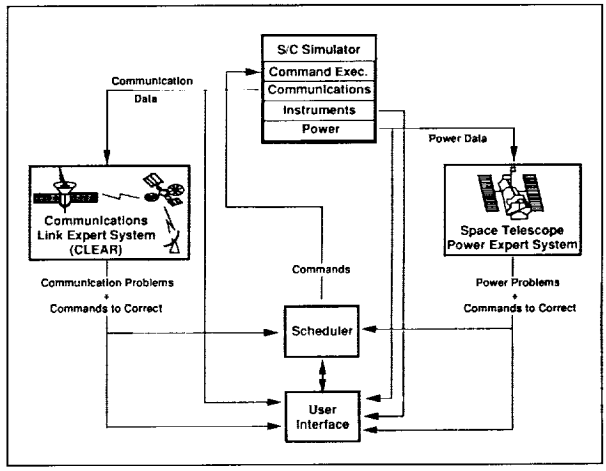

Testbed configuration for the distributed knowledge base.

Contact: Walter F. Truszkowski (Code 522.3)
(301) 286-8821
Sponsor: OAST

Mr. Walter F. Truszkowski, Head of the Automation Technology Section, holds degrees in mathematics and computer science. His professional interests include the cognitive aspects of human-machine systems, artificial intelligence, and approaches to information exchange.

EXPERT SYSTEM DEVELOPMENT METHODOLOGY

Expert System Development Methodology provides a solution to the problem of developing software that simulates the way human experts solve problems using rules of thumb, or heuristics. To develop an expert system, analysts must first acquire information from the human expert about how tasks are performed and then model the expert's reasoning capabilities in a form compatible with computers. This methodology addresses this issue of risk and acquires the data needed in an evolutionary fashion. The methodology presents a life cycle in which a prototype evolves through five stages of development. Each stage consists of five steps leading to a prototype for that stage. Development may proceed to a conventional development methodology at any time if enough has been learned about the problem to write requirements. Expert System Development Methodology drives out requirements so that a product may be built with a conventional development methodology.

This methodology is intended to be applied to the development of Goddard expert systems. It is based on a survey of existing methodologies, experience in developing a number of expert systems at Goddard, and an analysis of the expert system life cycle. A risk-driven methodology for conventional system development was introduced by Dr. Barry W. Boehm in his spiral model for software development. Expert System Development Methodology, while independently generated, is also a risk-driven methodology, which can be represented by a spiral model with the focus on knowledge acquisition as opposed to product development. The model is shown in the accompanying figure.

The methodology is comprised of a series of decisions that guide development. A metric, the test for application of risk-oriented technology, assists both managers and developers at each of these decision points. The methodology begins with an evaluation of the suitability of an expert system solution and an estimation of the risk involved. If the problem is a suitable candidate for an expert system, then work proceeds through the five stages of the methodology. Development does not proceed through all five stages if a stage question can be answered in an earlier stage or if the risk in proceeding with a conventional development has been reduced to an acceptable level. The methodology asks these five stage questions:

- Feasibility stage: Can one or more of the key functions performed by the expert be modeled?
- Research or extensibility stage: Can additional functions that are known be modeled?
- Field stage: Can the remaining functions be modeled so that the prototype can be used in a field setting?
- Production stage: Is it possible to refine the design, recode the program, or transport the system to a new host to achieve the desired functional and performance goals?
- Operational stage: Are the risks and costs of deploying the production prototype of an improved version acceptable?

At this stage in the methodology, the development team has learned that a system that simulates the human expert can be built. The goal of this stage is to make an exhaustive analysis and evaluation of the risks of deployment based on the production prototype.

Within each stage of expert system development, work proceeds through the following five highly iterative steps that are not necessarily performed in a simple, sequential fashion.

- Identification step: The knowledge engineer seeks to determine the problem that will be solved for the stage, identifies the sources knowledge, and begins to acquire the knowledge needed for the stage.
- Conceptualization step: Knowledge acquisition continues in this step. Concepts, relations, information-flow constraints, and problem-solving strategies are acquired from the expert. The knowledge gathered is organized and modeled on paper, using a modeling technique suitable to the problem.
- Formalization step: The prototype system is designed, the concepts defined in the conceptualization steps

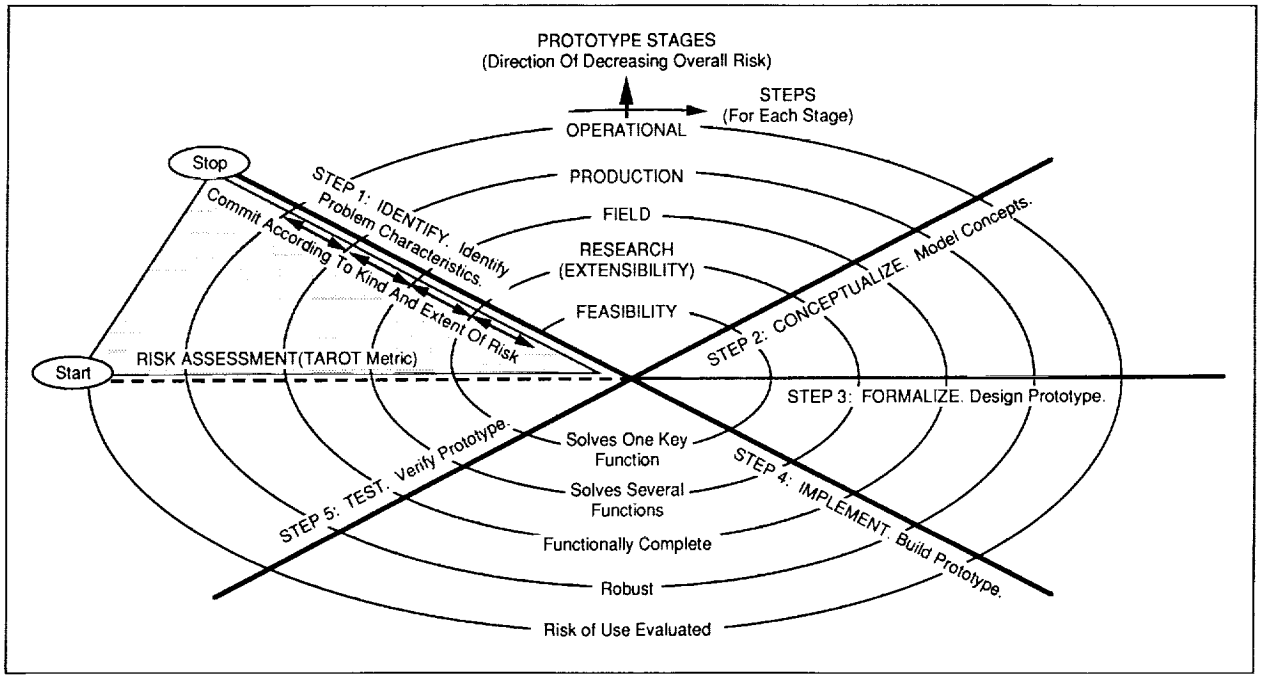

The spiral approach to expert system software development described by Expert System Development Methodology reduces risk.

are formalized, a tool or language is selected to represent these concepts, and the hardware is selected.

- Implementation step: The formalizations defined are coded using the selected tool or language to produce a prototype that will be tested.
- Test step: The focus in the early stages of the methodology is to compare the performance of the prototype with that of the expert. In later stages, the prototype is also tested for robustness, speed of execution, and risk of use in various modes of deployment.

An expert system development project terminates when the feasibility and use risks have been reduced to an acceptable level and enough is known about the problem to write requirements. The methodology's findings serve as the basis for a conventional systems development and are transferred to the developers in a formal review meeting. The project also terminates if the risks of either implementation or use are considered unacceptable or it is determined that the problem is not a suitable candidate for an expert system implementation.

Because developing specifications for an expert system at the start of the project is difficult, the manager is confronted with special problems in managing an expert system project. These problems are addressed in the methodology. It provides guidance on what reports to produce at the end of each stage and at the end of the project.

Expert System Development Methodology is intended to be a standard methodology to be applied to the development of Goddard expert systems. It is considered preliminary because it has not yet been applied to actual projects. It is nevertheless a synthesis of methodologies that have been used in conventional system development as well as in development of expert systems and has been evaluated in retrospect by comparing the methods used in two recent expert system development projects. These projects did not choose explicitly to use the methodology but provided useful additional insights into actual expert system development practices and problems. A future objective is to field-test and revise the methodology based on one or more pilot expert system projects.

Three documents describing Expert System Development Methodology have been generated. The *Expert System Development Methodology Standard* presents the methodology, includes background information on the life cycle of an expert system, and discusses the differences between expert system and conventional

system life cycles. The *Expert System Development Methodology User Guide* describes the methodology and presents a checklist of required actions for both developers and managers. The *Expert System Development Methodology Reference Manual* provides a description of the required activities organized according to topic and an appendix covering expert system development terminology. These documents have been revised based upon the retrospective evaluation and will be updated again to incorporate lessons learned from the pilot expert system projects.

Contact: Larry G. Hull (Code 522)
(301) 286-3009

Sponsor: Office of Space Operation

Mr. Larry G. Hull is a senior computer engineer with 23 years' experience at Goddard in areas such as real-time operational support for manned and unmanned spaceflight missions, computer performance and capacity management, discrete event simulation of computer and communications systems, expert systems, activity scheduling, and project management. He received an engineering degree and an MEA from George Washington University and holds a Certificate of Data Processing. Mr. Hull's primary research interests focus on artificial intelligence and activity scheduling.

USING PROTOTYPE SOFTWARE TO EVALUATE SCHEDULING ALGORITHMS

Automated scheduling systems have been developed to allocate resources to users with varying needs. To balance the success rate (the percentage of requests satisfied) and the scheduling system performance, scheduling algorithms are usually designed to build a good schedule without considering all of the possible combinations. Prototype software is being used to test different scheduling algorithms for the scheduling of the communications services.

The purpose of this prototype effort is to contribute to the design of a scheduling system to process generic scheduling requests. Such a system is being considered for implementation in the Network Control Center Data System. Generic requests provide a flexible format for specifying repetitive TDRSS service requests. The following is an English equivalent of a sample generic request:

- Schedule 16 15-min activities per day for 7 days.
- Schedule each activity to start within 90 min of the start of the previous activity.
- Activities must occur during TDRSS view periods.

The prototype system provides the operator with a selection of scheduling algorithms (or more specifically, a choice of skeleton "architectures" plus a choice of heuristics which plug into the architecture). The prototype generates a conflict-free schedule while recording the computer processing time expended and the number of events scheduled for each generic request. A report generator program tabulates the performance and success data for analysis.

Two scheduling algorithms have been implemented in the prototype to date. A third scheduling algorithm is currently being implemented. Weeklong schedules have been generated for each of the two algorithms for loads with and without the shuttle (see figure) and a preliminary analysis report has been prepared.

Also, a prototype data base has been created which models the TDRSS environment as accurately as possible, based on information provided by the Networks Division. The data base includes a set of realistic generic requests modeling 1995-era missions such as Cosmic Background Explorer (COBE), GRO, HST, Upper Atmospheric Research Satellite (UARS), X-ray Timing Explorer (XTE), and the shuttle. The data base also includes accurate view data, which represent times when the user spacecraft antennas can view TDRSS.

The two algorithms which have been implemented so far are named external expansion and repeat-expand cycles. The external expansion algorithm processes the whole group of generic requests by first expanding them into individual schedule requests, or instances, and then placing them on the time line. The repeat-expand cycles algorithm processes one generic request at a time, scheduling each instance of that generic request and then continuing to the next generic request.

The third algorithm to be implemented, internal-expansion, will process one generic request at a time, backtracking as necessary to select a set of time slots for the instances of the generic request.

Test results to date indicate that both the external expansion and repeat-expand cycles architectures were effective for

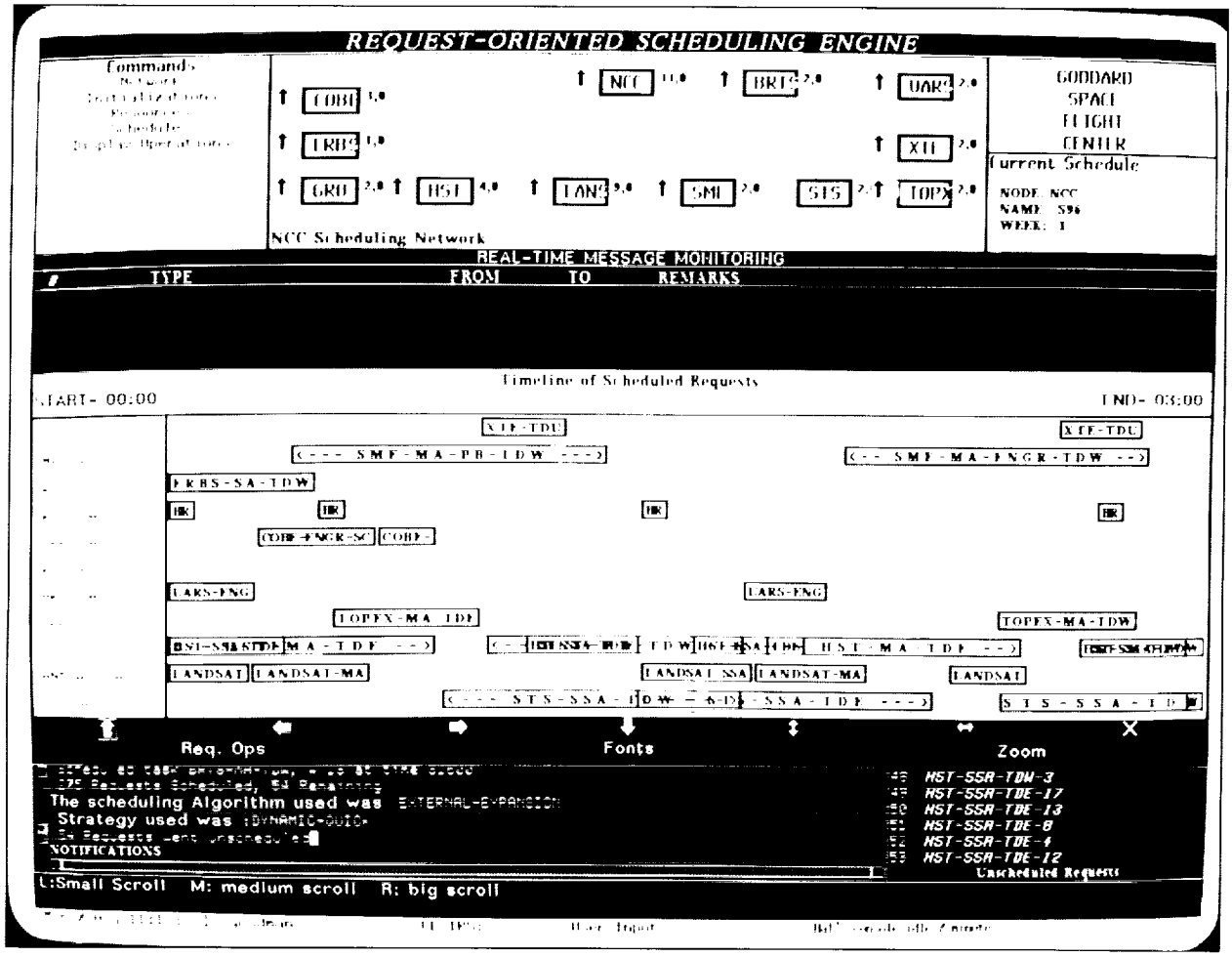

Display of TDRSS schedule.

scheduling TDRSS service, with neither architecture proving significantly better in terms of success rate or performance. Both algorithms produced schedules where about 86 percent of the primary requests were satisfied. An additional 0.4 percent to 1.5 percent of the requests were scheduled by less desirable alternate requests. The computer processing times varied by less than 10 percent for the two architectures. The computer took from 90 to 120 min to schedule and execute 1,500 to 1,700 events, which is the expected load for TDRSS in the 1995 time frame.

Future enhancements to the prototype include supporting wild-card designation in requests for the TDRS identifier, refining the existing architectures for performance, and providing a more intelligent time-slot selection by using resource usage estimates.*

**David Zoch and Jidé Odubiyi of Ford Aerospace implemented the two scheduling algorithms in the prototype. Todd Welden of Computer Sciences Corporation created a prototype data base which models the TDRSS environment.*

Contact: Nancy S. Goodman (Code 522)
(301) 286-6635

Sponsor: Office of Space Operations

Ms. Nancy S. Goodman is Technical Manager in the Systems Technology Applications Section of the Software and Automation Systems Branch. She has 9 years' experience at Goddard and is currently earning an MS in computer science at Johns Hopkins University.

CLEANROOM DEVELOPMENT METHODOLOGY

The Cleanroom software development methodology emphasizes human discipline in program verification rather than computer-aided program debugging to produce reliable software products. The methodology stresses producing correct software the first time, instead of relying on testing and debugging to identify and remove errors. This goal of error-free development is accomplished by applying verification formalisms and proofs of correctness and by separating developers and testers involved in the process. The key in applying the Cleanroom methodology to the software development process is focusing on defect prevention rather than defect removal.

The Cleanroom methodology incorporates several techniques that appear counter to current software engineering trends. These techniques have organizational implications such as the separation of development and test teams and life cycle implications such as incremental rather than sequential phases. Developers work in a desktop environment with no access to the computer. Systematic decomposition and verification techniques are applied by the development team before the code is delivered to the testers. Testing is implemented from an operational perspective using a statistical breakdown of operational scenarios.

The Cleanroom methodology as defined by Harlan Mills in the early 1980's was applied to several projects in the private sector with measured improvement in reliability and productivity. Experiments conducted at the University of Maryland also showed positive results in the reliability of the software product. The Systems Development Branch is conducting an experiment with the methodology by applying it to the in-house development of the Coarse/Fine Attitude Determination subsystem of the UARS Attitude Ground Support System. The goals of the project are to characterize and compare the process and products to standard Flight Dynamics projects and to tailor the methodology to better fit the Flight Dynamics environment.

Current analysis shows that about 28 percent of Flight Dynamics project efforts fall under the category of testing. Additionally, 35 to 45 percent of the total project effort can be classified as rework due to specification modifications, design flaws, and coding errors. The experiment was designed to determine if the Cleanroom methodology increases the quality and reliability of software significantly, decreases the test and debug time expended on a project, and minimizes the rework effort.

Preliminary analysis of the experiment indicates that the Cleanroom methodology may benefit the Flight Dynamics software development process. Its use confirms earlier Software Engineering Laboratory results, which emphasize the importance of code reading as a mechanism for identifying errors early in the software development process. Also, the development team's design walkthroughs proved effective in reducing design errors.

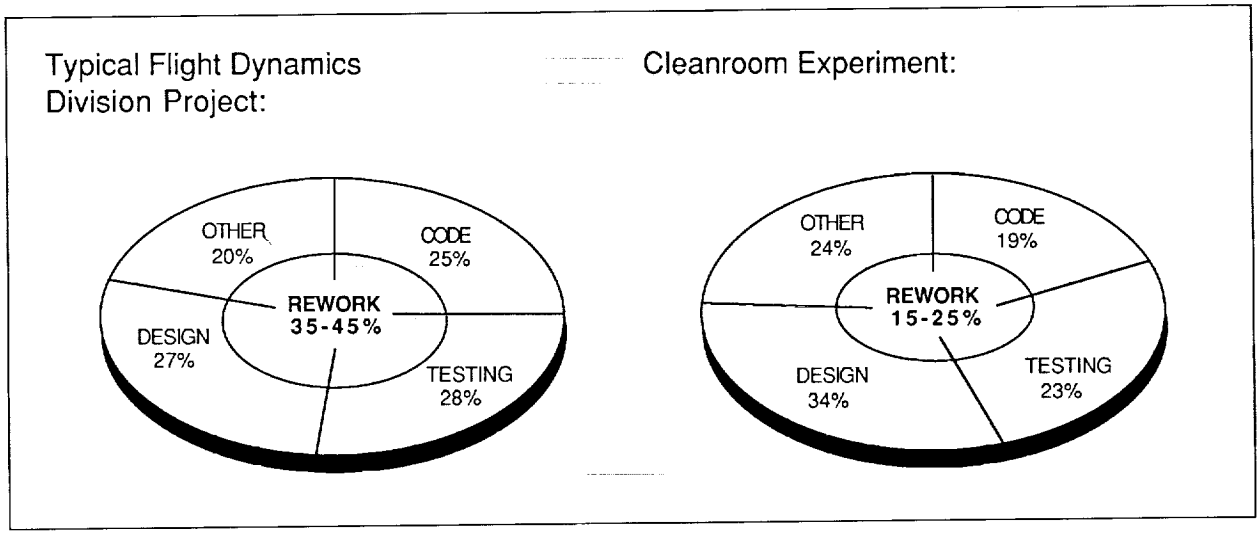

Comparison of effort breakdown.

Early analytical results indicate a first-time compilation success rate of 71 percent, which compares favorably with the 65-percent rate reported by a private sector firm. The experiment also indicates a potential reduction in rework effort by up to 50 percent and a reduction in the testing effort by 15 percent to 20 percent. The decrease in testing and coding phases is accompanied by a significant increase in design effort, implying the occurrence of early and less costly error detection (see figure).

Contact: Scott E. Green (Code 552)
(301) 286-5076

Sponsor: Office of Space Operations

Mr. Scott E. Green manages and develops Attitude Ground Support Systems and participates in research within the Software Engineering Laboratory of the Systems Development Branch. Mr. Green has worked at Goddard for 6 years and earned a BS in computer science at Loyola College.

NEURAL NETWORKS AND KNOWLEDGE-BASED SYSTEMS

Neural networks have the capability to learn and generalize input patterns based on training data. To date, a number of neural network systems have achieved pattern recognition and image processing capabilities. It is not difficult to extend neural networks to applications typically solved by rule-based expert systems. The advantage of the neural system is that it can be taught by examples, rather than through a hand-constructed knowledge base of if-then rules. A data base of examples can be constructed manually or gathered over time in an operational setting. These examples can then be presented to the neural network for training. Once a network has been trained, it will recognize input patterns and respond with the trained output result, which might be a response to some situation, a conclusion, or a fault classification.

One disadvantage of using neural networks instead of a rule-based expert system is that the knowledge inherent in the weights of the network is not easily presented for human verification and explanation. In other words, it is difficult to discover exactly what the neural network "knows." Goddard researchers have devised a general methodology for extracting the "rules" of a neural network. This four-step methodology consists of several strategies for pruning the search space (the number of possible rules for a given amount of inputs is extremely large), followed by a hypothesize-and-test loop. The methodology employs these steps:

(1) Prune the search space using various statistical methods, including sensitivity analysis, level curves, projection onto a basis, correlation, principal components, and determination of means, variance, and extremes.

(2) Generate hypothesized rules.

(3) Test hypothesized rules against the network.

(4) Keep the validated rules.

The methodology appears to be quite general and adaptable to many different types of applications. One of the most exciting aspects of neural network technology is its capacity for learning based on training data. This capability, coupled with the knowledge-extraction methodology, offers a potentially significant aid to knowledge acquisition for knowledge-based systems.

Contact: Robert E. Dominy (Code 522.3)
(301) 286-4196

Sponsor: Goddard Director's Discretionary Fund,
NASA Office of Space Operations,
Advanced Systems Program

Mr. Robert E. Dominy of the Automation Technology Section develops technology for distributed knowledge-based systems. The technical areas that interest him most are artificial intelligence and machine learning. He has 4 years' experience at Goddard and has a BA in computer science.

THE EVOLVING IMPACT OF ADA FOR FLIGHT DYNAMICS SOFTWARE

The Software Engineering Laboratory of the Flight Dynamics Division has been studying the effect of Ada on the development of flight dynamics software. These studies started in 1985 with the development of a pilot project, Gamma Ray Dynamics Simulator (GRODY), in Ada, which was completed in July 1988. GRODY is a system that models the attitude control laws used by GRO. The Software Engineering Laboratory's Ada research has continued by observing the use of Ada to develop production systems. These projects can be used to characterize how the use of Ada evolves as experience is gained.

The objective of the pilot project was to assess the Ada language and related technology by comparing an Ada software system to a FORTRAN system developed from the same specification. The GRODY development team was trained extensively in the Ada language and in modern programming practices to ensure that the team used the full capabilities of Ada, rather than merely developing a FORTRAN-like system using Ada. This training was successful, because the GRODY team used all the features (tasking, packages, generics, exceptions . . .) that make Ada a more advanced language. The GRODY team also produced the general object-oriented design methodology and several generic packages that have been reused in production projects.

In addition to the GRODY software development team, a group of researchers collected data and reported results for the GRODY project. Documents have been written detailing lessons learned for training, design, implementation, and testing. Of all the lessons learned, Goddard researchers identified three that were particularly significant. First, training is important because Ada's features should be used differently than FORTRAN's. Secondly, the design method should help analyze the use of data typing, because Ada provides more capabilities for user-defined types than FORTRAN and imposes stricter rules for how data types are used. In general, the design methodology used should exploit Ada's advanced features. The third lesson was that there are few differences in system testing between languages, as the underlying problem being solved is the same.

The GRODY pilot project was followed by the development of operational software for Geostationary Operational Environmental Satellites (GOES), UARS, and Extreme Ultraviolet Explorer (EUVE). The GOES projects were the first production Ada projects. A dynamics simulator similar to GRODY and a telemetry simulator (test telemetry generator) were started in 1987, while GRODY was still being implemented. Thus, they can be considered second-generation projects. The most interesting characteristic of the GOES projects is that they were able to reuse GRODY code to the same degree as FORTRAN simulators. As this was the first time Ada reuse was possible, these results were encouraging.

The UARS and EUVE simulators were built on the GRODY and GOES experience. Each of the development team leaders and a higher proportion of the programmers had experience from previous Ada projects.

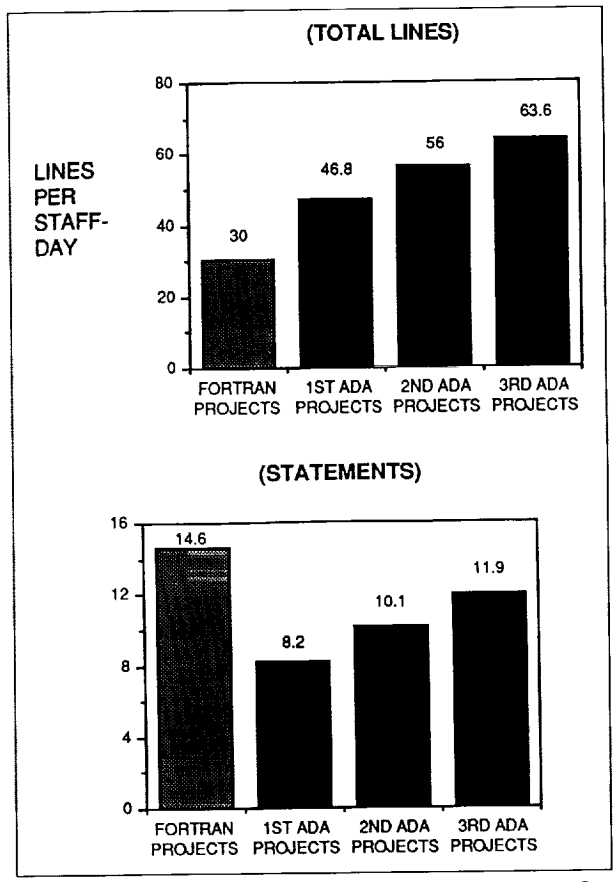

Two measures of productivity in using Ada compared to FORTRAN.

These third-generation projects have placed a greater emphasis on generics and software reuse.

The set of similar simulators developed from 1985 to 1989 has allowed the Software Engineering Laboratory to measure the changes in Ada use and the cost and quality of the Ada software delivered. Two measures of productivity (see the first figure) show that Ada development teams have become more productive over a period of time. Counting statements instead of lines gives a better comparison of Ada and FORTRAN sizes in the Flight Dynamics Division environment, because counting source lines is more sensitive to the two languages' different coding styles. There has been a similar positive trend in the reliability of Ada software.

In addition to observing the positive trends in cost and reliability, the Software Engineering Laboratory has measured changes in how the language is used. For

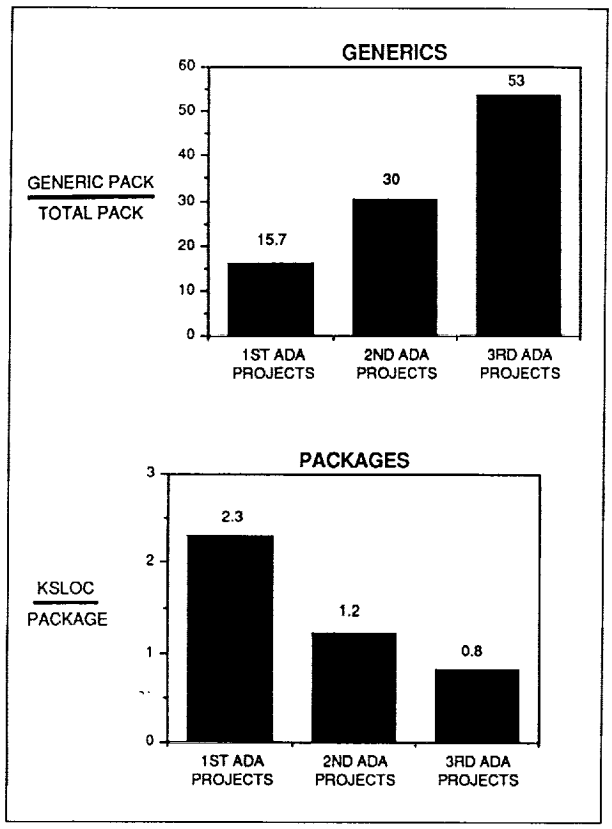

Packages written in Ada for Flight Dynamics Division simulations have become smaller with each set of projects, and increasing proportions are generic.

example, the second figure shows that packages implemented for Flight Dynamics Division simulators have become smaller and that a higher portion are generic. Similar data have been examined for Ada features such as tasking, data typing, and exceptions. The measurements taken to date show that the use of Ada has evolved with experience and that productivity and quality have also increased. The next step is to determine what trends in the use of the language have the greatest effect on productivity and quality. As more flight dynamics software is implemented in Ada, research will continue to explore how the use of the Ada language is evolving to meet NASA's needs.

Contact: Michael E. Stark (Code 552.2)
(301) 286-5048

Sponsor: Office of Space Operations

Mr. Michael E. Stark analyzes, develops, and manages support software and software engineering research in the Flight Dynamics Division of the Systems Development Branch. During his 9 years at Goddard, Mr. Stark has been honored with a NASA Group Achievement Award and was cowinner of a Code 500 Best Paper Award. He earned a BA in mathematics and economics from Oberlin College.

THE INTERIM CUSTOMER DATA AND OPERATIONS SYSTEM (CDOS) SOFTWARE SUPPORT ENVIRONMENT

CDOS is being built by the Mission Operations and Data Systems Directorate at Goddard to support ground-to-space communications for space-based platforms such as Space Station Freedom and Earth Observing System (Eos). The CDOS Support Environment supports the CDOS by providing a framework in which project information may be created, managed, and integrated. The system-support environment will cover the complete system life cycle from analyzing system requirements through implementation and fabrication to sustaining engineering.

The system-support environment goals are to reduce the costs of both system development and maintenance, promote the creation of the system in a timely manner, and improve the overall quality of the system. These goals are accomplished through this common environment, which supports effective group communication, use of documented procedures, and use of integrated computer applications (tools). This environment will replace paper-based operations with more flexible and powerful automated support.

The system-support environment not only enhances communication among current end users but also provides a bridge between the contractors developing the system and those who sustain, maintain, and enhance it. Because they use the same support environment, the ability to capture or trace the relationships between requirements, design, code, and other products is enhanced. For example, a requirement to handle data capture from a platform at a certain data rate was derived from a model. If the model is changed, the requirement and related design and code elements must all be changed. Changes are facilitated when they are all done in a common environment.

CDOS is divided into two phases: requirements analysis and preliminary design (phase B) and development

(phase C/D). The CDOS Support Environment for phase B is intended to be a pilot for the system-support environment to be created for phase C/D. The pilot or interim system-support environment is being created with the CDOS project staff so that the support-environment staff can understand how a project functions and formalize functions into procedures. These procedures then are documented, and if feasible and desirable, a tool is created to automate the process.

Currently, the CDOS Support Environment is composed of a group of Apple Macintosh work stations linked by Ethernet local area networks. The networks are linked over video broadband or other high-speed communications links. Each computer has access to a central file server tied to the network, which provides timely and accurate access to project information. Tools are either acquired off the shelf, e.g., Microsoft Word for document creation, or are built in-house when necessary.

As part of phase B work, the two phase B contractors analyzed the existing CDOS requirements document and reported their results in the form of change requests. During July and August of 1989, CDOS Support Environment provided a way to automate the processing of change requests. The phase B contractors and the project staff were provided with a package consisting of hard-copy documentation and diskette files. The package contained a style guide and documents for standards and procedures.

The style guide provides for consistency and compatibility within all system documentation. It is a formal standard for formatting system engineering documentation. It is limited to the types of output that can be created with Microsoft Word and compatible programs. Draft standards and procedures have been developed governing the submission of phase B products to the project. Procedure DM203 prescribes acceptable formats for electronic delivery of documentation and applies to all of CDOS contract deliverables. Procedure DM201 is specific to the phase B contract deliverables and describes how change requests (adding to or modifying the Level II requirements) should be embedded in a deliverable. Also included in the package was a Macintosh diskette in Microsoft Word format containing the style guide and the documents for standards.

A change request trace extractor tool and the Configuration Control Board (CCB) data base were created to help automate CDOS. The tool is a Macintosh application that uses the Microsoft Word file containing the contractor's change requests and extracts them into a format readable by the CCB data base.

The data base uses Apple HyperCard. The configuration management officer uses the data base to create, manipulate, and print the different forms associated with CCB activity. New forms are created based on information already in the data base. The data base also keeps track of relationships between forms (e.g., what change requests a document-change notice satisfies). At any time, the information may be printed in either a form or a report format.

By following the standards and procedures documents and using the Macintosh files, the phase B contractors provided the project staff with a Microsoft Word document from which the change requests were extracted automatically. The extracted change requests then were used as input to the CCB data base. Using the CCB data base, it was possible to generate over 500 forms for a review in 2 days. Most of this time was spent by the configuration management officer in classifying, grouping, and printing the change requests.

The CCB data base captures the results of the technical reviews by mapping each change request into one or more document change requests to the system requirements document. The data base allows the configuration management officer to create a document change request from one or more change requests. The relationships of document change request to change requests is maintained automatically by the data base.

In the near future, CDOS Support Environment will release the project data base and start the process of capturing the requirements and tracing them to the design work to be done during the rest of phase B. The staff are also beginning to support system phase C/D by preparing for a system requirements review.

Contact: Mark A. Stephens (Code 522)
(301) 286-5994

Sponsor: Office of Space Tracking and Data Systems

Mr. Mark A. Stephens is Project Manager of the CDOS Support Environment in the Data Systems Technology Division. He has 9 years' experience at Goddard and holds an MS.

ORIGINAL PAGE
COLOR PHOTOGRAPH

Engineering Technology

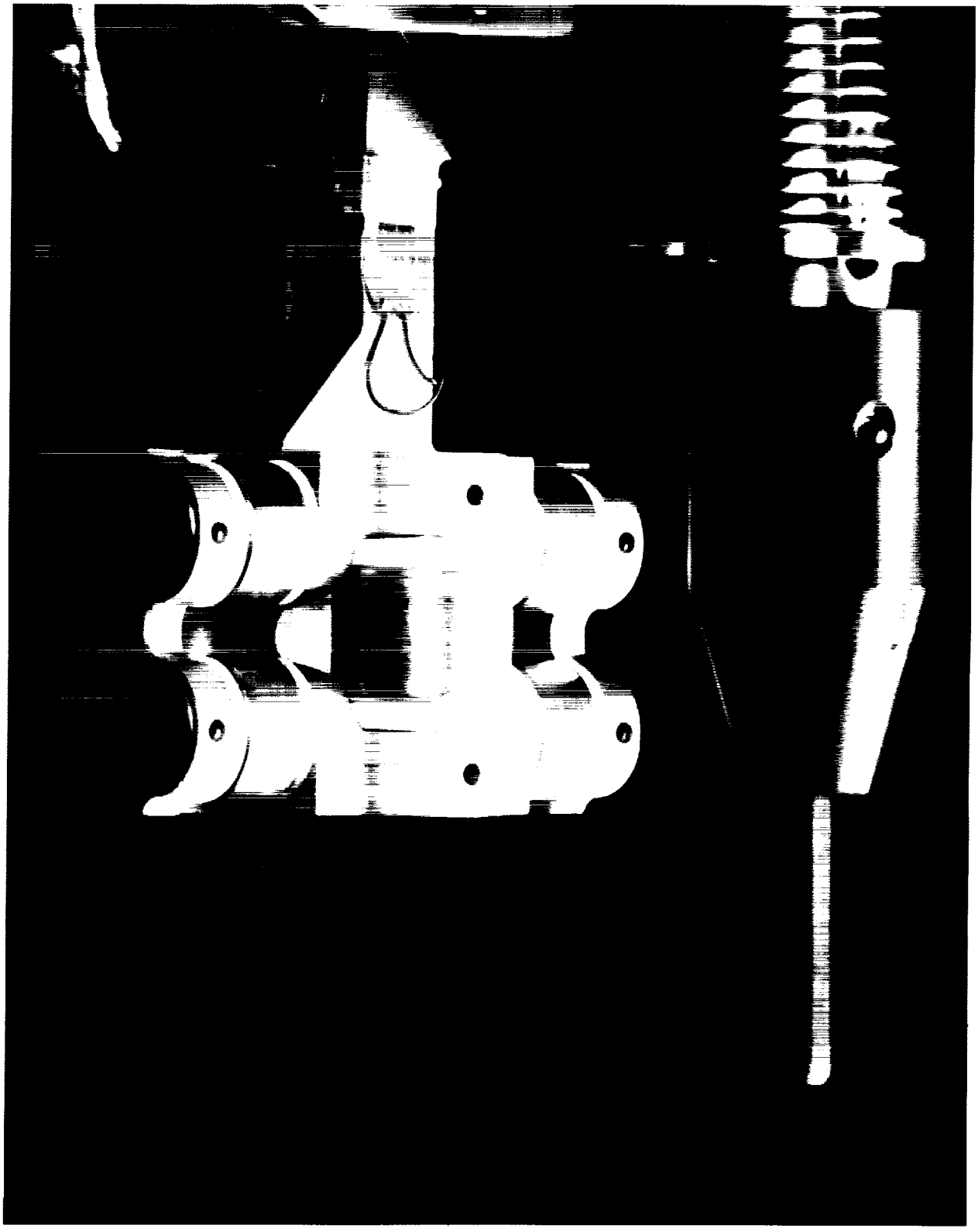

Engineering Technology is the key to progress in more sensitive instruments, more capable spacecraft, more reliable systems, and more cost-effective research.

—T. Huber

SENSORS AND SPACE TECHNOLOGY

PASSIVE HIGH TEMPERATURE SUPERCONDUCTOR (HTSC) BEARINGS FOR CRYOGENIC COOLERS

The lifetimes of NASA scientific flight missions that require cryogenic cooling on board for proper operation of sensors and other instruments is limited by the lifetime of stored cryogens. For example, the Infrared Astronomical Satellite launched in 1983 was in operation less than a year. The otherwise perfectly capable satellite ceased to function because the 0.5 m^3 of liquid helium that it carried boiled out due to inherent heat leaks. The contemplated Space Infrared Telescope Facility will have a projected lifetime of 2 years if 4 m^3 of liquid helium planned for its dewar last as long as expected.

Clearly, an improvement in cooling technology would significantly affect life expectancy in future NASA missions such as the Advanced X-Ray Astrophysics Facility, Astromag, Cassini, Space Infrared Telescope Facility, and others. There are three basic alternatives to increase the lifetime of cooling systems: (1) minimize the heat leaks in dewars; (2) develop a capability to replenish cryogens on orbit; and (3) use a mechanical, closed-loop, service-free refrigerator. Goddard researchers are examining the possibility of improving the performance of mechanical coolers by using noncontact passive HTSC magnetic bearings.

Present state-of-the-art means of centering the shafts in long-lifetime mechanical coolers are based on three types of bearings: electromagnetic, gas, and flexure bearings. Unfortunately, magnetic bearings employing permanent magnets alone cannot be used to suspend the shaft, because they do not provide stable equilibrium in all three axes, as demonstrated by Earnshaw in the last century and reconfirmed many times since then by various workers. Mechanical refrigerators employing active linear electromagnetic bearings (Philips Stirling cycle cooler) require complex electronic control systems that increase weight and cost and decrease the reliability of the coolers. Cryocooler systems based on gas-bearing turbomachines (rotary, ultra-high-speed turboexpander) appear to be quite reliable, but suffer low efficiency due to heat leaks. Flexure bearings (diaphragms, springs) suffer from heat leaks and are not reliable for long-life space applications due to metal fatigue.

HTSC material, when cooled below its critical temperature, exhibits a stable levitation effect resulting from a combination of the Meissner effect and flux pinning. Therefore, designing a passive magnetic bearing that can provide three-dimensional stable equilibrium is possible using HTSC oxides.

Closed-cycle mechanical refrigerators will be almost an ideal application for the new HTSC oxides. First, because they are already providing cooling for the scientific instruments, no additional cooling system is required to keep

An innovative finger design for space robot grippers. The finger design consists of an arrangement of alignment and seating rollers on each of the two gripper fingers, thus significantly improving the effectiveness of the gripper.

HTSC oxides below transition temperature. Second, the coolant is an inert gas (neon or helium, for example), the most desirable environment for the HTSC oxides, which are susceptible to degradation (i.e., one does not have to worry about adverse effects of the space environment).

A joint Goddard-Department of Defense Strategic Defense Initiative Office effort was initiated to develop, design, and build a passive HTSC magnetic bearing with characteristics suitable for application in cryogenic mechanical refrigerators.

The funding will be provided to Cornell University and a private firm to select HTSC material, establish a structure-properties relationship, design and build a prototype bearing, conduct bearing performance tests, provide preliminary and engineering designs of the engineering model, build the engineering model, and perform a test of the engineering model of the passive radial HTSC magnetic bearing-based device.

If this effort is successful, it is expected to reduce the input power in mechanical coolers by about 40 percent without reducing their cooling power. The reduction of input power also translates into reduction of the refrigerator's weight. Also, multistage cooling will be possible because HTSC bearings will allow the proper operation of the final, 5- to 10-°K range stages.

Contact: Yury Flom (Code 313)
(301) 286-3274

Sponsor: Director's Discretionary Fund, Office of Aeronautics and Space Technology (OAST), and Research and Technology Operating Plan

Dr. Yury Flom received his PhD in materials engineering from the University of Maryland. Dr. Flom is involved in materials engineering, testing, evaluation, and failure analysis services for Goddard and other NASA facilities. Recently, Dr. Flom has also been coordinating HTSC activities at Goddard.

AN ADAPTABLE HIGH VOLTAGE POWER SUPPLY FOR SPACE FLIGHT APPLICATIONS

There is a great demand for highly regulated high voltage power supplies in the 1- to 4-kV range for spacecraft scientific instruments. A number of upcoming projects—International Solar-Terrestrial Physics Project (ISTP), Cassini, X-ray Timing Explorer (XTE), and numerous balloon and rocket missions—have requested such supplies. A shortage of manpower prevents meeting the demand with individual custom designs, and such flight-qualified supplies are not commercially available.

A single, adaptable design is needed to satisfy the requirements of each project without reengineering the electrical or packaging design. It must satisfy the standard specifications commonly required and be adaptable to the individual needs of the instrument. The goal is to develop a design of proven reliability that can be used on other projects. An adaptable high voltage power supply has been developed for this purpose. A block diagram of the supply is shown in the first figure.

Special concerns in the design, layout, and assembly of the power supply further complicate the design process. Because the high voltage section is most susceptible to failure, the major design effort must be focused there. The reliability of high voltage supplies is determined by the integrity of the construction. To increase reliability, the high voltage section should be structurally simple, and voltage stress on the components must be reduced. Other factors must be considered, such as dielectric quality, component spacing, and assembly techniques.

The adaptable high voltage power supply design is composed of an oscillator/step-up transformer, a high voltage regulator, a voltage multiplier, output filters, and a feedback network. A +28-Vdc input feeds the oscillator, which was chosen for optimum reliability. The high voltage transformer, in series with the regulator, presents a stepped-up ac signal to the voltage multiplier. Its design minimizes the voltage stress on the windings, thus reducing the risk of voltage breakdown between them. Previous techniques required transformers to be hand wound, whereas a machine-wound method is employed here. This approach results in repeatability of transformer characteristics, making testing

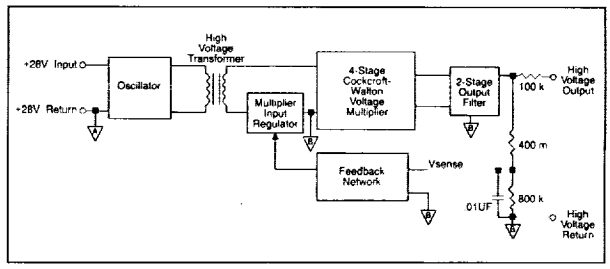

Block diagram of an adaptable high voltage power supply.

ORIGINAL PAGE
BLACK AND WHITE PHOTOGRAPH

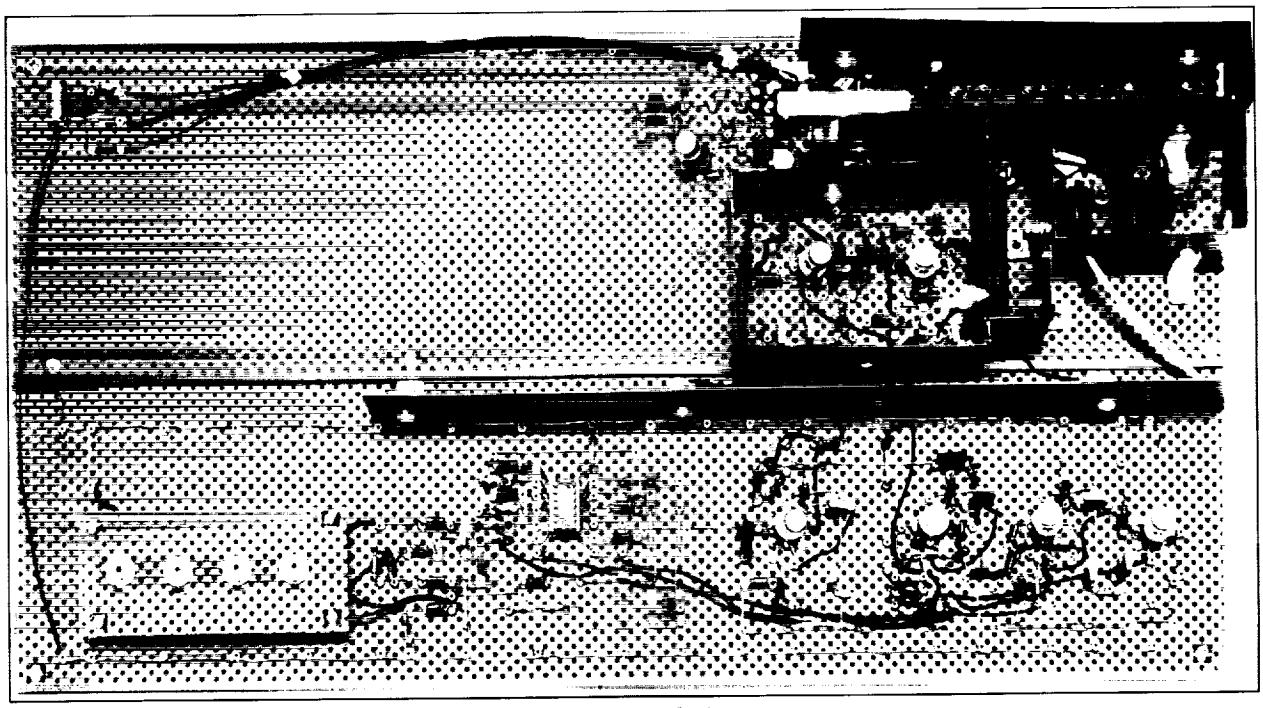

Testing of the breadboarded supply for the high voltage power design.

of the circuit less time consuming and minimizing the need for compensation within the circuit.

Simplicity, reliability, and flexibility were sought in selecting the high voltage regulator. This circuit, the multiplier input regulator, controls the output by changing the conduction of a single transistor in series with the transformer secondary at the input to the voltage multiplier. It offers many advantages over previous techniques. The high voltage assembly's simplicity is its most important feature because it will determine the unit's reliability. This regulator also provides a low parts count and low power dissipation. True isolation of the input power and high voltage returns is achieved since the regulation is done on the secondary side of the transformer. Voltage stress on regulator components can be maintained at acceptable levels while still using small component sizes. This regulator also requires less testing time than other methods to obtain adequate performance.

Flexibility is accomplished in this choice of high voltage regulation. Multiple-output voltages are easily attained by adding another secondary winding to the transformer along with a multiplier stack and the associated regulator. Only a +28-V input must be provided because all supply voltages for the circuitry are derived internally. While the basic supply will remain the same, component values in the voltage multiplier, output filters, and feedback network can be altered to accommodate different specification.

A straightforward layout of the high voltage compartments is one key feature of the packaging design. The supply is arranged in modular sections that allow their dimensions to be modified easily for different applications. Another benefit of this approach is the reduction of noise coupled to the output.

Testing of the breadboarded supply (shown in the second figure) has shown impressive results. Since the extensive testing and debugging on the supply are completed, future resources can be devoted to investigating possible improvements in the high voltage assembly.

Contact: Karen D. Castell (Code 711.4)
(301) 286-2383

Sponsor: XTE Project

Ms. Karen D. Castell received a BSEE from Duke University and an MSEE from Northeastern University. She is presently working in the Sensor Power Electronics Section of the Space Power Applications Branch.

CONTROL OF A 7-DEGREE-OF-FREEDOM (DOF) ROBOT SLAVE ARM USING A 6-DEGREE-OF-FREEDOM (DOF) FORCE-REFLECTING MASTER ARM

Researchers at Goddard's Development, Integration, and Test Facility are currently developing a Flight Telerobotic Servicer (FTS) engineering testbed to be used to provide the answers needed to design safe, reliable, and fully functional robotics for in-space operations. The engineering testbed will be used to resolve the following primary research issues:

- Human factors in robot teleoperation control.
- Robot control in microgravity.
- Dual-arm teleoperations.
- Task simulations.
- Hierarchical control using a high-level programming language.
- Robot safety.

The engineering testbed, shown in the first figure, consists of dual-arm, 7-DOF robot slave manipulators. Each arm on the robot has an extension of approximately 6 ft and is mounted on a stand 8 ft above the ground. The arms are 1.5 ft apart, simulating right and left arms.

The teleoperated control of the robot arms is accomplished with a pair of 6-DOF hand controllers shown in the second figure. Mounted on the ends of each arm are robot end effectors. Switches on the hand controller allow for control of these end effectors. Researchers are currently optimizing end-effector designs to enhance the gripping and material-handling capabilities of the robot. The end effectors incorporate force-torque sensors located between the end effector and the robot. Researchers have developed control algorithms (software code) that provide force feedback to the operator. When the robot end effector contacts an object or is in motion, the force-torque sensors provide force feedback, using Cartesian coordinates, through the hand controller to the operator. This capability provides a sensory perception to the operator of the magnitude of the forces generated by the end effector when in motion or in contact with an object. The hand controller will react with a force opposite and of scaled magnitude to the contact force or motion of the end effector.

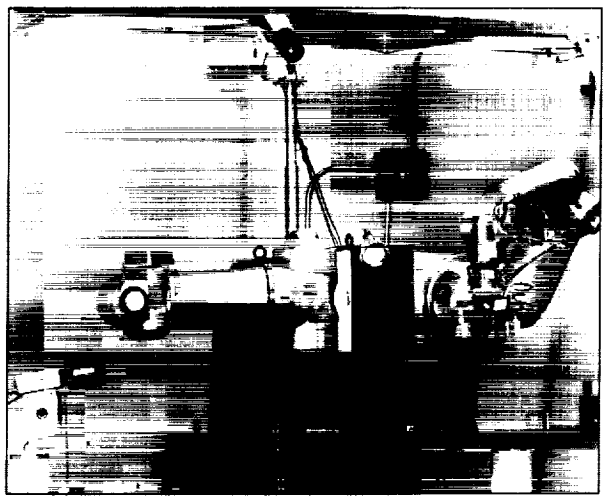

Engineering testbed consisting of dual-arm, 7-DOF robot slave manipulators.

Cameras are used on the engineering testbed to provide a view of the work area to the operator. One camera is mounted on each end effector, and the other near the base of the two manipulators. Researchers are presently planning to enhance the operator-viewing capability to at least two control views which are orthogonal, allowing the vision system's plane of orthogonality to correspond to the operator's base frame and to the base control plane for the hand controller. When the operator moves the hand controller, the robot should appear to move in the same direction in at least one of the camera views.

The control computer electronics consists of the following three INTEL 80386/80387 processor boards:

- Robot servo processor.
- Gravity compensation and inverse processor.
- Command and communications processor.

Researchers have developed algorithms for the processors to provide all coordinate transformations between 6-DOF and 7-DOF space and force feedback control schemes. There are basically two force feedback control schemes: (1) direct force feedback uses data from the end-effector force torque sensor to derive a Cartesian force torque vector that is transmitted to the robot arm, and (2) bilateral force feedback computes a force torque vector based on the error between the desired position and the archived trajectory of the robot arm. Researchers anticipate that both force feedback schemes will be implemented on the engineering testbed.

ORIGINAL PAGE
BLACK AND WHITE PHOTOGRAPH

ORIGINAL PAGE
BLACK AND WHITE PHOTOGRAPH

6-DOF hand controllers provide teleoperated control of the robot arms.

Researchers have developed a Watchdog Safety System that monitors the health and status of the engineering testbed control system, oversees robot and sensor data to ensure that the robot is operating within safe limits, and safely shuts down the robot when an unsafe condition exists.

In the future, the engineering testbed will incorporate a high level safety system that determines the safe operational and warning limits from its knowledge of the task being performed. These limits will be sent to the watchdog system, which exists at the servo level of telerobot control and monitors robot and sensor data to ensure that the data are within the safe limits determined by the safety system. The watchdog system is also responsible for monitoring the health of other computers in the engineering testbed robot control system such as the work station computer and the robot controller.

Future efforts will be directed at accomplishing the following goals established by the engineering testbed researchers:

- Improve force reflection techniques.
- Incorporate higher levels of NASA's Standard Reference Model for robotic control.
- Integrate end-effector controllers.
- Support dynamic simulation parameters.
- Integrate various sensor technologies.

Contact: Richard G. Schnurr (Code 745)
(301) 286-6069
Sponsor: Space Station Freedom FTS Project

Mr. Richard G. Schnurr, an electronics engineer in the Guidance and Control Branch, received his BS in electrical engineering from the University of Maryland. He has worked at Goddard on several Attached Shuttle Payload projects, including the Spartan freeflyer. He is currently involved in developing a robotics technology testbed for the FTS Project in the robotics laboratory of the Engineering Directorate.

HIGH PERFORMANCE, COMPACT HEAT EXCHANGER FOR A SPACE-QUALIFIED CRYOGENIC COOLER

Reverse-Brayton cycle cryocoolers will be relied upon routinely to meet NASA and Department of Defense space application refrigeration needs during the next decade and beyond. Design requirements dictate minimizing cryocooler physical parameters and input power to reduce on-orbit delivery costs. In the past, heat exchanger technology was an inherent weakness in the way of accomplishing these ends. However, breakthroughs in heat exchanger miniaturization have occurred that permit the fabrication of new, all-metal, highly efficient heat exchangers.

Until now, only heat exchangers built with organic material were able to achieve the high thermal performance values required for space cryocooler systems within the permitted size and weight constraints. Unfortunately, organic materials degrade cryocooler performance through several mechanisms: working fluid leakage and system contamination by organic fouling are two prominent ones. An efficient, compact, all-metal heat exchanger eliminates NASA and Department of Defense concerns about these problems.

Such a heat exchanger was developed. The heat exchanger consists of 600 copper disk-annular ring pairs soldered in a tube-in-tube configuration. Precision machining of more than 2,600 annular slots in each disk-ring pair is a factor crucial to achieving high performance. Each slot is about 0.005-in. wide by 0.125-in. long and must have uniform walls and spacing. The accompanying figure shows an end view of a completed disk-ring pair.

A computer design of an optimum all-metal heat exchanger was reported previously *(Research and Technology 1988)*. However, this design could not be fabricated using conventional manufacturing processes. Experiments had shown that an electric-discharge machining

method could produce the very small slots of the uniformity and surface finish that were specified, but too much time was needed to make the 1 million slots required to complete a single heat exchanger.

To solve this problem, an eight-station automated machine designed to fabricate the heat exchanger plates was developed and tested. The slots are machined one at a time by a plunge electric-discharge machining technique using thin molybdenum ribbons as the electrodes. Uniform width slots as narrow as 0.004 in. can be machined through copper plates up to 0.030-in. thick. The molybedenum electrodes are dressed before each cut to ensure the uniformity of the slots. The indexing-dressing-machining cycle time is about 1 min per slot, and the machine produces eight complete heat exchanger plates per day. This microprocessor-controlled robot machining system is fully automated and requires minimal human oversight. It produces identical parts 24 h per day; each part has the required precision, quality, and reproducibility required by the heat exchanger design. Machine setup and down times are negligible.

To achieve high thermal efficiency, axial conduction along the length of the heat exchanger had to be reduced to the lowest practical value. To do so, thin wall, low conductivity stainless steel tubes were used to support the disk-ring pairs. Bonding between the disk-ring pairs and the tubes is important to provide for high radial heat transfer. Organic materials could not be tolerated because of their loss of flexibility after cyclic cooling to cryogenic temperatures. The soldering technique devised for the assembly employs a freon vapor reflow process to achieve good bonding without displacing disks or rings in the process.

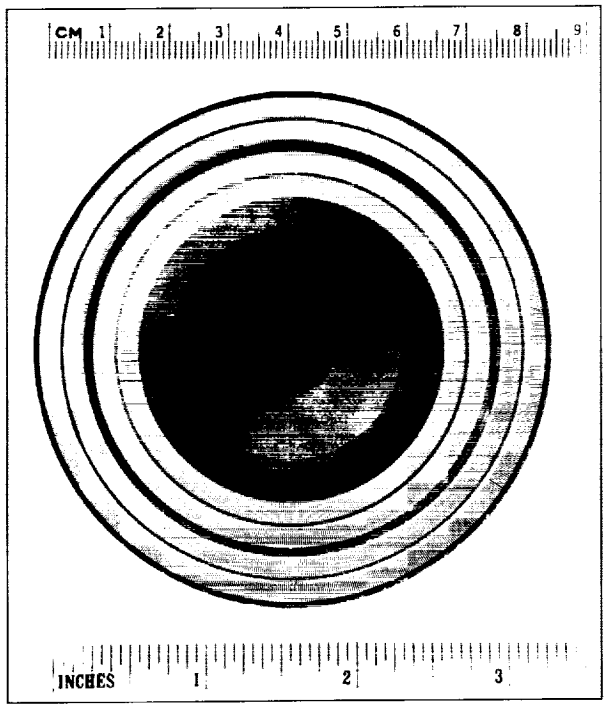

A disk-ring pair with more than 2,600 0.005-in. wide radial slots for a high performance, compact heat exchanger.

A special indexing jig was devised to assemble disk-ring pairs at precise axial locations along the length of the heat exchanger. Assembly of the prototype heat exchanger and performance testing was complete in November 1989.

Contact: Max G. Gasser (Code 713.1)
(301) 286-8378

Sponsor: Small Business Innovative Research Program

Mr. Max G. Gasser is an aerospace engineer with 24 years' experience at Goddard. Mr. Gasser, who received his BS in chemical engineering from Virginia Polytechnic Institute and State University, is involved in research and development of cryogenic cooler technology for space applications. He has received an Innovative Research-100 Award and holds a patent on the Stirling cycle cryogenic cooler.

ROLLING FRICTION FINGERS

At Goddard, a finger for robotic grippers has been designed that greatly improves effectiveness in grasping and manipulating objects by reducing the effects of friction. The design has been prototyped and is being tested as a component of Goddard's FTS and FTS Operations Simulator.

The design, shown in the first figure, uses an arrangement of rollers to grasp a handle designed to fit the fingers. This roller design has many advantages over the standard V-grooved fingers, including the following:

- Improved effective capture range, guidance, alignment, and seating capability.
- Elimination of damage to the grasped object due to burring or scraping.
- Improved force sensing and control.

ORIGINAL PAGE
BLACK AND WHITE PHOTOGRAPH

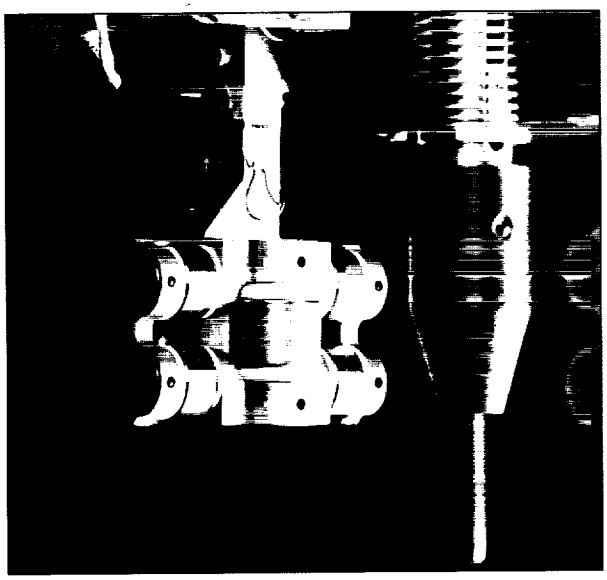

The rolling-finger design for robotic grippers.

- Enhanced gripper motor performance.
- Easy release of grasped objects, even in the presence of strong side torques.

Conventional fingers can damage an object as it is grasped, especially if the alignment of the fingers is not precise. With the Goddard design, the rollers roll along the surface of the object as it is grasped, guiding and aligning it, as the second figure shows. As the gripping process continues, the fingers align the object more precisely until it is firmly seated, as illustrated in the third figure. This roller action prevents damage to the object from scraping or burring.

The rolling fingers also aid gripper force control because the sensors do not have to contend with a large and unpredictable friction vector. The sensor readings become much clearer and more predictable. This is particularly beneficial in the thermal vacuum of space, where friction is especially unpredictable.

The effectiveness of the gripper motor is improved significantly because it no longer needs to use a large percentage of its power to overcome friction. This improved efficiency allows the motor to be smaller, consume less power, and generate less waste heat.

The final advantage is a very important safety consideration. Because the object is in contact only with rollers while it is held, it cannot become jammed, even in the presence of strong side torques. Any object grasped can be released quickly and easily.

The rolling friction fingers were developed at Goddard. The design is being refined and tested at the Center and is expected to be applied in the FTS program. The rolling friction fingers have very significant advantages over standard fingers and should be valuable in many other applications.

Contact: John M. Vranish (Code 716)
(301) 286-4031

Sponsor: Space Station Freedom FTS Project

Mr. John M. Vranish, an aerospace engineer in the Electromechanical Branch, holds several patents on robotic electromechanical systems, mechanisms, and tactile proximity force sensors. His invention, the Robotic Derivetor, was the top-rated Department of Defense robot innovation in fiscal year 1979. He received his MS in electrical engineering from George Washington University.

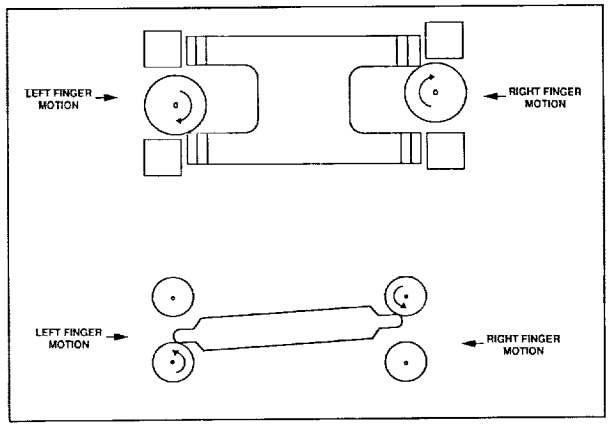

Rollers guiding and aligning the handle as the fingers close.

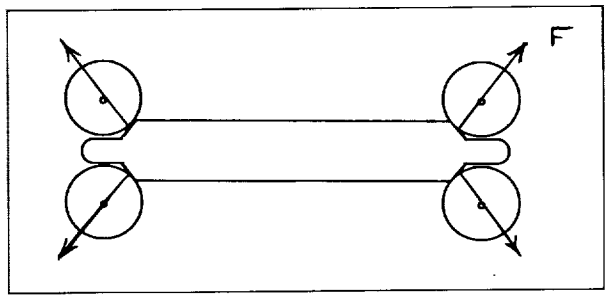

The fingers close as the handle is seated.

COLLISION-AVOIDANCE-MANAGEMENT SKIN FOR ROBOT ARMS

Safety is a primary concern for robots operating in space. Researchers at Goddard are addressing this concern by developing a collision-avoidance-management skin for use around robot arms. This project has been ongoing for 3 years. This report reflects the current state of development. The project has three objectives. First, such a skin should allow the robot to sense the presence of an object to a range of approximately 1 ft so that the robot has time to stop movement before contact. Second, the skin should detect the edges of an object to 1 in. at a 2-in. range. This permits the robot to go around an obstacle. Third, upon contact, the robot should be able to use tactile sensing to determine to 0.25 in. where on the robot arm such contact was made and how hard it was, to a threshold 8 oz, so the robot can manage the contact. During the past year, an approach was implemented using an array of dual-mode capacitive plates operating at a radio-frequency of 100 kHz. The sensing system design concept is shown in the first figure. The work is being done in-house at Goddard.

The proof-of-principle prototype for this phase is shown in the second figure. The sensor consistently detected a human hand at a 10-in. range and met the performance requirements listed in the preceding paragraph. Tactile and proximity signals were easily discriminated. The signal processing is based on frequency modulation techniques; thus, the prototype was able to operate in an electromagnetic-interference-intensive environment with no adverse effects. Also, the sensor was able to "see" through a thermal blanket; thus, it need not be exposed to the space environment.

The circuitry proved to be straightforward and stable despite the small capacitances involved. The capacitive array was simple and easy to fabricate and package around the robot arms. The sensor system approach lends itself to being built by integrated circuit and hybrid fabrication methods. Since the signals produce a continuous sensing field around the robot arms, the robot cannot be blinded by problems that normally handicap optical sensors, such as sun glint, reflections, and heat.

Researchers are continuing to optimize sensor performance. Hardware development will emphasize improving range, reducing crosstalk between the elements of the array in order to improve directionality, and developing self-calibration techniques so the sensor can function unattended in space for extended periods. In addition, analysis and modeling are establishing a basis for further optimizing sensor hardware and developing the range and edge detection algorithms. Finally, preparatory work has already begun to interface the proof-of-principle prototype to a robot control system and to establish the "fuzzy logic" algorithm needed to perform the automated collision-avoidance-management functions.

Future plans include using hybrid and integrated circuit techniques to further improve the circuitry and array construction. Researchers also expect to add a layer of heat-detecting polyvinylidene fluoride material to the sensor to detect the proximity of hot objects. The capacitive array will "see" through this layer and the thermal blanket.

Contact: John M. Vranish (Code 716)
(301) 286-4031

Sponsor: Director's Discretionary Fund

Mr. John M. Vranish, an aerospace engineer in the Electromechanical Branch, holds several patents on

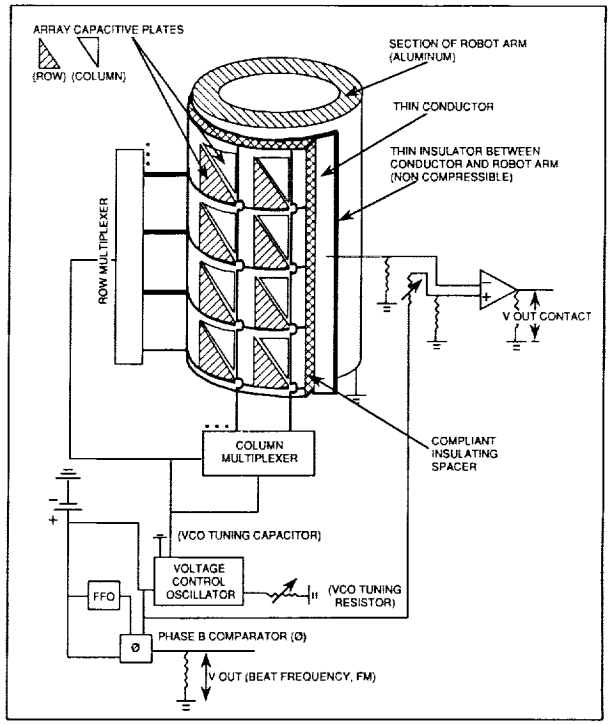

The sensing system design concept for the collision-avoidance-management skin for robot arms.

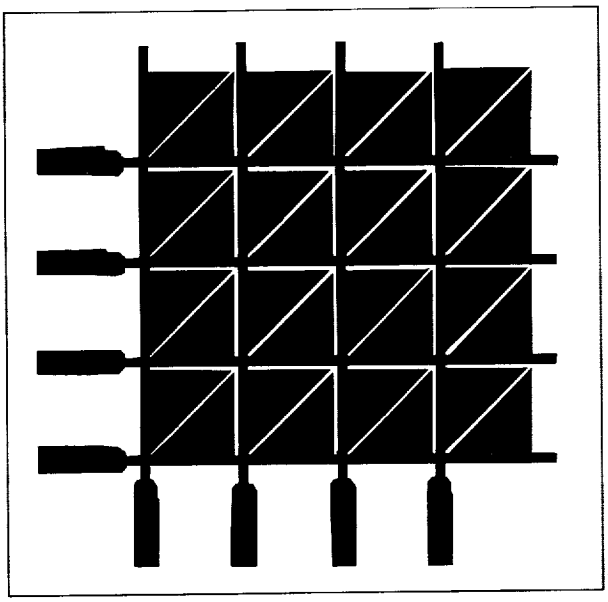

Proof-of-principle prototype for the sensing system design.

robotic electromechanical systems, mechanisms, and tactile proximity force sensors. His invention, the Robotic Derivetor, was the top-rated Department of Defense robot innovation in fiscal year 1979. He received his MS in electrical engineering from George Washington University.

HIGH-POWER, NEAR DIFFRACTION-LIMITED OUTPUT FROM ALUMINUM-GALLIUM-ARSENIDE LASER DIODE ARRAYS

Arrays of semiconductor aluminum-gallium-arsenide laser diodes are attractive for use in applications that require high-power optical sources such as solid-state laser pumping, free-space laser communications, and remote-sensing systems. These arrays offer the remote-sensing advantage of high optical power (>200 mW continuous power) with high electrical efficiency (50 percent) and can be modulated for communications by directly switching the drive current on and off to form a light pulse stream of 1's and 0's. Unfortunately, these arrays typically operate with several lobes in their intensity distribution or far-field pattern and also operate with many spectral modes, two characteristics which limit their uses for free-space communications and other applications. These undesirable properties result from incoherent (out-of-phase) operation of the individual array elements, making the array output seem to come from many different lasers instead of one large laser. Goddard research is centered on finding techniques to improve the output beam qualities of these laser diode arrays and therefore enhance their usefulness to many of NASA's laser applications.

Injection locking is one technique used to control externally the beam quality of a laser diode array. Originally developed by Dr. Lew Goldberg at the Naval Research Laboratory, this technique in theory can phase-lock an array of lasers to a single external laser by injecting light from the external or master laser into each array laser element simultaneously in a master-slave laser configuration. This action causes the array of lasers to operate in phase with each other and therefore emit coherent beams. As a result, the injection-locked laser array appears as a single high-power, coherent source that has become useful for many of the applications previously discussed.

In Goddard experiments, light from a single-stripe laser diode was passed through a Faraday optical isolator and focused down on the end of a 10-element laser diode array (100 μm wide) capable of producing 500 mW of continuous or pulsed optical power. The experimental configuration is shown in the first figure. A linear camera, spectrometer, and interferometer were also used to monitor the respective intensity distribution, wavelength

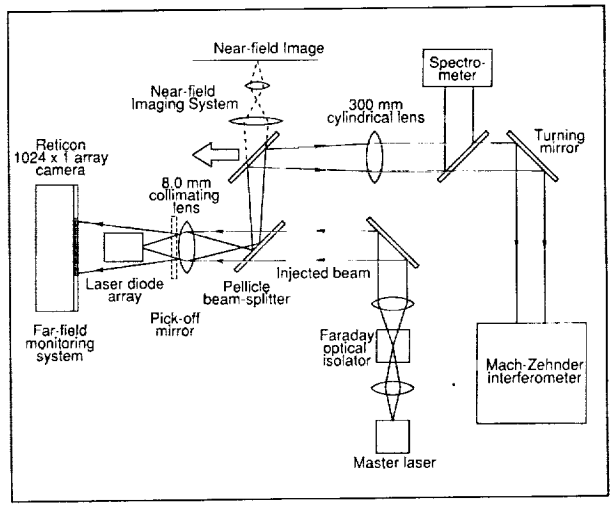

Experimental configuration for injection-locking experiments and subsequent diagnostic measurements. Light from the master laser is injected into the laser diode array.

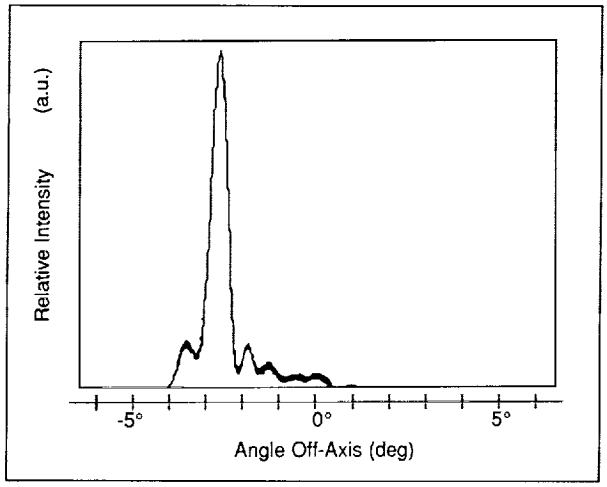

Intensity distribution of light from the injection-locked laser diode array. The main lobe contains 240 mW (77 percent) of the 340 mW total continuous power from the array. The light in the single lobe was also single wavelength. The injected power is 6.8 mW.

spectrum, and spatial coherence of the array output for both the free-running and injection-locked cases.

The free-running (i.e., uninjected) array operated at 340 mW of continuous power with typical multilobed intensity distribution and multiple-wavelength spectrum. Injection locking of the array occurred when 6.8 mW from the master laser was injected into an end element of the array at an angle of about 3°. The injection-locked array operated with 240 mW of continuous power optical power in a single-intensity lobe and at a single wavelength. The single lobe was emitted 3° from the array facet normal opposite to the injected beam and at the same wavelength as the master laser. The intensity distribution of the light is shown in the second figure. This observation leads Goddard researchers to believe that the injected array acts more like an amplifier of the master laser beam than as a phase-locked array of emitters. Other researchers have published similar results that lend support to this theory. Regardless of the actual physical mechanism, the desired result was achieved. Measurements of the phase-front quality of the injection-locked array output were made at Goddard and published, showing the 240-mW continuous power beam from injected array to be spatially coherent and almost diffraction limited ($\lambda/27$).

Subsequently, Goddard researchers have demonstrated injection locking of an array which was current modulated from 0 to 350 mW at 25 MHz and 50-percent duty cycle. The injection-locked array produced 230 mW of peak pulsed power in a single-intensity lobe and again at a single wavelength. Experiments to modulate the injected array at higher modulation rates and peak powers have been limited by the electronic current drivers. Further advancements in drivers may show that even faster and more intense single-lobe pulses may be achieved using injection locking in the future. Goddard researchers' results make these injection-locked arrays useful as solid-state laser pumps, as low-data-rate (25-Mbps) laser communications transmitters, and perhaps even as laser remote-sensing transmitters to measure amounts of atmospheric water vapor. Future work may further broaden the field of applications for these devices.

Contact: Donald M. Cornwell, Jr. (Code 723)
(301) 286-6542

Sponsor: OAST

Mr. Donald M. Cornwell, Jr., is currently working on the injection locking of high-power aluminum-gallium-arsenic gain-guided laser diode arrays for possible use as laser transmitters for NASA's Laser Communications Program. He earned his BS in physical sciences from the University of Maryland and in 1988 received the Best Student Paper Award in the Institute of Electrical and Electronics Engineers (IEEE) Region 2 for his work on the injection locking of index-guided semiconductor laser arrays. He has been with Goddard for 7 years.

LOW-FREQUENCY ELECTRIC AND MAGNETIC FIELDS

Goddard researchers used a state-of-the-art spectrum analyzer to measure low-frequency (3- to 30-Hz) electric and magnetic fields occurring in the Earth-ionosphere cavity (Spaniol and Sutton, 1988). The researchers have continued their investigation to determine sources, magnitudes, and frequencies that may occur in the cavity. The lowest cavity-resonant frequency is estimated to be about 8 Hz, but lower frequencies may be an important component of the electromagnetic environment.

The cavity-resonance study led to a review of the fundamental theories of the electron and its associated fields. The potential field frequencies produced by the electron were investigated with a classical model. During this investigation, the researchers discovered a relationship

between the high-frequency charge field and the extremely low frequency of the gravitational field. This relationship is expressed in terms of electron mass and is not corrected for relativistic effects:

$$m_e = (e/2C)\left\{ (h\,(1Hz)^2/(\pi\varepsilon_o{}^2\, GC) \right\}^{1/4} \qquad (1)$$

The numerical calculations agree with measured values at a surprisingly high level of precision. The researchers are continuing this investigation.

Development of a three-axis magnetic and electric field monitoring system is continuing with NASA support at West Virginia State College. The figure shows the college facility. The long-range plan is to establish monitoring systems at several historically black colleges and universities that would be connected to a data analysis center at West Virginia State through its existing uplink capability. Such a capability would permit both directional and phase information to be correlated to research the extremely low-frequency (ELF) electromagnetic activity of the Earth-ionosphere cavity. These data would be available to all NASA centers and any research center that has downlink capability. Correlation of solar activity, weather patterns, and aurora activity with cavity signals may lead to greater understanding of the Earth's overall electrical system.

The magnetic field sensor system incorporates a unique broadband active antenna capable of detecting fields as small as 1 pT in the 0.3- to 300-Hz range. In the past, search coils without feedback were employed only with great difficulty because of signal-to-noise ratio limitations. Also, the banks of low q-band-pass filters that were often employed could provide only crude spectral response information. With the new, more sensitive active antenna coupled to a Fast Fourier transform analyzer, both these limitations have been alleviated. The three-axis magnetic field measurement system now under development will incorporate three similar mutually orthogonal active antennas.

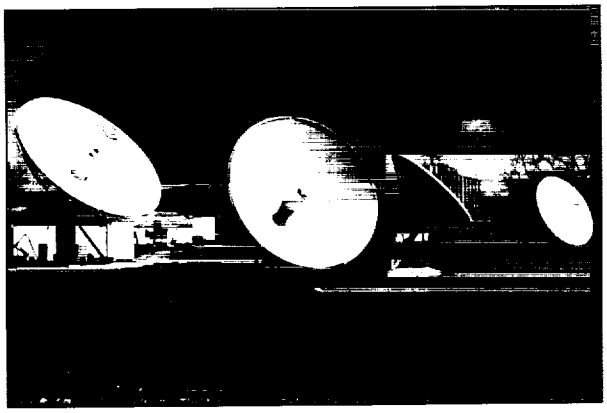

West Virginia State College Uplink Facility.

Contact: G. Craig Spaniol,
West Virginia State College (Code 728)
(301) 286-5454

John F. Sutton (Code 728)
(301) 286-5454

Sponsor: Summer Faculty Fellowship Program

Dr. G. Craig Spaniol, a graduate of West Virginia State College and Rensselaer Polytechnic Institute, is a professional engineer working with the Instrument Electronic System Branch. He is Chairman of the Department of Industrial Technology at West Virginia State College.

Dr. John F. Sutton designs low-noise electronic systems for satellite experiments. He is also developing therapy equipment for the treatment of leukemia and AIDS. Dr. Sutton has a PhD in physics and 29 years' experience at Goddard.

STABILITY STUDY OF A CONTROL SCHEME FOR TWO-PHASE THERMAL SYSTEMS

Two-phase thermal systems have a number of advantages over single-phase systems, such as isothermality, lower fluid inventory, smaller power needs, and less weight. As a result, two-phase systems have become the designated means of heat transfer for the space station and for other long-duration space facilities. One of the most common two-phase systems currently used on spacecraft is the heat pipe. A typical two-phase thermal loop consists of an evaporator plate for vaporizing the working fluid, a vapor header and transport line for transferring the vapor to the condenser, the condenser for removing heat and recondensing the fluid, a mechanical pump for supplying the pumping head, a reservoir for maintaining system pressure, and a liquid return line. Capillary wicking is sometimes used in the evaporator to supply pumping head for the system and to facilitate the separation of vapor and liquid. If the evaporator does have capillary wicks, then an isolator (a header which directs the liquid through a wick) is needed to prevent the

ORIGINAL PAGE
BLACK AND WHITE PHOTOGRAPH

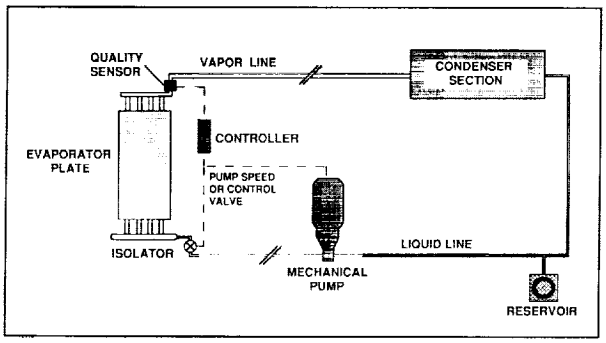

Two-phase thermal loop with quality controller
TWO PHASE THERMAL LOOP WITH QUALITY CONTROLLER

backflow of vapor. This configuration is shown in the accompanying figure.

Pumped two-phase systems tend to be harder to control than single-phase systems due to the lack of an adequate thermodynamic condition to use as feedback to the controller. Whereas single-phase systems can use temperature as the sensed property for a controller, two-phase systems are isothermal. One of the most important physical properties in a two-phase system is the percentage vapor (referred to as quality) of a stream. A measure of quality (or of another property that reflects quality) would be the ideal feedback for a controller. The technology that is the subject of the research reported here is based on using a nonazeotropic mixture of two refrigerants, rather than a single refrigerant such as ammonia. A nonazeotropic mixture is necessary since boiling temperature usually changes with composition, whereas azeotropic mixtures have a constant boiling temperature. The exit quality would then become a function of temperature and pressure, both of which can be determined by well-established techniques. Once the exit quality is sensed, the evaporator flow rate is regulated by a control valve (thermal expansion or solenoid) on the evaporator inlet or by adjusting the mechanical pump speed to maintain the exit quality at the desired value.

A computer model was constructed using the systems improved numerical differencing analyzer with the fluid integrator to determine under what conditions this control scheme could become unstable, how the system would respond, and what precautions could be taken to prevent this instability. A two-phase mechanically pumped loop with one wicked evaporator plate was used for the model. The quality in the vapor header was used as the feedback for a proportional-integral controller that adjusted the speed of the mechanical pump.

The results of the testing using the model indicate that a control system using the quality in the vapor header as the feedback property and flow rate as the control variable would be stable under a variety of load conditions. Step changes, sine wave variation, and a ramp increase in the heat load to the evaporator failed to show any sign of instability in the system. In addition, an increase in the condenser radiator temperature, a condition the controller was not meant to handle, did not result in a deviation of the header quality from the set point.

Contact: Steve M. Benner (Code 732)
(301) 286-4364

Frederick A. Costello,
Frederick A. Costello, Inc. (Code 732)
(703) 620-4942

Sponsor: Research and Technology Operating Plan

Dr. Steve M. Benner is responsible for the design, development, and testing of heat transfer systems, including capillary-pumped loops and heat pumps on the space station project. Dr. Benner is also interested in computer modeling of various thermal systems. He received his PhD in chemical engineering from The Ohio State University and has worked at Goddard for 2 years.

Dr. Frederick A. Costello designs and analyzes active and passive thermal control systems. Dr. Costello received a Small Business Innovative Research award for his nonazeotropic mixture concept. He earned his PhD in mechanical engineering from the University of Pennsylvania.

THE FATIGUE LIFE TESTING OF FLEXIBLE HOSES

Thermal control of large space facilities, such as the space station, will require the transport of large quantities of one- or two-phase fluid over considerable distances and through a variety of fittings. In the case of attached payloads, this transport may have to occur across joints that rotate or move in some manner. In addition, if the payload is tracking a celestial or terrestrial object, the joint could be in constant motion over the life of the space facility. This would place a tremendous strain on the fluid connection, requiring upwards of 150,000 cycles over a 10-year period with working fluids, such as anhydrous ammonia, on the inside and a space environment on the outside. One possible solution for making

this type of fluid connection is to use flexible hoses. This study was to determine whether flexible hoses, either teflon or corrugated metal, were capable of withstanding the large number of flexes under pressure that would be experienced on a long-term space facility.

A planetary design was chosen for the rotating pipe connection testing over the more common helical and spiral designs, because these require considerable hose length. Long lengths are needed to minimize buckling, kinking, and out-of-plane movement and especially to reduce the stress on the fittings. The long hose length adds significantly to the pressure loss and to parasitic heat transfer. Stress at the fittings is normally high and failures usually occur near or at these points; therefore, the flexing in this design is confined to areas away from the fittings. In addition, since the combined stresses caused by bending, hoop, and tensile stresses can cause local failure, the design isolates the bending caused by flexing. By minimizing stresses, the torque required to flex the joint is also minimized.

The flexible hose to be tested was wrapped around the sun and planetary pulleys, forming an "S" shape and resting in grooves in the pulleys. As the hose came off the lower section of the planetary pulley, it lay in a guide-track groove. The hose ends were held in place by fasteners. The end of the hose on the sun pulley was blocked, and the other end was attached to a pressure gauge, valve, and gas supply, which is used to pressurize the hose. A motor rotated the sun and planetary pulley via a system of gears and a drive arm. As the assembly operated, the hose was flexed back and forth along the section that passed between the two pulleys. Only about one foot of the hoses underwent flexing with little stress to the remainder of the hose.

The flexible hose was placed on the assembly as described above, then pressurized with nitrogen and checked for leaks. A current counter (used to monitor the length of time the motor was in operation) was set to zero and the motor turned on. Once the hose ruptured and its pressure dropped to zero, a pressure control sensor shut off the motor and the counter number recorder. The motor

Flexible Hose Test Results

(All sizes not marked are in inches)

Test	Type	Diam	Pres, psia	Hours	Cycles	Comments
1a	SS2*	0.375	175	72	50,000	Approximation
1b	SS2A	0.375	175	16	13,200	Without braid
1c	SS2	0.375	175	49	40,400	
2a	SS1A	0.50	175	<1	620	Without braid
2b	SS1	0.50	175	<1	620	
3a	Teflon1	0.50	35	230	189,750	No rupture
3b	Teflon1	0.50	145	230	189,750	No rupture
4a	Teflon2	0.375	55	239	197,200	No rupture
4b	Teflon2	0.375	130	239	197,200	No rupture
5a	SS3	0.25	55	118	97,400	
5b	SS3	0.25	130	76	62,700	
6a	SS1	0.50	55	37	30,500	
6b	SS2	0.375	55	41	33,800	
7	SS1	0.50	130	47	38,500	
8a	Teflon1	0.50	145	247	203,800	No rupture
8b	Teflon1	0.50	145	247	203,800	393,500 total cycles
8c	Teflon2	0.375	145	247	203,800	400,950 total cycles

**316L stainless steel*

operated at 13.75 rpm. The hoses tested were 1/2-, 3/8-, and 1/4-in. id corrugated metal (316L stainless steel), 1/2-in. id convoluted teflon, and 3/8-in. id smooth-bore teflon hoses. Aside from two test cases, the hoses had an exterior layer of stainless steel braid.

The 1/2- and 3/8-in. metal hoses used in this test study had fatigue lives of between 30,000 and 40,000 cycles, and the 1/4-in. hose had lives between 60,000 and 100,000 cycles, as shown in the accompanying table. There was no attempt to optimize the bend radius during the test because the equipment could not be altered in this way. All the hoses were subjected to the same bend radius of 5 in., even though the recommended minimum bend radius for the 1/2-in. metal hose was 5.9 in. This difference may have accounted for the short cycle life of the first 1/2-in. hose tested. In summary, the metal hoses of all three diameters fall far short of the desired life of 150,000 cycles and do not appear to be suitable for this application.

On the other hand, the teflon hoses withstood cycles as many as two and one-half times the desired cycles without rupturing. Whether the test was made continuously or not did not seem to affect the hose lives, but the hoses were not tested to total failure, and there may be some effect on the ultimate cycle life. There was an indication that failure of the convoluted teflon hoses might occur as a result of small leaks instead of rupturing, and this possibility will have to be studied further before teflon hoses can be considered for this application. There are some other possible drawbacks to the use of teflon hoses, such as permeability to ammonia, loss of flexibility due to temperature changes and ammonia exposure, cold creep at the fittings, and long-range durability, but if these problems can be addressed or corrected, then teflon hoses would seem to be the best choice of flexible hosing for use across rotating joints.

Contact: Steve M. Benner (Code 732.2)
(301) 286-4364
Frederick A. Costello,
Frederick A. Costello, Inc. (Code 732)
(301) 620-4942
Theodore D. Swanson (Code 732)
(301) 286-6952

Sponsor: Research and Technology Operating Plan

Dr. Steve M. Benner is responsible for the design, development, and testing of heat transfer systems, including capillary-pumped loops and heat pumps on the space station project. Dr. Benner is also interested in computer modeling of various thermal systems. He received his PhD in chemical engineering from The Ohio State University and has worked at Goddard for 2 years.

Dr. Frederick A. Costello designs and analyzes active and passive thermal control systems. Dr. Costello received a Small Business Innovative Research award for his nonazeotropic mixture concept. He earned his PhD in mechanical engineering from the University of Pennsylvania.

Mr. Theodore D. Swanson is a senior aerospace engineer with 5 years' experience at Goddard. Mr. Swanson, who holds an MS from the University of Maryland, designed the first ammonia-based, operational two-phase heat transfer testbed along with two ground-based photovoltaic power stations. He was also chairman of the Workshop on Two-Phase Fluid Behavior in a Space Environment.

CAPILLARY PUMPED LOOP FLIGHT EXPERIMENT (CAPL)

The CAPL is a follow-on to the Capillary Pumped Loop (CPL) Hitchhiker-G flight experiment described in *Research and Technology 1986*. The technology has been under development at Goddard for the past several years. This technology takes the latent heat of vaporization of ammonia in a closed thermal control system to transfer large amounts of heat over long distances. Two-phase systems like the CPL offer significant power and weight savings over single-phase systems currently in use. They also provide mounting interfaces (cold plates) that can be used to heat or cool electrical equipment, instruments, or other space-craft components. These cold plates are held at a nearly constant temperature over wide power ranges by the ammonia fluid that flows through them. Because the CPL has no moving parts, it has a higher inherent reliability than other mechanically pumped two-phase systems. Its main constraint is its limited pumping capability (approximately 0.5 psi), which is developed in the capillary pumps located in the cold plates.

The new experiment is designed to test the CPL-type of thermal control system that is baselined for the space station polar platforms. Flight validation of this technology in a microgravity environment is required before it can be implemented. Differences between the 1-g and micro-g

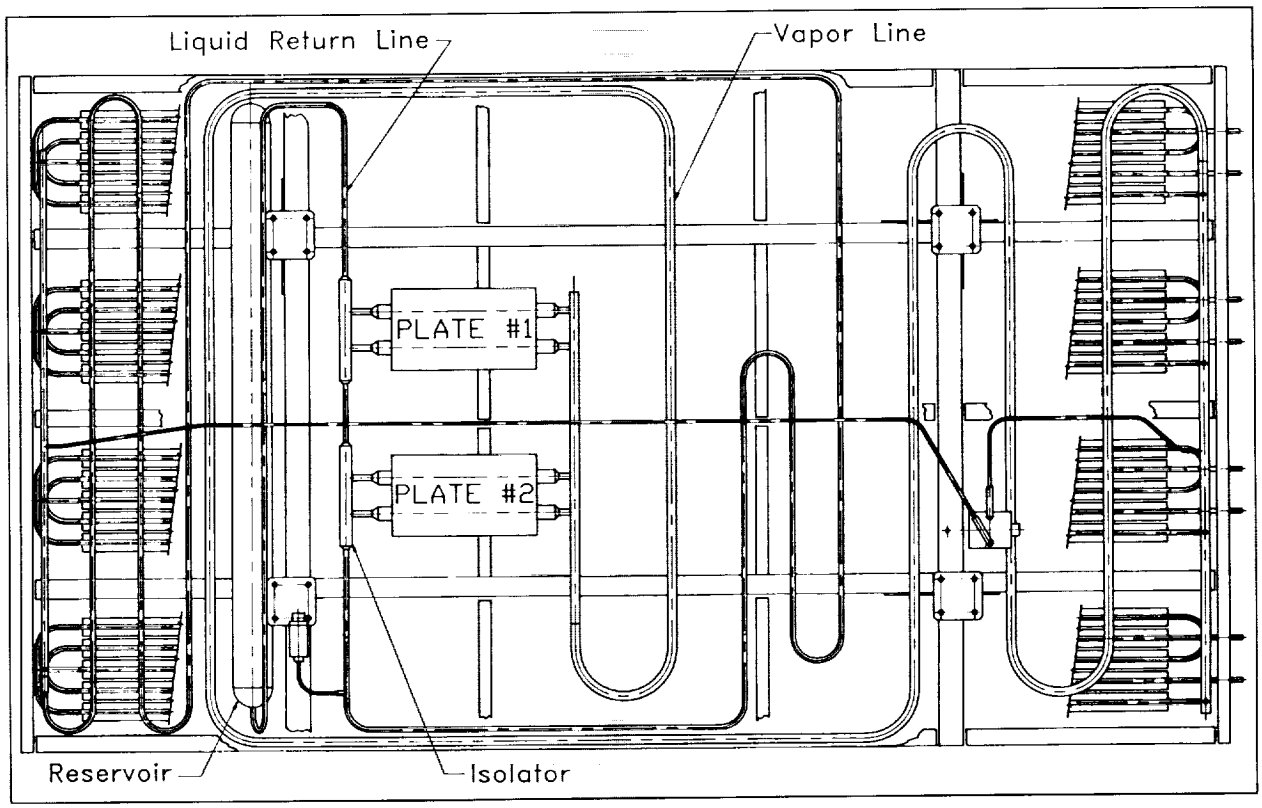

The CAPL current design.

operating characteristics in such areas as pressure losses, boiling and condensing heat transfer coefficients, and fluid management must be measured and tested. The initial CPL Hitchhiker-G experiment was a good first step in this direction and proved that the technology could be used in space. However, this experiment was only a small-scale representation of the device (14 in. by 14 in. by 4 in.) and had limited power and transport capability. Therefore, flight of a larger, full-size system is required for technology validation.

The CAPL experiment is shown as presently designed in the accompanying figure. It measures 56 in. by 100 in. by 13 in. and will be mounted to the Hitchhiker-G carrier system. One side is used as a radiator and faces into the shuttle bay; the other side contains the various experiment components sandwiched between the radiator and the plate. The CAPL has two cold plates with two capillary evaporator pumps mounted on each plate. Power levels up to 800 W per cold plate will be tested. The experiment also has a large thermally controlled reservoir and 10-m-long liquid and vapor transport lines (to simulate long transport distances on a large platform). Finally, there are four parallel radiator elements that condense the ammonia vapor and radiate the experiment heat load to space.

The experiment is currently being redesigned to reflect the latest polar platform thermal design concept. Enhancement and changes being evaluated include additional instrumentation, a heat pipe heat exchanger at the radiator interface, a smaller reservoir, a capillary starter pump, and increased liquid and vapor line transport distances. The additional instrumentation includes differential pressure transducers to measure the pressure losses along the transport lines and a flowmeter to measure the liquid ammonia flow rate. The heat pipe heat exchanger radiator will replace the direct condensation radiator in the current design. This heat rejection technique is required by the platform due to the vulnerability of the platform radiator to meteoroid hits, which could result in the loss of fluid inventory. A heat exchanger would use heat pipes to carry the heat from the CPL thermal control loop to the radiators. Since the heat pipes each have a separate self-contained fluid loop, a meteoroid puncture would result in the loss of only one radiator element, and not the

entire thermal control system (which would happen with the direct condensation radiator design). The smaller reservoir will be used to demonstrate CAPL operation with a reduced fluid inventory, thus lowering the ammonia charge requirement for future CPL systems. The starter pump will be used to assist startup operations and clear excess ammonia liquid that may accumulate in the vapor lines. Increases in the transport length from 10 to 15 m will simulate more accurately the latest platform configuration, and effects such as increased pressure drop and parasitic heat loss will be evaluated.

The new CPL experiment will be flown on the Hitchhiker-G carrier, which will provide shuttle power and real-time data and command capability. The experiment will be monitored on the ground with the heater power profiles controlled by ground commands. After completion of the redesign phase, the experiment will be fabricated, tested, and flight qualified. It is scheduled for a flight readiness date of June 1991.

Contacts: Dan Butler (Code 732)
(301) 286-5235
Roy McIntosh (Code 732.2)
(301) 286-3478

Sponsor: Office of Space Station

Mr. Dan Butler is a research and development engineer in the Thermal Engineering Branch, Applied Engineering Division, with 12 years' experience at Goddard. He holds a BS in aerospace engineering from Virginia Polytechnic Institute and State University. Mr. Butler currently serves as Program Manager for CAPL.

Mr. Roy McIntosh is Head of the Advanced Development and Flight Experiments Section in the Thermal Engineering Branch. Mr. McIntosh, who received his education at Antioch College, has acquired 27 years' experience at Goddard and earned two Exceptional Performance Awards and a NASA Exceptional Engineering Achievement Medal for work in two-phase heat transfer.

AN IMPROVED HIGH-POWER THERMAL CONTROL SYSTEM

Goddard is responsible for developing the thermal control system for Space Station Freedom's attached payloads, free-flying platforms, and payload servicing bay. This thermal system must be capable of acquiring tens of kilowatts worth of heat, which must then be carried up to 30 m to the heat sink. In addition, multiple users applying different heat loads must be maintained at the same operating temperature regardless of their relative location in the loop.

Two-phase heat transfer systems are being investigated as a means of meeting these thermal requirements. In a two-phase process, heat is acquired when a fluid changes phase from a liquid to vapor. Because refrigerants such as ammonia have a very high heat of vaporization, large amounts of heat can be transferred in a two-phase process with a relatively small mass flow rate. Since evaporation and condensation occur at nearly the same temperature, users would be unaffected by their position in the loop. Thus, a two-phase system is ideal for meeting the space station's external thermal control requirements.

Goddard researchers have investigated a variety of two-phase concepts over the past 5 years. One of the most promising candidates has been the Hybrid Capillary Pumped Loop (HCPL). The HCPL can operate as either a capillary-pumped system or a mechanically pumped loop. As a capillary system, the pressure head needed to circulate the fluid is derived solely from capillary action in a polyethylene wick. When the system requires more flow than can be derived from capillary action alone, a conventional mechanical pump is employed to provide the needed fluid flow.

One type of HCPL, called the High Power Spacecraft Thermal Management System (see figure), has been tested successfully by the Advanced Development Section at Goddard for over 2 years. In the most recent

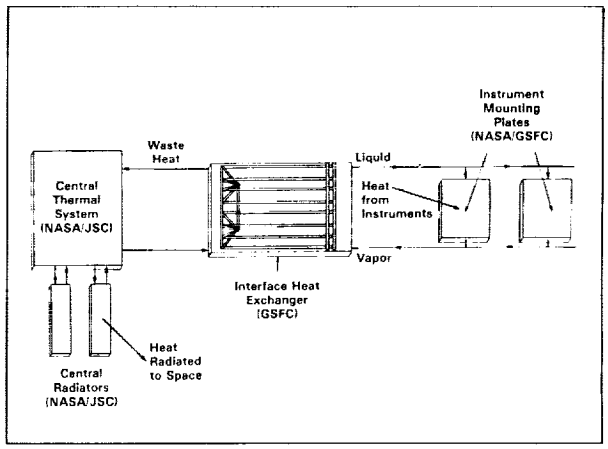

Space station thermal interface development.

testing phase, modifications were made to the facility and the system so that Goddard staff could demonstrate loop performance over a much broader range of operating conditions.

One of the more significant changes made to improve the system was the installation of a 25 kW-capacity refrigerator (prior tests were limited to 10 kW of steady-state cooling). The improved refrigerator permitted researchers to perform long-duration tests, during which the system was subjected to heat loads of 500 to 20,000 W continuously for over 2,000 h.

A coolant loop was added to one of the evaporator plates to quantify the capillary evaporator's ability to operate as either an evaporator or condenser. Tests were performed in which the regular condenser was closed using a valve, and one of the evaporator plates operated as the lone condenser in the High Power Spacecraft Thermal Management System. The ability to operate a capillary pump as either an evaporator or a condenser greatly increases design flexibility if the thermal control system is a HCPL.

An additional requirement that Goddard must meet to support the thermal control of Space Station Freedom is to minimize system weight. The amount of fluid required to operate the High Power Space Thermal Managment System will have a direct bearing on the overall system weight. One goal of the tests was to determine if the fluid inventory could be reduced. To meet this end, a capillary starter pump and reservoir load cells were added to the system. The starter pump is a uniquely designed capillary pump whose purpose is to sweep any liquid out of the vapor header before applying heat to the evaporator section. The load cell allowed operators to understand the reservoir's dynamics better. Tests showed that with an ammonia inventory less than what is required to flood the system, the starter pump effectively wetted the capillary evaporators' wicks, which had previously been dry. This wetting permitted the system to start normally when heat was applied to the plates. Without the starter pump, system startups with a dry wick were not always successful.

The improvements greatly increased the scope of tests that could be performed on the High Power Spacecraft Thermal Management System. The latest have improved understanding of how the HCPL operates. To verify the HCPL concept in a microgravity environment, Goddard will be flying a space shuttle experiment in the early 1990's.

Contacts: Michael E. McCabe (Code 732)
(301) 286-4363
Roy McIntosh (Code 732.2)
(301) 286-3478

Sponsor: Space Station Freedom

Mr. Michael E. McCabe has 4 years' experience testing and developing advanced spacecraft thermal control systems and components in the Thermal Engineering Branch. Mr. McCabe has a BS in mechanical engineering from the University of Maryland.

Mr. Roy McIntosh is Head of the Advanced Development and Flight Experiments Section in the Thermal Engineering Branch. Mr. McIntosh, who received his education at Antioch College, has acquired 27 years' experience at Goddard and earned two Exceptional Performance Awards and a NASA Exceptional Engineering Achievement Medal for work in two-phase heat transfer.

TWO-PHASE INTERFACE HEAT EXCHANGER

Heat exchangers are an integral element of any large thermal control system. These devices permit the transfer of heat across a boundary without mixing the two heat transfer fluids. This physical separation can be critical to fluid management, safety, and reliability. The two-phase thermal system proposed for the completed Space Station Freedom will rely on heat exchangers for several specific applications. The Interface Heat Exchanger developed in this effort is intended primarily to transfer heat from an instrument thermal bus to the central thermal bus. Heat is transferred by condensing the instrument bus heat transfer fluid (ammonia) on one side of the heat exchanger and boiling the central bus heat transfer fluid (also ammonia) on the other side. Specifications require a heat transfer rate of 8 kW at a temperature differential of 5 °C.

The Interface Heat Exchanger uses a tube-within-a-tube design with eight such tube pairs in parallel. The inner tube is used for boiling and the outer tube for condensation. Both tubes employ a spiral fin to enhance the heat transfer coefficient and to manage the fluid. In microgravity, the 11° spiral keeps liquid from the central thermal bus on the boiling side of the interface and vapor from the instrument thermal bus on the condensing side. The tubing is made from 6061 aluminum. The outer tube is 1 in. in diameter while the active length of each leg is 36 in.

ORIGINAL PAGE
BLACK AND WHITE PHOTOGRAPH

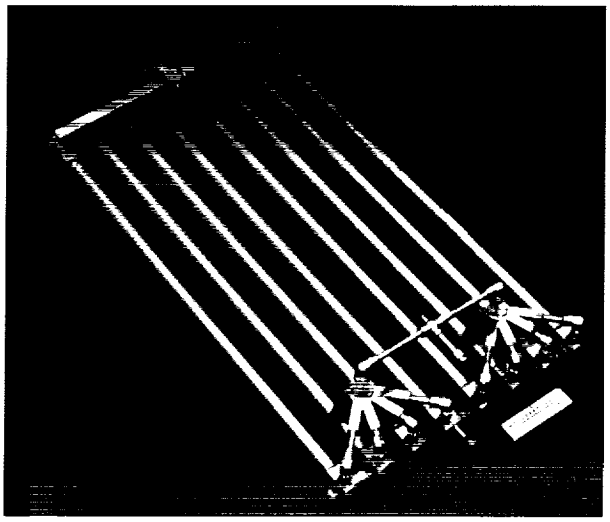

Two-phase interface heat exchanger.

The Interface Heat Exchanger underwent an extensive in-house testing program at Goddard. Each side was connected to a two-phase thermal bus charged with ammonia. This effort was the first realistic test involving the coupling of two two-phase thermal loops in the space station program. The Interface Heat Exchanger transferred 8.2 kW at a temperature differential of 5 °C. This performance exceeded specifications. However, researchers discovered that performance was affected by the flow rate of the liquid ammonia on the boiling side. When this flow rate was decreased to a point where the quality of the exit flow exceeded 30 percent, one or more of the eight parallel tubes dried out and a vapor blow-through occurred. This situation occurred regardless of total heat load or saturation temperature. This limitation may result from a flow distribution problem in the inlet header. Performance testing demonstrated that the heat exchanger was sensitive to adverse tilt. In addition, the maximum vapor exit quality was demonstrated to be a function of liquid inlet pressure drop. This behavior is characteristic of poor flow distribution.

Contact: Theodore D. Swanson (Code 732)
(301) 286-6952
Michael E. McCabe (Code 732)
(301) 286-4363

Sponsor: OAST

Mr. Theodore D. Swanson is a senior aerospace engineer with 5 years' experience at Goddard. Mr. Swanson, who holds an MS from the University of Maryland, designed the first ammonia-based, operational two-phase heat transfer testbed along with two ground-based photovoltaic power stations. He was also chairman of the Workshop on Two-Phase Fluid Behavior in a Space Environment.

Mr. Michael E. McCabe has 4 years' experience testing and developing advanced spacecraft thermal control systems and components in the Thermal Engineering Branch. Mr. McCabe has a BS in mechanical engineering from the University of Maryland.

OVERHEAD GANTRY ROBOT FOR FLIGHT TELEROBOTIC SERVICER (FTS) OPERATIONAL SIMULATIONS

NASA is developing an FTS through a contractor to assist astronauts in performing space station assembly and servicing tasks. The Goddard FTS Development, Integration, and Test Facility is responsible for performing simulations of space station scenarios using ground robots and full-size mockups of space station components to assist in the selection and validation of the tasks to be performed by the FTS. Since the FTS will perform tasks in conjunction with the shuttle and space station remote manipulator systems, an essential part of the FTS operational simulator is a Remote Manipulator System (RMS) simulator.

Goddard purchased a dual-arm gantry-style robot to simulate the RMS and installed in it the Development, Integration, and Test Facility. The robot is shown in the first figure. This gantry system includes two 6-DOF arms, each capable of lifting 4,000 lb and exerting 4,000 ft-lb of torque. Motions are repeatable to within 0.006 in. and 0.02° throughout the 46- × 25- × 8-ft work envelope. This strength and repeatability is achieved because of the high rigidity of the gantry system, which contrasts with the more flexible structure of the RMS. This difference is necessary because of the large load capacities required of the simulator to manipulate full-size mockups in a 1-g environment. The RMS is capable of manipulating these large structures in the microgravity environment of space, but on Earth it cannot support its own weight.

Because of the high rigidity and strength of the gantry system, some form of mechanical compliance is necessary to prevent damage to the mockups. This compliance is achieved through the use of a passive charge-coupled device (CCD), which is shown in the second figure. The device currently in use provides full 6-DOF compliance.

ORIGINAL PAGE
BLACK AND WHITE PHOTOGRAPH

Goddard researchers plan a future version that will allow the stiffness of the device to be varied and the exact deflection of the device to be measured. The CCD is connected to a quick-disconnect device, which allows the robot to easily grasp and release suitably outfitted mockups.

Goddard researchers have demonstrated capabilities for the robot to autonomously retrieve, position, and release mockups of a space station deck carrier and Station Interface Adapter (SIA). Goddard researchers have verified the robot's capability to perform various in-space tasks. This verification was achieved by retrieving and positioning the SIA using the gantry. The gantry allows a floor-mounted PUMA robot arm, which simulates the FTS, to deploy the SIA legs. Then the gantry moves the SIA so that each leg rests against a space station truss node, and the gantry holds the SIA in position while the PUMA attaches the legs to the nodes with a nut-driver mechanism. Then the gantry releases the SIA, grasps the deck carrier, transports it to a point above the SIA, and lowers it into position. An attachment mechanism is activated to join the deck carrier to the SIA. The gantry releases itself and moves away while two PUMA robots perform a number of tasks on the deck carrier and an attached Orbital Replacement Unit (ORU). The gantry is operated by a menu-driven software system that uses motion routines from the library supporting the robot. The motions are performed using taught points and programmed motions with predefined velocities and accelerations.

The two floor-mounted PUMA arms will be replaced by a pair of bilateral force-reflecting master-slave arms.

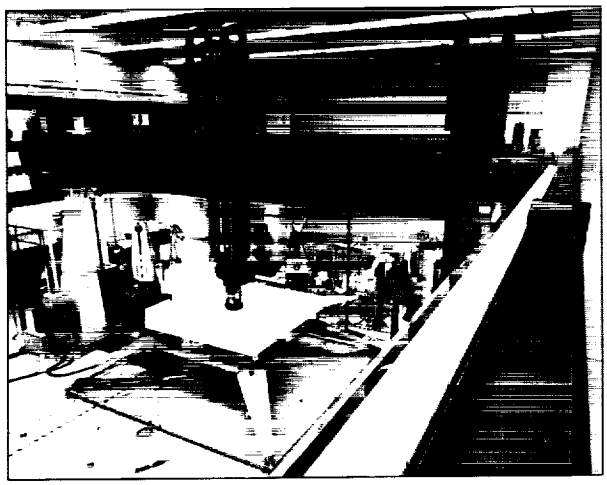

Dual-arm, gantry-style robot.

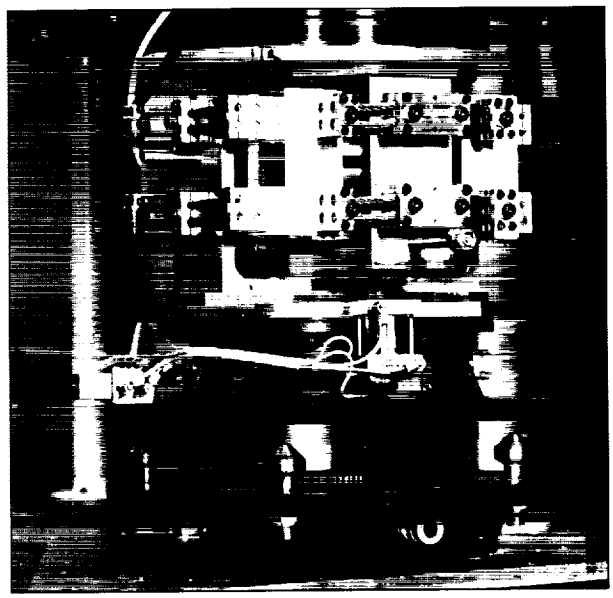

Passive CCD.

These arms will be mounted to a second gantry mast using a strongback and will soon be used to simulate the FTS. The gantry control system is also being upgraded to reflect more accurately the RMS-to-operator interface. To more accurately duplicate the RMS control interface, joystick control capability will be added to the system, and the operator interface will be moved into a mockup of the aft flight deck work station of the space shuttle orbiter. A new gantry control system is being developed to add this new capability. This control system will be an extension of the Hierarchical Ada Robotic Programming System currently under development. This system is an implementation of the NASA Standard Reference Model, which is a robot control architecture developed by National Institute of Standards and Technology (NIST) and NASA. The new gantry control system will allow for teleoperated or autonomous, as well as shared and force-position, control of the system. With this upgraded control, the gantry system will allow the simulation of additional space station tasks, such as the Astromag experiment deployment and radiator panel assembly.

The gantry system has proven its usefulness as an RMS system simulator. It is unique in its ability to allow end-to-end testing of various FTS tasks using full-scale mockups without the need for elaborate gravity-offset systems. This capability for end-to-end testing of proposed tasks is an invaluable aid in designing the flight system and planning the FTS tasks.*

**The CCD shown in the second figure was developed by Jim Kerley at Goddard. The Hierarchical Ada Robotic Programming System is being developed by Stephen Leake of NIST.*

Contact: Thomas C. Feild, Jr. (Code 735)
(301) 286-6686

Sponsor: Space Station Freedom FTS Project

Mr. Thomas C. Feild, Jr., is an electrical engineer in the Robotics Data Systems and Integration Section with 7 years' experience at Goddard. For the past several years, he has helped develop a laboratory to demonstrate use of robots for space station assembly and servicing tasks. Mr. Feild received his BS in electrical engineering from Virginia Polytechnic Institute and State University.

MODEL-BASED ROBOT VISION USING ALGEBRAIC IMAGE OPERATORS

Vision is one of the most important sensory resources of an autonomous/semi-autonomous robotic system. A vision system is required to process raw video data to determine an object's identification, pose, and location relative to the image plane. This information is used by other elements of the robot control system to determine the appropriate manipulator movement to perform the given task.

Goddard is developing a robust vision system to perform object-independent/ orientation-independent feature extraction and object identification. The system is divided into three processing tasks: (1) low-level scene analysis/edge detection; (2) linear feature extraction; (3) model matching/pose interpretation.

Previous Goddard research on a highly structured and compact algebraic representation of grey-level images viewed as fuzzy sets has been extended. Addition and multiplication are defined for the set of all grey level images and can then be described as polynomials of two variables.

If Z denotes the integers, then an image A may be represented as

$$A = \{ (x,y) \in Z \times Z \mid \mu_A (x,y) \in [0,1] \}, \qquad (1)$$

where μ_A (x,y), denoting the grey level of pixel (x,y), is a real number between 0 and 1 with the larger numbers corresponding to the darker grey levels. In this way A may be viewed as a fuzzy set.

Let A and B be grey-level images. The addition of A and B is defined as:

$$A + B = \{ (x,y) \in A \cup B \mid \mu_{A+B} = \min [\max (\mu_A (x,y) , \mu_B (x,y)) , \max (1 - \mu_A (x,y) , 1 - \mu_B (x,y))] \} \qquad (2)$$

Observe that in the binary case (with μ = either 1 or 0), the addition reduces to the "exclusive-or" addition. That is, in binary set theoretic addition of images A and B is

$$A + B = (A \cup B) \cap (\bar{A} \cup \bar{B}) \qquad (3)$$

where $\bar{A}$ and $\bar{B}$ are the inverse images of A and B respectively.

Multiplication of grey-level images A and B is defined by

$$A * B = \left\{ \sum (x_1 + x_2 , y_1 + y_2) \mid \mu_{A*B} (x_1 + x_2 , y_1 + y_2) = \min_{\substack{(x_1 , y_1) \in A , \\ (x_2 , y_2) \in B}} [\mu_A (x_1 , y_1) , \mu_B (x_2 , y_2)] \right\} \qquad (4)$$

where Σ denotes the addition performed by (2).

The operations of + and * are commutative and associative, thus making the set of all grey-level images a commutative semigroup under each of these operations.

Under the addition and multiplication operations defined above, an image A may be represented as the polynomial

$$A = \sum_{(m , n) \in A} \mu_{mn} x^m y^n \qquad (5)$$

where the coefficient is the grey-level of pixel (m,n) and the summation is defined by (2).

The new algebraic structure provides the basis for an innovative, efficient edge detection scheme.

The classical two-dimensional differential operator is defined as

$$D1 = (1 + x)(1 + y) \qquad (6)$$

This operator produces a spotty edge as seen in (a) of the first figure.

Then the classical differential operator was varied to the form

$$D2 = 1 + xy \qquad (7)$$

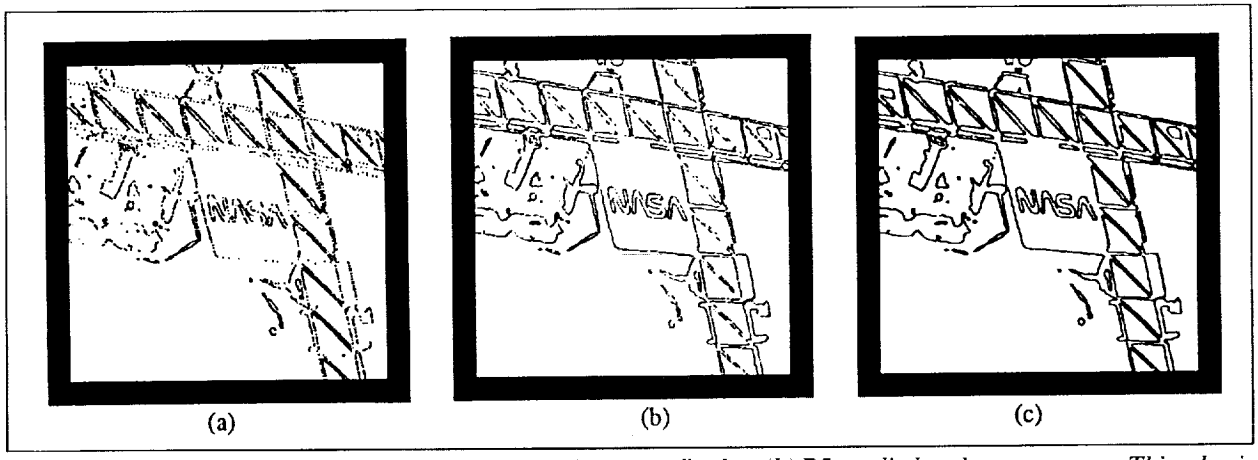

(a) The operation of D1 on a complex scene. Notice the "spotty" edge. (b) D2 applied to the same scene. This edge is better; however, the bias is apparent on the diagonal struts. (c) The operation of D3 on the scene. This operator contains no bias and produces a solid edge.

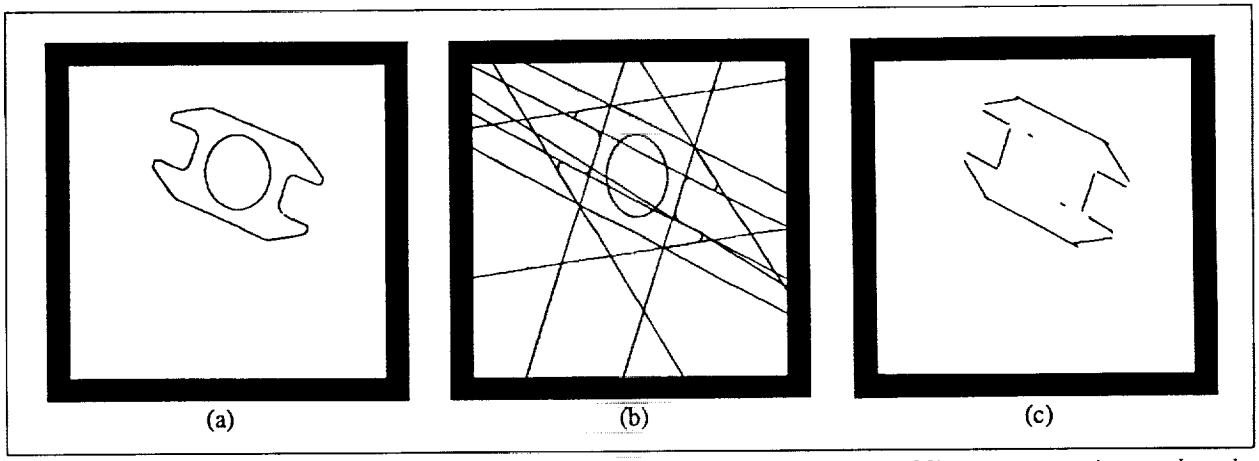

(a) The operation of D3 on an ORU handle scene. (b) The Hough-derived analytical lines are super-imposed on the edged image. Note the accuracy. (c) The line segments are determined by the line follower/line locator. This information is passed to a model matcher.

This new, more compact irreducible polynomial operator gave a substantially improved contour enhancement capability. Although *D*2 proved to be a simple, efficient operator for contour enhancement in images with a preponderance of vertical and horizontal lines, its major drawback was the introduction of a bias along the -45° lines. This is seen in (b) of the first figure.

To overcome this bias, the differential operator on an image A was varied to

$$D3 * A = \quad (8)$$
$$\{(m,n)\ \varepsilon\ (A + Axy) \cup (Ax + Ay) \mid \mu_{D3*A}(m,n) = \max[\mu_{A+Axy}(m,n), \mu_{Ax+Ay}(m,n)]\}$$

This *D*3 operating on a complicated scene is shown in (c) of the first figure.

The algebraic edge detector has been employed as the front end of a linear feature extraction system which is based on the Hough transform. The primary goal is to establish and maintain object independence and system invariance to object rotation, translation, and scaling in the image. The system takes the edge image as input and produces a list of line segments.

The Hough transform is a technique for placing parameters on binary image points. Then, these points are placed into a family of curves representing the analytical

equations of image features. The employed linear transform is based on the following equation.

$$\rho = x*\cos(\theta)+y*\sin(\theta), \quad (9)$$

Where x and y are the coordinates of the edge, θ is the evaluated orientation relative to the x axis (evaluated in the range of $-\pi/2$ to $\pi/2$), and ρ is the normal vector to the line of that orientation. The evaluation of equation (9) produces the transform parameter space.

Goddard scientists have thus developed an adaptable and reliable method for processing the Hough transform parameter space to extract unique image feature equations. The analytical feature representations are then used to locate actual feature segment endpoints via a line-following/segment-locating mechanism.

The processing sequence of the linear feature extraction system is shown in the second figure.

Contact: Bao-Ting Lerner,
U.S. Naval Academy (Code 735)
(301) 286-4817
Michael V. Morelli,
Fairleigh Dickinson University (Code 735)
(301) 286-8269

Dr. Bao-Ting Lerner is an Associate Professor of mathematics at the U.S. Naval Academy. For the past 2 years, she has been a visiting research professor at the Goddard Robotics Laboratory where she has directed research projects on computer vision and applications of multivalued logic to expert system development. She was named a Summer Faculty Fellow by the American Society for Engineering Education in 1987 and 1988 while working in the Robotics Laboratory.

Mr. Michael V. Morelli, a research intern and consultant at the Robotics Laboratory for the past 2 years, conducts vision research in the areas of statistical analysis and modeling of illumination effects. Currently, he is a graduate student at Fairleigh Dickinson University.

VISION AND FORCE CONTROL OF ROBOT GRASPING OPERATIONS

Researchers at the Goddard Development, Integration, and Test Facility have designed a two-finger robot gripper mechanism, which mounts on a PUMA 762 robot and uses a standardized handle for robotic grasping operations. With this gripper-handle combination, a variety of tasks can be performed, such as servicing or replacing an ORU. The vision and force control systems automate the grasping operation through the use of machine vision and a force-torque-controlled gripper.

The systems consist of a MicroVAX II running VAXELN for the image processing, a MicroVAX II running VMS for the robot control system, a wrist camera and force/torque sensor attached to the robot arm behind the gripper shown in the first figure, and a visual target mounted on the handle. The first step is to position the gripper fingers in relation to the ORU handle so that they can properly engage the handle. This part of the grasping operation is accomplished by the machine vision system.

The vision system positions the gripper through an iterative process. First, the robot arm is manipulated so that the gripper is near the handle and the target is in the field of view of the wrist camera. The target consists of four black spots forming a square on a white background with a black border and is shown in the second figure.

Next, a frame grabber board in the MicroVAX II digitizes a single video frame to identify the target. The frame grabber digitizes the target into a 256-bit gray scale and reduces it to a two-level black-and-white image based on a preselected threshold. Any pixel lighter than the threshold becomes white, and any pixel darker than the threshold becomes black. Then software on the MicroVAX II, with the help of the black border of the white target, searches for the target. Target candidates are sorted, then

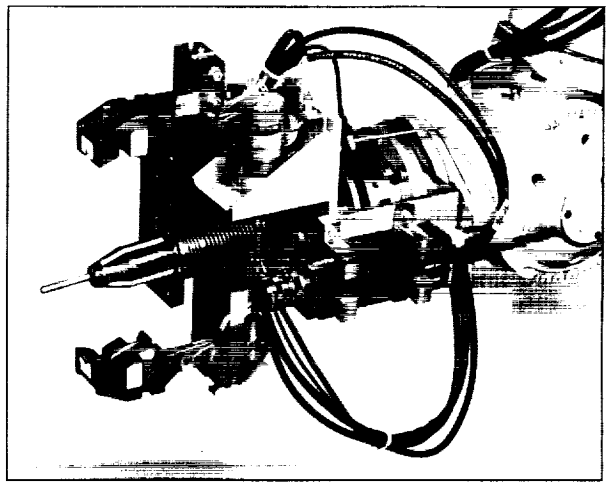

The two-finger robot gripper with force-torque sensor and wrist camera.

ORIGINAL PAGE
BLACK AND WHITE PHOTOGRAPH

examined from largest to smallest. The software starts with the largest candidate and searches it for a four-spot target. If the target is not found, the next-largest candidate is examined. The search halts when the target is found. If none of the candidates is correct, the software searches the whole image for the four spots.

Once identified, the apparent size and perspective of the four-spot target image and the focal length of the camera are used to determine the viewing angle and the distance of the camera from the target. The position and orientation data are then passed to the robot control MicroVAX. The entire process, from digitizing the video frame to determining the position and orientation, requires from 1 to 5 s.

The robot control computer responds to the vision system data by moving the gripper about 80 percent closer to the handle; then it starts the entire procedure again. Placing the gripper within 1 or 2 mm and 1° or 2° of its aligned position usually requires 5 iterations.

At this point, force control replaces vision to complete the grasping operation. In order to make force control of the gripper possible, its fingers are equipped with strain gauges and attached to the arm through a 6-DOF force-torque sensor. The strain gauges indicate the gripping force being exerted, and the force-torque sensor measures forces and torques about three orthogonal axes.

While the fingers close on the handle, the finger controller maintains a preselected force level. When the robot control computer sensed that the fingers' position is no longer changing, it starts to monitor the output from the force-torque sensor. The presence of forces or torques indicates a misalignment of the fingers and the handle. If any are detected, the robot control computer moves the arm to negate the forces or torques. This action continues until the forces and torques are within acceptable limits and the fingers are closed on the handle.

Sometimes the fingers catch on the handle, but no forces or torques are generated. In that case, the finger separation will not be within the specified limits of its closed value. If that happens, the robot goes to joystick mode, and an operator uses a joystick and cameras to manipulate the robot arm to free the fingers and allow them to continue to close. Once the fingers are free to close, the operator hits a button to return control to the robot control computer.

Several improvements to the vision system are now functioning in a test mode and will be integrated in the near future. Currently, the threshold level is selected manually. The vision system is very sensitive and will fail to identify the target if the threshold is not set properly for the existing lighting conditions. Human eyes are much less discriminating and cannot discern small changes that affect the system. This problem may be solved by selecting the threshold automatically for each image to be processed.

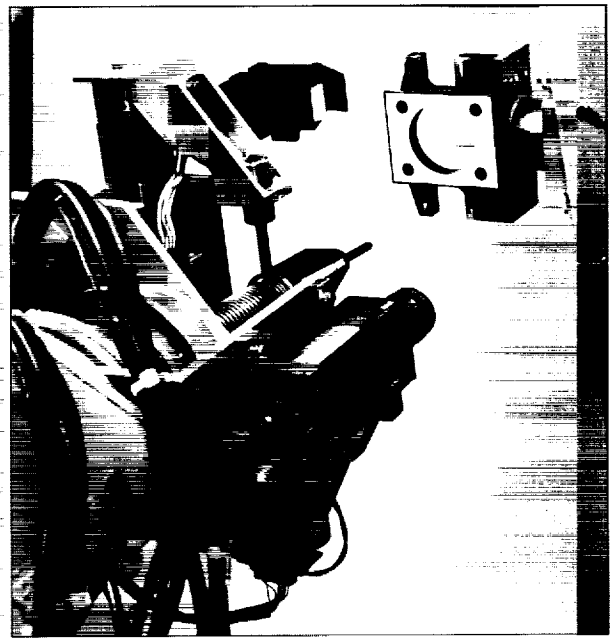

The robot gripper and its target.

In the future, a specialized image processing machine (Datacube) will replace the vision system MicroVAX. The new machine will include special hardware to speed the process of identifying potential targets in an image. This machine will greatly speed the target-recognition and position-determination process.

Another enhancement that will reduce processing time is programming the vision computer to remember the last position of the target in each iteration. The position of the target in the video frame can be predicted accurately as the arm closes in on the handle. The search would start at the most likely area based on the previous frame instead of from scratch as is now done in each iteration. Some time can be saved this way because target recognition is the most time-consuming part of the machine-vision process.

The vision and force control systems automate the fine guidance portion of the grasping operation. These systems

reduce operator workload significantly because fine guidance ordinarily requires a great deal of concentration and is fatiguing. Also, mistakes are more likely to cause damage to the objects being manipulated. Finally, the vision and force control systems can be incorporated easily into a totally autonomous robotic system.

Contact: Arlie D. Long (Code 735)
(301) 286-9717

Sponsor: Space Station Freedom FTS Project

Mr. Arlie D. Long, a computer engineer in the Robotics Data Systems and Integration Section, is currently involved in robot control systems and software development for robot assembly and maintenance of the space station. He received his BS in electrical engineering from the University of Maryland and has been at Goddard for 15 years.

THE USE OF TIMERS TO EXTEND MISSION LIFE

The PEGSAT spacecraft will be used to support a short-duration science mission involving chemical releases over northern latitude ground observation sites. The mission will accomplish the chemical release when the proper combination of time, weather, and science conditions exist. There will be approximately three windows of opportunity during the 3- to 4-month mission.

PEGSAT power is a limited resource; due to the lack of solar arrays, special operational and design considerations were made to maximize mission life. The total spacecraft power for the mission is about 1,000 W/h. Special low-power timing circuits and system operating modes were developed and implemented to control spacecraft subsystems and components. Three system operating modes cycle power to the spacecraft subsystems: full system on, command receiver on, and timers only.

In the full-system-on mode, telemetry is being sent to the ground station. The telemetry includes all temperature, battery monitors, status, magnetometer, and other signals. This mode uses the most power, approximately 84 W. This mode is on for only 10 min/day, which is about the amount of time of one ground station contact. To get into this mode, the ground station sends a command to turn on the 10-min contact timer.

The second mode, command receiver, is on for 3 h/day. This period is required to ensure a minimum of two good ground passes. With the command receiver on, engineers are able to send commands to the spacecraft. The power in this mode is about 0.5 W.

The last mode, timers only, is the lowest power mode. This mode needs only 0.006 W. This is the mode that the spacecraft is in for 21 h/day. The function of this mode is to enable and disable the command receiver mode.

All these modes are controlled by a set of timers. The periodic timer controls the command receiver, and the contact timer allows 10 min for the ground pass. With the use of timers, Goddard engineers are able to extend the mission life by powering only the systems that are required.

Contact: Timothy D. Gruner (Code 745.2)
(301) 286-3891

Sponsor: PEGSAT Project, Attitude Control Branch, Engineering Directorate

Mr. Timothy D. Gruner is an electronic engineer with the Electronics and Computer Development Section. He graduated with a BS from the University of Delaware and has 3 years' experience developing and implementing electronics hardware and associated software for the Spartan, PEGSAT, and Small Explorer projects.

PEGSAT ATTITUDE MONITORING SYSTEM

The PEGSAT satellite, which is to be placed in a polar orbit on the first launch of a Pegasus vehicle this year, will release large barium clouds during orbit passes over Fort Churchill, Canada. The objective is to allow ground observations of the electric and magnetic fields of the Earth in the vicinity of an aurora. To optimize effects due to orbital velocity on the cloud expansion, it is desired that the spacecraft, which is spin-stabilized at 6 rpm, pass through a predetermined spin angle with respect to the magnetic field at the moment the chemical cloud is released. With only a three-axis magnetometer and no onboard processing available, a capability was needed to process the magnetometer telemetry at the Fort Churchill ground station to allow the experimenter to correlate the spacecraft rotation and position with auroral activity. This capability would enable the cloud-release command to be uplinked at the correct time. To achieve this, a scheme has been implemented on a personal computer that processes telemetered magnetometer signals, first on an earlier pass so

that the direction of the spin axis can be ascertained, and then on the cloud-release pass to determine possible release times (one for each spin of the spacecraft) as well as the spacecraft latitude at those times.

During the cloud-release pass, after acquisition of signal, a time code generator and the magnetometer telemetry are sampled and processed every 7 ms to give a spin angle with respect to the magnetic field. When the computed angle exceeds 350°, a time versus angle function is fit to the data collected on that revolution using a linear least-squares fit. Then the function is solved for future times when the spacecraft will rotate through the desired spin angle. For each of these times, the spacecraft latitude is determined from a polynomial equation for latitude versus time whose coefficients are determined before the pass based on the latest North American Defense Command parameters. The resulting list of times and latitudes is then displayed and refreshed after the next revolution.

The experimenter can select a time of release by determining which corresponding latitude is closest to auroral activity he is observing with ground-based all-sky cameras. When the selection is made, as late as 1 min before release, the personal computer is armed and begins a countdown to the selected time. At $T = 0$, a signal is sent to the command transmitter which uplinks the command to the spacecraft to fire one of the two barium canisters.

Contact: David J. Olney (Code 745)
(301) 286-5350
Todd Shope (Code 740)
(301) 286-2369

Sponsor: Engineering Directorate

Mr. David J. Olney is currently Head of the Sensor Development and Flight Support Section. He has been an attitude control systems engineer working with Pegasus, Small Explorer, Combined Radiation and Release Experiment Satellite, Spartan, and several sounding rocket programs at Goddard. Mr. Olney earned an MS from George Washington University.

Mr. Todd Shope, a computer engineer at Goddard, received his BS in computer science from the University of Maryland and has participated in the Pegasus, Spartan, and Combined Radiation and Release Experiment Satellite programs.

SPACE COMMUNICATIONS SYSTEMS

EXTENDED LIFE TEST OF A 90-GHz HIGH-ELECTRON-MOBILITY TRANSISTOR MIXER PREAMPLIFIER

The High-Electron-Mobility Transistor Mixer Preamplifier is a part of the Differential Microwave Radiometer and will be operated at 140 °K while in flight. However, researchers have discovered that high-electron-mobility transistor devices fail after a few minutes of operation at 78 °K. Because no data were available about the operation of these devices at 140 °K, a test was needed to ensure that the mixer preamplifier would not fail after operating at a temperature of 140 °K for at least 3 months.

The test lasted from January 1988 to March 1989. In that time two 3-month periods of contiguous data were taken while the other data were interrupted because of external system failure. An external system failure generally meant that the device warmed to room temperature because the test setup failed to maintain a 140-°K test environment.

The mixer preamplifier was placed inside a cryogenic dewar, which was evacuated so that condensation would not occur when the device was cooled. A mechanical pump maintained the vacuum, and a timing circuit periodically released liquid nitrogen to maintain the desired temperature. Feedthrough connectors ensured a good electrical contact as well as a good vacuum. Two thermalcouples were placed on the mixer preamplifier to monitor its temperature. The thermalcouple outputs were recorded on a strip chart recorder and varied by less than 1.5 °K during the test. A semirigid coaxial cable with a feedthrough connector was used so that the intermediate frequency output could be measured, and a WR10 waveguide was used for the local oscillator input and the radiofrequency input.

High-Electron-Mobility Test Data

Date	Power Hot Target (W)	Power Cold Target (W)	Noise Figure (dB)
Jan. 6, 1988	9.44	8.72	9.91
Jan. 7	10.30	9.52	9.94
Jan. 11	9.87	9.06	9.59
Jan. 18	********Test Chamber Warm********		
Jan. 20	11.13	10.25	9.75
Feb. 1	10.38	9.62	10.09
Feb. 17	10.32	9.60	10.29
Mar. 6	******** Test Chamber Warm ********		
Mar. 10	8.66	8.02	10.00
Apr. 5	8.44	7.75	9.61
Apr. 20	8.28	7.52	9.11
Apr. 28	9.10	8.27	9.15
May 13	8.42	7.75	9.75
May 25	8.44	7.70	9.32
June 13	8.52	7.80	9.50
June 18	******** Test Chamber Warm ********		
June 27	8.28	7.60	9.58
July 5	7.55	6.79	8.70
July 11	7.68	6.96	9.01
July 18	7.17	6.48	8.89
July 25	7.05	6.39	9.01
Aug. 2	7.80	7.00	8.62
Aug. 9	7.50	6.80	9.03
Aug. 12	******** Test Chamber Warm ********		
Aug. 15	6.80	6.10	8.60
Sept. 14	7.23	6.45	8.40
Oct. 25	9.21	8.24	8.50
Nov. 6	******** Test Chamber Warm ********		
Nov. 8	8.82	8.04	9.26
Nov. 30	8.22	7.53	9.49
Dec. 18	******** Test Chamber Warm ********		
Jan. 9, 1989	9.37	8.34	8.31
Jan. 23	9.46	8.37	8.11
Feb. 16	9.46	8.44	8.40
Feb. 27	9.28	8.29	8.45
Mar. 11	9.48	8.56	8.86
Mar. 24	9.00	8.04	8.45
Apr. 11	******** Test Chamber Warm ********		

The waveguide used for the radiofrequency and local oscillator inputs was custom made to fit the dewar. Due to twists and bends in the guide, an insertion loss of about 4 dB was measured across 88 to 92 GHz. This insertion loss can be blamed for the relatively poor noise figures measured during the test. Because this was a failure test, a poor noise figure would not affect the outcome as long as it remained relatively constant. If the mixer preamplifier were to fail because of temperature, then its noise figure would reflect this by changing drastically. The data from the test are shown in the table.

The mixer preamplifier was tested at room temperature as a followup to the data that were taken at 140 °K. The results are as follows:

Date	Power Hot Target (μW)	Power Cold Target (μW)	Noise Figure (dB)
May 9	8.22	7.66	10.40

The test data from March 10 to June 13, 1988, and January 9 to March 24, 1989, fulfill the requirement for 3 contiguous months of data. The conclusion from these data is that the high-electron-mobility transistor devices in the mixer preamplifiers will not be a problem in flight.

Contact: Michael T. Bukowski (Code 727)
(301) 286-5936

Sponsor: Microwave Instrument and Radiofrequency Technology Branch

Mr. Michael T. Bukowski has been at Goddard for 6 years and currently works in the Microwave and Radio Frequency Technology Section. He holds a BSEE from Marquette University.

LOSSLESS DATA COMPRESSION CODER/DECODER SET FOR SPACE APPLICATIONS

Future NASA space platforms such as the Earth Observing System (Eos) will support a multitude of science instruments designed to observe specific properties of the Earth at different wavelengths. A complete 24-h observation using all the spectral bands will require communication channel capacity larger than what is currently available and will also create difficulty in the onboard network interface. Besides viable approaches such as instrument scheduling and spectral and data editing, which will hinder the transmission of useful information, an

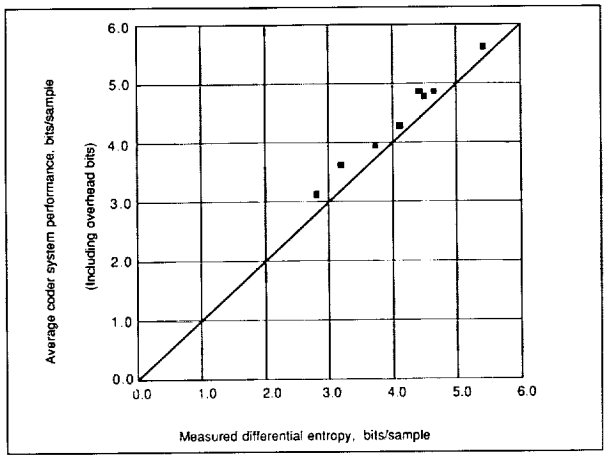

Coder performance on test images.

information-preserving technique can allow more imaging data to be accommodated in the communication channel. This technique will guarantee full reconstruction of the data before it is dispatched to the user community.

The information-preserving data-reduction technique is known as lossless data compression. This technique exploits the inherent correlation among the majority of either imaging or science data by first performing differential pulse code modulation on the data and then employing various reversible coding schemes to reduce the data rate. Such coding schemes assign fewer bits to more frequently occurring data and longer bit patterns to less frequent data. The achievable compression ratio depends mainly on the information content of the data, which is characterized as the data entropy.

A lossless data compression coder/decoder set is being developed in collaboration with Jet Propulsion Laboratory's High Resolution Imaging Spectrometer (HIRIS) project team. Specifically, through a contract with the University of Idaho, Goddard is responsible for the design, fabrication, and testing of the decoder. The developed hardware will be used on the first Eos platform to reduce the HIRIS sensor data rate to provide enough ground coverage.

The very large-scale integration (VLSI) chip set, designed with a pipeline architecture, will be fabricated using 1.5μ complementary metal oxide semiconductor technology. The chip set implements the modified Rice algorithm and adapts to scene statistics by processing every 16 samples as a block and choosing a most optimal code option for this block. Simulation of the algorithm on a set of test images reveals a close match of the coder's system performance to the data entropy, as depicted in the accompanying figure.

The chip set accepts data quantified from 4 to 14 bits and operates in both packet and continuous data modes. Current design projects a data throughput rate at 10 megasamples per s because of the simplicity of both the encoding and decoding algorithms.

Contact: Pen-Shu Yeh (Code 728)
(301) 286-4477
Warner H. Miller (Code 728)
(301) 286-8183

Sponsors: OAST, Office of Space Operations

Dr. Pen-Shu Yeh is completing her first year at Goddard. Her areas of interest include signal-image processing, computer vision, and biomedical applications. She earned her PhD in electrical engineering from Stanford University.

Mr. Warner H. Miller, who received an MS in applied science from George Washington University, has been at Goddard for 28 years. He designs advanced flight instruments for signal processing with the Instrument Electronics Branch. Mr. Miller has special interests in data processing, telemetry, channel encoding, and communications.

SYSTEM AND SOFTWARE ENGINEERING

THE INTERACTIVE CONTROL ANALYSIS (INCA) PROGRAM

Control system design engineers need analytic tools that are simple and quick to use and that provide accurate results. The INCA computer program was developed to provide this capability for control system design analysis engineers at Goddard. INCA has been used extensively at Goddard for spacecraft, instruments, pointing systems, and robotics control systems. Numerous flight-proven designs, including Earth Radiation Budget Satellite (ERBS) and the Advanced

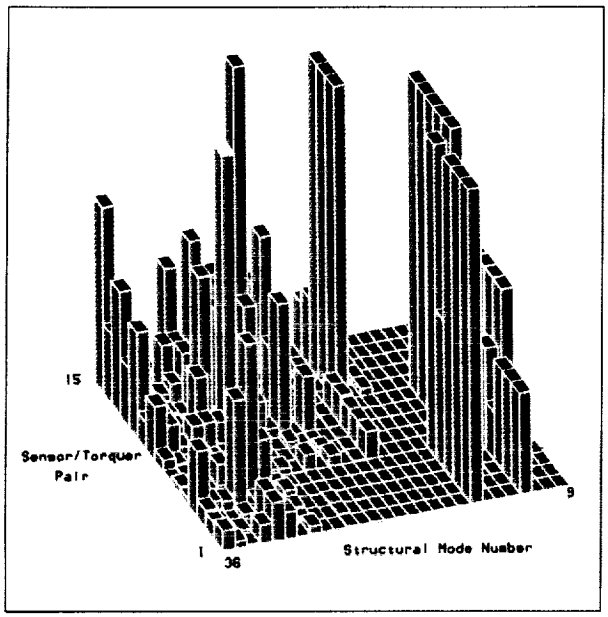

Linear time response analysis using INCA.

Television Infrared Observation Satellite-Nadir (ATN) weather satellite series, have been developed or validated using INCA's analytic capabilities.

Using INCA's command menu, the controls engineer can quickly generate system models. These models are then stored in transfer function form for single-input single-output systems or in matrix form for multi-input multi-output systems. INCA provides the capability to analyze continuous systems, sample data systems, and hybrid (continuous/sample data) systems. In addition, systems with computational delays or transport lags can be analyzed. The resultant linear models can be manipulated to modify the design or used to determine system stability, parameter robustness, or control system performance. Standard filter and control law templates have also been included to expedite system design.

INCA provides a comprehensive host of standard classical controls analysis techniques, including linear time response (as in the first figure), root locus, and frequency

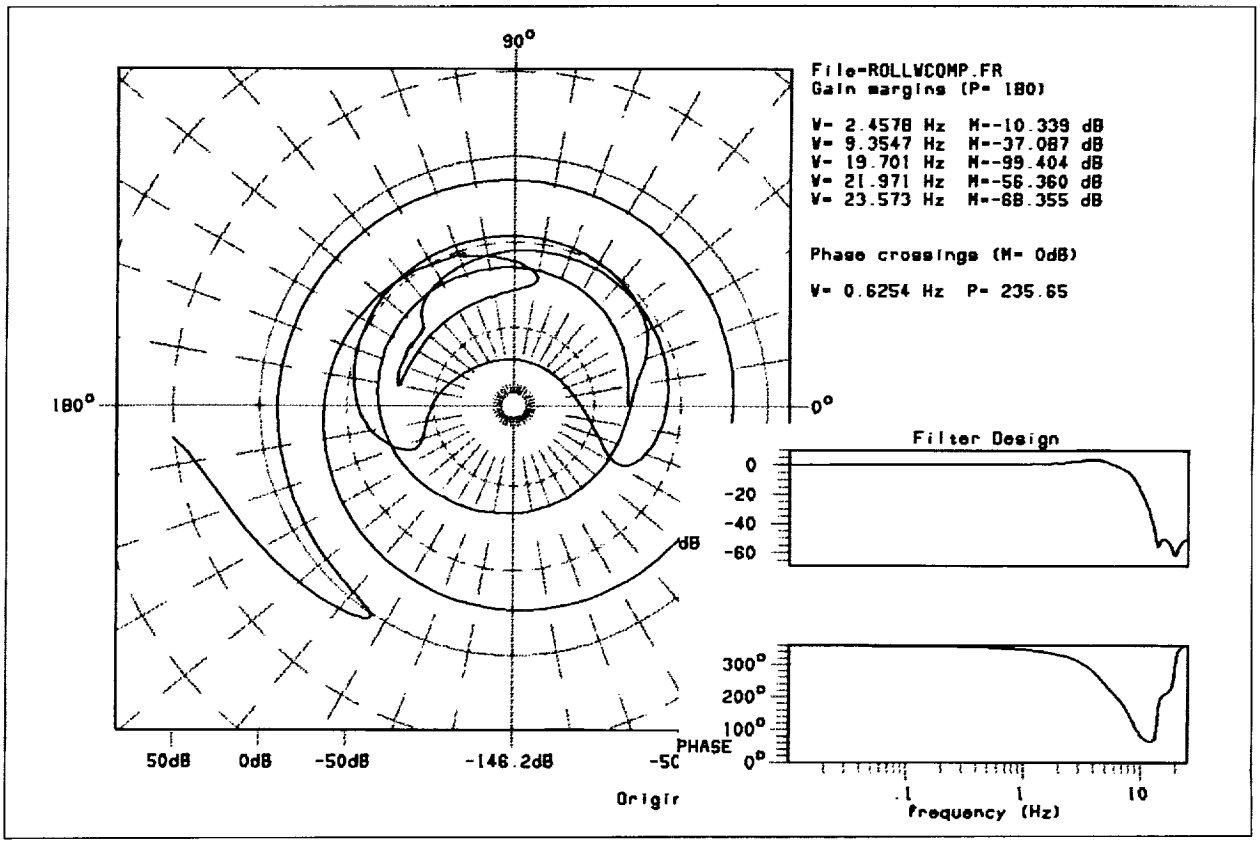

A Nyquist frequency response plot, with multiple-plot windows, generated using INCA.

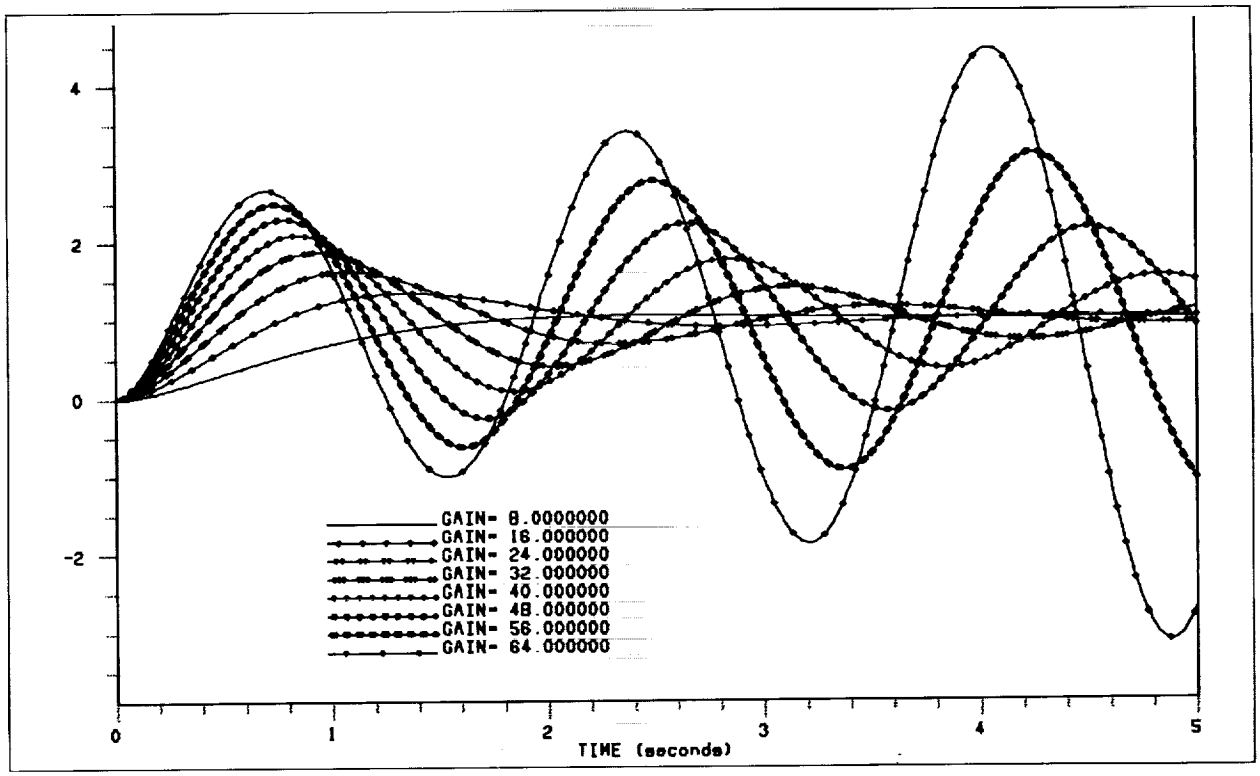

A sample sensitivity analysis generated using INCA.

response (Bode, Nichols, Nyquist) (as in the second figure) capabilities. In addition, frequency response analyses of nonlinear systems can be performed using the describing function method. As shown in the first figure, analysis results are presented as multicolored plots with a full range of simple plot manipulation command. Plot zooming and multiple-plot windows capabilities, shown in the second figure, and simple plot documentation capabilities are available. Analysis results can also be presented in tabular form.

Multi-input multi-output capabilities include transfer function to state variable form transformations, matrix arithmetic, eigenvalue-eigenvector determination, and singular value decomposition calculation. Moreover, a finite element model reduction capability has recently been added for controllers under the influence of structural flexibility (shown in the third figure).

INCA was developed for use on all VAX computers that use the VMS operating system. INCA graphics can be viewed on a wide variety of color and monochrome terminals including Tektronix color and monochrome graphics terminals, DEC VT terminals, and some Macintosh and IBM PC emulators. Graphic output devices include, but are not limited to, the Tektronix color graphics printers, DEC laser printers, and local terminal hardcopy devices.*

**INCA is available through COSMIC, NASA's software dissemination source.*

Contact: Frank H. Bauer (Code 712)
(301) 286-6392
John P. Downing (Code 712)
(301) 286-8204
Christopher J. Thorpe (Code 712)
(301) 286-8338

Sponsor: FTS/Space Station Project Office

Mr. Frank H. Bauer, Head of the Project Support Section of the Guidance and Control Branch, received his MS in aerospace engineering from Purdue University. Since 1979, he has been involved in the design, analysis, and technical oversight of spacecraft and the Instrument and Pointing Control Systems, most notably for the ERBS, Geostationary Operational Environmental Satellites (GOES), and Television Infrared Observation Satellite

Spacecraft Programs and for the Japanese Astronomy Spacelab payload.

Dr. John P. Downing has 7 years' experience at Goddard and currently works at the Guidance and Control Branch. He has developed software for a portable Television Infrared Observation Satellite Local User Terminal. Dr. Downing holds a PhD in physics from Wayne State University.

Mr. Christopher J. Thorpe, a software engineer, has worked at Goddard for 2 years. His most recent work includes the introduction of state space methods into Interactive Control Analysis. He holds a BSCS degree from the University of Maryland.

GODDARD MAN-MACHINE INTERACTION RESEARCH PROGRAM

Several ongoing research activities are being coordinated that allow human performance factors to be taken into account during the early design phase of man-operated mechanical equipment. The man-machine interaction problem requires an ability to model the machine mathematically, to quantify basic elements of human performance needed to operate the machine, and to couple the two studies together. The research objective is to use low-cost analysis methods to study man-machine interaction tradeoff options before expensive prototypes are built and tested.

The FTS project office is supporting the development of general-purpose multibody dynamics modeling software, namely Order N Integrating Our Wondrous Analysis (IOWA)/Dynamic Interaction Simulations of Controls and Structures (DISCOS) at the University of Iowa and a private research firm. These programs will provide an ability to model the machine. Special capabilities are being developed to allow man-in-the-control- loop commands. The end product will be a low-cost simulator. The operator will be able to evaluate different control design concepts while the machine designer evaluates the mechanical system's dynamic response and performance characteristics.

The Office of Commercial Programs along with the University of Iowa and a private corporation are developing such a simulator for a backhoe. Lessons learned on this project directly benefit the design of a simulator for the far more complex FTS system.

OAST is supporting the development of a library of multibody test and validation data at the University of Iowa. This library will not only provide a ready reference source of how-to-model information for a broad variety of mechanical system modeling problems, but it will also document program validity. This office is also supporting enhancements to the INCA program, which is Goddard's primary general-purpose control system design and analysis capability. Most recently, methods to create transfer functions from test data and their use for controls design purposes have been developed at Arizona State University and incorporated into INCA.

Goddard's controls research with the Massachusetts Institute of Technology, the University of Iowa, and the private research firm is focused on the objective of demonstrating that complex robotics control algorithms can be developed from a computational analysis base. Current robot modeling and validation efforts have exposed several multibody dynamics modeling shortcomings. These shortcomings are being addressed from the perspective of needs associated with the development of robot-translation, pick-and-put, dual-arm handoff, and fragile-surface-contact control algorithms.

Human factors research at the Universities of Texas and Iowa is attempting to build upon the extensive capabilities that exist in the field of rehabilitation engineering. The efforts are on two levels. First is the ability to quantify the basic elements of human performance. Researchers intend to use a backhoe to perform a detailed human performance study of coordinated hand, wrist, and forearm action, both with and without gloves. The objectives are to perform a detailed study on a complex, but still relatively simple operation before a more complex hand controller is attempted.

On the second, more detailed level, researchers are attempting to set the foundation for a biomechanical neuro-musculo-skeletal dynamics analysis capability. This work at the Universities of Texas, Iowa, Colorado, Case Western Reserve, and Johns Hopkins involves both the development of new analysis capability and the development of methods for obtaining the human body data needed by the analysis methods. The focus is on the development of a capability to predict muscle participation requirements needed to perform a prescribed task. The objective is the development of an analysis capability which will provide a quick pretest, first-order assessment

of man-operated machine controllers and astronaut work scenarios from the perspective of human factors.*

**Dr. Han Chun and Dr. James Turner of Cambridge Research contributed to the research reported in this article.*

Contact: Harold P. Frisch (Code 712)
(301) 286-8730

Sponsor: FTS Project, Office of Commercial Programs, OAST

Mr. Harold P. Frisch works in the Guidance and Control Branch at Goddard. He has developed many computer programs which have become industry standards for the design and analysis of spacecraft attitude control systems. He is currently engaged in supporting multidiscipline analysis in many subject areas by means of the Integrated Analysis Capability program.

SELF-HOSTED EMBEDDED MICROPROCESSOR (SHEMP)

During the integration of computer-based instrument control systems, there usually are many last-minute software changes. Physical access to the central processing unit (CPU) for in-circuit emulation to change and test code is often awkward because the CPU is located within the instrument and because the mechanical design is optimized for ruggedness and thermal properties instead of access. Disassembling a CPU to replace programmable read-only memories (PROM's) is both costly and time consuming because once a board is removed from the chassis, conformal coating must be removed from the board before the old PROM's can be removed. To reassemble the instrument, the new PROM's are inserted, and the procedure is reversed. In addition, each step of the reassembly is accompanied by very extensive inspection and vibration, thermal, and electrical testing to ensure the quality of the instrument.

The SHEMP was developed to demonstrate the advantages of developing flight software directly on target hardware. This prototype embedded computer is based on the SC32, a 32-bit Forth microprocessor developed by the Johns Hopkins Applied Physics Laboratory. SHEMP achieves the goal of supporting software development on target hardware by providing an interactive Forth programming environment hosted by the SC32 Forth engine. The excellent Forth-program throughput of the SC32 produces better performance than compiled code on conventional processors (8.4 times faster than a VAX 11/780 programmed in C). Yet this benefit is achieved with a simple CPU board that can easily become the basis of an embedded computer.

SHEMP consists of a CPU board containing the system's main memory and most of the input/output, as the figure shows. The circuit card contains the SC32, 32 KWords of erasable, programmable read-only memory (EPROM) that stores the bootstrap code and Forth kernel, 256 KWords of Random Access Memory (RAM), hard and soft resets, interrupt controller, dual Universal Asynchronous Receive Transmitters, real-time clock, watchdog timer, bus interface, and provisions for power cycling to conserve battery power. A second card contains a magnetic bubble memory mass storage unit, where the source code is stored. The unit can be copied into fast RAM on command. Now only a terminal is needed to modify software, rather than a development system, a logic analyzer, and an emulator.

System software supports interactive program development and testing on the target flight computer as well as traditional real-time control. SHEMP uses a Forth kernel developed at the Johns Hopkins Applied Physics Laboratory with multitasking extensions. The kernel uses a fully hashed dictionary structure and the compiled code is subroutine threaded. A rule-driven optimizing metacompiler has also been developed, and the

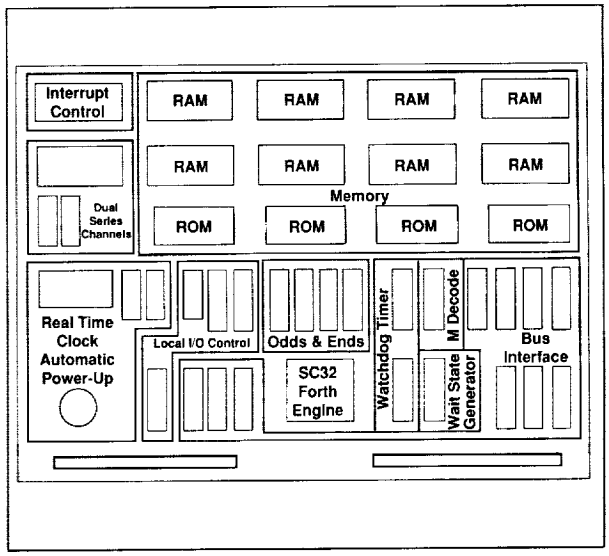

SHEMP CPU board layout.

optimizer is to be included as part of the interactive compiler. An editor and bubble memory file system are available as part of the system software.

The combination of a powerful target processor, mass storage, and suitable system software will lower the costs of implementing computer-based instrument control systems while increasing the instrument flexibility.

Contact: Lee W. Nearhoof (Code 743)
(301) 286-5287

Sponsor: Engineering Directorate, Instrumentation Branch

Mr. Lee W. Nearhoof, an electrical engineer, has 4 years' experience in the Payload Development Section at Goddard. He holds a BS from the University of Maryland and is the Lead Design Engineer for the Complex Autonomous Payloads Program.

CONTROLS ANALYSIS CAPABILITY FOR FLEXIBLE ROBOTIC SYSTEMS

Multibody dynamics software programs are currently used for an extremely broad range of simulation applications: robotics, tanks, the Strategic Defense Initiative, automotive vehicles, farm machinery, spacecraft, biomechanics, etc. It is well known that multibody software is not equally applicable to all possible modeling and simulation problems. For a very broad range of problems, the software is more than adequate; for others, special modeling needs preclude computationally efficient use. The objective of this study is to demonstrate conclusively that multibody software can be used to develop a robot dynamics simulation capability compatible with the needs of FTS control system design and performance evaluation work. Two simulation programs are being developed: one, Order N DISCOS, supports high-fidelity autonomous control; the second, Order N IOWA, supports lower fidelity real-time man-in-the-loop control. Both are to be theoretically and experimentally cross-validated for robotics application.

The research team includes investigators at the Industry/University Cooperative Research Center at the University of Iowa—which is sponsored by the National Science Foundation, The Department of Defense, Goddard, and the Department of Transportation—and their colleagues at the Massachusetts Institute of Technology and a private research firm. The University of Iowa is concentrating on the development of a special-purpose program based upon Order N IOWA. It will have a real-time man-in-the-loop control capability. It will also have the companion real-time graphics animation capability needed for telerobotic operator cueing. The private research firm is concentrating on the development of a pilot program called Order N DISCOS. It is to have all high-fidelity modeling capability necessary to robotics application. The Massachusetts Institute of Technology is concentrating on control system characterization. All work is being focused on the arm produced by another private firm in the Goddard Robotics Laboratory. To demonstrate that the developed analysis capabilities are representative of the actual physical system, they are to be validated through a series of tests in the Robotics Laboratory. All tests are to be simulated and test-versus-simulation results compared.

The most important realization achieved during the early phase of this study was that all existing multibody software codes lacked a fundamental capability essential for efficient robot simulation model development. The missing modeling component was a computationally efficient gearbox element. The angular momentum stored in rapidly spinning gears within each joint's gearbox must be taken into account in a full robot simulation model. During 1989, computational tests were performed with the Design Analysis for Dynamic Systems (DADS) program to demonstrate conclusively the need for this new capability. Inclusion of gearbox modeling for arm application using standard DADS modeling procedures makes computations four or five times less efficient. A computationally efficient gearbox modeling capability was developed during 1989 and incorporated into Order N DISCOS. It is also to be included within Order N IOWA. Since DADS is essentially equivalent in computational speed and capability to other commercially available software, the results can be applied also to them.

Testing for this project began in the Robotics Laboratory on June 26, 1989. A full complement of tests was performed for parameter identification and simulation validation purposes. Initial data reduction and simulation attempts are most encouraging. All single-DOF tests agree well with nonlinear simulation model predictions. Simulation and cross-validation for multiDOF tests are progressing, and excellent agreement is expected.

The new multibody algorithms are placing the ability to create low-cost, high-speed, and even real-time simulations of

complex mechanical equipment within the researchers' grasp. Ongoing work is directed toward providing all modeling capability needed to support FTS control system development. Mission capability is to be identified, theoretically developed, transformed to software code, theoretically cross-validated, and then experimentally validated in the Robotics Laboratory at Goddard.*

**Dr. Hon Chun and Dr. James Turner of Cambridge Research have contributed to this research in developing the pilot program called Order N Discos.*

Contact: Harold P. Frisch (Code 712)
(301) 286-8730

Sponsor: FTS Project, OAST

Mr. Harold P. Frisch works in the Guidance and Control Branch at Goddard. He has developed many computer programs which have become industry standards for the design and analysis of spacecraft attitude control systems. He is currently engaged in supporting multidiscipline analysis in many subject areas by means of the Integrated Analysis Capability program.

USER SPACE DATA SYSTEMS

CONFIGURABLE HIGH RATE PROCESSOR

The Configurable High Rate Processor System Program is part of the Civil Space Technology Initiative in OAST. Its goal is to provide the architecture, system control, and high rate data-handling interfaces needed to support onboard compression, information extraction, and automated operations of high-rate imaging missions. The system provides a flexible architecture for interconnecting the components of an onboard processing system. These components include instruments, telemetry, mass storage, processors, and system control (see the first figure). Onboard data rates in the 1- to 10-Gbps range will be accommodated.

The next generation of imaging sensors will provide measurement capability at finer spectral and spatial resolution, resulting in data rates exceeding the capability of the TDRSS and the capacity of ground processing systems and analysis teams. Interdisciplinary studies will require coordinated observations and integrated analysis of data from these sensors. The Civil Space Technology Data System Program is developing processor, storage, and network technology to support onboard data processing, formatting, and buffering for these high-rate missions.

The objective of the Configurable High Rate Processor System Program is to apply high-rate network technology and develop the packet telemetry handling interfaces to enable the processing and buffering components to be configurable for a range of tasks, from single instrument data compression to multisensor fusion and feature extractions. The development will include a phased testbed (shown in the second figure) to demonstrate technology components for the project applications, such as Eos, to support the integration of technology into space platform architectures and to support evaluation of onboard processing functions. Support is building within NASA and

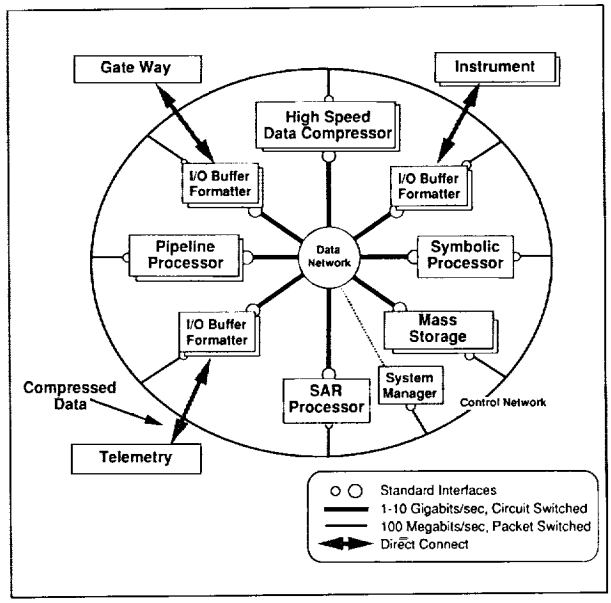

The Configurable High Rate Processor System concept.

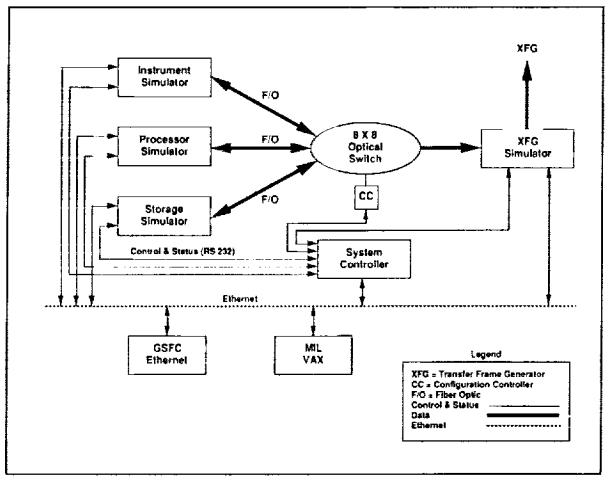

The Configurable High Rate Processor System initial testbed configuration.

the Department of Defense to use the testbed as a technology demonstration resource.

The system architecture accommodates heterogeneous computational, storage, and interface elements under one unified approach. Goddard staff are specifying and developing the testbed, which is expected to be operational in the 1990's. Control processors in each element will run control software based on the network operating system developed at Jet Propulsion Laboratory. The standardized hardware and software interfaces will allow developers of instruments, processors, and storage devices to bring their hardware to the testbed and operate it under data-load conditions similar to those encountered during flight. Breadboard versions of the lossless data compressor from Jet Propulsion Laboratory and of the spaceborne symbolic processor from Ames Research Center are expected by the end of fiscal year 1991.

The space optical disk recorder being developed at Langley Research Center is expected late in fiscal year 1992. Deliveries of a rad-hard 32-bit multicomputer from Langley and a rad-hard generic image processor prototype from Goddard are scheduled for fiscal year 1995.

During fiscal year 1989, the two contract study teams preparing Phase B designs for the Eos Data and Information System (EosDIS) began special emphasis studies under this program's sponsorship to derive project requirements for high-capacity processing on board the Eos platforms. A draft requirements document for the system was developed and reviewed. Based on this requirements document, a preliminary design review was presented in June 1989. Also during fiscal year 1989 the Data Compression Workshop, co-sponsored by Goddard and Jet Propulsion Laboratory (held in February 1988) to identify the technologies and scientific drivers for onboard data compression, published its proceedings.

Contact: Danny A. Dalton (Code 735)
(301) 286-5659

Sponsor: OAST

Mr. Danny A. Dalton, Head of the Flight Data Systems Branch, is responsible for data system technology development and flight project support. He has won a NASA Exceptional Service Medal and a Goddard Exceptional Performance Award. Mr. Dalton has 27 years' experience at Goddard and holds a BSEE.

TECHNIQUES

X-RAY CHARACTERIZATION OF HIGH TEMPERATURE SUPERCONDUCTOR (HTSC) YTTRIUM-BARIUM-COPPER OXIDE

The increasing use of the HTSC yttrium-barium-copper oxide requires that this material receive careful study. Superconductor quality has become an important concern in the industry. Methods are needed to evaluate this material easily in terms of purity and its ability to display the desired properties below the critical temperature. Yttrium-barium-copper oxide exhibits superconducting properties at reduced temperatures only for a small range of oxygen content. As the oxygen level is decreased from O7 to O6, the material undergoes a phase transition from orthorhombic to tetragonal and no longer superconducts at any temperature.

The intent of this research is to examine this material by x-ray diffraction, which is one of the most powerful techniques used in the phase identification of solid materials. Purity of the sample is established by comparing the measured x-ray diffraction data with that of a reference standard pattern published by researchers at NIST. Following the comparison, a series of oxygen-annealing and hydrogen-reduction steps is performed to provide samples with varying levels of oxygen content. Each sample is then analyzed by x-ray diffraction, and from the small but measurable shift in peak positions, a correlation curve is determined of unit cell volume versus oxygen level in the material. This process permits an important aspect of the superconductor quality to be determined fairly readily by x-ray diffraction analysis.

The type of data collection used is a time-averaging method, where multiple x-ray scans on the sample being analyzed are collected. The intensity data at each angle position for each scan are added together. At the end of data collection, each intensity is divided by the number of scans to arrive at the correct count rate. The entire data collection process is controlled by a VAX minicomputer. After the raw data are collected, a background intensity correction is performed, followed by lattice parameter calculation with a standard data reduction program.

The accompanying table shows the calculated unit cell volumes for the various stages of treatment corresponding to different oxygen content.

The distribution of oxygen level covers ranges from approximately 5 for the sample reduced at 650 °C to 7 for the oxygen-annealed specimen. The as-received sample has an oxygen level of 6.9, but those reduced at 400 °C and 550 °C correspond to levels of about 6.0 and 5.3 respectively. The unit cell volume systematically increases, though by a very small amount, as the oxygen content in the material decreases. As the oxygen content decreases from one level to another, the oxidation state of the copper changes, and an increase in the radius of the copper ions occurs. This increase correlates with the observed increase in unit cell volume with oxygen depletion. For all the samples that have undergone hydrogen reduction and have oxygen levels of 6 or less, the lattice parameters *a* and *b* have become nearly the same, indicating that the phase transformation from orthorhombic to tetragonal has occurred as expected. These samples are not superconducting at any temperature.

Therefore, this method provides a way to evaluate this material, by obtaining the unit cell volume with x-ray diffraction and determining the oxygen content from the developed correlation curve. It should be emphasized again that these changes in volume are very small and considerable care must be taken when examining this material with x-ray diffraction to ensure reasonable results. More work is being done to extract more data points for the curve, especially around the orthorhombic-tetragonal phase transition.

Contacts: Petar Arsenovic (Code 313)
(301) 286-8739
Yury Flom (Code 313)
(301) 286-3274

Sponsor: Office of Flight Assurance

Mr. Petar Arsenovic, in the Materials Branch, Office of Flight Assurance, has a special interest in the study of HTSC's and the microstructure of carbon fibers used in aerospace composites. He received his MS in materials science from the University of Rochester and is currently pursuing a PhD in materials science from Johns Hopkins University.

Dr. Yury Flom received his PhD in materials engineering from the University of Maryland. Dr. Flom is involved in materials engineering, testing, evaluation, and failure

Lattice Parameter Data (Angstroms)

	a	b	c	Vol
Oxygen-annealed sample	3.8105	3.8806	11.6695	172.56
As-received sample	3.8192	3.8852	11.6778	173.28
H2 reduced at 400 °C sample	3.8524	3.8518	11.8221	175.42
H2 reduced at 550 °C sample	3.8562	3.8558	11.8256	175.83
H2 reduced at 650 °C sample	3.8569	3.8574	11.8265	175.95

analysis services for Goddard and other NASA facilities. Recently, Dr. Flom has also been coordinating HTSC activities at Goddard.

SIMULATING THE EFFECTS OF ATOMIC OXYGEN ON MATERIALS

It has been shown that the presence of atomic oxygen in low Earth orbit causes severe damage to many types of exposed polymeric materials. This phenomenon has led to serious concerns about the long-term survival of materials on structures such as the Hubble Space Telescope (HST) and the Space Station Freedom. Laboratories around the country have expended large amounts of time and money attempting to simulate the low Earth environment and thus obtain reliable predictions of material degradation. At Goddard, there has been no development of an expensive atomic oxygen simulator, but staff members are attempting to provide a low-cost screening method which could provide semiquantitative data.

This method uses a radiofrequency atomic oxygen generator system (an asher), which is normally used to clean organic contaminants from semiconductor and ceramic materials. It has been shown that this system produces damage to polymeric surfaces that appears to be very similar to the damage seen from orbital exposure. The problem with these systems is that quantitative correlation between experiment and orbit is very poor because the asher environment is a poor simulation of low Earth orbit. Most asher systems have no directionality and no way to identify the reactive species or their energies. Quantitative correlations have been improved by making changes in operating power levels and total oxygen pressure in the system. This improvement involves alteration of the concentrations of reactive oxygen species in the system such as atomic oxygen, ionic oxygen, and various other possible radicals.

Goddard researchers have created a unique analytical capability by combining the oxygen plasma generator with a cryogenic trap. Since the system requires a continuous flow of low-pressure oxygen, the cryogenic trap on the exit port collects the volatile products of the degradation reactions as they are swept from the chamber. The collected products are then analyzed by mass spectrometry, infrared spectrometry, or scanning electron microscopy to gain insight into the nature of the atomic oxygen degradation processes. Results have shown that the primary reaction products are extremely reactive species, probably free radicals. This finding raises concern about possible secondary reactions that may occur in orbit over long time periods with large structures. If reactive products from the atomic oxygen reactions impinge on other sensitive surfaces, it is likely that unexpected damage will occur on those surfaces. This phenomenon has been observed in the Goddard system.

Future work will be focused on the use of a new parallel-plate type of the radiofrequency system that produces a directional flux. This system may allow a better definition of surface damage and may even allow measurement of reactive species in the system by an appropriately placed residual gas analyzer. It is expected that such data will clarify the position of the radiofrequency generator system as a useful tool for material screening. In addition, more studies of the fates of the reaction products should clarify concerns regarding their possible impact on flight structures.

Contact: Joe A. Colony (Code 313)
(301) 286-5288

Sponsor: Office of Flight Assurance

Mr. Joe A. Colony has a BA in chemistry from Reed College. He has been at Goddard for 27 years and is a Senior Analytical Chemist in the Materials Branch, Office of Flight Assurance. He has also been a thermal coatings specialist in the Thermal Engineering Branch.

HYDROGEN COLLECTORS FOR SPACE FLIGHT APPLICATIONS

Solid hydrogen cryostats are an efficient source of cooling for space-based instruments and sensors. They offer significant savings in weight and volume when compared to cryostats filled with other coolants. Unlike most cryogens, hydrogen boiloff is extremely flammable, so venting during ground handling and launch operations must be carefully controlled. A potential solution is to collect the hydrogen vapors in a canister filled with a hydride-forming metal alloy.

The phase 1 goal of this Small Business Innovative Research project is to demonstrate the feasibility of infiltrating a reticulated carbon foam with a hydrogen-absorbing metal alloy by chemical vapor infiltration, a variation of the chemical vapor deposition process. The resultant composite foam should be lightweight, have a large surface

area for collecting hydrogen, provide unrestricted flow of hydrogen vapor throughout the collector, and avoid some of the problems associated with caking of powdered metal hydrides. The carbon foam may also improve the heat transfer properties of the collector.

The materials studied during phase 1 were lanthanum nickel ($LaNi_5$) and magnesium. Lanthanum chloride ($LaCl_3$) and nickel chloride ($NiCl_2$) were codeposited on carbon foams. The following reduction reactions were used to produce the $LaNi_5$ compound desired for hydrogen absorption studies:

$$2\,LaCl_3 + 3\,Zn \rightarrow 2\,La + 3\,ZnCl_2$$

$$NiCl_2 + Zn \rightarrow Ni + ZnCl_2.$$

Magnesium was deposited as Bis (cyclopentadienyl) magnesium and similarly reduced to metallic magnesium on carbon foam. Studies of reaction time, temperature, pore size of the foam and surface area, and mass of deposited alloys were conducted prior to determining the hydrogen absorption of the samples. The amount of hydrogen absorbed was determined in relation to surface area, weight, and volume of the collector. An effort was made to optimize deposition parameters for maximum hydrogen absorption efficiency.*

**This project was conducted by Ultramet in Pacoima, California.*

Contact: Mark A. Domen (Code 313)
(301) 286-5954

Sponsor: Small Business Innovative Research Program

Mr. Mark A. Domen is a materials engineer in the Materials Assurance Office. He reviews materials and processes intended for use on space flight projects and provides technical guidance in the selection and testing of materials. He has an MS in chemical engineering and has been at Goddard for 4 years.

ACOUSTIC SPECTROMETER FACILITY AND SELECTED RESULTS

An acoustic spectrometer is a device for exciting a range of vibrational modes of a specimen and measuring the frequency (and therefore elastic moduli) and the damping of each excited mode. These measurements can serve many purposes: nondestructive quality assurance and testing, analysis of energy-flow processes occurring within the material, and development of models for structural vibrations due to applied time-dependent stresses.

The Goddard acoustic spectrometer uses a specimen prepared as a bar 2 to 12 in. long and up to 1 in. wide and high. Flexural, extensional, and torsional modes are studied. Drive frequencies cover the range 1 μHz to 20 MHz with a resolution of 1 μHz below 100 kHz and 1 mHz above 100 kHz.

The average strain amplitude ranges from about 1 to 30,000 μstrains. Measurements are made throughout this range to test for the strain dependence of the moduli and damping. All measurements are currently made at room temperature. The apparatus operates both in air and in a vacuum of better than 10^{-6} torr.

The damping of a mode is measured either by observing the half-width of a driven resonance or by observing the decay rate of a freely decaying mode; these usually agree to within 3 to 10 percent. Damping is reported using the damping factor $g \stackrel{def}{=} \Delta E/(2\pi[E])$, where ΔE is the energy lost during a vibration cycle, and $[E]$ is the average energy over that cycle. Moduli are typically determined to within 0.5 percent for specimens of good geometry.

Many internal processes have been related to material damping and then studied using acoustic spectrometry. Thermoelastic damping is relevant to the damping of the flexural vibrations of beams and plates made of metals because it usually dominates all others in the neighborhood of the fundamental beam resonance (Zener, 1948). It depends upon absolute temperature, heat capacity, thermal expansion, Young's modulus, and size and shape of the material. When other properties are known, this method can compute thermal diffusivity from measurements of damping or, conversely, damping from measures of thermal properties.

For 6061-T6 aluminum, flexural damping is well described by Zener's thermoelastic damping *with no adjustable parameters.* The addition of silicon carbide, either as whiskers or as particles, to the aluminum slightly modifies the Zener damping and adds further damping ($g \sim 10^{-4}$ for silicon carbide content of 20 to 40 percent). The damping of extensional and torsional modes is less than $g \sim 10^{-4}$ for 6061-T6 aluminum and increases with the addition of silicon carbide.

For graphite fiber/resin composites, researchers found only a slight dependence of the damping factor upon frequency and a substantial dependence upon layup, including a linear dependence upon the number of plies (consistent with a model in which damping is dominated by interply processes). For composites that had sustained thermal-cycling damage, the damping factor was proportional to the average strain, down to strains of 10^{-5} (consistent with a model in which damping is dominated by fiber-matrix sliding friction).

Specimens of Cosmic Background Explorer (COBE) faceplate material were tested before and after cold soaks to -120 °C, -130 °C, -140 °C, -150 °C, and -160 °C. Moduli were stable to 1 part in 500 and damping factors to 1 part in 50 (the respective uncertainties in these measurements). Hence, the cold soaks did not cause the skins of these faceplates to delaminate from their honeycomb cores. The nondestructive nature of these tests allowed them to be repeatedly extended to lower temperatures using the same specimens, which increased confidence in the conclusions.

Visual inspections of specimens of graphite fiber/resin composite used in solar panel assemblies showed voids in the resin-phase. Testing before and after thermal cycling showed greater decreases in moduli than the controls of standard resin-phase. The only available specimens were too small for conventional moduli testing.

Contact: Henning W. Leidecker (Code 313)
(301) 286-9180

Sponsor: Office of Flight Assurance

Dr. Henning W. Leidecker is a materials scientist in the Materials Branch, where he designs and conducts materials tests. He earned a PhD in physics from The Catholic University of America and taught physics at The American University before joining Goddard in 1985.

ENCODER LAMP TEST FACILITY AND RESULTS

The optical imaging system of GOES depends upon an optical encoder. Burnout of the incandescent lamp used in this encoder is fatal to the operation of the imager. While the lifetime of this type of lamp was expected to be several times the service life of a GOES (5 to 7 years), the imagers of four of the last seven GOES have failed prematurely due to lamp burnout.

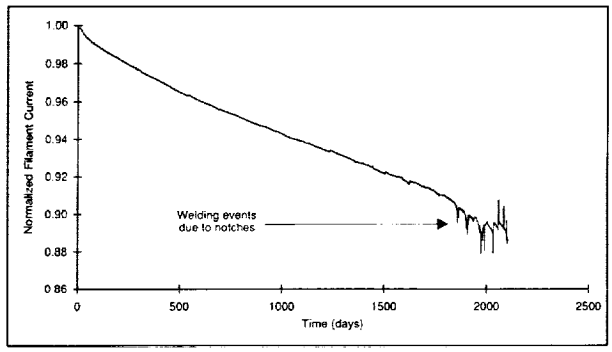

Typical plot of filament current versus time.

In 1982, a manually operated test facility was constructed to determine the expected lifetime of the lamps (which had already burned out) used in GOES-2 through GOES-4. Lamps were tested at different voltages (temperatures) to determine lifetime as a function of operating voltage. The voltage across each lamp, the current through each lamp, and the light output of each lamp in two directions were measured and recorded two or three times a week for the duration of the test. Data from this test showed that the lamps used in GOES-2 through GOES-4 should have lasted only 1 to 2 years (as they did). An empirical equation was derived for the lifetime of a lamp as a function of voltage and was used to accurately predict the lifetime of the lamps used in GOES-5 and GOES-6. While the data from this test produced accurate predictions, more testing was needed to completely understand the failure mechanism of these lamps.

In 1983, an automated test facility was constructed to continue studies on the behavior of these lamps and their lifetime as a function of filament operating voltage and filament materials. It was proposed that the lamps in GOES-G (destroyed on launch) and GOES-H (now GOES-7) be doped with other materials (rhenium or thoria) to extend their lifetime. The lamps in GOES-1 through GOES-6 had filaments made of pure tungsten (GE-218). Lamps were tested with filaments made of GE-218 tungsten doped with rhenium or thoria and Luma tungsten doped with rhenium or thoria. The lamps were operated at lower voltages since the encoders could now be operated with less light output.

The automated test facility operated 28 lamps at constant voltage while recording data on a daily basis. The data recorded each day were the same as those recorded with the manually operated facility. On a less frequent basis, the light output from each lamp was measured as

a function of position along the filament. Automation allowed for daily measurements at less cost than weekly manual measurements. Also, the error rate was reduced by two orders of magnitude.

The data from these life tests showed that the lifetime of lamps doped with thoria was slightly less than undoped filaments and the lifetime of lamps doped with rhenium, slightly more. The lifetime of the primary and backup lamps used in the current GOES-7 has been estimated using these data, and this estimate is greater than the service life of the satellite. This increase in lifetime is due to lowering the operating voltage.

The data from the automated test also allowed for a complete understanding of the failure mechanism associated with these lamps. This knowledge was made possible by daily measurements, which revealed events not previously observed. The center portion of the filament began to crystallize and eventually developed "notches" in the filament. As a notch became larger, the filament became hotter and decreased in diameter at that point. Eventually, a notch completely penetrated the filament; then either the filament failed or the notch disappeared and the filament welded at that point. If welding occurred, the filament continued to operate normally until another notch caused it to fail.

The development of these notches or "hot spots" was observed in real time with the automated facility. A plot of the filament current versus time, shown in the first figure, revealed a rapid decrease in current with the onset of a hot spot. This was caused by a decrease in the filament diameter at the hot spot, which increased the electrical resistance of the filament. After the notch welded, the current returned to the value it had before the onset of the hot spot. The onset of a hot spot and then welding took place over 3 to 5 days. These hot spots were also observed using the scans of light output versus filament position, as shown in the second and third figures. The temperature at the hot spot was higher than along the rest of the filament, which caused an increase in light output at that point. A plot of light output versus filament position revealed the location of the notch.

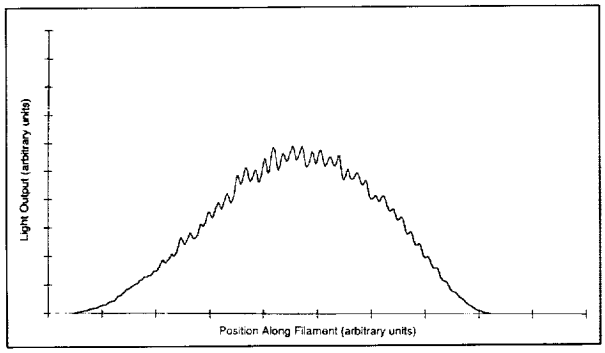

Scan of light output versus filament position before the development of notches.

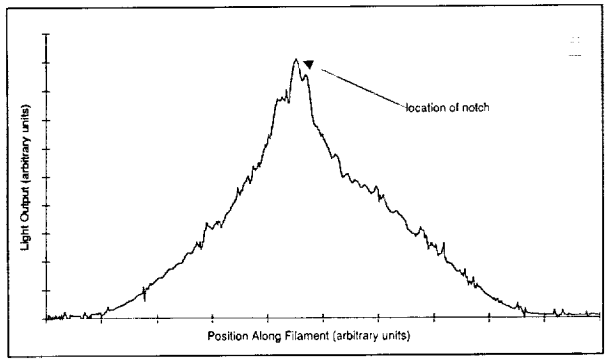

Scan of light output versus filament position just before the welding of a notch.

Contact: Charles E. Powers (Code 313)
(301) 286-8061

Sponsor: Office of Flight Assurance

Mr. Charles E. Powers currently works in the Materials Branch, Office of Flight Assurance, where he supports materials testing. During his 6 years at Goddard, he has been active in the use of computers for the automatic control and monitoring of experiments and data reduction. Mr. Powers earned his MS in physics.

NONCONTACT/ROOM TEMPERATURE EVALUATION OF YTTRIUM-BARIUM-COPPER OXIDE SUPERCONDUCTING MATERIALS

The recently discovered class of materials that superconduct at temperatures greater than that of liquid nitrogen (77 °K) has the potential for use in spacecraft applications. These applications might include thick films, bearings, and electrical wires. Because stringent processing requirements are needed to manufacture components from this material, a technique should be available to verify the quality of the produced components quickly and nondestructively and with minimum effort. A technique that satisfies

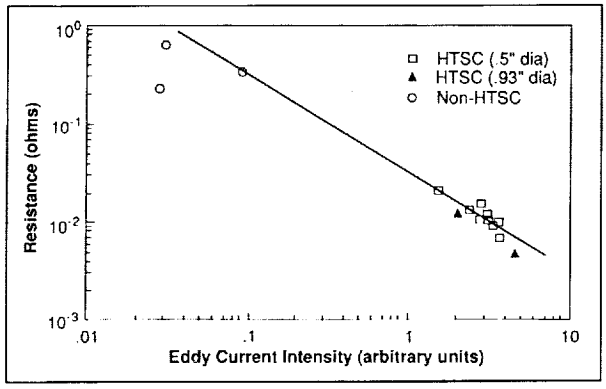

Room temperature resistance of superconducting and nonsuperconducting pellets measured with mechanically attached leads and with the eddy current technique.

these requirements has been achieved with the use of an off-the-shelf eddy current tester.

The ability of yttrium-barium-copper oxide to superconduct at low temperatures is very sensitive to the amount of oxygen it contains. The superconducting transition temperature has been correlated to the room temperature resistivity of superconducting oxides. Lower electrical resistance at room temperature is indicative of higher transition temperature. Resistivity measurements are typically made by mechanically attaching leads to the material. During the production of a superconducting component, mechanically attaching leads to the product may not be feasible, or the attachment of these leads may damage the component. An alternative method of evaluating resistivity or conductivity is through the use of eddy current techniques.

Several yttrium-barium-copper oxide pellets were manufactured at Goddard. All but three of these pellets were oxygen annealed. The superconducting ability of each pellet was verified by observing that it could create the Meissner effect when immersed in liquid nitrogen by levitating a small samarium cobalt magnet. The nonannealed pellets could not levitate the magnet. The resistivity of the pellets was then measured using a four-point probe configuration. The accompanying figure shows that the room temperature resistance of the pellets increased from approximately 10 μΩ for the superconducting pellets to 400 μΩ for the nonsuperconducting pellets.

The specimens were then measured with an eddy current inspection device using a 100-kHz probe at a gain of 30 dB. The magnitude of the response was recorded in output voltage that was indicative of the maximum response of the probe to interaction with the pellet. The probe response is represented on an oscilloscope cathode ray tube screen as a trace. The output voltage from the eddy current device agrees well with the resistance measurements. Slight variations in both eddy current response and resistivity of the superconducting pellets are due to slight variations in processing parameters.

The eddy current testing technique has potential applications in processing environments. It is nondestructive, noncontacting, and portable and requires minimal time to perform tests and provide feedback.

Contact: Michael J. Viens (Code 313)
(301) 286-2049

Sponsor: Office of Flight Assurance

Mr. Michael J. Viens of the Materials Branch has an MS in mechanical engineering and has worked at Goddard for 3 years. Mr. Viens conducts mechanical testing of ceramic, metallic, and polymeric materials and evaluates test results. He is also involved in nondestructive, ultrasonic evaluation of materials and optical emission spectroscopy.

A BALLOON STUB DUCT DESIGN AND ANALYSIS MODEL

Some scientific experiments flown aboard zero-pressure balloons, e.g., those performing in situ atmospheric measurements employing aspirated instruments, require a rapid (approximately 305-m/min) controlled descent from float altitude to accomplish flight objectives. To meet this requirement, a technique involving a large venting duct, or stub duct, has been developed. The duct is installed in the balloon envelope slightly below its equator. Once the duct opens at float altitude, it discharges a large quantity of inflation gas over a brief time span to induce a high descent rate. After the stub duct closes automatically, when the gas zero-pressure line within the balloon rises to the level of the duct opening, a much smaller control valve in the top of the balloon opens to continue gas venting and sustain the descent.

The computations required to predict the balloon response to the discharge of gas from the stub duct are complicated by the change in the shape and size of the balloon

as gas is vented and by the adiabatic heating of the remaining gas produced by compression upon rapid descent into denser air. A simulation model accounting for these phenomena has been developed in two steps, a partially manual procedure and a refinement to fully automated simulation.

The process of modeling the performance of a given balloon stub duct configuration is given in the first figure. The primary computation loop begins with a description of the balloon configuration, including size, envelope weight, gross inflation (lift), etc., provided as input to an existing model named Stress Index. This model determines the shape of the balloon at any stage of the flight, in the form of height and radius coordinates to points on the envelope surface, and the buoyancy per unit volume, as a function of the height coordinate. Height is referenced to the balloon zero-pressure line, the level at which differential pressure across the envelope wall is zero. The height coordinate at the stub duct opening and the buoyancy are used to compute the available pressure head at the stub duct level. The pressure head is needed to compute duct flow rate. The duct mass flow rate computation is a manual step which occurs next in the process; the rate then is input to the balloon vertical performance model, Altime.

Altime consists of several differential time equations, including the vertical equation of motion, the mass rate equation, the gas and balloon-envelope heat-flow equations, and the gas and envelope temperature. All equations are solved by a Runge-Kutta integrator for each simulation time step. The gas discharge rate through the stub duct is not computed within Altime and thus requires user input. Altime then is used to simulate 30 s or so of real time, at which point two of the Altime outputs, the gas mass and volume, must be used in the next block. This step requires external manual computation. The gas density and balloon gross inflation are computed and fed into

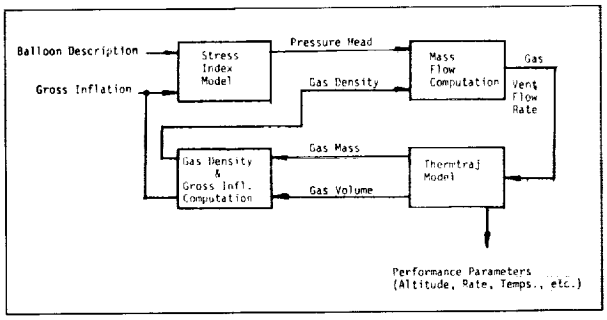

Balloon stub duct performance modeling procedure.

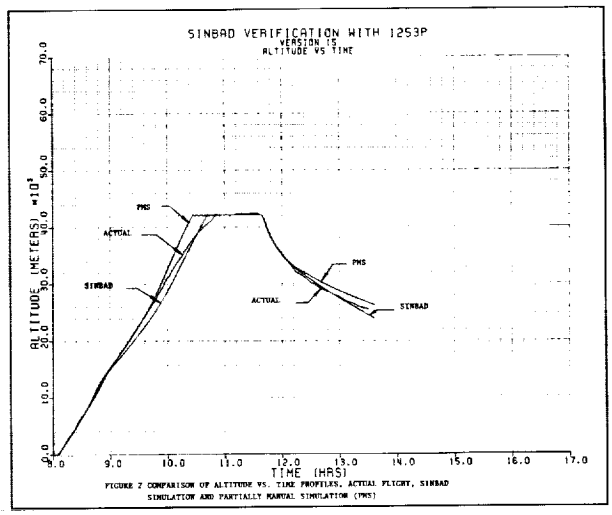

A comparison of altitude versus time profiles computed using actual flight data, Sinbad simulation, and partially manual simulation.

the Stress Index and gas mass flow steps, and the cycle repeats. The process is completed when the available pressure head is reduced to zero and duct flow ceases. Throughout the process, Altime provides outputs of other key parameters such as altitude, descent rate, and gas and envelope temperatures that define the balloon's response to the venting of gas. The same procedure is employed to model the performance during the interval when the top valve is opened after the stub duct closes.

Because the procedure requires manual intervention, it is tedious and labor intensive. This problem has been addressed by additional work, recently completed, which combines the balloon shape computation capabilities of Stress Index and the manual computations of gas mass flow, gas density, and gross inflation into the Altime performance model to create a new model named Sinbad, which automatically performs all of the steps described in the first figure.

The quality of the simulation capabilities inherent in Sinbad is shown in the second figure. A comparison of the altitude-versus-time profiles was performed for an actual balloon flight, Flight 1253P, using a stub duct with a simulation using the partly manual procedure described herein, and another using the new Sinbad model. The improved match of Sinbad is due to more frequent updating of the balloon shape definition at each simulation time step and other recent vertical performance model improvements included in Sinbad.

The stub duct modeling and analysis procedures provide effective and convenient means for generating specific stub duct designs, predicting performance, and conducting parametric studies to determine the importance of various design parameters.

Contact: George R. Conrad (Code 842)
(804) 824-1675

Sponsor: Office of Space Science and Applications

Mr. George R. Conrad received his MS in mechanical engineering from New Mexico State University and has over 25 years' experience as a development engineer. He is currently working at the university's Physical Services Laboratory in support of the Balloon Project Branch at Wallops.

BLOWN FILM EXTRUSION OPTIMIZATION

The NASA balloon program uses very thin polyethylene films in the manufacture of its scientific balloons. These specialized films are produced using the blown film extrusion process with the relationships between the key processing variables being quite complex. Adjustments to one processing variable may, and most often do, influence the other variables and the final mechanical properties of the film.

Extensive research has been conducted on determining the effects extrusion processing variables have on final film mechanical properties. The research has generally approached the problem assuming an isolation of variables, not their interdependence. No reported research has investigated the combination of process variables needed to produce an optimum film as determined by a desired final film property. Recent research by The Pennsylvania State University in support of the NASA balloon program has demonstrated an optimization technique that can be employed to determine the process variable values required to produce a superior-quality film keyed to any quantifiable final property.

The research was performed using a Killion 1.25-in. extruder equipped with a blown film tower, a 24:1 length-to-diameter screw with a Maddock mixing head, and a low-density polyethylene resin. The film thickness was fixed, and four of the most influential extrusion variables were identified for interdependency and control: screw speed, nip speed, bubble diameter, and frostline height.

The resulting films were tested and optimized for toughness, a film property defined as the area under the uniaxial load deformation curve.

The optimization technique determines the relationship between the extrusion variables and the desired film property—in this case, toughness. The relationship, known as a merit function, is described mathematically as a function of the four extrusion variables. Evaluating the function precisely is complex; however, the solution can be made more manageable using trust regions.

A trust region is a subset of the operating range of a variable within which the merit function is accurately described by a linear relationship. The function is modified so that each of the four variables can be represented by a trust region. Hence, any combination of the four variables within this region provides an accurate value of film toughness, and the coefficients of the variables will be valid anywhere in the trust region set.

Determination of the coefficients is accomplished by performing multiple film runs of known variable values within a trust region set, measuring the toughness of the resulting films, and, using a least-squares fit, evaluating the four coefficients. Represented algebraically, the

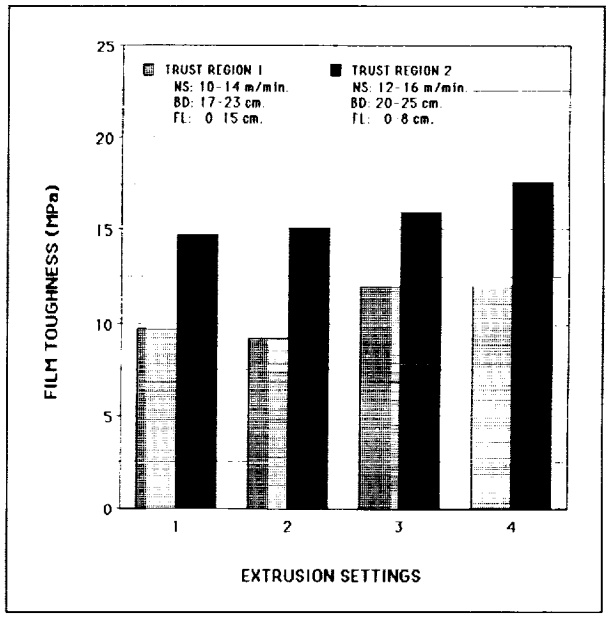

Results of the blown film extrusion process optimization technique through the first two trust regions. The balloon film toughness is increased by increasing nip speed and bubble diameter and decreasing frostline height.

merit function is easily optimized by computer using the Simplex method.

Simplex evaluates $n + 1$ points within the trust region set with the merit function, where n is the number of variables. The lowest value point is then replaced with a point closer to higher valued points and reevaluated. The iteration process is repeated until the steps toward the optimum become sufficiently small. The result is a maximum toughness within the trust region set and the variables that produced it.

These values then serve as the midpoints of the next trust region set. This process is repeated, with each trust region representing a step toward global optimum settings. Global optimums are determined by approaching a range boundary (i.e., equipment limitations) or crossing over a dependence maximum as indicated by a sign change in the corresponding coefficient.

Trust regions were established as ±10 percent of each parameter's operating range with resulting merit functions accurate to within 0.5 percent with experimental data. Trust Region 1 was located by running a random series of films across the range of variable values and using the settings for the toughest resulting film as the midpoint of Trust Region 1.

The accompanying figure summarizes the results of the optimization through the first two trust regions. Trust Region 1 yielded an average toughness of 10 MPa. Optimization of the merit function predicted an increase in toughness could be achieved with an increase in nip speed and bubble diameter and a decrease in frostline height. The midpoints of Trust Region 2 were obtained from the optimum value of Trust Region 1. As can be seen, Trust Region 2 yielded films with an increase in toughness of approximately 50 percent. Additional trust regions yielded no further increases in toughness due to bubble stability problems as a result of physical equipment limitations.

Future work will concentrate on the application of this optimization technique to other polyethylene resins. Optimization toward target values using trial-and-error or parametric extrusion runs can be significantly reduced by use of this technique, which should be applicable to similar processes. As a result, research can be accelerated and development costs reduced.

Contact: I. Steve Smith, Jr. (Code 842)
(804) 824-1669

Sponsor: Office of Space Science and Applications

Mr. I. Steve Smith, Jr., received a BS in aerospace engineering from Texas A&M University. He joined Goddard in 1983 as part of the Balloon Projects Branch at Wallops. Mr. Smith has worked with scientific ballooning for over 15 years and is responsible for research and development activities of the balloon program.

ORIGINAL PAGE
COLOR PHOTOGRAPH

Institutional Technology

The Management Operations Directorate represents Institutional Technology for Goddard Space Flight Center. During 1989, the Directorate maintained its high quality support for Goddard's vital space, science, and conservation missions. At the beginning of the year, after looking closely at how the Center does business and how to do it better, the Directorate reaffirmed its basic purpose—to provide high quality, responsive, innovative Center support. Highlights of some specific Directorate innovations are set forth here.

INSTITUTIONAL TECHNOLOGY

QUANTITY PURCHASES OF MICROCOMPUTERS

At the close of fiscal year 1983, with more than 1,000 microcomputers in use at Goddard, the use of microcomputers for word processing, spreadsheet construction, data base management, telecommunications, and graphics applications was expanding rapidly. Significant productivity improvements related to the automation and enhancement of office functions were being realized almost daily, with no apparent end in sight.

A survey conducted at that time revealed that there was significant, widespread interest in the office automation aspects of microcomputing and that 100 microcomputers would be needed. To encourage and facilitate these automation initiatives at Goddard, an acquisition plan was initiated and approved to buy an initial order of 50 units with a subsequent indefinite purchase quantity of up to $980,000. The contract was awarded in May 1984 for a 2-year period, but was exhausted within 8 months with 250 units having been ordered. It was evident that a new, larger scale procurement was needed. Because mass-buy arrangements establish the level of distributed computing capability available to a significant portion of the computing community for several years, these purchases must be carefully crafted to ensure that they respond to the technical requirements of the community, both immediately and within the technological life span of the hardware or software involved. While the lower prices, standardization, ease of maintenance, reduced paperwork, and shortened procurement cycle attained through large-scale procurements are important benefits, they are secondary compared to the technical propriety of the equipment selected.

In spring 1986, a new requirements survey and analysis was conducted. The survey confirmed a continuing and expanding need for the further enhancement of Goddard's distributed computing capability. A comprehensive plan was developed to estimate Goddard's office automation and distributed administrative computing requirements, determine methods of funding, ascertain the complement of equipment and services to be obtained, determine the delivery logistics, specify the administration of the procurement, and govern the development and production of a thorough procurement package.

Changes in microcomputer technology were so swift that specifications needed to be changed as soon as they were developed. The Goddard staff felt that the Intel 80386 microprocessor was the chip of the near future and that the older Intel 8086/8088-based technologies would fade away rapidly once the 386 became reasonably available. The issuance of a large contract, covering a long period of time, was considered. However, the staff felt that fast-changing technology would render a long-term contract obsolete before it could be exhausted, if not before it

Computer work stations throughout the directorate have vastly improved the efficiency, accuracy, and ease of management operations.

could be implemented. Pending the full arrival of the 386, the Goddard staff decided to provide the available Intel 80286 technology to personnel. It was, therefore, proposed to issue a lessor contract covering the immediately available technology, to be followed later by acquisition plans covering the evolving technology.

Using the Small Business Administration 8(a) process, a fixed-price, variable-quantity, microcomputer hardware purchase contract was awarded on September 18, 1987, to a private firm.

The contract, as subsequently modified, authorized the acquisition of $2.5 million of microcomputer hardware over a 1-year period, with an option for a second year but without any further increase in the funding limitation of the contract. When the funding limitation was reached on March 27, 1989, a total of 614 8-MHz Intel 80286-based microcomputer systems and peripherals had been purchased.

The procurement was developed and implemented at an approximate cost to the Government of $27,000, including both procurement and technical personnel resources. Post-implementation contract administration expenses were estimated at $25,000. Using a more conventional contract and small-purchase procedures, the procurement of equivalent equipment would have required the processing of 169 individual procurement actions at a cost to the Government of approximately $338,000. In addition, an equivalent quantity of equipment purchased with ordinary discounts would have cost an estimated $3.62 million.

Due to the 8(a) process, combined with large-quantity discounts, reduced handling, and heavily automated order processing, the cost savings to the Government totaled approximately $1.4 million in personnel and equipment costs. The transaction allowed Goddard to achieve significant long-term, post-purchase efficiencies in terms of hardware standardization, single-vendor responsibility, and reduced maintenance costs.

Major developments in microcomputer technology in the fall of 1988 significantly altered the technical direction of long-term acquisition plans. In concert with fiscal factors, this development suggested that it was premature to enter into a large-scale, long-term contract before spring 1990. Consequently, Goddard management determined to conduct another procurement of the existing Intel 80286-based, AT-bus technology which would support needs through spring and summer of 1990. Another fixed-price, variable-quantity, microcomputer hardware mass-buy contract, again using the Small Business Administration 8(a) process, was awarded on September 1, 1989, to the same private firm. This contract will provide Goddard with approximately 400 12-MHz microcomputer systems over the next year.

Despite the obvious success of the recently exhausted contract, as well as the substantial early interest shown in the contract awarded September 1, 1989, the lead times associated with procurements of this scale and mechanism limit the ability of these contracts to provide contemporary equipment. Organizations are constantly lagging with respect to the acquisition and use of cost-effective improvements in technology. To facilitate a more timely quantification of Goddard's evolving microcomputing requirements and purchasing patterns, the Automation and Planning Branch proposed a pilot program to monitor, for statistical purposes, all of Goddard's procurements of microcomputer hardware. To further assist in the prompt identification and communication of Goddard's needs, the branch has proposed that the Center Information Resources Oversight Committee establish an inter-Directorate advisory panel. Goddard management anticipates that the next large-scale procurement of microcomputer hardware will be along conventional competitive lines, but less conventional methods are being studied which will enable the Center to enter into more technologically responsive purchases. These plans will hopefully be ready for consideration hand-in-hand with the practical arrival of 80486 technology in late 1991.

Contact: Ronald E. Shoupe (Code 251)
(301) 286-5879
Sponsor: Management Operations Directorate

Mr. Ronald E. Shoupe is a Senior Hardware and Systems Analyst specializing in office automation and management information systems technology. He is Leader of the Microcomputing Group in the Automation and Planning Branch and primary staff consultant to the Center Information Resources Oversight Committee. He has received the Information Management Division Peer Award and numerous Performance Awards. Mr. Shoupe, who has been with Goddard for 4 years, holds a BS from the University of Maryland and is a graduate of the Civil Service Management Institute at Kings Point Coast Guard Academy.

THE GODDARD SPACE FLIGHT CENTER ENVIRONMENTAL PROGRAM

The Health and Safety Branch assumed formal responsibility for the Center Environmental Program in fiscal year 1987. The initial goal was to manage effectively Goddard's hazardous wastes in accord with environmental regulations and minimize the cost and liabilities associated with the handling, storage, and disposal of hazardous materials at both the Greenbelt and Wallops locations. Goddard has constructed a new hazardous waste storage facility at each location and will add a small neutralization room to Greenbelt's hazardous waste storage facility. Recyclable oils and other materials are now stored in covered and secured storage areas to lessen the likelihood of contamination.

Shortly after the construction of storage facilities, the Center hired a contractor Environmental Specialist to perform the line function necessary to bring the Center into complete compliance. The provision of a full-time Wallops Environmental Engineer in May 1989 facilitated the implementation of the program at that location. Over the past year, the Center has properly disposed of approximately 19 tons of hazardous wastes at a cost of $30,000. The specialist's efficiencies through consolidation, neutralization, and recycling covered more than the total cost of his position.

In accord with environmental law, the Comprehensive Environmental Response Compensation and Liability Act, Goddard completed field work associated with a site investigation at both locations to determine the effect of past environmental practices. Test results indicate that Wallops has soil and groundwater contamination at the old fuel farm, the scrap yard, the fire-fighter training area, and the old waste oil dump site. Separate from the site investigation, other areas of environmental concern have been identified at Wallops. Some of these concerns are the potential contamination of the drinking water wells, the silver discharge at the sewage treatment outfall, the cleanup of fuel-soaked soil at past fueling stations, and the removal of unused underground heating fuel tanks.

Goddard is identifying its environmental concerns, working closely with the Region III of the Environmental Protection Agency, the States of Maryland and Virginia, and local governments to identify Goddard's problems and develop appropriate, timely corrective action. By fiscal year 1991, estimates indicate that Goddard will have spent nearly $15 million on identifying and correcting environmental problems. Goddard has made significant strides since 1987 and is meeting its new environmental challenges. Goddard will support the environmental program with the necessary resources. NASA will support Goddard's efforts with its fiscal year 1989, 1990, and 1991 environmental budgets of $25, $30, and $32 million, respectively. Goddard is committed to taking a proactive posture with respect to environmental compliance and setting an example for other Federal facilities.

Contact: Joseph H. Letourneau (Code 205)
(301) 286-7444

Sponsor: Health and Safety Branch

Mr. Joseph H. Letourneau, coordinator of the Goddard environmental program, has been with Goddard for 10 years and has a BS in mechanical engineering.

THE COMPUTER SERVICES BRANCH (CSB) CONFIGURATION MANAGEMENT PROGRAM

The CSB of the Information Management Division provides administration data processing services to Goddard. Applications encompass financial management, human resource management, procurement management, and information resources management. These CSB objectives are grouped into two areas, the Configuration Management Program, shown in the first figure, and the system development life cycle. Although these activities have been ongoing, these formal objectives and guidelines for these programs have recently been established. The Configuration Management Program consists of five disciplines: performance measurement and capacity planning, quality assurance and control, data administration, change control management, and distributed processing.

These disciplines have been integrated into a unique program with the following goals: providing better, more efficient service to the user community; enhancing the quality of products and services provided to the user community; reducing or avoiding costs in all areas, such as the system development and maintenance activities; and improving productivity in all areas.

The first discipline, performance measurement and capacity planning, includes measuring the various aspects

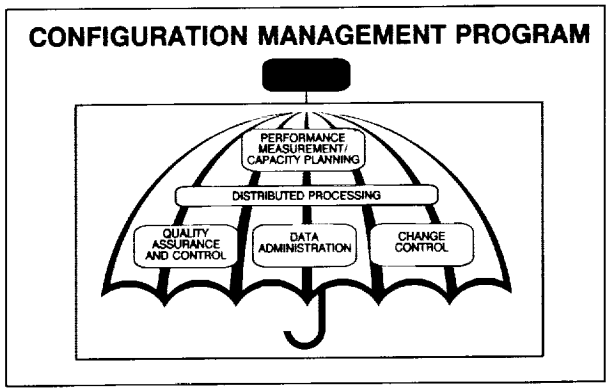

Configuration Management Program's five disciplines.

of the mainframe's performance in response time, central processing unit (CPU) activity, direct access storage device activity, and many other aspects of the computer where performance of the system is an issue. (CSB operates an Amdahl 580/5850 CPU, has 160 Gbytes of online storage, and supports communications capable of handling up to 150 concurrent users, using IBM's MVS operating system.) Performance measurement refers to the practice of monitoring mainframe systems to track usage and trends so that the CSB is able to do the following: identify candidates for improvement in system inefficiencies, fine-tune and maximize the use of existing equipment (both hardware and software), identify contention spots in the current system and suggest cost-effective solutions, and establish a performance baseline for accurately projecting growth.

Capacity planning is a methodology that uses established formulas of capacity limits and growth forecasts to allow the staff to project and manage growth of the mainframe systems effectively. The program is designed to monitor and track all aspects of the system performance as well as growth of new software applications. The methodology is shown in the second figure. By combining the current performance levels with forecasted growth, CSB will be able to plan accurately and ensure that the system's capacity will be sufficient for providing prompt reliable service for its users.

During the past year, the CSB established a performance data base and implemented standard performance reports for all new systems. These reports came from the current performance monitoring packages, which include the Resource Measurement Facility, the Monitor for the Customer Information Control System, and the TRIM software performance monitor for ADABAS. These monitors and reports provide input to guide the branch tuning applications as well as establishing service level agreements for new and existing systems. The purpose of these service level agreements is to outline the level of expected service that can be reasonably provided for an application system based upon its performance configuration. Besides standard identification, these service level agreements contain standard indexes that the CSB uses for making workload projections. These indexes include the use of data processing units such as CPU use; ADABAS calls, file structures, and usage of data elements; and physical inputs-outputs and disk storage requirements. Also, workload projections are based upon natural forecasting units such as number of users, number of terminals, number of screens, and access patterns.

In the future, the performance measurement and capacity planning program will establish a schedule for tuning critical systems and systems that are lacking in performance. In addition, the CSB plans to invest in an automated capacity-planning modeling tool to assist in producing more accurate workload projections. The CSB also plans to build an interface between its automated data dictionary system, Predict, and the ADABAS performance monitor, TRIM, to track performance data on a data element level. This interface will also be useful in constructing data elements based workload projections for new systems.

Quality assurance and control are closely associated with the application software system life-cycle development methods. Quality assurance is the planned and systematic process of assuring conformance of software products to

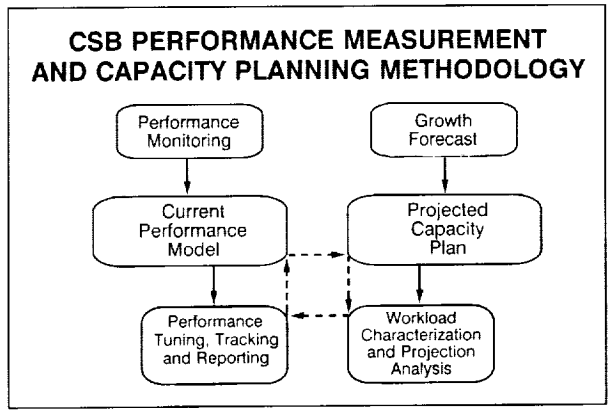

CSB capacity plan and performance measurement methodology.

established requirements, methods, and standards. The process involves a program of review and test activities that will become a regular part of any new system development activity. Occurring at various points throughout the system development cycle, these activities are designed to provide a way to ensure that the software system is following the requirements defined by its user and meeting standards for software development.

The third discipline in the Configuration Management Program is data administration. Data administration is a centralized policy, planning, and coordination function focusing on the standardization of data resources, the elimination or control of redundant data items, and the definition and collection of data items. Data administration at the CSB, as shown in the third figure, will establish data as a resource to be planned, managed, and controlled so that it can be shared effectively by the users of administration information at Goddard.

The CSB has realized some significant benefits from data administration. These benefits include high-level data architecture, a model for incorporating all of the branch's applications into the program, and an effective data dictionary. Next year, the program's objectives will be to develop user dictionaries, develop standards for computer-aided software engineering tools, and interface the dictionaries with system-wide performance data to track data element usage.

The fourth discipline is change control management. Change control refers the branch's application systems requirement for constant changes or modifications. These changes may be simple, limited to one program, or they may be complex, affecting several systems. Change control management maintains the integrity and traceability of the product by controlling and tracking the product throughout the system life cycle. The system provides the mechanics for performing effective quality control and verification, validation, and testing. This program was established to manage potential change conflicts and impose a central method to avoid potential problems that can result from quick fixes.

The final discipline is distributed processing. This discipline involves analyzing and establishing policies and standards for distribution of processing using the mainframe as the central accessible storehouse for most of Goddard's administration data. A variety of remote terminals retrieves the centralized data and then manipulates it

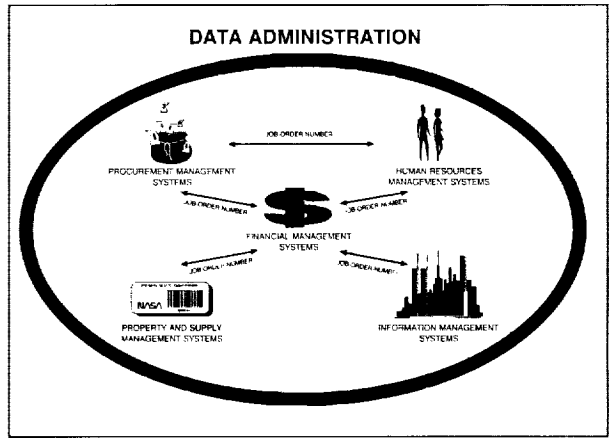

Administrative data needs to be shared effectively by many users.

using a dedicated terminal such as a personal computer. This system is shown in the fourth figure.

Currently at Goddard, directly connected terminals and the Rolm telephone system link the administrative mainframe to its users. Many users employ personal computers as remote terminals to access the mainframe. The structure resembles a star with the mainframe at the center and peripheral terminals radiating out in all directions. The CSB is investigating a cost-effective use of resources that involves distribution of processing, a form of distributed processing common to management information systems. This distribution would divide each function so that each component of the Goddard administrative system would be used for the operations it does best, the mainframe for efficient data base access and the personal computer for interactive manipulation of data. In addition, off-loading processing through distributed processing represents a performance savings to the mainframe. The Configuration Management Program's success has been due, in part, to the overlap and interaction between its various disciplines.

These five disciplines could not function practically by themselves. To have an effective Configuration Management Program, the branch established an improved systems development life cycle methodology where the five disciplines could be integrated into the branch's daily work activities. The new system development life cycle has become the vehicle of operation for the various disciplines. The goals of the system development life cycle methodology are establishing a standard for the most effective business solutions in support of the administration

of Goddard's mission, developing reliable, high quality application software systems for the end-users of the CSB computer, increasing the level of end-user participation throughout all phases of systems development, increasing productivity for both the CSB and its end-users, and decreasing costs for application development efforts.

These goals focus on an increased level of involvement for the users of data processing services, for the analysts and programmers responsible for developing these systems, and for all levels of management. Although this involvement will require more lead time in the development process for all participants, the result will be a higher quality product and less time and money spent on maintenance.

In January 1989, the Software Engineering Analysis Team was established. The team's purpose was to review a variety of possible application software development life cycle methodologies, and compare and contrast them with current practices and procedures. The team was divided into an analysis panel, a review panel, and the Configuration Management Program team. Guidelines for the team's analysis were established in a charter given to the panels.

The analysis panel recommended unanimously that the CSB adopt and modify the NASA-sponsored Automated Information Management System life cycle. This program provides a framework for the development, implementation, operation, and maintenance of agencywide administrative information systems. The program encompasses data processing and telecommunications capabilities as they relate to administrative support across NASA.

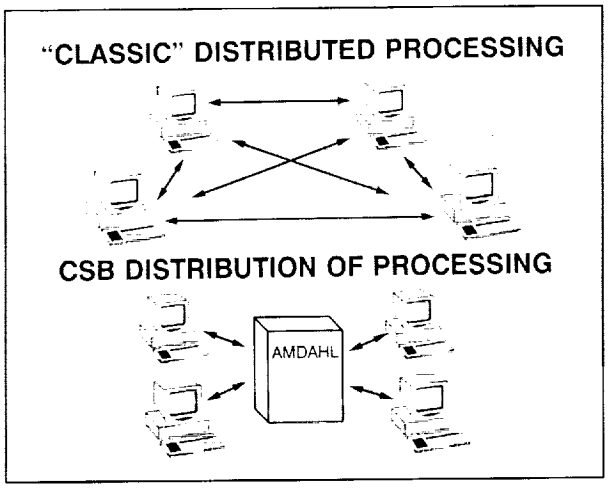

The CSB showed a performance savings by using a mainframe in the distribution of processing instead of the classic method of distributing processing.

The life cycle, shown in figure five, is divided into five phases: predefinition, project definition, system development, implementation, and operations and support. The system development framework is intended to be flexible. Feasibility, cost, and complexity of a project will be the major factors in determining the extent to which the procedures, techniques, and documentation required are employed in a particular project.

The CSB Automated Information Management System life cycle has several advantages: adherence to NASA standards combined with knowledge of the unique needs of the Goddard business community; enhanced user involvement; completely documented formats, schedules, and milestones for all deliverable products; and increased quality assurance and change control built into the methodology.

Following the adoption of the system development life cycle, the Configuration Management Program developed a series of end-user classes to familiarize the Goddard community with the new procedures and practices that make up the CSB methodology. The classes cover the entire system development life cycle: the predefinition and project definition phases, the system development phase, and the implementation, operations, and support phases. The objective of these is to familiarize the user community with the goals, documentation, reviews, methods, and techniques of the system development life cycle. The staff continues to modify and adjust the new system development life cycle methodology for existing production systems and for all new development efforts. Both the Configuration Management Program and analysis teams continue to meet regularly to review and track the progress made during the implementation process and discuss the technological issues of software development, management, and maintenance.

Quality, productivity, and efficiency are of importance to the CSB. The Configuration Management Program, using an integrated team approach, has enabled the branch to incorporate these important elements into its routine workday. The CSB views this innovative approach to doing business as a significant step forward in a practical implementation of the Information Management Division

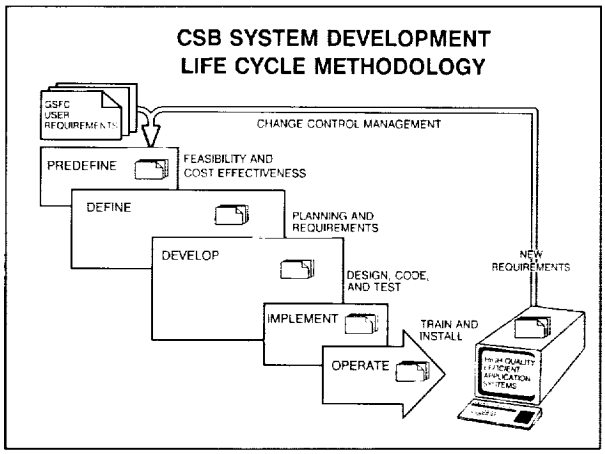

The five stages of the life cycle methodology.

policy: "Quality services, at least cost, and on schedule from a team committed to customers."

Contact: Patricia A. Bavis (Code 254)
(301) 286-9483

Edward B. Klem (Code 254)
(301) 286-5826

Ronald D. Lear (Code 254.6)
(301) 286-8050

Michael E. McCann (Code 254.6)
(301) 286-5360

Roy W. Queen (Code 254.6)
(301) 286-3674

Paul Watts (Code 254)
(301) 286-4311

Sponsor: CSB

Ms. Patricia A. Bavis, in the CSB Information Management Division, has earned a BS in business administration and currently is working on another in information systems management. She has won an award for her configuration management presentations to Goddard management personnel.

Dr. Edward B. Klem is Senior Systems Analyst supporting Goddard's administrative computer center in the CSB. He has received the Management Operations Directorate Contractor Award and has 5 years' experience at Goddard.

Mr. Ronald D. Lear holds a BS in technical writing and works on the performance measurement and capacity planning program for the mainframe environment in the CSB.

Mr. Michael E. McCann, a Data Administrator working at the CSB in the Information Management Division, develops and implements a program designed to recognize and manage data as a valuable resource. He holds a BS in oceanography and has worked at Goddard for 5 years.

Mr. Roy W. Queen works in the CSB, where he sets up quality assurance and change control programs for system software development. Mr. Queen has an AA in business administration.

Mr. Paul Watts holds a BA in business administration and economics and is currently working on an MS in business management and information systems. He is a member of the Configuration Management Program team in the CSB.

CENTER-WIDE LOCAL AREA NETWORK SUPPORT

Recently, the Information Resources Oversight Committee delegated responsibility for Goddard's network environment to the Network Steering Committee. The Network Steering Committee provides the management, engineering, operations, and maintenance of Goddard's network environment, including user support. The Network Support for Small Systems was formed in March 1988 to assist user organizations that participate in Goddard's network environment.

The Network Support Group for Small Systems has played a prominent role in advocating, installing, and supporting microcomputer-based local area networks. The group convinced a large number of organizations to adopt a common local area network, a development that has led to increased efficiency in office operations by sharing resources throughout Goddard. The number of users of Goddard's predominant microcomputer local area network has increased by 230 percent since August 1988, with a 100-percent increase in the number of division-level organizations acquiring a microcomputer local area network.

Aside from the resource-sharing benefits provided by compatible networks, the network support group provides the following services to Goddard organizations:

- Assistance in preparing requirements for the acquisition and installation of local area networks.
- Recommendation of a network design based on specific organizational requirements.

- Assistance with the procurement process, including identifying technical specifications for the network hardware, software, and installation.
- Assistance with training in the use and administration of a network.
- Assistance in problem identification and resolution.
- Assistance with the installation, operation, and fine tuning of the network hardware and software.
- Assistance in connecting the local network to the Goddard network.

To further encourage use of a common microcomputer local area network, the Network Support Group has established shared network services that are available to organizations through the Goddard network. The first service is a Center-wide name service that provides a directory of all users and file servers, making it possible for a user to send an electronic mail message without knowing the recipient's address. A centralized name service also makes more Random Access Memory (RAM) available on individual servers, freeing them to run other network services. A second service is a central server that is set up to provide a platform for shared software. One software package available through this server acts as a terminal emulator program, allowing an IBM personal computer or compatible computer to work as an American Standard Code for Information Interchange (ASCII) terminal, connecting to remote host applications such as GSFCmail. A third service is an electronic mail gateway that allows messages to be sent transparently and automatically between users of different electronic mail systems.

Through the establishment of the Network Support Group, significant improvements have been made in the personal and group office productivity. As a result, the overall institutional services provided to the Goddard community have been strengthened.

Contact: Deborah L. Sharpe (Code 251)
(301) 286-8519

Sponsor: Management Operations Directorate

Ms. Deborah L. Sharpe is a Communication Management Specialist in the Automation and Planning Branch of the Information Management Division. She manages the Xerox Network Service, helps design and implement microcomputer local area networks, and serves as Directorate representative on the Centerwide Network Steering Committee. Ms. Sharpe has received several performance awards during her 3 years with Goddard.

INVOICE PAYMENT SYSTEM OVERVIEW

The Invoice Payment System, which was implemented in fiscal year 1989, provides system users in Goddard's Financial Management Division with the means to enter, examine, and process vendor payments on line. The menu-driven system maintains vendor payment addresses, processes individual invoices, creates payment schedule reports, and tracks invoices from receipt to payment.

Invoices are entered into the system by way of an invoice entry screen. Once an invoice has been entered, voucher examination is performed on line through the Voucher Examination Module. After an invoice has been examined, it is reviewed by the verifying officer and scheduled for payment. An enhancement to the system that will soon be implemented will generate Automated Clearing House Tapes, so that vendor payments can be made by direct deposit.

Management tools provided by the system include reports of unpaid invoices (by examiner), reports tracking invoices through the system, invoice status reports, and late-early payment report data. The system will also assist managers in meeting Prompt Payment Act requirements by scheduling payment dates as soon as invoices are received.

Contact: Susan Trelease (Code 210)
(301) 286-4404

Sponsor: Financial Management Division

Ms. Susan Trelease is a systems accountant in the Financial Management Division. Ms. Trelease helps provide systems support to operational areas such as accounts payable, payroll, travel, general ledger, and budget. She has 3 years' experience with NASA and has a BS in accounting.

COGENERATION POWER PLANT

Cogeneration is the sequential generation of electrical and thermal power using one energy source. Cogeneration is not a new technology. It was prevalent at the turn of the century. More than 59 percent of the total

U.S. power-generating capacity was at industrial sites in 1900. With the increase in reliability and economics of commercial power, the cogeneration plants became extinct. Only in recent years has cogeneration been considered a viable technology again. Cogeneration provides energy users with an opportunity to reduce their overall energy costs through an investment in a high-efficiency on-site power generating system.

Goddard is served by a 30-year-old power plant that produces steam, chilled water, and emergency power (see first figure). Most of the major components of the plant are scheduled for replacement or extensive rehabilitation. Rehabilitation of the plant will require a significant capital expenditure. Additionally, the annual cost of energy, which now totals $7.0 million, is likely to increase. There is also an increased demand for backup power for real-time support beyond the present capacity. Goddard conducted a feasibility study to analyze energy data, energy requirements, and alternate power plant configurations that included a cogeneration system. This system will produce power and heat for the center at a reduced cost. The study also reviewed sensitivity analyses to identify the relationship between key factors and overall results.

As the second figure illustrates, the feasibility study modeled the performance of alternative cogeneration systems, each sized to different criteria. The smallest system examined consisted of a single Allison 571-KA gas turbine with a site capacity of approximately 5,600 W. The cogeneration system was equipped with a heat-recovery boiler and duct burner. The system size was based on Goddard's thermal loads and, when base loaded, would supply most (70.4 percent) of the Center's steam requirements, with little need to release any of the turbine's exhaust heat to the atmosphere. It would also supply over 20 percent of Goddard's peak electrical requirement and almost 40 percent of the Center's electrical usage.

This system could be operational in 1992 and would require a $6.1 million capital investment. The first year's savings were projected to total almost $1.3 million and, based on a 20-year economic life and a discount rate of 9.875 percent, would produce savings with a net present value (NPV) of $13.3 million. Included in this savings was $2.6 million for deferral in replacing the existing boiler plant.

The primary economic assumption was that natural gas prices for a nonseasonal, increased load such as a cogeneration plant would be $2.78 per million Btu as compared to the rate of $3.20 per million Btu under the current contract with Washington Gas. It was also assumed that Potomac Electric Power Company (PEPCO)'s current rate structure would remain in place with purchased power increasing at a rate of 1.4 percent above inflation. Boiler fuel was assumed to increase at 2 percent above inflation, which was assumed to be 5 percent per year. The cost of cogeneration fuel under a long-term contract as developed by a third party was assumed to increase at the rate of inflation. Finally, it was assumed that there were no incremental operational steam system costs (manpower, chemicals, etc.) associated with the cogeneration system. The costs of operating a cogeneration/boiler plant were equal to those of a boiler plant only.

Because this option met only a small fraction of Goddard's requirements, the economics of a larger cogeneration system were examined. A Solar Mars turbine generator set with a site rating of approximately 8,350 kW was selected. The generator more closely matched the Center's minimum electrical requirement of 9,300 to 9,400 kW. This system would provide approximately 35 percent of the Center's peak demand requirement and almost 60 percent of the electrical usage. More than 50 million kWh would be purchased from PEPCO. While this system would provide most of the thermal energy required by Goddard, it would not have adequate capacity to satisfy all needs, and approximately 6 percent of the steam would be raised in the conventional boilers.

The capital cost for this system would be approximately $9.27 million, and it would result in savings of $1.4 million in the first year of operation. The resulting NPV of $13.2 million would be slightly less attractive than the thermally base-loaded system.

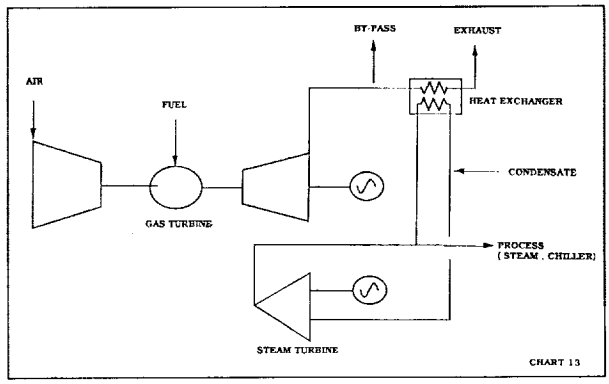

Schematic of the Goddard power plant.

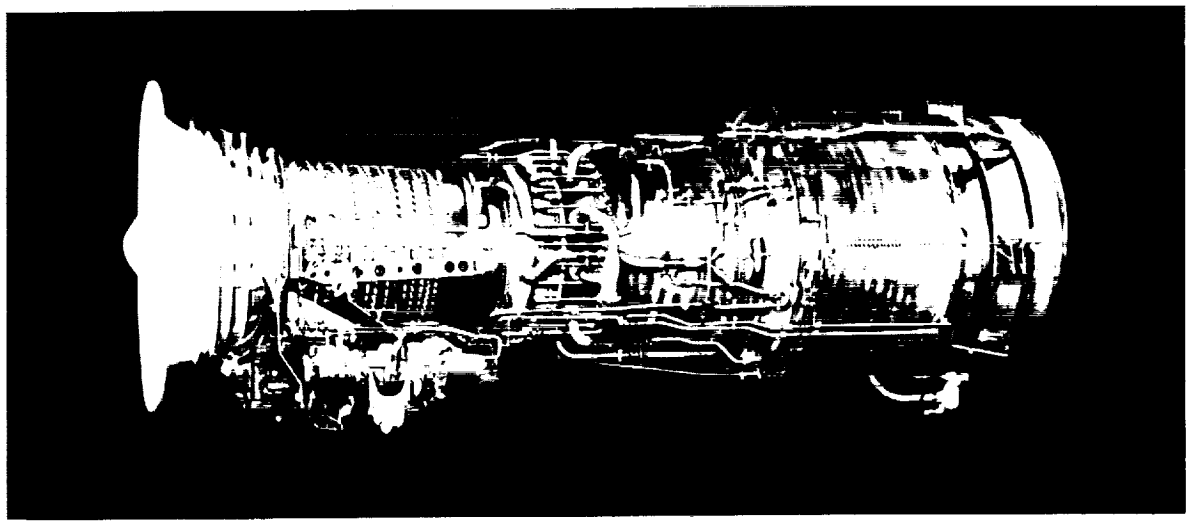

Power Turbine Speed (RPM)	3600	3000
Output (SHP)	30,400	29,500
(Kw_S)	22,669	21,998
Heat Rate (BTU/SHP-hr)(LHV)	6872	7052
(BTU/Kw_S-hr)(LHV)	9216	9457
Exhaust Gas Flow (lb/sec)	150.4	151.5
Exhaust Gas Temp (°F)	982	985

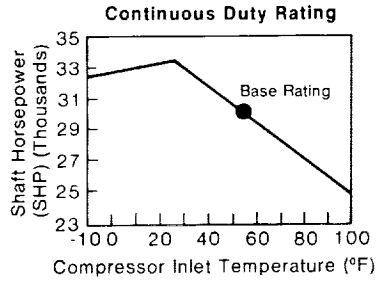

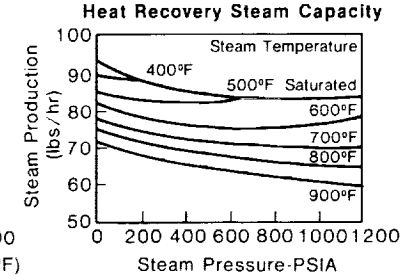

Sample performance summary for one of the systems studied.

While this turbine exhaust could not satisfy the Center's peak thermal requirements, it would have excess capacity during the summer with a combined cycle system. This option consisted of the Mars combustion turbine combined with a 600-kW steam turbine that would operate on excess steam from the heat-recovery boiler. This turbine increased the project NPV to $13.7 million.

Because the 571-KA is more efficient electrically than the Mars, an electrically base-loaded system consisting of two 571-KA turbines was also examined. This system would provide more than half of the required peak capacity and more than 75 percent of the required electrical energy. It would also provide almost all the required steam. This system would produce an NPV of $16.9 million and, if a 1,000-kW steam turbine were included, would produce an NPV of $18.3 million. The primary reason for the better return shown by the two 571-KA turbines was its higher electrical efficiency.

The last option examined was a larger cogeneration system sized to supply most of the Center's electrical requirements. This system, built around a General Electric LM 2500, would provide more than 85 percent of the peak demand during the summer and all required capacity during the winter. It would also provide most of the energy required on site with more than 50 million kWh hours of energy available for sale to PEPCO. The price for this power would be negotiated with the company; however, the rate paid to small cogeneration systems was used as a starting point in the analysis, and 1992 revenues of $1.8 million were projected. As an option, the Center's load growth might provide an alternative market for this power, further improving the project's economics.

The cost of "reserving" standby capacity from PEPCO at $6,500 per month was included as a cogeneration cost. Securing an acceptable standby contract would require negotiation with the company and development of

an agreement for any sale of excess power. The overall cost reduction to the Center in 1992 would be almost $2.8 million after an initial investment of $14.8 million. The resulting NPV would be $25.6 million.

Goddard officials considered a 3,000-kW steam turbine in a combined cycle mode because of excess thermal energy. This system would produce additional power for sale to PEPCO, reduce the need for power purchases from the utility, and produce an NPV of $29.1 million. Should the utility get its requested rate increase, the NPV would improve to $30.8 million. Options for improving the system's economics by cooling the turbine inlet, for example, were not considered.

Goddard officials analyzed the economic performance of the same LM 2500 turbine system, assuming that all cogenerated power would be sold to PEPCO. This option produced an NPV of $19.2 million for the simple cycle and $27.4 million for the combined cycle and was not preferable to the use of power site.

Finally, several sensitivity analyses were performed to identify the relationship between the following key factors and overall results:

- A range in budget from -25 to +100 percent of the base case.
- A relative change in electric costs, as compared to fuel, ranging from -5 to +5 percent.
- A change in all energy costs relative to inflation of -2 to +2 percent.
- A change in the discount rate of -5 to +5 percent.

The project remained viable under these broad alternatives, either singly or in combination.

The best option available to Goddard is the LM 2500 combined cycle plant. This project could be viable with either NASA or third-party ownership. Assuming typical third-party financing of 15 years with 25-percent equity and a 10-percent interest rate, Goddard could retain 30 percent of the resulting operational savings under a shared savings contract. The NPV of the Center's savings under this contractual arrangement would be $14.6 million. The value of the lost revenue to Goddard totaling $14.5 million would be offset partially by increased Federal taxes with an NPV of $5.0 million, reducing the net loss to $9.5 million.

Under this type of arrangement, Goddard could transfer much of the risk and the economic gain associated with a cogeneration project to the third party. Because of the critical nature of the Center's mission, any third-party contract would require special terms and conditions covering control of the operation of the cogeneration facility if the third party's performance failed to meet contract requirements. A key to any successful contract would be Goddard's ability to use the existing backup systems as required.

Also, staffing is a key issue with third-party ownership. If the third party is responsible for maintenance and operation of the cogeneration plant and the Goddard staff is responsible for maintenance and operation of the existing boiler plant, savings would be substantially reduced. The NPV of the resulting savings would be reduced to $3.4 million if NASA retained control and responsibility for the existing boiler plant.

A second third-party alternative is based on a leasing agreement, and under this type of arrangement, Goddard's share of the savings might have an NPV of $21.3 million. This type of arrangement would also allow the Center to operate the plant and would eliminate any penalty associated with two operating crews. It would provide the Center with the best overall economics combined with maximum control.

Goddard is also faced with the replacement of the existing electrical chillers. Electric chillers with a coefficient of performance of 4.69 (0.75 kW hours/ton hour) and absorption chillers with coefficient of performance of 0.6 were compared based on peak shaving operation of the absorption chillers and base-loaded operation of the electric chillers. Economics were examined, both under the existing PEPCO rates and under the rates which PEPCO recently requested. While this rate petition included a request for an increase, it also included a significant restructuring of the GT rate. The cost of peak energy in the summer would be significantly increased, while the winter rate would be decreased. This restructuring would have the greatest impact on chiller economics.

The analysis was based on a $170-per-ton differential in total installed costs for the absorption chillers. Additionally, it was based on an assumption that any differences in nonenergy operating costs were so small as to be negligible.

If 1,500 tons of the existing electric chillers were replaced with absorption chillers and if these absorption chillers were operated as peakers, for approximately 180 hours per year, under existing PEPCO rates, the payback would be 4.7 years based on natural gas at $3.20 per million Btu. If the absorption chiller were operated in a base-loaded mode, the payback would be unacceptably long. More importantly, under the PEPCO proposed rate restructuring, the simple payback would decrease to 3.1 years. If lower-cost summer gas priced at $2.78 per million Btu were assumed, the paybacks would be 4.4 years under existing PEPCO rates and 2.7 years with the proposed PEPCO rates.

Any decision regarding chiller replacement should be deferred until the PEPCO rate structure can be predicted more confidently.

The primary conclusions resulting from this analysis were that cogeneration would be a viable option at Goddard and would produce significant savings to NASA. The maximum economic return would result from a combined cycle consisting of a General Electric LM 2500 gas turbine with a site rating of 20,950 kW and a 3,000-kW steam turbine.

This system could be developed with either NASA or third-party ownership. Third parties have shown a strong interest in the development of gas-fired cogeneration in the PEPCO service area. Both a shared-savings contract and a leasing arrangement would be viable, with the lease producing a better economic return to the Center while also providing better control of the cogeneration facility and the existing boiler plant.

Contact: Pradeep Sinha (Code 290)
(301) 286-3171

Sponsor: Management Operations Directorate

Mr. Pradeep Sinha, a professional engineer and Assistant Chief of the Plant Operations and Maintenance Division, directs all contracted activities, conducts management and engineering evaluations of the physical plant, and manages maintenance and operating programs with large-scale facilities impact. Mr. Sinha earned one MS in industrial engineering and is currently pursuing another in engineering administration. He has won several Special Achievement Awards and a Management and Recognition System Performance Award during his 10 years with Goddard.

ANTICIPATED MAJOR COMPETITIVE PROCUREMENTS LISTING:

AN AID TO PROSPECTIVE CONTRACTORS
A MICROCOMPUTER SYSTEM FOR INFORMATION RETRIEVAL AND COMPILATION

The importance of highly qualified contractor support for NASA's mission cannot be emphasized strongly enough. NASA published a handbook for contractors, *Selling To NASA* (1986), which was designed to assist the prospective contractor. This publication provides useful general information describing the type of work done by NASA. However, it cannot provide information regarding the specific contracts being let by a particular NASA installation during a specific time period. In response to this need, in 1984 Goddard published a listing of anticipated 8(a) procurements and disseminated the list to prospective contractors. The listing has since been expanded to include all anticipated major competitive procurements. The report encourages and helps industry plan to respond to Goddard's requirements.

In producing a procurements list, the Goddard author sought to automate the procedures for gathering data and producing a report. The procedures described below were used successfully to prepare the "Anticipated Major Competitive Procurements" report, a 132-page listing, which was published early in fiscal year 1989.

At Goddard, each procurement listed in the "Anticipated Major Competitive Procurements" report meets the following three criteria:

- Cost of over $100,000.
- Activity during specified fiscal years. For example, the report issued in October 1988 includes procurements anticipated for fiscal years 1989 and 1990.
- Designation as either competitive, which could include a small business setaside, or an 8(a) procurement action.

The information presented in Goddard's report is provided by the organizations initiating the procurement actions. The information consists of (1) the code and name of the initiating organization; (2) a one-line title of the procurement action; (3) estimated person years where appropriate; (4) the name, code, and telephone number of both the technical representative and the contracting officer; (5) the estimated request-for-proposal/ invitation-for-bid release

date; (6) the estimated award date; and (7) a one- or two-paragraph description of the action (up to 1,200 characters).

Data have always been gathered from the resource staff of each directorate. In most cases, the resource staff pass along these data to the technical organizations. In the past, this information was gathered by paper transfer; the resource organizations typed information and forwarded it to the report's researchers who then edited and retyped the information into a single file. Information was frequently gathered through interviews with the resource or technical staffs and was a time-consuming process.

Report preparation was done by word processor; the entire document had to be retyped each year. Thus, it was practical to disseminate the report only once a year, due to the effort required to gather data and produce the report.

The report's compiler recently wrote a computer program to help streamline these tasks. Diskettes containing the program and previously submitted data files are now distributed to the Directorate Resource Managers, who then forward them to the pertinent personnel for completion. The information need not be completely retyped if submitted during previous data-gathering efforts; it is edited or deleted as appropriate, new actions are added, and then the diskette is returned in a protective mailer to the Procurement Analysis Branch for compilation. Here, the data files on more than 20 incoming diskettes are sorted into one file. A program is then run against this file, compiling the data into its final printed output form as a text file. The text file is then edited and printed from a word processor. Because the computer programs needed to perform these tasks have all been prepared, only the editing procedure requires a notable amount of time; the rest of the work is performed in a matter of minutes.

The system was written for IBM-compatible microcomputers. It was written in dBASE III+ and compiled using Clipper, so it can be used on all IBM-compatibles without requiring dBASE. It starts with a main menu and features fill-in-the-blank data prompts and edits that help ensure the completeness and validity of data. The main menu has the following options:

1) Read instructions. One page of instructions is included as the menu default choice, always at the fingertips of the user.

2) Add new procurement action. This option includes all of the items listed in the report, as well as data entry edits to help ensure the quality of the input.

3) Edit previously added action.

4) Delete previously added action.

5) Print. This option takes the user to a print menu that allows the printing of a single procurement action or all procurement actions for a specified code. Both information contained in this printout and its format are the same as the final report.

6) Exit.

Goddard's "experiment" in automating the Major Competitive Procurements listing data collection and report writing seems to have been very successful. This microcomputer system was used in September and October of 1989. As an option, data providers were allowed to send information in a typewritten form, yet almost all responses were by diskette. Suggestions for improvement were solicited and many suggestions have been incorporated through program modifications.

This automated approach provides a useful tool in strengthening the response of contractors to NASA's needs.

Contacts: Dennis E. Reed (Code 263.3)
(301) 286-5313

Sponsor: Operations Analysis Branch, Procurement Support Division

Dr. Dennis E. Reed is Program Analyst in the Operations Analysis Section of the Procurement Analysis Branch. He holds a PhD in evaluation research and teaches in the Applied Behavioral Science Program at Johns Hopkins University. He has 7 years' experience at Goddard and has received an Innovation Award.

Acronyms

ABLE	Amazon Boundary Layer Experiment above 10 TeV
ACAD	Attitude Control and Determination
AIPS	Astronomical Image Processing System
AIRS	Atmospheric Infrared Sounder
AMSU	Advanced Microwave Sounding Unit Antimatter
ASCII	American Standard Code for Information Interchange
ATN	Advanced Television Infrared Observation Satellite (TIROS)-N
AVHRR (-LAC)	Advanced Very-High-Resolution Radiometer(-Local)
BCAUS	Backup Control Mode Analysis and Utility System
BGO	bismuth germanium
CAPL	Capillary Pumped Loop Flight Experiment
CCB	Configuration Control Board
CCD	charge-coupled device
CD-ROM	compact disk read-only memory
CDAW	Coordinated Data Analysis Workshop
CDDIS	Crustal Dynamics Data Information System
CDF	Common Data Format
CDHF	Central Data Handling Facility
CDOS	Customer Data and Operations System
CL	Common Lisp
CLAES	Cryogenic Limb Array Etalon Spectrometer
CLASS	Communications Link Analysis Simulations System
COBE	Cosmic Background Explorer
CPL	Capillary Pumped Loop
CPU	central processing unit
CSB	Computer Services Branch
DADS	Design Analysis for Dynamic Systems
DIRBE	Diffuse Infrared Background Experiment
DISCOS	Dynamic Interaction Simulations of Controls and Structures
DMR	Differential Microwave Radiometer
DOF	degree of freedom
ECL	emitter-coupled logic
EGRET	Energetic Gamma Ray Experiment Telescope
ELF	extremely low frequency
ELV	expendable launch vehicle
Eos	Earth Observing System
EosDIS	Eos Data and Information System
EPROM	erasable, programmable read-only memory
ERB(E)	Earth Radiation Budget (Experiment)
ERBS	Earth Radiation Budget Satellite
ERS	Earth Resources Satellite
ESMR	Electrically Scanning Microwave Radiometer
EUV	extreme ultraviolet
EUVE	Extreme Ultraviolet Explorer
FCOM	fluorescent components of organic matter
FIFE	First ISLSCP Field Experiment
FIRAS	Far Infrared Absolute Spectrophotometer
FIRE	First ISCCP Regional Experiment
FTS	Flight Telerobotic Servicer
FUSE	Far Ultraviolet Spectroscope Explorer
FWHM	full width half maximum
GCM	General Circulation Model
GEOS	Geostationary Earth Orbiting Satellite
GLRS	Geoscience Laser Ranging System
GOES	Geostationary Operational Environmental Satellites
GRIS	Gamma-Ray Imaging Spectrometer
GRO	Gamma Ray Observatory
GRODY	Gamma Ray Dynamics Simulator
GTE	Global Tropospheric Experiment
HCPL	Hybrid Capillary Pumped Loop
HIRIS	High Resolution Imaging Spectrometer

PRECEDING PAGE BLANK NOT FILMED

PAGE 270 INTENTIONALLY BLANK

Acronyms

HST	Hubble Space Telescope
HTSC	high temperature superconductor
HV	high voltage
IDL	Interactive Data Language
IEEE	Institute of Electrical and Electronics Engineers
IFC	Intensive Field Campaigns
IMP	Interplanetary Monitoring Platform
IMS	interference mitigation schedule
INCA	Interactive Control Analysis
IOWA	Integrating Our Wondrous Analysis
ISCCP	International Satellite Cloud Climatology Project
ISLSCP	International Satellite Land Surface Climatology Project
ISO	International Standards Organization
ISTP	International Solar-Terrestrial Physics Project
LAWS	Laser Atmospheric Wind Sounder
LISA	Large Isotope Spectrometer for Astromag
LSA	Land System Analysis
LZP	level zero processing
MEDS	Modular Environment for Data Systems
MODIS	Moderate-Resolution Imaging Spectrometer
MPP	Massively Parallel Processor
MSS	Matrix Switch System
NAE	Nuclear Astrophysics Explorer
NCAR	National Center for Atmospheric Research
NCDC	National Climate Data Center
NCDS	NASA Climate Data System
NGS	NSSDC Graphics System
NIST	National Institute of Standards and Technology
NOAA	National Oceanic and Atmospheric Administration
NPV	net present value
NSSDC	National Space Science Data Center
OAST	Office of Aeronautics & Space Technology
ORU	Orbital Replacement Unit
PEPCO	Potomac Electric Power Company
PLDS	Pilot Land Data System
PROM	programmable read-only memory
PROMIS	Polar Regions Outer Magnetosphere International Study
PSD	power spectral density
RAC	Remote Analysis Computer
RAM	random access memory
RGB	Red Giant Branch
RMS	Remote Manipulator Systems
ROSAT	Roentgen Satellite
SAGE	Stratospheric Aerosol and Gas Experiment
SAR	Synthetic Aperture Radar
SBUV	Solar Backscatter Ultraviolet Radiometer
SCINATT	Spectra, Composition, and Interactions of Nuclei above 10 TeV
SCR	Surface Contour Radar
SEM	Space Environment Monitor
SHEMP	Self-Hosted Embedded Microprocessor
SIA	Station Interface Adapter
SME	Solar Mesospheric Explorer
SMM	Solar Maximum Mission
SMMR	Scanning Multichannel Microwave Radiometer
SOPS	Spacelab Output Processing System
SPAN	Space Physics Analysis Network
SPOT	Satellite pour L'Observation de la Terre
SSIS	Space Station Information System
SSM/I	Special Sensor Microwave/Imager
STOL	Systems Test and Operations Language
STS	Space Transportation System (Shuttle)

Acronyms

TAC	time-to-amplitude converter
TAE	Transportable Applications Environment
TDRS(S)	Tracking and Data Relay Satellite (System)
TIMS	Thermal Infrared Multispectral Scanner
TM	Thematic Mapper
TOMS	Total Ozone Mapping Spectrometer
TTL	transistor-to-transistor logic
UARS	Upper Atmospheric Research Satellite
VCDU	Virtual Channel Data Unit
VCSM	Virtual Channel Sorter Multiplexer
VEI	volcanic explosivity index
VLBI	very long baseline interferometry
VLSI	very large-scale integration
WDC	Wildcard Display Creator
WiZard	Measurements of Cosmic Rays Including AntiProtons, Positrons, AntiNuclei and a Search for Primordial Antimatter
XCAL	external calibrator
XTE	X-Ray Timing Explorer

Index

Author	Page
Abshire, Dr. James B.	18
Adamec, Dr. David D.	12
Alcorn, Dr. George E.	169, 177
Allison, Dr. Michael D.	79
Ames, Troy J.	200
Arsenovic, Petar	246
Atlas, Dr. Robert M.	57
Bailey, Steven A.	145
Baker, Dr. Daniel N.	91, 104
Barbier, Dr. Louis M.	106
Basile, Lisa	200
Bauer, Frank H.	239
Bavis, Patricia A.	259
Bell, Lynda J.	43
Benner, Dr. Steve M.	223, 224
Bergeson-Willis, Samuel E.	160
Bindschadler, Dr. Robert A.	5, 8
Blackstone, Michael	194
Bliven, Dr. Larry F.	14
Bonavito, Dr. N.L.	75
Bukowski, Michael T.	237
Burlaga, Dr. Leonard F.	96
Bush, Joy L.	192
Butler, Dan	226
Cahalan, Dr. Robert F.	60
Campbell, William J.	140
Canuto, Dr. Vittorio M.	80
Carlton, Douglas	192
Castell, Karen D.	214
Cavalieri, Dr. Donald J.	3
Chesters, Dr. Dennis	128
Clark, Dr. Thomas A.	43
Colony, Joe A.	248
Comberiate, Michael A.	166
Conrad, George R.	252
Cornwell, Donald M., Jr.	221
Costello, Dr. Frederick A.	223, 224
Dalton, Danny A.	245
Doiron, Scott D.	38
Domen, Mark A.	248
Dominy, Robert E.	208
Dorband, Dr. John E.	142
Douglass, Dr. Anne R.	50
Downing, Dr. John P.	239
Epstein, Dr. Gabriel L.	82
Feild, Thomas C., Jr.	230
Ferrare, Richard A.	71
Fichtel, Dr. Carl E.	110
Flom, Dr. Yury	213, 246
Frisch, Harold P.	242, 244
Garvin, Dr. James B.	18, 33
Garza-Robles, Raul	151
Gasser, Max G.	217
Gehrels, Dr. Neil A.	111
Goodman, Nancy S.	205
Goucher, Gregory W.	137
Greatorex, Scott A.	190
Green, Scott E.	207
Gruner, Timothy D.	236
Hall, Dr. Forrest G.	20
Hand, Sarah L.	183
Harris, Dr. Isadore	73
Hartke, Dr. Gregory J.	80
Hartley, Jonathan B.	173, 174
Heirtzler, Dr. James R.	41
Herrero, Dr. Fred A.	73, 101
Hoge, Dr. Frank E.	7
Horner, Ward P.	184
Hull, Larry G.	172, 203
Hunter, Dr. Stanley D.	115
Jackman, Dr. Charles H.	50
Jeletic, James F.	190
Jones, Jeffrey A.	96
Kalb, Virginia L.	45
Keller, Dr. John W.	98, 101
Kelley, Dr. Richard L.	117

PRECEDING PAGE BLANK NOT FILMED

Index

Author	Page
Kelly, Angelita C.	200
Kim, Hongsuk H.	31
Kimes, Dr. Daniel S.	25
King, Dr. Joseph H.	147
Klem, Dr. Edward B.	259
Klimas, Dr. Alexander J.	91
Kniffen, Dr. Donald A.	154
Koblinsky, Dr. Chester J.	10
Korb, Dr. Lawrence	68
Kram, Howard M.	181
Krueger, Dr. Arlin J.	38
Kyle, Dr. H. Lee	127
Lear, Ronald D.	259
Leidecker, Dr. Henning W.	249
Lepping, Dr. Ronald P.	96, 104
Lerner, Dr. Bao-Ting	232
Letourneau, Joseph H.	259
Long, Arlie D.	234
Mackenzie, Charles M.	161
Mandl, Daniel J.	192
Margolies, Donald L.	155
Markham, Brian L.	29
Mattson, Roger A.	153
Mayr, Dr. Hans G.	73, 87
McCabe, Michael E.	228, 229
McCann, Michael E.	259
McGarry, Jan L. F.	18
McGee, Dr. Thomas J.	53
McGuire, Dr. Robert E.	135
McIntosh, Roy	226, 228
Meeson, Dr. Blanche W.	133
Melfi, Dr. Samuel H.	71
Melson, W. Edward, Jr.	67
Miller, George N.	101
Miller, Warner H.	238
Morelli, Michael V.	232
Muller, Ronald M.	164
Murray, Henry L.	194
Nava, Dr. David F.	105
Nearhoof, Lee W.	243
Negri, Andrew J.	16
Neupert, Dr. Werner M.	82
Noll, Carey E.	124
O'Brien, John J.	160
Olney, David J.	236
Olsen, Lola M.	130
Ormes, Dr. Jonathan F.	106, 168
Owe, Dr. Manfred	27
Parkinson, Dr. Claire L.	3
Payne, Dr. Walter A., Jr.	105
Phenix, James E.	168
Pickering, Dr. Kenneth E.	58
Pisarski, Dr. Ryszard L.	122
Potler, Laura A.	122
Powers, Charles E.	250
Prather, Dr. Michael J.	52
Pritchard, Dr. James A.	192
Queen, Roy W.	259
Rash, James L.	187
Rawley, Dr. Gayle L.	117
Reber, Dr. Carl A.	47
Reed, Dr. Dennis E.	268
Roberts, Dr. D. Aaron	89
Sabia, Stephen	197
Salichs, Luis G.	181
Sauber, Dr. Jeanne M.	43
Schaefer, William H.	18
Schatten, Dr. Kenneth H.	87
Schmidlin, Francis J.	55
Schnetzler, Dr. Charles C.	38
Schnurr, Richard G.	216
Schulz, Dale F.	159
Schwemmer, Geary K.	68
Sellers, Dr. Piers J.	20
Sharpe, Deborah L.	263
Shope, Todd S.	236

Index

Author	Page
Shoupe, Ronald E.	257
Sinha, Pradeep	264
Slavin, Dr. James A.	104
Smith, I. Steve, Jr.	254
Smith, Nancy D.	189
Spaniol, Dr. G. Craig	222
Stark, Michael E.	208
Stecker, Dr. Floyd W.	114
Stephens, Mark A.	210
Stothers, Dr. Richard B.	40
Strong, Dr. James P.	146
Sud, Dr. Yogesh C.	62
Sutton, Dr. John F.	222
Swanson, Theodore D.	224, 229
Swartz, Marvin	85
Sweigart, Dr. Allen V.	84
Szczur, Martha R.	198
Tao, Dr. Wei-Kuo	64
Thomas, Edward F., Jr.	170
Thomas, Dr. Roger J.	82
Thompson, Dr. Anne M.	58
Thompson, Dr. William T.	85
Thorpe, Christopher J.	239
Tilton, Dr. James C.	143
Treinish, Lloyd A.	130, 137, 148
Trelease, Susan	264
Truszkowski, Walter F.	201
Tueller, Dr. Jack	108
Viens, Michael J.	251
Vranish, John M.	218, 220
Walsh, Dr. Edward J.	13
Walter, Dr. Louis S.	38
Walton, Barbara A.	175
Wasilewski, Dr. Peter J.	93
Watts, Paul	259
Weaver, Steven J.	192
White, Dr. Richard A.	121
Whiteman, David N.	71
Wong, Yen F.	187
Yeh, Dr. Pen-Shu	238
Zuber, Dr. Maria T.	18
Zwally, Dr. H. Jay	5